

EXTRACTION AND POLYMERIZATION OF BIOAROMATICS FROM MEGACROPS

By

STEVEN SHEN

A DISSERTATION PRESENTED TO THE GRADUATE SCHOOL
OF THE UNIVERSITY OF FLORIDA IN PARTIAL FULFILLMENT
OF THE REQUIREMENTS FOR THE DEGREE OF
DOCTOR OF PHILOSOPHY

UNIVERSITY OF FLORIDA

2019

© 2019 Steven Shen

If you have faith like a grain of mustard seed, you will say to this mountain, 'Move from here to there,' and it will move, and nothing will be impossible for you.

ACKNOWLEDGMENTS

First of all, I would like to thank my parents for their continuous support and unconditional love. I have gotten this far through their hard work from the early morning until late night, which they gave everything on my education and spent nothing on themselves. I thank my younger brother, Stanley Shen, who is an example on his calm and gentle attitudes. I thank my sister, Shirley Shen, for always spamming the family group chat with positive and cheerful messages. I also want to thank my family, especially my aunt, Gek Kim, for her immeasurable help during my struggles to get into University of Florida. I especially want to thank my girlfriend, Joanna Nadia, for all her prayers and support giving me perseverance throughout all my ups and downs. She motivates me, with her sweetest personality, to work hard and go the extra yard. She has been such a blessing to my life.

I would like to acknowledge my undergraduate research advisor, Dr. Eng. Yessi Permana, who first opened door and showed me the polymer world. He also connected me with Dr. Shogo Shimazu at Chiba University in Japan where I had the opportunity to do internship in his laboratory for three months. I thank my undergraduate research partners for the friendship and support during my final year of undergraduate.

I would like to thank all my former students and teacher coworkers at SMAK1 BPK Penabur Bandung for making me realize how I love teaching chemistry. Then, I would like to express my sincere gratitude to all my former students at University of Florida who I was trying to inspire but ended up inspiring me. I also thank Dr. Tammy Davidson for being a compassionate orgo lab coordinator, binding and building a solid team of orgo lab TAs.

I thank all the former graduates, undergraduates, and interns in the Miller Unit, Dr. Alexander Pemba, Dr. John Garcia, Dr. Ha Nguyen, Dr. Mayra Rostagno, Dr. Nicole Powell, Dr. Amr Feteha, Dr. Pengxu Qi, Dr. Olivier Nsengiyumva, Dr. Gabriel Short, Dr. Hipassia Moura, Khalid Alqahtani, Erik Price, Patricia Scheurle, Haley Donow, Marcus Reis, Enita Rastoder, Julie Chevillard, Fabio Ferrari, Amandine Heckmann, Lisa-Ann Ridley, and Jessica Thomas who I always admired; I truly had countless enjoyable discussion on life and research with everyone. I thank Dr. Mayra Rostagno who was my remarkable mentor on my first project and who I definitely learned a lot from. I thank Jessica Thomas who was the best undergraduate research ever. Her hard work, input, and positive personalities propelled all projects into completion. I also wish to thank the current Miller Group, Justin Smith, Yohei Yoshinaka, Jordan Torgunrud, Yu-Kai Su, Shih-Hsien Hsu, Alejandro Faria, Caroline Coxwell, Harper Cassady, Stephen Sangster, and Florian Diot-Néant for being my second family who I can rely on.

I would like to thank SPARC (Southeast Partnership for Advanced Renewables from Carinata) project for providing a platform for big collaborations. I am really grateful to be a part of something bigger than myself. I especially thank Dr. Sheeja George, Dr. Ian Small, Dr. David Wright, Dr. Nicolas DiLorenzo, Dr. Jon Stewart, Dr. Zhaohui Tong, and Edward N. Coppola, for providing us materials, instruments, suggestions, and supports on my Carinata projects. Of course, I would also like to thank USDA (United States Department of Agriculture) #1012948 and NSF (National Science Foundation) #1607263 for their financial supports which made all of these things possible.

I wish to thank my research committee: Dr. Alexander J. Greening, Dr. Lisa McElwee-White, Dr. Benjamin W. Smith, and Dr. Jennifer Andrew for taking the time out

of their schedules to help me reaching my goals. I also would like to thank Dr. Florent Allais who was very supportive during my internship at Chaire ABI in Reims, France. I thank everyone for being researchers that I can always look up to.

Finally, I would like to express my heartfelt gratitude to my advisor, Dr. Stephen A. Miller, for being an extraordinary advisor. I thank him for believing in me and allowing me to work in the Miller Unit. I thank him for his continuous guidance and support. Indeed, he has taught me polymer and organic chemistry, but more importantly, he taught me to push my limit, to develop a passion for learning, and to build the personal confidence. I will certainly carry this with me throughout my professional career development. I could not imagine a better person to work under for my PhD.

I started my PhD journey five years ago and I cannot believe that now I am almost at the end of it. The path was not smooth or even clearly marked, and sometimes there were weird detours. However, I thank the Lord God for blessing me with some of the most amazing people along the way. My growth as a PhD student definitely came from surrounding myself with incredibly capable people and having supportive network of family and friends. I was very fortunate to have such wonderful labmates and supervisor on my PhD study. This journey was indeed beautiful.

TABLE OF CONTENTS

| | <u>page</u> |
|---|-------------|
| ACKNOWLEDGMENTS..... | 4 |
| LIST OF TABLES..... | 10 |
| LIST OF FIGURES..... | 11 |
| LIST OF ABBREVIATIONS..... | 31 |
| ABSTRACT..... | 32 |
| CHAPTER | |
| 1 BIORENEWABLES FROM <i>BRASSICA CARINATA</i> BIOMILL..... | 34 |
| Background..... | 34 |
| Biofuels from <i>Brassica carinata</i> | 37 |
| Biorenewables from <i>Brassica carinata</i> | 39 |
| Erucic acid for biorenewables..... | 39 |
| Glucosinolates..... | 41 |
| Sinapic acid..... | 42 |
| Results and discussion..... | 44 |
| Extraction of sinapic acid from <i>Brassica carinata</i> meal..... | 45 |
| Synthesis of polyethylene sinapate and congeners..... | 48 |
| Synthesis of polyethylene sinapate from extracted sinapic acid..... | 53 |
| Conclusions..... | 54 |
| 2 WEAK LINKS IN SINAPIC ACID-BASED POLYMERS..... | 56 |
| Background..... | 56 |
| Experimental..... | 61 |
| Materials..... | 61 |
| Characterization..... | 61 |
| Synthesis..... | 62 |
| Results and discussion..... | 69 |
| Monomer design..... | 69 |
| Optimization of polymerization conditions..... | 72 |
| Polymer synthesis..... | 74 |
| Accelerated degradation studies..... | 83 |
| Conclusions..... | 85 |
| 3 EXTRACTION OF HYDROXYCINNAMIC ACIDS FROM SUGARCANE AND CORN..... | 87 |
| Background..... | 87 |

| | |
|--|-----|
| Experimental..... | 89 |
| Materials..... | 89 |
| Characterization | 89 |
| Extraction procedure | 90 |
| Reflux extraction | 90 |
| Pressurized extraction | 90 |
| Ultrasound-assisted extraction..... | 91 |
| Microwave-assisted extraction | 92 |
| Results and discussion | 92 |
| Sugarcane bagasse and lignin paste | 92 |
| Corn bran, cob, silk, and tassel | 96 |
| Conclusions | 98 |
| | |
| 4 SUSTAINABLE POLYVINYL ACETALS FROM BIOAROMATIC ALDEHYDES | 99 |
| Background..... | 99 |
| Experimental..... | 104 |
| Materials..... | 104 |
| Characterization | 104 |
| Polyvinyl acetal synthesis..... | 105 |
| Kinetic studies | 107 |
| Hydrolysis experiments | 108 |
| Results and discussion | 109 |
| Bioaromatic aldehydes employed..... | 109 |
| Acetalization optimization | 110 |
| Kinetic studies | 111 |
| Structure and acetal determination by NMR..... | 114 |
| Level of acetalization..... | 115 |
| Thermal properties | 117 |
| Effect of PVA molecular weight on polyvinyl acetal properties | 120 |
| Heterogeneous degradation studies..... | 120 |
| Conclusions | 122 |
| | |
| 5 RENEWABLE POLYMERS VIA THE BIGINELLI MULTICOMPONENT REACTION | 124 |
| Background..... | 124 |
| Results and discussion | 126 |
| Poly-DHMP analogue from cyclopentanone..... | 126 |
| Poly-DHMP analogue from dimethyl 3-oxoglutarate..... | 129 |
| Conclusions | 132 |
| | |
| 6 EXPERIMENTAL | 133 |
| Chapter 1 | 133 |
| Chapter 2..... | 142 |
| Chapter 3..... | 154 |

| | |
|--|-----|
| Chapter 4..... | 158 |
| Chapter 5..... | 167 |
| APPENDIX | |
| A SUPPLEMENTARY INFORMATION FOR CHAPTER 1..... | 172 |
| TGA Spectra | 172 |
| DSC Spectra..... | 179 |
| GPC Spectra..... | 186 |
| NMR Spectra | 188 |
| B SUPPLEMENTARY INFORMATION FOR CHAPTER 2..... | 204 |
| TGA Spectra | 204 |
| DSC Spectra..... | 219 |
| GPC Spectra..... | 234 |
| NMR Spectra | 238 |
| C SUPPLEMENTARY INFORMATION FOR CHAPTER 3..... | 264 |
| NMR Spectra | 264 |
| D SUPPLEMENTARY INFORMATION FOR CHAPTER 4..... | 270 |
| TGA Spectra | 270 |
| DSC Spectra..... | 278 |
| GPC Spectra..... | 286 |
| NMR Spectra | 292 |
| E SUPPLEMENTARY INFORMATION FOR CHAPTER 5..... | 304 |
| TGA Spectra | 304 |
| DSC Spectra..... | 309 |
| GPC Spectra..... | 312 |
| NMR Spectra | 316 |
| BIOGRAPHICAL SKETCH..... | 320 |
| LIST OF REFERENCES | 321 |

LIST OF TABLES

| <u>Table</u> | <u>page</u> |
|--------------|---|
| 1-1 | Polymerization results for polyalkylene sinapates 49 |
| 1-2 | Copolymerization results of the copoly(hydroxyethyl dihydrosinapic acid/hydroxyethylsinapic acid) series 51 |
| 2-1 | Optimization study of polyhexyleneglycolate dihydrosinapate and polyhexyleneglycolate sinapate 72 |
| 2-2 | Copolymerization results of copoly(ethyleneglycolate dihydrosinapate/ethyleneglycolate sinapate) series 73 |
| 2-3 | Homopolymerization results of polyalkyleneglycolate sinapates. ^a 76 |
| 2-4 | Copolymerization results of the copoly(ethylenelactate dihydrosinapate/ethylenelactate sinapate) series 78 |
| 2-5 | Polymerization results of ferulic acid based polymers, <i>p</i> -coumaric acid-based polymers, sinapic acid based-polyamide, and sinapic acid-based polyesteramide 79 |
| 2-6 | Degradation studies of polyethyleneglycolate dihydrosinapate (PEGHS), polyethylenelactate dihydrosinapate (PELHS), and polylactic acid (PLA) 84 |
| 3-1 | Iterative extraction results on dried lignin paste and sugarcane bagasse..... 94 |
| 3-2 | Extraction results of ferulic acid and <i>p</i> -coumaric acid from corn bran, cob, silk and tassel 97 |
| 4-1 | Polyvinyl acetals from polyvinyl alcohol (PVA) and 13 different aldehydes, along with isolated yield and characterization data..... 117 |
| 5-1 | Optimization study of poly-DHMP from van-2-van, cyclopentanone, and urea. 128 |
| 5-2 | Polymerization results of poly-DHMP analogues from bioaromatic dialdehyde monomers, dimethyl 3-oxoglutarate, and urea 130 |
| 6-1 | Various extraction results 141 |

LIST OF FIGURES

| <u>Figure</u> | <u>page</u> |
|---------------|---|
| 1-1 | Biofuels and biorenewables from <i>Brassica carinata</i> 36 |
| 1-2 | Extraction and polymerization of sinapic acid from <i>Brassica carinata</i> 44 |
| 1-3 | Basic aqueous hydrolysis and extraction of sinapic acid from <i>carinata</i> meal. 46 |
| 1-4 | Extraction and basic aqueous hydrolysis of sinapine. 47 |
| 1-5 | Synthetic route of polyalkylene sinapate (blue, left) and polyethylene dihydrosinapate (orange, right)..... 48 |
| 1-6 | Comparison of glass transition temperatures for the copoly(hydroxyethyl dihydrosinapic acid/hydroxyethyl sinapic acid) series observed by Differential Scanning Calorimetry (light blue diamonds) to those calculated by the Fox equation (light grey circles). 52 |
| 1-7 | Comparison between polyethylene sinapate (PES) from extracted sinapic acid and from commercial petroleum sinapic acid. 53 |
| 2-1 | Polyethylene terephthalate (PET) alternatives from sinapic acid exhibit superior glass transition temperatures (T_g) vs. petroleum-based PET. 59 |
| 2-2 | Synthesis of dimethylglycolate sinapate, dimethylglycolate dihydrosinapate, dimethyl lactate sinapate, and dimethyl lactate dihydrosinapate from sinapic acid, which can be extracted from <i>Carinata</i> seed meal. 70 |
| 2-3 | Synthetic route to copoly(ethyleneglycolate dihydrosinapate/ethyleneglycolate sinapate) (R = H), copoly(ethylenelactate dihydrosinapate/ethylenelactate sinapate) (R = Me), polyalkyleneglycolate sinapate ($n = 2-10$), and polyalkyleneglycolate dihydrosinapate ($n = 2$ and 6). . 71 |
| 2-4 | Glass transition temperatures observed and plotted for copoly(ethyleneglycolate dihydrosinapate/ethyleneglycolate sinapate). 75 |
| 2-5 | Glass transition temperatures observed and plotted for polyalkyleneglycolate sinapates. 78 |
| 2-6 | Comparison of glass transition temperatures between copoly(ethyleneglycolate dihydrosinapate/ethyleneglycolate sinapate) (light green circles) and copoly(ethylenelactate dihydrosinapate/ethylenelactate sinapate) (light orange squares). 81 |

| | | |
|-----|---|-----|
| 2-7 | Hydrolysis of polyethyleneglycolate dihydrosinapate and polyethylenelactate dihydrosinapate generated glycolic sinapic diacid and lactic sinapic diacid as shown by ¹ H NMR | 84 |
| 3-1 | Simplified extraction flowchart for sugarcane bagasse and lignin paste resulting in <i>p</i> -coumaric acid and ferulic acid..... | 93 |
| 3-2 | Yield comparison on reflux, pressurized, ultrasound-assisted, microwave-assisted extraction of lignin paste (blue) and sugarcane bagasse (orange). | 95 |
| 3-3 | Extraction of <i>p</i> -coumaric acid and ferulic acid from corn components (silk, tassel, bran, cob)..... | 96 |
| 3-4 | ¹ H NMR spectrum of commercial <i>p</i> -coumaric acid and ferulic acid and extracted <i>p</i> -coumaric acid (triangles) and ferulic acid (dots) from corn cob..... | 97 |
| 4-1 | The acetalization of polyvinyl alcohol (PVA) with formaldehyde (R = H) or butyraldehyde (R = Pr) yields polyvinyl formal (PVF) or polyvinyl butyral (PVB), respectively. | 100 |
| 4-2 | Polyvinyl alcohol (PVA) is herein condensed with bioaromatic aldehydes that are lignin-derived (HB , VV , SY), synthetic (EV), naturally occurring (OV , IV , SA , OA , PA , BZ , CI , CU), or glucose-derived (HMF). | 103 |
| 4-3 | The acetalization of PVA with vanillin is catalysed by <i>p</i> -TSA and yields polyvinyl vanillin acetal (PV-VV-A) with 63.3% of the –OH groups converted to acetals. | 107 |
| 4-4 | Acetalization of PVA with vanillin versus time measured by ¹ H NMR: (a) acetal peak integration (5.4 ppm, arbitrary units) versus time over 17 hours; (b) NMR spectra cascade for the acetal region (5.2–5.7 ppm) and the methylene region (1.2–1.7 ppm) every 12 minutes for the first 3 hours, and every hour until the end of the experiment (16.8 hours). | 111 |
| 4-5 | Glass transition temperature (°C, circles) and degree of acetalization (% , squares) vs. time measured for aliquots removed from the bulk acetalization of PVA with vanillin. | 113 |
| 4-6 | For the seven homologous benzaldehydes with increasing substitution at the 3, 4, and 5 positions (X, Y, Z), the extent of acetalization ($2x/[2x+y]$) decreases with increasing sterics, as measured by the aldehyde molecular weight. | 116 |
| 4-7 | The glass transition temperature (<i>T</i> _g) of PVA is increased via acetalization (ranging from 54 to 75%) with bioaromatic aldehydes and the measured <i>T</i> _g value can be correlated to aldehyde structure and functionality. Hydrogen bonding is key to high <i>T</i> _g values (139 to 157 °C)..... | 118 |

| | | |
|------|--|-----|
| 4-8 | Heterogeneous hydrolysis study of PV-VV-A with 54.0 % initial acetalization. 24-hour exposure to deionized water or pH = 5 aqueous buffer effected no hydrolysis, but hydrolysis was significant in more acidic aqueous media with residual acetalization of 28.4, 3.2, or 0.8 % for pH = 3, 2, or 1, respectively. ... | 121 |
| 5-1 | Previous work on (a) conventional Biginelli reaction and (b) modified Biginelli reaction..... | 125 |
| 5-2 | Preliminary study: synthesis of dihydropyrimidinone (DHMP) analogue via a modified Biginelli reaction by Hu <i>et al.</i> | 126 |
| 5-3 | Synthesis of bioaromatic dialdehyde monomers. | 127 |
| 6-1 | Comparison of crude product and purified product using activated charcoal. ... | 157 |
| A-1 | TGA Thermogram of polyethylene dihydrosinapate (Table 1-1, Entry 2 and Table 1-2, Entry 1)..... | 172 |
| A-2 | TGA Thermogram of copoly(hydroxyethyl dihydrosinapic acid/hydroxyethylsinapic acid) [90:10] (Table 1-2, Entry 2) | 172 |
| A-3 | TGA Thermogram of copoly(hydroxyethyl dihydrosinapic acid/hydroxyethylsinapic acid) [80:20] (Table 1-2, Entry 3) | 173 |
| A-4 | TGA Thermogram of copoly(hydroxyethyl dihydrosinapic acid/hydroxyethylsinapic acid) [70:30] (Table 1-2, Entry 4) | 173 |
| A-5 | TGA Thermogram of copoly(hydroxyethyl dihydrosinapic acid/hydroxyethylsinapic acid) [60:40] (Table 1-2, Entry 5) | 174 |
| A-6 | TGA Thermogram of copoly(hydroxyethyl dihydrosinapic acid/hydroxyethylsinapic acid) [50:50] (Table S3, Entry 6) | 174 |
| A-7 | TGA Thermogram of copoly(hydroxyethyl dihydrosinapic acid/hydroxyethylsinapic acid) [40:60] (Table 1-2, Entry 7) | 175 |
| A-8 | TGA Thermogram of copoly(hydroxyethyl dihydrosinapic acid/hydroxyethylsinapic acid) [30:70] (Table 1-2, Entry 8) | 175 |
| A-9 | TGA Thermogram of copoly(hydroxyethyl dihydrosinapic acid/hydroxyethylsinapic acid) [20:80] (Table 1-2, Entry 9) | 176 |
| A-10 | TGA Thermogram of copoly(hydroxyethyl dihydrosinapic acid/hydroxyethylsinapic acid) [10:90] (Table 1-2, Entry 10) | 176 |
| A-11 | TGA Thermogram of polyethylene sinapate (Table 1-1, Entry 1 and Table 1-2, Entry 11)..... | 177 |
| A-12 | TGA Thermogram of polypropylene sinapate (Table 1-1, Entry 3) | 177 |

| | | |
|------|---|-----|
| A-13 | TGA Thermogram of polyhexalene sinapate (Table 1-1, Entry 4) | 178 |
| A-14 | TGA Thermogram of polyethylene sinapate from extracted sinapic acid..... | 178 |
| A-15 | DSC Thermogram of polyethylene dihydrosinapate (Table 1-1, Entry 2 and Table 1-2, Entry 1)..... | 179 |
| A-16 | DSC Thermogram of copoly(hydroxyethyl dihydrosinapic acid/hydroxyethylsinapic acid) [90:10] (Table 1-2, Entry 2) | 179 |
| A-17 | DSC Thermogram of copoly(hydroxyethyl dihydrosinapic acid/hydroxyethylsinapic acid) [80:20] (Table 1-2, Entry 3) | 180 |
| A-18 | DSC Thermogram of copoly(hydroxyethyl dihydrosinapic acid/hydroxyethylsinapic acid) [70:30] (Table 1-2, Entry 4) | 180 |
| A-19 | DSC Thermogram of copoly(hydroxyethyl dihydrosinapic acid/hydroxyethylsinapic acid) [60:40] (Table 1-2, Entry 5) | 181 |
| A-20 | DSC Thermogram of copoly(hydroxyethyl dihydrosinapic acid/hydroxyethylsinapic acid) [50:50] (Table 1-2, Entry 6) | 181 |
| A-21 | DSC Thermogram of copoly(hydroxyethyl dihydrosinapic acid/hydroxyethylsinapic acid) [40:60] (Table 1-2, Entry 7) | 182 |
| A-22 | DSC Thermogram of copoly(hydroxyethyl dihydrosinapic acid/hydroxyethylsinapic acid) [30:70] (Table 1-2, Entry 8) | 182 |
| A-23 | DSC Thermogram of copoly(hydroxyethyl dihydrosinapic acid/hydroxyethylsinapic acid) [20:80] (Table 1-2, Entry 9) | 183 |
| A-24 | DSC Thermogram of copoly(hydroxyethyl dihydrosinapic acid/hydroxyethylsinapic acid) [10:90] (Table 1-2, Entry 10) | 183 |
| A-25 | DSC Thermogram of polyethylene sinapate (Table 1-1, Entry 1) | 184 |
| A-26 | DSC Thermogram of polypropylene sinapate (Table 1-1, Entry 3)..... | 184 |
| A-27 | DSC Thermogram of polyhexalene sinapate (Table 1-1, Entry 4)..... | 185 |
| A-28 | DSC Thermogram of polyethylen sinapate from extracted sinapic acid. | 185 |
| A-29 | GPC Chromatogram of polyethylene dihydrosinapate (Table 1-1, Entry 2 and Table 1-2, Entry 1)..... | 186 |
| A-30 | GPC Chromatogram of copoly(hydroxyethyl dihydrosinapic acid/hydroxyethylsinapic acid) [90:10] (Table 1-2, Entry 2). | 186 |
| A-31 | GPC Chromatogram of polyhexalene sinapate (Table 1-1, Entry 4)..... | 187 |

| | | |
|------|---|-----|
| A-32 | ¹ H NMR Spectrum of commercial sinapic acid. | 188 |
| A-33 | ¹ H NMR Spectrum of extracted sinapic acid from base hydrolysis. | 188 |
| A-34 | ¹ H NMR Spectrum of extracted sinapic acid from sonication..... | 188 |
| A-35 | ¹ H NMR Spectrum of extracted sinapine from MeOH hydrolysis..... | 189 |
| A-36 | ¹ H NMR Spectrum of extracted sinapic acid from MeOH hydrolysis. | 189 |
| A-37 | ¹ H NMR Spectrum of extracted sinapine from EtOH hydrolysis. | 189 |
| A-38 | ¹ H NMR Spectrum of extracted sinapic acid from EtOH hydrolysis. | 190 |
| A-39 | ¹ H NMR Spectrum of combined extracted sinapic acid for polymerization. | 190 |
| A-40 | ¹ H NMR Spectrum of hydroxyethylsinapic acid. | 190 |
| A-41 | ¹ H NMR Spectrum of hydroxyethyldihydrosinapic acid..... | 191 |
| A-42 | ¹ H NMR Spectrum of hydroxypropylsinapic acid. | 191 |
| A-43 | ¹ H NMR Spectrum of hydroxyhexylsinapic acid..... | 191 |
| A-44 | ¹ H NMR Spectrum of hydroxyethylsinapic acid from extracted sinapic acid..... | 192 |
| A-45 | ¹ H NMR Spectrum of polyethylene dihydrosinapate (Table 1-1, Entry 2 and Table 1-2, Entry 1)..... | 192 |
| A-46 | ¹ H NMR Spectrum of copoly(hydroxyethyldihydrosinapic acid/hydroxyethylsinapic acid) [90:10] (Table 1-2, Entry 2) | 192 |
| A-47 | ¹ H NMR Spectrum of copoly(hydroxyethyldihydrosinapic acid/hydroxyethylsinapic acid) [80:20] (Table 1-2, Entry 3) | 193 |
| A-48 | ¹ H NMR Spectrum of copoly(hydroxyethyldihydrosinapic acid/hydroxyethylsinapic acid) [70:30] (Table 1-2, Entry 4) | 193 |
| A-49 | ¹ H NMR Spectrum of copoly(hydroxyethyldihydrosinapic acid/hydroxyethylsinapic acid) [60:40] (Table 1-2, Entry 5) | 193 |
| A-50 | ¹ H NMR Spectrum of copoly(hydroxyethyldihydrosinapic acid/hydroxyethylsinapic acid) [50:50] (Table 1-2, Entry 6) | 194 |
| A-51 | ¹ H NMR Spectrum of copoly(hydroxyethyldihydrosinapic acid/hydroxyethylsinapic acid) [40:60] (Table 1-2, Entry 7) | 194 |
| A-52 | ¹ H NMR Spectrum of copoly(hydroxyethyldihydrosinapic acid/hydroxyethylsinapic acid) [30:70] (Table 1-2, Entry 8) | 194 |

| | | |
|------|---|-----|
| A-53 | ¹ H NMR Spectrum of copoly(hydroxyethyl-dihydro-sinapic acid/hydroxyethylsinapic acid) [20:80] (Table 1-2, Entry 9) | 195 |
| A-54 | ¹ H NMR Spectrum of copoly(hydroxyethyl-dihydro-sinapic acid/hydroxyethylsinapic acid) [10:90] (Table 1-2, Entry 10) | 195 |
| A-55 | ¹ H NMR Spectrum of polyethylene sinapate (Table 1-2, Entry 1 and Table 1-2, Entry 11) | 195 |
| A-56 | ¹ H NMR Spectrum of polypropylene sinapate (Table 1-2, Entry 3)..... | 196 |
| A-57 | ¹ H NMR Spectrum of polyhexalene sinapate (Table 1-2, Entry 4)..... | 196 |
| A-58 | ¹ H NMR Spectrum of polyethylene sinapate from extracted sinapic acid. | 196 |
| A-59 | ¹³ C NMR Spectrum of commercial sinapic acid | 197 |
| A-60 | ¹³ C NMR Spectrum of extracted sinapic acid | 197 |
| A-61 | ¹³ C NMR Spectrum of hydroxyethylsinapic acid | 197 |
| A-62 | ¹³ C NMR Spectrum of hydroxyethyl-dihydro-sinapic acid | 198 |
| A-63 | ¹³ C NMR Spectrum of hydroxypropylsinapic acid | 198 |
| A-64 | ¹³ C NMR Spectrum of hydroxyhexalene sinapic acid | 198 |
| A-65 | ¹³ C NMR Spectrum of hydroxyethylsinapic acid from extracted sinapic acid..... | 199 |
| A-66 | ¹³ C NMR Spectrum of polyethylene dihydro-sinapate (Table 1-1, entry 2, Table 1-2, entry 1). | 199 |
| A-67 | ¹³ C NMR Spectrum of copoly(hydroxyethyl-dihydro-sinapic acid/hydroxyethylsinapic acid) [90:10] (Table 1-2, Entry 2) | 199 |
| A-68 | ¹³ C NMR Spectrum of copoly(hydroxyethyl-dihydro-sinapic acid/hydroxyethylsinapic acid) [80:20] (Table 1-2, Entry 3) | 200 |
| A-69 | ¹³ C NMR Spectrum of copoly(hydroxyethyl-dihydro-sinapic acid/hydroxyethylsinapic acid) [70:30] (Table 1-2, Entry 4) | 200 |
| A-70 | ¹³ C NMR Spectrum of copoly(hydroxyethyl-dihydro-sinapic acid/hydroxyethylsinapic acid) [60:40] (Table 1-2, Entry 5) | 200 |
| A-71 | ¹³ C NMR Spectrum of copoly(hydroxyethyl-dihydro-sinapic acid/hydroxyethylsinapic acid) [50:50] (Table 1-2, Entry 6) | 201 |

| | | |
|------|---|-----|
| A-72 | ¹³ C NMR Spectrum of copoly(hydroxyethyl dihydro sinapic acid/hydroxyethyl sinapic acid) [40:60] (Table 1-2, Entry 7) | 201 |
| A-73 | ¹³ C NMR Spectrum of copoly(hydroxyethyl dihydro sinapic acid/hydroxyethyl sinapic acid) [30:70] (Table 1-2, Entry 8) | 201 |
| A-74 | ¹³ C NMR Spectrum of copoly(hydroxyethyl dihydro sinapic acid/hydroxyethyl sinapic acid) [20:80] (Table 1-2, Entry 9) | 202 |
| A-75 | ¹³ C NMR Spectrum of copoly(hydroxyethyl dihydro sinapic acid/hydroxyethyl sinapic acid) [10:90] (Table 1-2, Entry 10) | 202 |
| A-76 | ¹³ C NMR Spectrum of polyethylene sinapate (Table 1-1, entry 1 and Table 1-2, entry 11) | 202 |
| A-77 | ¹³ C NMR Spectrum of polypropylene sinapate (Table 1-2, entry 3)..... | 203 |
| A-78 | ¹³ C NMR Spectrum of polyhexalene sinapate (Table S2, entry 4)..... | 203 |
| A-79 | ¹³ C NMR Spectrum of polyethylene sinapate from extracted sinapic acid..... | 203 |
| B-1 | TGA Thermogram of polyethyleneglycolate dihydro sinapate (Table 2-2, entry 1) | 204 |
| B-2 | TGA Thermogram of copoly(ethyleneglycolate dihydro sinapate/ethyleneglycolate sinapate) [90:10] (Table 2-2, entry 2)..... | 204 |
| B-3 | TGA Thermogram of copoly(ethyleneglycolate dihydro sinapate/ethyleneglycolate sinapate) [80:20] (Table 2-2, entry 3)..... | 205 |
| B-4 | TGA Thermogram of copoly(ethyleneglycolate dihydro sinapate/ethyleneglycolate sinapate) [70:30] (Table 2-2, entry 4)..... | 205 |
| B-5 | TGA Thermogram of copoly(ethyleneglycolate dihydro sinapate/ethyleneglycolate sinapate) [60:40] (Table 2-2, entry 5)..... | 206 |
| B-6 | TGA Thermogram of copoly(ethyleneglycolate dihydro sinapate/ethyleneglycolate sinapate) [50:50] (Table 2-2, entry 6)..... | 206 |
| B-7 | TGA Thermogram of copoly(ethyleneglycolate dihydro sinapate/ethyleneglycolate sinapate) [40:60] (Table 2-2, entry 7)..... | 207 |
| B-8 | TGA Thermogram of copoly(ethyleneglycolate dihydro sinapate/ethyleneglycolate sinapate) [30:70] (Table 2-2, entry 8)..... | 207 |
| B-9 | TGA Thermogram of copoly(ethyleneglycolate dihydro sinapate/ethyleneglycolate sinapate) [20:80] (Table 2-2, Entry 9) | 208 |

| | | |
|------|---|-----|
| B-10 | TGA Thermogram of copoly(ethyleneglycolate dihydrosinapate/ethyleneglycolate sinapate) [10:90] (Table 2-2, entry 10)..... | 208 |
| B-11 | TGA Thermogram of polyethyleneglycolate sinapate (Table 2-2, entry 11)..... | 209 |
| B-12 | TGA Thermogram of polypropyleneglycolate sinapate (Table 2-3, entry 2) | 209 |
| B-13 | TGA Thermogram of polybutyleneglycolate sinapate (Table 2-3, entry 3)..... | 210 |
| B-14 | TGA Thermogram of polypentyleneglycolate sinapate (Table 2-3, entry 4)..... | 210 |
| B-15 | TGA Thermogram of polyhexyleneglycolate dihydrosinapate (Table 2-1, entry 2). | 211 |
| B-16 | TGA Thermogram of polyhexyleneglycolate sinapate (Table 2-3, entry 5)..... | 211 |
| B-17 | TGA Thermogram of polyoctyleneglycolate sinapate (Table 2-3, entry 6)..... | 212 |
| B-18 | TGA Thermogram of polynonyleneglycolate sinapate (Table 2-3, entry 7)..... | 212 |
| B-19 | TGA Thermogram of polydecyleneglycolate sinapate (Table 2-3, entry 8)..... | 213 |
| B-20 | TGA Thermogram of polyethylenelactate dihydrosinapate (Table 2-4, entry 1). | 213 |
| B-21 | TGA Thermogram of copoly(ethylenelactate dihydrosinapate/ethylenelactate sinapate) [70:30] (Table 2-4, entry 2) | 214 |
| B-22 | TGA Thermogram of copoly(ethylenelactate dihydrosinapate/ethylenelactate sinapate) [50:50] (Table 2-4, Entry 3) | 214 |
| B-23 | TGA Thermogram of copoly(ethylenelactate dihydrosinapate/ethylenelactate sinapate) [30:70] (Table 2-4, entry 4) | 215 |
| B-24 | TGA Thermogram of polyethylenelactate sinapate (Table 2-4, entry 5) | 215 |
| B-25 | TGA Thermogram of polyethyleneglycolate ferulate (Table 2-5, entry 1). | 216 |
| B-26 | TGA Thermogram of polyethyleglycolate coumarate (Table 2-5, entry 2) | 216 |
| B-27 | TGA Thermogram of polyethylenelactate ferulate (Table 2-5, entry 3)..... | 217 |
| B-28 | TGA Thermogram of polyethylenelactate coumarate (Table 2-4, entry 4)..... | 217 |
| B-29 | TGA Thermogram of polyethyleneglycolate dihydrosinapamide (polyesteramide) (Table 2-5, entry 5). | 218 |
| B-30 | TGA Thermogram of polyethyleneglycolaamide dihydrosinapamide (polyamide) (Table 2-5, entry 6). | 218 |

| | | |
|------|---|-----|
| B-31 | DSC Thermogram of polyethyleneglycolate dihydrosinapate (Table 2-2, entry 1). | 219 |
| B-32 | DSC Thermogram of copoly(ethyleneglycolate dihydrosinapate/ethyleneglycolate sinapate) [90:10] (Table 2-2, entry 2)..... | 219 |
| B-33 | DSC Thermogram of copoly(ethyleneglycolate dihydrosinapate/ethyleneglycolate sinapate) [80:20] (Table 2-2, entry 3)..... | 220 |
| B-34 | DSC Thermogram of copoly(ethyleneglycolate dihydrosinapate/ethyleneglycolate sinapate) [70:30] (Table 2-2, entry 4)..... | 220 |
| B-35 | DSC Thermogram of copoly(ethyleneglycolate dihydrosinapate/ethyleneglycolate sinapate) [60:40] (Table 2-2, entry 5)..... | 221 |
| B-36 | DSC Thermogram of copoly(ethyleneglycolate dihydrosinapate/ethyleneglycolate sinapate) [50:50] (Table 2-2, entry 6)..... | 221 |
| B-37 | DSC Thermogram of copoly(ethyleneglycolate dihydrosinapate/ethyleneglycolate sinapate) [40:60] (Table 2-2, entry 7)..... | 222 |
| B-38 | DSC Thermogram of copoly(ethyleneglycolate dihydrosinapate/ethyleneglycolate sinapate) [30:70] (Table 2-2, entry 8)..... | 222 |
| B-39 | DSC Thermogram of copoly(ethyleneglycolate dihydrosinapate/ethyleneglycolate sinapate) [20:80] (Table 2-2, entry 9)..... | 223 |
| B-40 | DSC Thermogram of copoly(ethyleneglycolate dihydrosinapate/ethyleneglycolate sinapate) [10:90] (Table 2-2, entry 10)..... | 223 |
| B-41 | DSC Thermogram of polyethyleneglycolate sinapate (Table 2-2, entry 11) | 224 |
| B-42 | DSC Thermogram of polypropyleneglycolate sinapate (Table 2-3, entry 2) | 224 |
| B-43 | DSC Thermogram of polybutyleneglycolate sinapate (Table 2-3, entry 3) | 225 |
| B-44 | DSC Thermogram of polypentyleneglycolate sinapate (Table 2-3, entry 4) | 225 |
| B-45 | DSC Thermogram of polyhexyleneglycolate dihydrosinapate (Table 2-1, entry 2) | 226 |
| B-46 | DSC Thermogram of polyhexyleneglycolate sinapate (Table 2-3, entry 5)..... | 226 |
| B-47 | DSC Thermogram of polyoctyleneglycolate sinapate (Table 2-3, entry 6)..... | 227 |
| B-48 | DSC Thermogram of polynonyleneglycolate sinapate (Table 2-3, entry 7) | 227 |
| B-49 | DSC Thermogram of polydecyleneglycolate sinapate (Table 2-3, entry 8)..... | 228 |

| | | |
|------|---|-----|
| B-50 | DSC Thermogram of polyethylenelactate dihydrosinapate (Table 2-4, entry 1) | 228 |
| B-51 | DSC Thermogram of copoly(ethylenelactate dihydrosinapate/ethylenelactate sinapate) [70:30] (Table 2-4, entry 2) | 229 |
| B-52 | DSC Thermogram of copoly(ethylenelactate dihydrosinapate/ethylenelactate sinapate) [50:50] (Table 2-4, entry 3) | 229 |
| B-53 | DSC Thermogram of copoly(ethylenelactate dihydrosinapate/ethylenelactate sinapate) [30:70] (Table 2-4, entry 4) | 230 |
| B-54 | DSC Thermogram of polyethylenelactate sinapate (Table 2-4, entry 5) | 230 |
| B-55 | DSC Thermogram of polyethyleneglycolate ferulate (Table 2-5, entry 1) | 231 |
| B-56 | DSC Thermogram of polyethyleglycolate coumarate (Table 2-5, entry 2) | 231 |
| B-57 | DSC Thermogram of polyethylenelactate ferulate (Table 2-5, entry 3) | 232 |
| B-58 | DSC Thermogram of polyethylenelactate coumarate (Table 2-5, entry 4) | 232 |
| B-59 | DSC Thermogram of polyethyleneglycolate dihydrosinapamide (polyesteramide) (Table 2-5, entry 5) | 233 |
| B-60 | DSC Thermogram of polyethyleneglycolamide dihydrosinapamide (polyamide) (Table 2-5, entry 6) | 233 |
| B-61 | GPC Chromatogram of polyethyleneglycolate dihydrosinapate (Table 2-2, entry 1) | 234 |
| B-62 | GPC Chromatogram of copoly(ethyleneglycolate dihydrosinapate/ethyleneglycolate sinapate) [90:10] (Table 2-2, Entry 2) | 234 |
| B-63 | GPC Chromatogram of copoly(ethyleneglycolate dihydrosinapate/ethyleneglycolate sinapate) [80:20] (Table 2-2, Entry 2) | 235 |
| B-64 | GPC Chromatogram of polyhexyleneglycolate dihydrosinapate (Table 2-1, Entry 2) | 235 |
| B-65 | GPC Chromatogram of polyethylenelactate dihydrosinapate (Table 2-4, Entry 1) | 236 |
| B-66 | GPC Chromatogram of polyethyleneglycolate dihydrosinapamide (polyesteramide) (Table 2-5, entry 5) | 236 |
| B-67 | GPC Chromatogram of polyethyleneglycolamide dihydrosinapamide (polyamide) (Table 2-5, entry 6) | 237 |
| B-68 | ¹ H NMR Spectrum of dimethylglycolate sinapate | 238 |

| | | |
|------|--|-----|
| B-69 | ¹ H NMR Spectrum of dimethylglycolate dihydrosinapate. | 238 |
| B-70 | ¹ H NMR Spectrum of dimethylactate sinapate. | 238 |
| B-71 | ¹ H NMR Spectrum of dimethylactate dihydrosinapate. | 239 |
| B-72 | ¹ H NMR Spectrum of dimethylglycolate ferulate. | 239 |
| B-73 | ¹ H NMR Spectrum of dimethylactate ferulate. | 239 |
| B-74 | ¹ H NMR Spectrum of dimethylglycolate coumarate. | 240 |
| B-75 | ¹ H NMR Spectrum of dimethylactate coumarate. | 240 |
| B-76 | ¹ H NMR Spectrum of polyethyleneglycolate dihydrosinapate (Table 2-2, entry 1). | 240 |
| B-77 | ¹ H NMR Spectrum of copoly(ethyleneglycolate dihydrosinapate/ethyleneglycolate sinapate) [90:10] (Table 2-2, entry 2)..... | 241 |
| B-78 | ¹ H NMR Spectrum of copoly(ethyleneglycolate dihydrosinapate/ethyleneglycolate sinapate) [80:20] (Table 2-2, entry 3)..... | 241 |
| B-79 | ¹ H NMR Spectrum of copoly(ethyleneglycolate dihydrosinapate/ethyleneglycolate sinapate) [70:30] (Table 2-2, entry 4)..... | 241 |
| B-80 | ¹ H NMR Spectrum of copoly(ethyleneglycolate dihydrosinapate/ethyleneglycolate sinapate) [60:40] (Table 2-2, entry 5)..... | 242 |
| B-81 | ¹ H NMR Spectrum of copoly(ethyleneglycolate dihydrosinapate/ethyleneglycolate sinapate) [50:50] (Table 2-2, entry 6)..... | 242 |
| B-82 | ¹ H NMR Spectrum of copoly(ethyleneglycolate dihydrosinapate/ethyleneglycolate sinapate) [40:60] (Table 2-2, entry 7)..... | 242 |
| B-83 | ¹ H NMR Spectrum of copoly(ethyleneglycolate dihydrosinapate/ethyleneglycolate sinapate) [30:70] (Table 2-2, entry 8)..... | 243 |
| B-84 | ¹ H NMR Spectrum of copoly(ethyleneglycolate dihydrosinapate/ethyleneglycolate sinapate) [20:80] (Table 2-2, entry 9)..... | 243 |
| B-85 | ¹ H NMR Spectrum of copoly(ethyleneglycolate dihydrosinapate/ethyleneglycolate sinapate) [10:90] (Table 2-2, entry 10)..... | 243 |
| B-86 | ¹ H NMR Spectrum of polyethyleneglycolate sinapate (Table 2-2, entry 11) | 244 |
| B-87 | ¹ H NMR Spectrum of polypropyleneglycolate sinapate (Table 2-1, entry 2)..... | 244 |
| B-88 | ¹ H NMR Spectrum of polybutyleneglycolate sinapate (Table 2-3, entry 3). | 244 |

| | | |
|-------|--|-----|
| B-89 | ¹ H NMR Spectrum of polypentylenglycolate sinapate (Table 2-3, entry 4) | 245 |
| B-90 | ¹ H NMR Spectrum of polyhexylenglycolate sinapate (Table 2-3, entry 5) | 245 |
| B-91 | ¹ H NMR Spectrum of polyhexylenglycolate dihydrosinapate (Table 2-1, entry 1) | 245 |
| B-92 | ¹ H NMR Spectrum of polyoctylenglycolate sinapate (Table 2-3, entry 6) | 246 |
| B-93 | ¹ H NMR Spectrum of polynonylenglycolate sinapate (Table 2-3, entry 7) | 246 |
| B-94 | ¹ H NMR Spectrum of polydecylenglycolate sinapate (Table 2-3, entry 8) | 246 |
| B-95 | ¹ H NMR Spectrum of polyethylenelactate dihydrosinapate (Table 2-4, entry 1) | 247 |
| B-96 | ¹ H NMR Spectrum of copoly(ethylenelactate dihydrosinapate/ethylenelactate sinapate) [70:30] (Table 2-4, entry 2) | 247 |
| B-97 | ¹ H NMR Spectrum of copoly(ethylenelactate dihydrosinapate/ethylenelactate sinapate) [50:50] (Table 2-4, entry 3) | 247 |
| B-98 | ¹ H NMR Spectrum of copoly(ethylenelactate dihydrosinapate/ethylenelactate sinapate) [30:70] (Table 2-4, entry 4) | 248 |
| B-99 | ¹ H NMR Spectrum of polyethylenelactate sinapate (Table 2-4, entry 5)..... | 248 |
| B-100 | ¹ H NMR Spectrum of polyethyleneglycolate ferulate (Table 2-5, entry 1)..... | 248 |
| B-101 | ¹ H NMR Spectrum of polyethyleneglycolate coumarate (Table 2-5, entry 2).... | 249 |
| B-102 | ¹ H NMR Spectrum of polyethylenelactate ferulate (Table 2-5, entry 3) | 249 |
| B-103 | ¹ H NMR Spectrum of polyethylenelactate coumarate (Table 2-5, entry 4) | 249 |
| B-104 | ¹ H NMR Spectrum of polyethyleneglycolate dihydrosinapamide (polyesteramide) (Table 2-5, entry 5) | 250 |
| B-105 | ¹ H NMR Spectrum of polyethyleneglycolamide dihydrosinapamide (polyamide) (Table 2-5, entry 6) | 250 |
| B-106 | ¹³ C NMR Spectrum of dimethylglycolate sinapate | 251 |
| B-107 | ¹³ C NMR Spectrum of dimethylglycolate dihydrosinapate | 251 |
| B-108 | ¹³ C NMR Spectrum of dimethyl lactate sinapate | 251 |
| B-109 | ¹³ C NMR Spectrum of dimethyl lactate dihydrosinapate..... | 252 |

| | | |
|-------|--|-----|
| B-110 | ¹³ C NMR Spectrum of dimethylglycolate ferulate | 252 |
| B-111 | ¹³ C NMR Spectrum of dimethylactate ferulate | 252 |
| B-112 | ¹³ C NMR Spectrum of dimethylglycolate coumarate..... | 253 |
| B-113 | ¹³ C NMR Spectrum of dimethylactate coumarate | 253 |
| B-114 | ¹³ C NMR Spectrum of polyethyleneglycolate dihydrosinapate (Table 2-2, entry 1) | 253 |
| B-115 | ¹³ C NMR Spectrum of copoly(ethyleneglycolate dihydrosinapate/ethyleneglycolate sinapate) [90:10] (Table 2-2, entry 2)..... | 254 |
| B-116 | ¹³ C NMR Spectrum of copoly(ethyleneglycolate dihydrosinapate/ethyleneglycolate sinapate) [80:20] (Table 2-2, entry 3)..... | 254 |
| B-117 | ¹³ C NMR Spectrum of copoly(ethyleneglycolate dihydrosinapate/ethyleneglycolate sinapate) [70:30] (Table 2-2, entry 4)..... | 254 |
| B-118 | ¹³ C NMR Spectrum of copoly(ethyleneglycolate dihydrosinapate/ethyleneglycolate sinapate) [60:40] (Table 2-2, entry 5)..... | 255 |
| B-119 | ¹³ C NMR Spectrum of copoly(ethyleneglycolate dihydrosinapate/ethyleneglycolate sinapate) [50:50] (Table 2-2, entry 6)..... | 255 |
| B-120 | ¹³ C NMR Spectrum of copoly(ethyleneglycolate dihydrosinapate/ethyleneglycolate sinapate) [40:60] (Table 2-2, entry 7)..... | 255 |
| B-121 | ¹³ C NMR Spectrum of copoly(ethyleneglycolate dihydrosinapate/ethyleneglycolate sinapate) [30:70] (Table 2-2, entry 8)..... | 256 |
| B-122 | ¹³ C NMR Spectrum of copoly(ethyleneglycolate dihydrosinapate/ethyleneglycolate sinapate) [20:80] (Table 2-2, entry 9)..... | 256 |
| B-123 | ¹³ C NMR Spectrum of copoly(ethyleneglycolate dihydrosinapate/ethyleneglycolate sinapate) [10:90] (Table 2-2, entry 10)..... | 256 |
| B-124 | ¹³ C NMR Spectrum of polyethyleneglycolate sinapate (Table 2-2, entry 11).... | 257 |
| B-125 | ¹³ C NMR Spectrum of polypropyleneglycolate sinapate (Table 2-3, entry 2).... | 257 |
| B-126 | ¹³ C NMR Spectrum of polybutyleneglycolate sinapate (Table 2-3, entry 3)..... | 257 |
| B-127 | ¹³ C NMR Spectrum of polypentyleneglycolate sinapate (Table 2-3, entry 4).... | 258 |
| B-128 | ¹³ C NMR Spectrum of polyhexyleneglycolate sinapate (Table 2-3, entry 5)..... | 258 |

| | | |
|-------|---|-----|
| B-129 | ¹³ C NMR Spectrum of polyhexyleneglycolate dihydrosinapate (Table 2-1, entry 2) | 258 |
| B-130 | ¹³ C NMR Spectrum of polyoctyleneglycolate sinapate (Table 2-3, entry 6) | 259 |
| B-131 | ¹³ C NMR Spectrum of polynonyleneglycolate sinapate (Table 2-3, entry 7)..... | 259 |
| B-132 | ¹³ C NMR Spectrum of polydecyleneglycolate sinapate (Table 2-3, entry 8) | 259 |
| B-133 | ¹³ C NMR Spectrum of polyethylenelactate dihydrosinapate (Table 2-4, entry 1) | 260 |
| B-134 | ¹³ C NMR Spectrum of copoly(ethylenelactate dihydrosinapate/ethylenelactate sinapate) [70:30] (Table 2-4, entry 2) | 260 |
| B-135 | ¹³ C NMR Spectrum of copoly(ethylenelactate dihydrosinapate/ethylenelactate sinapate) [50:50] (Table 2-4, entry 3) | 260 |
| B-136 | ¹³ C NMR Spectrum of copoly(ethylenelactate dihydrosinapate/ethylenelactate sinapate) [30:70] (Table 2-4, entry 4) | 261 |
| B-137 | ¹³ C NMR Spectrum of polyethylenelactate sinapate (Table 2-4, entry 5) | 261 |
| B-138 | ¹³ C NMR Spectrum of polyethyleneglycolate ferulate (Table 2-5, entry 1) | 261 |
| B-139 | ¹³ C NMR Spectrum of polyethyleneglycolate coumarate (Table 2-5, entry 2) .. | 262 |
| B-140 | ¹³ C NMR Spectrum of polyethylenelactate ferulate (Table 2-5, entry 3)..... | 262 |
| B-141 | ¹³ C NMR Spectrum of polyethylenelactate coumarate (Table 2-5, entry 4) | 262 |
| B-142 | ¹³ C NMR Spectrum of polyethyleneglycolate dihydrosinapamide (polyesteramide) (Table 2-5, entry 5) | 263 |
| B-143 | ¹³ C NMR Spectrum of polyethyleneglycolamide dihydrosinapamide (polyamide) (Table 2-5, entry 6) | 263 |
| C-1 | ¹ H NMR spectrum of crude product from large scale extraction on lignin paste..... | 264 |
| C-2 | ¹ H NMR spectrum of recrystallized product from large scale extraction on lignin paste. | 264 |
| C-3 | ¹ H NMR spectrum of 1 st cycle product from reflux extraction on lignin paste (Table 3-1, entry 1). | 264 |
| C-4 | ¹ H NMR spectrum of 2 nd cycle product from reflux extraction on lignin paste (Table 3-1, entry 2). | 265 |

| | | |
|------|--|-----|
| C-5 | ¹ H NMR spectrum of 3 rd cycle product from reflux extraction on lignin paste (Table 3-1, entry 3). | 265 |
| C-6 | ¹ H NMR spectrum of 1 st cycle product from pressurized extraction on lignin paste (Table 3-1, entry 1). | 265 |
| C-7 | ¹ H NMR spectrum of 1 st cycle product from ultrasound extraction on lignin paste (Table 3-1, entry 1). | 266 |
| C-8 | ¹ H NMR spectrum of 1 st cycle product from microwave extraction on lignin paste (Table 3-1, entry 1). | 266 |
| C-9 | ¹ H NMR spectrum of 1 st crop purified product from reflux extraction on sugarcane bagasse (Table 3-1, entry 6–9)..... | 266 |
| C-10 | ¹ H NMR spectrum of 2 nd crop purified product from reflux extraction on sugarcane bagasse (Table 3-1, entry 6–9)..... | 267 |
| C-11 | ¹ H NMR spectrum of 1 st cycle product from pressurized extraction on sugarcane bagasse (Table 3-1, entry 6)..... | 267 |
| C-12 | ¹ H NMR spectrum of 1 st cycle product from ultrasound extraction on sugarcane bagasse (Table 3-1, entry 6)..... | 267 |
| C-13 | ¹ H NMR spectrum of 1 st cycle product from microwave extraction on sugarcane bagasse (Table 3-1, entry 6)..... | 268 |
| C-14 | ¹ H NMR spectrum of purified product from ultrasound extraction on lignin paste using activated charcoal. | 268 |
| C-15 | ¹ H NMR spectrum of product from corn bran extraction(Table 3-2, entry 1)..... | 268 |
| C-16 | ¹ H NMR spectrum of product from corn cob extraction(Table 3-2, entry 2) | 269 |
| C-17 | ¹ H NMR spectrum of product from corn silk extraction(Table 3-2, entry 3)..... | 269 |
| C-18 | ¹ H NMR spectrum of product from corn tassel extraction(Table 3-2, entry 4)... | 269 |
| D-1 | TGA Thermogram of PV-VV-A (Table 4-1, entry 1)..... | 270 |
| D-2 | TGA Thermogram of PV-HB-A (Table 4-1, entry 2)..... | 270 |
| D-3 | TGA Thermogram of PV-SY-A (Table 4-1, entry 3)..... | 271 |
| D-4 | TGA Thermogram of PV-EV-A (Table 4-1, entry 4)..... | 271 |
| D-5 | TGA Thermogram of PV-OV-A (Table 4-1, entry 5)..... | 272 |
| D-6 | TGA Thermogram of PV-IV-A (Table 4-1, entry 6). | 272 |

| | | |
|------|---|-----|
| D-7 | TGA Thermogram of PV-SA-A (Table 4-1, entry 7)..... | 273 |
| D-8 | TGA Thermogram of PV-OA-A (Table 4-1, entry 8)..... | 273 |
| D-9 | TGA Thermogram of PV-PA-A (Table 4-1, entry 9)..... | 274 |
| D-10 | TGA Thermogram of PV-BZ-A (Table 4-1, entry 10). | 274 |
| D-11 | TGA Thermogram of PV-CI-A (Table 4-1, entry 11). | 275 |
| D-12 | TGA Thermogram of PV-CU-A (Table 4-1, entry 12)..... | 275 |
| D-13 | TGA Thermogram of PV-VV-A High MW (Table 4-1, entry 13). | 277 |
| D-14 | TGA Thermogram of PVA High MW (Table 4-1, entry 14). | 276 |
| D-15 | TGA Thermogram of PV-VV-A High MW (Table 4-1, entry 15). | 277 |
| D-16 | DSC Thermogram of PV-VV-A (Table 4-1, entry 1)..... | 278 |
| D-17 | DSC Thermogram of PV-HB-A (Table 4-1, entry 2)..... | 278 |
| D-18 | DSC Thermogram of PV-SY-A (Table 4-1, entry 3)..... | 279 |
| D-19 | DSC Thermogram of PV-EV-A (Table S1, Entry 4). | 279 |
| D-20 | DSC Thermogram of PV-OV-A (Table 4-1, entry 5). | 280 |
| D-21 | DSC Thermogram of PV-IV-A (Table 4-1, entry 6). | 280 |
| D-22 | DSC Thermogram of PV-SA-A (Table 4-1, entry 7)..... | 281 |
| D-23 | DSC Thermogram of PV-OA-A (Table 4-1, entry 8). | 281 |
| D-24 | DSC Thermogram of PV-PA-A (Table 4-1, entry 9)..... | 282 |
| D-25 | DSC Thermogram of PV-BZ-A (Table 4-1, entry 10)..... | 282 |
| D-26 | DSC Thermogram of PV-CI-A (Table 4-1, entry 11)..... | 283 |
| D-27 | DSC Thermogram of PV-CU-A (Table 4-1, entry 12). | 283 |
| D-28 | DSC Thermogram of PV-HMF-A (Table 4-1, entry 13)..... | 284 |
| D-29 | DSC Thermogram of PVA High MW (Table 4-1, entry 14). | 284 |
| D-30 | DSC Thermogram of PV-VV-A High MW (Table 4-1, entry 15) | 285 |
| D-31 | GPC Chromatogram of PVA (Table 4-1, entry 0). | 286 |

| | | |
|------|--|-----|
| D-32 | GPC Chromatogram of PV-VV-A (Table 4-1, entry 1). | 286 |
| D-33 | GPC Chromatogram of PV-HB-A (Table 4-1, entry 2). | 287 |
| D-34 | GPC Chromatogram of PV-SY-A (Table 4-1, entry 3). | 287 |
| D-35 | GPC Chromatogram of PV-EV-A (Table 4-1, entry 4). | 288 |
| D-36 | GPC Chromatogram of PV-OV-A (Table 4-1, entry 5). | 288 |
| D-37 | GPC Chromatogram of PV-IV-A (Table 4-1, entry 6). | 289 |
| D-38 | GPC Chromatogram of PV-SA-A (Table 4-1, entry 7). | 289 |
| D-39 | GPC Chromatogram of PV-OA-A (Table 4-1, entry 8). | 290 |
| D-40 | GPC Chromatogram of PV-PA-A (Table 4-1, entry 9). | 290 |
| D-41 | GPC Chromatogram of PV-BZ-A (Table 4-1, entry 10). | 291 |
| D-42 | ¹ H NMR Spectrum PV-VV-A (Table 4-1, entry 1). | 292 |
| D-43 | ¹ H NMR Spectrum PV-HB-A (Table 4-1, entry 2). | 292 |
| D-44 | ¹ H NMR Spectrum PV-SY-A (Table 4-1, entry 3). | 292 |
| D-45 | ¹ H NMR Spectrum PV-EV-A (Table 4-1, entry 4). | 293 |
| D-46 | ¹ H NMR Spectrum PV-OV-A (Table 4-1, entry 5). | 293 |
| D-47 | ¹ H NMR Spectrum PV-IV-A (Table 4-1, entry 6). | 293 |
| D-48 | ¹ H NMR Spectrum PV-SA-A (Table 4-1, entry 7). | 294 |
| D-49 | ¹ H NMR Spectrum PV-OA-A (Table 4-1, entry 8). | 294 |
| D-50 | ¹ H NMR Spectrum PV-PA-A (Table 4-1, entry 9). | 294 |
| D-51 | ¹ H NMR Spectrum PV-BZ-A (Table 4-1, entry 10). | 295 |
| D-52 | ¹ H NMR Spectrum PV-CI-A (Table 4-1, entry 11). | 295 |
| D-53 | ¹ H NMR Spectrum PV-CU-A (Table 4-1, entry 12). | 295 |
| D-54 | ¹ H NMR Spectrum PV-HMF-A (Table 4-1, entry 13). | 296 |
| D-55 | ¹ H NMR Spectrum PV-VV-A* High MW (Table 4-1, entry 15) | 296 |
| D-56 | ¹³ C NMR Spectrum of PV-VV-A (Table 4-1, entry 1). | 297 |

| | | |
|------|---|-----|
| D-57 | ¹³ C NMR Spectrum of PV-HB-A (Table 4-1, entry 2)..... | 297 |
| D-58 | ¹³ C NMR Spectrum of PV-SY-A (Table 4-1, entry 3)..... | 298 |
| D-59 | ¹³ C NMR Spectrum of PV-EV-A (Table 4-1, entry 4)..... | 298 |
| D-60 | ¹³ C NMR Spectrum of PV-OV-A (Table 4-1, entry 5)..... | 299 |
| D-61 | ¹³ C NMR Spectrum of PV-IV-A (Table 4-1, entry 6). | 299 |
| D-62 | ¹³ C NMR Spectrum of PV-SA-A (Table 4-1, entry 7)..... | 300 |
| D-63 | ¹³ C NMR Spectrum of PV-OA-A (Table 4-1, entry 8)..... | 300 |
| D-64 | ¹³ C NMR Spectrum of PV-PA-A (Table 4-1, entry 9)..... | 301 |
| D-65 | ¹³ C NMR Spectrum of PV-BZ-A (Table 4-1, entry 10). | 301 |
| D-66 | ¹³ C NMR Spectrum of PV-CI-A (Table 4-1, entry 11). | 302 |
| D-67 | ¹³ C NMR Spectrum of PV-CU-A (Table 4-1, entry 12)..... | 302 |
| D-68 | ¹³ C NMR Spectrum of PV-HMF-A (Table 4-1, entry 13)..... | 303 |
| D-69 | ¹³ C NMR Spectrum of PV-VV-A* (Table 4-1, entry 15)..... | 303 |
| E-1 | TGA thermogram of poly-DHMP analogue from van-2-van and cyclopentanone (Figure 5-1, entry 1)..... | 304 |
| E-2 | TGA thermogram of poly-DHMP analogue from 4HB-2-4HB and dimethyl 3- oxoglutarate (Figure 5-2, entry 1). | 304 |
| E-3 | TGA thermogram of poly-DHMP analogue from van-2-van and dimethyl 3- oxoglutarate (Figure 5-2, entry 2). | 305 |
| E-4 | TGA thermogram of poly-DHMP analogue from syr-2-syr and dimethyl 3- oxoglutarate (Figure 5-2, entry 3). | 305 |
| E-5 | TGA thermogram of poly-DHMP analogue from evan-2-evan and dimethyl 3- oxoglutarate (Figure 5-2, entry 4). | 306 |
| E-6 | TGA thermogram of poly-DHMP analogue from 4HB-3-4HB and dimethyl 3- oxoglutarate (Figure 5-2, entry 5). | 306 |
| E-7 | TGA thermogram of poly-DHMP analogue from van-3-van and dimethyl 3- oxoglutarate (Figure 5-2, entry 6). | 307 |
| E-8 | TGA thermogram of poly-DHMP analogue from syr-3-syr and dimethyl 3- oxoglutarate (Figure 5-2, entry 7). | 307 |

| | | |
|------|--|-----|
| E-9 | TGA thermogram of poly-DHMP analogue from evan-3-evan and dimethyl 3-oxoglutarate (Figure 5-2, entry 8). | 308 |
| E-10 | DSC thermogram of poly-DHMP analogue from van-2-van and dimethyl 3-oxoglutarate (Figure 5-2, entry 2). | 309 |
| E-11 | DSC thermogram of poly-DHMP analogue from syr-2-syr and dimethyl 3-oxoglutarate (Figure 5-2, entry 3). | 309 |
| E-12 | DSC thermogram of poly-DHMP analogue from evan-2-evan and dimethyl 3-oxoglutarate (Figure 5-2, entry 4). | 310 |
| E-13 | DSC thermogram of poly-DHMP analogue from van-3-van and dimethyl 3-oxoglutarate (Figure 5-2, entry 6). | 310 |
| E-14 | DSC thermogram of poly-DHMP analogue from syr-3-syr and dimethyl 3-oxoglutarate (Figure 5-2, entry 7). | 311 |
| E-15 | DSC thermogram of poly-DHMP analogue from evan-3-evan and dimethyl 3-oxoglutarate (Figure 5-2, entry 8). | 311 |
| E-16 | GPC chromatogram of poly-DHMP analogue from 4HB-2-4HB and dimethyl 3-oxoglutarate (Figure 5-2, entry 1). | 312 |
| E-17 | GPC chromatogram of poly-DHMP analogue from van-2-van and dimethyl 3-oxoglutarate (Figure 5-2, entry 2). | 312 |
| E-18 | GPC chromatogram of poly-DHMP analogue from syr-2-syr and dimethyl 3-oxoglutarate (Figure 5-2, entry 3). | 313 |
| E-19 | GPC chromatogram of poly-DHMP analogue from evan-2-evan and dimethyl 3-oxoglutarate (Figure 5-2, entry 4). | 313 |
| E-20 | GPC chromatogram of poly-DHMP analogue from 4HB-3-4HB and dimethyl 3-oxoglutarate (Figure 5-2, entry 5). | 314 |
| E-21 | GPC chromatogram of poly-DHMP analogue from van-3-van and dimethyl 3-oxoglutarate (Figure 5-2, entry 6). | 314 |
| E-22 | GPC chromatogram of poly-DHMP analogue from syr-3-syr and dimethyl 3-oxoglutarate (Figure 5-2, entry 7). | 315 |
| E-23 | GPC chromatogram of poly-DHMP analogue from evan-3-evan and dimethyl 3-oxoglutarate (Figure 5-2, entry 8). | 315 |
| E-24 | ¹ H NMR spectrum of van-2-van. | 316 |
| E-25 | ¹ H NMR spectrum of poly-DHMP analogue from van-2-van and cyclopentanone (Table 5-1, entry 1). | 316 |

| | | |
|------|--|-----|
| E-26 | ¹ H NMR spectrum of poly-DHMP analogue from 4HB-2-4HB and dimethyl 3-oxoglutarate (Table 5-2, entry 1). | 316 |
| E-27 | ¹ H NMR spectrum of poly-DHMP analogue from van-2-van and dimethyl 3-oxoglutarate (Table 5-2, entry 2). | 317 |
| E-28 | ¹ H NMR spectrum of poly-DHMP analogue from syr-2-syr and dimethyl 3-oxoglutarate (Table 5-2, entry 3). | 317 |
| E-29 | ¹ H NMR spectrum of poly-DHMP analogue from evan-2-evan and dimethyl 3-oxoglutarate (Table 5-2, entry 4). | 317 |
| E-30 | ¹ H NMR spectrum of poly-DHMP analogue from 4HB-3-4HB and dimethyl 3-oxoglutarate (Table 5-2, entry 5). | 318 |
| E-31 | ¹ H NMR spectrum of poly-DHMP analogue from van-3-van and dimethyl 3-oxoglutarate (Table 5-2, entry 6). | 318 |
| E-32 | ¹ H NMR spectrum of poly-DHMP analogue from syr-3-syr and dimethyl 3-oxoglutarate (Table 5-2, entry 7). | 318 |
| E-33 | ¹ H NMR spectrum of poly-DHMP analogue from evan-3-evan and dimethyl 3-oxoglutarate (Table 5-2, entry 8). | 319 |

LIST OF ABBREVIATIONS

| | |
|-------------------|-----------------------------------|
| CDCl ₃ | Deuterated chloroform |
| DHMP | Dihydropyrimidinone |
| DMSO | Dimethyl sulfoxide |
| DSC | Differential Scanning Calorimetry |
| GPC | Gel Permeation Chromatography |
| HCl | Hydrochloric acid |
| HFIP | Hexafluoroisopropanol |
| M_n | Number average molecular weight |
| M_w | Weight average molecular weight |
| PES | Polyethylene sinapate |
| PET | Polyethylene terephthalate |
| PLA | Poly(lactic acid) |
| PMMA | Polymethylmethacrylate |
| PP | Polypropylene |
| PS | Polystyrene |
| PVA | Polyvinyl alcohol |
| T_g | Glass transition temperature |
| T_m | Melting temperature |
| TGA | Thermogravimetric analysis |

Abstract of Dissertation Presented to the Graduate School
of the University of Florida in Partial Fulfillment of the
Requirements for the Degree of Doctor of Philosophy

EXTRACTION AND POLYMERIZATION OF BIOAROMATICS FROM MEGACROPS

By

Steven Shen

October 2019

Chair: Stephen A. Miller
Major: Chemistry

Petroleum is a non-renewable resource, and yet it is vital for our world. However, from the emission of greenhouse gasses from fuel production and utilization to the generation of non-degradable plastic waste that flows into the ocean, every step of petroleum processing damages the environment whether in the short or long term. Although biorefineries from crops have been developed as potential solutions to this problem, the biofuel cost is still unable to compete with the cost of petroleum-based fuel. One part of this study focused on the extraction of hydroxycinnamic acids, which are high value added co-products, from sugarcane, corn, and specifically *Brassica carinata* that has recently gained popularity among other cash crops due to its bio-jet fuel application. From sugarcane and corn crops, ferulic acid and *p*-coumaric acid were extracted in tandem. Meanwhile, sinapic acid was extracted from *Brassica carinata* meal. All of these hydroxycinnamic acids have been studied for their antioxidant and nutraceutical properties which can potentially be used for the natural additives/preservatives industry.

Moreover, this study investigated several series of synthesized bioplastics that can be derived from megacrops, which allowed us to address two current plastic

problems: (1) most plastics are derived from non-renewable resources (petroleum and natural gas), and (2) most plastics are non-degradable. Several series of sinapic acid-based polymers were obtained, such as polyalkylene sinapate, polyalkylene glycolate sinapate, and polyalkylene lactate sinapate. Additionally, several lignin-derived materials were utilized for polyvinyl acetal synthesis. Lastly, a modified Biginelli multicomponent reaction was applied to several renewable monomers creating a series of poly(dihydropyrimidinone) polymers. Most of these sustainable polymers displayed thermal properties that overlap those of current commodity plastics.

CHAPTER 1
BIORENEWABLES FROM *BRASSICA CARINATA* BIOMILL*

Background

The present world is highly dependent on petroleum owing to its usage as fuels and precursors to synthesize a wide variety of essential products, such as olefins and aromatics for pharmaceuticals and plastics.¹ As an inexpensive and highly efficient source of energy, petroleum oil dominates a third of the world energy consumption.² However, each step of petroleum production does a lot of harm to the environment. For example, the drilling process can potentially contaminate bodies of water with oil and drilling mud, and the refinery process emits volatile toxic organic compounds and greenhouse gasses.³ Additionally, petroleum oil tends to cause political and economic instability among the oil-rich countries, known as “the resource curse”.⁴ In most cases, oil producing countries suffer from the price variability of crude oil. In the worst-case scenario, it will bring an economic collapse to those oil revenue countries when these prices plummet.⁵ Moreover, as a finite resource, the decline of crude oil production will be inevitable as the demand for energy will also keep increasing over the years.⁶ Consequently, this will result in the peak oil and the prices of the petroleum oil will rise to the point that it is unaffordable as a daily energy source.⁷

For the past few decades, renewable energies have been fostered and developed as an alternative to the conventional energy from fossil fuels. One of the most readily available and reliable renewable energies in the market is biomass feedstock energy due to its high energy density and value-added by-products.⁸ *Brassica*

* This work will be submitted to Green Chemistry as a perspective article.

carinata, commonly known as Abyssinian or Ethiopian mustard, is a sympatric speciation between *B. nigra* (black mustard) and *B. oleracea* (wild cabbage plants that include many common vegetables such as cabbage, broccoli, cauliflower, and kale).⁹ *Carinata* has been cultivated in Ethiopia since around 4000 BC.¹⁰ The modern cultivation of the *carinata* crop has been seen as a potential oilseed crop globally, and it has been commercially grown in semi-arid climates such as in the southern Canadian prairie and the northern US plains.¹¹ Some of the agronomic benefits of *carinata* include: large seed size, resistance to seed shattering, resistance to most pathologies, and low bird predation.¹² Furthermore, it is not only heat and drought tolerant,¹³ but also frost tolerant.¹⁴ As a matter of fact, in recent years, *carinata* has been studied as a winter crop in the southern US (Mississippi, Alabama, Georgia, South Carolina, North Carolina, and Florida) and Uruguay.¹⁵ As a winter cash crop, *carinata* will add some economic and ecological benefits to the existing agricultural systems; it will increase the revenue of the commercial farms while promoting the health of soils via crop rotation.¹⁶

The leaf of *carinata* is edible and a suitable source of micronutrients for humans.¹⁷ The seed contains 25–36% oil, 31–41% protein, and low fiber content according to a study by Warwick *et al.*,¹⁸ Furthermore, *carinata* contains several key chemicals that are unique to brassica species such as glucosinolates and sinapic acid. Comparing to other brassica species (*B. juncea*, *B. napus*, *B. rapa*), *Brassica carinata* has a higher meal protein content, but the oilseed is 3–10% less than those from other brassica species. Importantly, and a point often overlooked, is that *carinata* has a larger seed size; thus in some cases, it actually has a higher yield than other brassicas.¹⁹ On average, the oilseed primarily consists of inedible 42% erucic acid (C22:1) and other

common and edible fatty acids such as 8% oleic acid (C18:1), 16% linoleic acid (C18:2), 13% linolenic acid (C18:3), 8% eicosenoic acid (C20:1), 3% nervonic acid (C24:1), 4% other unsaturated fatty acids, and 6% saturated fatty acids.¹⁸

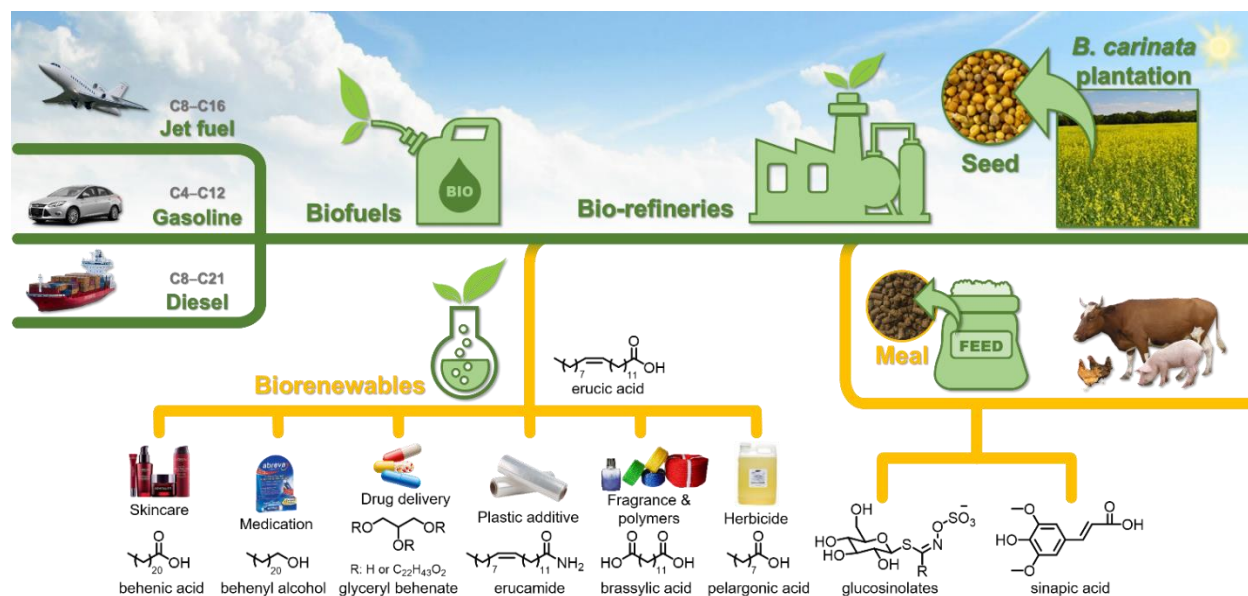


Figure 1-1. Biofuels and biorenewables from *Brassica carinata*

In general, a safe and nutritional oilseed for humans' consumption should not contain more than 2% erucic acid.²⁰ A high exposure to erucic acid poses a potential risk of high blood cholesterol levels that will lead to myocardial lipidoses or heart disease.²¹ In order to fulfil the requirement of edible *carinata* seed oils, zero erucic acid *carinata* has been developed.²² However, high erucic acid *carinata* seed is prominent for the industrial application, particularly in the biofuel and biorenewables industries.²³ At the same time, this will also avoid the highly criticized “food versus oil” problem which is problematic to the biofuel production from other megacrops, such as sugar, corn, or soybean crops.²⁴ In addition to biofuel production, the meal and sinapic acid, from the post-oil extraction seed, is also essential to give the best environmental and economic impact for the non-food oil crop from *B. carinata*.²⁵ Therefore, in regard to energy and

chemical production, the cultivation of *B. carinata* delivers a substantial prospect as an alternative to petroleum (Figure 1-1).

Biofuels from *Brassica carinata*

Erucic acid is a long, 22 carbon chain, monounsaturated omega-9 fatty acid. The length of its carbons chain contributes two things to biofuel production: (1) a higher energy density oil than those without erucic acid,²⁶ and (2) production of a high-value biofuel product, particularly in jet fuel production.²⁷ Jet fuel requires the long hydrocarbon chain mixtures to prevent the fuel to freeze when a jet reaches high altitude. The oil from *Brassica carinata* is readily processed into the advanced “drop-in” hydrocarbon biofuel since it has a high amount of long chain unsaturated fatty acids and a low amount of saturated fatty acids. Out of all of the biomass-based fuels, drop-in biofuels provide the best possible scenario for production and commercialization, due to the similarity of their chemical compositions and energy levels compared to their petroleum fuels counterpart.²⁸ There is a potential of second generation bioethanol production from *carinata* via enzymatic pathways,²⁹ however this might not be the most ideal case since ethanol has lower energy density compared to hydrocarbon fuels.

The biomass-based jet fuel production has a great prospect in the global market. The International Air Transportation (IATA) suggested a goal to reduce the net aviation CO₂ emissions of 50% by 2050 relative to 2005 levels by endorsing the development of sustainable alternative fuels for aviation. Similarly, the U.S. Air Force has pursued the consumption of bio-jet fuel to replace half of its petroleum-based jet fuel, which translates to 1.2 billion gallon of bio-jet fuel consumption per year.³⁰ There were some attempts to substitute petroleum-based jet fuel with other sustainable energy resources, such as battery and solar power; however those alternatives lack energy for heavier

duties due to their much lower energy density compared to hydrocarbon-based fuels. As a non-food oil that contains high amounts of erucic acid (a long chain fatty acid), *carinata* is ultimately the best candidate for replacing petroleum-based jet fuel.

At this time, one of the most commercially successful bio-jet fuels from *carinata* in the world market is ReadiJet®, a 100% drop-in bio-jet fuel. ReadiJet® is produced by Applied Research Associates (ARA) and Chevron Lummus Global (CLG) from Agrisoma's *carinata* feedstock under the Resonance™ brand name.³¹ The new technology, which is called as Biofuels Isoconversion (BIC), was introduced for the biofuel refinery process. In general, the steps in the process include: (1) hydrothermal clean-up (HCU) which removes metals and other impurities and hydrolyses to obtain free fatty acids, (2) catalytic hydrothermolysis (CH) converts the clean free fatty acids oil into crude hydrocarbon oil (paraffin, isoparaffin, cycloparaffin, and aromatics) by cracking, isomerization, and cyclization, (3) hydrotreating step hydrogenates the olefins and removes the oxygen, sulfur, nitrogen, and metal contents in the liquid fuel, (4) distillation separates the naphta, diesel, and jet fuel components based on the range of their boiling points.³² ReadiJet® is certified through the American Society for Testing and Materials (ASTM) for commercial use and Navy's Military Specification (MILSPEC) for the operational use by the US Navy. In October 2012, the flight test by National Research Canada (NRC) using ReadiJet® in their Falcon 20 aircraft marked the world's first flight that was fueled by 100% drop-in renewable fuel.³³ In January 2018, Qantas Airways, partnered with Agrisoma and World Energy accomplished the world's first US-Australia bio-jet fuel flight (QF96) powered by 10% *carinata*-based jet fuel blend.³⁴ Later

in September 2018, Agrisoma, World Energy, and United Airlines completed the longest transatlantic bio-jet fuel flight powered by 30% *carinata*-based jet fuel blend.³⁵

Biorenewables from *Brassica carinata*

Currently, the estimated cost of jet fuel from *B. carinata* is up to US\$0.60 per liter, meanwhile the jet fuel from petroleum costs US\$0.40 per liter. Indeed, the production of *carinata*-based jet fuel is still too expensive to be profitable.³⁶ However, the production revenue can still be increased by two pathways: blending with low value oil such as grease and used cooking oil; or producing *carinata*-based value added co-products.²⁵ The byproducts from biofuel refinery processes are highly useful as precursors for chemical industries. Some of the most common byproducts are glycerine, acetic acid, ethyl acetate, and n-paraffins. N-paraffins (linear alkanes) can be extracted from the jet fuel fraction and the process will also improve the properties of bio-jet fuel. At the same time, n-paraffins can potentially be used to synthesize linear alkyl benzene, which is one of main ingredients for detergent products with the global market production of 4.3 million tonnes per year.³⁷ The post-oil extraction *carinata* seeds contain high crude protein (40%) and low glucosinolates (28 mmol/kg); this *carinata* meal can be used as cattle feed, as suggested by DiLorenzo *et al.*³⁸ According to the cost analysis study by Millar *et al.*, *carinata* protein meal plays a crucial role with at least 34% of total revenue of *B. carinata* cultivation in addition to the biofuel production.³⁶ Additionally, *carinata* meal can potentially be used for bio-plastics production by directly mixing the meal with 10–30% glycerol via a compression molding process.³⁹

Erucic acid for biorenewables

Oil seed with a high content of erucic acid can be directly used as a natural and biodegradable lubricant.⁴⁰ In addition, there is a relatively big market for utilizing erucic

acid as a precursor for several industrial chemicals, such as behenic acid, behenyl alcohol, glyceryl behenate, erucamide, pelargonic acid, and brassylic acid.

Commercially, behenic acid can be infused into a skincare formula due to its soothing and moisturizing properties for the skin.⁴¹ Behenyl alcohol exhibits antiviral activity against herpes simplex virus,⁴² and it is currently sold as a medication cream named Abreva® to treat cold sores caused by the herpes simplex virus.⁴³ Glyceryl behenate finds a great application in drug delivery systems, such as the preparation of solid lipid nanoparticles as a drug carrier.⁴⁴ About 33% of erucic acid production translates into the synthesis of erucamide,⁴⁵ since erucamide serves as an indispensable plastic film additive, particularly as a slip-promoting agent. In other words, the presence of erucamide in the plastic films will prevent the layers of the film from being glued together and thus enable films to slide over each other.⁴⁶

Both pelargonic acid and brassylic acid can be obtained directly from oxidative cleavage via ozonolysis of erucic acid.⁴⁷ Pelargonic acid is one of the least toxic herbicidal soaps⁴⁸ and is sold under the brand name Scythe® which contains 57% pelargonic acid.⁴⁹ In the market, brassylic acid is found in the form of its macrocyclic ester, ethylene brassylate, which has a strong pleasant odor and it is one of the most common musk compounds in the fragrance industry.⁵⁰ As a matter of fact, the ethylene brassylate-based fragrance named Astrotrone® from DuPont was included in the “Children of Recovery” list, due to the product’s contribution promoting economic growth during the US recovery period, 1934–1935.⁵¹ Another potential application of brassylic acid is nylon 13,13 production which was studied to a scale-up level synthesis in the 1970s.⁵² Some of the first polyamides that were synthesized and characterized were

nylon 13,13 ($T_g = 41\text{ }^\circ\text{C}$, $T_m = 175\text{ }^\circ\text{C}$), nylon 12,13 ($T_g = 42\text{ }^\circ\text{C}$, $T_m = 175\text{ }^\circ\text{C}$), nylon 10,13 ($T_g = 45\text{ }^\circ\text{C}$, $T_m = 176\text{ }^\circ\text{C}$), nylon 8,13 ($T_g = 46\text{ }^\circ\text{C}$, $T_m = 192\text{ }^\circ\text{C}$), and nylon 6,13 ($T_g = 51\text{ }^\circ\text{C}$, $T_m = 208\text{ }^\circ\text{C}$). Although their glass transition and melting temperatures are lower than that of nylon 6,6 ($T_g = 54\text{ }^\circ\text{C}$, $T_m = 260\text{ }^\circ\text{C}$), these nylons from brassylic acid showed promising results regarding their mechanical properties and hydrophobicity which could potentially be an alternative to current commodity nylons.⁵³ Lastly, erucic acid can also be utilized in producing poly(3-hydroxyalkanoates), a biodegradable polymer ($T_g = -46\text{ }^\circ\text{C}$, $T_m = 50\text{ }^\circ\text{C}$) produced by *Pseudomonas aeruginosa*.⁵⁴

Glucosinolates

Glucosinolates are biologically inactive and stable compounds that exist in many parts of the *Brassicaceae* species, such as stem, root, and seed. However, they generate active compounds, such as isothiocyanates, upon hydrolysis catalysed by myrosinase (thioglucoside glucohydrolase) as a plant self-defense mechanism.⁵⁵ This mechanism contributes to the bitter flavor and pungency of *Brassica* vegetables (kale, mustard, and broccoli). Indeed, *Brassicaceae* species generally have high resistance to diseases and pests mainly due to the production of isothiocyanates, since isothiocyanates are potent natural pesticides against nematodes,⁵⁶ bacteria, and fungi.⁵⁷ In recent years, glucosinolates have been studied for their potential anticancer properties. This is most likely related to the induction of the glutathione S-transferase enzyme for the purpose of detoxification in the human digestive system. One study from Egner *et al.* found that the daily consumption of a broccoli sprout-derived beverage that is rich in glucoraphanin (4-methylsulfinylbutyl glucosinolate) increased the excretion of carcinogen and pollutant.⁵⁸ Similarly, the therapeutic benefits of sinigrin (allyl

glucosinolate) abundant in wasabi and horse-radish have been widely studied, such as anticancer, antibacterial, antifungal, antioxidant, anti-inflammatory, wound healing properties, and biofumigation.⁵⁹

For human consumption, there is no specific dietary recommendations for glucosinolates, although one study revealed that the daily consumption of glucosinolates can reach up to 46 mg per person in Germany.⁶⁰ On the other hand, glucosinolates in the *Brassica* meal cause severe harmful effects to livestock, including hypothyroidism, growth retardation, organ damage, disruption in eating behavior, and even death. The limit intake of glucosinolate for pigs is 1 mmol/kg meal, for poultry is up to 4 mmol/kg meal, and for cows is up to 31 mmol/kg meal.⁶¹ In order to be utilized as animal feed, several benign extraction methods of glucosinolates in *Brassica* meals have been developed, for example: extraction of glucosinolates by water,⁶² ethanol 75%,⁶³ and methanol.⁶⁴ Another effective method to reduce the level of glucosinolates is by baking the *Brassica* meal through the desolventizer-toaster (DT) process.⁶⁵

Sinapic acid

Sinapic acid naturally exists in its choline ester form, sinapine, and it serves as an essential precursor of lignin and flavonoid synthesis in *Brassicaceae* species.⁶⁶ The presence of sinapine is undesirable in animal feeds due to its tangy odour and bitter taste interfering with the livestock eating behavior. Conversely, sinapic acid and its derivatives are beneficial in human daily life since sinapic acid and its derivatives exhibit antioxidant, anti-inflammatory, anticancer, antimutagenic, antimicrobial, anti-anxiety, and antihyperglycemic properties.^{67,68,69,70,71,72} In the market, the lowest price of sinapic acid was recently US\$550 per kg (Henan Tianfu Chemical Co., Ltd. via Alibaba.com), which makes it a high value added co-product for the *B. carinata* bio-refinery. Moreover,

since sinapic acid can be obtained from the waste of the *carinata* seed after oil extraction, the end cost of extracted sinapic acid can be much more inexpensive and thus more profitable. Due to its antioxidant properties, there is a potential for use as an alternative to current commercial preservatives in food, cosmetics, and pharmaceuticals such as butylatedhydroxytoluene (BHT) or butylatedhydroxyanisole (BHA). The BHT market is predicted to grow from US\$250 million in 2018 to US\$380 million (75 million kg) by 2025⁷³ despite the growing concern over its potential carcinogenic properties.⁷⁴

Several extraction methods for sinapine from *Brassica* seed meals have been developed, such as water, ethanol, alkaline hydrolysis,^{75,76,77} and ultrasound-assisted hydrolysis.⁷⁰ The most recent work on extraction of sinapine was from Allais *et al.* where they used mustard residue of industrial production that mainly consisted of *Brassica juncea* (90%), resulting in more than 10 mg sinapic acid per gram of defatted and dried meal.⁷⁸ According to Mailer *et al.*, the overall range for sinapine in *Brassica* meals was from 5.2 to 16.2 mg/g, while the range of sinapine in *B. carinata* was from 8.5 – 14.5 mg/g.⁷⁹ As can be seen, the extraction methods and conditions of glucosinolates and sinapine are very similar; this theoretically can be done in tandem extracting both compounds together from the *B. carinata* meal. Consequently, the extraction of the *B. carinata* meal will increase the quality of the meal while isolating value added co-products at the same time.

Another potential market for sinapic acid is the synthesis of bioplastics as alternatives to petroleum-based plastics. The current global bioplastic production represents less than 1% of 348 million tonnes in annual plastic production. However, the global production of bioplastics is poised to rise 20% per year from 2018 to 2023,

equating to 2.6 million tonnes of bioplastics produced by 2023.⁸⁰ As the demand for bioplastics will keep increasing over the years, bioplastics will make a good long-term investment for the economy and environmental benefits. There are several sinapic acid-based polymers that have been made. First, a patent from Bezwada Biomedical, LLC introduced weak link moieties in sinapic acid-based biopolymers that are biodegradable for medical application.⁸¹ Second, Allais and co-workers synthesized norbornene dihydrosinapate via enzymatic catalysis *Candida antartica* Lipase B of norbornene and dihydrosinapic acid; then ring opening metathesis polymerization was performed, resulting in bioplastics with a T_g value up to 56 °C.⁸² Last, the same group (Allais *et al.*) produced a sinapic acid-based bisphenol (syringaresinol) as a safer and renewable alternative to bisphenol A via *laccase* *Trametes versicolor* which was reacted with epichlorohydrin resulting in a syringaresinol with two epoxy moieties (diglycidyl ether of syringaresinol). This monomer was then polymerized with diamines (e.g. isophorone diamine) resulting in thermosets of bioplastics with the T_g is up to 126 °C.⁸³

Results and discussion

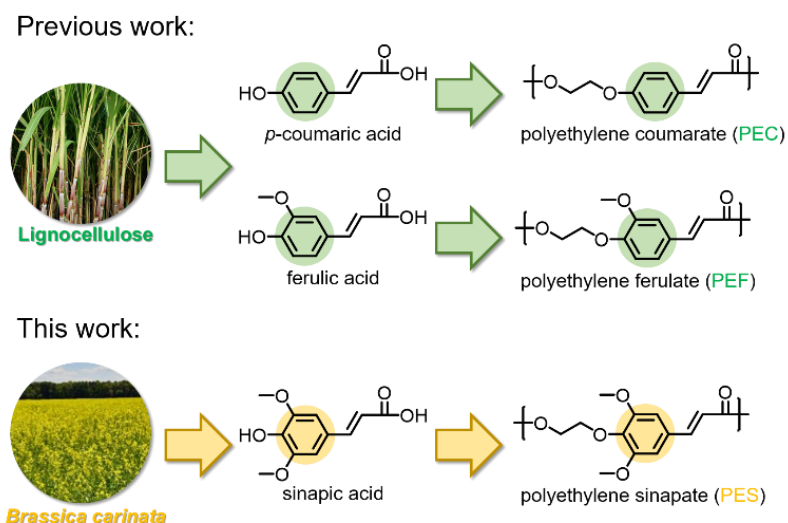


Figure 1-2. Extraction and polymerization of sinapic acid from *Brassica carinata*

Our studies were part of Southeast Partnership for Advanced Renewables from *Carinata* (SPARC) program. SPARC is a collaboration of universities, institutions, and industries that focuses on *B. carinata* as a viable winter crop in the southeast US, resulting in a *carinata* centered fuels and renewables supply chain with national and global impact.¹⁵ In this study, we focused on extraction of sinapic acid from *carinata* meal using various conditions adapted from conventional methods of extracting sinapic acid and derivative compounds from *Brassica* feedstocks.^{73,74,75} Then, we continued with the synthesis of polyethylene sinapate and its congeners from the commercial sinapic acid that we purchased; the polymerization methods were adapted from the previous work by Miller *et al.* in polyethylene ferulate synthesis.⁸⁴ Finally, we also attempted polymerization of polyethylene sinapate from extracted sinapic acid that was obtained directly from *carinata* meal (Figure 1-2).

Extraction of sinapic acid from *Brassica carinata* meal

The pellets of low glucosinolate and hexanes pre-washed *Brassica carinata* meal were obtained from Agrisoma Biosciences, Inc.; the same samples were used on cattle feed studies by DiLorenzo *et al.*³⁸ Prior to the extraction of sinapic acid, the meal was pulverized using a coffee grinder in order to increase the surface area of the biomass. The extraction was then carried out by a simple hydrolysis step of the pulverized *carinata* meal in basic aqueous media, and followed by the liquid-liquid extraction using ethyl acetate (Figure 1-3). In the hydrolysis step, the solute was given enough energy in order to depolymerize the lignin material, which can be accomplished by heating or sonicating the solution. The basic solution of *Brassica* meal was stirred at 60 °C for a

specified time, and the result from Table 6-1 suggested that increasing the amount of *Brassica* meal lowered the yield of extraction (entries 1, 4, and 5).

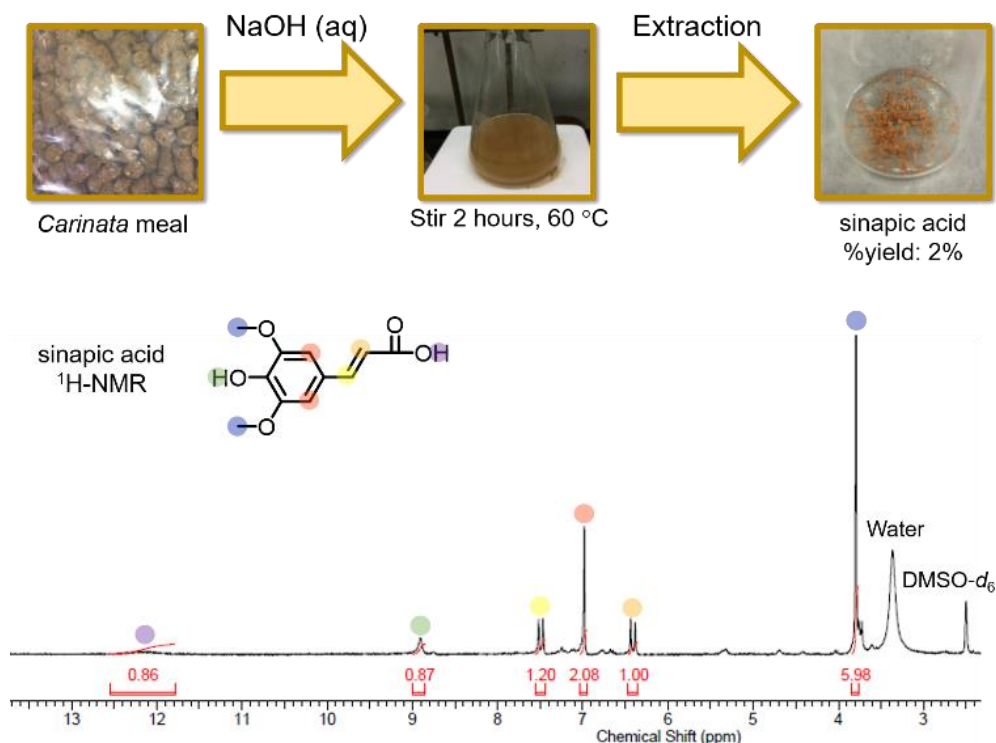


Figure 1-3. Basic aqueous hydrolysis and extraction of sinapic acid from *carinata* meal.

One possible explanation was the large scale needed more energy and time in order to fully hydrolyse the meal. Another possible explanation was the amount of aqueous solvent that was used hindered the efficiency of sinapic acid to move to the ethyl acetate layer on a larger scale. Indeed, the extraction yield on a large scale can be improved by increasing the amount of stirring time as can be seen from entries 2 and 4, or entries 5 and 6. In addition, the yield can also be improved by increasing the temperature of hydrolysis to reflux the solution (entry 15). Meanwhile, ultrasound-assisted hydrolysis in basic aqueous solution did not seem to help the hydrolysis step since it did not improve and even lowered the yield (entries 12, 13, and 14). According to the ¹H-NMR, the extracted sinapic acid was fairly pure (Figure 1-3). Some peaks of

impurities in the 1.20–2.30 ppm region are usually identified as “brown substances” or Maillard compounds, which are commonly found in the extraction of phenolic acids from plant-based biomass; however these can be removed by using activated charcoal.^{85,86}

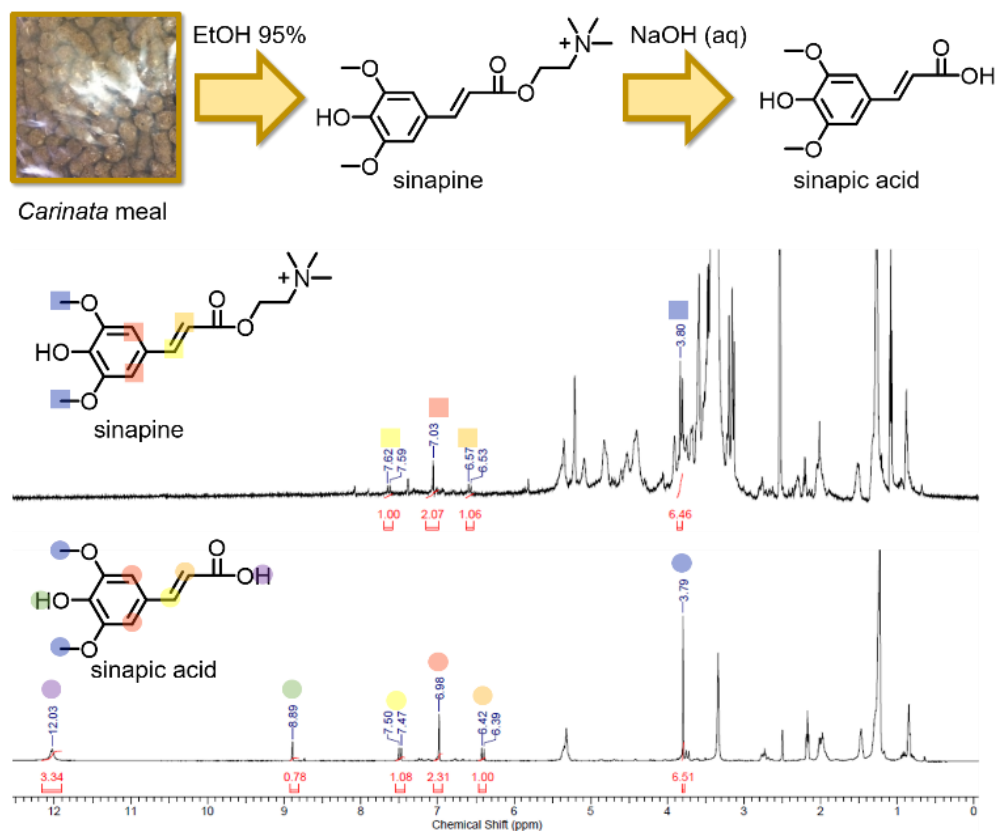


Figure 1-4. Extraction and basic aqueous hydrolysis of sinapine.

Alkali treated meal can potentially cause kidney failure to cattle;⁸⁷ for this reason neutral alcohols were used as a green and safe alternative⁸⁸ to wash the *carinata* meal to obtain sinapine solution, which can be further hydrolysed, separately, into sinapic acid. Methanol 70% (entry 15) and ethanol 95% (entry 16) were chosen due to their volatility, hence a relatively easy removal from the meal. Based on the ¹H NMR, the alcohol solution showed some notable peaks of sinapine, such as 6H from two methoxy groups (3.80 ppm), 2H from the trans double bond (6.55 ppm, 7.61 ppm), and 2H from aromatic (7.03 ppm). The highest yield of 3.60% is obtained by ethanol 95% washing;

however it is also important to note that this method also amplifies the content of impurities in extracted sinapic acid (Figure 1-4).

Synthesis of polyethylene sinapate and congeners

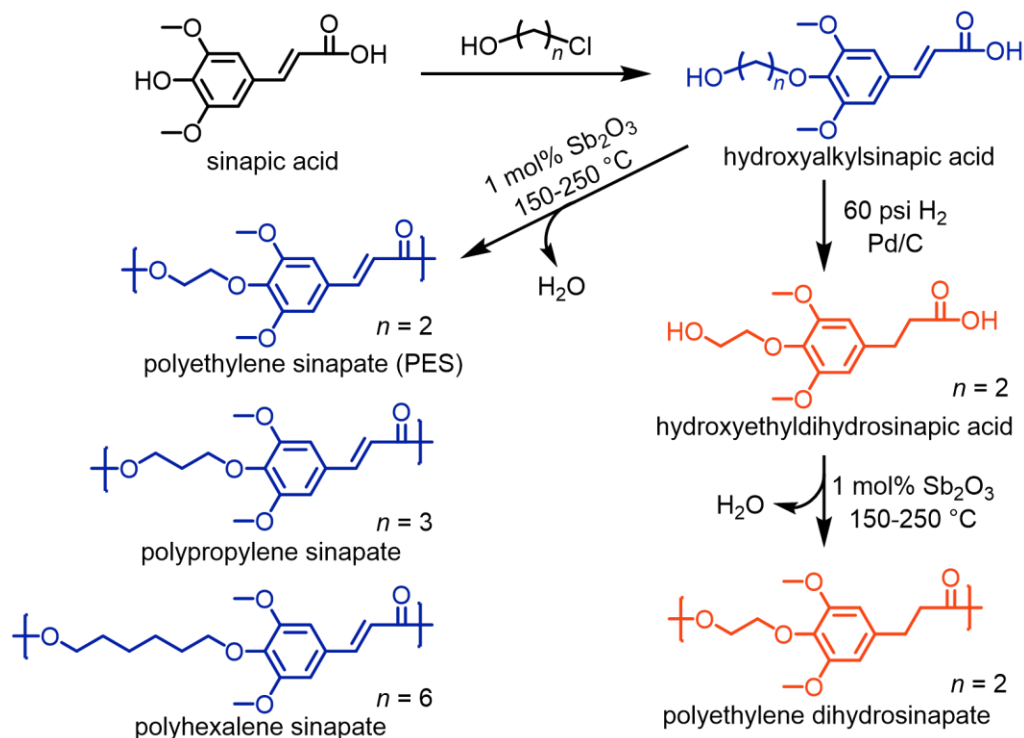


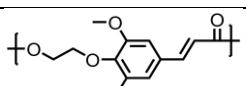
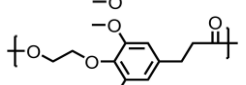
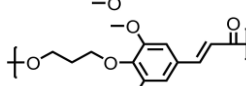
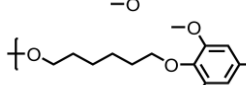
Figure 1-5. Synthetic route of polyalkylene sinapate (blue, left) and polyethylene dihydrosinapate (orange, right)

Previously, our research group published the synthesis of polyethylene ferulate, polyethylene coumarate, and their derivatives (Figure 1-2).⁸⁴ Ferulic acid and *p*-coumaric acid were used as the monomers to afford these biorenewable polymers with various thermal properties. Both monomers are hydroxycinnamic acids that can be obtained from lignocellulose materials, such as sugarcane and corn. One of the aims of this project is the continued pursuit of tunable thermal properties for biopolymers from sinapic acid, a distinct hydroxycinnamic acid that exists in the *Brassicaceae* plant family. Sinapic acid was then converted to hydroxyethylsinapic acid via a reaction of sinapic

acid and 2-chloroethanol. The reason for extending sinapic acid was to increase the nucleophilicity of monomers by providing a primary alcohol group instead of a phenolic group, thus increasing the reactivity of the monomers. Moreover, the methylene spacer would also provide some flexibility in the main chain of the synthesized polymers that could potentially increase the processability and tractability of the polymers.

Hydroxyethylidihydrosinapic acid was made by subjecting the hydroxyethylsinapic acid into hydrogenation using Pd on carbon catalyst. This would provide a low T_g polymer due to the lower conformational barriers from the additional methylene spacers by hydrogenation of the double bond. In addition to the saturation, other flexible monomers were also made by introducing methylene spacers of different length by reacting sinapic acid with 3-chloro-1-propanol or 6-chloro-1-hexanol, resulting in hydroxypropylsinapic acid and hydroxyhexylsinapic acid monomers, respectively (Figure 1-5).

Table 1-1. Polymerization results for polyalkylene sinapates ^a

| Entry | Polymer | Yield (%) | M_n^b (Da) | M_w^b (Da) | \mathcal{D}^b | T_g^c (°C) | $T_{5\%}^d$ (°C) | $T_{50\%}^e$ (°C) |
|-------|---|-----------|--------------|--------------|-----------------|--------------|------------------|-------------------|
| 1 |  | 60.2 | <i>f</i> | <i>f</i> | <i>f</i> | 118 | 338 | 390 |
| 2 |  | 74.8 | 8,000 | 37,000 | 4.6 | 41 | 330 | 379 |
| 3 |  | 69.7 | <i>f</i> | <i>f</i> | <i>f</i> | 90 | 346 | 392 |
| 4 |  | 74.2 | 4,500 | 24,000 | 5.3 | 43 | 350 | 396 |

^aReaction conducted in neat conditions using 1 mol% Sb_2O_3 ; mixtures were melted with a temperature ramp from 150 °C – 250 °C for 4 hours, then 8 hours of dynamic vacuum at 250 °C, except as noted. See the experimental method for exact temperature profile. ^bObtained by GPC in HFIP at 40 °C versus PMMA standards. ^cDetermined by DSC. ^dTemperature reported upon 5% mass loss. ^eTemperature reported upon 50% mass loss. ^fPolymers were insoluble in GPC solvents

Polyalkylene sinapates were synthesized using 1 mol% Sb_2O_3 as the typical melt polycondensation catalyst. The monomers were melted under a nitrogen atmosphere

and gradually heated from 150 °C to 250 °C for 4 hours. The byproduct from the polycondensation was water and the system was placed under dynamic vacuum for 6 hours to remove the byproduct and thus increase the degree of polymerization. The polymers were melted and recovered from round bottom flask using a spatula. According to Table 1-1, the yield of recovered polymers was in the range of 60.2–74.8%; the low T_g polymers were easier to recover and thus, had higher yield. The characterizable molecular weight of polymers was low; polyhexylene sinapate had a M_n value of 4,500 and dispersity index (\mathcal{D}) of 5.3, and polyethylenedihydro sinapate had a M_n value of 8,000 and \mathcal{D} of 4.6; meanwhile, the rest of the homopolymers that had high rigidity did not dissolve in the hexafluoroisopropanol (HFIP) for GPC characterization.

On the other hand, the polymers exhibited excellent thermal properties, the temperature of 5% mass loss under nitrogen ($T_{5\%}$) was in the range of 330–350 °C, and the temperature of 50% mass loss under nitrogen ($T_{50\%}$) was in the range of 379–396 °C. Additionally, there were structure-thermal property relationships among the polymers that can be assessed depending on the number of methylene spacers, such as the length of n carbons between alcohol and phenol or the hydrogenated double bond. These provided the conformational flexibility of polymers and thus lowered the T_g . Comparing to our previous reported work, the observed T_g of polyethylene sinapate was higher than the reported T_g of polyethylene ferulate and polyethylene coumarate, with the T_g values of 118 °C, 113 °C, and 109 °C, respectively. Likewise, the T_g of polyethylenedihydro sinapate was also higher than the reported T_g of polyethylene dihydroferulate and polyethylene dihydrocoumarate, with T_g values of 41 °C, 32 °C, 24 °C, respectively.⁸⁴ This was most likely due to the effect from conformational barriers

outweighing the free volume effect of the additional methoxy groups. This could mean that the polymers from *Brassica* generally have superior thermal properties due to the additional methoxy group of sinapic acid compared to ferulic acid- and coumaric acid-based polymers that derive from lignocellulose biomass.

Table 1-2. Copolymerization results of the copoly(hydroxyethyl dihydro sinapic acid/hydroxyethyl sinapic acid) series

| Entry | Monomer feed % | | SA ^b (mol %) | Yield (%) | M _n ^c (Da) | Đ ^c | T _g ^d (°C) | T _g ^{Fox} _e (°C) | T _{5%} ^f (°C) |
|-------|----------------|------|----------------------------|-----------|-------------------------------------|----------------|-------------------------------------|--|--------------------------------------|
| | HEHSA | HESA | | | | | | | |
| 1 | 100 | 0 | 0 | 74.8 | 8,000 | 4.6 | 41 | 41 | 330 |
| 2 | 90 | 10 | 9 | 80.5 | 14,000 | 6.3 | 43 | 44 | 341 |
| 3 | 80 | 20 | 21 | 88.0 | <i>g</i> | <i>g</i> | 48 | 48 | 338 |
| 4 | 70 | 30 | 28 | 92.5 | <i>g</i> | <i>g</i> | 53 | 50 | 336 |
| 5 | 60 | 40 | 37 | 88.8 | <i>g</i> | <i>g</i> | 57 | 54 | 335 |
| 6 | 50 | 50 | 47 | 91.2 | <i>g</i> | <i>g</i> | 65 | 59 | 339 |
| 7 | 40 | 60 | 56 | 91.4 | <i>g</i> | <i>g</i> | 71 | 65 | 332 |
| 8 | 30 | 70 | 65 | 92.8 | <i>g</i> | <i>g</i> | 77 | 71 | 333 |
| 9 | 20 | 80 | 75 | 97 | <i>g</i> | <i>g</i> | 89 | 80 | 324 |
| 10 | 10 | 90 | 85 | 90.5 | <i>g</i> | <i>g</i> | 95 | 92 | 332 |
| 11 | 0 | 100 | 100 | 60.2 | <i>g</i> | <i>g</i> | 118 | 118 | 338 |

^aReaction conducted in neat conditions using 1 mol% Sb₂O₃; mixtures were melted with a temperature ramp from 150 °C – 250 °C for 4 hours, then 8 hours of dynamic vacuum at 250 °C, except as noted. See the experimental method for exact temperature profile. ^bIncorporation of hydroxyethyl sinapic acid and hydroxyethyl dihydro sinapic acid in the copolymers was determined by ¹H NMR. ^cObtained by GPC in HFIP at 40 °C versus PMMA standards. ^dDetermined by DSC. ^eCalculated by the Fox equation. ^fTemperature reported upon 5% mass loss. ^gPolymers were insoluble in GPC solvents.

A series of controlled glass transition temperature copolymers was synthesized by taking advantage of the high *T_g* of polyethylene sinapate and the low *T_g* of polyethylene dihydro sinapate, particularly by employing different ratios of hydroxyethyl sinapic acid (HESA) and hydroxyethyl dihydro sinapic acid (HEHSA) monomers. Indeed, there was a positive correlation between the *T_g* of copolymers versus feed fraction of unsaturated monomer, as illustrated by Figure 1-6.

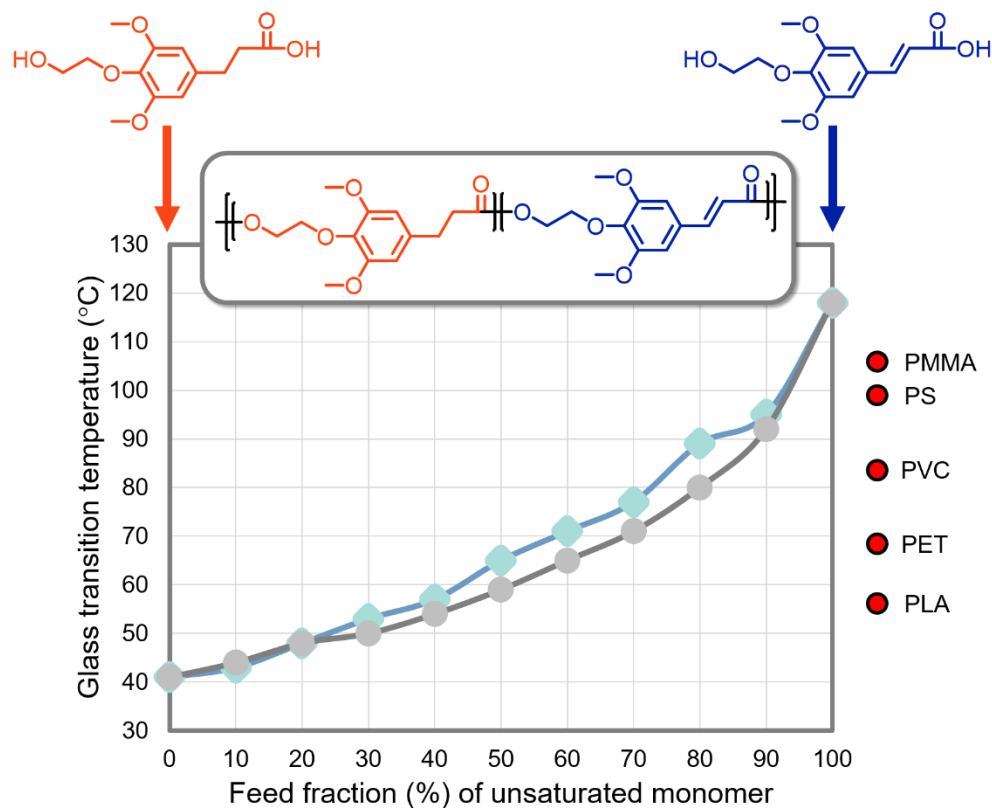


Figure 1-6. Comparison of glass transition temperatures for the copoly(hydroxyethylidihydroxy sinapic acid/hydroxyethylsinapic acid) series observed by Differential Scanning Calorimetry (light blue diamonds) to those calculated by the Fox equation (light grey circles).

As tabulated in Table 1-2, the T_g values observed by Differential Scanning Calorimetry (DSC) were close to the T_g values predicted by the Fox equation for binary blend copolymers.⁸⁹ The T_g range of the copolymer series is 41 °C to 118 °C, spanning the T_g values of several high demand commodity plastics, including polymethyl methacrylate ($T_g = 105$ °C), polystyrene ($T_g = 100$ °C), polyvinyl chloride ($T_g = 82$ °C), polyethylene terephthalate ($T_g = 67$ °C), and polylactic acid ($T_g = 55$ °C). Similarly, the percentage of incorporated monomers feed was confirmed by the ^1H NMR spectroscopy. The relative integration for the methylene peaks of the HEHSA moiety

(2.7 and 2.9 ppm) and the methylene peaks of both HEHSA and HESA moieties (4.2, 4.3, 4.4, 4.5 ppm) were particularly used for determining the values given in Table 1-2.

Synthesis of polyethylene sinapate from extracted sinapic acid

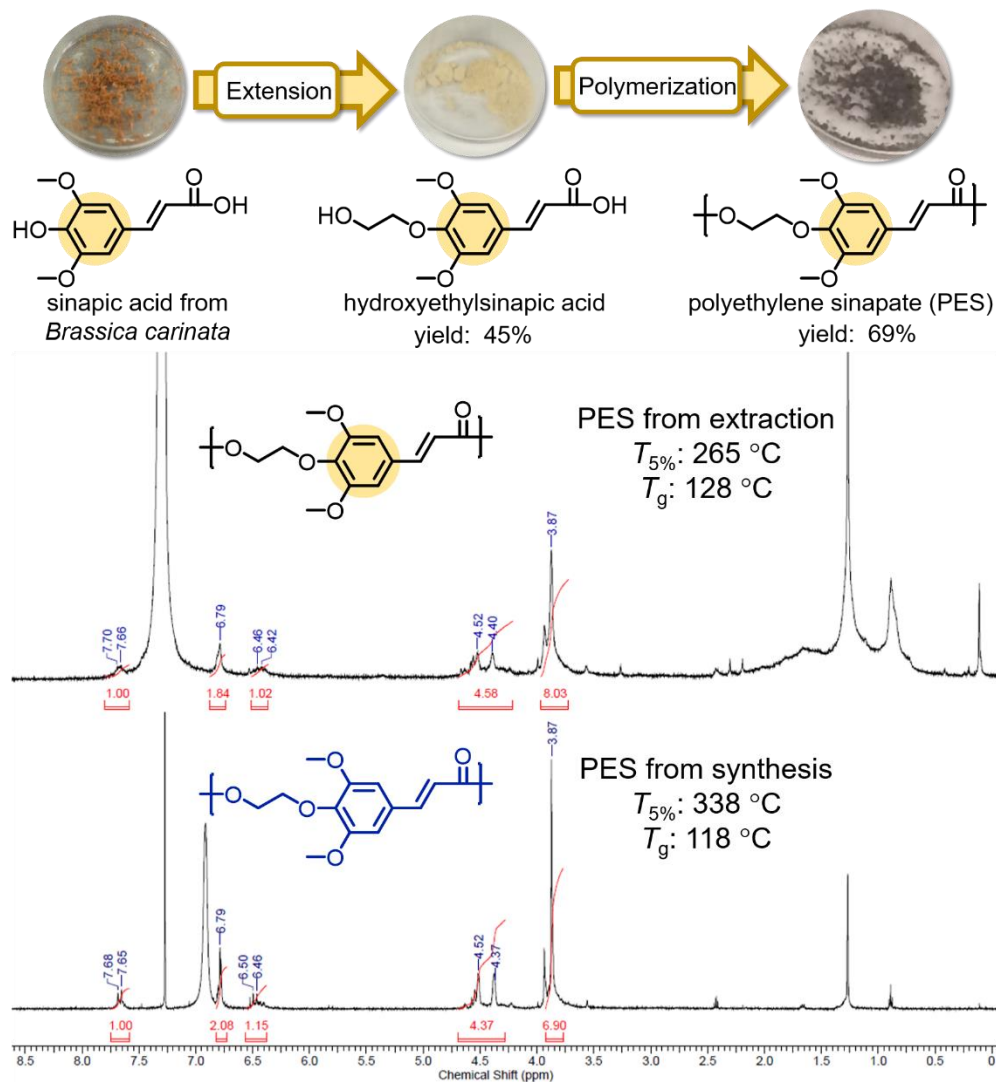


Figure 1-7. Comparison between polyethylene sinapate (PES) from extracted sinapic acid and from commercial petroleum based sinapic acid.

The last part on this project was the synthesis of polyethylene sinapate using the extracted sinapic acid that we obtained directly from *carinata* meal. All of the obtained sinapic acid from various extraction methods was accumulated into a round bottom

flask; then the extracted sinapic acid was converted into hydroxyethylsinapic acid monomer. Then, the synthesized monomer was polymerized using the same protocol used for the initial polymer that we made from commercial sinapic acid, but with a smaller scale. The ^1H NMR spectrum confirmed that the synthesized polymer was indeed the polyethylene sinapate. This polymer exhibited a $T_{5\%}$ of 265 °C and a T_g of 128 °C (Figure 1-7). The difference of thermal properties for this polymer use the polyethylene sinapate from commercial sinapic acid was probably due to the small scale reaction that we used; the small scale of the polymerization amplified the effects of the impurities and provided somewhat anomalous result. Still, this polymer is likely one of the first if not the first synthetic polymer made from *Brassica carinata* based sinapic acid.

Conclusions

As the future of petroleum becomes bleak, *Brassica carinata* brings an enormous number of opportunities as the future bio-refinery alternative. For farmers, *carinata* will increase incomes for its agronomic benefits, and has potential as a winter cash crop. For the transportation industry, *carinata* has one of highest non-food oil seed contents, which has been converted to advanced bio-jet fuel. For animal farm, the defatted seed can be used as the livestock meal due to its high protein and low fiber content. For the chemicals industry, *carinata*-based chemicals can provide great diversification of the chemical portfolio for human daily life products, including fragrance, skincare, pharmaceuticals, herbicides, preservatives, and bioplastics.

In the current market, sinapic acid is a high value added co-product (US\$550 per kg); therefore, the extraction of sinapic acid from the meal will greatly increase revenue

for the *carinata* biomill, while at the same time increasing the quality of the meal. If one acre of *carinata* plantation yields 1,800 kg of seed or 900 kg of meal,¹⁵ and the average yield of sinapic acid in the meal is 1.5%, then there is a possible additional value of US\$7500 per acre from sinapic acid. However, the price of this extracted sinapic acid has a flexible true value and can be adjusted according to the demand of the market since this sinapic acid is initially a by-product from the low value product, *carinata* meal. As has been suggested by numerous studies⁶⁶⁻⁸³ and this work, sinapic acid fits into the global preservatives and bioplastics market, which both will have an increasing demand in the future.

By exploiting structure-property relationships, the synthesized polyalkylene sinapates showed excellent thermal stability and a wide range of glass transition temperatures that overlap with several current commodity plastics. Although the degradation studies on these polymers were not conducted, the structures' similarity to that of lignin and polyesters suggested that there is a potential biodegradation pathway that can breakdown these polymers into non-toxic small molecules.⁹⁰ In the most ambitious scenario, perhaps when every flight uses *carinata*-based jet fuel and the plantation of *carinata* covers millions of acres of land, then the *carinata*-based polymers will definitely enter the global market to replace current petroleum-based plastics.

CHAPTER 2 WEAK LINKS IN SINAPIC ACID-BASED POLYMERS[†]

Background

Global plastic production has continued to increase over the years due to the ever-growing demand and consumption of plastic materials. In 2017 alone, the world produced 348 billion kg of plastics which consisted of commodity plastics, engineering plastics, and high-performance plastics. Household commodity plastics made up to 90% of the entire plastics' market share, including polyethylene terephthalate (PET, 7%), high-density polyethylene (HDPE, 15%), polyvinyl chloride (PVC, 16%), low-density polyethylene (LDPE, 17%), polypropylene (PP, 23%), and polystyrene (PS, 7%).⁹¹ In addition, about 40% of these commodity plastics were designed for single use packaging materials.⁹² This high dependence on plastics comes at two great costs to the environment: (1) most plastics are derived from non-renewable resources (petroleum and natural gas),⁹³ (2) most plastics are non-degradable and plastics waste will keep accumulating over the years.⁹⁴ One of the concrete solutions to these problems is the synthesis of bioplastic, which is either a bio-based or degradable plastic.⁹⁵ Presently, there is a substantial untapped market for bioplastic development and production, as current bioplastics constitute only one percent of total global plastic production.⁸⁰ Polylactic acid (PLA) is one of the most commercially successful bio-based and biodegradable plastic,⁹⁶ under the trade names of Ingeo® from NatureWorks⁹⁷ and Luminy® from Total Corbion.⁹⁸ PLA is synthesized from a ring-opening polymerization of L-lactide obtained from the fermentation of corn, cassava,

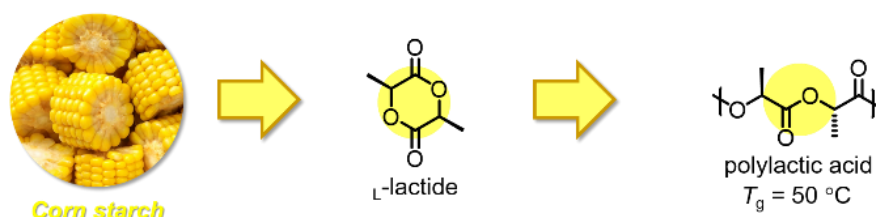
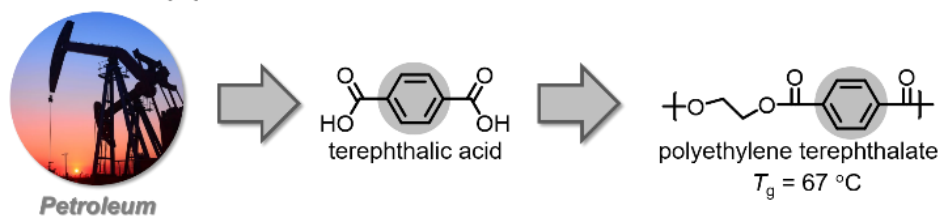
[†] This work will be submitted to Polymer Chemistry as a paper

sugarcane, or beet starch.^{96–98} One analogue of PLA is polyglycolic acid (PGA) a bioplastic under the trade name of Kuredux® from Kureha.⁹⁹ Additionally, PGA is synthesized from a ring-opening polymerization of glycolide resembling the synthesis of PLA.¹⁰⁰ Owing to their biocompatibility and biodegradability,¹⁰¹ both PLA and PGA have been manufactured for medical applications such as absorbable medical sutures.^{102,103} Nevertheless, due to a higher demand of packaging bioplastics (65% of total bioplastics market in 2018),⁸⁰ PLA has found a more lucrative market in packaging applications.^{104,105} Moreover, PLA and PGA have mechanical properties that are comparable to current commodity plastics.^{95–100} PLA exhibits a glass transition temperature (T_g) of 50 °C and a melting temperature (T_m) of 160 °C,¹⁰⁶ while PGA has a T_g of 35 °C and a T_m of 231 °C.¹⁰⁷ Although PLA and PGA are semi-crystalline polymers that offer high T_m , for packaging applications high T_g amorphous biopolymers are still preferred due to their greater optical transparency, toughness, and susceptibility to hydrolysis.¹⁰⁸

Several studies have been carried out to increase the thermal properties of PLA and PGA by copolymerizing PLA or PGA with cyclic and aryl groups that can impede the conformational mobility of polymers. Baker and co-workers synthesized a series of substituted PLA and PGA to study the effect on their degradation and thermal properties. Two notable copolymers were poly(lactic acid-co-mandelide) with a T_g of 86 °C and poly(lactic acid-co-cyclohexyllactide) with a T_g of 73 °C.^{109,110} In other study, Hillmyer *et al.* polymerized various spiro lactide derivatives, including poly(isoprene-lactide), poly(norbornane-lactide), and poly(cyclohexadiene-lactide), displaying T_g values of 77 °C, 107 °C, and 119 °C, respectively.¹¹¹ Comparatively, Vert *et al.* introduced a bulky ketal pendant group from gluconic acid into PGA and PLA

derivatives and substantially increased the T_g of those polymers.^{112,113} For instance, polymerization of 3-(1,2,3,4-tetraoxobutylidene)diisopropylidene)dioxane-2,5-dione (DIPAGYL) yielded poly-DIPAGYL with a T_g of 97 °C.¹¹² On the other hand, the copolymers of poly-DIPAGYL and PLA (70% lactide) exhibited a T_g of 73 °C.¹¹³ There were also several studies on the copolymerization of PLA and PGA with PET ($T_g = 67$ °C) by Olewnik *et al.*^{114,115} They depolymerized post-consumer PET into bis(2-hydroxyl terephthalate) (BHET); then poly(lactic acid-co-ethylene terephthalate) ($T_g = 60$ °C) was obtained by melt polymerization of BHET and L-lactic acid oligomers.¹¹³ Later, the same method was also utilized to produce poly(glycolic acid-co-ethylene terephthalate) with a T_m of 166 °C; there was no reported T_g in this paper.¹¹⁵ For the past few decades, furan-based polymers have been extensively studied as a greener alternative of PET plastic. Perhaps the most prevalent example is polyethylene furanoate (PEF) by Avantium¹¹⁶ which unfortunately is not biodegradable.¹¹⁷ Recent work from Zhu and co-workers was the introduction of a weak link (glycolate moiety) into a furan-based polyester, particularly the copolyester of poly(glycolic acid-co-butylene furandicarboxylate) with a T_g up to 38 °C.¹¹⁸ Lastly, in 2017, our group published a paper on copolymers of L-lactide and bioaromatics (syringic acid, vanillic acid, ferulic acid, and coumaric acid-based polymers) with T_g values ranging from 68 °C to 107 °C.¹¹⁹

Commodity plastics:



This work:

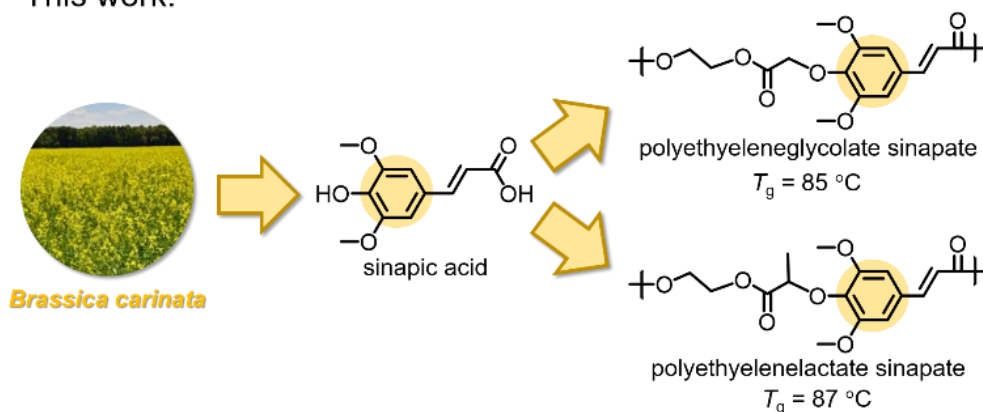


Figure 2-1. Polyethylene terephthalate (PET) alternatives from sinapic acid exhibit superior glass transition temperatures (T_g) vs. petroleum-based PET.

In the Miller group, we valorize readily available biobased monomers to obtain high T_g and T_m plastics as alternatives to current commodity plastics. One particular renewable monomer that has recently caught our interest is sinapic acid. Sinapic acid is a naturally occurring substance in the Brassicaceae, or commonly known as the mustard plant family.¹²⁰ The extractions of sinapic acid or its choline ester form, sinapine, from plants have been widely developed.^{78,79,121,122,123} There are two motivations behind this extraction development: (1) the presence of sinapic acid (in the form of sinapine) in the plant is anti-nutritional for animals, hence it is crucial to remove

sinapine from the mustard seeds used as livestock feed; however (2) for humans, sinapic acid is a high-value medicinal and supplementary product due to its antioxidant, anti-inflammatory, antibacterial, and antimutagenic properties.^{67,69,71,72} Although the current price of sinapic acid is still high (US\$550 per kg), it is important to note that sinapic acid can be obtained from plant waste materials, particularly the post oil extraction of seed meal.^{78,79,121,122,123} Currently, under the SPARC (Southeast Partnership for Advanced Renewables from Carinata) project, *Brassica carinata* has been seen and studied as, arguably, the plant with the most potential for biofuel production.^{11,15} As a matter of fact, Applied Research Associates (ARA), partnering with Chevron Lummus Global (CLG) and Agrisoma, has produced a 100% drop-in bio-jet fuel, under the brand name ReadJet®.³¹ As the demand of drop-in biofuel increases over the years, *B. carinata* may be capable of driving down the price of sinapic acid to be affordable enough as an abundant biorenewable resource for polymer synthesis.¹²⁴ Nevertheless, on a small scale industry, sinapic acid still contributes as a high-value added co-product from the *Brassica carinata* biorefinery. Up to this date, there are several published sinapic acid-based bioplastics, such as: (1) Bezwada Biomedical, LLC patented a series of degradable sinapic acid-based biopolymers for biomedical applications;⁸¹ (2) Allais *et al.* published a ring opening polymerization of norbornene dihydrosinapate (NDS) which yielded bioplastics with T_g values up to 56 °C;⁸² (3) The same research group (Allais *et al.*) synthesized a sinapic acid-based bisphenol resulting a series of bioplastics with T_g values up to 126 °C;⁸³ (4) Our research group also recently contributed on our polyethylene sinapate (PES) series with T_g values ranging from 41 °C to 118 °C.^{123,124} Herein, we sought to install lactate and glycolate moieties

into sinapic acid-based polymers. Lactate and glycolate act as the weak links that facilitate the degradation of polymers while having tunable T_g owing to the presence of sinapic acid moiety in the main chain.

Experimental

Materials

Sinapic acid was purchased from Henan Tianfu Chemical Co., Ltd. via Alibaba.com. Ferulic acid and *p*-coumaric acid were purchased from Nanjing Zelang Medical Technology Co., Ltd. via Alibaba.com. Methyl chloroacetate, 1,3-propanediol, and 1,9-nonanediol were purchased from Sigma Aldrich. Methyl 2-chloropropionate, and 1,6-hexanediol were purchased from Alfa Aesar. Ethylene glycol, 1,4-butanediol, 1,5-pentanediol, 1,8-octanediol, and 1,10-decanediol were purchased from Acros Organics. Acetone, ethyl acetate, methanol, hydrochloric acid, sodium hydroxide, sodium iodide, sodium bicarbonate, sodium chloride, and potassium carbonate anhydrous were purchased from Fisher Chemical. Ethylenediamine was purchased from Honeywell Fluka. Ethanolamine and NMR solvents, including deuterated chloroform (CDCl_3), and deuterated dimethyl sulfoxide ($\text{DMSO}-d_6$) were purchased from Cambridge Isotope Laboratories. Polylactic acid (PLA) sample was obtained from dissolving “Eco cup” in dichloromethane and reprecipitated in hexanes ($M_n = 12,000$, $\bar{D} = 3.7$). Seawater was obtained from Siesta Key, Florida ($27^\circ 16' 31''\text{N}$, $82^\circ 33' 9''\text{W}$). All the chemicals, unless expressly mentioned, were utilized without further purification.

Characterization

Proton nuclear magnetic resonance (^1H NMR) and carbon nuclear magnetic resonance (^{13}C NMR) were recorded using an Inova 500 MHz spectrometer. Chemical shifts are reported in parts per million (ppm) downfield relative to tetramethylsilane

(TMS, 0.0 ppm). Coupling constants (J) are reported in Hertz (Hz). Multiplicities are reported using the following abbreviations: s, singlet; d, doublet; t, triplet; q, quartet; m, multiplet; br, broad.

Thermogravimetric analyses (TGA) were measured under nitrogen with a TGA Q5000 (TA Instruments). About 5–7 mg of each sample were heated at 20 °C/min from room temperature (25 °C) to 600 °C.

Differential scanning calorimetry (DSC) thermograms were obtained with a DSC Q1000 (TA instruments). Typically 4–6 mg of a sample were massed and added to a sealed pan that passed through a heat-cool-heat cycle at 10 °C min⁻¹. Reported data are from the second full cycle. The temperature ranged from 0 to 250 °C.

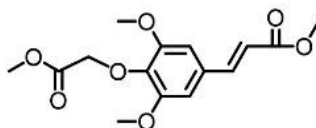
Gel permeation chromatography (GPC) was performed at 40 °C using an Agilent Technologies 1260 Infinity Series liquid chromatography system with an internal differential refractive index detector, and a two Waters Styragel HR-5E columns (7.8 mm i.d., 300 mm length, guard column 7.8 mm i.d., 25 mm length) using a solution of 0.1% potassium triflate (K(OTf)) in HPLC grade hexafluoroisopropanol (HFIP, purchased from SynQuest Laboratories, Alachua, Florida) as the mobile phase flow rate of 0.5 mL min⁻¹. Calibration was performed with narrow polydispersity polymethyl methacrylate standards.

Synthesis

Sinapic acid was converted into methyl sinapate and then into its subsequent monomers. A series of homopolymers and copolymers was then synthesized by reacting with ethylene glycol and other longer chains of linear diols. The methods for dimethylglycolate sinapate (MGS), dimethylglycolate dihydrosinapate (MGHS),

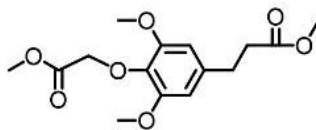
dimethylacrylate sinapate (MLS), dimethylacrylate dihydrosinapate (MLHS), polyethyleneglycolate dihydrosinapate (PEGHS), polyethyleneglycolate sinapate (PEGS), polyethylenelactate dihydrosinapate (PELHS), and polyethylenelactate sinapate (PELS) follow below and all other monomer syntheses are provided in Chapter 6.

Synthesis of dimethylglycolate sinapate (MGS).



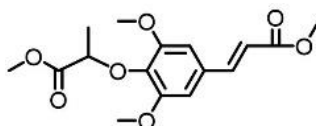
A mixture of methyl sinapate (39.0 g, 0.164 mol), sodium iodide (1.55 g, 10.35 mmol), and potassium carbonate (27.8 g, 0.202 mol) was suspended in 350 mL acetone. The solution was stirred and heated at reflux for 30 mins. Then, methyl chloroacetate (11.04 mL, 0.126 mol) was slowly added into the solution. The solution was then refluxed for 24 hours at reflux. Upon completion, the mixture was cooled down to room temperature, then acetone was removed by a rotatory evaporation. The resulting crude product was dissolved in 500 mL of ethyl acetate and washed with 2 x 250 mL of 0.5 M sodium hydroxide solution, 2 x 150 mL of deionized water, and 150 mL of brine. The organic portion was dried over magnesium sulfate anhydrous and filtered, then ethyl acetate was removed by a rotatory evaporation resulting in white powder. 35.37 g of dry white powder was obtained in 90.6% yield. ^1H NMR (DMSO- d_6) δ ppm 3.68 (s, 2 H), 3.72 (s, 3 H), 3.80 (s, 6 H), 4.57 (s, 2 H), 6.67 (d, 1 H), 7.08 (s, 2 H), 7.59 (d, 1 H). ^{13}C NMR (DMSO- d_6) δ ppm 51.4, 51.5, 56.2, 64.0, 106.1, 116.3, 128.1, 137.5, 144.6, 152.3, 166.8, 168.2.

Synthesis of dimethylglycolate dihydrosinapate (MGHS).



Dimethylglycolate sinapate (15.0 g, 0.048 mol) and 10% Pd on Carbon (1.03 g, 0.967 mmol) were mixed in 225 mL of THF. The mixture was hydrogenated for 24 hours under 60 psi of H₂ gas. The reaction was then vacuum filtered through a celite filter bed. The filtrate was dried by a rotary evaporator and diluted in ethyl acetate. The product was then precipitated upon addition of cold hexane and was isolated by gravity filtration. After drying under vacuum, 14.215 g of dry white powder was obtained in 94.16% yield. ¹H NMR (CDCl₃) δ ppm 2.63 (t, 2 H), 2.79 (t, 2 H), 3.60 (s, 3 H), 3.68 (s, 3 H), 3.73 (s, 6 H), 4.45 (s, 2 H), 6.54 (s, 2 H). ¹³C NMR (CDCl₃) δ ppm 30.6, 34.9, 51.4, 51.5, 55.9, 68.8, 105.5, 136.8, 152.1, 156.5, 169.2, 172.7.

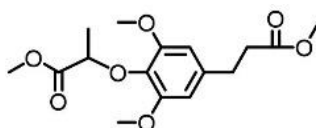
Synthesis of dimethyl lactate sinapate (MLS).



A mixture of methyl sinapate (39.0 g, 0.164 mol), sodium iodide (1.55 g, 10.35 mmol), and potassium carbonate (27.8 g, 0.202 mol) was suspended in 350 mL acetone. The solution was stirred and heated at reflux for 30 mins. Then, methyl 2-chloropropionate (14.36 mL, 0.126 mol) was slowly added into the solution. The solution was then refluxed for 3 days at reflux. Upon completion, the mixture was cooled down to room temperature, then acetone was removed by a rotatory evaporation. The resulting crude product was combined with 750 mL of 1 M hydrochloric acid solution. The acidic solution was then extracted with 2 x 350 mL of ethyl acetate. The organic portion was

washed with 2 x 250 mL of 1 M sodium hydroxide solution, 2 x 150 mL of deionized water, and 150 mL of brine. The organic portion was dried over magnesium sulfate anhydrous and filtered, then ethyl acetate was removed by a rotatory evaporation resulting in white powder. 26.748 g of dry white powder was obtained in 48.0% yield. ^1H NMR ($\text{DMSO-}d_6$) δ ppm 1.38 (d, 3 H), 3.65 (s, 3 H), 3.70 (s, 3 H), 3.78 (s, 6 H), 4.59 (q, 1 H), 3.90 (t, 2 H), 6.67 (d, 1 H), 7.08 (s, 2 H), 7.60 (d, 1 H). ^{13}C NMR ($\text{DMSO-}d_6$) δ ppm 18.1, 51.4, 51.5, 56.1, 76.3, 105.9, 117.2, 129.7, 137.0, 144.6, 152.6, 166.8, 171.4.

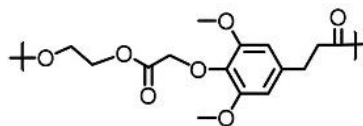
Synthesis of dimethyl lactate dihydrosinapate (MLHS).



A mixture of methyl dihydrosinapate (17.339 g, 0.072 mol), sodium iodide (0.685 g, 4.57 mmol), and potassium carbonate (12.277 g, 0.089 mol) was suspended in 200 mL acetone. The solution was stirred and heated at reflux for 30 mins. Then, methyl 2-chloropropionate (6.33 mL, 0.05552 mol) was slowly added into the solution. The solution was then refluxed for 2 days at reflux. Upon completion, the mixture was cooled down to room temperature, then acetone was removed by a rotatory evaporation. The resulting crude product was combined with 500 mL of 1 M hydrochloric acid solution. The acidic solution was then extracted with 2 x 250 mL of ethyl acetate. The organic portion was washed with 2 x 150 mL of 1 M sodium hydroxide solution, 2 x 100 mL of deionized water, and 100 mL of brine. The organic portion was dried over anhydrous magnesium sulfate and filtered; then ethyl acetate was removed by a rotatory evaporation resulting in a colorless oil. 14.97 g of colorless oil was obtained in 63.7% yield. ^1H NMR ($\text{DMSO-}d_6$) δ ppm 1.35 (d, 3 H), 2.63 (t, 2 H), 2.79 (t, 2 H), 3.60 (s, 3 H),

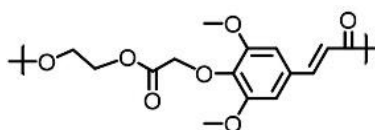
3.65 (s, 3 H), 3.72 (s, 6 H), 4.43 (q, 1 H), 6.53 (s, 2 H). ^{13}C NMR (DMSO- d_6) δ ppm 18.0, 30.6, 34.9, 51.4, 51.5, 55.8, 76.4, 105.4, 133.4, 136.5, 152.4, 171.6, 172.7.

Synthesis of polyethyleneglycolate dihydrosinapate (PEGHS).



Dimethylglycolate dihydrosinapate (1.50 g, 4.803 mmol), ethylene glycol (0.358 g, 5.764 mmol), and Sb_2O_3 (28.0 mg, 2 mol%) were loaded into a 50 mL round bottom flask. This flask was fitted with a bump trap and attached to the Schlenk line. The system was then purged with a nitrogen and vacuum three times. The mixture was melted under a nitrogen atmosphere at 160 °C for 2 hours, at 180 °C for 16 hours, and at 200 °C for 2 hours. Later, the system was placed under dynamic vacuum and was heated gradually from 200 °C to 215 °C for 5 hours to remove the condensation byproduct, thus increasing the degree of the polymerization. Once cool, the polymer was melted for removal from the flask and used without further purification. 1.306 g of polymer was obtained in 87.6% yield. ^1H NMR (CDCl_3) δ ppm 2.63 (t, 2 H), 2.88 (t, 2 H), 3.81 (s, 6 H), 4.28 (t, 2 H), 4.41 (t, 2 H), 4.61 (s, 2 H), 6.40 (s, 2 H). ^{13}C NMR (CDCl_3) δ ppm 31.1, 35.7, 56.1, 62.4, 63.2, 69.3, 105.3, 132.6, 141.5, 152.6, 169.8, 176.0.

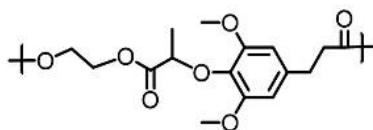
Synthesis of polyethyleneglycolate sinapate (PEGS).



Dimethylglycolate sinapate (1.50 g, 4.834 mmol), ethylene glycol (0.360 g, 5.801 mmol), and Sb_2O_3 (28.2 mg, 2 mol%) were loaded into a 50 mL round bottom flask. This flask was fitted with a bump trap and attached to the Schlenk line. The system was then

purged with a nitrogen and vacuum three times. The mixture was melted under a nitrogen atmosphere at 180 °C for 1 hour, and at 200 °C for 16 hours. Later, the system was placed under dynamic vacuum and was heated gradually from 200 °C to 240 °C for 7 hours to remove the condensation byproduct, thus increasing the degree of the polymerization. Once cool, the polymer was melted for removal from the flask and used without further purification. 1.303 g of polymer was obtained in 87.5% yield. ¹H NMR (CDCl₃) δ ppm 3.87 (s, 6 H), 4.43, 4.49 (m, 4 H), 4.72 (d, 2 H), 6.35 (d, 1 H), 6.74 (s, 2 H), 7.58 (d, 1 H). ¹³C NMR (CDCl₃) δ ppm 56.0, 62.2, 62.4, 69.0, 105.1, 116.6, 129.7, 137.9, 145.0, 152.5, 166.3, 168.8.

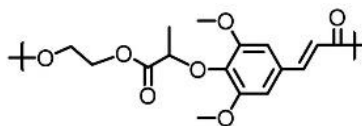
Synthesis of polyethylenelactate dihydrosinapate (PELHS).



Dimethyl lactate dihydrosinapate (1.50 g, 4.60 mmol), ethylene glycol (0.2855 g, 4.60 mmol), and Sb₂O₃ (27.82 mg, 2 mol%) were loaded into a 50 mL round bottom flask. This flask was fitted with a bump trap and attached to the Schlenk line. The system was then purged with a nitrogen and vacuum three times. The mixture was melted under a nitrogen atmosphere at 160 °C for 2 hours, at 180 °C for 16 hours, and at 200 °C for 2 hours. Later, the system was placed under dynamic vacuum and was heated gradually from 200 °C to 215 °C for 10 hours to remove the condensation byproduct, thus increasing the degree of the polymerization. Once cool, the polymer was melted for removal from the flask and used without further purification. 1.081 g of polymer was obtained in 72.5% yield. ¹H NMR (CDCl₃) δ ppm 1.53 (d, 3 H), 2.63 (t, 2 H), 2.86 (t, 2 H), 3.78 (s, 6 H), 4.27, 4.37 (m, 4 H), 4.61 (s, 1 H), 6.38 (s, 2 H). ¹³C NMR

(CDCl₃) δ ppm 18.4, 31.1, 35.6, 56.0, 62.16, 62.22, 77.1, 105.2, 134.3, 136.4, 152.9, 172.0, 172.5.

Synthesis of polyethylenelactate sinapate (PELS).



Dimethyl lactate sinapate (1.492 g, 4.60 mmol), ethylene glycol (0.2855 g, 4.60 mmol), and Sb₂O₃ (26.82 mg, 2 mol%) were loaded into a 50 mL round bottom flask. This flask was fitted with a bump trap and attached to the Schlenk line. The system was then purged with a nitrogen and vacuum three times. The mixture was melted under a nitrogen atmosphere at 180 °C for 3 hour, and at 200 °C for 16 hours. Later, the system was placed under dynamic vacuum and was heated gradually from 200 °C to 240 °C for 6 hours to remove the condensation byproduct, thus increasing the degree of the polymerization. Once cool, the polymer was melted for removal from the flask and used without further purification. 1.163 g of polymer was obtained in 78.4% yield. ¹H NMR (CDCl₃) δ ppm 1.59 (m, 3 H), 3.86 (s, 6 H), 4.43, 4.52 (m, 4 H), 4.77 (m, 1 H), 6.35 (d, 1 H), 6.81 (s, 2 H), 7.58 (d, 1 H). ¹³C NMR (CDCl₃) δ ppm 18.5, 56.4, 61.7, 62.4, 78.5, 105.1, 114.2, 128.3, 139.6, 144.8, 155.2, 167.2, 170.1.

Accelerated hydrolysis experiment

Effect of aqueous base solution. 0.1 g of PEGHS, PELHS, and PLA were placed in 12 mL of 1 M aqueous sodium hydroxide. These three vials were placed on a water bath at 80 °C. After 12 hours the pH was neutralized, liquid-liquid extraction was performed using chloroform (3 x 10 mL), the organic layers were combined and

evaporated, and the remaining solids were dried and then dissolved in DMSO- d_6 for ^1H NMR and ^{13}C NMR analysis and in HFIP for GPC analysis.

Effect of aqueous acid solution. 0.1 g of PEGHS, PELHS, and PLA were placed in 12 mL of 1 M aqueous hydrochloric acid. These three vials were placed on a water bath at 80 °C. After 12 hours the pH was neutralized and the remaining solids were dried and then dissolved in DMSO- d_6 for ^1H NMR and ^{13}C NMR analysis and in HFIP for GPC analysis.

Effect of deionized water and seawater. 30 mg of PEGHS, PELHS, and PLA were placed in 10 mL of deionized water and seawater. These six vials were placed on a water bath at 80 °C. After 72 hours the remaining solids were washed with deionized water and were dried overnight, then the solids were dissolved in DMSO- d_6 for ^1H NMR and ^{13}C NMR analysis and in HFIP for GPC analysis.

Results and discussion

Monomer design

Sinapic acid is versatile in creating various sinapic acid-based monomers due to its functionality. In this work, the double bond was hydrogenated creating a saturated monomer. Furthermore, the phenol group was elaborated with alkanoate groups. For instance, synthesis of dimethylglycolate sinapate and dimethyl lactate sinapate monomers involved methyl chloroacetate and methyl 2-chloropropionate. Methyl chloroacetate was converted into the glycolate moiety while methyl 2-chloropropionate was converted into the lactate moiety. It is noteworthy to mention that both haloester compounds can be derived from the byproducts, acetic acid and propionic acid, of

petroleum refinery processes.¹²⁵ This synthesis pathway fits into the SPARC narration, as both haloester compounds can be produced from *B. carinata* biorefineries.

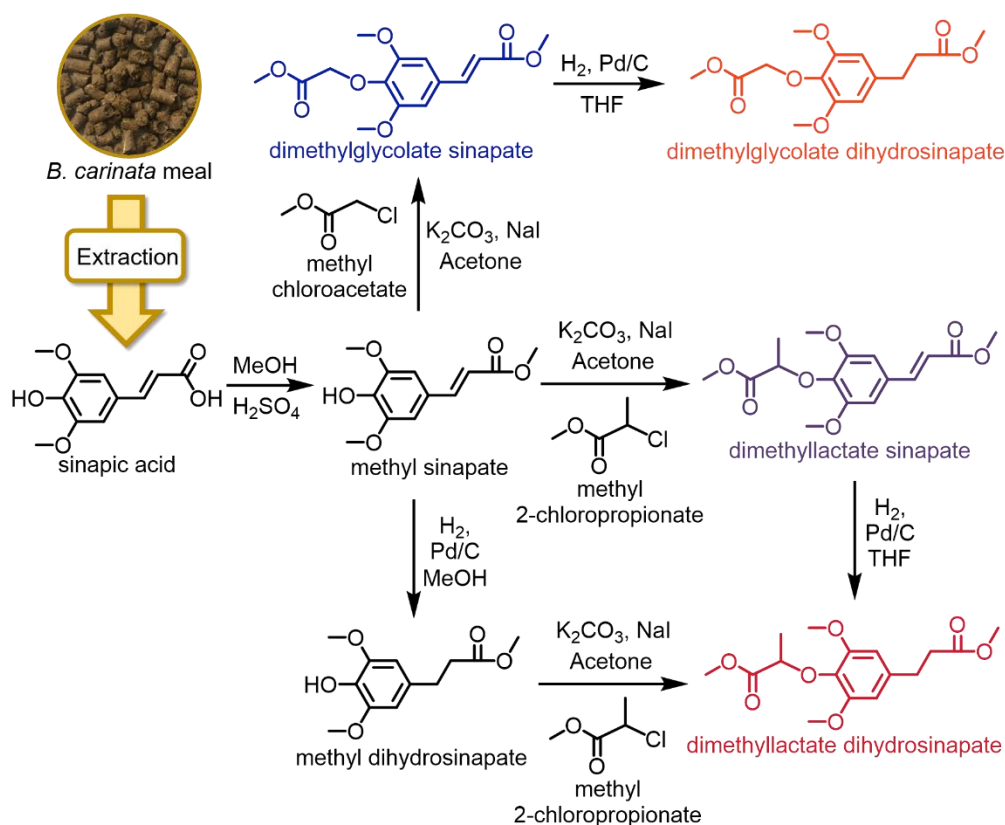


Figure 2-2. Synthesis of dimethylglycolate sinapate, dimethylglycolate dihydrosinapate, dimethyl lactate sinapate, and dimethyl lactate dihydrosinapate from sinapic acid, which can be extracted from *carinata* seed meal.

As can be seen, diester monomers were used for polymerization instead of using diacid counterparts. The original approach was to synthesize the diacid monomers instead of diester form. In fact, there had been several attempts for polycondensation of synthesized diacids with several diols, but to no avail. The diacid monomers did not melt despite reaction temperatures up to 240 °C. Meanwhile, the diols rapidly volatilized, and hence the polymerization was prevented. Since ester groups generally have a lower melting point than their carboxylic acid counterparts, diester monomers should melt and react more readily. Furthermore, the methanol byproduct generated by the

polycondensation reaction should be easier to remove than water (from the original approach) from the equilibrium;¹²⁶ this suggests that diester monomers should be superior to the diacid monomers.

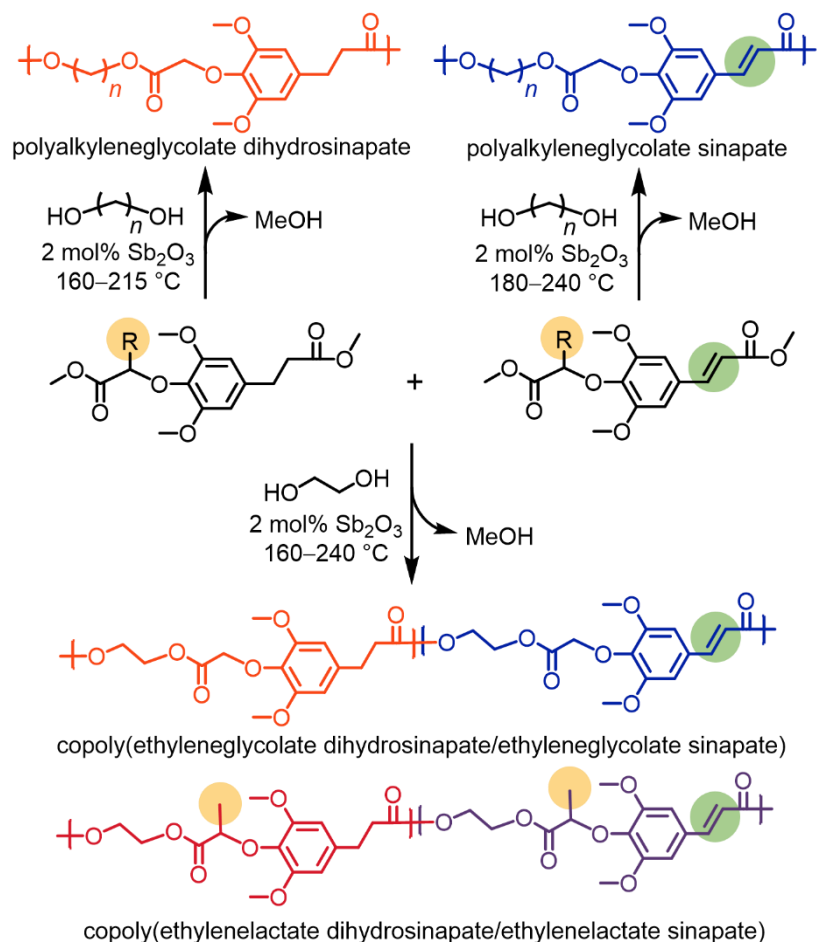
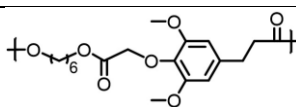
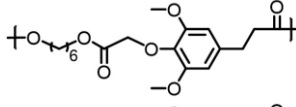
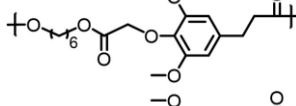
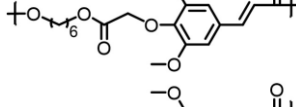
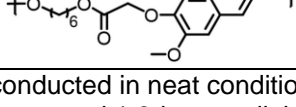


Figure 2-3. Synthetic route to copoly(ethyleneglycolate dihydrosinapate/ethyleneglycolate sinapate) (R = H), copoly(ethylenelactate dihydrosinapate/ethylenelactate sinapate) (R = Me), polyalkyleneglycolate sinapate ($n = 2-10$), and polyalkyleneglycolate dihydrosinapate ($n = 2$ and 6).

Table 2-1. Optimization study of polyhexyleneglycolate dihydrosinapate and polyhexyleneglycolate sinapate ^a

| Entry | Polymer | [Cat.] ^b (mol%) | T _{ramp} ^c (°C) | Yield (%) | M _n ^d (Da) | Đ ^d | T _g ^e (°C) | T _{5%} ^e (°C) |
|-------|---|-------------------------------|--|--------------|-------------------------------------|----------------|-------------------------------------|--------------------------------------|
| 1 |  | 1 | 160–215 | 73.2 | 11,500 | 2.5 | 0 | 294 |
| 2 |  | 2 | 160–215 | 82.0 | 15,200 | 2.4 | 4 | 295 |
| 3 |  | 2 | 160–240 | 73.0 | 20,000 | 4.1 | 7 | 294 |
| 4 |  | 2 | 180–215 | 70.1 | 5,800 | 2.9 | 32 | 289 |
| 5 |  | 2 | 180–240 | 96.7 | <i>g</i> | <i>g</i> | 49 | 301 |

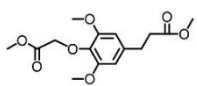
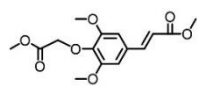
^aReaction conducted in neat condition using dimethylglycolate sinapate or dimethylglycolate dihydrosinapate and 1,6-hexanediol; mixtures were melted with a temperature ramp under nitrogen then switch to a dynamic vacuum. See the experimental method for exact temperature profile. ^bConcentration of Sb₂O₃ as the catalyst. ^cTemperature ramp of polymerization. ^dObtained by GPC in HFIP at 40 °C versus PMMA standards. ^eDetermined by DSC. ^fTemperature reported upon 5% mass loss. ^gPolymers were insoluble in GPC solvents.

Optimization of polymerization conditions

Dimethylglycolate dihydrosinapate (MGHS), dimethylglycolate sinapate (MGS), and 1,6-hexanediol were selected as the monomers because of their homopolymers, polyhexyleneglycolate sinapate and polyhexyleneglycolate dihydrosinapate—most likely to be soluble in HFIP for molecular weight characterization by GPC. There were two parameters that were used for the optimization study: catalyst loading and temperature. Several studies from our group suggested that Sb₂O₃ was indeed the most suitable catalyst for high temperature (above 180 °C) polycondensation reactions,^{84,119,126,127,128,129,130} so the optimization focused on the amount of catalyst loading needed (1 mol% versus 2 mol%) instead. Based on Table 1, 2 mol% Sb₂O₃ (Table 2-1, entry 2) gave a better result than that from 1 mol% Sb₂O₃ (Table 2-1, entry

1) using the same temperature ramp (160 °C – 215 °C). On the other hand, when the maximum temperature ramped to 240 °C (Table 2-1, entry 3), there was a broadening of \bar{D} to 4.1, although there was also an increased M_n (number average molecular weight) to 20,000 Da. Conversely, the polymerization of polyhexyleneglycolate sinapate yielded a low M_n (5,800 Da) when the maximum reaction temperature was 215 °C (Table 2-1, entry 4). The polymerization seemed to be sluggish and the ramp temperature needed to be increased to have a lower viscosity mixture. For this reason, reaction temperature was ramped to 240 °C (Table 2-1, entry 5), which was also the maximum temperature of the silicone oil bath before it degraded. The overall superior thermal properties indicated that this condition (entry 5) gave a better result than that from entry 4; the missing molecular weight data was only due to the insolubility of the polymer in HFIP for GPC characterization.

Table 2-2. Copolymerization results of copoly(ethyleneglycolate dihydrosinapate/ethyleneglycolate sinapate) series. ^a

| Entry | Monomer feed % | | MGS ^b (mol %) | Yield (%) | M_n ^c (Da) | \bar{D} ^c | T_g ^d (°C) | $T_{5\%}$ ^e (°C) | $T_{50\%}$ ^f (°C) |
|-------|---|---|--------------------------------|-----------|----------------------------|------------------------|----------------------------|--------------------------------|---------------------------------|
| |  |  | | | | | | | |
| 1 | 100 | 0 | 0 | 87.6 | 16,600 | 2.6 | 33 | 289 | 360 |
| 2 | 90 | 10 | 16 | 90.2 | 13,600 | 2.8 | 35 | 290 | 373 |
| 3 | 80 | 20 | 26 | 86.3 | 9,600 | 2.7 | 36 | 284 | 365 |
| 4 | 70 | 30 | 34 | 94.0 | <i>g</i> | <i>g</i> | 42 | 265 | 266 |
| 5 | 60 | 40 | 44 | 85.8 | <i>g</i> | <i>g</i> | 49 | 287 | 392 |
| 6 | 50 | 50 | 50 | 87.5 | <i>g</i> | <i>g</i> | 52 | 286 | 397 |
| 7 | 40 | 60 | 58 | 83.3 | <i>g</i> | <i>g</i> | 58 | 289 | 415 |
| 8 | 30 | 70 | 72 | 87.6 | <i>g</i> | <i>g</i> | 65 | 292 | 412 |
| 9 | 20 | 80 | 83 | 82.6 | <i>g</i> | <i>g</i> | 69 | 290 | 418 |
| 10 | 10 | 90 | 92 | 85.4 | <i>g</i> | <i>g</i> | 74 | 292 | 414 |
| 11 | 0 | 100 | 100 | 87.5 | <i>g</i> | <i>g</i> | 85 | 291 | 424 |

^aReaction conducted with no solvent using 2 mol% Sb_2O_3 ; mixtures of dimethylglycolate sinapate or dimethylglycolate dihydrosinapate and ethylene glycol were melted with a temperature ramp under nitrogen, then switch to a dynamic vacuum. See the experimental method for exact temperature profile. ^bIncorporation of MGS in the copolymers was determined by 1H NMR. ^cObtained by GPC in HFIP at 40 °C versus PMMA standards. ^dDetermined by DSC. ^eTemperature reported upon 5% mass loss. ^fTemperature reported upon 50% mass loss. ^gPolymers were insoluble in GPC solvents, THF and HFIP.

Polymer synthesis

Homopolymerization of polyethyleneglycolate dihydrosinapate (PEGHS) used the same condition as Table 2-1, entry 2. Meanwhile, homopolymerization of polyethyleneglycolate sinapate (PEGS) used the same condition as Table 2-1, entry 4. To accommodate the difference of melting points and reactivity, the copolymerization of saturated monomer and unsaturated monomer was conducted with different temperature ramps, depending on the feed ratio of the monomers employed. An excess amount (1.2 equivalents) of diols was typically used due to the high volatility of the diols at high temperature, compared to the other monomers. The mixtures were melted and stirred for 16 hours at 180 °C – 200 °C yielding a pre-polymer. Then, the polymerization was continued under dynamic vacuum conditions and a high temperature gradient to remove byproducts—such as methanol from the polycondensation and remaining unreacted diols—thus effectively increasing the molecular weight of polymer. All copolymerization results of PEGHS and PEGS with various monomer feed ratio were tabulated in Table 2-2. Based on ¹H NMR, the percentage of incorporated monomers feed aligned with the feed fractions of the monomers employed, which confirmed by the plot of MGS monomer feed % versus incorporated mol% resulted in $R^2 = 0.9945$. To enumerate, the ratio integration of four methylene protons for the MGHS repeat unit and six methoxy protons for both the MGHS and MGS unit were counted to determine the percentage of the MGHS portion in the copolymers. Furthermore, the overall satisfactory yields of 83–94% were obtained from the mass of recovered polymer.

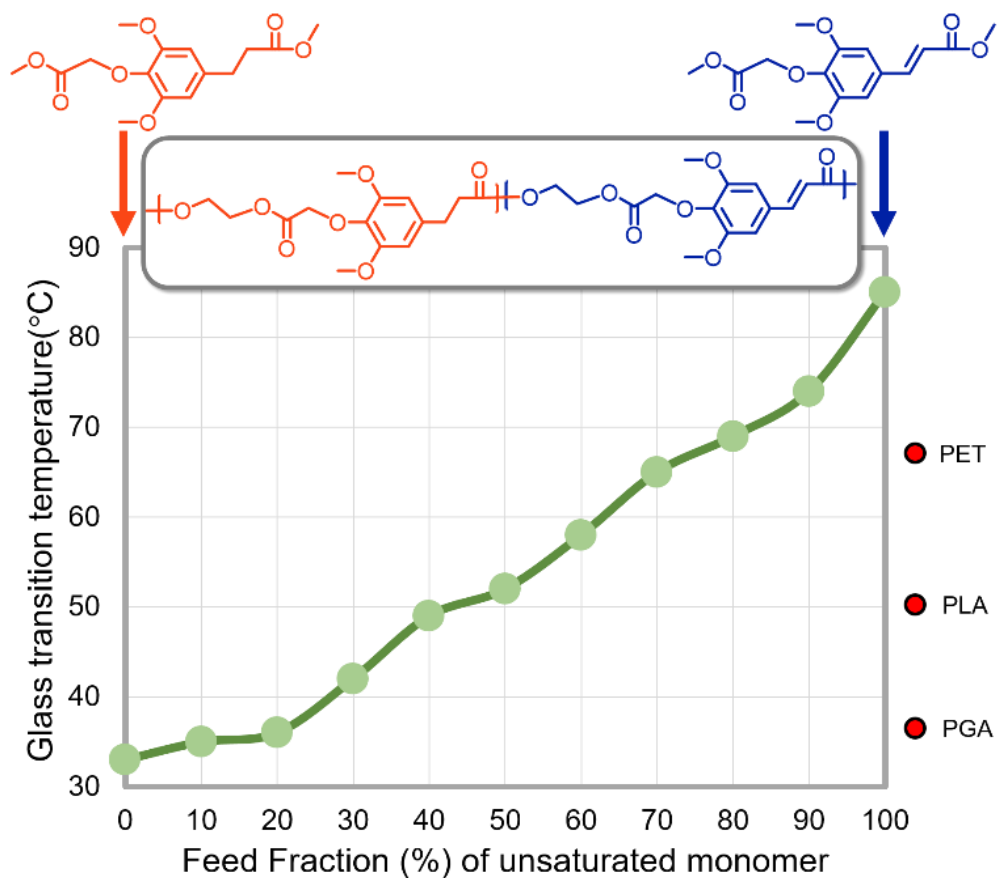


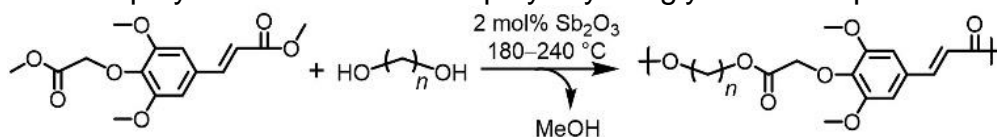
Figure 2-4. Glass transition temperatures observed and plotted for copoly(ethyleneglycolate dihydrosinapate/ethyleneglycolate sinapate).

Homopolymerization of PEGHS (Table 2-2, entry 1) resulting polymer with high M_n of 16,600 g/mol and \bar{D} (dispersity index) of 2.6. Comparatively, copolymers with the MGS:MGHS feed ratio of 90:10 and 80:20 resulted in polymers with M_n of 13,600 g/mol and 9,600 g/mol, respectively. The trend suggested that a higher percentage of unsaturated monomer yielded a higher molecular weight. One important point to remember is that this was only possible due to the lower viscosity and more homogeneous mixtures during polymerization, thus yielding a higher molecular weight polymers. Consequently, the temperature of the copolymerization needed to be adjusted according to the monomer feed ratio. In other words, copolymerization with a

higher percentage of unsaturated monomer (MGS) used a higher temperature to lower the viscosity during polymerization. The insolubility of the copolymers with MGS:MGHS feed ratio above 80:20 in HFIP prevented GPC analysis.

The synthesized PEGS-PEGHS copolymers exhibited excellent thermal degradation temperatures. In particular, the highest temperature of 5% mass loss ($T_{5\%}$) was up to 292 °C and the highest temperature of 50% mass loss ($T_{50\%}$) was up to 424 °C. PEGS and PEGHS have T_g values of 85 °C and 33 °C, respectively. Furthermore, a series of copolymers with T_g ranging from 33 °C to 85 °C was synthesized by employing different monomeric MGS:MGHS ratios. For the synthesized copolymers, as the MGS feed fraction increases from 0% to 100% with 10% increments, there was an observed positive linearity of T_g versus the increased MGS (unsaturated comonomer) contents in the copolymer. The plot confirmed this structure-property relationship; the saturated portion of copolymers in Figure 2-4 allowed this facile movement for long-range segmental motions of the polymer chains. Likewise, the unsaturated portion of copolymers limited the conformational mobility by increasing the conformational barriers

Table 2-3. Homopolymerization results of polyalkyleneglycolate sinapates. ^a



| Entry | Length of diol (n) | Yield (%) | T_g ^d (°C) | $T_{5\%}$ ^e (°C) | $T_{50\%}$ ^f (°C) |
|-------|--------------------|-----------|-------------------------|-----------------------------|------------------------------|
| 1 | 2 | 87.5 | 85 | 291 | 424 |
| 2 | 3 | 92.7 | 72 | 298 | 413 |
| 3 | 4 | 99.0 | 61 | 298 | 391 |
| 4 | 5 | 90.0 | 54 | 301 | 378 |
| 5 | 6 | 96.7 | 49 | 301 | 378 |
| 6 | 8 | 95.6 | 38 | 303 | 377 |
| 7 | 9 | 91.5 | 31 | 302 | 374 |
| 8 | 10 | 95.5 | 25 | 306 | 380 |

^aReaction conducted without solvent using 2 mol% Sb_2O_3 ; see the experimental method for exact temperature profile. ^bDetermined by DSC. ^cTemperature reported upon 5% mass loss. ^dTemperature reported upon 50% mass loss.

For another approach, MGS monomer was reacted with different length diols ranging from $n = 2$ to $n = 10$ (with the exception of $n = 7$), generating a series of polyalkyleneglycolate sinapate (PAGS). As shown in Table 3-3, the polymerization yields ranged from 88% to 99%; however there was no molecular weight data on this series due to the insolubility of the polymers in HFIP. The degradation temperatures $T_{5\%}$ were as high as 306 °C and $T_{50\%}$ was as high as 424 °C. The synthesized PAGS exhibited T_g values ranging from 25 °C ($n = 10$) to 85 °C ($n = 2$). Indeed, the length of methylene spacers affected the T_g of the polymers; PAGS with longer carbon chains exhibited lower T_g values as illustrated by Figure 2-5. The less polar PAGS created more spatial arrangements and lower aromatic content in the main chain, thus the macromolecular chain found it easier to fold and flow, lowering the T_g values for any additional methylene spacers. There were no observed melting temperatures (T_m) from the Differential Scanning Calorimetry (DSC), perhaps due to random copolymerization that occurred between head and tail of the monomer, decreasing the crystallinity of the polymers. There might be a possibility to increase the crystallinity by an annealing process for the long chain diol polymers to exhibit melting points, or by incorporating longer diols into the main chain of the polymer.

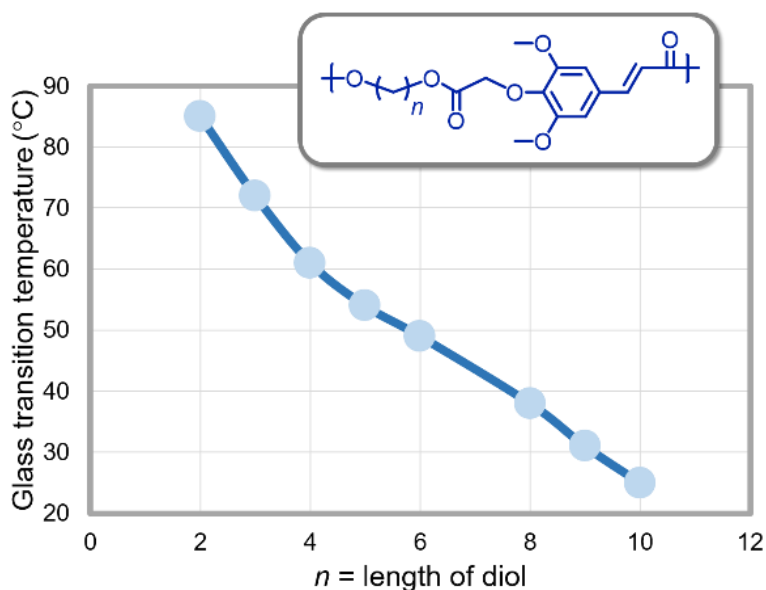
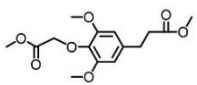
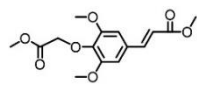


Figure 2-5. Glass transition temperatures observed and plotted for polyalkyleneglycolate sinapates.

Table 2-4. Copolymerization results of the copoly(ethylenelactate dihydrosinapate/ethylenelactate sinapate) series. ^a

| Entry | Monomer feed % | | MLS ^b (mol %) | Yield (%) | M_n ^c (Da) | \bar{D} ^c | T_g ^d (°C) | $T_{5\%}$ ^e (°C) | $T_{50\%}$ ^f (°C) |
|-------|---|---|--------------------------------|-----------|----------------------------|------------------------|----------------------------|--------------------------------|---------------------------------|
| |  |  | | | | | | | |
| 1 | 100 | 0 | 0 | 72.5 | 9,200 | 3.2 | 23 | 271 | 340 |
| 2 | 70 | 30 | 32 | 77.4 | <i>g</i> | <i>g</i> | 37 | 275 | 344 |
| 3 | 50 | 50 | 48 | 83.1 | <i>g</i> | <i>g</i> | 49 | 276 | 357 |
| 4 | 30 | 70 | 65 | 80.8 | <i>g</i> | <i>g</i> | 68 | 280 | 356 |
| 5 | 0 | 100 | 100 | 78.4 | <i>g</i> | <i>g</i> | 87 | 292 | 371 |

^aReaction conducted neat using 2 mol% Sb_2O_3 ; mixtures of dimethyl lactate sinapate or dimethyl lactate dihydrosinapate and ethylene glycol were melted with a temperature ramp under nitrogen, then switch to a dynamic vacuum. See the experimental method for exact temperature profile. ^bIncorporation of dimethyl lactate sinapate in the copolymers were determined by 1H NMR. ^cObtained by GPC in HFIP at 40 °C versus PMMA standards. ^dDetermined by DSC. ^eTemperature reported upon 5% mass loss. ^fTemperature reported upon 50% mass loss. ^gPolymers were insoluble in GPC solvents.

HFIP. The copolymer series exhibited degradation temperature $T_{5\%}$ up to 292 °C and $T_{50\%}$ up to 371 °C. In addition, the T_g values of the copolymers naturally were increased following the increased percentage of unsaturated monomer (MLS), ranging from 23 °C to 87 °C. Interestingly, comparing to the PEGS/PEGHS copolymers series on a low percentage of unsaturated monomer, PELS/PELHS copolymers exhibited lower T_g . Meanwhile, the T_g of both copolymers series on high percentage of unsaturated monomer were relatively the same as shown by Figure 2-6. Based on PLA ($T_g = 50$ °C)¹⁷ and PGA ($T_g = 35$ °C),^{100,107} our initial expectation was PELHS ($T_g = 23$ °C) would have a higher T_g than PEGHS ($T_g = 33$ °C), due to the additional methyl group that normally raised the conformational energy barriers. However, the additional methyl group on PELHS actually seemed to cause a lower than expected T_g of PELHS, possibly by contributing to the free volume effect on the flexible polymer (PELHS) from saturated monomer (MLHS). One example was from the work of Heise *et al.* on the preparation of poly(4-methylcaprolactone) with a T_g of -68 °C; meanwhile, the synthesized polycaprolactone exhibited T_g of -57 °C.¹³¹ Interestingly, with an increased of unsaturated portion (MLS), the free volume effect from this additional methyl group of MLHS seemed to diminish, in addition to the negligible contribution raising its conformational energy.

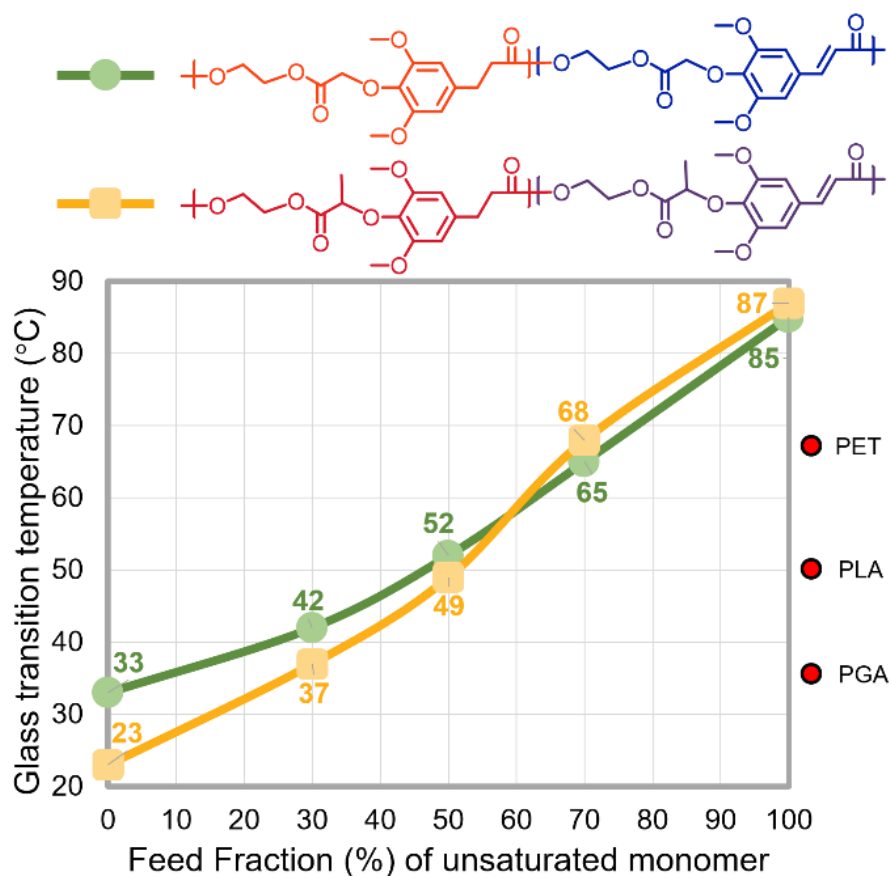


Figure 2-6. Comparison of glass transition temperatures between copoly(ethyleneglycolate dihydro-sinapate/ethylene glycolate sinapate) (light green circles) and copoly(ethylenelactate dihydro-sinapate/ethylenelactate sinapate) (light orange squares).

The effects of methoxy groups on the main chain can be investigated by comparing ferulic acid and *p*-coumaric acid. Ferulic acid and *p*-coumaric acid are hydroxycinnamic acids derived from lignocellulosic biomass; these have been extensively used in our group to synthesize bioplastics.^{84,119,127–130} As tabulated in Table 2-5, polyethyleneglycolate ferulate (PEGF), polyethyleneglycolate coumarate (PEGC), polyethylenelactate ferulate (PELF), and polyethylenelactate coumarate (PELC) were synthesized with yields of 67%, 80%, 74%, and 74%, respectively. These polymers showed $T_{5\%}$ up to 327 °C, and $T_{50\%}$ up to 420 °C. The obtained T_g of these polymers

confirmed the structure-property relationship. The methoxy group played a vital role in increasing the glass transition temperature of polymers, as can be seen from PEGS, PEGF, and PEGC that exhibited T_g values of 85 °C, 75 °C, and 58 °C, respectively, and also from PELS, PELF, PELC that exhibited T_g values of 87 °C, 72 °C, and 67 °C, respectively. Each additional methoxy group seems to raise conformational barriers and have a smaller effect on the free volume of the polymers. It is noteworthy to point out that the effect of the methyl group from the lactate moiety in unsaturated homopolymers was significant when there was no methoxy group. This was confirmed by the difference of T_g between PELC (67 °C) and PEGC (58 °C), which was 9 °C. On the other hand, the existence of methoxy group in the main chain seemed to contribute more and overshadowed the effect of the methyl group from the lactate moiety.

As can be seen, the prepared monomers from this work were an AA type monomer. A series of polyesters had been made by reacting with diols. Furthermore, by reacting with a diamine or an alcoholamine, we extended the polymers' scope into polyamide and polyesteramide, respectively. Dimethylglycolate dihydrosinapate was selected as the monomer and reacted with ethylenediamine and ethanolamine to yield polyethyleneglycolamide dihydrosinapamide (PEGAHSA) and polyethyleneglycolate dihydrosinapamide (PEGEHSA). Of course, the polyesteramide could be a mixture of polyethyleneglycolamide dihydrosinapate and PEGEHSA since the polymerization was a random polycondensation; PEGEHSA was used as a representative for both existing polyesteramides forms, for the sake of simplicity. Both synthesized polyamide and polyesteramide had a medium recovered yield 61% and 68% and a low M_n of 2,500 g/mol and 5,800 g/mol, respectively. This was likely due to the extraordinarily high melt

viscosity during polymerization, thus impeding the polymer chains to grow further. Nevertheless, there was a significant increase of T_g for both polymers versus their polyester (PEGHS) counterparts. PEGAHS and PEGEHS exhibited T_g values of 108 °C and 56 °C, respectively. Obviously, the presence of chain-chain interactions increased conformational barriers and also increased the rigidity of the polymers.

Accelerated degradation studies

Preliminary degradation studies were conducted on polyethyleneglycolate dihydrosinapate (PEGHS), polyethylenelactate dihydrosinapate (PELHS), and polylactic acid (PLA). These polymers were suspended into 1 M NaOH(aq), 1 M HCl (aq), deionized water (DIW), and seawater at 80 °C. Heterogeneous degradation studies as a direct comparison between the two end spectra of pH used 1 M NaOH(aq) and 1 M HCl(aq). According to our visual observation in hot 1 M NaOH(aq) solution, PELHS degraded completely within 2 hours, then followed by PLA in 5 hours, and finally PEGHS degraded in 12 hours. Meanwhile, all of the samples in HCl solution did not fully degrade after 12 hours; PLA seemed to maintain its initial shape while PEGHS and PELHS became gel-like substances. Both basic and acidic media degraded the polymers which confirmed by GPC analysis. However, these polymers were degraded much faster in aqueous base due to the presence of hydroxy (OH^-) species saponifying the ester linkages. Furthermore, diacid monomers versions of dimethylglycolate dihydrosinapate (MGHS) and dimethylactate dihydrosinapate (MLHS) were recovered from the degradation study in NaOH solution, as observed by ^1H NMR analysis (Figure 2-7). Interestingly, PLA was degraded significantly slower in hot acidic media than the synthesized PEGHS and PELHS.

Table 2-6. Degradation studies of polyethyleneglycolate dihydrosinapate (PEGHS), polyethylenelactate dihydrosinapate (PELHS), and polylactic acid (PLA).

| Entry | Polymer | M_n I ^a (Da) | % M_n NaOH ^b (%) | % M_n HCl ^c (%) | % M_n DIW ^d (%) | % M_n Sea ^e (%) |
|-------|---------|------------------------------|----------------------------------|---------------------------------|---------------------------------|---------------------------------|
| 1 | PEGHS | 16,600 | 0 | 0.5 | 16.9 | 5.4 |
| 2 | PELHS | 9,200 | 0 | 1.0 | 9.8 | 5.4 |
| 3 | PLA | 12,000 | 0 | 77.5 | 37.5 | 43.3 |

^aInitial number average molecular weight. ^bPercentage of maintained M_n after hydrolysis in 80 °C 1 M NaOH(aq) for 12 hours. ^cPercentage of maintained M_n after hydrolysis in 80 °C 1 M HCl(aq) for 12 hours. ^dPercentage of maintained M_n after hydrolysis in 80 °C deionized water for 72 hours. ^ePercentage of maintained M_n after hydrolysis in 80 °C seawater for 72 hours.

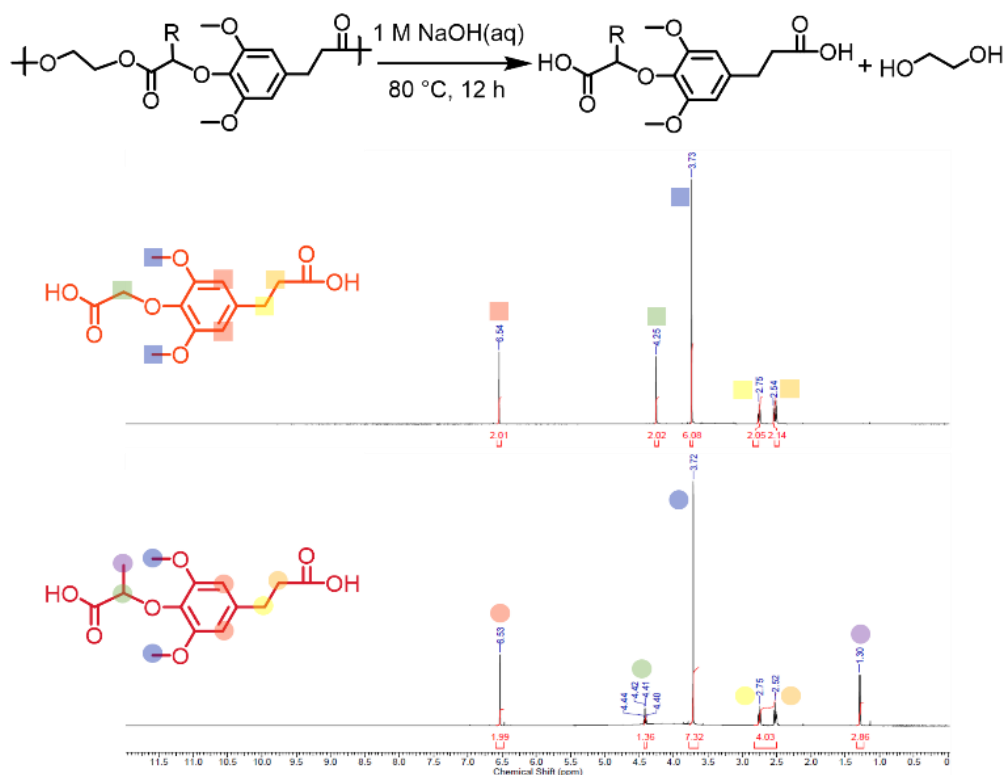


Figure 2-7. Hydrolysis of polyethyleneglycolate dihydrosinapate and polyethylenelactate dihydrosinapate generated glycolic sinapic diacid and lactic sinapic diacid as shown by ¹H NMR

Based on HFIP GPC analysis, after 12 hours PLA maintained 77.5% of its M_n , on the other hand PEGHS and PELHS had 99.5% and 99.0% of their M_n degraded, respectively. The degradation studies in hot DIW and hot seawater media were conducted for 72 hours. Again, PEGHS and PELHS were more extensively hydrolysed

than PLA under both conditions. PLA maintained 37.5% and 43.3% of its M_n in hot DIW and seawater, respectively. PEGHS and PELHS showed a slightly better degradation in hot seawater than hot DIW. One possible explanation was the pH of seawater is slightly basic (pH = 8) versus DIW (pH = 6), thus providing more hydroxy species as hydrolytic agents. Additionally, PELHS showed the best degradation rate in all media; it seemed to be the free volume effect on methyl group played a vital role in providing spaces for all aqueous media to penetrate and hydrolyse the bulk polymer.

Conclusions

Polyethyleneglycolate sinapate and analogues were prepared from sinapic acid, a hydroxycinnamic acid that exists in the *Brassicaceae* plant family. The versatility of sinapic acid made it possible to create a series of diester monomers that readily reacts with diols via transesterification, yielding sinapic acid-based polymers with fine control of glass transition temperatures. There were several approaches in tuning glass transition temperatures, including: (1) copolymerization of saturated and unsaturated monomers, (2) addition of a methyl group in the monomer, (3) extension of methylene spacers by employing diols of varying length, (4) substitution of sinapic acid monomers with other hydroxycinnamic acid-based monomers, and (5) utilization of ethylenediamine or ethanolamine creating a polyamide or polyesteramide. The copoly(ethyleneglycolate dihydrosinapate/ethyleneglycolate sinapate) and copoly(ethylenelactate dihydrosinapate/ethylenelactate sinapate) series exhibited T_g values ranging from 33 °C to 85 °C and from 23 °C to 87 °C, respectively. Furthermore, dimethylglycolate sinapate was polymerized with linear diols of various length ($n = 2-10$) created a polyalkyleneglycolate sinapate series with T_g ranging from 25 °C ($n = 10$) to 85 °C ($n =$

2). The effect of a methoxy group on the glass transition temperature was also investigated using ferulic acid and p-coumaric acid-based monomers; the presence of a methoxy group on the aromatic substituent apparently increased the T_g of the polymers. In addition, sinapic acid-based polyamide exhibited a high T_g value of 108 °C which surpasses the T_g of polystyrene (95 °C).

The targeted polymers degraded more readily versus PLA. In particular, both polyethyleneglycolate dihydrosinapate and polyethylenelactate dihydrosinapate maintained only 5.4% of their initial M_n ; meanwhile, PLA maintained 43.3% of its M_n after heterogeneous hydrolysis in 80 °C seawater after 72 hours. Although these temperatures would not naturally exist in an ocean surface environment, these preliminary accelerated degradation studies indicated a potential degradation in a sea environment. Moreover, the synthesized polymers were readily hydrolysed in 1 M NaOH aqueous medium into diacid monomers. This provides an opportunity for upcycling the degraded polymer under benign conditions, back to monomers which can be repurposed for repolymerization.

CHAPTER 3 EXTRACTION OF HYDROXYCINNAMIC ACIDS FROM SUGARCANE AND CORN‡

Background

Biomass feedstock-based fuels have gained interest over the years as a prospective alternative energy to replace petroleum-based fuel.⁸ Sugarcane and corn crops are currently the major biomass feedstocks for bioethanol, an alcohol-based biofuel, production. Currently, the United States (corn) and Brazil (sugarcane) are the two world's largest bioethanol producers, representing 90% of global bioethanol production.^{132,133} Worldwide, sugarcane covers 65 million acres of land which Brazil accounts for 41% of its total.¹³⁴ Besides bioethanol production, sugarcane contributes over 75% of global sugar production.¹³⁵ After the extraction of sugar juice, the crop will generate a dry matter which is called as bagasse. This bagasse is mostly burned onsite as for energy production, but the pulp is actually useful for paper production.¹³⁶ It is noteworthy to mention that sugarcane is also the highest yielding amongst other crops.¹³⁷ On the other hand, corn (or maize according to the agricultural term) is the second most planted crop after wheat covering over 400 million acres of land. The largest corn plantation can be found in United States with over 90 million acres of corn crop area are planted annually.¹³⁸ Although the ethanol production capacity of corn is lower than that of sugarcane (495 gal/acre vs 2105 gal/acre),¹³³ corn crop has a more diversified portfolio than that of sugarcane owing to the presence of protein in corn that can meet demands for corn-based animal feed.¹³⁹

‡ This portion of work was submitted as a US Patent Application, Serial No. 16/374,262; filed April 3, 2019.

As lignocellulose biomass, sugarcane and corn bioethanol processes generate lignin-rich waste. This lignin material contains hydroxycinnamic acids, ferulic acid (FA) and *p*-coumaric acid (pCA), which can be harvested via a simple hydrolysis step. They occur in cell walls as the “glue-like” substances binding cell wall polymers through carboxylic and phenolic sites.¹⁴⁰ The presence of these hydroxycinnamic acids in cell wall polymers affect the hardness of a plant, while at the same time provide growth to the living plants and give the biodegradability property to the dead plants.^{141,142} Both ferulic acid and *p*-coumaric acid display antioxidant, antimicrobial, anti-inflammatory and anti-cancer properties.^{143,144,145,146,147} As a matter of fact, some of the traditional herbal remedies to treat various diseases contain ferulic acid or *p*-coumaric acid, such as corn silk, dune wormwood, and *Xanthium* species.^{148,149,150} Ferulic acid, extracted from rice bran, has found its market in the dietary supplement industry.¹⁵¹ Moreover, due to its biocompatibility to the human body, ferulic acid has also secured some market shares in the pharmaceutical and cosmetic industries. Ferulic acid penetrates well into the skin and it facilitates the photostage inhibition, reducing wrinkles and discoloration of the skin.¹⁵² For these reasons, both ferulic acid and *p*-coumaric acid are definitely high value added co-products on biorefinery processes.

Extraction of ferulic acid or *p*-coumaric acid have been extensively studied. Conventional extraction includes enzymatic,¹⁵³ acidic,¹⁵⁴ and alkaline extraction.^{155,156,157} Furthermore, several extraction methods have been developed to accelerate the extraction time, including pulsed-electric field,¹⁵⁸ supercritical fluid,¹⁵⁹ sonication,¹⁶⁰ and microwave-assisted extraction.¹⁶¹ Herein, we performed extraction of ferulic acid and *p*-coumaric acid on sugarcane bagasse, lignin paste, corn cob, corn

tassel, corn bran, and corn silk, adapting various existing methods. Our goals were obtaining the highest yield and finding the greatest time efficiency using the one parameter at a time strategy. This study also complements the ferulic acid and *p*-coumaric acid-based polymer series that have been reported in our group.^{159–161}

Experimental

Materials

Sugarcane bagasse and its dried lignin paste were donated from a local cellulosic bioethanol facility in Brazil. Corn tassel was obtained from a local farm in Indiana, US. Corn cob “Branch Gourmet” was purchased from a Publix store. Corn silk “Frontier co-op” was purchased from Amazon.com. Corn Bran was purchased from Honeyville. All samples were grounded into fine powders before use. Ethyl acetate, sodium hydroxide, sodium iodide, sodium bisulfite, charcoal® Norit SA3, and sodium chloride were purchased from Fisher Chemical. NMR solvents including deuterated chloroform (CDCl₃) and deuterated dimethyl sulfoxide (DMSO-*d*₆) were purchased from Cambridge Isotope Laboratories. All chemicals, unless expressly mentioned, were utilized without further purification.

Characterization

Proton nuclear magnetic resonance (¹H NMR) and carbon nuclear magnetic resonance (¹³C NMR) were recorded using an Inova 500 MHz spectrometer. Chemical shifts are reported in parts per million (ppm) downfield relative to tetramethylsilane (TMS, 0.0 ppm). Coupling constants (*J*) are reported in Hertz (Hz). Multiplicities are reported using the following abbreviations: s, singlet; d, doublet; t, triplet; q, quartet; m, multiplet; br, broad.

Extraction procedure

Ferulic acid and *p*-coumaric acid were extracted via alkaline hydrolysis, such as using pressure, ultrasound, microwaves, and normal heat aqueous reflux at 100 °C. The extraction of lignin paste follow below, and all other materials; sugarcane bagasse, corn cob, corn tassel, corn bran, and corn silk, are provided in Chapter 6.

Reflux extraction

2.00 g of dried lignin powder, and 50 mL of NaOH 0.5 M (aq) were loaded in a closed 100 mL round bottom flask. The reaction was conducted for 2 hours at 100 °C. Upon completion, the solution was acidified to pH = 1 with 50 mL HCl 1 M (aq). The solids were filtered out and washed with DIW; then the remaining solution was extracted with 3 x 100 mL portions of ethyl acetate. The organic (ethyl acetate) portion was washed with copious amounts of water, followed by brine (saturated NaCl solution), and then dried over anhydrous MgSO₄. The ethyl acetate was then removed by rotary evaporation leaving behind crude para-coumaric acid (pCA) and ferulic acid (FA). The identity and the purity of the product were confirmed by ¹H NMR analysis. The extraction procedure, as given above, was repeated twice using the lignin solids from the previous extraction and two additional extractions were performed on lignin solids with heating for 20 hours and 24 hours.

Pressurized extraction

2.00 g of dried lignin powder, and 50 mL of NaOH 0.5 M (aq) were loaded in a closed 100 mL glass reactor vessel. The reaction was conducted for 2 hours at 150 °C, resulting in an extra 20 psi from steam pressure. Upon completion, the solution was acidified to pH = 1 with 50 mL HCl 1 M (aq). The solids were filtered out and washed

with DIW; then the remaining solution was extracted with 3 x 100 mL portions of ethyl acetate. The organic (ethyl acetate) portion was washed with copious amounts of water, followed by brine (saturated NaCl solution), and then dried over anhydrous MgSO₄. The ethyl acetate was then removed by rotary evaporation leaving behind crude para-coumaric acid (pCA) and ferulic acid (FA). The identity and the purity of the product were confirmed by ¹H NMR analysis. The extraction procedure, as given above, was repeated twice using the lignin solids from the previous extraction and two additional extractions were performed on lignin solids with heating for 16 hours and 18 hours.

Ultrasound-assisted extraction

2.00 g of dried lignin powder, and 50 mL of NaOH 0.5 M (aq) were sonicated in a 100 mL round-bottom flask for 2 hours at room temperature. Upon completion, the solution was acidified to pH = 1 with 50 mL HCl 1 M (aq). The solids were filtered out and washed with DIW; then they were loaded in a 100 mL round-bottom flask for the next cycle of sonication. Meanwhile, the remaining solution was extracted with 3 x 100 mL portions of ethyl acetate. The organic (ethyl acetate) portion was washed with copious amounts of water, followed by brine (saturated NaCl solution), and then dried over anhydrous MgSO₄. The ethyl acetate was then removed by rotary evaporation leaving behind crude para-coumaric acid (pCA) and ferulic acid (FA). The identity and the purity of the product were confirmed by ¹H NMR analysis. Then, the leftover lignin, and 50 mL of NaOH 0.5 M (aq) were sonicated in a 100 mL round-bottom flask for 5 hours. The mixture was treated following the same procedure as mentioned above. The hydrolysis was repeated until there was no longer pCA and FA peaks in the ¹H NMR analysis.

Microwave-assisted extraction

2.00 g of dried lignin powder, and 50 mL of NaOH 0.5 M (aq) were loaded in a 100 mL round bottom flask. The reaction was set on dynamic procedure with a power of 50 Watts, maximum temperature of 90 °C, and the total time was 15 mins. Upon completion, the solution was acidified to pH = 1 with 50 mL HCl 1 M (aq). The solids were filtered out and washed with DIW; then the remaining solution was extracted with 3 x 100 mL portions of ethyl acetate. The organic (ethyl acetate) portion was washed with copious amounts of water, followed by brine (saturated NaCl solution), and then dried over anhydrous MgSO₄. The ethyl acetate was then removed by rotary evaporation leaving behind crude para-coumaric acid (pCA) and ferulic acid (FA). The hydrolysis of leftover lignin solids was repeated for four more times using the same procedure as mentioned above.

Results and discussion

Sugarcane bagasse and lignin paste

Sugarcane bagasse was harvested from post-extraction of sugar juice on sugarcane and fermentation to bioethanol in a biorefinery in Brazil. This bagasse usually ended up in a burner to generate power for a plant; however the production of bagasse outweigh electricity needed for a plant which made accumulated bagasse an upstream waste. Similarly, lignin paste was obtained by removing cellulose and hemicellulose from the bagasse (lignocellulose material). This lignin paste was dried and formed into blocks. Therefore, the extraction of *p*-coumaric acid and ferulic acid that were trapped in the bagasse will potentially add some revenue to the bioethanol facility.

Prior to the extraction, bagasse and lignin were grounded into fine powders in order to increase the surface area allowing solvent to penetrate into the material. The

hydrolysis step was performed in alkaline solution cutting and saponifying the network of phenolic ester crosslinks by hydroxy species. Upon addition of alkaline solution, the lignin paste became homogeneous, suggesting the deprotonation of lignin took place and made it soluble in water. Moreover, in order to find the optimized method for lignin depolymerization, various form of energy were investigated, including normal reflux at 100 °C, pressure in a glass reactor vessel, sonication, and microwaves, as can be seen from Figure 3-1.

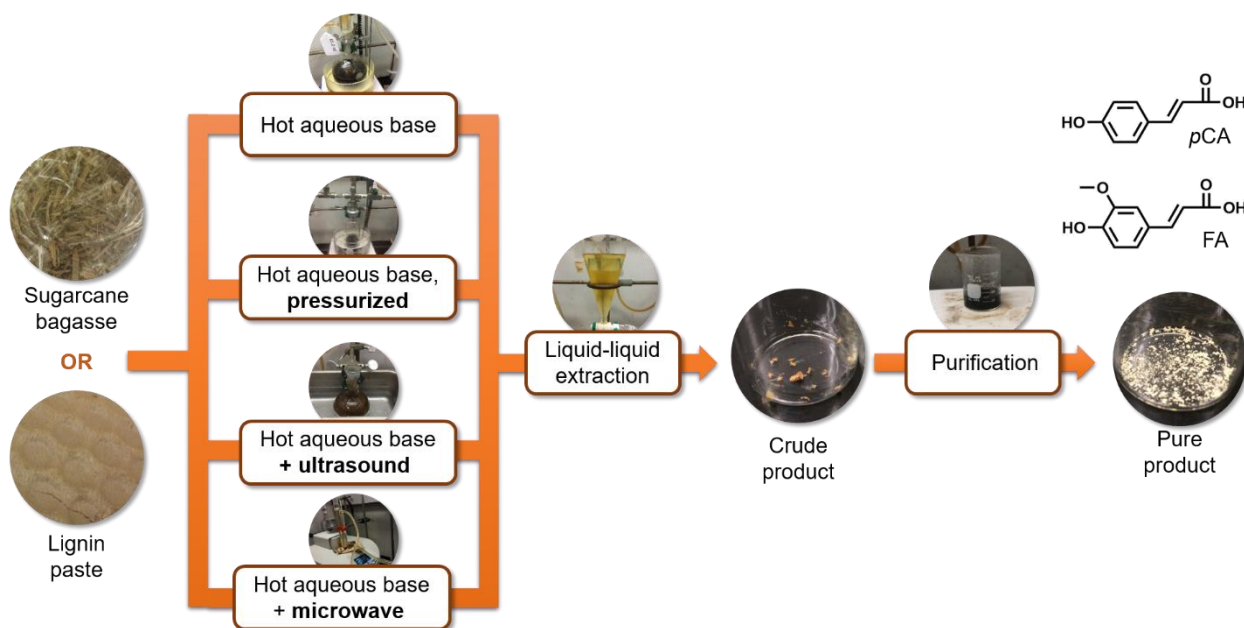


Figure 3-1. Simplified extraction flowchart for sugarcane bagasse and lignin paste resulting in *p*-coumaric acid and ferulic acid.

After the hydrolysis step, acid solution was added into the mixture to protonate the hydrolysed *p*-coumaric acid and ferulic acid so that those hydroxycinnamic acids were able to move into the organic layer during the extraction step. Furthermore, the acidification step also facilitated the precipitation of leftover lignin which then was removed by filtration. The filtration process could be accelerated by using centrifugation at 3500 rpm for 10 minutes. Centrifugation was especially useful for a large scale

extraction. On a large scale reaction, concentrated H₃PO₄ was used instead of 1 M HCl for the acidification process to minimize the volume of the aqueous portion.

Additionally, concentrated H₃PO₄ gave the best yield compared to any other concentrated acids tested. One possible reason was other concentrated acids, upon addition, burned the materials in solution thus lowered the yield of recovered products (see Chapter 6 for more information on the large scale extraction). Some chemical shift peaks in the ¹H-NMR analysis that we regarded as the most important were 6.28 ppm (doublet) and 6.35 ppm (doublet) from vinylic of *p*-coumaric acid and ferulic acid, respectively.

Table 3-1. Iterative extraction results on dried lignin paste and sugarcane bagasse ^a

| Lignin paste ^b | | | | | | | | |
|---------------------------|-----------------------|----------------------|--------------------------|----------------------|-------------------------|----------------------|------------------------|----------------------|
| Entry | Reflux ^c | | Pressurized ^d | | Ultrasound ^e | | Microwave ^f | |
| | Yield <i>g</i> (%) | pCA : FA <i>h</i> | Yield <i>g</i> (%) | pCA : FA <i>h</i> | Yield <i>g</i> (%) | pCA : FA <i>h</i> | Yield <i>g</i> (%) | pCA : FA <i>h</i> |
| 1 | 2.95 | 88 : 12 | 5.85 | 83 : 17 | 5.20 | 80 : 20 | 3.95 | 86 : 14 |
| 2 | 3.90 | 84 : 16 | 2.50 | 74 : 26 | 4.70 | 86 : 14 | 3.50 | 84 : 16 |
| 3 | 2.10 | 70 : 30 | 1.00 | 56 : 44 | 3.30 | 88 : 12 | 3.20 | 84 : 16 |
| 4 | <i>i</i> | <i>i</i> | 1.40 | 37 : 63 | 1.95 | 83 : 17 | 3.15 | 76 : 24 |
| 5 | <i>i</i> | <i>i</i> | 2.40 | 37 : 63 | <i>i</i> | <i>i</i> | <i>i</i> | <i>i</i> |
| Total | 8.95 | 82 : 18 | 13.15 | 66 : 34 | 15.15 | 84 : 16 | 13.80 | 83 : 17 |

| Sugarcane bagasse ^j | | | | | | | | |
|--------------------------------|-----------------------|----------------------|--------------------------|----------------------|-------------------------|----------------------|------------------------|----------------------|
| Entry | Reflux ^c | | Pressurized ^d | | Ultrasound ^e | | Microwave ^f | |
| | Yield <i>g</i> (%) | pCA : FA <i>k</i> | Yield <i>g</i> (%) | pCA : FA <i>h</i> | Yield <i>g</i> (%) | pCA : FA <i>h</i> | Yield <i>g</i> (%) | pCA : FA <i>h</i> |
| 6 | 4.55 | <i>k</i> | 7.80 | 76 : 24 | 4.00 | 67 : 33 | 2.70 | 74 : 26 |
| 7 | 0.98 | <i>k</i> | 5.20 | 67 : 33 | 3.90 | 74 : 26 | 3.80 | 72 : 28 |
| 8 | 2.95 | <i>k</i> | <i>i</i> | <i>i</i> | 3.20 | 100 : 0 | 2.75 | 66 : 34 |
| 9 | 0.06 | <i>k</i> | <i>i</i> | <i>i</i> | <i>i</i> | <i>i</i> | <i>i</i> | <i>i</i> |
| 10 | <i>i</i> | <i>i</i> | <i>i</i> | <i>i</i> | <i>i</i> | <i>i</i> | <i>i</i> | <i>i</i> |
| Total | 8.54 | 73 : 27 | 13.00 | 72 : 28 | 11.10 | 79 : 21 | 9.25 | 71 : 29 |

^aIterative extraction was performed until there were no longer observed pCA and FA in ¹H-NMR spectrum. All extraction entries were only performed once. ^bLignin paste was dried and ground before use. ^cHeated at 100 °C. ^dHydrolysis step in a glass reactor vessel. ^eUltrasound was from L&R sonicator water bath at 23 kHz. ^fMicrowave reactor: CEM Discover S class, with attached reflux condenser. ^gCrude yield obtained from recovered solids. ^h*p*-coumaric acid (pCA) and ferulic acid (FA) that were observed from ¹H-NMR, the total pCA : FA was calculated from the ratio of each steps. ⁱNo observable pCA or FA. ^jSugarcane bagasse was grounded before use. ^kNMR analysis was skipped in each steps in order to save samples for purification, ratio pCA : FA was calculated from the ratio of purified samples.

As tabulated in Table 3-1, the extraction on lignin and bagasse resulted in crude percent yield ranging from 8.95 to 15.15% and from 8.54 to 13%, respectively. As can be seen, lignin paste yielded more than its bagasse counterparts; perhaps this was due to the existence of hemicellulose and cellulose which decreased the density of lignin in bagasse, thus lowering the yield of extraction, overall. Interestingly, lignin paste seemed to have a higher content of *p*-coumaric acid than sugarcane bagasse. Out of all methods, pressurized method gave the highest yield on the first extraction cycle. The general trend on the iterative extraction was the increase of ferulic acid composition for each extraction cycle. One highlighted method was the pressurized extraction on lignin paste.

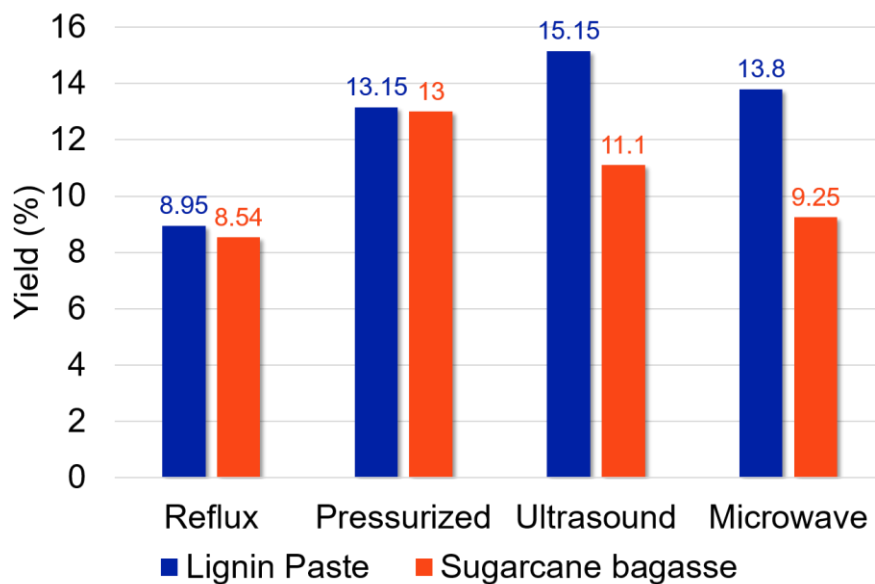


Figure 3-2. Yield comparison on reflux, pressurized, ultrasound-assisted, microwave-assisted extraction of lignin paste (blue) and sugarcane bagasse (orange).

The bar chart on Figure 3-2 suggests that the highest yield on lignin extraction was obtained from the ultrasound method; meanwhile the highest yield on bagasse

extraction was obtained from pressurized method. On the other hand, a normal reflux (100 °C) method gave the lowest yield for both lignin and bagasse extraction. Although microwave-assisted extraction was the fastest (15 minutes per extraction) out of all methods, it did not give the lowest yield.

Corn bran, cob, silk, and tassel

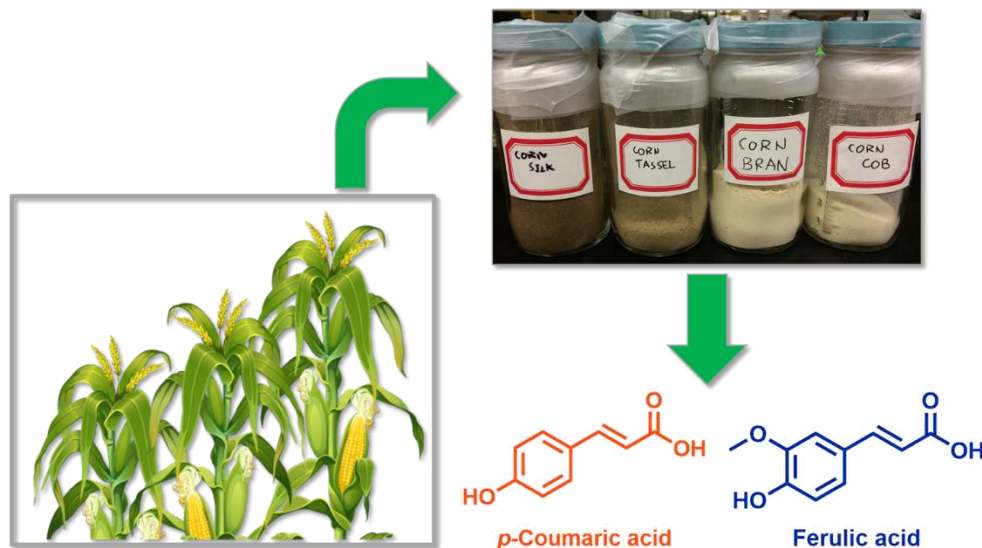


Figure 3-3. Extraction of *p*-coumaric acid and ferulic acid from corn components (silk, tassel, bran, cob).

Each component of corn was investigated for its ferulic acid and *p*-coumaric acid components as depicted by the simplified flowchart on Figure 3-3. The extraction procedure was adapted from the previous extraction on sugarcane materials where the mixtures were agitated in alkaline solution to hydrolyze the ester linkages on the lignocellulose, thus releasing hydroxycinnamic acids. In this case, ultrasound was selected as the extraction method, due to the less complicated set up for the hydrolysis step, in addition to the higher purity versus other methods based on ¹H-NMR analysis.

According to the results of the extractions, there was a higher percentage of ferulic acid in corn than in sugarcane. Table 3-2 suggested that corn bran gave the

highest yield of 4.3% which consisted of 94.3% ferulic acid and 5.7% *p*-coumaric acid. In corn cob, ferulic acid and *p*-coumaric acid existed together with a similar percentage of 55.4% and 44.6%, respectively. Furthermore, as can be seen from Figure 3-4, the extraction gave a relatively high ¹H NMR purity of *p*-coumaric acid and ferulic acid. Interestingly, corn silk yielded exclusively ferulic acid with a yield of 2.3%. The only part of the corn components that afforded more *p*-coumaric acid than ferulic acid was corn tassel with 33.3% ferulic acid and 66.7% *p*-coumaric acid.

Table 3-2. Extraction results of ferulic acid and *p*-coumaric acid from corn bran, cob, silk and tassel. ^a

| Entry | Corn component | mass initial (g) | mass product (g) | Yield ^b (%) | pCA : FA ^c |
|-------|----------------|------------------|------------------|------------------------|-----------------------|
| 1 | Bran | 2 | 0.085 | 4.30 | 6 : 94 |
| 2 | Cob | 2 | 0.053 | 2.60 | 45 : 55 |
| 3 | Silk | 2 | 0.046 | 2.30 | 0 : 100 |
| 4 | Tassel | 2 | 0.023 | 1.20 | 67 : 33 |

^aExtraction was performed using an L&R sonicator water bath at 23 kHz. ^bCrude yield obtained from recovered solids. ^c*p*-coumaric acid (pCA) and ferulic acid (FA) that were observed by ¹H-NMR.

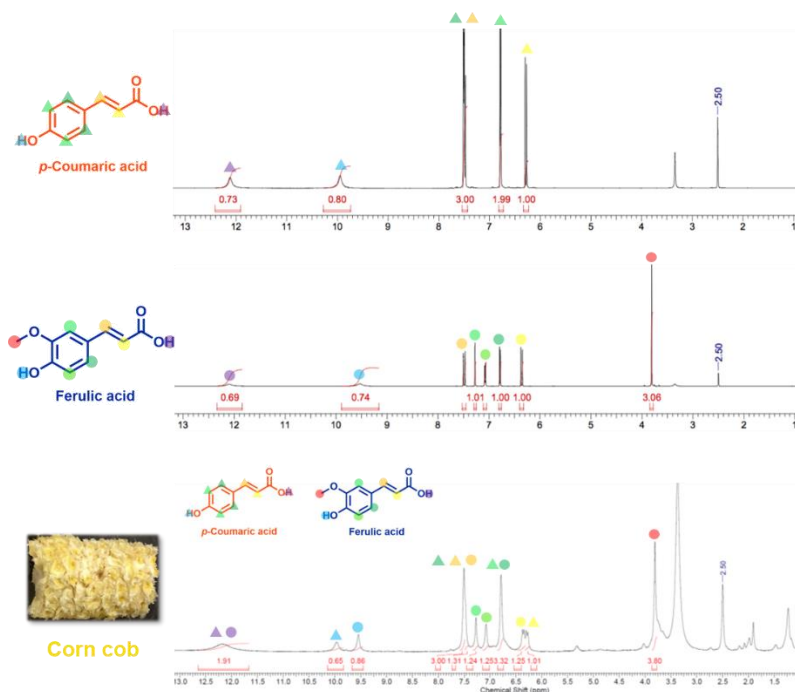


Figure 3-4. ¹H NMR spectrum of commercial *p*-coumaric acid and ferulic acid and extracted *p*-coumaric acid (triangles) and ferulic acid (dots) from corn cob.

Conclusions

Bioethanol is an alternative to petroleum-based fuels due to its low toxicity, acceptable energy density, and relatively lower overall carbon emission. In the present world, sugarcane and corn plantations contribute to the majority of global bioethanol production. As the total area for both plantations is more than 500 million acres, there are several products, mainly for food consumption, that meet the global demand. However, ferulic acid and *p*-coumaric acid have not been among them. Both substances provide proven benefits that potentially have a big market, such as the preservatives or bioplastics market.

Our work investigated ferulic acid and *p*-coumaric acid that were contained in sugarcane and corn components. Lignin paste and sugarcane bagasse yielded up to 15.15% and 13.0% respectively with the majority of them consisting of *p*-coumaric acid. Likewise, corn bran, cob, silk, and tassel afforded yields of 4.3%, 2.6%, 2.3%, and 1.2% with the majority of them consisted of ferulic acid, except for corn tassel that gave more *p*-coumaric acid than ferulic acid. Indeed, some of the brown substances (possibly wax material) were also extracted giving a coloration on the product, however this can be removed by utilizing charcoal, yielding a relatively pure hydroxycinnamic acids.

The motivation of this study was to give an idea of the potential of upstream waste from sugarcane and corn creating co-products, which in the best scenario can increase the revenue of a bioethanol refinery. Of course, there are some potential area of improvements on this study. One example is utilizing a statistical approach as an analytical method for optimization, in particular response surface methodology (RSM). Such a sophisticated optimization model will definitely be beneficial for upscaling the extraction process.

CHAPTER 4 SUSTAINABLE POLYVINYL ACETALS FROM BIOAROMATIC ALDEHYDES[§]

Background

The need for increasing the sustainability of packaging plastics is imminent. While commodity plastic production is ever increasing, recycling efforts are seemingly static.¹⁶² Global plastic production exceeds 300 billion kg per year, averaging more than 40 kg of plastic per person on planet Earth.¹⁶³ Astonishingly, annual plastic production is approaching the mass of 5 billion humans. More alarming is that almost a third of all plastic waste reaches neither recycling facilities nor landfills, finding its final residency in the environment, including the oceans.¹⁶⁴ Current efforts toward truly sustainable plastics must focus on two factors: establishing renewability of the starting materials without a dependence on finite fossil fuels and identifying degradation pathways that operate under various environmental conditions.⁹⁵

Polyvinyl alcohol (PVA) is an interesting commercial polymer with combined production over 1.2 billion kg annually¹⁶⁵ including its derivatives polyvinyl formal and polyvinyl butyral.¹⁶⁶ The highest production water-soluble polymer in the world, PVA is usually manufactured via the polymerization of vinyl acetate in methanol followed by hydrolysis in the presence of sodium hydroxide.¹⁶⁷ Vinyl acetate itself is synthesized by the reaction of acetic acid and ethylene in the presence of oxygen. Both starting materials can be obtained sustainably from bioethanol.¹⁶⁸ Furthermore, a patent is available describing vinyl acetate manufacture from acetic acid exclusively.¹⁶⁹ PVA itself is non-toxic,^{170,171} biodegradable,^{172,173,174} biocompatible,^{172,174,175} and inexpensive

[§] Reproduced from M. Rostagno, Shen, S., I. Ghiviriga, and S. A. Miller, *Polym. Chem.*, 2017, **8**, 5049–5059 with permission from The Royal Society of Chemistry.

(~\$2.23 per kilogram),¹⁷⁶ making it a promising potential component of sustainable and degradable commodity plastics.

The condensation of PVA with formaldehyde or butyraldehyde yields polyvinyl formal (PVF) or polyvinyl butyral (PVB), respectively (Figure 4-1). These polyvinyl acetals have been known and studied for many years and produced industrially since the 1930s.¹⁷⁷ PVF occupies only a small part of the polyvinyl acetals market, with tradenames Vinylec® (Chisso)¹⁷⁸ and Pioloform® (Kuraray),¹⁷⁹ and has applications in coatings and insulation for electronics.¹⁷⁷ PVB is known by several trademark names including Butvar® (Eastman),¹⁸⁰ Butacite® (Dupont),¹⁸¹ and Mowital® (Kuraray).¹⁷⁹ It has several specialty applications, including shatter-proof glass interlayering for vehicles, coatings, inks, binders and adhesives, and military applications.^{177,182}

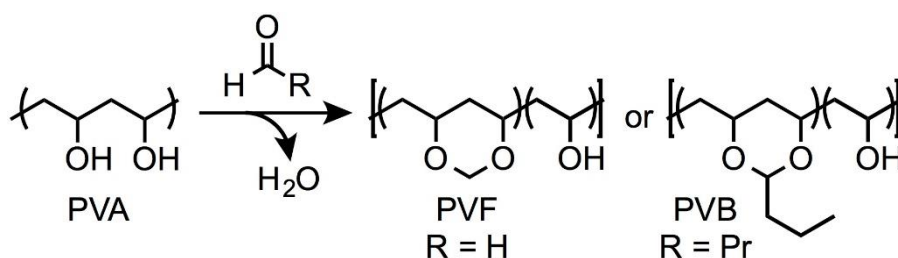


Figure 4-1. The acetalization of polyvinyl alcohol (PVA) with formaldehyde (R = H) or butyraldehyde (R = Pr) yields polyvinyl formal (PVF) or polyvinyl butyral (PVB), respectively.

PVB demonstrates the facile structural modification of PVA, leading to quite different properties and applications. In commercial PVB (Butvar), the typical level of acetalization is 80%, giving amorphous polymers with glass transition temperature (T_g) values ranging from 62–78 °C.¹⁸³ This T_g range is suitable for the aforementioned applications, but higher T_g values would be desirable for the consideration of polyvinyl acetals for general packaging applications. For example, a T_g value around 100 °C would match that of the highly versatile commodity plastic polystyrene (PS).

Synthetic approaches for the acetalization of PVA to PVB and PVF have been extensively studied in the literature, exploring methods in water^{184,185,186} and other solvents including ethanol¹⁸² or *N*-methylpyrrolidone.¹⁸⁷ Beyond butyraldehyde and formaldehyde, a variety of aliphatic and aromatic aldehydes have been explored for the synthesis of polyvinyl acetals. These include condensation of PVA with furfural in dimethyl sulfoxide or water with acetalization around 55%,¹⁸⁸ or 25% with a reported T_g of 87 °C.¹⁸⁹ Alternatively, furfural and butyraldehyde can be incorporated into the same product.¹⁹⁰ Another report describes a rather high level of acetalization with benzaldehyde (>90%) in a solution of dimethylformamide and dimethylsulfoxide; while a melting temperature (T_m) of 205 °C was reported, the T_g remained low at 70 °C.¹⁹¹ The aromatic pesticide 2,6-dichlorobenzaldehyde was attached to PVA with up to 68% efficiency, and its hydrolysis was studied in dioxane.¹⁹² In pursuit of cosmetic applications and evaluation of polymeric shininess, a collection of aliphatic and aromatic aldehydes was studied. Most reactions were conducted in tetrahydrofuran and acetalization reached 80%, but no T_g values were reported for the formed polyvinyl acetals.¹⁹³ Interestingly, the direct acetalization of polyvinyl acetate (the usual precursor to PVA) with butyraldehyde or other aldehydes can be accomplished in supercritical CO₂. The other aldehydes include the aliphatics 3,3-dimethyl butyraldehyde or dodecylaldehyde, or the aromatics benzaldehyde (no T_g values determined) or 2,3,5,6-tetrafluorobenzaldehyde (T_g of 58 °C with 60% acetalization and 33% remaining acetate).¹⁹⁴

In the past two decades, researchers have increasingly exploited naturally occurring aromatic molecules as building blocks for sustainable polymers.¹⁹⁵ The

inclusion of such bioaromatics often confers improved thermal^{119,196} and mechanical properties.¹⁹⁷ The aromatic components typically increase T_g values because of quadrupolar interactions, π stacking, and increased conformational barriers. One approach is to incorporate the bioaromatic within the main-chain of the polymer.^{84,130} An alternative approach is to incorporate the bioaromatic onto the polymer as pendant groups, in a fashion similar to polystyrene. An example is the polymerization of acrylates derived from bio-based phenolics such as guaiacol, creosol, 4-ethylguaiacol, vanillin,¹⁹⁸ and syringol.¹⁹⁹ Obtained T_g values were competitive with that of polystyrene (100 °C) starting at 92 °C for guaiacol but reaching 205 °C for syringol. The pendant bioaromatic strategy has also been reported for functionalized polyacrylamides; however, the attachment of vanillin decreased the T_g of polyacrylamide from 165 °C to 101 °C.²⁰⁰

While PVA-derived polyvinyl acetals bear side-chain acetals, main-chain polyacetals from bio-based monomers have been pursued recently with vigor.⁴ For example, crystalline aliphatic polyacetals have been synthesized from renewable α,ω -diols and formaldehyde equivalents in pursuit of degradable polyethylene mimics.^{201,202} A similar strategy provided semi-crystalline polyacetals of isosorbide (or its isomers) with T_m values up to 156 °C.²⁰³ Copolyacetals were also obtained employing both isosorbide and α,ω -diols, yielding materials with tunable degradability.²⁰⁴ Another interesting molecule used to prepare main-chain polyacetals is glycolaldehyde, which is readily obtained from the pyrolysis of lignocellulosic feedstocks. Dimerization of glycolaldehyde forms a cyclic bis-hemiacetal that can be polymerized via an acetalization step, yielding a crystalline thermoplastic material with a T_m near 80 °C.²⁰⁵

Finally, rather rigid polyacetals have been synthesized from bioaromatic dialdehydes (from, e.g. vanillin or syringaldehyde) and tetraols—including naturally occurring erythritol—providing acid-degradable materials with T_g values up to 159 °C.^{206,207}

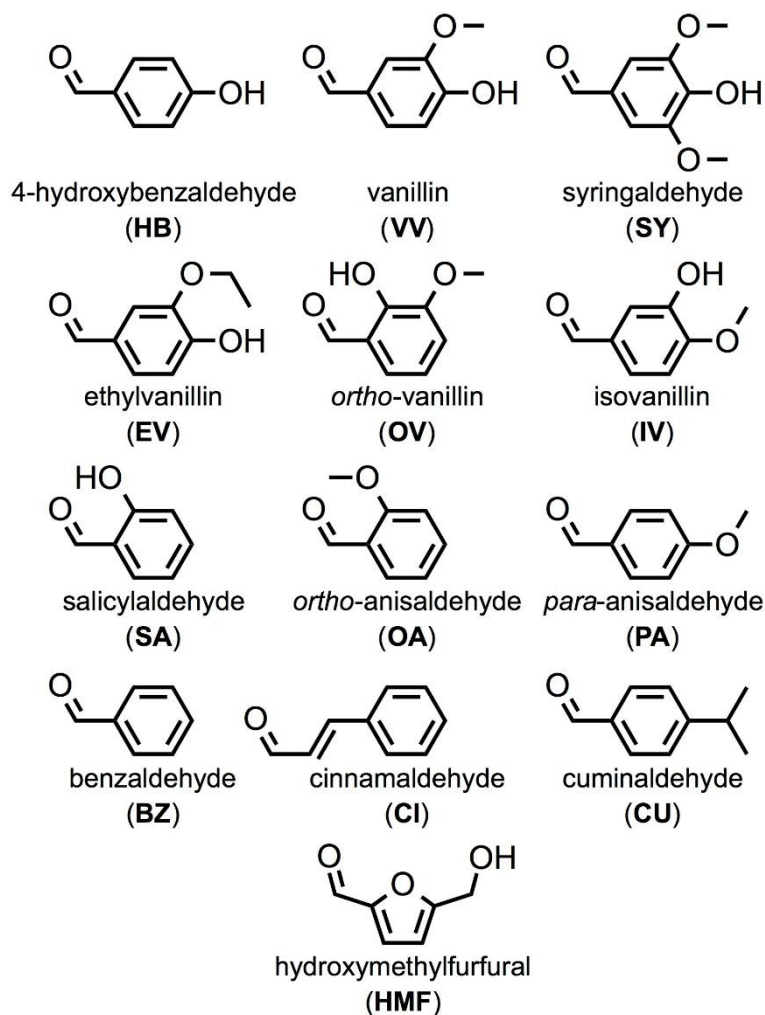


Figure 4-2. Polyvinyl alcohol (PVA) is herein condensed with bioaromatic aldehydes that are lignin-derived (**HB**, **VV**, **SY**), synthetic (**EV**), naturally occurring (**OV**, **IV**, **SA**, **OA**, **PA**, **BZ**, **CI**, **CU**), or glucose-derived (**HMF**).

This study reports the synthesis of novel polyvinyl acetal/ polyvinyl alcohol copolymers obtained from the condensation of commercially available PVA with a collection of thirteen aldehydes that are either naturally occurring, biorenewable, and/or edible and non-toxic (Figure 4-2.). Structure-property relationships are established

between the bioaromatic aldehyde and the polymeric glass transition temperature. Additionally, experiments are performed that reveal details of the rate and equilibrium position of acetal formation between PVA and vanillin. Lastly, heterogeneous degradation studies demonstrate that polyvinyl vanillin acetals hydrolyze readily under acidic aqueous conditions at room temperature.

Experimental

Materials

Sodium bicarbonate, sodium hydroxide, acetone, dimethyl sulfoxide (DMSO), *N*-methyl-2-pyrrolidone (NMP) (VWR), *para*-toluenesulfonic acid (*p*-TSA), benzaldehyde, *ortho*-anisaldehyde, cuminaldehyde (Sigma-Aldrich), 4-hydroxybenzaldehyde, *para*-anisaldehyde, salicylaldehyde (Acros Organics), syringaldehyde (Alfa Aesar), ethylvanillin (SAFC), *ortho*-vanillin (TCI), *trans*-cinnamaldehyde (Lancaster), isovanillin (Oakwood Chemical), vanillin (Borregaard Ind. Ltd. from *Picea abies*, Norway spruce), and hydroxymethylfurfural (HMF, Ench Industry Co. Ltd.), were purchased and used without further purification. Polyvinyl alcohol (PVA), with average molecular weight 13,000–23,000 Da and 98% hydrolyzed, and PVA, with average molecular weight 146,000–186,000 Da and 99+% hydrolyzed (Sigma-Aldrich), were ground before use. NMR solvent deuterated dimethyl sulfoxide (DMSO- d_6 , Cambridge Isotope Laboratories) was stored over activated 4 Å molecular sieves (Sigma-Aldrich). All other chemicals, unless expressly mentioned, were used as received.

Characterization

Proton nuclear magnetic resonance (^1H NMR), carbon nuclear magnetic resonance (^{13}C NMR), gradient Heteronuclear Multiple-Bond Correlation (*g*HMBC), gradient Heteronuclear Single Quantum Correlation (*g*HSQC), and gradient

Heteronuclear Single Quantum Coherence-Total Correlation Spectroscopy (gHSQC-TOCSY) were recorded using an Inova 500 MHz spectrometer. Chemical shifts are reported in parts per million (ppm) downfield relative to tetramethylsilane (TMS, 0.0 ppm) or residual proton in the specified solvent. Coupling constants (J) are reported in Hertz (Hz). Multiplicities are reported using the following abbreviations: s, singlet; d, doublet; t, triplet; q, quartet; m, multiplet; br, broad.

Differential scanning calorimetry (DSC) thermograms were obtained with a DSC Q1000 (TA instruments). Typically 4–6 mg of a sample were massed and added to a sealed pan that passed through a heat-cool-heat cycle at 10 °C min⁻¹. Reported data are from the second full cycle. The temperature ranged from 0 to 250 °C.

Thermogravimetric analyses (TGA) were measured under nitrogen with a TGA Q5000 (TA Instruments). About 10–15 mg of each sample were heated and held at 100 °C for 50–75 min. Then, 5 mg portions of these samples were heated at 20 °C min⁻¹ from 25 to 600 °C.

Gel permeation chromatography (GPC) was performed at 40 °C using an Agilent Technologies 1260 Infinity Series liquid chromatography system with an internal differential refractive index detector, and two Waters Styragel HR-5E columns (7.8 mm i.d., 300 mm length, guard column 7.8 mm i.d., 25 mm length) using a solution of 0.1% potassium triflate (K(OTf)) in HPLC grade hexafluoroisopropanol (HFIP) as the mobile phase at a flow rate of 0.5 mL min⁻¹. Calibration was performed with narrow polydispersity polymethyl methacrylate standards.

Polyvinyl acetal synthesis

Polyvinyl alcohol, reported as 98% hydrolyzed polyvinyl acetate, with molecular weight averaging 13,000–23,000 Da, was condensed with thirteen aromatic aldehydes

to yield thirteen modified PVA polymers. The method for polyvinyl vanillin acetal (**PV-VV-A**) follows below and all other methods are provided in the ESI.

Synthesis of polyvinyl vanillin acetal PV-VV-A. On a Schlenk line, a 250 mL round bottom flask (Flask A) was charged with 1.00 g (22.50 mmol) polyvinyl alcohol and 0.077 g (0.45 mmol) *p*-TSA. This flask was fitted with a bump trap and attached to the Schlenk line and the other openings were sealed with rubber septa. The system was evacuated and backfilled with nitrogen before injection of 7.5 mL of DMSO via syringe. Full dissolution was accomplished by heating to 90 °C under nitrogen. A second 250 mL round bottom flask (Flask B) was charged with 4.45 g (29.25 mmol) vanillin. The flask was fitted with a bump trap and rubber septa were attached to the Schlenk line before evacuation and backfilling with nitrogen. Flask B was then injected with 5 mL of DMSO via syringe and stirring effected complete dissolution at room temperature. This vanillin solution was then transferred to Flask A via syringe. The reaction was heated under nitrogen at 60 °C for 2 hours. The crude product was precipitated by adding the cooled reaction to 350 mL aqueous sodium bicarbonate. The precipitate was isolated by decanting, washed twice with 150 mL deionized water, and air dried overnight. NMR analysis of the crude product (4.22 g, 169% yield) showed the presence of water and unreacted vanillin. Purified product was obtained by dissolving 0.40 g of crude product in 15 mL of DMSO, stirring overnight, and reprecipitating in 350 mL of aqueous sodium bicarbonate. The precipitate was isolated by decanting, washed twice with 150 mL deionized water, and air dried overnight. The final product was obtained as a white powder in 19% purification yield (0.08 g). The isolated yield was 31.1% (purification was conducted on a fraction of the crude product, therefore isolated yield is based on

extrapolated numbers). ^1H NMR (DMSO- d_6) δ ppm 1.1–1.8 (m, $-\text{CH}_2-$, 6.32 H), 3.26 (br, OH, 1.65 H), 3.69 (m, $-\text{OCH}_3$, 3 H), 3.90 (m, $\text{CH}-\text{OR}$, 3.36 H), 5.35, 5.56, 5.65 (m, $-\text{OCArHO}-$, 1H), 6.68, 6.76, 6.87 (m, Ar-H, 3 H) (see ESI, Fig. S47). The small peak in the region 1.8–2.0 ppm was ignored since it belongs to the non-hydrolyzed acetyl $-\text{CH}_3$ groups.²⁰⁸ ^{13}C NMR (DMSO- d_6) δ ppm 37.6, 38.3, 44.6, 44.9, 46.3, 46.7, 56.1, 63.3, 64.3, 73.1, 73.6, 100.5, 110.7, 115.3, 119.3, 130.9, 147.3, 147.5. The net reaction yield was computed to be 31%, which accounts for the incomplete acetalization of PVA, combined with mass loss during the purification steps. By ^1H NMR, the degree of acetalization was found to be 63.3%—meaning that 63.3% of the original PVA hydroxy groups are now acetals and 36.7% of the hydroxy groups remain free. In the case of Figure 4-3, $x = 0.633/2 = 0.317$ and $y = 0.367$.

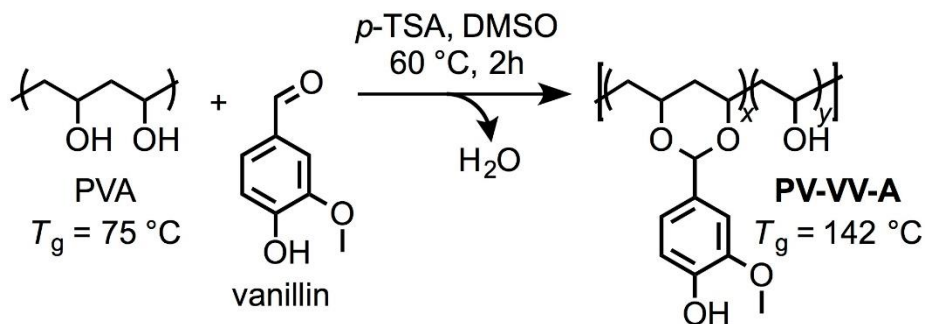


Figure 4-3. The acetalization of PVA with vanillin is catalysed by $p\text{-TSA}$ and yields polyvinyl vanillin acetal (**PV-VV-A**) with 63.3% of the $-\text{OH}$ groups converted to acetals.

Kinetic studies

Two kinetic studies were performed in order to understand the reaction timescale and the optimal reaction duration. First, a small-scale, NMR reaction was conducted at room temperature with excess aromatic aldehyde; this allowed for *in situ* analysis of the timescale to reach equilibrium and the position of equilibrium. Second, a large-scale

reaction was conducted at 60 °C for 48 hours, during which sizeable aliquots were extracted and analyzed for extent of acetalization and polymer T_g .

NMR kinetic study. Polyvinyl alcohol (~1 mg) was dissolved in 1 mL DMSO- d_6 . Then, an excess of vanillin (~15 mg) was added, ensuring at least a ten-fold excess of the aldehyde. The solution was transferred to an NMR tube and an initial ^1H NMR spectrum was obtained to calculate the relative concentration of vanillin versus PVA. The sample was ejected from the NMR spectrometer and one crystal of *p*-TSA (<1 mg) was added to the NMR tube. ^1H NMR spectra were taken continuously and entries recorded every 12 minutes for 1008 minutes (16.8 hours) at 25 °C.

Large-scale kinetic study. This method is a larger scale version of the **PV-VV-A** synthesis described above. In this case, Flask A contained 20.0 g (450 mmol) polyvinyl alcohol and 1.54 g (9.0 mmol) *p*-TSA dissolved in 150 mL of DMSO. Flask B contained 89.03 g (585 mmol) vanillin dissolved in 100 mL of DMSO. After the solution from Flask B was transferred to Flask A via syringe, the reaction was heated and stirred under nitrogen at 60 °C for 48 hours. 25 mL aliquots were extracted at $T = 1, 2, 3, 4, 6, 8, 12, 24,$ and 48 hours. Each aliquot was precipitated and purified as described above for **PV-VV-A**.

Hydrolysis experiments

Long heterogeneous study. A long hydrolysis study was performed by placing 10 mg of **PV-VV-A** in 10 mL of aqueous media: buffers with pH 1, 2, 3, and 5; deionized water; and seawater. These six vials were agitated on an orbital shaker at room temperature. Photographs were taken initially, every hour during the first day, daily during the first week, and weekly for the term of a month.

24 hour heterogeneous study. 30 mg of **PV-VV-A** were placed in 10 mL of aqueous media: buffers with pH 1, 2, 3, 5, and deionized water. These five vials were agitated on an orbital shaker at room temperature. After 24 hours the pH was neutralized, water was evaporated, and the remaining solids were dissolved in DMSO- d_6 for ^1H NMR analysis.

Accelerated study. 0.4 g of purified **PV-VV-A** polymer were placed in 50 mL of 1M aqueous hydrochloric acid and heated to reflux for 4 hours. After reaction, the free vanillin was extracted with diethyl ether (3 x 20 mL), the organic layers were combined and washed with brine, dried over MgSO_4 , and evaporated under reduced pressure, and the free vanillin was recovered. The aqueous layer was evaporated to recover PVA, which was subjected to NMR analysis to confirm that no vanillin acetal groups remained.

Results and discussion

Bioaromatic aldehydes employed

Polyvinyl alcohol (PVA) was reacted with thirteen bioaromatic aldehydes to yield polyvinyl aromatic acetals. The first three of Figure 4-2 are 4-hydroxybenzaldehyde (**HB**), vanillin (**VV**), and syringaldehyde (**SY**), which can be obtained from the pyrolysis of lignin.^{209,210} Ethylvanillin (**EV**), a synthetic analogue of vanillin, is not found in nature, but is used as a vanillin flavouring alternative.²¹¹ The next eight of Figure 4-2 are all naturally occurring aldehydes which can be extracted from different natural sources in small quantities and are generally used in the flavour and fragrance industry:²¹¹ *ortho*-vanillin (**OV**),²¹² isovanillin (**IV**),²¹³ salicylaldehyde (**SA**), *ortho*-anisaldehyde (**OA**), *para*-anisaldehyde (**PA**), benzaldehyde (**BZ**), cinnamaldehyde (**CI**), and cuminaldehyde (**CU**). Finally, hydroxymethylfurfural (HMF) is an upstart biogenic platform molecule²¹⁴ made

via the dehydration of hexoses, and has been particularly appealing as a precursor to polyethylene furanoate (PEF),²¹⁵ a potential biorenewable replacement for polyethylene terephthalate (PET).²¹⁶

Acetalization optimization

The reaction of PVA with vanillin was chosen as a model for optimizing the acetalization conditions. Prior reported methods for the synthesis of polyvinyl acetals utilized water and/or ethanol,¹⁸² N-methylpyrrolidone (NMP) for polyvinyl butyral,¹⁸⁷ water for polyvinyl formal,¹⁸⁶ dimethyl sulfoxide (DMSO) for polyvinyl furfural,¹⁸⁸ among other examples. Among the acid catalysts HCl, acetic acid, methane sulfonic acid, sulfuric acid, and *para*-toluene sulfonic acid, only the last two yielded appreciable polyvinyl acetal. While sulfuric acid works only in NMP, *p*-TSA was effective in both NMP and DMSO. Different concentrations and ratios were explored as well, following guidance from the PVB example of Zhang and Yu.¹⁶⁸ With vanillin, a similar excess of the aldehyde (2.6:1) gave optimal results. Of the explored solvents ethanol, DMSO, and NMP, only the last two allowed a noticeable reaction, but DMSO was chosen since it is a considerably more benign solvent than NMP,²¹⁷ and is a better solvent for vanillin as well. As we have previously reported,^{206,207} drying agents can increase polymer molecular weight for acetalization polymerization by capturing evolved water. To test the efficacy of this strategy for acetalization of PVA, drying agents were either added directly to the reaction (4 Å molecular sieves or MgSO₄) or suspended in a porous bag above the reaction (MgSO₄ or Na₂SO₄). Inclusion of a drying agent did not improve the % acetalization or polymer *T*_g, hence, drying agents were not employed for subsequent reactions. Additional details of the optimization study are available in the ESI.

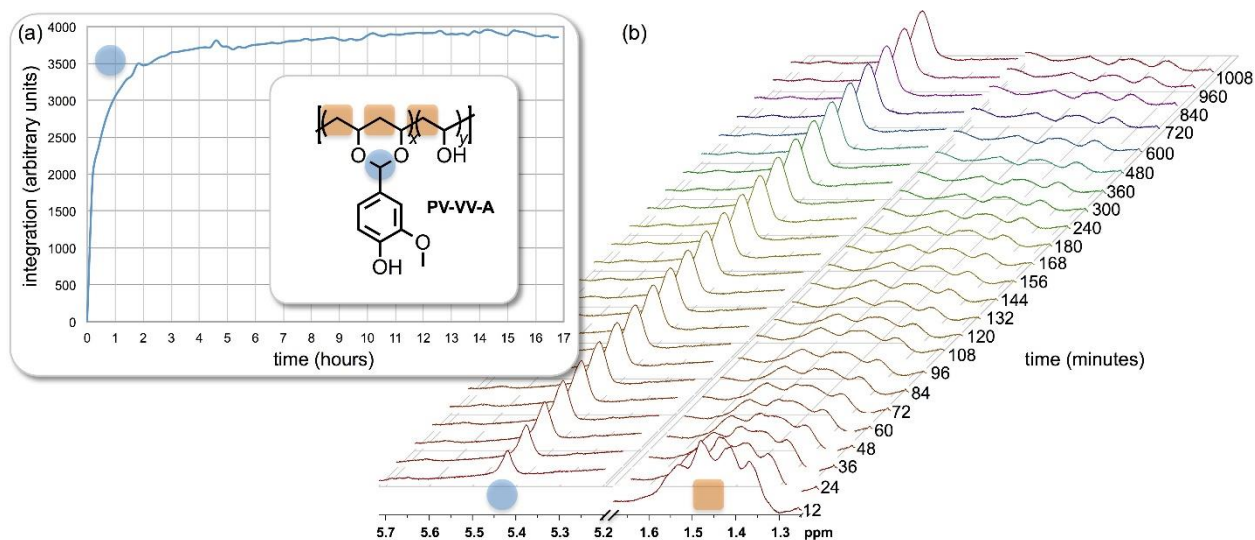


Figure 4-4. Acetalization of PVA with vanillin versus time measured by ^1H NMR: (a) acetal peak integration (5.4 ppm, arbitrary units) versus time over 17 hours; (b) NMR spectra cascade for the acetal region (5.2–5.7 ppm) and the methylene region (1.2–1.7 ppm) every 12 minutes for the first 3 hours, and every hour until the end of the experiment (16.8 hours).

Kinetic studies

Two different experiments were designed to understand the dependence of PVA acetalization with time. First, an experiment was prepared in an NMR tube with $\text{DMSO-}d_6$ saturated with PVA, a tenfold excess of vanillin, and a small crystal of *p*-TSA as the acid catalyst; this was monitored in the NMR spectrometer for about 17 hours at 25 °C (Figure 4-4). The peak observed near 5.4 ppm corresponds to the acetal proton, which originated as the aldehyde proton; this peak was compared to the broad multiplet at 1.2–1.7 ppm, which corresponds to the backbone methylene protons. Figure 4-4(a) plots the integration of the acetal peak over 17 hours. Acetalization occurs as soon as the catalyst is added, with half of the reaction accomplished in the first 12 minutes. The reaction proceeds exponentially over the first 2 hours and reaches a plateau after 4 or 5 hours. Figure 4-4(b) compares the growing acetal peaks (5.2–5.7 ppm) with the broadening methylene region (1.2–1.7 ppm). A substantial increase in the peak area at

5.4 ppm is easily seen within the first 5 spectra (first hour), while the upfield methylene peaks lose definition and broaden as the PVA yields to a copolymer of PVA and polyvinyl acetal having a mixture of methylene environments among free and reacted –OH groups. The final NMR integration (T = 16.8 hours) showed an acetalization of 70.8%. Under these conditions in an NMR tube, acetalization is facile, even without water removal. At room temperature, equilibrium is reached after about 5 hours, but about 29% of the PVA hydroxy groups ultimately remain unreacted, even with a tenfold excess of vanillin.

The second kinetic experiment was a large-scale reaction, conducted under conditions similar to bulk PVA acetalization. The reaction was performed on 20 grams of PVA at 60 °C over 48 hours, with *p*-TSA as the catalyst and 2.6 theoretical equivalents of vanillin. Aliquots were extracted periodically and analyzed for % acetalization and polymer glass transition temperature (T_g). Figure 4-5 plots the results of this study, where the % acetalization begins low (around 32%) after 1 hour, but subsequent aliquots show the increase of acetalization, reaching ~50% after just 2 hours and levelling in this range thereafter. The T_g shows a similar time dependence. Lower T_g values of 134–136 °C are obtained in the first two hours of reaction. Thereafter, the T_g reaches a plateau in the range of 137–139 °C. Under the conditions of this large-scale reaction, equilibrium is mostly achieved after 2 hours.

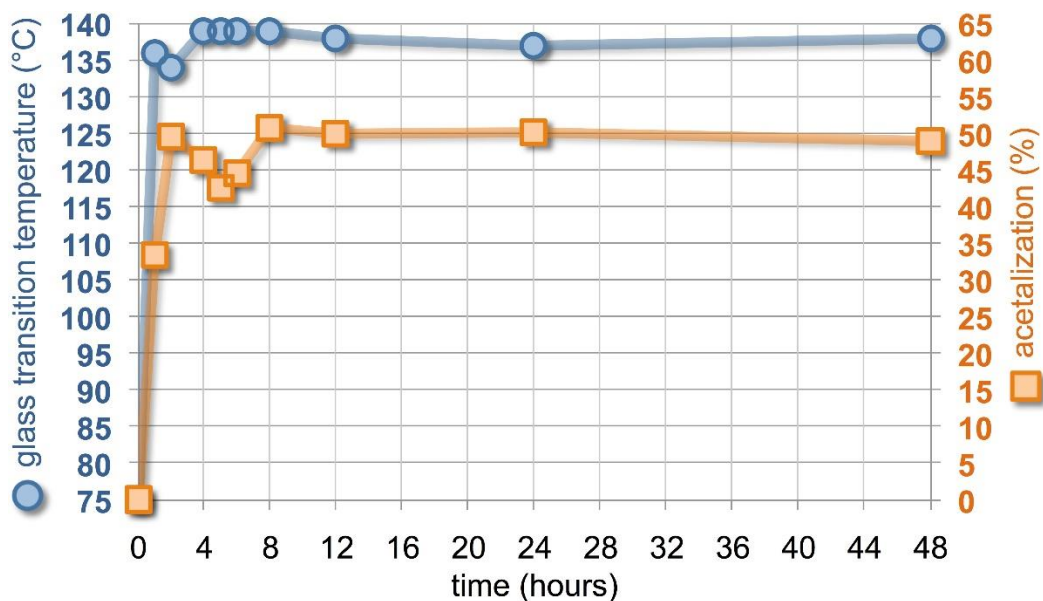


Figure 4-5. Glass transition temperature (°C, circles) and degree of acetalization (% , squares) vs. time measured for aliquots removed from the bulk acetalization of PVA with vanillin.

Acetalization of PVA with bioaromatic aldehydes

Table 4-1 compiles polymerization details and polymer characterization data for the reaction of PVA with thirteen different bioaromatic aldehydes. The aforementioned kinetic studies on vanillin suggested that two hours should be a sufficient reaction time for other aldehydes as well. This was true except for hydroxymethylfurfural and benzaldehyde, which gave low yields (<40%) for this duration; hence, these two aldehydes were reacted for 6 hours. To ensure reaction homogeneity, the PVA and *p*-TSA were dissolved in DMSO at 60 °C and the aldehyde solution was added via syringe. The reaction was terminated by pouring the cooled, homogeneous reaction into saturated aqueous sodium bicarbonate solution. These basic conditions neutralized the *p*-TSA catalyst and ensured the stability of the acetals in the presence of water. The initially precipitated polymer was generally comingled with unreacted aldehyde, necessitating a dissolution/re-precipitation procedure.

As described below, the % acetalization was analyzed by NMR and the thermal properties were studied by DSC and TGA. Gel permeation chromatography (GPC) in hexafluoroisopropanol (HFIP) was performed on several polyvinyl acetal samples, but showed little difference compared to the polyvinyl alcohol employed as starting material. Oddly, the number average molecular weight (M_n) and polydispersity index (PDI) values were unperturbed by substantial acetalization. The homogeneity of the GPC results could be explained in two ways. First, hydrolysis in the in HFIP solvent could occur to regenerate the original PVA, as has been invoked previously.²⁰⁷ Second, the mass added via acetalization could be counter-balanced by a smaller hydrodynamic volume. Logically, the hydrodynamic radius of pure PVA is large since hydrogen bonding with alcoholic solvent is pervasive; but the hydrodynamic radius is expected to shrink with increasing acetalization, as polymer hydrophobicity increases. Therefore Table 4-1 reports only *calculated* M_n values, starting with the measured M_n value of 22,300 for PVA and adding mass prescribed by the mass of the aldehyde (minus water) multiplied by the % acetalization.

Structure and acetal determination by NMR

Extensive NMR studies were performed on **PV-VV-A**. Multiple ^{13}C NMR signals appeared for the polymer backbone, but this multiplicity is ascribed to the atactic polymer stereochemistry, naturally present in the PVA starting material as well.²¹⁸ Assignments were made for all the observed peaks in the ^1H and ^{13}C NMR spectra. It was possible to quantify the acetal abundance by integrating peaks corresponding to the acetal hydrogen ($-\text{OCArHO}-$, 5.4–5.6 ppm), compared to all backbone methylene hydrogens ($-\text{CH}_2-$, 1.1–1.8 ppm). For each incorporated aldehyde molecule, 4 methylene PVA hydrogens are converted to polyvinyl acetal methylene hydrogens

because two $-\text{[CH}_2\text{CHOH]}-$ repeat units are required to generate the cyclic acetal. Thus, multiplying 4 by the quotient $[\text{acetal-H}]/[\text{total } -\text{CH}_2-]$ yields the percent acetalization on a molar basis.

The acetal region is somewhat complicated by local stereochemistry. In addition to a major peak near 5.4 ppm, a minor peak appears near 5.6 ppm. In analogy to our previously reported main-chain polyacetals (derived from erythritol and dialdehydes),²⁰⁷ the major acetal peak corresponds to $-\text{OCArHO}-$ with aryl located equatorial and the minor peak corresponds to $-\text{OCArHO}-$ with aryl located axial in the newly formed 6-member ring. Even though the minor ^1H NMR peaks can be observed in all thirteen of the spectra from Table 4-1, they are more pronounced for entries 2, 5, and 7–12. There is no clear structure-property relationship regarding this stereochemical nuance.

Level of acetalization

For the reaction of PVA ($M_n = 22,300$) and vanillin at 60 °C, the maximum acetalization achieved was about 63% (Table 4-1, entry 1). Several studies are available discussing the kinetics of forming polyvinyl acetals from PVA and aldehydes or ketones.^{219,220} For *irreversible* 1,3 functionalization, the maximum theoretical acetalization possible is of 86.5%.²²¹ The balance (13.5%) pertains to those isolated $-\text{OH}$ groups that remain unreacted because there is no neighboring $-\text{OH}$ group for acetal formation. However, this limit of 86.5% can be broken in cases of *reversible* functionalization, since de-acetalization can regenerate an $-\text{OH}$ group next to a formerly stranded one. For example, the reaction of PVA with formaldehyde can yield polymers with over 90% acetalization.²²²

In the present case, acetalization is presumably reversible and the values approaching 75% are not a kinetic limit, but likely a thermodynamic limit. Minimal steric

congestion in the aforementioned case of formaldehyde allows for a high degree of acetalization, with comparatively little mass added. In contrast, two of the largest aldehydes in Table 4-1, syringaldehyde (**SY**) and cuminaldehyde (**CU**), yield the lowest level of acetalization, 54.1 and 57.6 %, respectively. Fittingly, two of the smallest aldehydes in Table 4-1, benzaldehyde (**BZ**) and *ortho*-anisaldehyde (**OA**), yield the highest level of acetalization, 74.8 and 73.4 %, respectively. Thus, it seems that voluminous aldehydes present steric bulk, blocking free –OH groups from reaction and lowering the level of acetalization.²²⁰ For the acetalization level of PVA with benzaldehyde (**BZ**), literature values of 90%¹⁹¹ and 65%¹⁹³ flank the value of 74.8% in Table 4-1 (entry 10). One conclusion is that acetalization levels can vary considerably, but under comparable reaction conditions, smaller aldehydes add to PVA with a larger equilibrium constant. Support for this conclusion is seen in Figure 4-6, which shows that the acetalization % is inversely proportional to the formula weight of the seven homologous benzaldehydes with increasing substitution (sterics) at the 3, 4, and 5 positions.

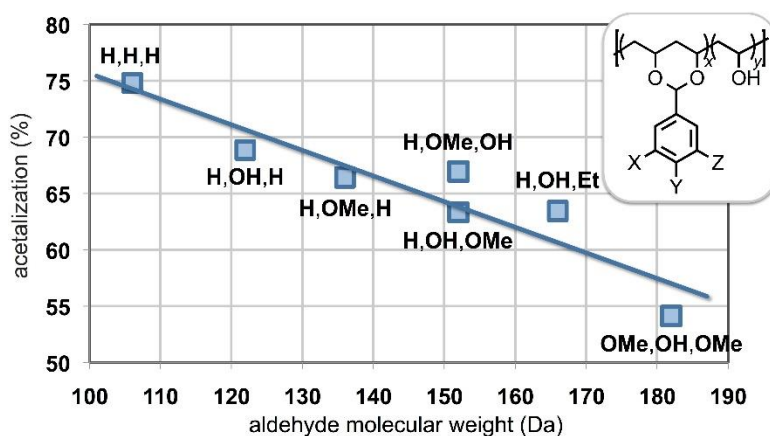
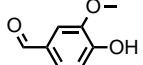
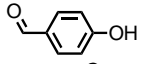
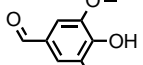
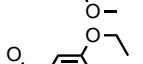
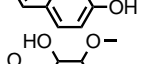
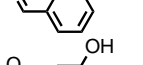
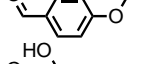
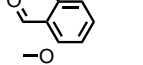
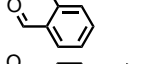
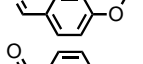
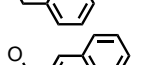
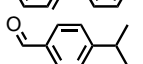
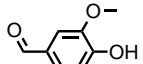


Figure 4-6. For the seven homologous benzaldehydes with increasing substitution at the 3, 4, and 5 positions (X, Y, Z), the extent of acetalization ($2x/[2x+y]$) decreases with increasing sterics, as measured by the aldehyde molecular weight.

Table 4-1. Polyvinyl acetals from polyvinyl alcohol (PVA) and 13 different aldehydes, along with isolated yield and characterization data.^a

| Entry | Aldehyde | Yield (%) | Acetal (%) | T_g (°C) ^b | T_{95} (°C) ^c | M_n (Da) ^d |
|-------|---|-----------|------------|-------------------------|----------------------------|----------------------------------|
| 0 | None | - | None | 75 | 222 | 22,300 ^e |
| 1 |  | 31.1 | 63.3 | 142 | 199 | 43,700 |
| 2 |  | 37.6 | 68.8 | 157 | 224 | 40,400 |
| 3 |  | 54.9 | 54.1 | 139 | 224 | 44,700 |
| 4 |  | 44.7 | 63.5 | 114 | 185 | 46,000 |
| 5 |  | 54.4 | 57.6 | 139 | 234 | 41,800 |
| 6 |  | 46.9 | 66.9 | 139 | 278 | 45,000 |
| 7 |  | 55.7 | 64.0 | 150 | 241 | 39,100 |
| 8 |  | 70.5 | 73.4 | 121 | 296 | 44,300 |
| 9 |  | 55.7 | 66.4 | 116 | 241 | 42,100 |
| 10 |  | 84.6 | 74.8 | 129 | 298 | 38,900 |
| 11 |  | 55.5 | 68.3 | 117 | 215 | 42,000 |
| 12 |  | 57.2 | 57.6 | 137 | 308 | 41,200 |
| 13 |  | 80.0 | 58.5 | 144 | 286 | 38,200 |
| 14 | none | - | None | 70 | 120 | 146,000– 186,000 ^g |
| 15 |  | 64.4 | 73.8 | 145 | 235 | 310,000– 395,000 |

^aReaction conducted in dimethyl sulfoxide at 60° C for two hours (except as noted) with 2 mol% *p*-TSA. Ratio of [aldehyde]/[1,3-diol] = 2.6. ^bDetermined by DSC. ^cTemperature reported upon 5% mass loss by TGA. ^dCalculated number average molecular weight (M_n) from initial M_n = 22,300 Da of PVA (or 146,000–186,000 for entry 15) augmented by % acetalization as determined by ¹H NMR. ^e M_n of PVA obtained by GPC in hexafluoroisopropanol (HFIP) at 40 °C versus PMMA standards. ^fReaction conducted for 6 hours. ^g M_n range, as reported by the manufacturer.

Thermal properties

Polyvinyl alcohol is a semi-crystalline, water-soluble polymer with relatively low T_g of 75 °C (Table 4-1, entry 0), and a high T_m of 230 °C, above its initial degradation temperature.¹⁶⁶ By introducing pendent aromatic rings via acetalization, the T_g of PVA is

substantially increased. As graphed in Figure 4-7, the thirteen amorphous polyvinyl aromatic acetals exhibited T_g values ranging from 114 to 157 °C, offering an increase of 39 to 82 °C versus PVA itself.

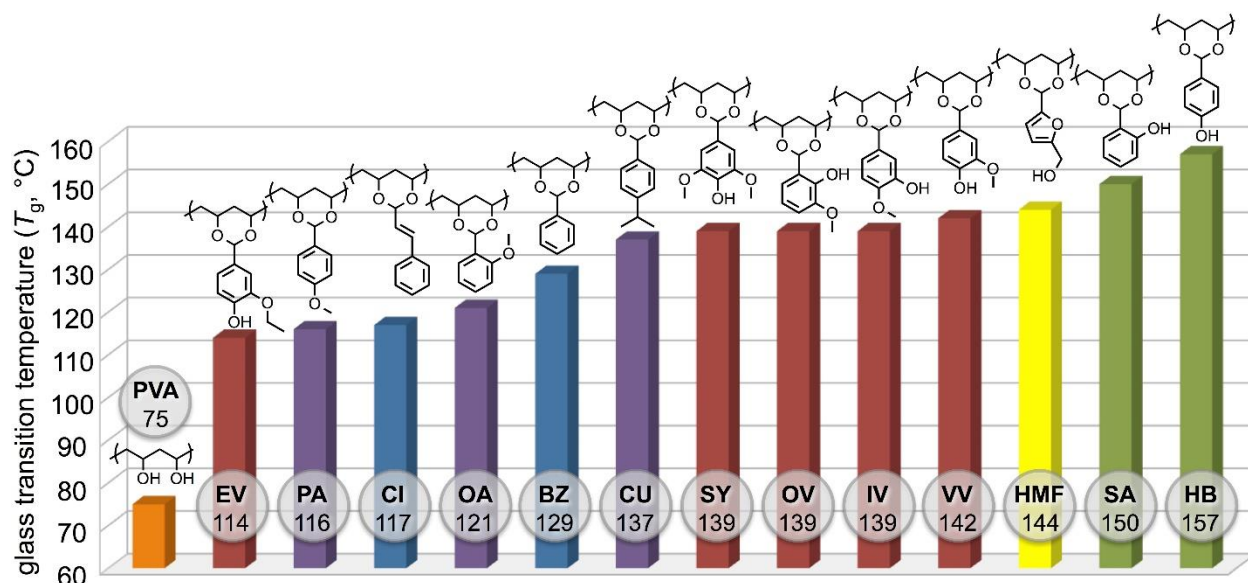


Figure 4-7. The glass transition temperature (T_g) of PVA is increased via acetalization (ranging from 54 to 75%) with bioaromatic aldehydes and the measured T_g value can be correlated to aldehyde structure and functionality. Hydrogen bonding is key to high T_g values (139 to 157 °C).

Polymer structure-property relationships can be assessed depending on the nature of the aldehyde attached to PVA. Aldehydes possessing a single hydroxy group showed remarkably higher T_g values than their counterparts bearing a methoxy group in the same position. Specifically, the polymer from 4-hydroxybenzaldehyde (**HB**) showed a T_g of 157 °C—the highest of the entire series—whereas the polymer from *para*-anisaldehyde (**PA**) showed a T_g of 116 °C, a 41 °C difference. The same effect is observed when comparing salicylaldehyde (**SA**) and *ortho*-anisaldehyde (**OA**) with T_g = 150 and 121 °C respectively, a difference of 29 °C. These stark differences can be attributed to pervasive hydrogen bonding with hydroxy groups from the aldehyde. With just ethereal aromatic groups, hydrogen bonding is limited to only the unreacted

hydroxy groups on the main chain. The polymer from **HMF** also exhibits a high T_g of 144 °C. Although hydrogen bonding is fully available to this polymer, perhaps the free volume introduced by the flexible hydroxymethyl group is responsible for a lower T_g value compared to the phenolic alcohols **HB** and **SA**.

The polymers derived from vanillin (**VV**), isovanillin (**IV**), *o*-vanillin (**OV**), and syringaldehyde (**SY**) exhibit similar T_g values in the range of 139 to 142 °C. Although each of these possesses a phenolic hydroxy substituent, it is flanked by one or more methoxy groups in each case. Thus, the somewhat diminished T_g values compared to **HB** and **SA** can be attributed to steric interference with hydrogen bonding and/or increased free volume originating with the conformationally flexible methoxy groups.

Five polymers from Figure 4-7 have been created with aromatic aldehydes inherently incapable of hydrogen bonding: cuminaldehyde (**CU**), benzaldehyde (**BZ**), *ortho*-anisaldehyde (**OA**), cinnamaldehyde (**CI**), and *para*-anisaldehyde (**PA**). For these, the measured T_g ranges from 116 to 137 °C—all below the seven aforementioned polymers capable of hydrogen bonding via the pendent aromatic. It is perhaps anomalous that the highest T_g member of this series is cuminaldehyde (**CU**) because an isopropyl group is not expected to increase the T_g compared to hydrogen substitution. For example, the T_g of poly(4-isopropylstyrene) (87 °C)²²³ is lower than that of unsubstituted polystyrene (100 °C).²²⁴ One explanation—which should be considered when comparing all polyvinyl acetals herein—is that the T_g is affected by hydrogen bonding of the unreacted PVA portion. The polymer prepared with the smaller benzaldehyde (**BZ**) is 74.8 % acetalized, leaving unreacted only 25.2 % of the original hydroxy groups. The polymer prepared with the larger cuminaldehyde (**CU**) is

only 57.6 % acetalized, leaving unreacted 42.4 % of the original hydroxy groups, the highest level in this series. Thus, the comparatively high T_g of this polymer might be related to its high degree of hydrogen bonding among the unreacted main-chain hydroxy groups.

Finally, note that the lowest T_g of the polyvinyl acetals in Figure 4-7 is from ethylvanillin (**EV**) (114 °C), markedly lower than that from vanillin (**VV**) (142 °C). The induced free volume of an ethoxy group, compared to that of a methoxy group, is known to considerably diminish polymeric T_g values.²⁰⁶

Effect of PVA molecular weight on polyvinyl acetal properties

For creating the polymers of Table 4-1, entries 1–13, low molecular weight PVA (reported as 13,000–23,000 Da; measured as $M_n = 22,300$) was chosen to minimize problems related to polymer solubility and viscosity. For comparison, a higher molecular weight polyvinyl acetal was prepared from vanillin and PVA having a sevenfold higher molecular weight (Table 4-1, entry 14, reported as 146,000–186,000 Da). Table 4-1, entry 15 labels this polymer as **PV-VV-A*** and provides comparative characterization data. The higher molecular weight polymer has 73.8 % acetalization, about 10 % higher than the lower molecular weight version (63.3 %, Table 4-1, entry 1). The T_g value of 145 °C is merely 3 °C higher for **PV-VV-A***, suggesting that the lower molecular weight analogue suitably reveals this thermal property.

Heterogeneous degradation studies

A heterogeneous degradation study was performed on polyvinyl vanillin acetal with 63.3 % acetalization (**PV-VV-A**, Table 4-1, entry 1) in aqueous buffers with pH = 1, 2, 3, and 5, as well as deionized water and seawater. Visual inspection confirmed the eventual dissolution of the three most acidic samples. More acidic conditions effected

faster dissolution, with the sample at pH = 3 dissolving in 48 hours, the sample at pH = 2 dissolving in 24 hours, and the sample at pH = 1 dissolving in 2 hours. Presumably the acetals were hydrolyzed to regenerate water-soluble polyvinyl alcohol. Although the samples were monitored for 12 weeks, no visual changes were noted after the initial 48 hours. Apparently, the samples in pH = 5 buffer, deionized water, and seawater did not hydrolyze substantially over this time.

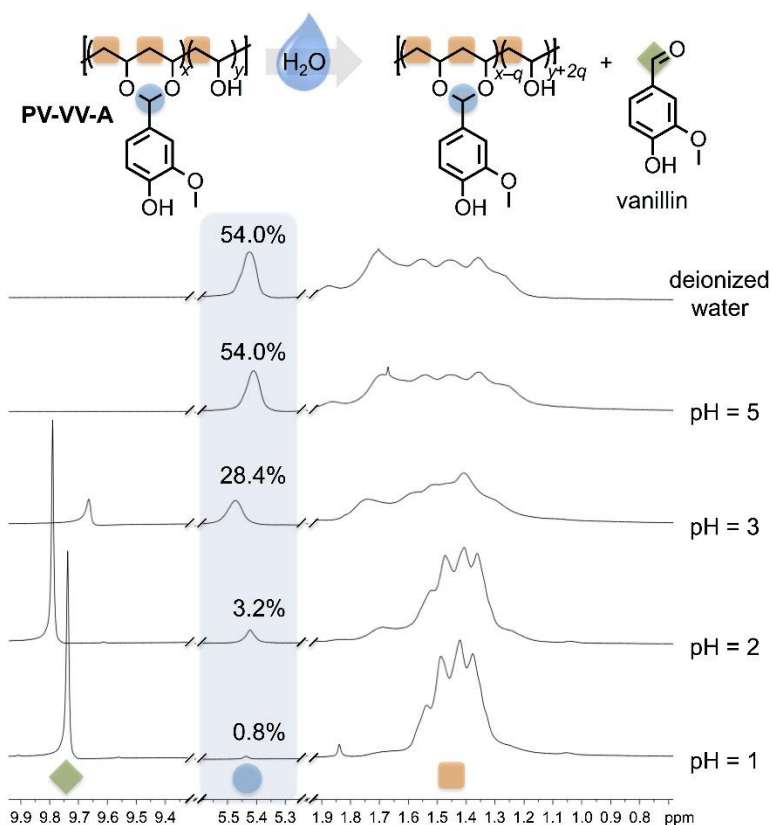


Figure 4-8. Heterogeneous hydrolysis study of **PV-VV-A** with 54.0 % initial acetalization. 24-hour exposure to deionized water or pH = 5 aqueous buffer effected no hydrolysis, but hydrolysis was significant in more acidic aqueous media with residual acetalization of 28.4, 3.2, or 0.8 % for pH = 3, 2, or 1, respectively.

A different **PV-VV-A** sample with 54.0 % acetalization was subjected to similar media (pH = 1, 2, 3, 5, and deionized water) on an orbital shaker for 24 hours, then neutralized, isolated, and analyzed by ^1H NMR. The results shown in Figure 4-8

corroborate those from visual inspection noted above. After 24 hours, no hydrolysis is observed in deionized water or at pH = 5; the level of acetalization is unchanged at 54.0 %. At pH = 3, about half of the initial acetals have hydrolyzed, yielding a polymer with 28.4 % acetalization and a prominent peak corresponding to the aldehydic proton of free vanillin at 9.7 ppm. Hydrolysis is quite advanced at pH = 2, for which residual acetalization is small at 3.2 %. Lastly, the sample at pH = 1 has hydrolyzed almost completely; the acetal peak at 5.4 ppm indicates a meager 0.8 % residual acetalization. Note that **PV-VV-A** can be fully hydrolyzed back to polyvinyl alcohol (PVA) by refluxing in 1 M aqueous hydrochloric acid for four hours. Although such conditions are uncommon in the environment, it is important to demonstrate the complete hydrolysis of high glass transition temperature polyvinyl aromatic acetals under initially heterogeneous conditions. For example, the stomach pH of mammals, fish, and birds is suitably low to fully digest **PV-VV-A** into innocuous PVA and vanillin.

Conclusions

Polyvinyl acetals were prepared from polyvinyl alcohol (PVA) and sustainable aromatic aldehydes. PVA is an attractive ingredient since it is non-toxic, water soluble, biodegradable, and potentially biorenewable. Acetalization with thirteen benign aromatic aldehydes, including vanillin and hydroxymethylfurfural, markedly boosts the glass transition temperature (T_g) of PVA from 75 °C to the range of 114 – 157 °C, surpassing the key benchmark of 100 °C for polystyrene (PS).²²⁴ PVA acetalization was incomplete because of steric limitations and the equilibrium level (54 – 75 % acetalization) seemed inversely proportional to the size of the aldehyde employed. Another targeted property of these polyvinyl acetals is their susceptibility to hydrolytic degradation in aqueous media. An aqueous buffer solution with pH = 5 showed no hydrolysis after 24 hours, but

more acidic media were effective. Over this timeframe at pH = 1, hydrolysis was nearly complete with acetalization dropping from the initial 54.0 % to 0.8 %.

With this work, we introduce a library of sustainable materials with excellent thermal properties and degradation behaviors. In particular, the useful temperature range matches or exceeds that of many commodity plastics, encouraging their future investigation as substitutes for polyethylene terephthalate (PET), polyvinyl chloride (PVC), or polystyrene (PS). Moreover, these polymers are designed for self-remediation in the environment, hydrolyzing to degradable PVA and benign aromatic aldehydes. Even though polyvinyl acetals have been known for more than 75 years and some are sold commercially, these are the first examples focused on sustainability and the utilization of renewable aromatic aldehydes.

CHAPTER 5 RENEWABLE POLYMERS VIA THE BIGINELLI MULTICOMPONENT REACTION

Background

Throughout the history of organic chemistry, multicomponent reactions (MCRs) have already been studied due to their atom economical reactions, despite the complexity of the chemical composition that they present. In particular, MCRs generate a single compound by combining three or more starting materials in one-pot facile synthesis under mild conditions. Furthermore, the final products include the components of all starting materials as their scaffolds, which leads to the diversity of target molecules by merely changing the starting materials. Hence, in pharmaceutical chemistry, the discovery of drug molecules immediately underwent a massive growth since the first integration of MCRs with the combinatorial chemistry was developed.²²⁵

Over the past few years, MCRs have been established as a novel method for polymerizations. The first group who integrated MCRs into polymer science was Crescenzi *et al.* in 1999. They performed the crosslinking of polysaccharides via IMCRs (isocyanide-based MCRs) resulting in the transparent networks with amide or aldehyde linkages between the cellulose chains.²²⁶ In 2003, the group of Wright reported sequential reactions of an Ugi-4CR (Ugi four-component reaction) of norbornenyl aldehydes or carboxylic acids and a ring-opening metathesis polymerization (ROMP) to obtain a highly functionalized polymer.²²⁷ However, the utilization of MCRs in the polymeric synthesis field was limited for nearly a decade, until Meier *et al.* brought the MCRs back into polymer chemistry in 2011. By integrating Passerini-3CR (the Passerini three-component reaction) and olefin metathesis to synthesize a polyester with amide side chain, there were three noteworthy discoveries that they successfully

demonstrated: (1) preparation of the monomers by the Passerini-3CR and then followed by acyclic diene metathesis (ADMET) polymerization, (2) synthesis of bifunctional monomers by self-metathesis and then followed by the direct polycondensation of the Passerini-3CR, (3) post-polymerization functionalization via grafting-onto strategy of the Passerini-3CR.²²⁸ It was believed that the successful work by Meier *et al.* has flourished the integration of MCRs in the polymer synthesis field.

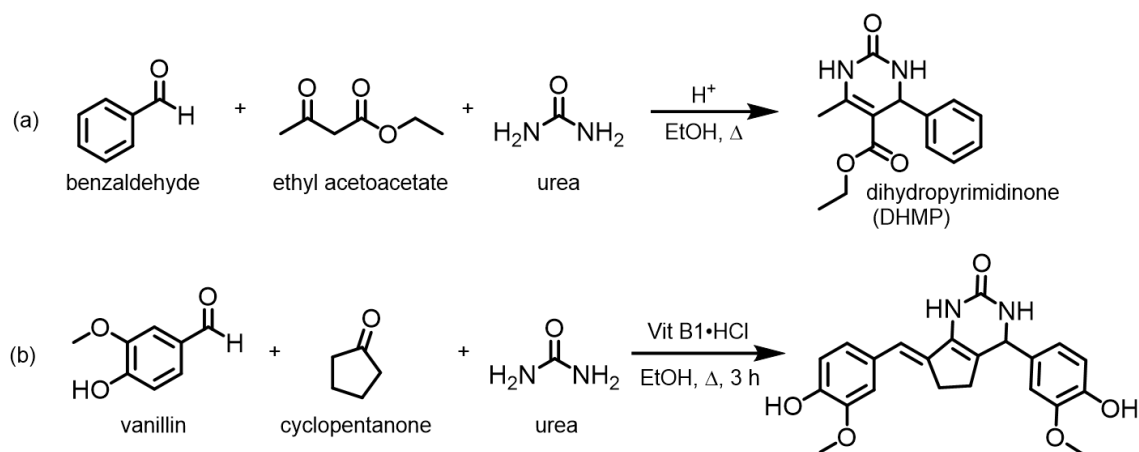


Figure 5-1. Previous work on (a) conventional Biginelli reaction and (b) modified Biginelli reaction.

This project was inspired by one of the famous named MCRs, the Biginelli reaction. In 1891, Biginelli employed small molecules such as benzaldehyde, ethylacetoacetate, and urea, yielding a dihydropyrimidinone (DHMP) compound that exhibited pharmacological activity.²²⁹ Furthermore, Hu *et al.* synthesized a derivative compound of DHMP, by substituting ethylacetoacetate (β -ketoester) with a cyclopentanone (ketone).²³⁰ It is noteworthy to mention that cyclopentanone provides two nucleophilic sites whereas ethylacetoacetate has only one nucleophilic site for the Biginelli reaction. Previously, our group synthesized a series of high glass transition temperatures (T_g) polyacetal ethers utilizing dialdehyde monomers and sugar

molecules, such as erythritol.²⁰⁶ As we continue on our pursuit to obtain high glass transition temperature, sustainable polymers, this work utilized two nucleophilic sites from a ketone reacted with bioaromatic dialdehyde monomers creating sustainable poly-DHMPs (polydihydropyrimidinones) series (Figure 5-1).

Results and discussion

Poly-DHMP analogue from cyclopentanone

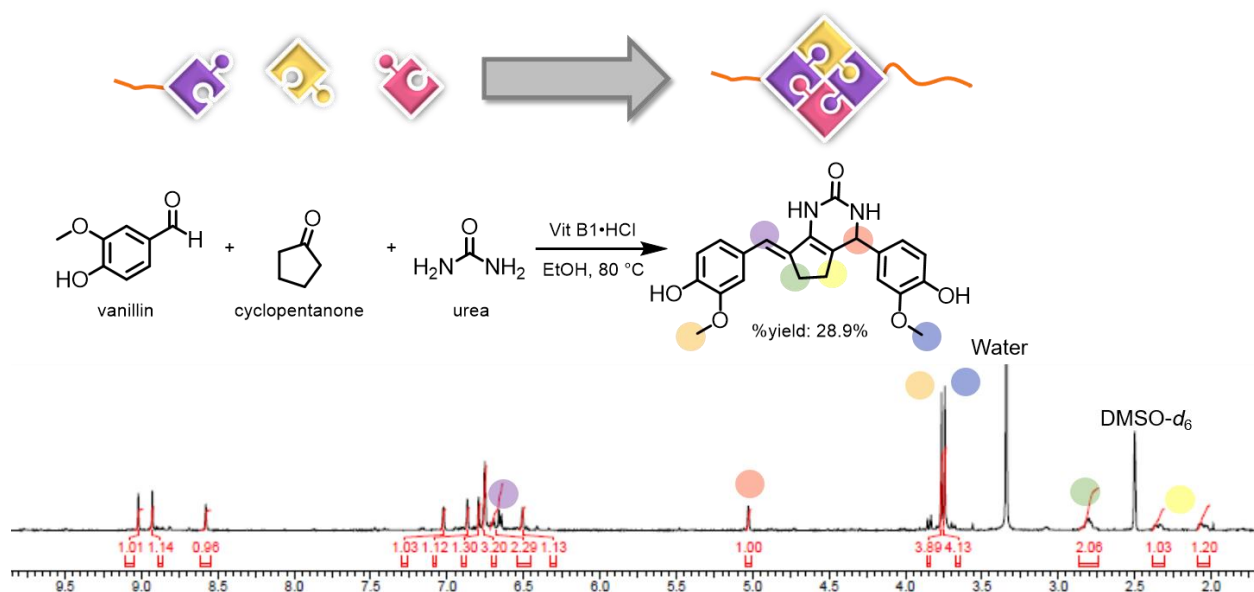


Figure 5-2. Preliminary study: synthesis of dihydropyrimidinone (DHMP) analogue via a modified Biginelli reaction by Hu *et al.*²³⁰

First of all, a preliminary study was conducted to find the most suitable conditions for polymerization by investigating various conditions to synthesize the DHMP analogue. This started by replicating the synthesis of DHMP compound from Hu *et al.* using ethanol as the solvent and vitamin B1 as the catalyst; a yield of 29% was obtained.²³⁰ Then, dimethylsulfoxide (DMSO) was selected as the alternative solvent because the polymerization could only be carried out in hot DMSO; dialdehyde monomers did not dissolve in hot ethanol. The Biginelli reaction that was carried under these conditions afforded 42% yield. Indeed, vitamin B1 was an attractive catalyst since

it is readily available in nature and gave an additional sustainability to the overall reaction. Vitamin B1 acts as a Lewis acid and promotes the Knoevenagel condensation step by activating the aldehyde carbonyl.²³¹ However, vitamin B1 has a low stability at high temperatures, which some polymerizations require because of the high viscosity of polymer solutions at low temperature. For this reason, para-toluenesulfonic acid (pTSA) was used as an alternative option of Lewis acid catalyst; these reaction conditions gave a yield of 24%.

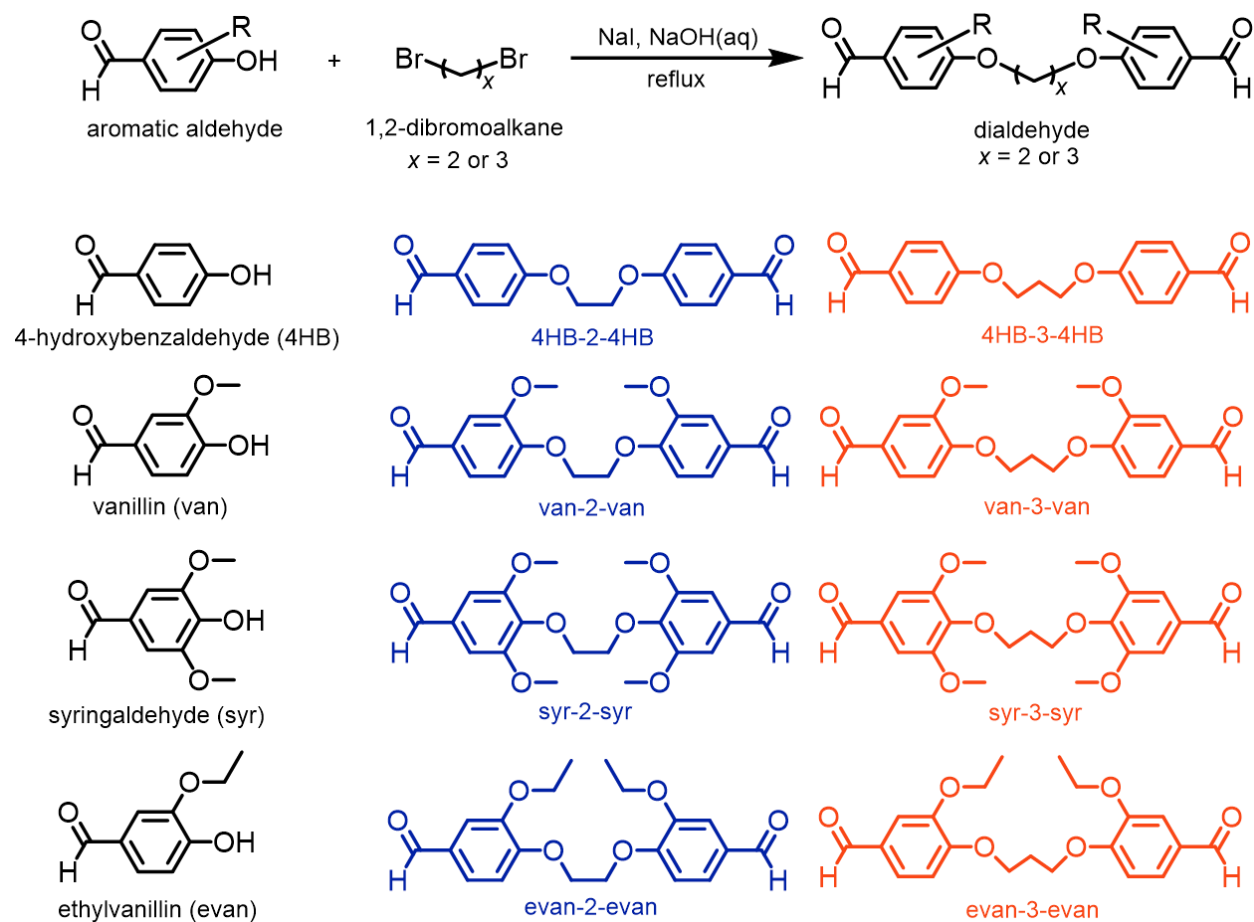
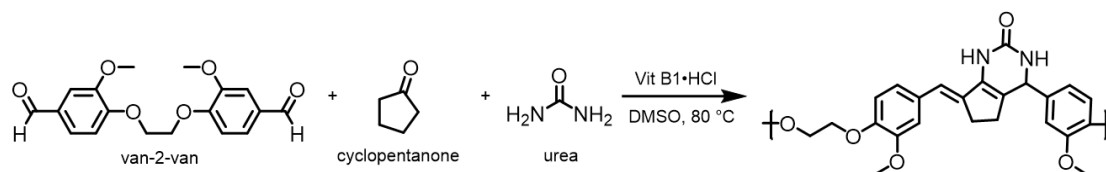


Figure 5-3. Synthesis of bioaromatic dialdehyde monomers.

A series of dialdehyde monomers was inherited from a previous project on polyacetal ethers, including 4HB-2-4HB, van-2-van, syr-2-syr, evan-2-evan, 4HB-3-4HB, van-3-van, syr-3-syr, and evan-3-evan (Figure 5-3).²⁰⁶ These dialdehyde components

were relatively simple to synthesize utilizing dibromoalkane as the alkylene linker and under alkaline aqueous media. Notice that all of the aromatic aldehydes were either readily available or derived from natural occurring compounds. Furthermore, these bioaromatic dialdehyde series allowed us to study the structure-property relationship of the synthesized polymer series due to the presence of different substituents (methoxy group versus ethoxy group) or the length of methylene spacers between aromatic groups while boosting the glass transition temperatures (T_g) at the same time.

Table 5-1. Optimization study of poly-DHMP from van-2-van, cyclopentanone, and urea. ^a



| Entry | Vit B1 ^b (mol%) | m prod. ^c (g) | Yield (%) | M_n ^d (Da) | M_w ^d (Da) | \bar{D} ^d | $T_{5\%}$ ^e (°C) |
|-------|-------------------------------|-----------------------------|--------------|----------------------------|----------------------------|------------------------|--------------------------------|
| 1 | 6 | 0.78 | 92.9 | 13,000 | 58,500 | 4.5 | 262 |
| 2 | 3 | 0.66 | 78.6 | 8,600 | 27,000 | 3.1 | 265 |
| 3 | 1 | 0.40 | 47.3 | 1,800 | 3,800 | 2.2 | 242 |

^aReaction conducted in DMSO using various mol% of catalyst at 80 °C for 24 hours. ^bVitamin B1·HCl used as the catalyst. ^cMass of recovered product. ^dDetermined by HFIP GPC. ^eTemperature reported upon 5% mass loss.

Polymerization optimization was performed using different amounts of catalyst, including 6 mol%, 3 mol%, and 1 mol% vitamin B1. The non-variable conditions were 10 mL of DMSO for 24 hours at a relatively low temperature 80 °C. The additional stoichiometry of cyclopentanone (2 mol eq.) and urea (2.4 mol eq.) was matched to the dialdehyde monomer (van-2-van), following the procedure from the synthesis of the DHMP small molecule where 1 mol eq. vanillin required 1 mol eq. cyclopentanone and 1.2 mol eq. urea. According to our observation, for a concentration higher than 2 mmol van-2-van employed, the mixture started turning into a red-colored gel thus preventing

the stirring process. Another important observation is that the polymer solution in DMSO could be precipitated in water, but this caused a much higher water content in the polymer, interfering with the actual yield of polymerization. Acetone was a more desirable solvent to precipitate the polymers, as it removed impurities including leftover DMSO and starting materials, in addition to the volatility, requiring less energy to dry the polymer samples.

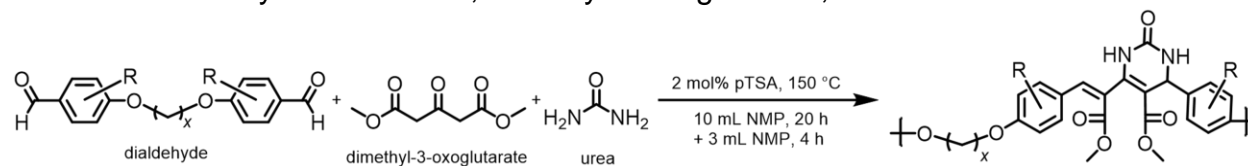
As tabulated in Table 5-1, the polymerization conditions that employed 6, 3, and 1 mol% vitamin B1 afforded polymers with: number average molecular weight (M_n) of 13,000, 8,000, and 2,000 Da; dispersity indices (\mathcal{D}) of 4.5, 3.1, and 2.1; and yields of 92.9%, 47.3%, and 78.6%, respectively. The temperature upon 5% mass loss ($T_{5\%}$) was up to 265 °C; all of the $T_{5\%}$ data were obtained after drying at 130 °C under nitrogen for 30 minutes in the TGA (thermogravimetric analysis) instrument. However, there were neither T_g nor T_m observed with DSC (differential scanning calorimetry) analysis of this polymer series. Consequently, the project shifted to a different type of ketone that also has two nucleophilic sites: dimethyl 3-oxoglutarate.

Poly-DHMP analogue from dimethyl 3-oxoglutarate

Dimethyl 3-oxoglutarate is a β -ketoester that can be derived from citric acid which naturally exists in citrus fruits.²³² The conditions of the reactions were adapted from the reaction using cyclopentanone above, except NMP (N-methyl-2-pyrrolidone) was used as the solvent, and 2 mol% pTSA as the catalyst. These changes were due to the polymerization using dimethyl 3-oxoglutarate requiring a much higher temperature than cyclopentanone (150 °C versus 80 °C).

Later, several polymerizations using different conditions were attempted (see Chapter 6). However, the \mathcal{D} values of the synthesized polymers were broad. Our assumption was the high viscosity of the polymers in the solution after reaching a certain molecular weight size impeded the stirring process. Thus, a small additional amount of NMP (3 mL) was added after 20 hours of reaction in order to dilute the polymer and lower the viscosity of solution; then the reaction was continued for four more hours. This definitely solved the viscosity issue as the synthesized poly-DHMP from van-2-van had a \mathcal{D} of 2.8 and a reasonably high M_n of 11,700 using this adaptation condition.

Table 5-2. Polymerization results of poly-DHMP analogues from bioaromatic dialdehyde monomers, dimethyl 3-oxoglutarate, and urea. ^a



| Entry | Dialdehyde | Yield ^b (%) | M_n ^c (Da) | M_w ^c (Da) | \mathcal{D} ^c | $T_{5\%}$ ^d (°C) | T_g ^e (°C) |
|-------|-------------|---------------------------|-------------------------|-------------------------|----------------------------|--------------------------------|----------------------------|
| 1 | 4HB-2-4HB | 48.6 | 8,400 | 55,600 | 6.8 | 261 | ^f |
| 2 | van-2-van | 31.9 | 11,700 | 33,500 | 2.8 | 283 | 180 |
| 3 | syr-2-syr | 34.3 | 14,500 | 49,200 | 3.4 | 272 | 198 |
| 4 | evan-2-evan | 27.2 | 12,000 | 36,900 | 3.1 | 293 | 169 |
| 5 | 4HB-3-4HB | 40.5 | 8,400 | 33,400 | 4.0 | 245 | ^f |
| 6 | van-3-van | 35.8 | 9,000 | 30,900 | 3.4 | 292 | 177 |
| 7 | syr-3-syr | 16.3 | 13,600 | 37,200 | 2.7 | 283 | 194 |
| 8 | evan-3-evan | 24.0 | 11,600 | 39,100 | 3.4 | 264 | 159 |

^aReaction conducted in NMP using 2 mol% pTSA at 80 °C for 24 hours. ^bYield of recovered product. ^cDetermined by HFIP GPC. ^dTemperature reported upon 5% mass loss. ^eDetermined by DSC.

Table 5-2 depicts a series of poly-DHMP analogues synthesized from dimethyl 3-oxoglutarate, urea, and bioaromatic dialdehyde monomers. There is apparently some correlation between the aromatic substituents with the obtained M_n . The polymers derived from 4HB (4-hydroxybenzaldehyde) had the lowest M_n and broadest \mathcal{D} ;

particularly, 4HB-2-4HB had a M_n of 8,200 with a broad \mathcal{D} of 6.8. As the number of methoxy groups increased, it seemed to also increase the obtained M_n , such as van-2-van ($M_n = 11,700$) versus syr-2-syr ($M_n = 14,500$), and van-3-van ($M_n = 9,000$) versus syr-3-syr ($M_n = 13,600$). One possible explanation was the methoxy substituent acted as an electron donating group that activated the aromatic ring thus facilitating the polymerization reaction.

The polymer series exhibited excellent thermal properties with $T_{5\%}$ ranging from 245 °C to 293 °C and T_g ranging from 159 °C to 198 °C. There was no observed T_g or T_m for polymers from 4HB-2-4HB and 4HB-3-4HB. This coincided with the reported work on polyacetal ethers, where there was also no observed T_g for 4HB-2-4HB polymers.⁷ On the other hand, the rest of the polymer series followed the logical structure–property relationship. Again, each additional methoxy group increased T_g by raising conformational energy barriers while ignoring its contribution to free volume. As a comparison, polymers from syr-2-syr (two methoxy groups per aromatic ring) and van-2-van (one methoxy group per aromatic ring) displayed T_g values of 198 °C and 180 °C, respectively; the difference was 18 °C. Meanwhile, the ethoxy group lowered the T_g of polymers due to the effect of free volume, as can be seen from the evan-2-evan polymer with a T_g of 169 °C. Lastly, there was also an observable change of T_g for the additional methylene spacer. Indeed, the longer methylene spacers have more long range polymer mobility while providing additional flexibility to the main chain, thus lowering the overall T_g . Polymers from van-3-van ($T_g = 177$ °C), evan-3-evan ($T_g = 159$ °C), and syr-3-syr ($T_g = 194$ °C) exhibited lower T_g values versus their shorter methylene spacer counterparts.

Conclusions

The concept of multicomponent reaction has existed since 1850, when Strecker introduced the well-known Strecker synthesis.²³³ Later, the Biginelli multicomponent reaction was published in 1891.²²⁹ Nevertheless, the application of multicomponent reaction to polymerization did not occur until much later in 1999.²²⁶ Multicomponent polymerization is indeed a versatile method of reacting small molecules, creating tunable polymer series. In this work, we produced a series of biorenewable polymers that displayed excellent thermal properties via a modified Biginelli reaction.

The optimization study was directed by a viscosity observation, which resulted in the additional of a small amount of solvent that could facilitate the polymerization. This procedure was then applied to eight types of dialdehyde components that were used for polymer series from dimethyl 3-oxoglutarate. The synthesized polymer series had a decent number average molecular weight (M_n) ranging from 8,200 to 14,500 Da and a glass transition temperature (T_g) ranging from 159 °C to 198 °C. These thermal properties far surpass the current household commodity plastics for high temperature packaging application such as polystyrene ($T_g = 100$ °C). However, further study on the mechanical properties and degradation studies are needed for these polymers in order to fully assess their viabilities as commodity plastics.

CHAPTER 6 EXPERIMENTAL

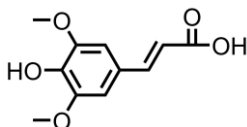
Chapter 1

Materials

Brassica carinata meal pellets were donated by Agrisoma Biosciences, Inc., Gatineau, Quebec, and were ground before use. Sinapic acid was purchased from Henan Tianfu Chemical Co., Ltd. via Alibaba.com. 2-Chloroethanol and 3-chloropropanol were purchased from Acros Organics. 6-Chlorohexanol was purchased from Alfa Aesar. Ethyl acetate, sodium hydroxide, sodium iodide, and sodium chloride were purchased from Fisher Chemical. NMR solvents, including deuterated chloroform (CDCl_3), deuterated dimethyl sulfoxide ($\text{DMSO}-d_6$), and deuterated trifluoroacetic acid ($\text{TFA}-d$) were purchased from Cambridge Isotope Laboratories. All the chemicals, unless expressly mentioned, were utilized without further purification.

Extraction

Extraction of sinapic acid using base hydrolysis



20 g of dried, ground, low-glucosinolate *carinata* meal, and 500 mL of 1 M NaOH (aq), were stirred in a 1 L Erlenmeyer flask for 48 hours at 60 °C. Upon completion, the solution was acidified to pH = 1 with 35 mL of concentrated H_3PO_4 . The resulting mixture was centrifuged at 3500 rpm for 10 mins. The solids were filtered out, and the remaining solution was extracted with 3 x 100 mL portions of ethyl acetate. The organic (ethyl acetate) portion was washed with copious amounts of water, followed by brine (saturated NaCl solution), and then dried over anhydrous MgSO_4 . The ethyl acetate was

then removed by rotary evaporation leaving behind 0.322 g of fairly pure sinapic acid (SA) in 1.61% yield. ^1H NMR ($\text{DMSO-}d_6$) δ ppm 3.80 (s, 6 H), 6.41 (d, 1 H), 6.98 (s, 2 H), 7.49 (d, 1 H), 8.89 (br. s., 1 H), 12.13 (br. s., 1 H). ^{13}C NMR ($\text{DMSO-}d_6$) δ ppm 56.1, 106.1, 116.1, 123.8, 138.1, 144.8, 153.1, 168.0.

Extraction of sinapic acid using sonication

10 g of dried, ground, low-glucosinolate carinata meal, and 250 mL of 1 M NaOH (aq) were loaded into a 500 mL round bottom flask. The solution was then sonicated using the sonication water bath for 16 hours. Upon completion, the solution was acidified to pH = 1 with 35 mL of concentrated H_3PO_4 . The resulting mixture was centrifuged at 3500 rpm for 10 mins. The solids were filtered out, and the remaining solution was extracted with 3 x 100 mL portions of ethyl acetate. The organic (ethyl acetate) portion was washed with copious amounts of water, followed by brine (saturated NaCl solution), and then dried over anhydrous MgSO_4 . The ethyl acetate was then removed by rotary evaporation leaving behind 0.105 g of fairly pure sinapic acid (SA) in 1.05% yield. ^1H NMR ($\text{DMSO-}d_6$) δ ppm 3.80 (s, 6 H), 6.41 (d, 1 H), 6.98 (s, 2 H), 7.49 (d, 1 H), 8.90 (br. s., 1 H), 12.19 (br. s., 1 H).

Extraction of sinapic acid using methanol

4 g of dried and ground low-glucosinolate carinata meal, and 100 mL of 70% v/v MeOH/ H_2O , were stirred in a 250 mL Erlenmeyer flask for 2 hours at 60 °C. The solids were then filtered out using gravity filtration, and the solvents were then removed by rotatory evaporation leaving behind a brown oil. Based on ^1H NMR ($\text{DMSO-}d_6$) characterization, some notable peaks of the brown oil were 3.80 (s, 6 H), 6.55 (d, 1 H), 7.03 (s, 2 H), 7.61 (d, 1 H), 8.04 (br. s., 0.43 H). After obtaining the brown oil, 50 mL of

0.5 M NaOH (aq) was added into the oil and the solution was transferred into a 100 mL Erlenmeyer flask. The solution was stirred for 2 hours at 60 °C. Upon completion, the solution was acidified with 1 M HCl until it reached pH = 1. The precipitates were filtered out using gravity filtration, and the remaining solution was extracted with 3 x 50 mL portions of ethyl acetate. The organic (ethyl acetate) portion was washed with copious amounts of water, followed by brine (saturated NaCl solution), and then dried over anhydrous MgSO₄. The ethyl acetate was then removed by rotary evaporation leaving behind 60 mg of fairly pure sinapic acid (SA) in 1.5% yield. ¹H NMR (DMSO-*d*₆) δ ppm 3.81 (s, 6 H), 6.43 (d, 1 H), 7.00 (s, 2 H), 7.50 (d, 1 H), 8.91 (br. s., 1 H), 12.15 (br. s., 1 H).

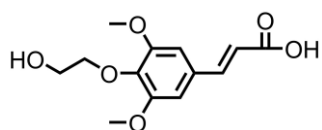
Extraction of sinapic acid using ethanol

5 g of dried and ground low-glucosinolate carinata meal was placed in a thimble, and was then loaded into a main chamber of Soxhlet extractor apparatus. The Soxhlet extractor was fitted with a 250 mL round bottom flask containing 125 mL of 95% v/v EtOH/H₂O. The Soxhlet extraction was performed by refluxing the solvent for 24 hours. Upon completion, the solvents were removed by rotary evaporation leaving behind a brown oil. Based on its ¹H NMR (DMSO-*d*₆) characterization, some notable peaks of the brown oil were 3.80 (s, 6 H), 6.55 (d, 1 H), 7.03 (s, 2 H), 7.61 (d, 1 H). After obtaining the brown oil, 50 mL of 0.5 M NaOH (aq) was added into the oil and the solution was transferred into a 100 mL Erlenmeyer flask. The solution was stirred for 2 hours at 60 °C. Upon completion, the solution was acidified with 1 M HCl until it reached pH = 1. The precipitates were filtered out using gravity filtration, and the remaining solution was extracted with 3 x 50 mL portions of ethyl acetate. The organic (ethyl acetate) portion

was washed with copious amounts of water, followed by brine (saturated NaCl solution), and then dried over anhydrous MgSO₄. The ethyl acetate was then removed by rotary evaporation leaving behind 0.18 g of fairly pure sinapic acid (SA) in 3.6% yield. ¹H NMR (DMSO-*d*₆) δ ppm 3.79 (s, 6 H), 6.41 (d, 1 H), 6.98 (s, 2 H), 7.49 (d, 1 H), 8.89 (br. s., 1 H), 12.03 (br. s., 1 H).

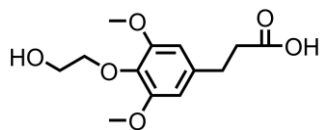
Monomer Synthesis

Synthesis of hydroxyethylsinapic acid



A mixture of sinapic acid (28.92 g, 0.129 mol) and sodium iodide (3.35 g, 0.022 mol) was dissolved in 270 mL of 1.1 M NaOH (aq) solution. The solution was stirred and heated at 85 °C. After 30 minutes of heating, 2-chloroethanol (12.6 mL, 0.185 mol) was slowly loaded into the solution. The solution was then refluxed for 36 hours at 105 °C. Next, the solution was washed with ethyl acetate and the aqueous layer was acidified with concentrated hydrochloric acid until the desired product precipitated as a white powder. The product was isolated by gravity filtration, titrated with ethanol, and vacuum dried for 5 hours. 25.233 g of dry white powder was obtained in 74.03% yield. ¹H NMR (DMSO-*d*₆) δ ppm 3.61 (t, 2 H), 3.81 (s, 6 H), 3.90 (t, 2 H), 4.56 (br. s., 1 H), 6.53 (d, 1 H), 7.03 (s, 2 H), 7.53 (d, 1 H), 12.27 (br. s., 1 H). ¹³C NMR (DMSO-*d*₆) δ ppm 56.1, 60.2, 74.2, 105.8, 116.3, 128.7, 137.8, 144.2, 153.1, 167.7.

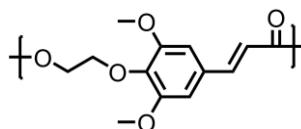
Synthesis of hydroxyethylidihydrosinapic acid



Hydroxyethylsinapic acid (22.0 g, 0.083 mol) and 10% Pd on Carbon (1.77 g, 0.00167 mol) were mixed in 78 mL of methanol and 145 mL of THF. The mixture was hydrogenated for 4 hours under 60 psi of H₂ gas. The reaction was then vacuum filtered through a celite filter bed. The filtrate was dried by a rotary evaporator and dissolved in THF. The product was then precipitated upon addition of cold hexane and was isolated by gravity filtration. After drying under vacuum, 7.697 g of dry white powder was obtained in 35.51% yield. ¹H NMR (CDCl₃) δ ppm 2.68 (t, 2 H), 2.91 (t, 2 H), 3.72 (t, 2 H), 3.85 (s, 6 H), 4.12 (t, 2 H), 6.45 (s, 2 H). ¹³C NMR (CDCl₃) δ ppm 30.8, 35.3, 55.8, 61.1, 74.9, 105.0, 134.5, 136.2, 152.9, 175.7.

Polymer Synthesis

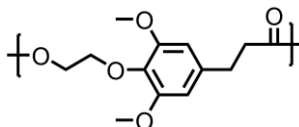
Polyethylene sinapate



Hydroxyethylsinapic acid (1.50 g, 5.7 mmol) and Sb₂O₃ (16.6 mg, 1 mol%) were loaded into a 50 mL round bottom flask. This flask was fitted with a bump trap and attached to the Schlenk line. The system was then purged with nitrogen and vacuum three times. The mixture was melted under a nitrogen atmosphere gradually from 200 °C to 250 °C for 4 hours. Later, the system was placed under dynamic vacuum for 6 hours to remove the condensation byproduct, thus increasing the degree of the polymerization. Once cool, the polymer was melted for removal from the flask and used

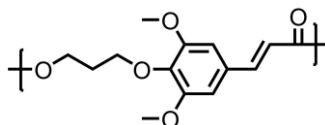
without further purification. 0.841 g of polymer was obtained in 60.2% yield. ^1H NMR ($\text{CDCl}_3/\text{TFA}-d$) δ ppm 3.87 (s, 6 H), 4.37 (t, 2 H), 4.52 (t, 2 H), 6.48 (d, 1 H), 6.79 (s, 2 H), 7.67 (d, 1 H). ^{13}C NMR ($\text{CDCl}_3/\text{TFA}-d$) δ ppm 56.4, 63.0, 70.0, 105.6, 113.5, 115.8, 134.3, 139.1, 153.6, 179.7.

Polyethylene dihydrosinapate



Hydroxyethyl dihydrosinapic acid (1.00 g, 3.76 mmol) and Sb_2O_3 (11 mg, 1 mol%) were loaded into a 50 mL round bottom flask. This flask was fitted with a bump trap and attached to the Schlenk line. The system was then purged with nitrogen and vacuum three times. The mixture was melted under a nitrogen atmosphere gradually from 150 °C to 200 °C for 4 hours. Later the system was placed under dynamic vacuum for 6 hours to remove the condensation byproduct, thus increasing the degree of the polymerization. Once cool, the polymer was melted for removal from the flask and used without further purification. 0.702 g of polymer was obtained in 74.8% yield. ^1H NMR (CDCl_3) δ ppm 2.68 (t, 2 H), 2.91 (t, 2 H), 3.80 (s, 6 H), 4.17 (t, 2 H), 4.36 (t, 2 H), 6.43 (s, 2 H). ^{13}C NMR (CDCl_3) δ ppm 31.3, 36.0, 56.1, 63.9, 70.8, 105.3, 134.9, 136.8, 153.2, 172.8.

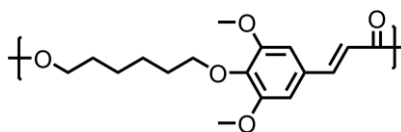
Polypropylene sinapate



Hydroxypropyl sinapic acid (1.50 g, 5.3 mmol) and Sb_2O_3 (15.5 mg, 1 mol%) were loaded into a 50 mL round bottom flask. This flask was fitted with a bump trap and

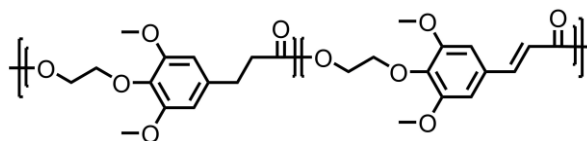
attached to the Schlenk line. The system was then purged with nitrogen and vacuum three times. The mixture was melted under a nitrogen atmosphere gradually from 180 °C to 220 °C for 5 hours. Later, the system was placed under dynamic vacuum for 8 hours to remove the condensation byproduct, thus increasing the degree of the polymerization. Once cool, the polymer was melted to for removal from the flask and used without further purification. 0.979 g of polymer was obtained in 69.7% yield. ¹H NMR (CDCl₃) δ ppm 2.16 (m, 2 H), 3.88 (s, 6 H), 4.20 (t, 2 H), 4.51 (t, 2 H), 6.42 (d, 1 H), 6.77 (s, 2 H), 7.66 (d, 1 H). ¹³C NMR (CDCl₃) δ ppm 29.1, 56.2, 62.8, 70.2, 105.6, 115.6, 130.1, 138.6, 146.1, 153.4, 166.7.

Polyhexylene sinapate



Hydroxyhexylsinapic acid (1.50 g, 4.62 mmol) and Sb₂O₃ (13.5 mg, 1 mol%) were loaded into a 50 mL round bottom flask. This flask was fitted with a bump trap and attached to the Schlenk line. The system was then purged with nitrogen and vacuum three times. The mixture was melted under a nitrogen atmosphere gradually from 155 °C to 200 °C for 5 hours. Later, the system was placed under dynamic vacuum for 8 hours to remove the condensation byproduct, thus increasing the degree of the polymerization. Once cool, the polymer was melted for removal from the flask and used without further purification. 1.173 g of polymer was obtained in 74.2% yield. ¹H NMR (CDCl₃) δ ppm 1.49 (m, 2 H), 1.55 (m, 4 H), 1.75 (m, 2 H), 3.87 (s, 6 H), 4.01 (t, 2 H), 4.22 (t, 2 H), 6.34 (d, 1 H), 6.75 (s, 2 H), 7.60 (d, 1 H). ¹³C NMR (CDCl₃) δ ppm 25.5, 28.5, 29.8, 55.9, 64.3, 73.1, 105.1, 117.1, 129.5, 139.2, 144.3, 153.4, 166.8.

Copoly(hydroxyethyldihydroxysinapic acid/hydroxyethylsinapic acid) [50:50]



Hydroxyethyldihydroxysinapic acid (0.532 g, 2 mmol), hydroxyethylsinapic acid (0.528 g, 2 mmol), and Sb_2O_3 (12 mg, 1 mol%) were loaded into a 50 mL round bottom flask. This flask was fitted with a bump trap and attached to the Schlenk line. The system was then purged with nitrogen and vacuum three times. The mixture was melted under a nitrogen atmosphere gradually from 170 °C to 220 °C for 4 hours. Later, the system was placed under dynamic vacuum for 6 hours to remove the condensation byproduct, thus increasing the degree of the polymerization. Once cool, the polymer was melted for removal from the flask and used without further purification. 0.901 g of polymer was obtained in 91.2% yield. ^1H NMR ($\text{CDCl}_3/\text{TFA}-d$) δ ppm 2.75, 2.93 (m, 5.96 H), 3.82, 3.89 (m, 18.01 H), 4.26, 4.33, 4.41, 4.52 (m, 11.15 H), 6.47 (m, 1.42 H), 6.51 (d, 1 H), 6.82 (m, 2.05 H), 7.73 (d, 1 H). ^{13}C NMR ($\text{CDCl}_3/\text{TFA}-d$) δ ppm 31.1, 36.0, 56.0, 64.6, 71.0, 105.6, 111.0, 113.3, 115.6, 134.0, 137.0, 152.7, 175.6.

Summary of Extraction Data

Table 6-1. Various extraction results. ^a

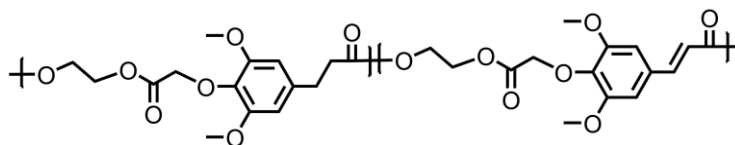
| Entry | m carinata (g) | [NaOH] (M) | V solution (mL) | Time (h) | m sinapic acid (g) ^f | Yield (%) ^g |
|-----------------|----------------|------------|-----------------|----------|---------------------------------|------------------------|
| 1 | 2 | 0.5 | 50 | 2 | 0.040 | 2.00 |
| 2 | 10 | 1 | 250 | 2 | 0.131 | 1.31 |
| 3 | 10 | 1 | 250 | 24 | 0.134 | 1.34 |
| 4 | 10 | 1 | 250 | 24 | 0.153 | 1.53 |
| 5 | 20 | 1 | 500 | 24 | 0.171 | 0.86 |
| 6 | 20 | 1 | 500 | 48 | 0.322 | 1.61 |
| 7 | 20 | 1 | 500 | 48 | 0.188 | 0.94 |
| 8 | 20 | 1 | 500 | 48 | 0.185 | 0.93 |
| 9 | 20 | 1 | 500 | 48 | 0.172 | 0.86 |
| 10 | 20 | 1 | 500 | 48 | 0.183 | 0.92 |
| 11 | 20 | 1 | 500 | 48 | 0.255 | 1.28 |
| 12 ^b | 2 | 0.5 | 50 | 2 | 0.046 | 2.30 |
| 13 ^b | 2 | 0.5 | 50 | 2 | 0.026 | 1.30 |
| 14 ^b | 10 | 1 | 250 | 16 | 0.105 | 1.05 |
| 15 ^c | 10 | 2 | 250 | 20 | 0.253 | 2.53 |
| 16 ^d | 4 | 0.5 | 50 | 2 | 0.060 | 1.50 |
| 17 ^e | 5 | 0.5 | 50 | 2 | 0.180 | 3.60 |

^aThe hydrolysis was performed in basic aqueous solution at 60 °C and stirred for a certain amount of time, as noted. ^bUltrasound-assisted hydrolysis in basic aqueous solution. ^cThe solution was heated to reflux at 117 °C. ^dCarinata was washed with 70% MeOH, and the dissolved portion was further used for the hydrolysis in basic aqueous solution at 60 °C and stirred for 2 hours. ^eCarinata was washed with 95% EtOH using Soxhlet apparatus, and the dissolved portion was further used for the hydrolysis in basic aqueous solution at 60 °C and stirred for 2 hours. ^fMass of recovered solid after the extraction. ^gPercent yield was from the mass of sinapic acid divided by the mass of carinata seed meal.

Chapter 2

Polymer synthesis

Copoly(ethyleneglycolate dihydrosinapate/ethyleneglycolate sinapate) [90:10]



Dimethylglycolate dihydrosinapate (1.124 g, 3.60 mmol), dimethylglycolate sinapate (0.124 g, 0.40 mmol), ethylene glycol (0.298 g, 4.80 mmol), and Sb_2O_3 (23.3 mg, 2 mol%) were loaded into a 50 mL round bottom flask. This flask was fitted with a bump trap and attached to the Schlenk line. The system was then purged with nitrogen and vacuum three times. The mixture was melted under a nitrogen atmosphere at 160 °C for 2 hours, at 180 °C for 16 hours, and at 200 °C for 2 hours. Later, the system was placed under dynamic vacuum and was heated gradually from 200 °C to 215 °C for 5 hours to remove the condensation byproduct, thus increasing the degree of polymerization. Once cool, the polymer was melted for removal from the flask and used without further purification. 1.119 g of polymer was obtained in 90.2% yield. ^1H NMR (CDCl_3) δ ppm 2.64, 2.88 (m, 84.53 H), 3.81, 3.87 (m, 150.09 H), 4.28, 4.41, 4.61, 4.70 (m, 140.10 H), 6.35 (d, 2.39 H), 6.40 (s, 41.40 H), 6.75 (s, 3.52 H), 7.60 (d, 1 H). ^{13}C NMR (CDCl_3) δ ppm 31.1, 35.7, 56.1, 62.3, 63.0, 69.3, 105.2, 105.3, 112.5, 117.8, 127.7, 129.4, 136.2, 137.9, 152.6, 160.8, 167.0, 169.7, 177.0.

Copoly(ethyleneglycolate dihydrosinapate/ethyleneglycolate sinapate) [70:30]

Dimethylglycolate dihydrosinapate (0.874 g, 2.80 mmol), dimethylglycolate sinapate (0.372 g, 1.20 mmol), ethylene glycol (0.298 g, 4.80 mmol), and Sb_2O_3 (23.3 mg, 2 mol%) were loaded into a 50 mL round bottom flask. This flask was fitted with a

bump trap and attached to the Schlenk line. The system was then purged with nitrogen and vacuum three times. The mixture was melted under a nitrogen atmosphere at 170 °C for 1 hour, at 185 °C for 16 hours, and at 200 °C for 2 hours. Later, the system was placed under dynamic vacuum and was heated gradually from 200 °C to 220 °C for 5 hours to remove the condensation byproduct, thus increasing the degree of polymerization. Once cool, the polymer was melted for removal from the flask and used without further purification. 1.164 g of polymer was obtained in 94.0% yield. ¹H NMR (CDCl₃) δ ppm 2.63, 2.87 (m, 12.76 H), 3.80, 3.86 (m, 29.07 H), 4.27, 4.41, 4.60, 4.69 (m, 26.74 H), 6.34 (d, 1.03 H), 6.40 (s, 6.18 H), 6.74 (s, 2.29 H), 7.60 (d, 1 H). ¹³C NMR (CDCl₃) δ ppm 31.1, 35.6, 56.1, 62.2, 63.5, 69.3, 105.2, 105.3, 112.4, 120.8, 130.0, 134.6, 136.5, 145.2, 152.6, 162.5, 169.2, 172.4, 177.0.

Copoly(ethyleneglycolate dihydrosinapate/ethyleneglycolate sinapate) [50:50]

Dimethylglycolate dihydrosinapate (0.6246 g, 2.0 mmol), dimethylglycolate sinapate (0.6206 g, 2.0 mmol), ethylene glycol (0.298 g, 4.80 mmol), and Sb₂O₃ (23.3 mg, 2 mol%) were loaded into a 50 mL round bottom flask. This flask was fitted with a bump trap and attached to the Schlenk line. The system was then purged with nitrogen and vacuum three times. The mixture was melted under a nitrogen atmosphere at 170 °C for 1 hour, at 185 °C for 16 hours, and at 200 °C for 2 hours. Later, the system was placed under dynamic vacuum and was heated gradually from 200 °C to 225 °C for 5 hours to remove the condensation byproduct, thus increasing the degree of polymerization. Once cool, the polymer was melted for removal from the flask and used without further purification. 1.082 g of polymer was obtained in 87.5% yield. ¹H NMR (CDCl₃) δ ppm 2.63, 2.88 (m, 5.06 H), 3.81, 3.86 (m, 15.07 H), 4.32, 4.42, 4.61, 4.70

(m, 13.75 H), 6.34 (d, 0.89 H), 6.40 (s, 2.15 H), 6.74 (s, 1.97 H), 7.59 (d, 1 H). ^{13}C NMR (CDCl_3) δ ppm 31.0, 35.9, 56.4, 62.6, 64.1, 69.4, 105.50, 105.54, 113.4, 121.9, 130.4, 134.8, 135.9, 144.8, 152.8, 162.5, 171.2, 174.2, 177.0.

Copoly(ethyleneglycolate dihydrosinapate/ethyleneglycolate sinapate) [30:70]

Dimethylglycolate dihydrosinapate (0.3748 g, 1.20 mmol), dimethylglycolate sinapate (0.8668 g, 2.80 mmol), ethylene glycol (0.298 g, 4.80 mmol), and Sb_2O_3 (23.3 mg, 2 mol%) were loaded into a 50 mL round bottom flask. This flask was fitted with a bump trap and attached to the Schlenk line. The system was then purged with nitrogen and vacuum three times. The mixture was melted under a nitrogen atmosphere at 180 °C for 1 hour, at 190 °C for 16 hours, and at 200 °C for 2 hours. Later, the system was placed under dynamic vacuum and was heated gradually from 200 °C to 230 °C for 5 hours to remove the condensation byproduct thus increasing the degree of polymerization. Once cool, the polymer was melted for removal from the flask and used without further purification. 1.082 g of polymer was obtained in 87.6% yield. ^1H NMR (CDCl_3) δ ppm 2.65, 2.87 (m, 1.96 H), 3.81, 3.87 (m, 10.47 H), 4.28, 4.43, 4.61, 4.70 (m, 9.53 H), 6.34 (d, 0.85 H), 6.40 (s, 1.13 H), 6.74 (s, 2.11 H), 7.59 (d, 1 H). ^{13}C NMR (CDCl_3) δ ppm 31.1, 35.6, 56.2, 62.4, 64.1, 69.2, 105.1, 105.3, 111.5, 116.8, 130.0, 133.6, 137.9, 141.9, 152.6, 162.3, 167.1, 169.7, 178.1.

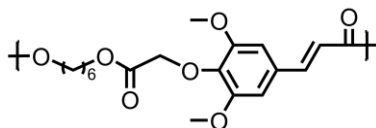
Copoly(ethyleneglycolate dihydrosinapate/ethyleneglycolate sinapate) [10:90]

Dimethylglycolate dihydrosinapate (0.1249 g, 0.40 mmol), dimethylglycolate sinapate (1.1171 g, 3.60 mmol), ethylene glycol (0.298 g, 4.80 mmol), and Sb_2O_3 (23.3 mg, 2 mol%) were loaded into a 50 mL round bottom flask. This flask was fitted with a bump trap and attached to the Schlenk line. The system was then purged with nitrogen

and vacuum three times. The mixture was melted under a nitrogen atmosphere at 180 °C for 1 hour, and at 200 °C for 16 hours. Later, the system was placed under dynamic vacuum and was heated gradually from 200 °C to 235 °C for 7 hours to remove the condensation byproduct, thus increasing the degree of polymerization. Once cool, the polymer was melted for removal from the flask and used without further purification.

1.054 g of polymer was obtained in 85.4% yield. ¹H NMR (CDCl₃) δ ppm 2.63, 2.88 (m, 0.49 H), 3.81, 3.87 (m, 8.67 H), 4.32, 4.43, 4.61, 4.70 (m, 7.38 H), 6.35 (d, 0.85 H), 6.40 (s, 0.46 H), 6.74 (s, 2.13 H), 7.56 (d, 1 H). ¹³C NMR (CDCl₃) δ ppm 33.3, 38.0, 56.2, 62.4, 63.8, 69.2, 105.3, 105.4, 112.5, 116.8, 130.0, 134.4, 138.2, 145.2, 152.7, 162.3, 169.0, 172.3, 176.2.

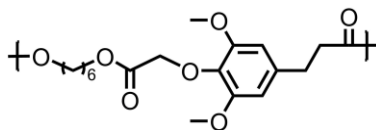
Polyhexyleneglycolate sinapate



Dimethylglycolate sinapate (1.50 g, 4.834 mmol), 1,6-hexanediol (0.6856 g, 5.801 mmol), and Sb₂O₃ (28.2 mg, 2 mol%) were loaded into a 50 mL round bottom flask. This flask was fitted with a bump trap and attached to the Schlenk line. The system was then purged with nitrogen and vacuum three times. The mixture was melted under a nitrogen atmosphere at 180 °C for 1 hour, and at 200 °C for 16 hours. Later, the system was placed under dynamic vacuum and was heated gradually from 200 °C to 240 °C for 7 hours to remove the condensation byproduct, thus increasing the degree of polymerization. Once cool, the polymer was melted for removal from the flask and used without further purification. 1.702 g of polymer was obtained in 96.7% yield. ¹H NMR (CDCl₃) δ ppm 1.43 (m, 4 H), 1.70 (m, 4 H), 3.87 (s, 6 H), 4.21 (m, 4 H), 4.68 (s, 2 H),

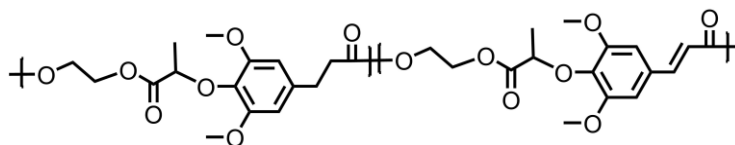
6.34 (d, 1 H), 6.75 (s, 2 H), 7.58 (d, 1 H). ^{13}C NMR (CDCl_3) δ ppm 19.4, 21.7, 24.5, 27.1, 56.2, 61.7, 65.8, 69.3, 105.3, 112.5, 127.3, 141.7, 147.8, 156.8, 165.8, 168.2.

Polyhexyleneglycolate dihydrosinapate



Dimethylglycolate dihydrosinapate (1.50 g, 4.803 mmol), 1,6-hexanediol (0.6807 g, 5.760 mmol), and Sb_2O_3 (28.0 mg, 2 mol%) were loaded into a 50 mL round bottom flask. This flask was fitted with a bump trap and attached to the Schlenk line. The system was then purged with nitrogen and vacuum three times. The mixture was melted under a nitrogen atmosphere at 160 °C for 2 hours, at 180 °C for 16 hours, and at 200 °C for 2 hours. Later, the system was placed under dynamic vacuum and was heated gradually from 200 °C to 215 °C for 5 hours to remove the condensation byproduct, thus increasing the degree of polymerization. Once cool, the polymer was melted for removal from the flask and used without further purification. 1.442 g of polymer was obtained in 82.0% yield. ^1H NMR (CDCl_3) δ ppm 1.36 (m, 4 H), 1.62, 1.67 (m, 4 H), 2.60 (t, 2 H), 2.88 (t, 2 H), 3.81 (s, 6 H), 4.07 (t, 2 H), 4.18 (t, 2 H), 4.58 (s, 2 H), 6.40 (s, 2 H). ^{13}C NMR (CDCl_3) δ ppm 25.4, 28.5, 31.3, 35.9, 56.1, 64.4, 69.6, 105.2, 134.7, 136.6, 152.6, 169.5, 172.8.

Copoly(ethylenelactate dihydrosinapate/ethylenelactate sinapate) [70:30]



Dimethyl lactate dihydrosinapate (1.0508 g, 3.22 mmol), dimethyl lactate sinapate (0.4476 g, 1.38 mmol), ethylene glycol (0.2855 g, 4.60 mmol), and Sb_2O_3 (26.82 mg, 2 mol%) were loaded into a 50 mL round bottom flask. This flask was fitted with a bump trap and attached to the Schlenk line. The system was then purged with nitrogen and vacuum three times. The mixture was melted under a nitrogen atmosphere at 170 °C for 2 hours, 185 °C for 15 hours, and at 200 °C for 2 hours. Later, the system was placed under dynamic vacuum and was heated gradually from 200 °C to 220 °C for 5 hours to remove the condensation byproduct, thus increasing the degree of polymerization. Once cool, the polymer was melted for removal from the flask and used without further purification. 1.153 g of polymer was obtained in 77.4% yield. ^1H NMR (CDCl_3) δ ppm 1.53 (m, 18.16 H), 2.63, 2.86 (m, 20.10 H), 3.79, 3.84 (m, 44.36 H), 4.31, 4.38, 4.61, 4.76 (m, 32.39 H), 6.32 (m, 1.06 H), 6.39 (m, 9.61 H), 6.73 (m, 2.10 H), 7.59 (d, 1 H). ^{13}C NMR (CDCl_3) δ ppm 18.3, 29.2, 34.7, 56.1, 62.2, 63.0, 68.9, 73.9, 103.1, 105.2, 115.1, 123.8, 127.7, 137.0, 139.6, 141.6, 157.0, 166.2, 167.1, 173.2.

Copoly(ethylenelactate dihydrosinapate/ethylenelactate sinapate) [50:50]

Dimethyl lactate dihydrosinapate (0.7506 g, 2.30 mmol), dimethyl lactate sinapate (0.7459 g, 2.30 mmol), ethylene glycol (0.2855 g, 4.60 mmol), and Sb_2O_3 (26.82 mg, 2 mol%) were loaded into a 50 mL round bottom flask. This flask was fitted with a bump trap and attached to the Schlenk line. The system was then purged with nitrogen and vacuum three times. The mixture was melted under a nitrogen atmosphere at 170 °C for

2 hours, 185 °C for 15 hours, and at 200 °C for 2 hours. Later, the system was placed under dynamic vacuum and was heated gradually from 200 °C to 225 °C for 5 hours to remove the condensation byproduct, thus increasing the degree of polymerization.

Once cool, the polymer was melted for removal from the flask and used without further purification. 1.236 g of polymer was obtained in 83.1% yield. ¹H NMR (CDCl₃) δ ppm 1.54 (m, 7.55 H), 2.62, 2.88 (m, 8.14 H), 3.79, 3.84 (m, 23.58 H), 4.31, 4.38, 4.61, 4.74 (m, 15.05 H), 6.32 (m, 1.06 H), 6.39, 6.42 (m, 4.13 H), 6.73 (m, 2.32 H), 7.59 (d, 1 H). ¹³C NMR (CDCl₃) δ ppm 19.6, 30.2, 36.6, 56.0, 62.4, 63.8, 68.8, 73.7, 103.3, 105.5, 114.4, 122.8, 125.7, 137.9, 139.8, 143.3, 157.1, 165.7, 166.2, 172.6.

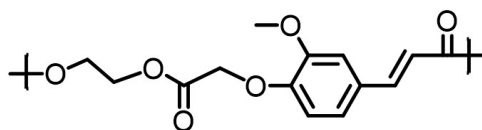
Copoly(ethylenelactate dihydrosinapate/ethylenelactate sinapate) [30:70]

Dimethylactate dihydrosinapate (0.4504 g, 1.38 mmol), dimethylactate sinapate (1.0443 g, 3.22 mmol), ethylene glycol (0.2855 g, 4.60 mmol), and Sb₂O₃ (26.82 mg, 2 mol%) were loaded into a 50 mL round bottom flask. This flask was fitted with a bump trap and attached to the Schlenk line. The system was then purged with nitrogen and vacuum three times. The mixture was melted under a nitrogen atmosphere at 180 °C for 2 hours, at 190 °C for 15 hours, and at 200 °C for 2 hours. Later, the system was placed under dynamic vacuum and was heated gradually from 200 °C to 230 °C for 5 hours to remove the condensation byproduct, thus increasing the degree of polymerization.

Once cool, the polymer was melted for removal from the flask and used without further purification. 1.20 g of polymer was obtained in 80.8% yield. ¹H NMR (CDCl₃) δ ppm 1.53 (m, 2.60 H), 2.62, 2.86 (m, 2.89 H), 3.79, 3.84 (m, 12.35 H), 4.38, 4.50, 4.63, 4.75 (m, 7.90 H), 6.35 (m, 0.67 H), 6.39 (m, 1.73 H), 6.73 (m, 2.07 H), 7.59 (d, 1 H). ¹³C NMR

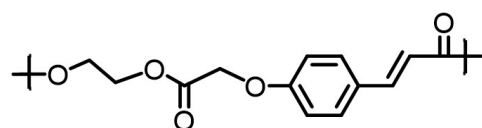
(CDCl₃) δ ppm 18.6, 27.9, 34.2, 54.3, 60.1, 62.2, 68.3, 73.4, 103.2, 105.4, 115.5, 123.5, 126.8, 137.7, 141.1, 142.3, 157.1, 166.2, 167.1, 173.0.

Polyethyleneglycolate ferulate



Dimethylglycolate ferulate (1.33 g, 4.745 mmol), ethylene glycol (0.3534 g, 5.694 mmol), and Sb₂O₃ (27.7 mg, 2 mol%) were loaded into a 50 mL round bottom flask. This flask was fitted with a bump trap and attached to the Schlenk line. The system was then purged with nitrogen and vacuum three times. The mixture was melted under a nitrogen atmosphere at 180 °C for 1 hour, and at 200 °C for 16 hours. Later, the system was placed under dynamic vacuum and was heated gradually from 200 °C to 240 °C for 7 hours to remove the condensation byproduct, thus increasing the degree of polymerization. Once cool, the polymer was melted for removal from the flask and used without further purification. 0.886 g of polymer was obtained in 67.1% yield. ¹H NMR (CDCl₃) δ ppm 3.90 (s, 3 H), 4.43, 4.52 (m, 4 H), 4.70, 4.77 (d, 2 H), 6.31 (m, 1 H), 6.80 (m, 1 H), 7.05 (m, 2 H), 7.58 (m, 1 H). ¹³C NMR (CDCl₃) δ ppm 55.9, 62.6, 63.0, 65.9, 110.5, 110.6, 113.5, 122.2, 128.6, 144.9, 149.2, 149.6, 166.6, 168.3.

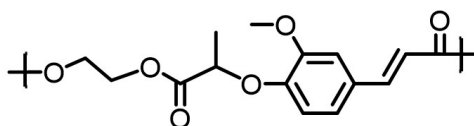
Polyethyleneglycolate coumarate



Dimethylglycolate coumarate (1.33 g, 5.315 mmol), ethylene glycol (0.3959 g, 6.378 mmol), and Sb₂O₃ (31.0 mg, 2 mol%) were loaded into a 50 mL round bottom flask. This flask was fitted with a bump trap and attached to the Schlenk line. The

system was then purged with nitrogen and vacuum three times. The mixture was melted under a nitrogen atmosphere at 180 °C for 1 hour, and at 200 °C for 16 hours. Later, the system was placed under dynamic vacuum and was heated gradually from 200 °C to 240 °C for 7 hours to remove the condensation byproduct, thus increasing the degree of polymerization. Once cool, the polymer was melted for removal from the flask and used without further purification. 1.059 g of polymer was obtained in 80.3% yield. ¹H NMR (CDCl₃) δ ppm 4.46 (m, 4 H), 4.63, 4.70 (m, 2 H), 6.30 (m, 1 H), 6.90 (m, 2 H), 7.46 (m, 2 H), 7.61 (m, 1 H). ¹³C NMR (CDCl₃) δ ppm 62.6, 64.9, 68.7, 114.9, 115.6, 127.9, 129.8, 144.8, 159.4, 166.7, 168.3.

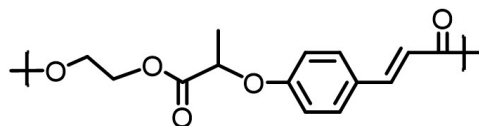
Polyethylenelactate ferulate



Dimethylacrylate ferulate (1.50 g, 5.10 mmol), ethylene glycol (0.3166 g, 5.10 mmol), and Sb₂O₃ (26.82 mg, 2 mol%) were loaded into a 50 mL round bottom flask. This flask was fitted with a bump trap and attached to the Schlenk line. The system was then purged with nitrogen and vacuum three times. The mixture was melted under a nitrogen atmosphere at 180 °C for 3 hours, and at 200 °C for 16 hours. Later, the system was placed under dynamic vacuum and was heated gradually from 200 °C to 240 °C for 6 hours to remove the condensation byproduct, thus increasing the degree of polymerization. Once cool, the polymer was melted for removal from the flask and used without further purification. 1.098 g of polymer was obtained in 73.6% yield. ¹H NMR (CDCl₃) δ ppm 1.62, 1.67 (m, 3 H), 3.87 (s, 3 H), 4.37, 4.47 (m, 4 H), 4.85 (m, 1 H), 6.29 (m, 1 H), 6.81 (m, 1 H), 7.03 (m, 2 H), 7.59 (m, 1 H). ¹³C NMR (CDCl₃) δ ppm 18.5,

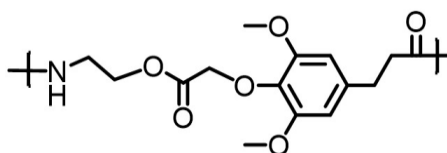
56.0, 61.9, 62.8, 73.6, 110.8, 115.0, 115.8, 122.2, 128.7, 145.0, 149.0, 150.0, 166.7, 171.4.

Polyethylenelactate coumarate



Dimethyl lactate coumarate (1.50 g, 5.67 mmol), ethylene glycol (0.3519 g, 5.67 mmol), and Sb_2O_3 (33.0 mg, 2 mol%) were loaded into a 50 mL round bottom flask. This flask was fitted with a bump trap and attached to the Schlenk line. The system was then purged with nitrogen and vacuum three times. The mixture was melted under a nitrogen atmosphere at 180 °C for 3 hours, and at 200 °C for 16 hours. Later, the system was placed under dynamic vacuum and was heated gradually from 200 °C to 240 °C for 6 hours to remove the condensation byproduct, thus increasing the degree of polymerization. Once cool, the polymer was melted for removal from the flask and used without further purification. 1.10 g of polymer was obtained in 74.0% yield. ^1H NMR (CDCl_3) δ ppm 1.58, 1.65 (m, 3 H), 4.37, 4.45 (m, 4 H), 4.83 (m, 2 H), 6.33 (m, 1 H), 6.86 (m, 2 H), 7.42 (m, 2 H), 7.58 (m, 1 H). ^{13}C NMR (CDCl_3) δ ppm 18.4, 61.7, 62.7, 72.3, 115.3, 115.6, 127.6, 129.8, 144.7, 159.2, 166.6, 171.3.

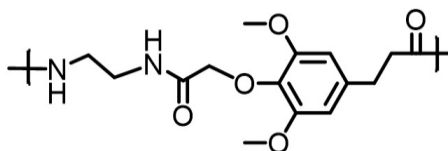
Polyethyleneglycolate dihydrosinapamide (polyesteramide)



Dimethylglycolate dihydrosinapate (1.50 g, 4.803 mmol), ethanolamine (0.3521 g, 5.764 mmol), and Sb_2O_3 (28.0 mg, 2 mol%) were loaded into a 50 mL round bottom

flask. This flask was fitted with a bump trap and attached to the Schlenk line. The system was then purged with nitrogen and vacuum three times. The mixture was melted under a nitrogen atmosphere at 150 °C for 2 hours, at 160 °C for 3 hours, at 180 °C for 16 hours, and at 200 °C for 2 hours. Later, the system was placed under dynamic vacuum and was heated gradually from 200 °C to 215 °C for 5 hours to remove the condensation byproduct, thus increasing the degree of polymerization. Once cool, the polymer was melted for removal from the flask and used without further purification. 1.017 g of polymer was obtained in 68.4% yield. ¹H NMR (DMSO-*d*₆) δ ppm 2.63, 2.89 (m, 4 H), 3.59 (m, 2 H), 3.82 (m, 6 H), 4.20 (m, 2 H), 4.47 (m, 2 H), 6.42 (s, 2 H), 7.90 (m, 0.66 H). ¹³C NMR (DMSO-*d*₆) δ ppm 31.1, 35.7, 37.8, 56.0, 63.2, 72.7, 105.1, 112.4, 135.0, 137.0, 152.1, 170.3, 172.4.

Polyethyleneglycolamide dihydrosinapamide (polyamide)



Dimethylglycolate dihydrosinapate (1.50 g, 4.803 mmol), ethylene diamine (0.3464 g, 5.764 mmol), and Sb₂O₃ (28.0 mg, 2 mol%) were loaded into a 50 mL round bottom flask. This flask was fitted with a bump trap and attached to the Schlenk line. The system was then purged with nitrogen and vacuum three times. The mixture was melted under a nitrogen atmosphere at 100 °C for 1.5 hours, at 120 °C for 1.5 hours, at 140 °C for 1 hour, at 160 °C for 1 hour, at 180 °C for 16 hours, and at 200 °C for 2 hours. Later, the system was placed under dynamic vacuum and was heated gradually from 200 °C to 215 °C for 5 hours to remove the condensation byproduct, thus

increasing the degree of polymerization. Once cool, the polymer was melted for removal from the flask and used without further purification. 0.910 g of polymer was obtained in 61.4% yield. ^1H NMR ($\text{DMSO-}d_6$) δ ppm 2.31, 2.36 (m, 2 H), 2.66, 2.75 (m, 2.20 H), 3.77 (m, 6 H), 4.24, 4.33 (m, 2 H), 6.54 (m, 2 H), 7.99 (m, 1.53 H). ^{13}C NMR ($\text{DMSO-}d_6$) δ ppm 31.4, 33.5, 37.0, 50.6, 55.8, 71.8, 105.3, 134.0, 137.7, 151.9, 168.6, 171.5.

Chapter 3

Large scale extraction

10.00 g of dried lignin powder, 250 mL of NaOH 2 M (aq) and 100 mg of NaHSO₃ were stirred in a 500 mL round-bottom flask for 20 hours at reflux temperature under a nitrogen atmosphere. Upon completion, the resulting dark brown solution was allowed to cool to room temperature. In order to precipitate the unreacted lignin, the solution was acidified to pH = 1 with concentrated H₃PO₄. The resulting mixtures were centrifuged at 3500 rpm for 10 mins. The solids were filtered out, and the remaining solution was extracted with 3 x 100 mL portions of ethyl acetate. The organic (ethyl acetate) portion was washed with copious amounts of water, followed by brine (saturated NaCl solution), and then dried over anhydrous MgSO₄. The ethyl acetate was then removed by rotary evaporation leaving behind crude para-coumaric acid (pCA). The crude pCA could be further purified by recrystallization from water. First, the crude product was dissolved in minimum amount of ethanol before adding hot boiling water little by little until the solution became cloudy. The remaining solution was refrigerated overnight until the pCA precipitated. Solvent reduction by rotatory evaporation may also help to precipitate the product. High purity of pCA was obtained by filtration and drying. The identity and the purity of the product were confirmed by ¹H NMR analysis.

Corn Silk

2.00 g of dried and grounded corn silk and 50 mL of NaOH 0.5 M (aq) were sonicated in a 100 mL round-bottom flask for 2 hours at room temperature. Upon completion, the solution was acidified to pH = 1 with 50 mL HCl 1 M (aq). The solids were filtered out and washed with DIW. Meanwhile, the remaining solution was extracted with 3 x 100 mL portions of ethyl acetate. The organic (ethyl acetate) portion

was washed with copious amounts of water, followed by brine (saturated NaCl solution), and then dried over anhydrous MgSO₄. The ethyl acetate was then removed by rotary evaporation leaving behind crude ferulic acid (FA) (mass = 0.046 g, yield = 2.3%). The identity and the purity of the product were confirmed by ¹H NMR analysis.

Corn Bran

2.00 g of dried and grounded corn bran and 50 mL of NaOH 0.5 M (aq) were sonicated in a 100 mL round-bottom flask for 2 hours at room temperature. Upon completion, the solution was acidified to pH = 1 with 50 mL HCl 1 M (aq). The solids were filtered out and washed with DIW. Meanwhile, the remaining solution was extracted with 3 x 100 mL portions of ethyl acetate. The organic (ethyl acetate) portion was washed with copious amounts of water, followed by brine (saturated NaCl solution), and then dried over anhydrous MgSO₄. The ethyl acetate was then removed by rotary evaporation leaving behind crude ferulic acid (FA) (mass = 0.085 g, yield = 4.3%). The identity and the purity of the product were confirmed by ¹H NMR analysis

Corn Cob

2.00 g of dried and grounded corn cob and 50 mL of NaOH 0.5 M (aq) were sonicated in a 100 mL round-bottom flask for 2 hours at room temperature. Upon completion, the solution was acidified to pH = 1 with 50 mL HCl 1 M (aq). The solids were filtered out and washed with DIW. Meanwhile, the remaining solution was extracted with 3 x 100 mL portions of ethyl acetate. The organic (ethyl acetate) portion was washed with copious amounts of water, followed by brine (saturated NaCl solution), and then dried over anhydrous MgSO₄. The ethyl acetate was then removed by rotary evaporation, leaving behind crude *p*-coumaric acid (pCA) and ferulic acid (FA) (mass =

0.0527 g, yield = 2.6%). The identity and the purity of the product were confirmed by ^1H NMR analysis.

Corn Tassel

2.00 g of dried and grounded corn tassel and 50 mL of NaOH 0.5 M (aq), were sonicated in a 100 mL round-bottom flask for 2 hours at room temperature. Upon completion, the solution was acidified to pH = 1 with 50 mL HCl 1 M (aq). The solids were filtered out and washed with DIW. Meanwhile, the remaining solution was extracted with 3 x 100 mL portions of ethyl acetate. The organic (ethyl acetate) portion was washed with copious amounts of water, followed by brine (saturated NaCl solution), and then dried over anhydrous MgSO_4 . The ethyl acetate was then removed by rotary evaporation leaving behind crude p-coumaric acid (pCA) and ferulic acid (FA) (mass = 0.023 g, yield = 1.15%). The identity and the purity of the product were confirmed by ^1H NMR analysis.

Purification using activated carbon

140 mg of crude product and 5 mL of acetone were added to a 100 mL beaker. Then, 25 mL of warm HCl pH 3 (aq) was added to the beaker slowly while heating on a hotplate, resulting a dark-brown solution. The dark-brown solution was heated for 15 mins at 80 °C to remove acetone from the solution. A pea-size amount of activated carbon (charcoal) was added to the solution and the solution was stirred for 1 hour at 80 °C. The charcoal was filtered out by gravity filtration and washed with 10 mL of HCl pH 3 (aq), resulting in a light yellow filtrate. Then, the filtrate was extracted with 2 x 10 mL portions of ethyl acetate. The organic (ethyl acetate) portion was washed with 15 mL of water, followed by brine (saturated NaCl solution), and then dried over anhydrous

MgSO₄. The ethyl acetate was then removed by rotary evaporation leaving behind an off white powder (mass = 59 mg, purification yield = 42.1%). The identity and the purity of the product were confirmed by ¹H NMR analysis (See Figure C-14).

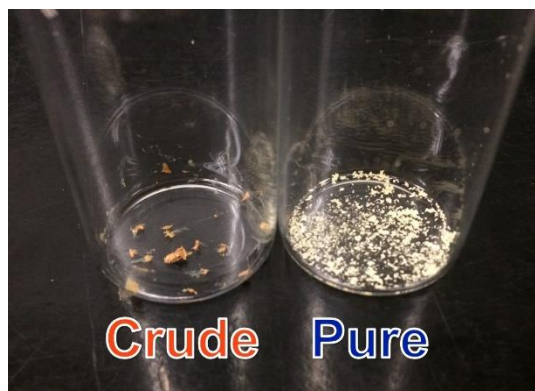


Figure 6-1. Comparison of crude product and purified product using activated charcoal.

Chapter 4

Synthesis of polyvinyl vanillin acetal *PV(VV)A*.

This technique was performed in the Schlenk line. Two 250 mL three necked round-bottom flasks (flask A and flask B) were used. Flask A was added with 1.00 g (22.50 mmol) PVA and 0.077 g (0.45 mmol) *p*-TSA. The system was purged under a nitrogen atmosphere and under vacuum three times. Flask A was injected with 7.5 mL of DMSO, and then heated to 90 °C under nitrogen to dissolve the mixture completely. Meanwhile, flask B was added with 4.45 g (29.25 mmol) vanillin. The system was purged under alternating nitrogen and vacuum. Flask B was injected with 5 mL of DMSO using a syringe through the septum and then the system was stirred under nitrogen until vanillin dissolved completely. When the contents from both flasks were homogeneous, the solution from flask B was transferred to flask A using a syringe. The reaction was heated under nitrogen at 60 °C for 2 hours. The crude product was precipitated in 350 mL aqueous sodium bicarbonate. The precipitate was washed twice with 150 mL deionized water, isolated by decantation and air dried overnight. The crude product was obtained in 169% yield (4.22 g). The purified product was obtained by dissolving 0.40 g of crude product in 15 mL of DMSO, stirring overnight and reprecipitating in 350 mL of aqueous sodium bicarbonate. The precipitate was washed twice with 150 mL deionized water, isolated by decantation and air dried overnight. The final product was obtained as a powder in 18.8% purification yield (0.08 g). The overall reaction yield was 31.1%. The degree of acetalization was found to be of 63.3% from NMR. ¹H NMR (DMSO-*d*₆) δ ppm 1.44 (m, 6.32 H), 3.26 (m, 1.65 H), 3.69 (m, 3 H), 3.90 (m, 3.16 H), 5.35, 5.56, 5.65 (m, 1 H), 6.68, 6.76, 6.87 (m, 3 H). The small peak at in the

region 1.8–2.0 ppm was not incorporated into the integration since it belongs to non-hydrolyzed acetyl –CH₃ groups. Methoxy peaks at 3.9 ppm were considered to be for 3 H, even though the integration was bigger in most cases due to the overlap with –OH peaks from PVA. ¹³C NMR (DMSO-*d*₆) δ ppm 37.6, 38.2, 44.5, 45.0, 46.2, 46.7, 56.0, 73.0, 73.5, 100.6, 110.8, 115.4, 119.4, 130.5, 147.52, 147.56.

Synthesis of polyvinyl *ortho*-vanillin acetal PV(OV)A.

This product was synthesized using the same procedure as for PV(VV)A. Flask A was added with 1.00 g (22.50 mmol) PVA, 0.077 g (0.45 mmol) *p*-TSA and 7.5 mL DMSO. Flask B was added with 4.46 g (29.25 mmol) OV and 5 mL DMSO. Contents of flask B were transferred to flask A. The reaction was heated under nitrogen at 60 °C for 2 hours. The crude product was obtained in 233% yield (5.82 g). The purified product was obtained in a similar fashion to PV(VV)A, 0.40 g were utilized. The final product was obtained as a powder in 23.8% purification yield (0.10 g). The overall reaction yield was 54.4%. ¹H NMR (DMSO-*d*₆) δ ppm 1.44 (m, 6.94 H), 3.77 (s, 3 H), 3.96 (m, 3.47 H), 5.74, 6.02 (m, 1 H), 6.73, 6.89, 6.97 (m, 3 H), 8.58 (br, s, 1 H), showing a degree of acetalization of 57.6%. ¹³C NMR (DMSO-*d*₆) δ ppm 36.4, 37.0, 42.4, 44.1, 44.6, 46.1, 55.9, 62.9, 63.7, 72.7, 73.4, 96.1, 111.7, 118.5, 119.1, 125.6, 143.7, 147.4.

Synthesis of polyvinyl isovanillin acetal PV(IV)A.

This product was synthesized using the same procedure as for PV(VV)A. Flask A was added with 1.00 g (22.50 mmol) PVA, 0.077 g (0.45 mmol) *p*-TSA and 7.5 mL DMSO. Flask B was added with 4.45 g (29.25 mmol) IV and 5 mL DMSO. Contents of flask B were transferred to flask A. The reaction was heated under nitrogen at 60 °C for 2 hours. The crude product was obtained in 201% yield (5.01 g). The purified product

was obtained in a similar fashion to PV(VV)A, 0.40 g were utilized. The final product was obtained as a powder in 23.7% purification yield (0.10 g). The overall reaction yield was 46.9%. ^1H NMR (DMSO- d_6) δ ppm 1.46 (m, 5.98 H), 3.73 (s, 3 H), 3.93 (m, 2.99 H), 4.42 (m, 1.42 H), 5.38, 5.56, 5.67 (m, 1 H), 6.82 (m, 3 H), 8.99 (br, s, 1 H), showing a degree of acetalization of 66.9%. ^{13}C NMR (DMSO- d_6) δ ppm 37.1, 37.8, 43.9, 44.6, 46.3, 46.9, 55.6, 62.7, 64.5, 72.3, 73.0, 99.8, 111.5, 113.5, 117.1, 131.9, 146.0, 147.7.

Synthesis of polyvinyl syringaldehyde acetal PV(SY)A.

This product was synthesized using the same procedure as for PV(VV)A. Flask A was added with 1.00 g (22.50 mmol) PVA, 0.077 g (0.45 mmol) *p*-TSA and 7.5 mL DMSO. Flask B was added with 5.33 g (29.25 mmol) SY and 5 mL DMSO. Contents of flask B were transferred to flask A. The reaction was heated under nitrogen at 60 °C for 2 hours. The crude product was obtained in 141% yield (3.99 g). The purified product was obtained in a similar fashion to PV(VV)A, 0.40 g were utilized. The final product was obtained as a powder in 39.8% purification yield (0.16 g). The overall reaction yield was 54.9%. ^1H NMR (DMSO- d_6) δ ppm 1.44 (m, 7.39 H), 3.27 (m, 2.63 H) 3.68 (m, 6 H), 3.92 (m, 3.69 H), 4.34 (m, 1H), 5.36, 5.62 (m, 1 H), 6.61 (s, 2 H), showing a degree of acetalization of 54.1%. ^{13}C NMR (DMSO- d_6) δ ppm 37.2, 37.9, 44.0, 44.5, 45.8, 46.3, 56.0, 62.9, 63.8, 72.8, 73.3, 100.2, 103.8, 129.5, 135.7, 147.6.

Synthesis of polyvinyl ethylvanillin acetal PV(EV)A.

This product was synthesized using the same procedure as for PV(VV)A. Flask A was added with 1.00 g (22.50 mmol) PVA, 0.077 g (0.45 mmol) *p*-TSA and 7.5 mL DMSO. Flask B was added with 4.87 g (29.25 mmol) EV and 5 mL DMSO. Contents of flask B were transferred to flask A. The reaction was heated under nitrogen at 60 °C for

2 hours. The crude product was obtained in 212% yield (5.64 g). The purified product was obtained in a similar fashion to PV(VV)A, 0.40 g were utilized. The final product was obtained as a powder in 21.4% purification yield (0.09 g). The overall reaction yield was 44.7%. ^1H NMR (DMSO- d_6) δ ppm 1.29 (s, 3 H), 1.46 (m, 6.31 H), 3.42 (m, 2.24 H), 3.90 (m, 2 H), 3.95 (m, 3.15 H), 4.33 (br, s, 1 H), 5.36, 5.59, 5.65 (m, 1 H), 6.72, 6.79, 6.88 (m, 3H), showing a degree of acetalization of 63.4%. ^{13}C NMR (DMSO- d_6) δ ppm 14.8, 37.1, 37.8, 44.0, 44.6, 45.8, 46.2, 63.0, 63.9, 72.5, 73.1, 73.8, 100.0, 111.8, 115.0, 118.9, 130.0, 146.3, 147.5.

Synthesis of polyvinyl benzaldehyde acetal *PV(BZ)A*.

This product was synthesized using a similar procedure to PV(VV)A. Flask A was added with 1.00 g (22.50 mmol) PVA, 0.077 g (0.45 mmol) *p*-TSA and 7.5 mL DMSO. Flask B was added with 3.10 g (29.25 mmol) BZ and 5 mL DMSO. Contents of flask B were transferred to flask A. The reaction was heated under nitrogen at 60 °C for 6 hours. The crude product was obtained in 218% yield (4.32 g). The purified product was obtained in a similar fashion to PV(VV)A, 0.40 g were utilized. The final product was obtained as a powder in 39.4% purification yield (0.158 g). The overall reaction yield was 84.6%. ^1H NMR (DMSO- d_6) δ ppm 1.54 (m, 5.35 H), 4.06 (m, 2.68 H), 4.50 (m, 0.85 H), 5.50, 5.76 (m, 1 H), 7.37 (m, 5 H), showing a degree of acetalization of 74.8%. ^{13}C NMR (DMSO- d_6) δ ppm 37.0, 37.7, 42.2, 43.9, 44.3, 47.2, 62.3, 68.2, 72.5, 73.1, 99.6, 126.1, 127.9, 128.3, 139.1.

Synthesis of polyvinyl 4-hydroxybenzaldehyde acetal *PV(HB)A*.

This product was synthesized using the same procedure as for PV(VV)A. Flask A was added with 1.00 g (22.50 mmol) PVA, 0.077 g (0.45 mmol) *p*-TSA and 7.5 mL

DMSO. Flask B was added with 3.58 g (29.25 mmol) HB and 5 mL DMSO. Contents of flask B were transferred to flask A. The reaction was heated under nitrogen at 60 °C for 2 hours. The crude product was obtained in 166% yield (3.59 g). The purified product was obtained in a similar fashion to PV(VV)A, 0.40 g were utilized. The final product was obtained as a powder in 22.9% purification yield (0.09 g). The overall reaction yield was 37.6%. ¹H NMR (DMSO-*d*₆) δ ppm 1.47 (m, 5.81 H), 3.88, 3.99, 4.33 (m, 2.91 H), 5.40, 5.60, 5.68 (m, 1 H), 6.70 (s, 2 H), 7.19 (s, 2 H), 9.47 (br, s, 1 H), showing a degree of acetalization of 68.8%. ¹³C NMR (DMSO-*d*₆) δ ppm 37.6, 38.4, 44.7, 45.0, 46.3, 46.7, 63.1, 64.3, 72.8, 73.4, 100.4, 115.0, 127.6, 130.4, 157.8.

Synthesis of polyvinyl salicylaldehyde acetal PV(SA)A.

This product was synthesized using the same procedure as for PV(VV)A. Flask A was added with 1.00 g (22.50 mmol) PVA, 0.077 g (0.45 mmol) *p*-TSA and 7.5 mL DMSO. Flask B was added with 3.58 g (29.25 mmol) SY and 5 mL DMSO. Contents of flask B were transferred to flask A. The reaction was heated under nitrogen at 60 °C for 2 hours. The crude product was obtained in 245% yield (5.29 g). The purified product was obtained in a similar fashion to PV(VV)A, 0.40 g were utilized. The final product was obtained as a powder in 23.2% purification yield (0.09 g). The overall reaction yield was 55.7%. ¹H NMR (DMSO-*d*₆) δ ppm 1.44 (m, 6.25 H), 3.79, 3.96, 4.27, 4.42 (m, 3.12 H), 5.70, 5.98 (m, 1 H), 6.77 (s, 2 H), 7.10 (s, 1 H), 7.32 (s, 1 H), 9.32 (br. s, 1 H), showing a degree of acetalization of 64.0%. ¹³C NMR (DMSO-*d*₆) δ ppm 37.1, 37.9, 44.2, 44.5, 45.8, 46.2, 62.8, 63.7, 72.6, 73.3, 96.0, 115.4, 118.6, 125.1, 127.3, 129.3, 154.4.

Synthesis of polyvinyl *para*-anisaldehyde acetal PV(PA)A.

This product was synthesized using the same procedure as for PV(VV)A. Flask A was added with 1.00 g (22.50 mmol) PVA, 0.077 g (0.45 mmol) *p*-TSA and 7.5 mL DMSO. Flask B was added with 3.99 g (29.25 mmol) PA and 5 mL DMSO. Contents of flask B were transferred to flask A. The reaction was heated under nitrogen at 60 °C for 2 hours. The crude product was obtained in 166% yield (3.85 g). The purified product was obtained in a similar fashion to PV(VV)A, 0.40 g were utilized. The final product was obtained as a powder in 33.8% purification yield (0.14 g). The overall reaction yield was 55.7%. ¹H NMR (DMSO-*d*₆) δ ppm 1.46 (m, 6.02 H), 3.74 (s, 3 H), 4.02 (m, 3.01 H), 4.43 (m, 1 H), 5.46, 5.64, 5.75 (m, 1 H), 6.88 (s, 2 H), 7.32 (s, 2 H), showing a degree of acetalization of 66.4%. ¹³C NMR (DMSO-*d*₆) δ ppm 37.0, 37.7, 42.3, 44.5, 45.8, 46.2, 55.1, 62.8, 63.9, 72.4, 73.0, 99.7, 113.2, 127.4, 131.6, 159.2.

Synthesis of polyvinyl *ortho*-anisaldehyde acetal PV(OA)A.

This product was synthesized using the same procedure as for PV(VV)A. Flask A was added with 1.00 g (22.50 mmol) PVA, 0.077 g (0.45 mmol) *p*-TSA and 7.5 mL DMSO. Flask B was added with 3.98 g (29.25 mmol) OA and 5 mL DMSO. Contents of flask B were transferred to flask A. The reaction was heated under nitrogen at 60 °C for 2 hours. The crude product was obtained in 155% yield (3.60 g). The purified product was obtained by dissolving 0.40 g of crude product in 15 mL of DMSO, stirring overnight and reprecipitating in 350 mL of methanol, and isolated by decantation and air dried overnight. The final product was obtained as a powder in 58.6% purification yield (0.24 g). The overall reaction yield was 70.5%. ¹H NMR (DMSO-*d*₆) δ ppm 1.49 (m, 5.43 H), 3.72 (s, 3 H), 3.93 (m, 1.72 H), 4.29 (m, 0.97 H), 5.70, 5.97 (m, 1 H), 6.93 (m, 2 H), 7.29

(m, 1 H), 7.43 (m, 1 H), showing a degree of acetalization of 73.7%. ^{13}C NMR (DMSO- d_6) δ ppm 36.3, 36.9, 42.0, 42.1, 43.8, 44.2, 55.5, 62.9, 68.4, 72.7, 73.4, 95.3, 111.1, 120.1, 126.9, 127.0, 129.7, 156.2.

Synthesis of polyvinyl cuminaldehyde acetal *PV(CU)A*.

This product was synthesized using the same procedure as for *PV(VV)A*. Flask A was added with 1.00 g (22.50 mmol) PVA, 0.077 g (0.45 mmol) *p*-TSA and 7.5 mL DMSO. Flask B was added with 4.33 g (29.25 mmol) CU and 5 mL DMSO. Contents of flask B were transferred to flask A. The reaction was heated under nitrogen at 60 °C for 2 hours. The crude product was obtained in 158% yield (3.88 g). The purified product was obtained by dissolving 0.40 g of crude product in 15 mL of DMSO, stirring overnight and reprecipitating in 350 mL of deionized water. The precipitate was stirred with 15 mL ethanol overnight, isolated by decantation and air dried overnight. The final product was obtained as a powder in 36.7% purification yield (0.15 g). The overall reaction yield was 57.2%. ^1H NMR (DMSO- d_6) δ ppm 1.07, 1.16 (s, 6H), 0.74–1.77 (m, 6.94 H), 2.81 (m, 1 H), 3.93 (m, 3.47 H), 5.46, 5.65, 5.74 (m, 1 H), 7.26 (m, 4 H), showing a degree of acetalization of 57.6%. ^{13}C NMR (DMSO- d_6) δ ppm 23.8, 33.2, 37.6, 38.1, 41.5, 42.0, 43.5, 44.6, 62.7, 64.2, 73.0, 73.3, 99.9, 125.7, 126.1, 136.9, 148.6. (Peaks at 18.6 and 56.0 come from leftover ethanol).

Synthesis of polyvinyl cinnamaldehyde acetal *PV(CI)A*.

This product was synthesized using the same procedure as for *PV(VV)A*. Flask A was added with 1.00 g (22.50 mmol) PVA, 0.077 g (0.45 mmol) *p*-TSA and 7.5 mL DMSO. Flask B was added with 3.86 g (29.25 mmol) CI and 5 mL DMSO. Contents of flask B were transferred to flask A. The reaction was heated under nitrogen at 60 °C for

2 hours. The crude product was obtained in 243% yield (5.52 g). The purified product was obtained in a similar fashion to PV(VV)A, 0.40 g were utilized. The final product was obtained as a powder in 23.1% purification yield (0.09 g). The overall reaction yield was 55.5%. ¹H NMR (DMSO-*d*₆) δ ppm 1.46 (m, 5.86 H), 3.94 (m, 2.94 H), 4.44 (m, 1.30 H), 5.15, 5.43 (m, 1 H), 6.23 (s, 1 H), 6.68 (s, 1 H), 7.36 (m, 5 H), showing a degree of acetalization of 68.3%. ¹³C NMR (DMSO-*d*₆) δ ppm 37.1, 37.9, 44.0, 44.5, 45.9, 46.2, 62.8, 63.9, 72.0, 72.8, 99.6, 126.6, 128.1, 128.7, 132.2, 135.7.

Synthesis of polyvinyl phenylacetaldehyde acetal *PV(PH)A*.

This product was synthesized using the same procedure as for PV(VV)A. Flask A was added with 1.00 g (22.50 mmol) PVA, 0.077 g (0.45 mmol) *p*-TSA and 7.5 mL DMSO. Flask B was added with 3.51 g (29.25 mmol) PH and 5 mL DMSO. Contents of flask B were transferred to flask A. The reaction was heated under nitrogen at 60 °C for 2 hours. The crude product was obtained in 186% yield (3.97 g). The purified product was obtained in a similar fashion to PV(VV)A, 0.40 g were utilized. The final product was obtained as a powder in 39.1% purification yield (0.16 g). The overall reaction yield was 71.8%. ¹H NMR (DMSO-*d*₆) δ ppm 1.46 (m, 13.50 H), 2.80 (m, 2 H), 3.77 (m, 5.80 H), 4.25, 4.46, 4.68 (m, 5.02 H), 5.02 (m, 1 H), 7.23 (m, 5 H), showing a degree of acetalization of 29.6%. ¹³C NMR (DMSO-*d*₆) δ ppm 38.5, 38.9, 40.8, 44.0, 44.4, 48.0, 49.5, 62.9, 64.0, 72.1, 72.7, 101.0, 104.0, 126.2, 127.9, 129.1, 129.9, 138.4. (Peaks from leftover phenylacetaldehyde are still present; further purification are needed).

Synthesis of polyvinyl floramelon acetal *PV(FL)A*.

This product was synthesized using the same procedure as for PV(VV)A. Flask A was added with 1.00 g (22.50 mmol) PVA, 0.077 g (0.45 mmol) *p*-TSA and 7.5 mL

DMSO. Flask B was added with 5.62 g (29.25 mmol) FL and 5 mL DMSO. Contents of flask B were transferred to flask A. The reaction was heated under nitrogen at 60 °C for 2 hours. The crude product was obtained in 241% yield (7.09 g). The purified product was obtained in a similar fashion to PV(VV)A, 1.00 g were utilized. The final product was obtained as a powder in 24.5% purification yield (0.26 g). The overall reaction yield was 58.3%. ¹H NMR (DMSO-*d*₆) δ ppm 0.90 (d, 3 H), 1.46 (m, 5.19 H), 2.21, 2.66 (m, 2 H), 3.79 (m, 2 H), 4.21 (m, 1 H), 5.91 (m, 2 H), 6.64 (m, 3 H), showing a degree of acetalization of 77.1%. ¹³C NMR (DMSO-*d*₆) δ ppm 12.7, 35.5, 37.0, 37.5, 44.1, 44.6, 45.8, 46.2, 47.2, 62.6, 63.2, 72.5, 72.8, 100.7, 108.0, 109.3, 121.9, 132.8, 145.2, 145.5, 147.2. (Peaks from floramelon are still present; further purification are needed).

Synthesis of polyvinyl hydroxymethylfurfural acetal *PV(HMF)A*.

This product was synthesized using the same procedure as for PV(VV)A, except the reaction time was of 6 hours. Flask A was added with 1.00 g (22.50 mmol) PVA, 0.077 g (0.45 mmol) *p*-TSA and 7.5 mL DMSO. Flask B was added with 4.33 g (29.25 mmol) HMF and 5 mL DMSO. Contents of flask B were transferred to flask A. The reaction was heated under nitrogen at 60 °C for 6 hours. The crude product was obtained in 158% yield (3.88 g). The purified product was obtained in a similar fashion to PV(VV)A, 0.40 g were utilized. The final product was obtained as a powder in 37.4% purification yield (0.16 g). The overall reaction yield was 80.0%. ¹H NMR (DMSO-*d*₆) δ ppm 1.44 (m, 6.84 H), 3.79 (m, 1.26 H), 3.97 (s, 2 H), 4.43 (m, 3.42 H), 5.24 (br. s, 1 H), 5.52, 5.77 (m, 1 H), 6.26 (m, 2 H), showing a degree of acetalization of 58.5%. ¹³C NMR (DMSO-*d*₆) δ ppm 37.0, 37.9, 39.9, 43.8, 44.1, 44.4, 46.3, 55.6, 61.5, 62.5, 72.4, 73.4, 94.8, 107.3, 108.2, 150.5, 155.0.

Chapter 5

Materials

All of the dialdehyde monomers (4HB-2-4HB, 4HB-3-4HB, van-2-van, van-3-van, syr-2-syr, syr-3-syr, evan-2-evan, evan-3-evan) were inherited from alumni (Dr. Alexander Pemba and Dr. Mayra Rostagno) of previous projects. Vitamin B1-HCl was purchased from TCI. Dimethyl sulfoxide (DMSO), *para*-toluenesulfonic acid (*p*-TSA), cyclopentanone, and dimethyl 3-oxoglutarate from Sigma-Aldrich. *N*-methyl-2-pyrrolidone (NMP) was purchased from VWR. Acetone was purchased from Fisher Chemical. NMR solvents, including deuterated chloroform (CDCl₃) and deuterated dimethyl sulfoxide (DMSO-*d*₆) were purchased from Cambridge Isotope Laboratories. All the chemicals, unless expressly mentioned, were utilized without further purification.

Poly-DHMP analogue from van-2-van and cyclopentanone

The polymerizations were typically carried out in a round bottom flask and connected to a reflux condenser under nitrogen. 2 mmol of van-2-van, 4 mmol of cyclopentanone, 4.8 mmol of urea, 6 mol% of vitamin B1.HCl, and 10 mL of DMSO were charged to a 50 mL round bottom flask. The mixture was then stirred for 24 hours at 80 °C. Upon completion, the reaction was poured into 150 mL cold acetone, then stirred for 30 minutes to yield an orange powder precipitate. The precipitate was filtered by gravity filtration, and the resulting orange powder was collected on a watch glass to dry in the hood overnight. 0.7812 g of polymer was obtained in 93% yield. The identity of the polymer was confirmed by ¹H NMR analysis.

Poly-DHMP analogue from 4HB-2-4HB and dimethyl 3-oxoglutarate

The polymerizations were typically carried out in a round bottom flask and connected to a reflux condenser under nitrogen. 2 mmol of 4HB-2-4HB, 4 mmol of dimethyl 3-oxoglutarate, 4.8 mmol of urea, 2 mol% of pTSA, and 10 mL of NMP were charged to a 50 mL round bottom flask. The mixture was stirred for 20 hours at 150 °C. Later, 3 mL of NMP was added to the mixture, and it was stirred for another 4 hours. Upon completion, the reaction was poured into 150 mL cold acetone, then stirred for 30 minutes to yield an orange powder precipitate. The precipitate was filtered by gravity filtration, and the resulting orange powder was collected on a watch glass to dry in the hood overnight. 0.4382 g of polymer was obtained in 49% yield. The identity of the polymer was confirmed by ¹H NMR analysis.

Poly-DHMP analogue from van-2-van and dimethyl 3-oxoglutarate

The polymerizations were typically carried out in a round bottom flask and connected to a reflux condenser under nitrogen. 2 mmol of van-2-van, 4 mmol of dimethyl 3-oxoglutarate, 4.8 mmol of urea, 2 mol% of pTSA, and 10 mL of NMP were charged to a 50 mL round bottom flask. The mixture was stirred for 20 hours at 150 °C. Later, 3 mL of NMP was added to the mixture, and it was stirred for another 4 hours. Upon completion, the reaction was poured into 150 mL cold acetone, then stirred for 30 minutes to yield an orange powder precipitate. The precipitate was filtered by gravity filtration, and the resulting orange powder was collected on a watch glass to dry in the hood overnight. 0.326 g of polymer was obtained in 32% yield. The identity of the polymer was confirmed by ¹H NMR analysis.

Poly-DHMP analogue from syr-2-syr and dimethyl 3-oxoglutarate

The polymerizations were typically carried out in a round bottom flask and connected to a reflux condenser under nitrogen. 2 mmol of syr-2-syr, 4 mmol of dimethyl 3-oxoglutarate, 4.8 mmol of urea, 2 mol% of pTSA, and 10 mL of NMP were charged to a 50 mL round bottom flask. The mixture was stirred for 20 hours at 150 °C. Later, 3 mL of NMP was added to the mixture, and it was stirred for another 4 hours. Upon completion, the reaction was poured into 150 mL cold acetone, then stirred for 30 minutes to yield an orange powder precipitate. The precipitate was filtered by gravity filtration, and the resulting orange powder was collected on a watch glass to dry in the hood overnight. 0.3918 g of polymer was obtained in 34% yield. The identity of the polymer was confirmed by ¹H NMR analysis.

Poly-DHMP analogue from evan-2-evan and dimethyl 3-oxoglutarate

The polymerizations were typically carried out in a round bottom flask and connected to a reflux condenser under nitrogen. 2 mmol of evan-2-evan, 4 mmol of dimethyl 3-oxoglutarate, 4.8 mmol of urea, 2 mol% of pTSA, and 10 mL of NMP were charged to a 50 mL round bottom flask. The mixture was stirred for 20 hours at 150 °C. Later, 3 mL of NMP was added to the mixture, and it was stirred for another 4 hours. Upon completion, the reaction was poured into 150 mL cold acetone, then stirred for 30 minutes to yield an orange powder precipitate. The precipitate was filtered by gravity filtration, and the resulting orange powder was collected on a watch glass to dry in the hood overnight. 0.2926 g of polymer was obtained in 27% yield. The identity of the polymer was confirmed by ¹H NMR analysis.

Poly-DHMP analogue from 4HB-3-4HB and dimethyl 3-oxoglutarate

The polymerizations were typically carried out in a round bottom flask and connected to a reflux condenser under nitrogen. 2 mmol of 4HB-3-4HB, 4 mmol of dimethyl 3-oxoglutarate, 4.8 mmol of urea, 2 mol% of pTSA, and 10 mL of NMP were charged to a 50 mL round bottom flask. The mixture was stirred for 20 hours at 150 °C. Later, 3 mL of NMP was added to the mixture, and it was stirred for another 4 hours. Upon completion, the reaction was poured into 150 mL cold acetone, then stirred for 30 minutes to yield an orange powder precipitate. The precipitate was filtered by gravity filtration, and the resulting orange powder was collected on a watch glass to dry in the hood overnight. 0.376 g of polymer was obtained in 40% yield. The identity of the polymer was confirmed by ¹H NMR analysis.

Poly-DHMP analogue from van-3-van and dimethyl 3-oxoglutarate

The polymerizations were typically carried out in a round bottom flask and connected to a reflux condenser under nitrogen. 2 mmol of van-3-van, 4 mmol of dimethyl 3-oxoglutarate, 4.8 mmol of urea, 2 mol% of pTSA, and 10 mL of NMP were charged to a 50 mL round bottom flask. The mixture was stirred for 20 hours at 150 °C. Later, 3 mL of NMP was added to the mixture, and it was stirred for another 4 hours. Upon completion, the reaction was poured into 150 mL cold acetone, then stirred for 30 minutes to yield an orange powder precipitate. The precipitate was filtered by gravity filtration, and the resulting orange powder was collected on a watch glass to dry in the hood overnight. 0.3759 g of polymer was obtained in 36% yield. The identity of the polymer was confirmed by ¹H NMR analysis.

Poly-DHMP analogue from syr-3-syr and dimethyl 3-oxoglutarate

The polymerizations were typically carried out in a round bottom flask and connected to a reflux condenser under nitrogen. 2 mmol of syr-3-syr, 4 mmol of dimethyl 3-oxoglutarate, 4.8 mmol of urea, 2 mol% of pTSA, and 10 mL of NMP were charged to a 50 mL round bottom flask. The mixture was stirred for 20 hours at 150 °C. Later, 3 mL of NMP was added to the mixture, and it was stirred for another 4 hours. Upon completion, the reaction was poured into 150 mL cold acetone, then stirred for 30 minutes to yield an orange powder precipitate. The precipitate was filtered by gravity filtration, and the resulting orange powder was collected on a watch glass to dry in the hood overnight. 0.190 g of polymer was obtained in 16% yield. The identity of the polymer was confirmed by ¹H NMR analysis.

Poly-DHMP analogue from evan-3-evan and dimethyl 3-oxoglutarate

The polymerizations were typically carried out in a round bottom flask and connected to a reflux condenser under nitrogen. 2 mmol of evan-3-evan, 4 mmol of dimethyl 3-oxoglutarate, 4.8 mmol of urea, 2 mol% of pTSA, and 10 mL of NMP were charged to a 50 mL round bottom flask. The mixture was stirred for 20 hours at 150 °C. Later, 3 mL of NMP was added to the mixture, and it was stirred for another 4 hours. Upon completion, the reaction was poured into 150 mL cold acetone, then stirred for 30 minutes to yield an orange powder precipitate. The precipitate was filtered by gravity filtration, and the resulting orange powder was collected on a watch glass to dry in the hood overnight. 0.2657 g of polymer was obtained in 24% yield. The identity of the polymer was confirmed by ¹H NMR analysis.

APPENDIX A
SUPPLEMENTARY INFORMATION FOR CHAPTER 1

TGA Spectra

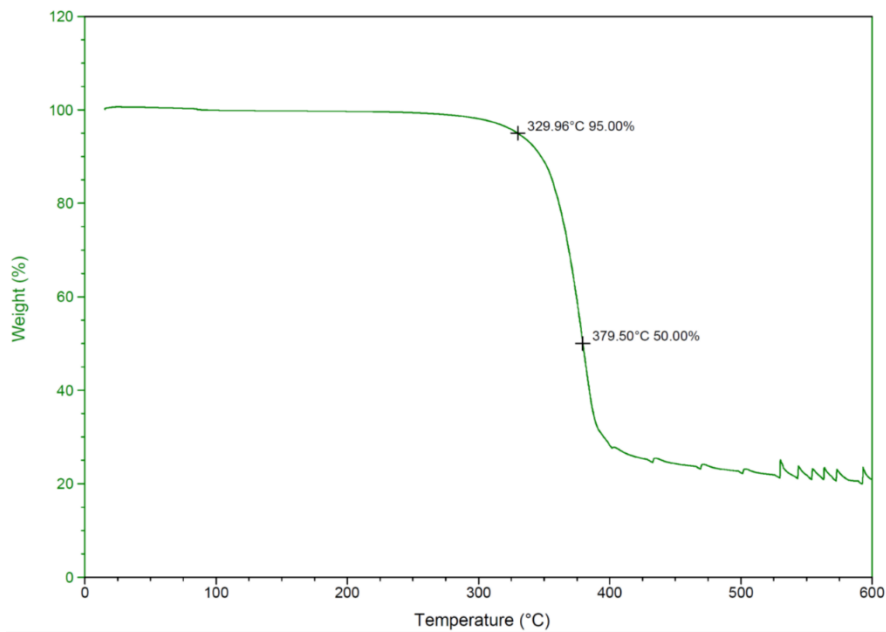


Figure A-1. TGA Thermogram of polyethylene dihydrosinapate (Table 1-1, Entry 2 and Table 1-2, Entry 1)

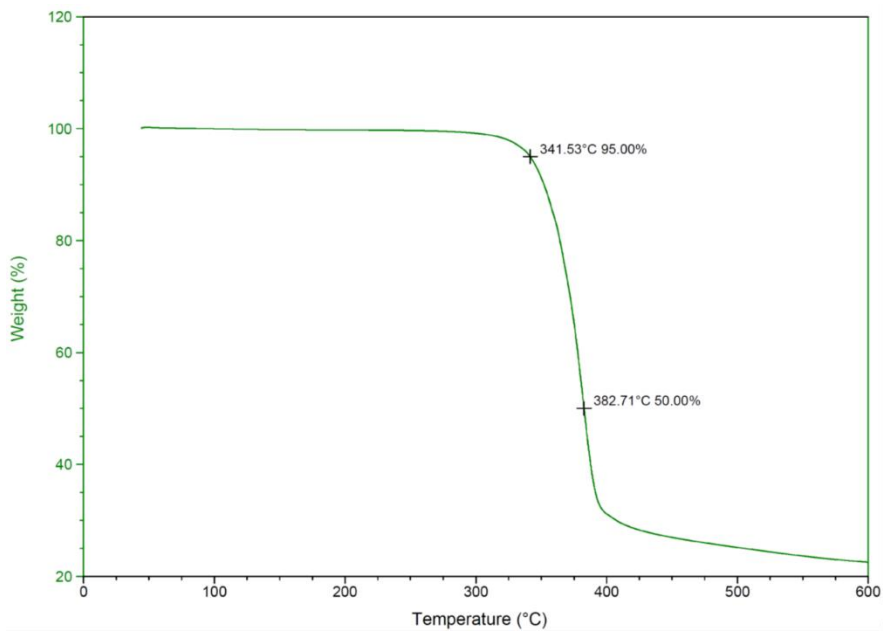


Figure A-2. TGA Thermogram of copoly(hydroxyethyldihydrosinapic acid/hydroxyethylsinapic acid) [90:10] (Table 1-2, Entry 2)

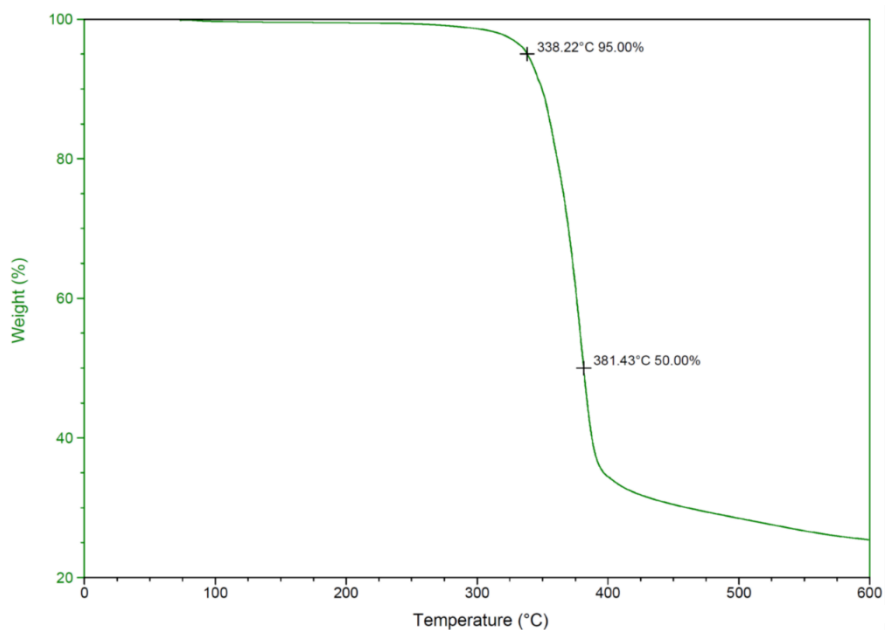


Figure A-3. TGA Thermogram of copoly(hydroxyethyldihydroxynapic acid/hydroxyethylsinapic acid) [80:20] (Table 1-2, Entry 3)

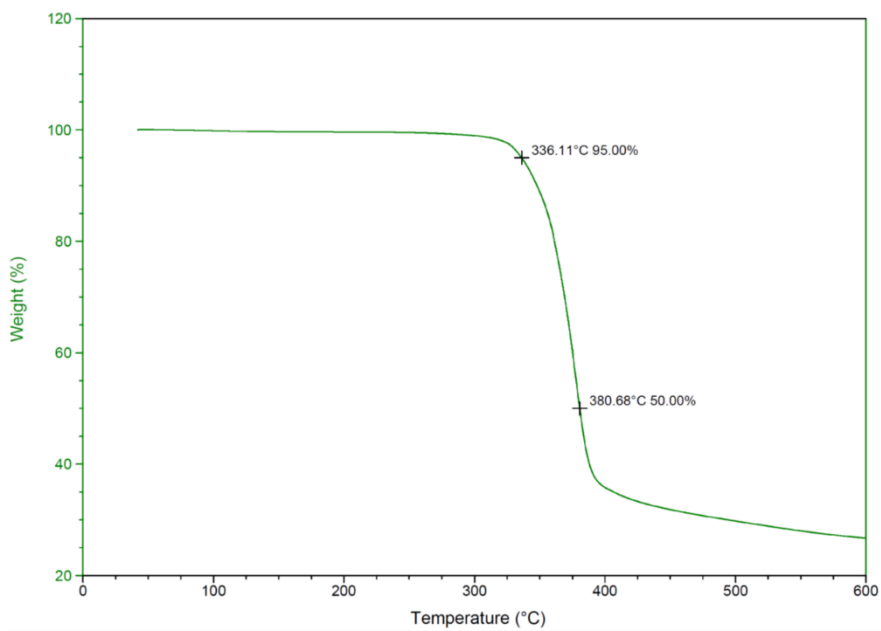


Figure A-4. TGA Thermogram of copoly(hydroxyethyldihydroxynapic acid/hydroxyethylsinapic acid) [70:30] (Table 1-2, Entry 4)

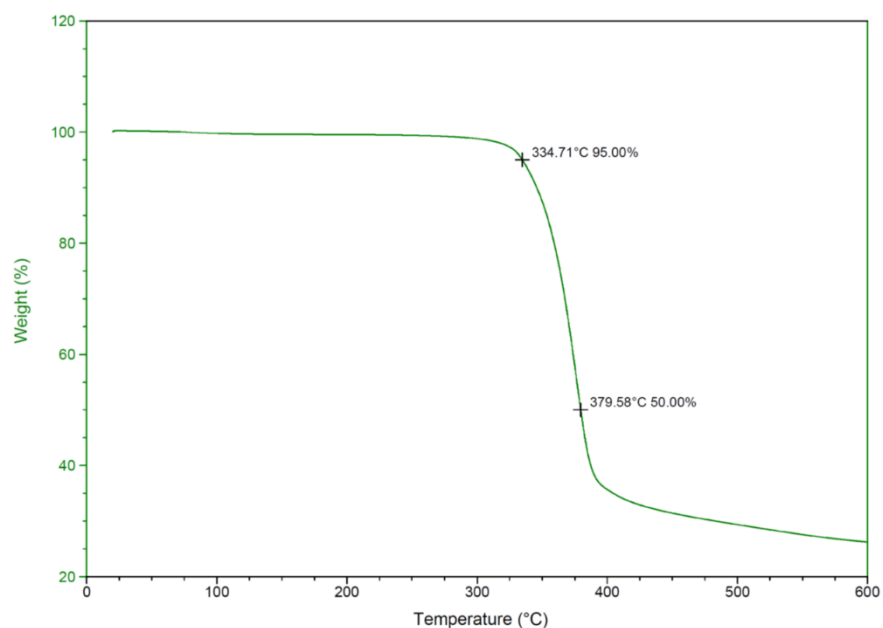


Figure A-5. TGA Thermogram of copoly(hydroxyethyldihydroxynapic acid/hydroxyethylsinapic acid) [60:40] (Table 1-2, Entry 5)

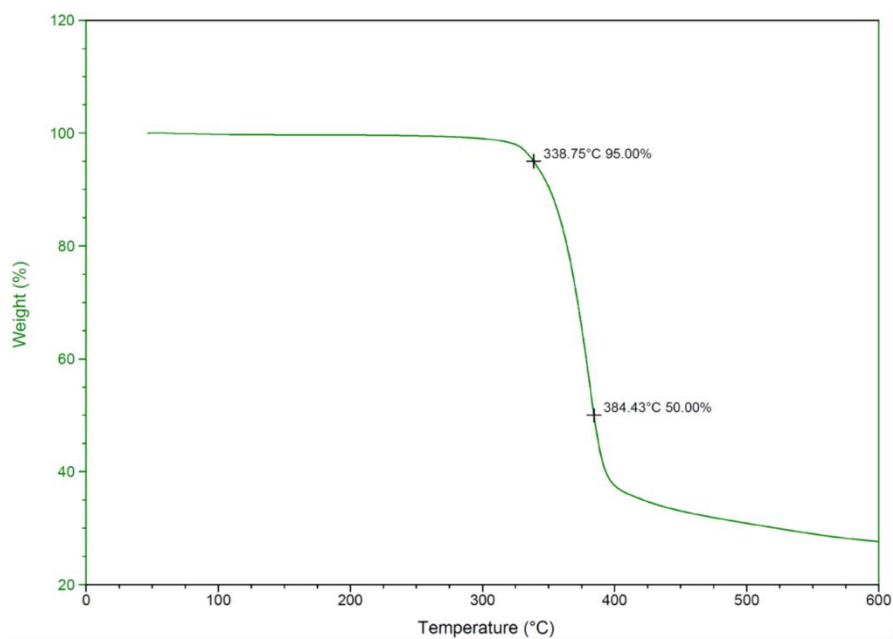


Figure A-6. TGA Thermogram of copoly(hydroxyethyldihydroxynapic acid/hydroxyethylsinapic acid) [50:50] (Table S3, Entry 6)

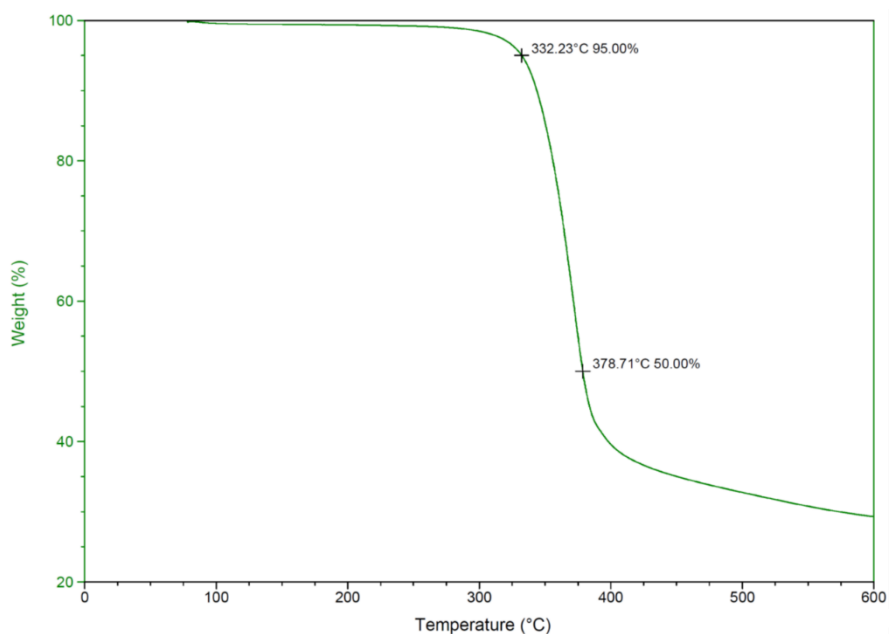


Figure A-7. TGA Thermogram of copoly(hydroxyethyldihydroxynapic acid/hydroxyethylsinapic acid) [40:60] (Table 1-2, Entry 7)

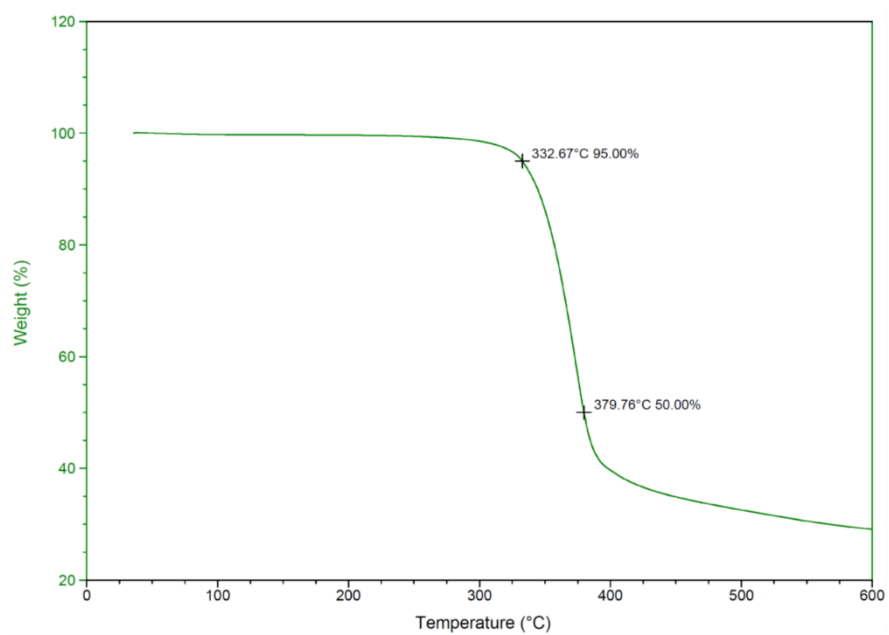


Figure A-8. TGA Thermogram of copoly(hydroxyethyldihydroxynapic acid/hydroxyethylsinapic acid) [30:70] (Table 1-2, Entry 8)

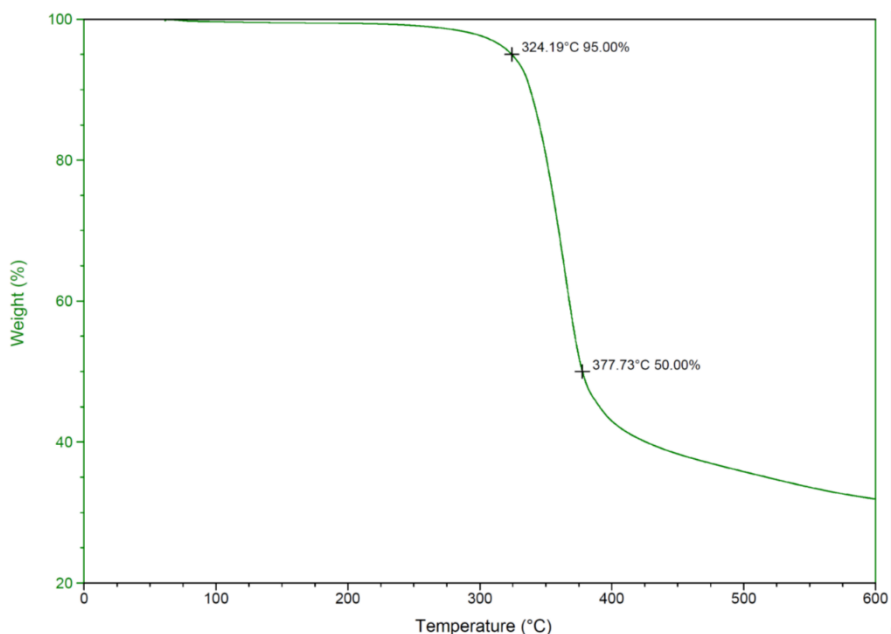


Figure A-9. TGA Thermogram of copoly(hydroxyethyldihydroxynapic acid/hydroxyethylsinapic acid) [20:80] (Table 1-2, Entry 9)

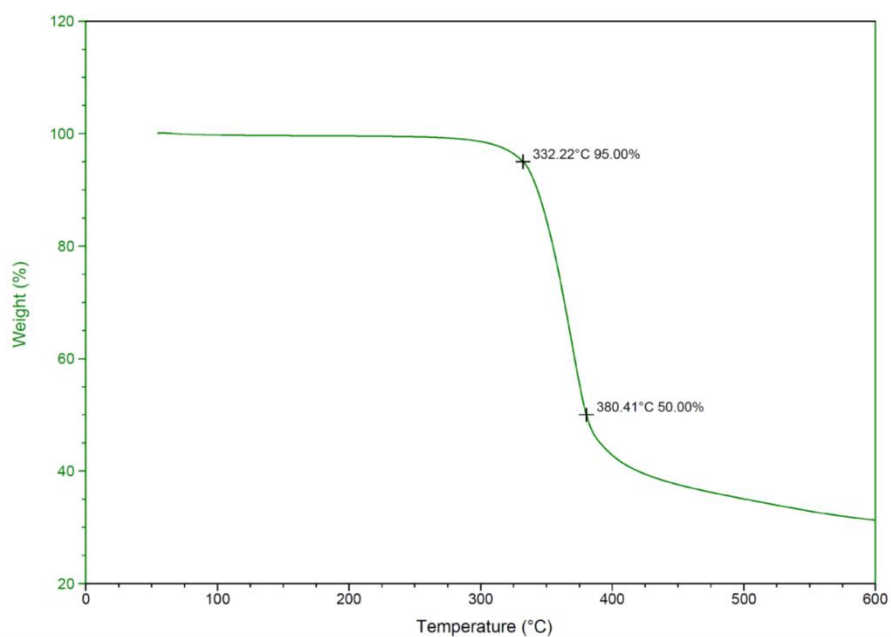


Figure A-10. TGA Thermogram of copoly(hydroxyethyldihydroxynapic acid/hydroxyethylsinapic acid) [10:90] (Table 1-2, Entry 10)

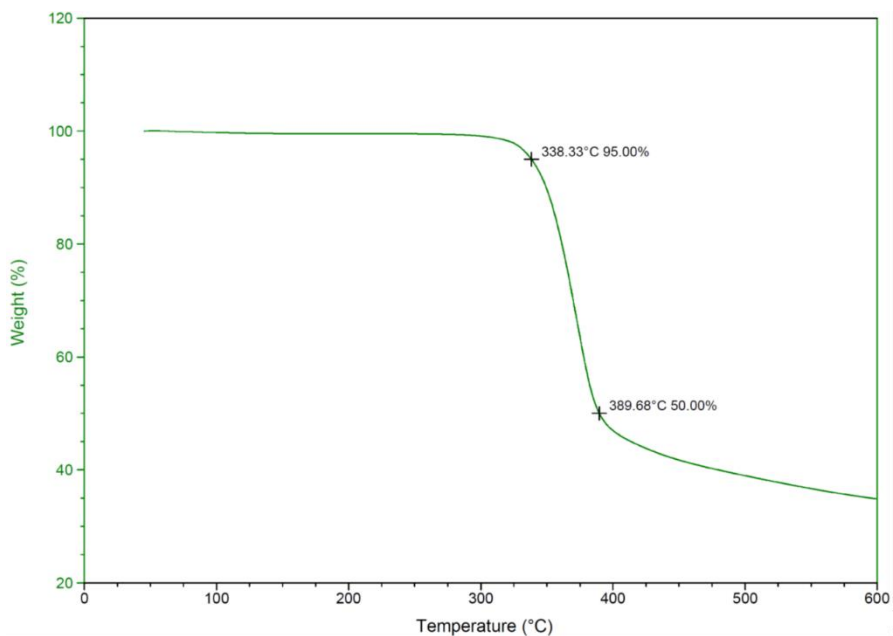


Figure A-11. TGA Thermogram of polyethylene sinapate (Table 1-1, Entry 1 and Table 1-2, Entry 11)

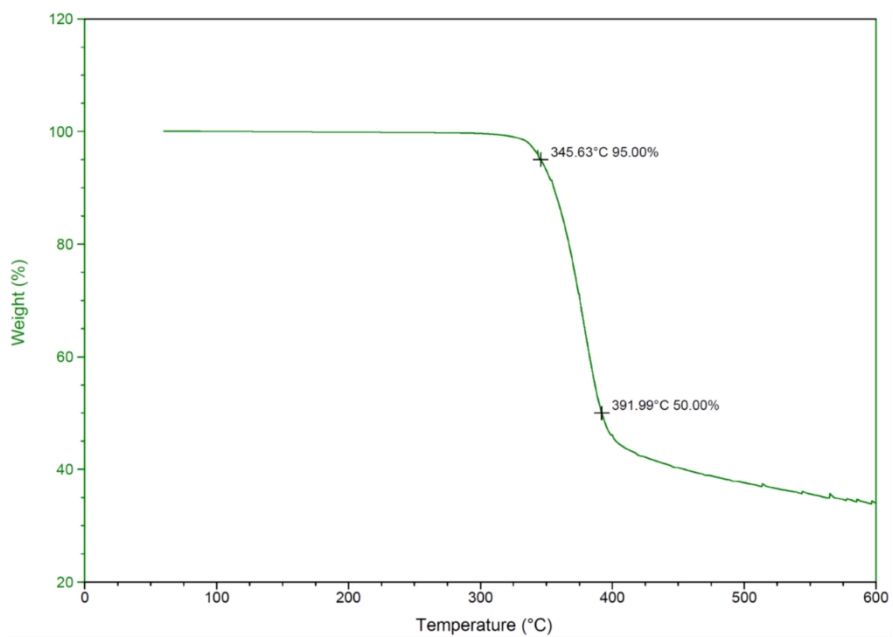


Figure A-12. TGA Thermogram of polypropylene sinapate (Table 1-1, Entry 3)

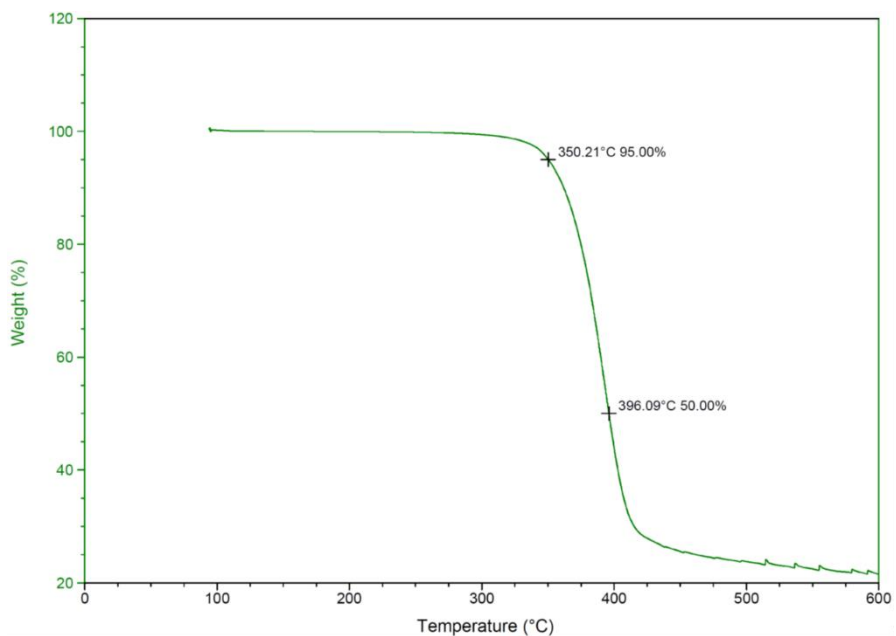


Figure A-13. TGA Thermogram of polyhexalene sinapate (Table 1-1, Entry 4)

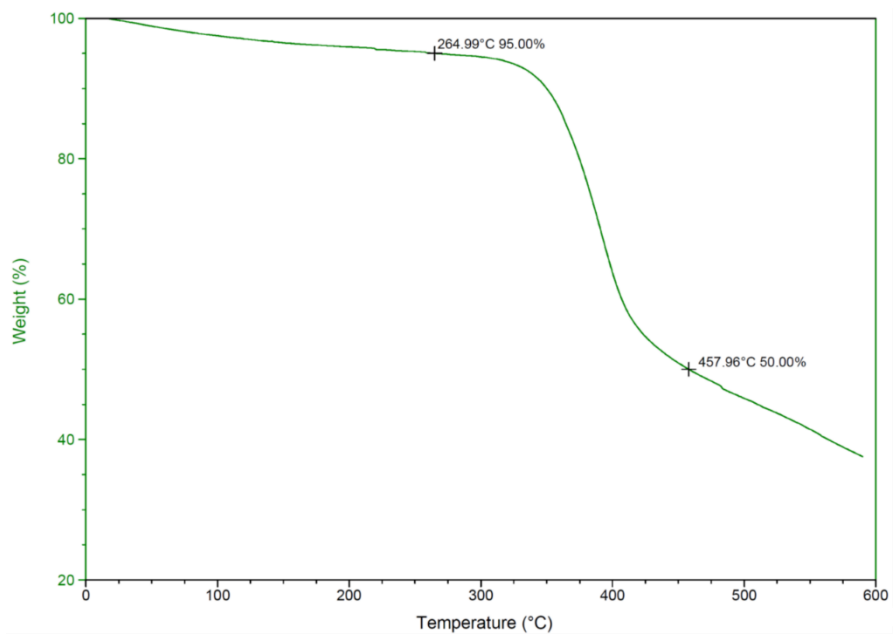


Figure A-14. TGA Thermogram of polyethylene sinapate from extracted sinapic acid.

DSC Spectra

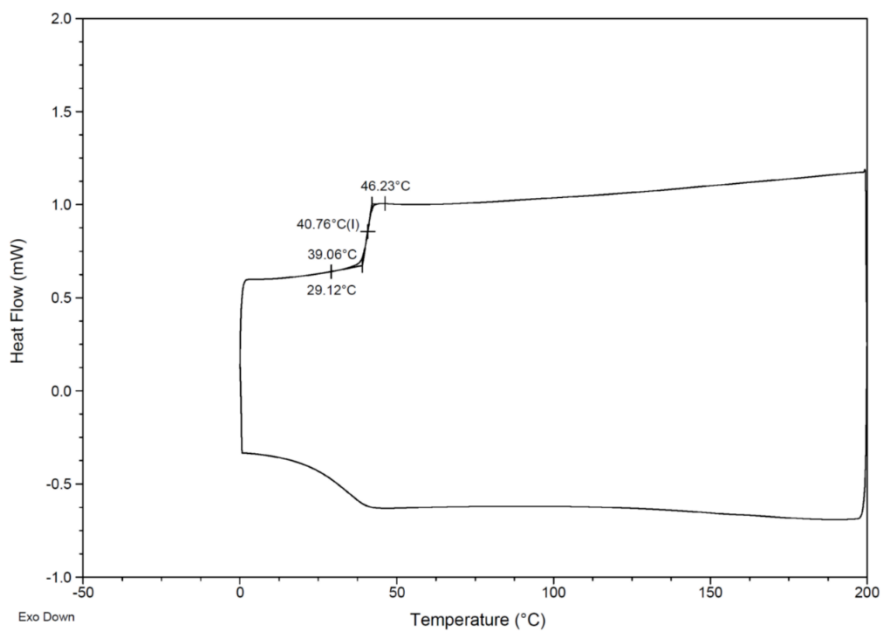


Figure A-15. DSC Thermogram of polyethylene dihydrosinapate (Table 1-1, Entry 2 and Table 1-2, Entry 1)

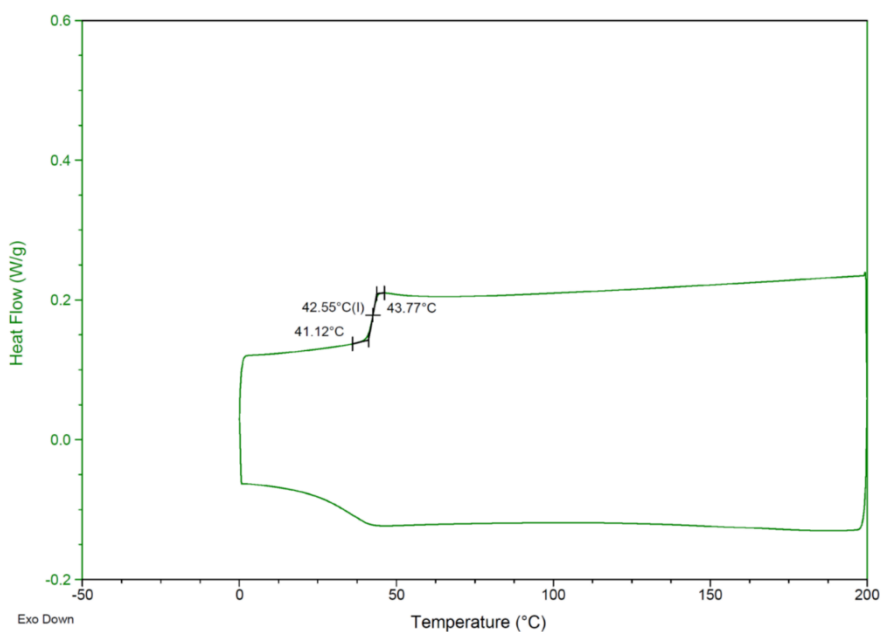


Figure A-16. DSC Thermogram of copoly(hydroxyethyl dihydrosinapic acid/hydroxyethylsinapic acid) [90:10] (Table 1-2, Entry 2)

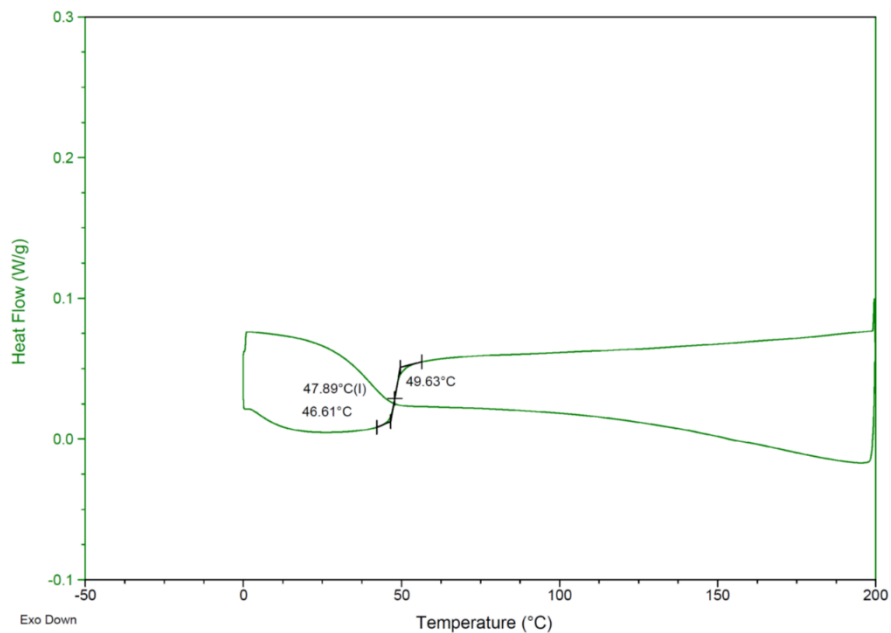


Figure A-17. DSC Thermogram of copoly(hydroxyethyldihydrosinapic acid/hydroxyethylsinapic acid) [80:20] (Table 1-2, Entry 3)

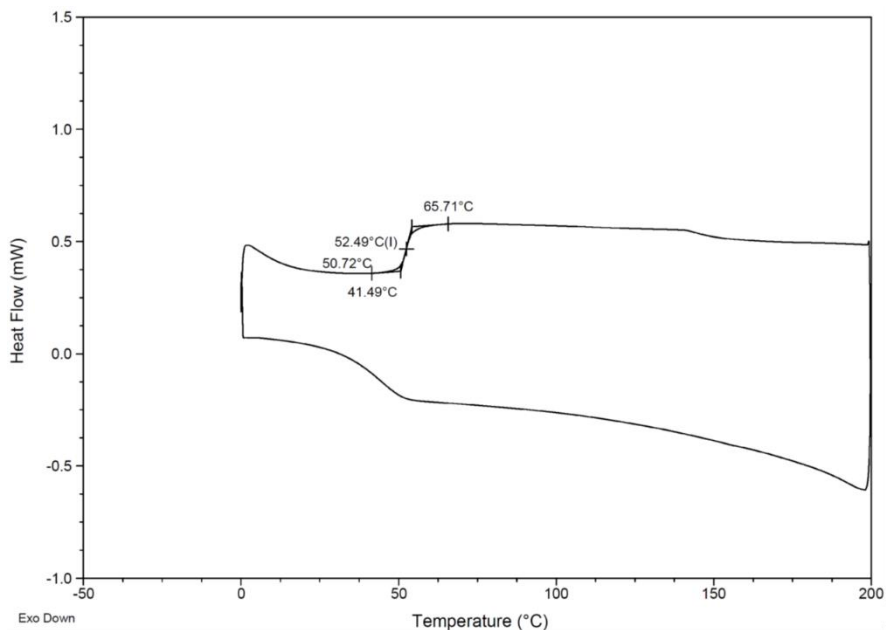


Figure A-18. DSC Thermogram of copoly(hydroxyethyldihydrosinapic acid/hydroxyethylsinapic acid) [70:30] (Table 1-2, Entry 4)

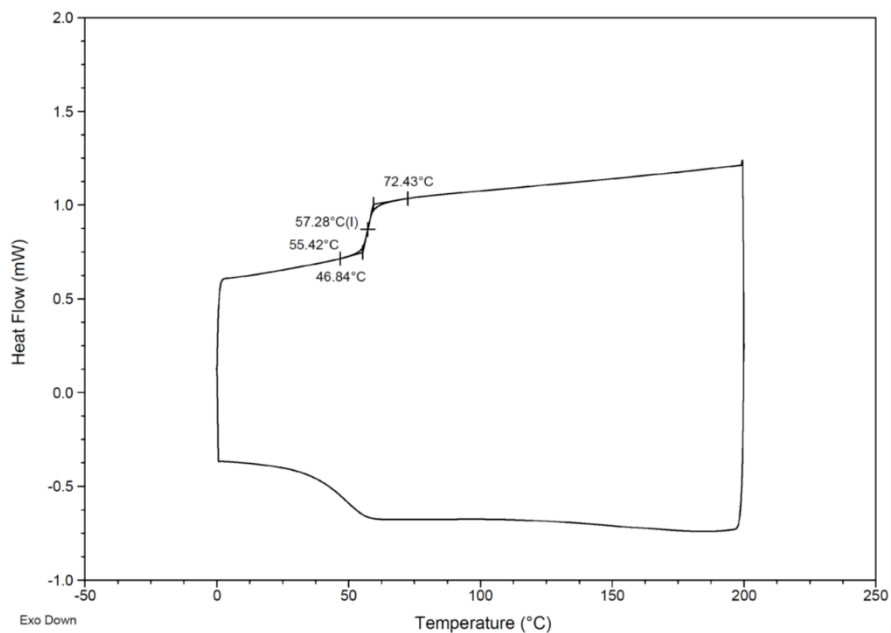


Figure A-19. DSC Thermogram of copoly(hydroxyethylidihydrosinapic acid/hydroxyethylsinapic acid) [60:40] (Table 1-2, Entry 5)

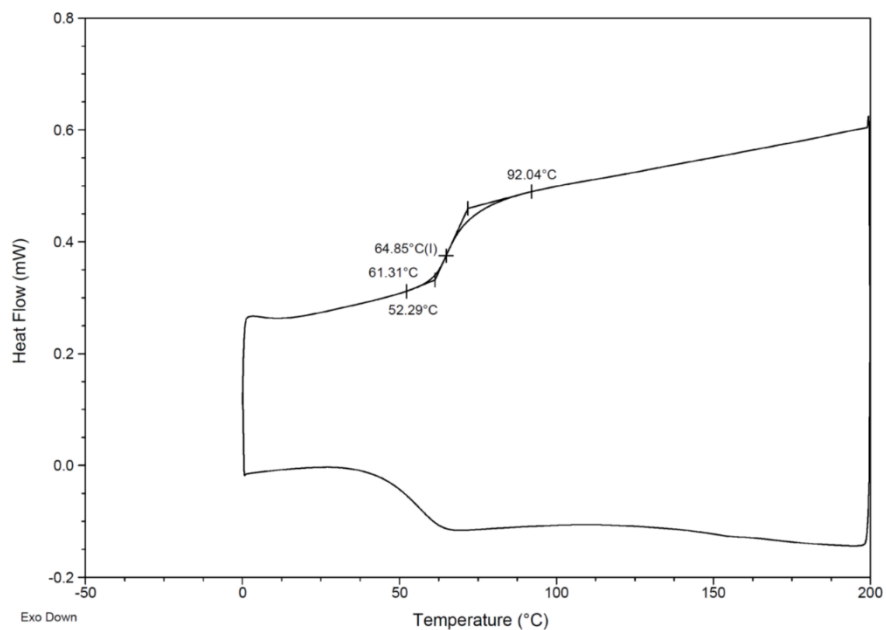


Figure A-20. DSC Thermogram of copoly(hydroxyethylidihydrosinapic acid/hydroxyethylsinapic acid) [50:50] (Table 1-2, Entry 6)

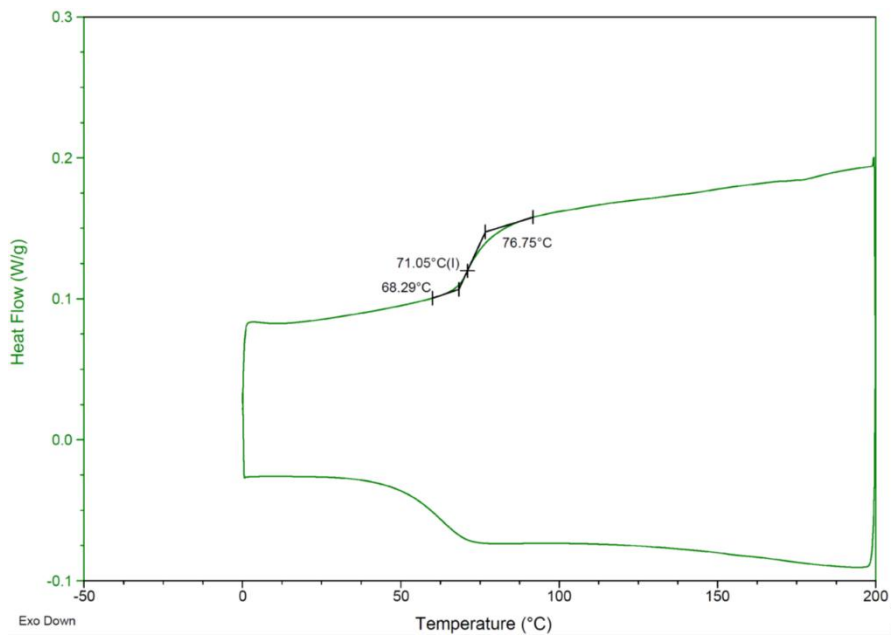


Figure A-21. DSC Thermogram of copoly(hydroxyethylidihydroxynapic acid/hydroxyethylsinapic acid) [40:60] (Table 1-2, Entry 7)

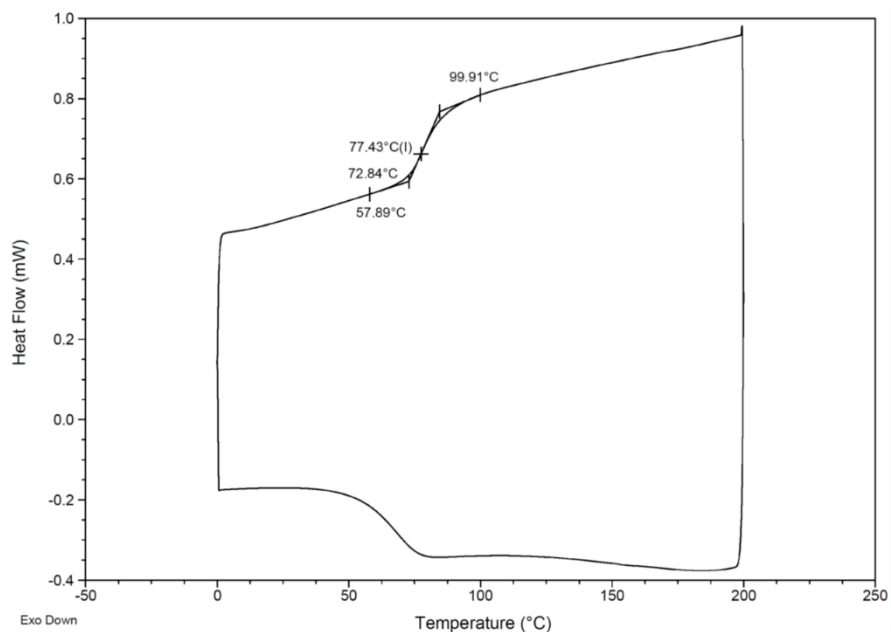


Figure A-22. DSC Thermogram of copoly(hydroxyethylidihydroxynapic acid/hydroxyethylsinapic acid) [30:70] (Table 1-2, Entry 8)

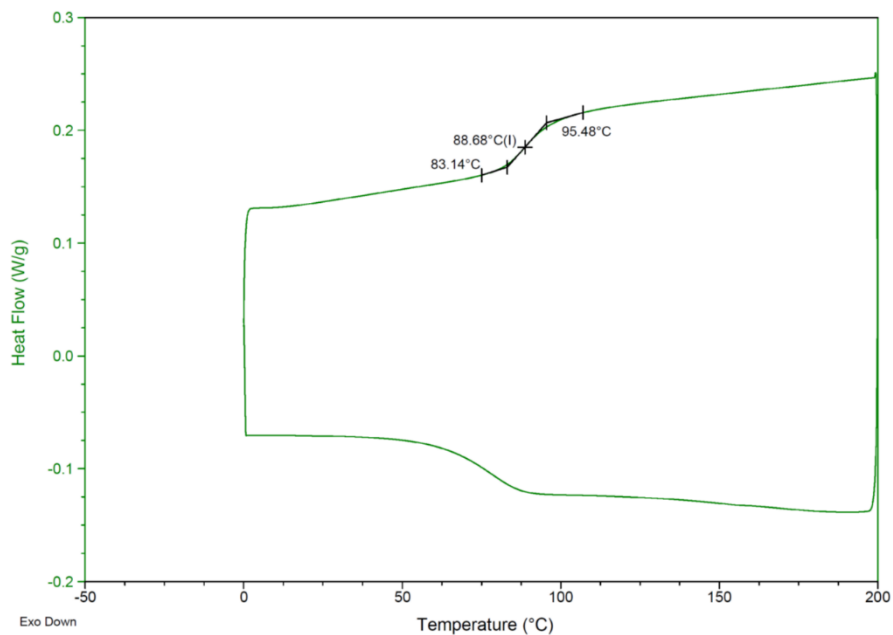


Figure A-23. DSC Thermogram of copoly(hydroxyethylidihydroxynapic acid/hydroxyethylsinapic acid) [20:80] (Table 1-2, Entry 9)

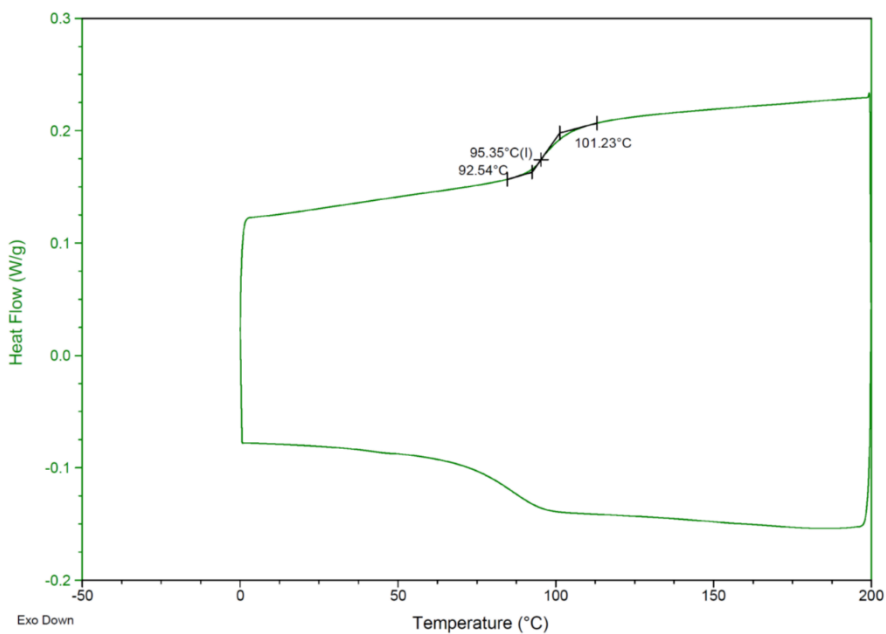


Figure A-24. DSC Thermogram of copoly(hydroxyethylidihydroxynapic acid/hydroxyethylsinapic acid) [10:90] (Table 1-2, Entry 10)

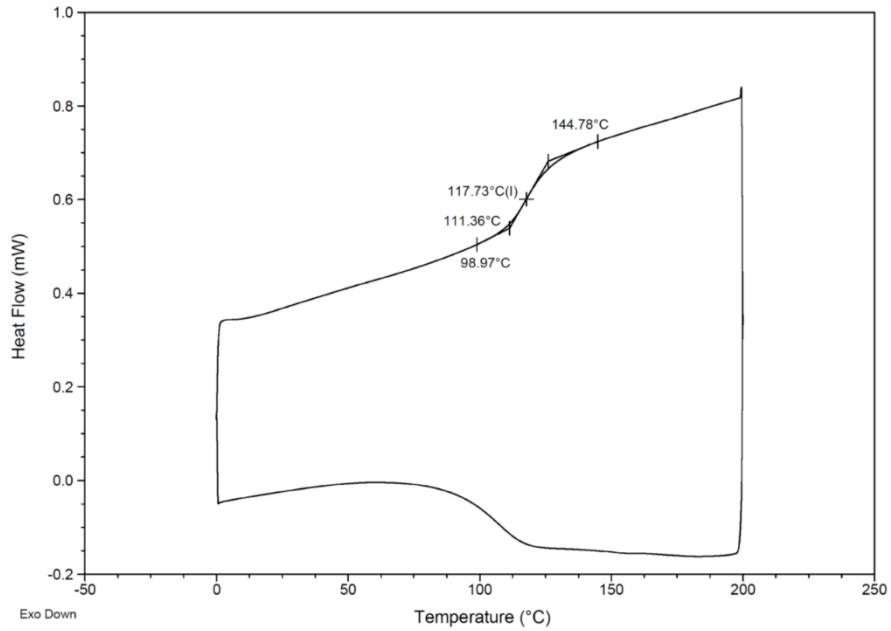


Figure A-25. DSC Thermogram of polyethylene sinapate (Table 1-1, Entry 1)

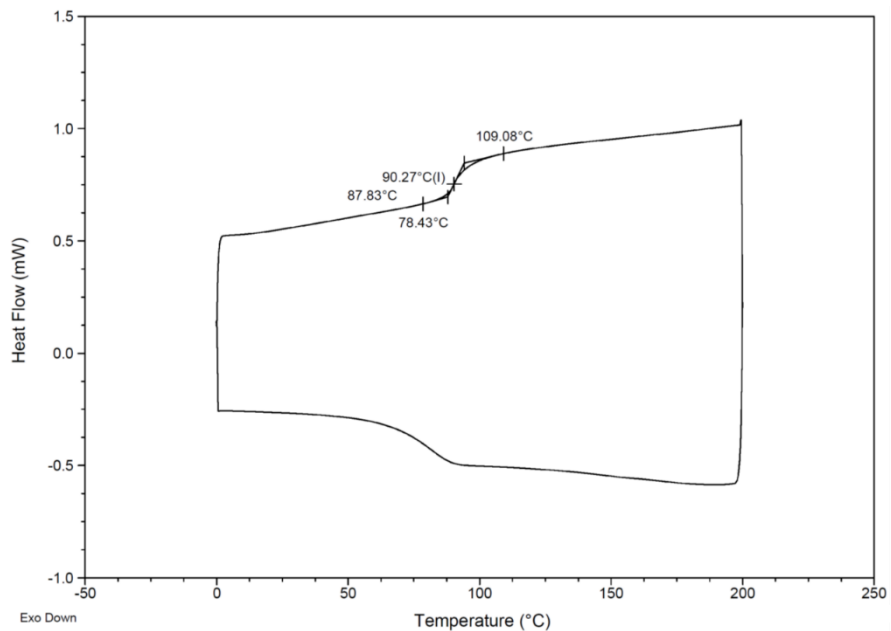


Figure A-26. DSC Thermogram of polypropylene sinapate (Table 1-1, Entry 3)

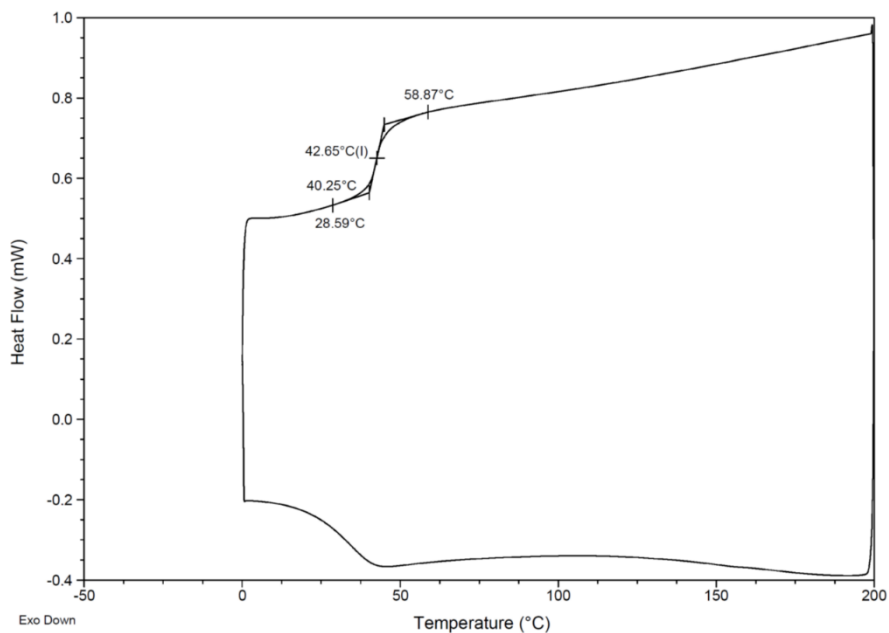


Figure A-27. DSC Thermogram of polyhexalene sinapate (Table 1-1, Entry 4)

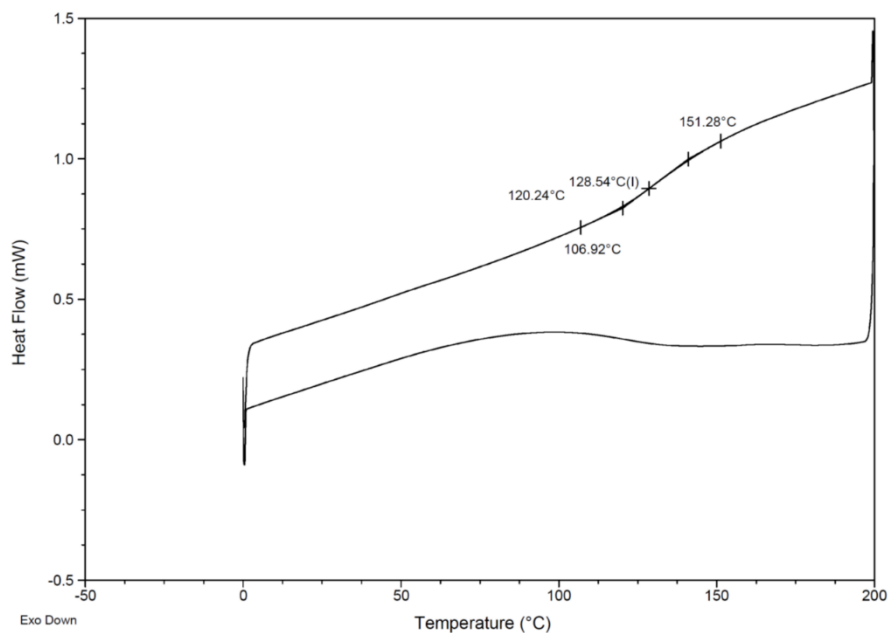


Figure A-28. DSC Thermogram of polyethylen sinapate from extracted sinapic acid.

GPC Spectra

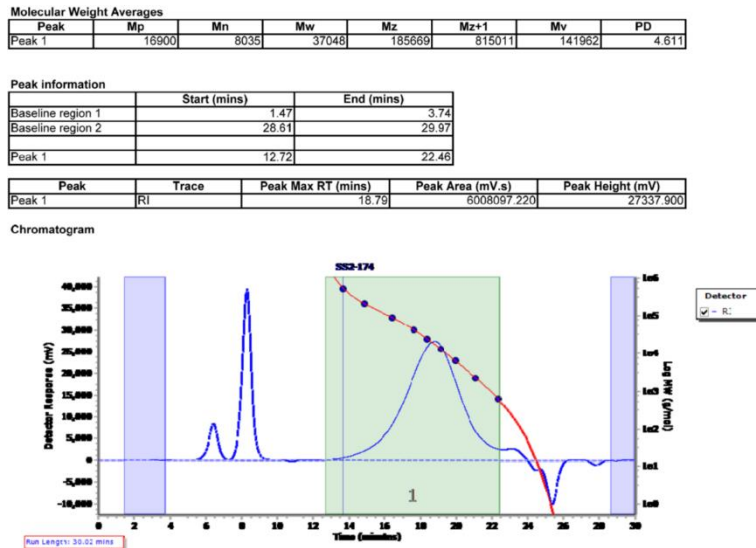


Figure A-29. GPC Chromatogram of polyethylene dihydrosinapate (Table 1-1, Entry 2 and Table 1-2, Entry 1).

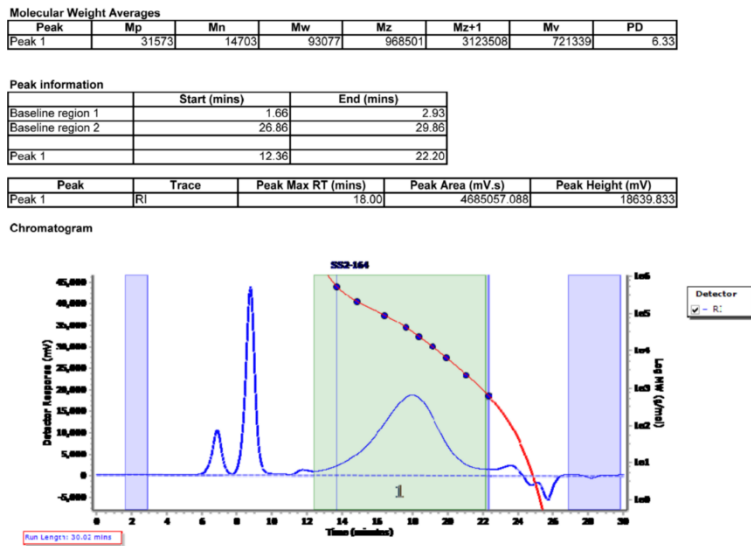


Figure A-30. GPC Chromatogram of copoly(hydroxyethyl dihydrosinapic acid/hydroxyethylsinapic acid) [90:10] (Table 1-2, Entry 2).

| Molecular Weight Averages | | | | | | | |
|---------------------------|------|------|-------|-------|--------|-------|-------|
| Peak | Mp | Mn | Mw | Mz | Mz+1 | Mv | PD |
| Peak 1 | 8693 | 4513 | 23933 | 83239 | 174703 | 72429 | 5.303 |

| Peak information | | |
|-------------------|--------------|------------|
| | Start (mins) | End (mins) |
| Baseline region 1 | 1.26 | 2.87 |
| Baseline region 2 | 26.77 | 29.97 |
| Peak 1 | 13.73 | 23.04 |

| Peak | Trace | Peak Max RT (mins) | Peak Area (mV.s) | Peak Height (mV) |
|--------|-------|--------------------|------------------|------------------|
| Peak 1 | R1 | 19.57 | 5691350.828 | 25360.101 |

Chromatogram

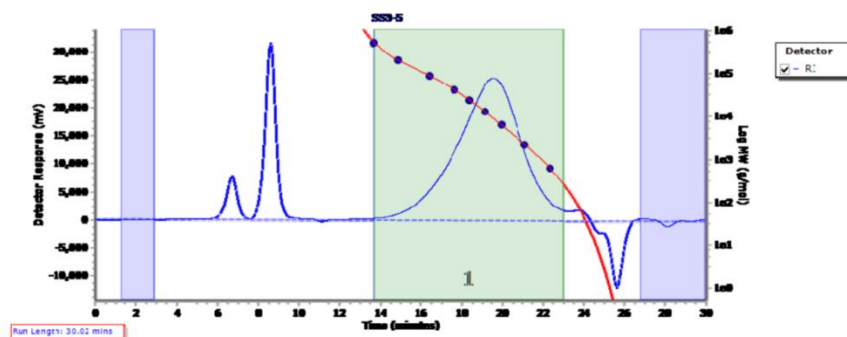


Figure A-31. GPC Chromatogram of polyhexalene sinapate (Table 1-1, Entry 4).

NMR Spectra

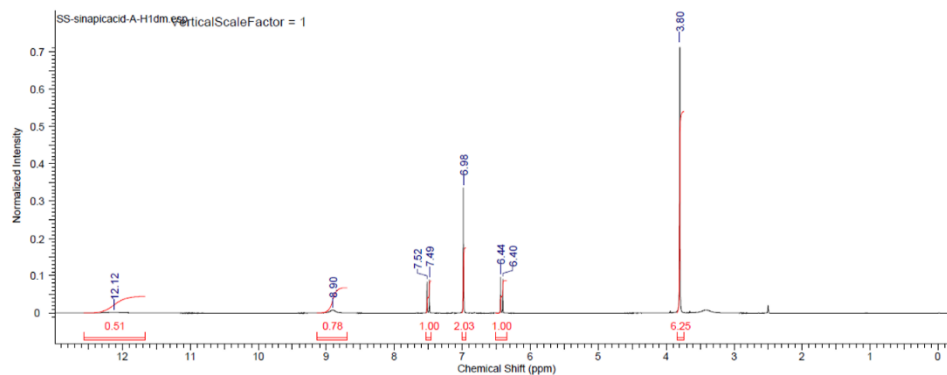


Figure A-32. ^1H NMR Spectrum of commercial sinapic acid.

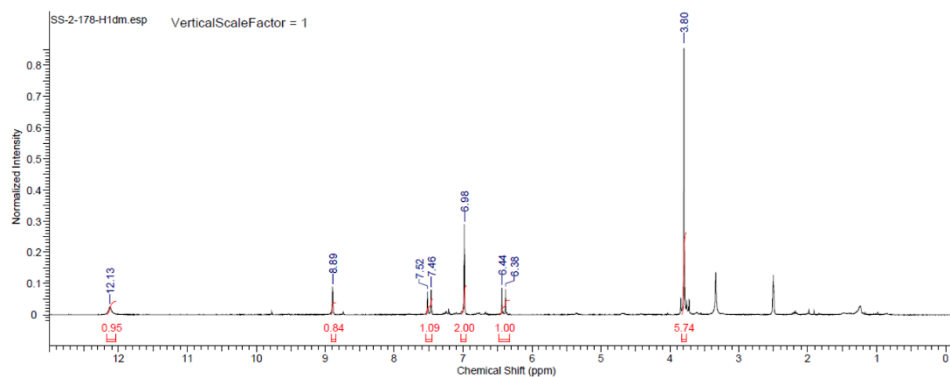


Figure A-33. ^1H NMR Spectrum of extracted sinapic acid from base hydrolysis.

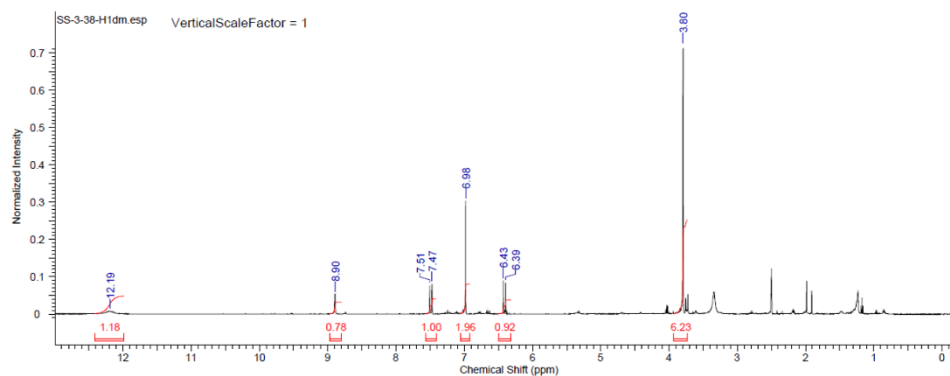


Figure A-34. ^1H NMR Spectrum of extracted sinapic acid from sonication.

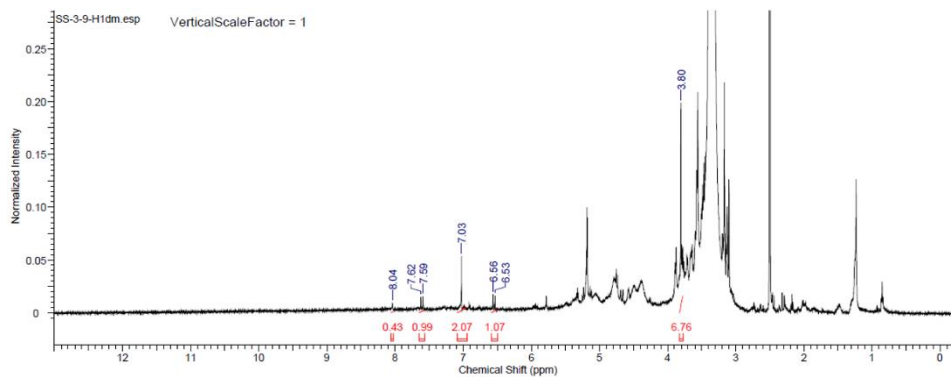


Figure A-35. ¹H NMR Spectrum of extracted sinapine from MeOH hydrolysis

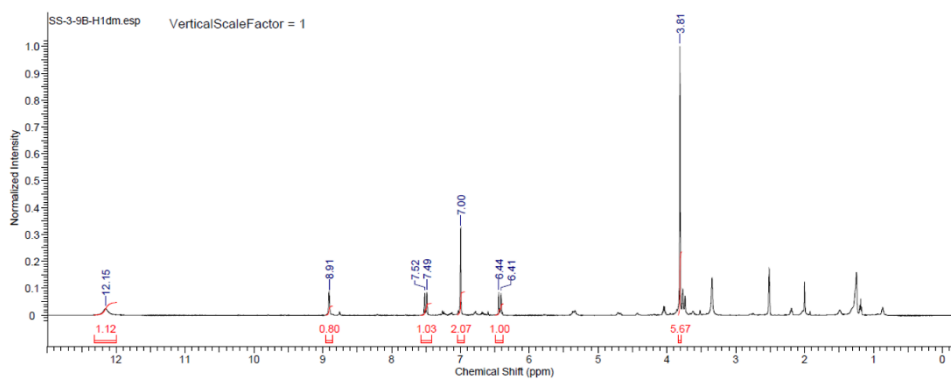


Figure A-36. ¹H NMR Spectrum of extracted sinapic acid from MeOH hydrolysis.

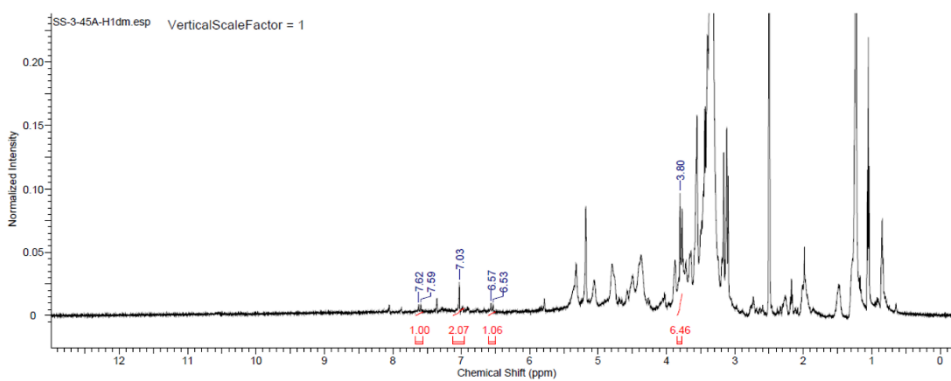


Figure A-37. ¹H NMR Spectrum of extracted sinapine from EtOH hydrolysis.

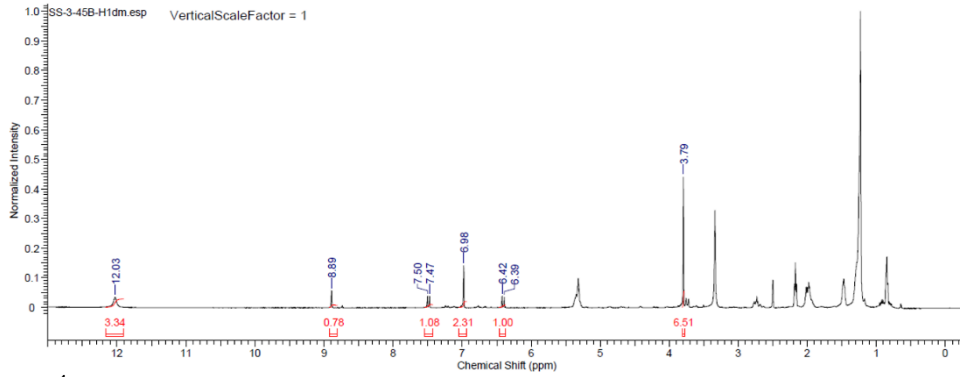


Figure A-38. ¹H NMR Spectrum of extracted sinapic acid from EtOH hydrolysis.

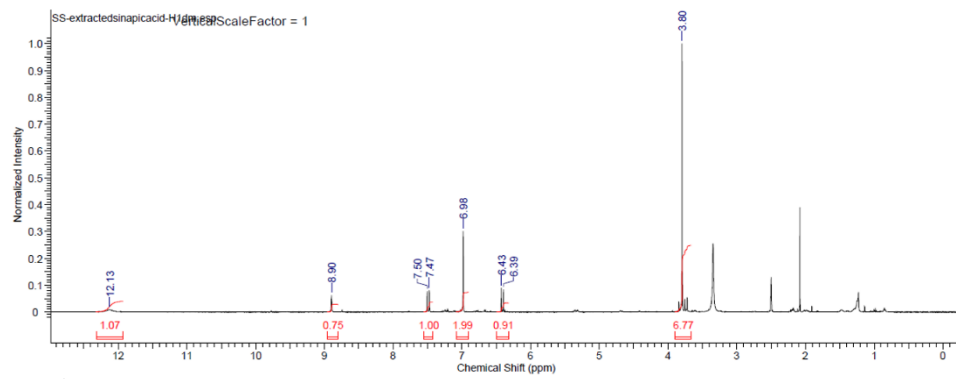


Figure A-39. ¹H NMR Spectrum of combined extracted sinapic acid for polymerization.

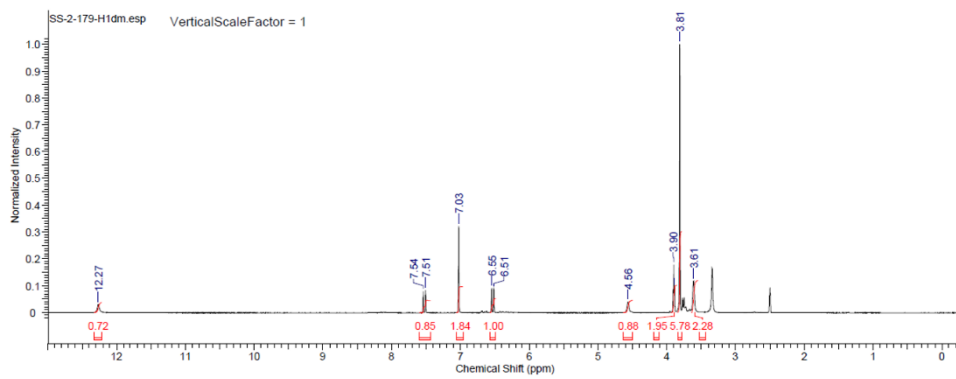


Figure A-40. ¹H NMR Spectrum of hydroxyethylsinapic acid.

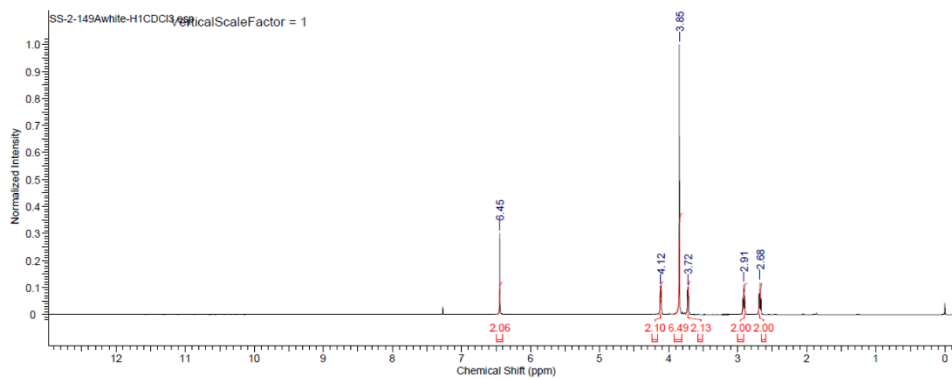


Figure A-41. ¹H NMR Spectrum of hydroxyethylidihydrosinapic acid.

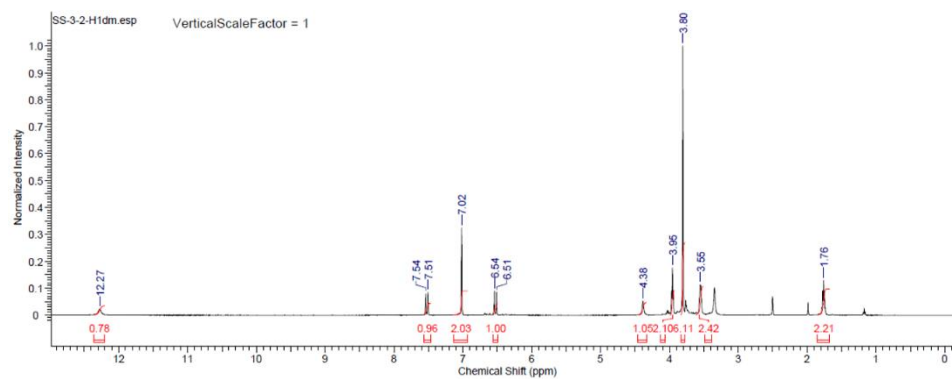


Figure A-42. ¹H NMR Spectrum of hydroxypropylsinapic acid.

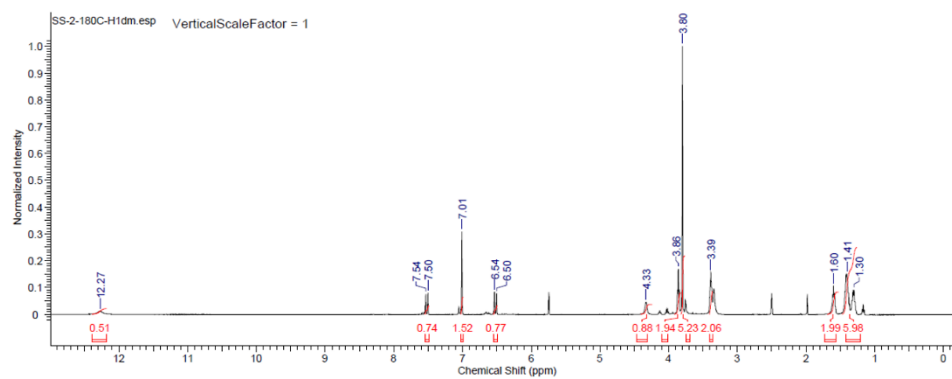


Figure A-43. ¹H NMR Spectrum of hydroxyhexylsinapic acid

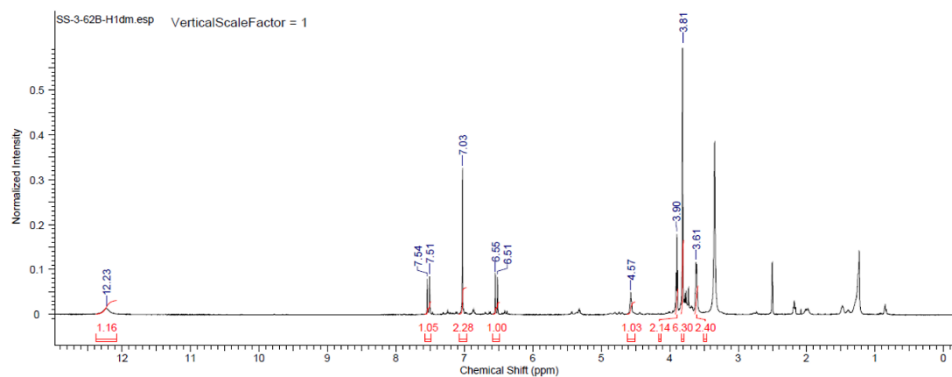


Figure A-44. ¹H NMR Spectrum of hydroxyethylsinapic acid from extracted sinapic acid

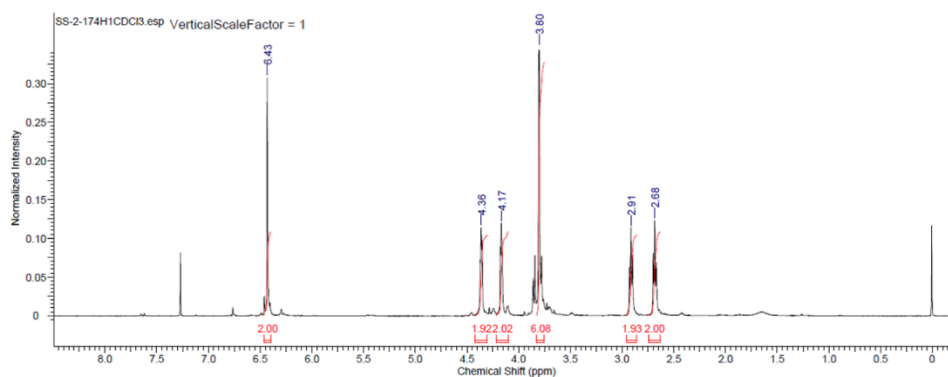


Figure A-45. ¹H NMR Spectrum of polyethylene dihydrosinapate (Table 1-1, Entry 2 and Table 1-2, Entry 1)

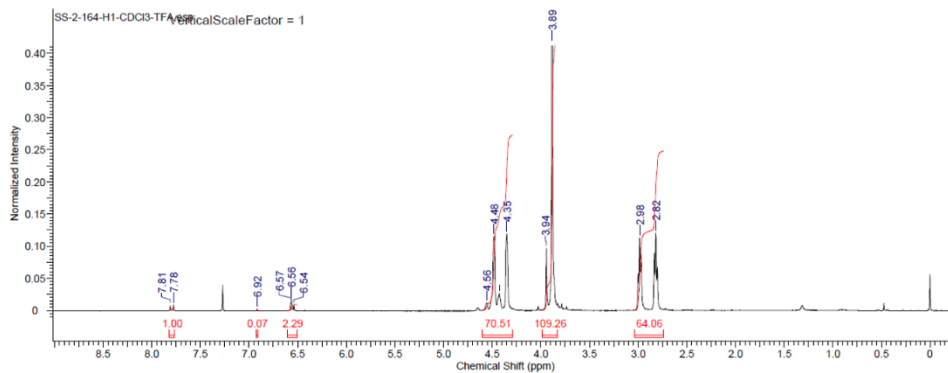


Figure A-46. ¹H NMR Spectrum of copoly(hydroxyethyl dihydrosinapic acid/hydroxyethylsinapic acid) [90:10] (Table 1-2, Entry 2)

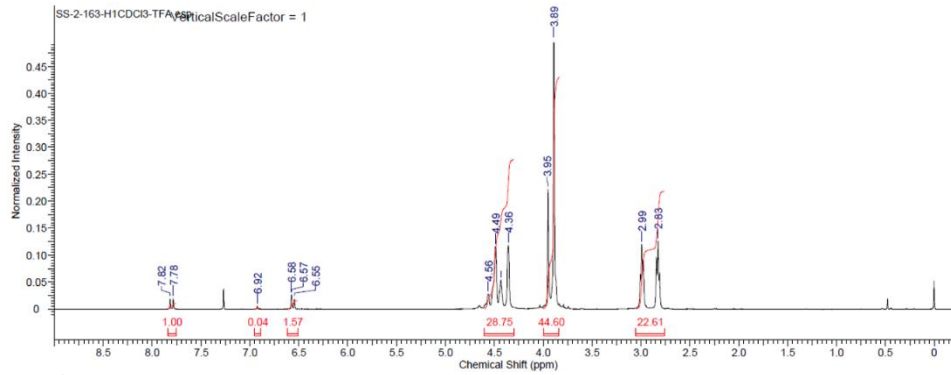


Figure A-47. ¹H NMR Spectrum of copoly(hydroxyethylidihydroxynapic acid/hydroxyethylsinapic acid) [80:20] (Table 1-2, Entry 3)

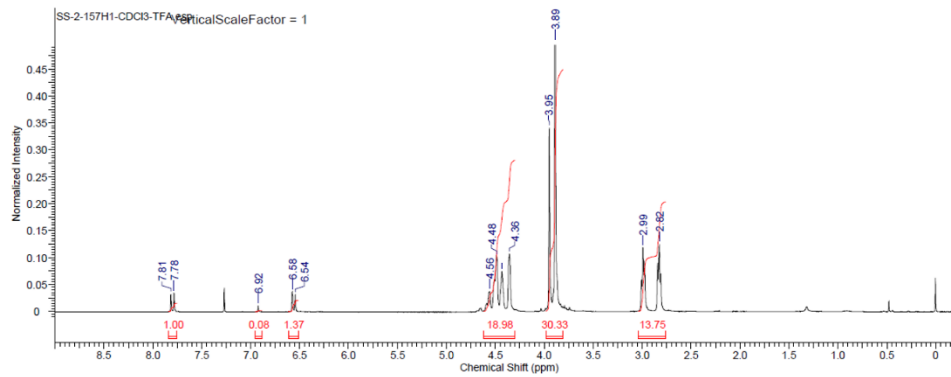


Figure A-48. ¹H NMR Spectrum of copoly(hydroxyethylidihydroxynapic acid/hydroxyethylsinapic acid) [70:30] (Table 1-2, Entry 4)

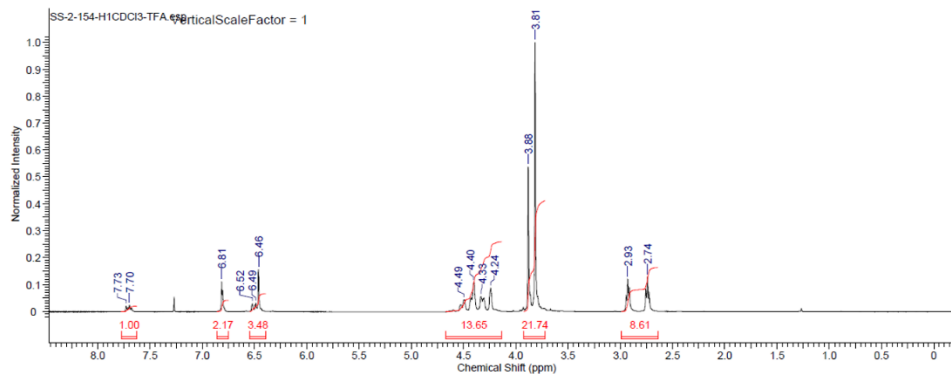


Figure A-49. ¹H NMR Spectrum of copoly(hydroxyethylidihydroxynapic acid/hydroxyethylsinapic acid) [60:40] (Table 1-2, Entry 5)

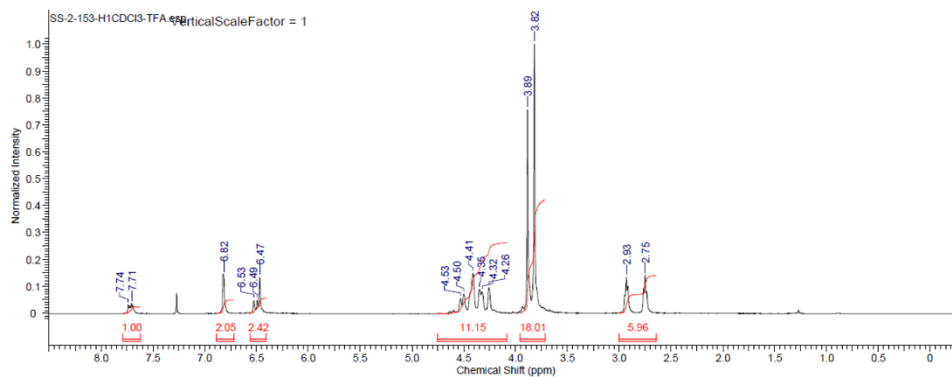


Figure A-50. ¹H NMR Spectrum of copoly(hydroxyethylidihydroxynipic acid/hydroxyethylsinipic acid) [50:50] (Table 1-2, Entry 6)

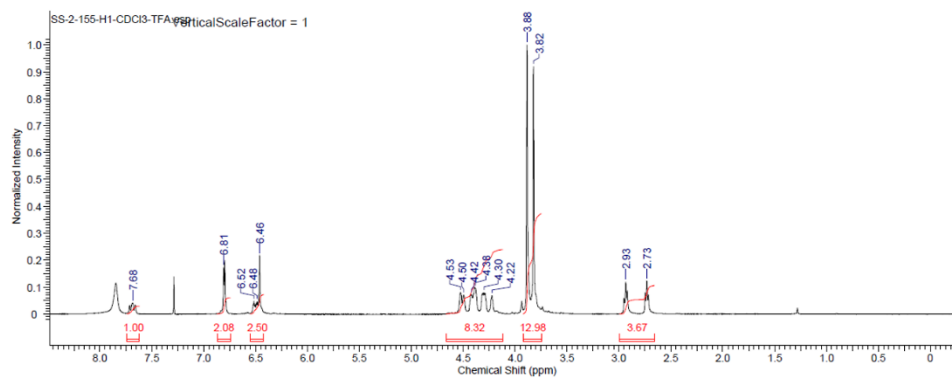


Figure A-51. ¹H NMR Spectrum of copoly(hydroxyethylidihydroxynipic acid/hydroxyethylsinipic acid) [40:60] (Table 1-2, Entry 7)

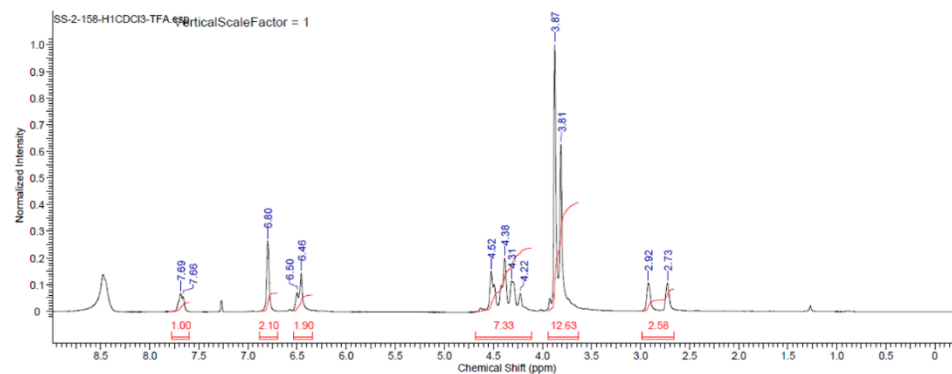


Figure A-52. ¹H NMR Spectrum of copoly(hydroxyethylidihydroxynipic acid/hydroxyethylsinipic acid) [30:70] (Table 1-2, Entry 8)

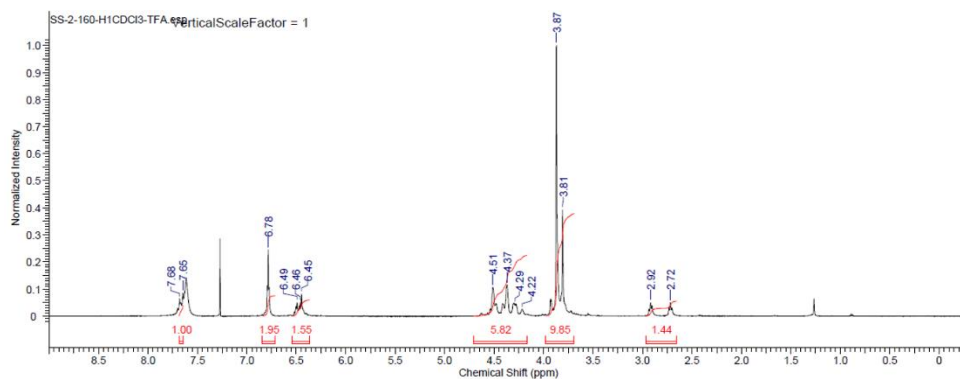


Figure A-53. ¹H NMR Spectrum of copoly(hydroxyethylidihydroxynapic acid/hydroxyethylsinapic acid) [20:80] (Table 1-2, Entry 9)

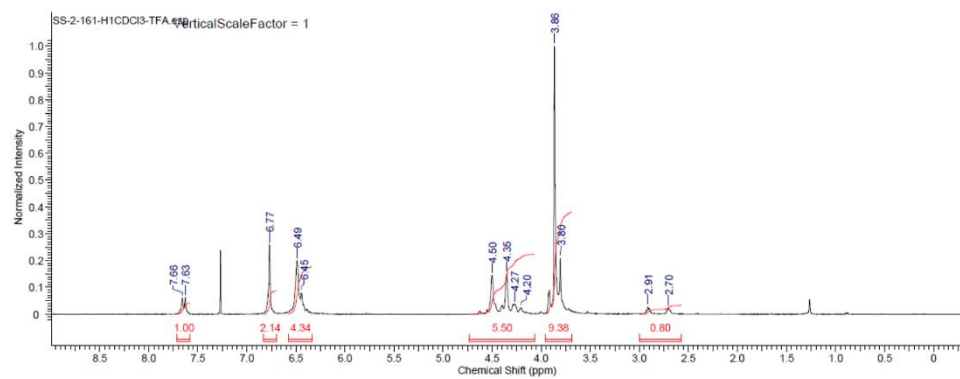


Figure A-54. ¹H NMR Spectrum of copoly(hydroxyethylidihydroxynapic acid/hydroxyethylsinapic acid) [10:90] (Table 1-2, Entry 10)

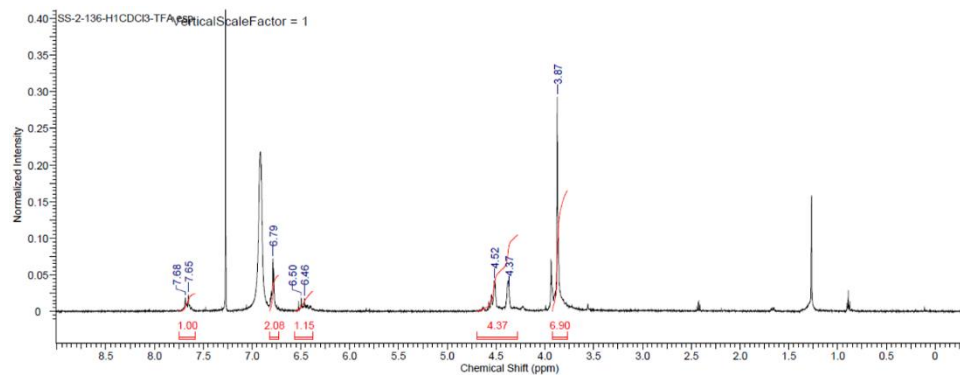


Figure A-55. ¹H NMR Spectrum of polyethylene sinapate (Table 1-2, Entry 1 and Table 1-2, Entry 11)

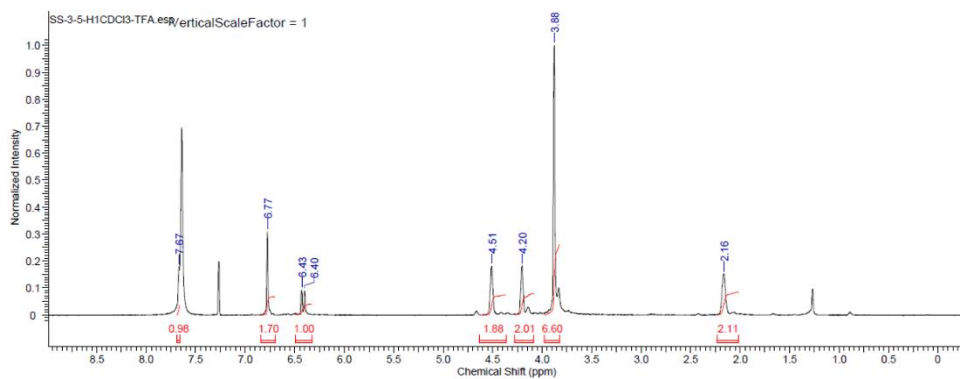


Figure A-56. ¹H NMR Spectrum of polypropylene sinapate (Table 1-2, Entry 3)

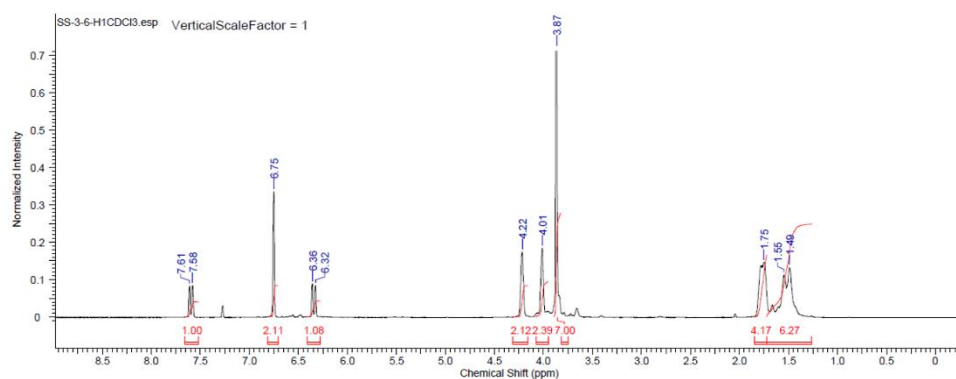


Figure A-57. ¹H NMR Spectrum of polyhexalene sinapate (Table 1-2, Entry 4).

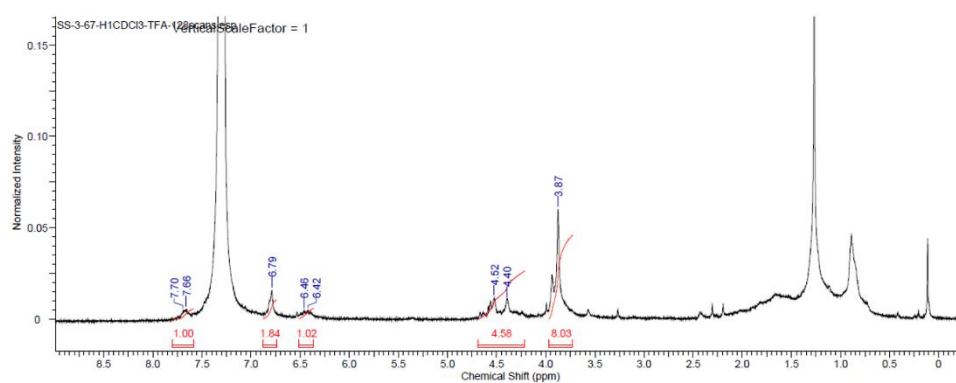


Figure A-58. ¹H NMR Spectrum of polyethylene sinapate from extracted sinapic acid.

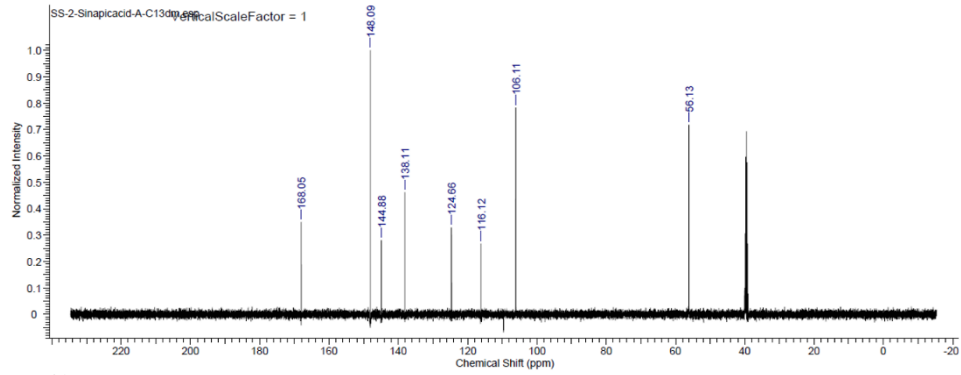


Figure A-59. ¹³C NMR Spectrum of commercial sinapic acid

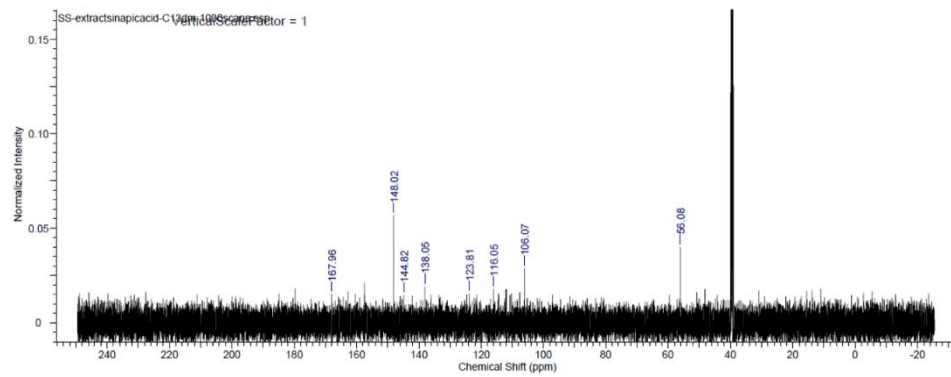


Figure A-60. ¹³C NMR Spectrum of extracted sinapic acid

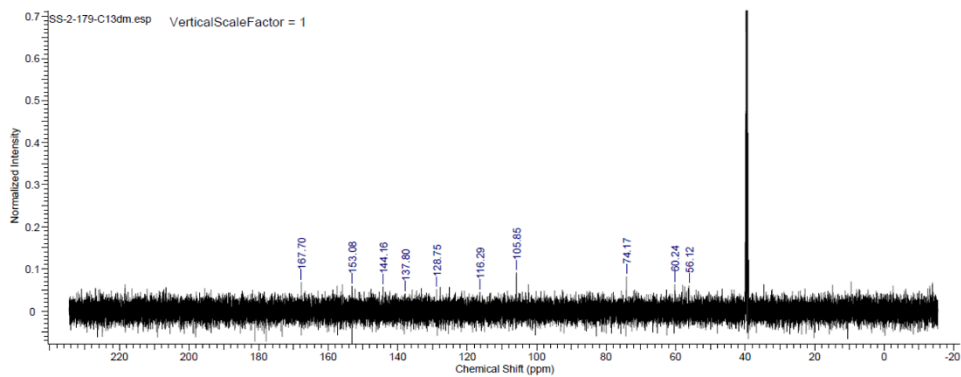


Figure A-61. ¹³C NMR Spectrum of hydroxyethylenesinapic acid

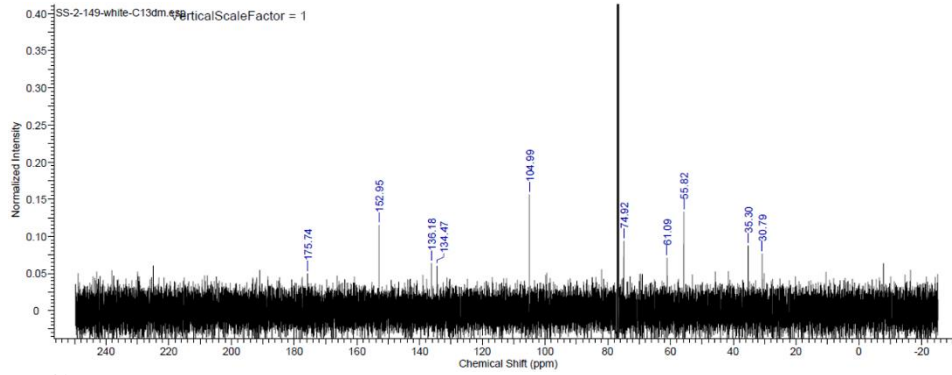


Figure A-62. ^{13}C NMR Spectrum of hydroxyethylenedihydrosinapic acid

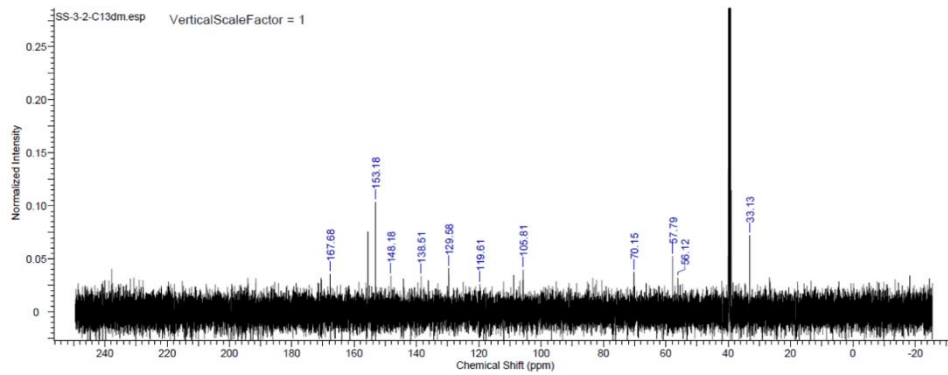


Figure A-63. ^{13}C NMR Spectrum of hydroxypropylenesinapic acid

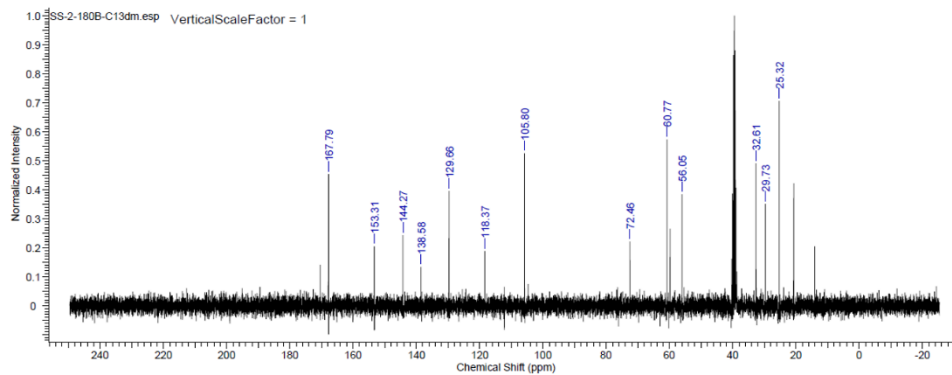


Figure A-64. ^{13}C NMR Spectrum of hydroxyhexalenesinapic acid

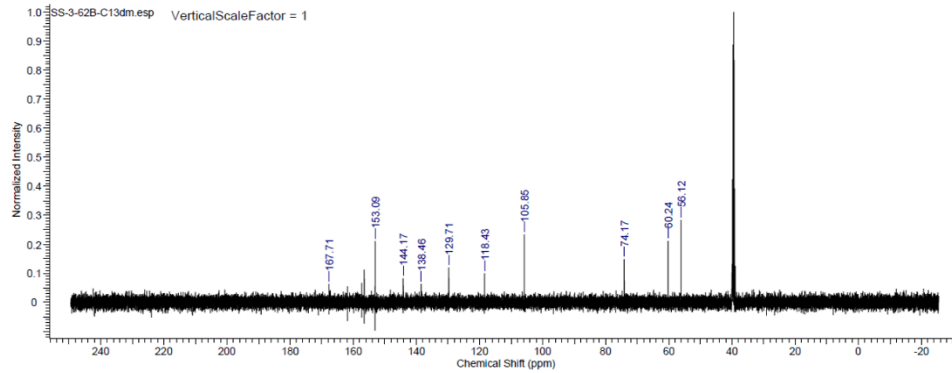


Figure A-65. ^{13}C NMR Spectrum of hydroxyethylenesinapic acid from extracted sinapic acid

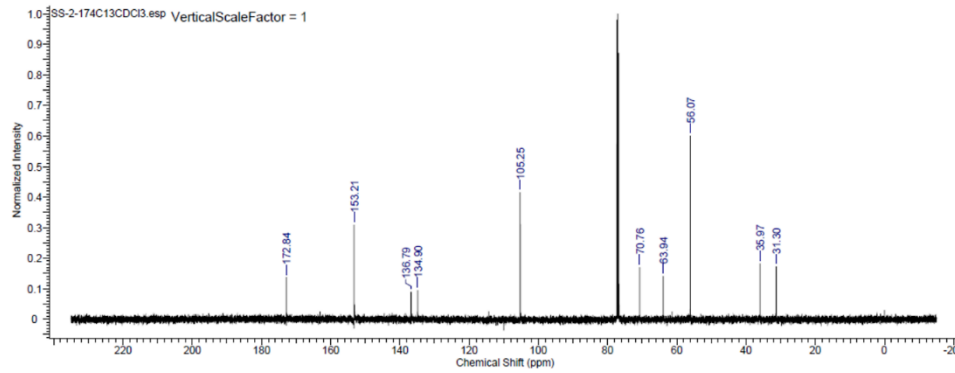


Figure A-66. ^{13}C NMR Spectrum of polyethylene dihydrosinapate (Table 1-1, entry 2, Table 1-2, entry 1).

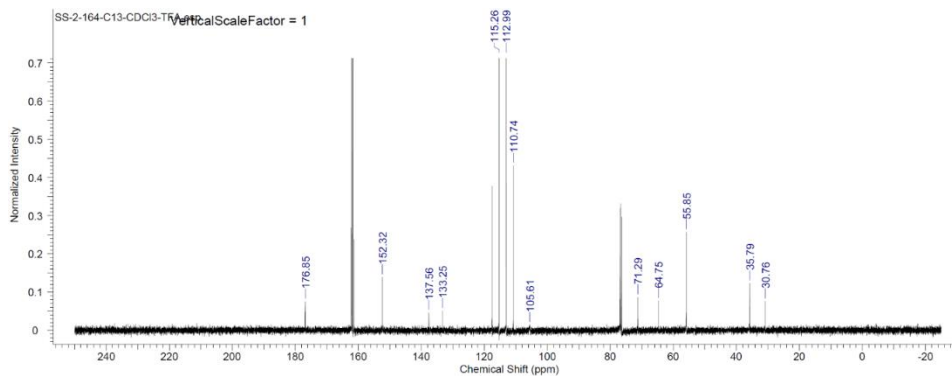


Figure A-67. ^{13}C NMR Spectrum of copoly(hydroxyethyl dihydrosinapic acid/hydroxyethylsinapic acid) [90:10] (Table 1-2, Entry 2)

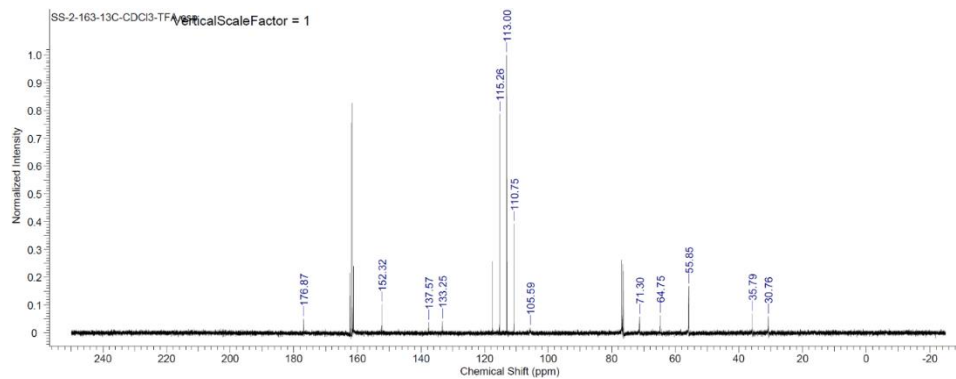


Figure A-68. ¹³C NMR Spectrum of copoly(hydroxyethylidihydrosinapic acid/hydroxyethylsinapic acid) [80:20] (Table 1-2, Entry 3)

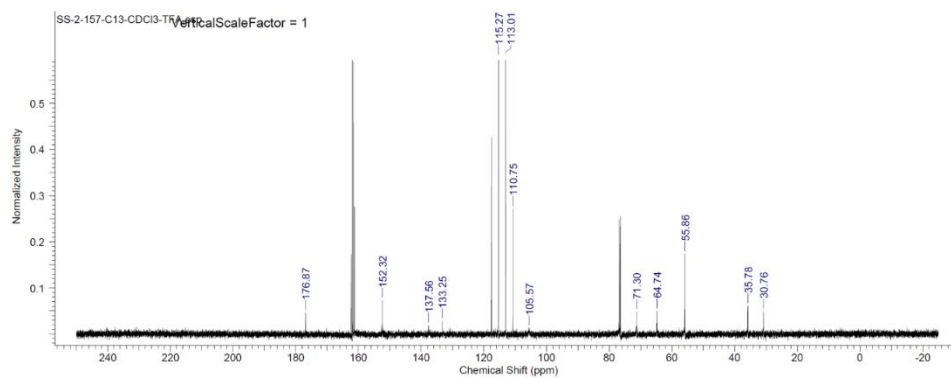


Figure A-69. ¹³C NMR Spectrum of copoly(hydroxyethylidihydrosinapic acid/hydroxyethylsinapic acid) [70:30] (Table 1-2, Entry 4)

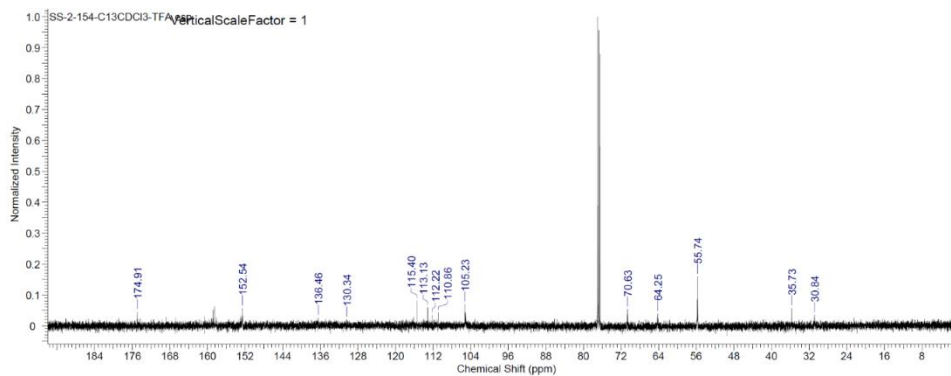


Figure A-70. ¹³C NMR Spectrum of copoly(hydroxyethylidihydrosinapic acid/hydroxyethylsinapic acid) [60:40] (Table 1-2, Entry 5)

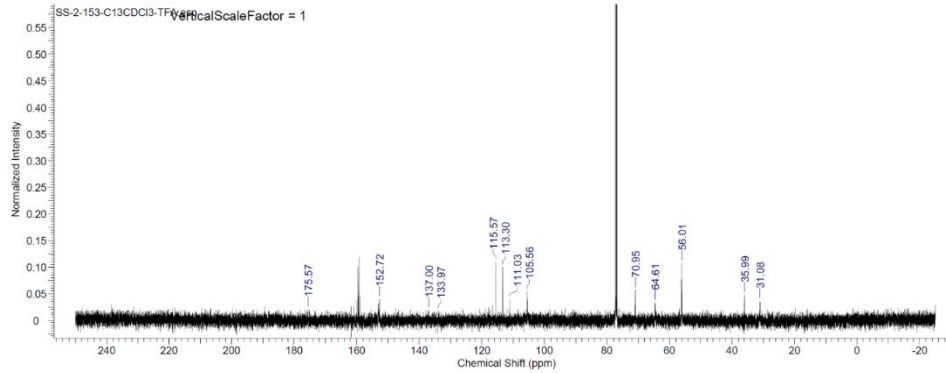


Figure A-71. ¹³C NMR Spectrum of copoly(hydroxyethylidihydrosinapic acid/hydroxyethylsinapic acid) [50:50] (Table 1-2, Entry 6)

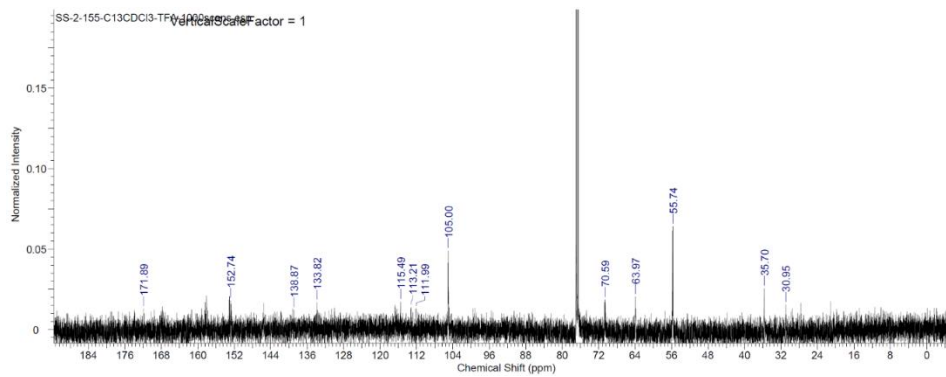


Figure A-72. ¹³C NMR Spectrum of copoly(hydroxyethylidihydrosinapic acid/hydroxyethylsinapic acid) [40:60] (Table 1-2, Entry 7)

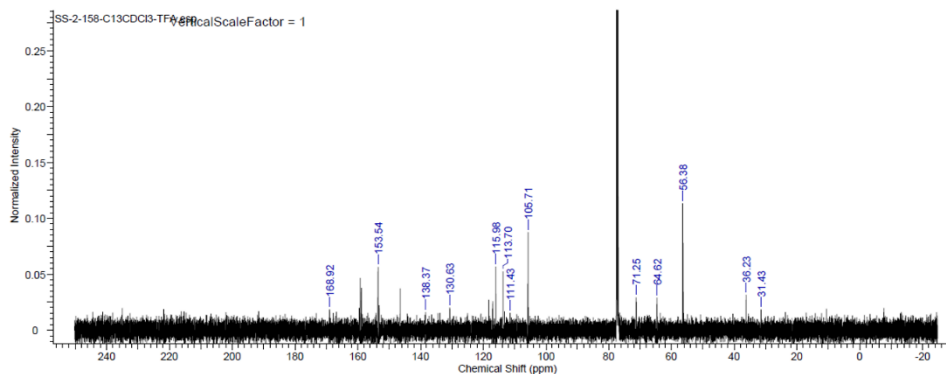


Figure A-73. ¹³C NMR Spectrum of copoly(hydroxyethylidihydrosinapic acid/hydroxyethylsinapic acid) [30:70] (Table 1-2, Entry 8)

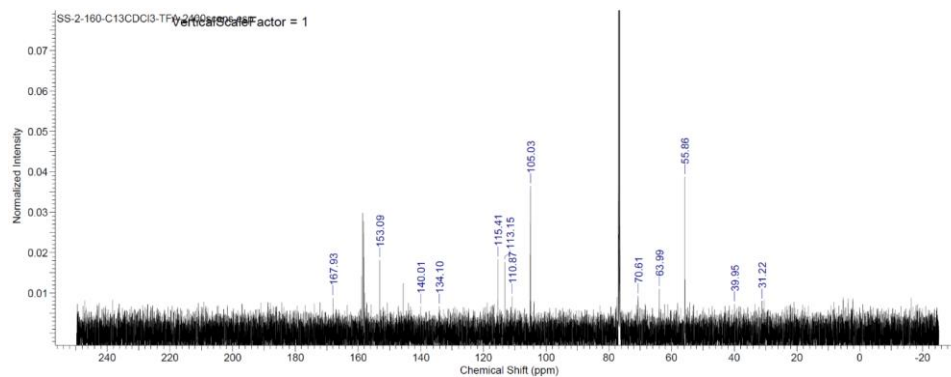


Figure A-74. ¹³C NMR Spectrum of copoly(hydroxyethylidihydroxynapic acid/hydroxyethylsinapic acid) [20:80] (Table 1-2, Entry 9)

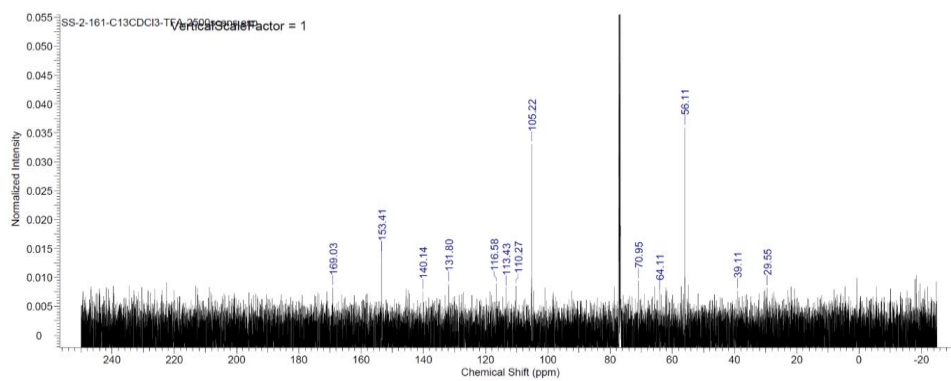


Figure A-75. ¹³C NMR Spectrum of copoly(hydroxyethylidihydroxynapic acid/hydroxyethylsinapic acid) [10:90] (Table 1-2, Entry 10)

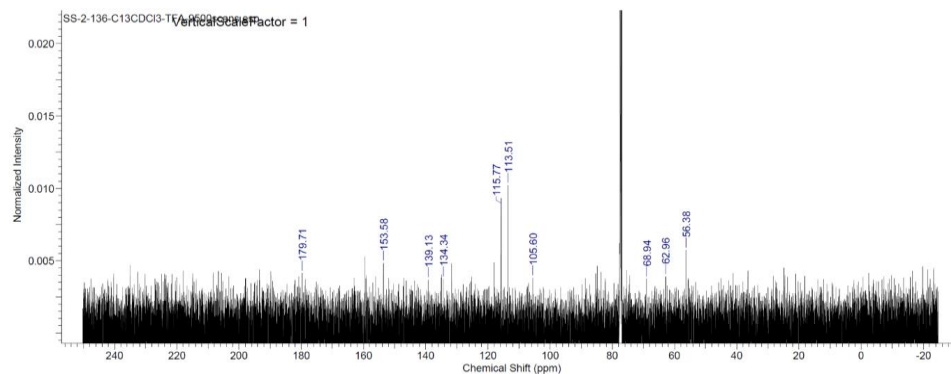


Figure A-76. ¹³C NMR Spectrum of polyethylene sinapate (Table 1-1, entry 1 and Table 1-2, entry 11)

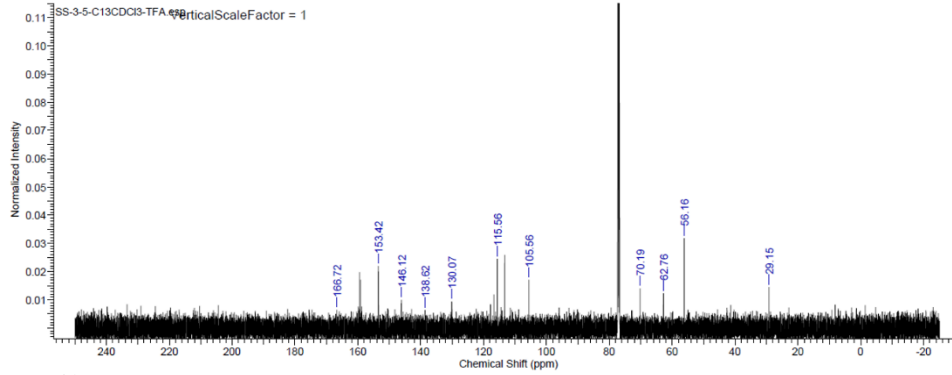


Figure A-77. ^{13}C NMR Spectrum of polypropylene sinapate (Table 1-2, entry 3).

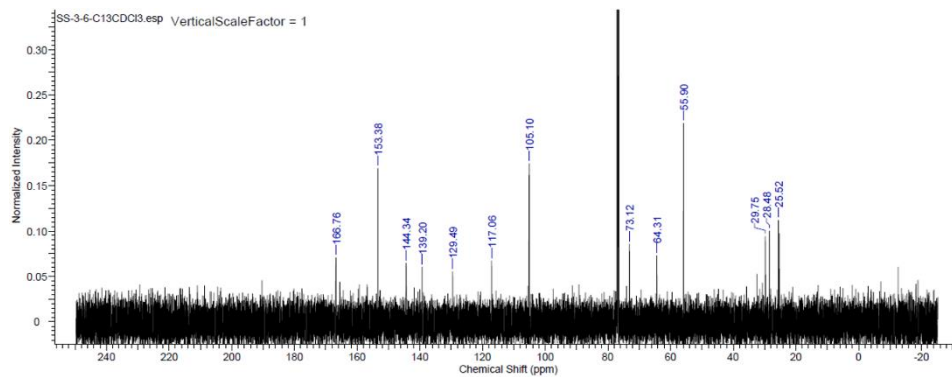


Figure A-78. ^{13}C NMR Spectrum of polyhexalene sinapate (Table S2, entry 4).

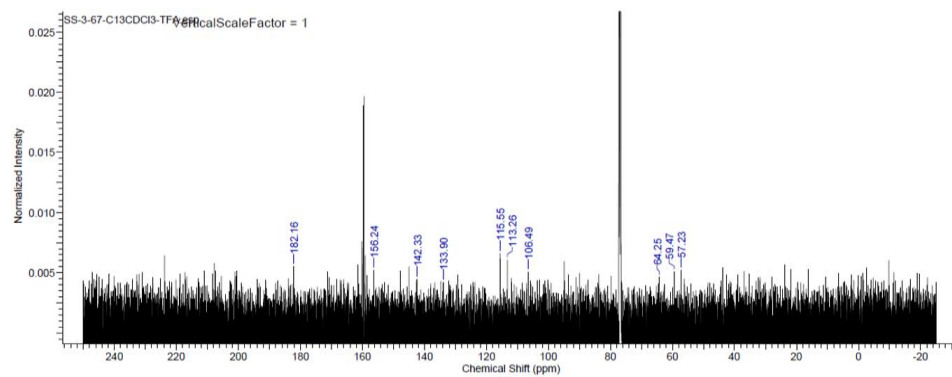


Figure A-79. ^{13}C NMR Spectrum of polyethylene sinapate from extracted sinapic acid.

APPENDIX B
SUPPLEMENTARY INFORMATION FOR CHAPTER 2

TGA Spectra

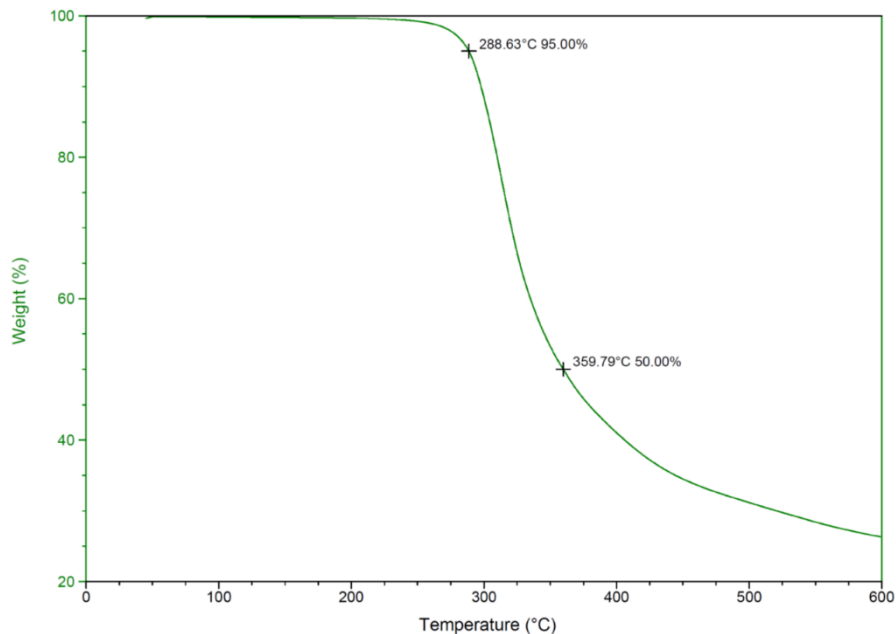


Figure B-1. TGA Thermogram of polyethyleneglycolate dihydrosinapate (Table 2-2, entry 1)

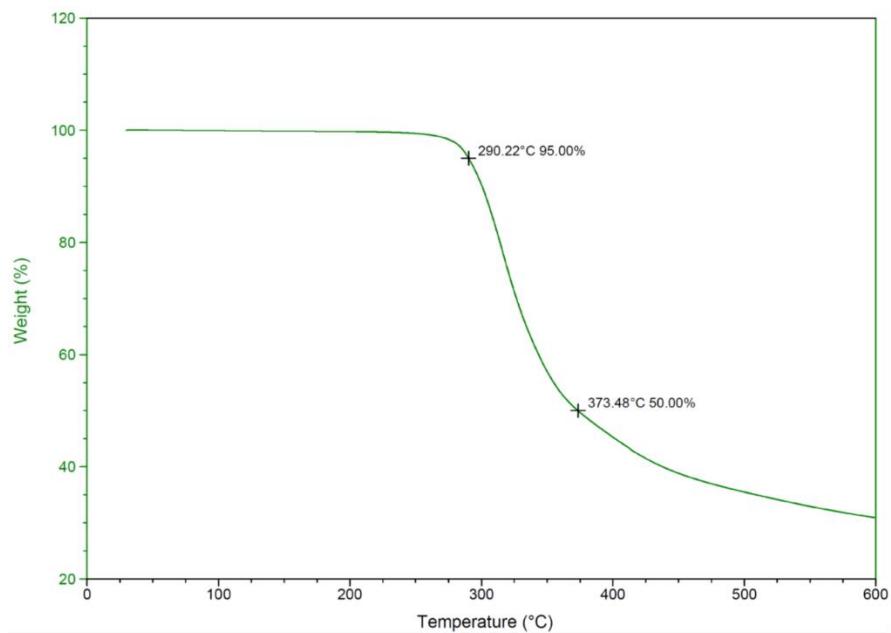


Figure B-2. TGA Thermogram of copoly(ethyleneglycolate dihydrosinapate/ethyleneglycolate sinapate) [90:10] (Table 2-2, entry 2).

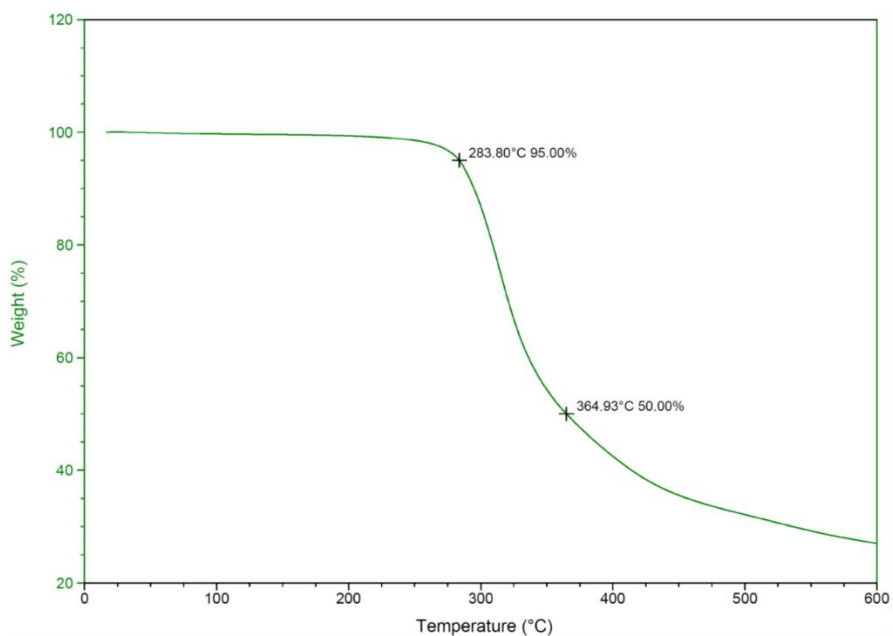


Figure B-3. TGA Thermogram of copoly(ethyleneglycolate dihydrosinapate/ethyleneglycolate sinapate) [80:20] (Table 2-2, entry 3).

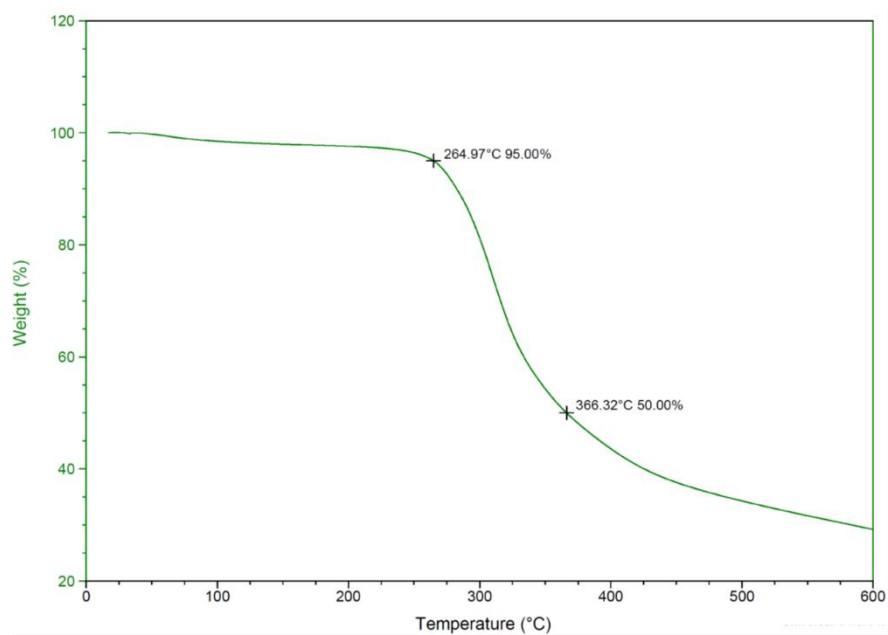


Figure B-4. TGA Thermogram of copoly(ethyleneglycolate dihydrosinapate/ethyleneglycolate sinapate) [70:30] (Table 2-2, entry 4).

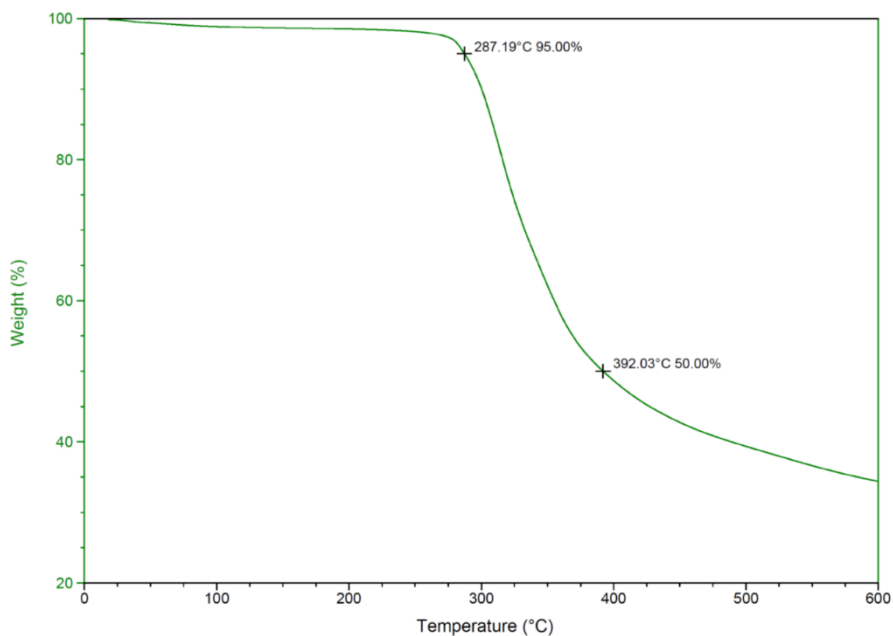


Figure B-5. TGA Thermogram of copoly(ethyleneglycolate dihydrosinapate/ethyleneglycolate sinapate) [60:40] (Table 2-2, entry 5)

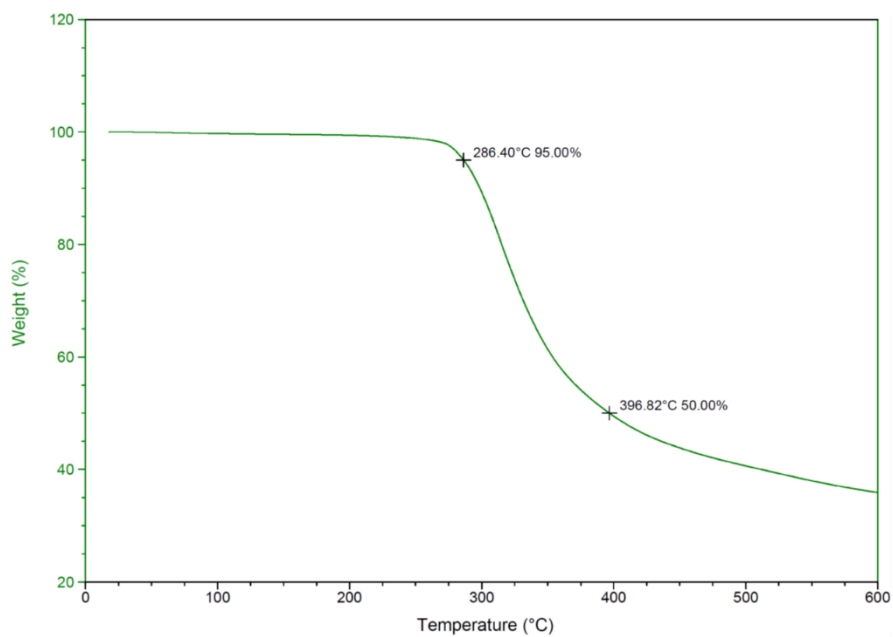


Figure B-6. TGA Thermogram of copoly(ethyleneglycolate dihydrosinapate/ethyleneglycolate sinapate) [50:50] (Table 2-2, entry 6).

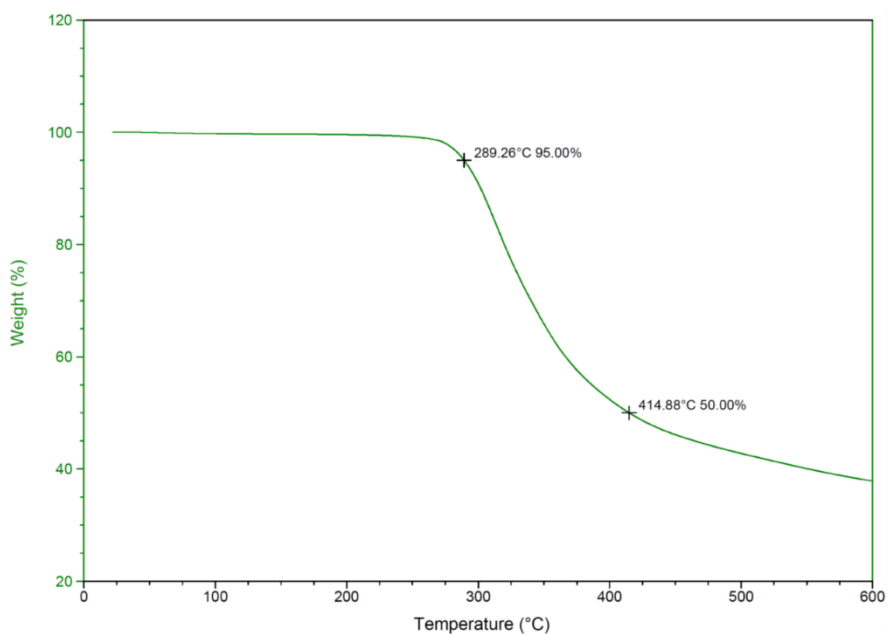


Figure B-7. TGA Thermogram of copoly(ethyleneglycolate dihydrosinapate/ethyleneglycolate sinapate) [40:60] (Table 2-2, entry 7)

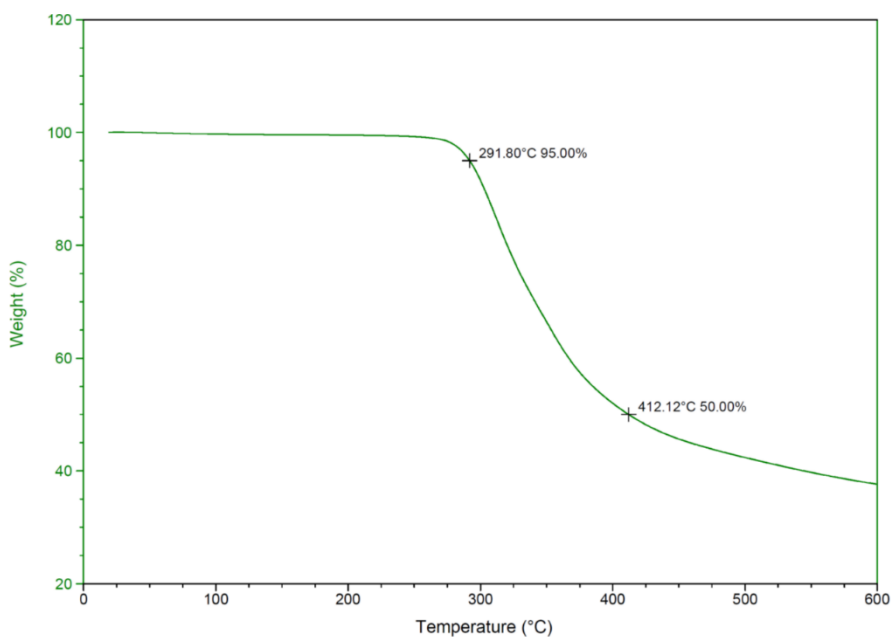


Figure B-8. TGA Thermogram of copoly(ethyleneglycolate dihydrosinapate/ethyleneglycolate sinapate) [30:70] (Table 2-2, entry 8).

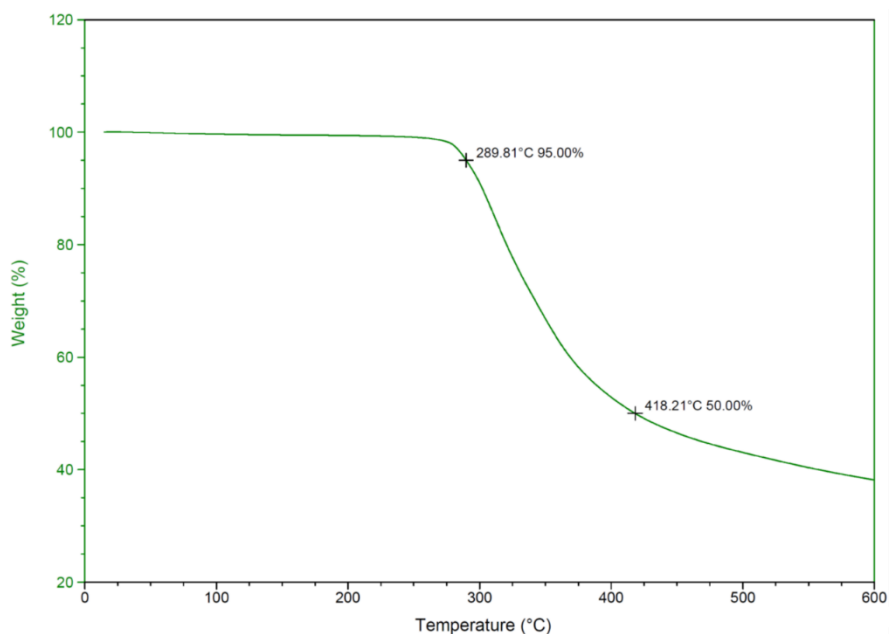


Figure B-9. TGA Thermogram of copoly(ethyleneglycolate dihydrosinapate/ethyleneglycolate sinapate) [20:80] (Table 2-2, Entry 9)

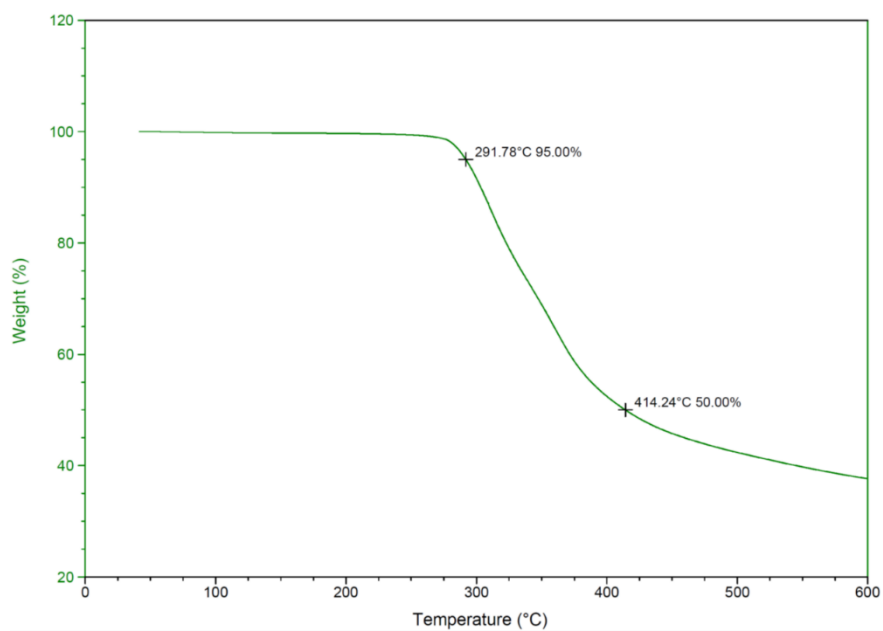


Figure B-10. TGA Thermogram of copoly(ethyleneglycolate dihydrosinapate/ethyleneglycolate sinapate) [10:90] (Table 2-2, entry 10).

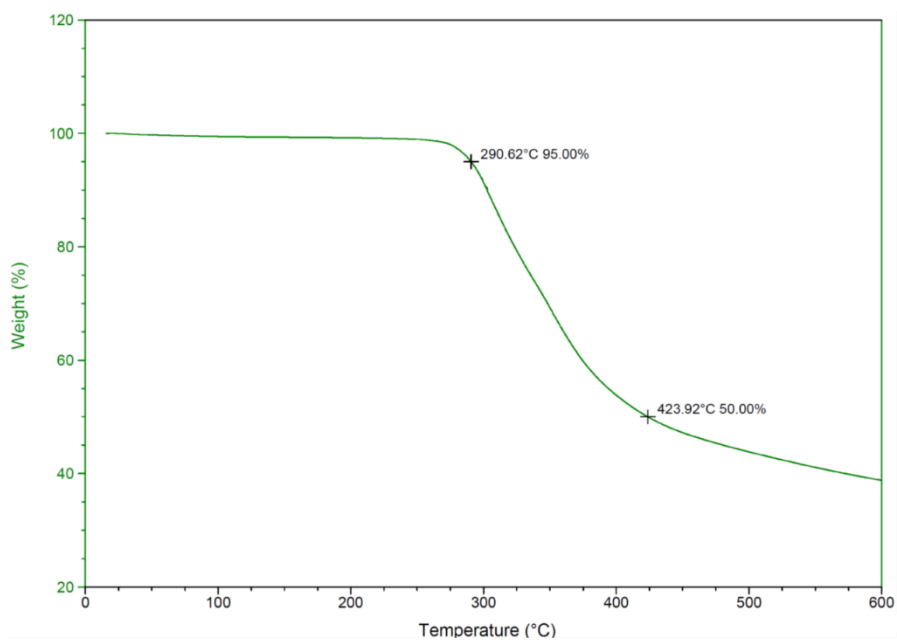


Figure B-11. TGA Thermogram of polyethyleneglycolate sinapate (Table 2-2, entry 11).

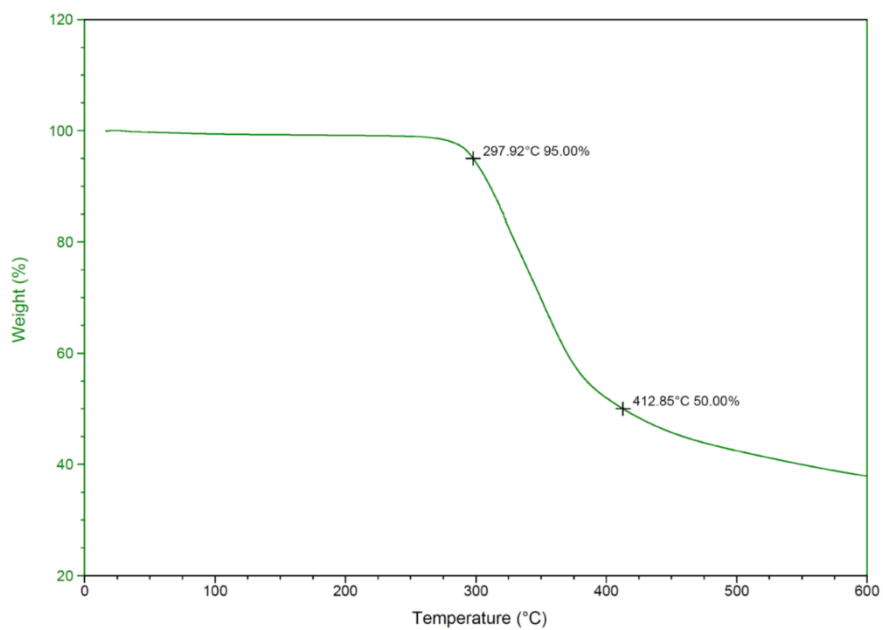


Figure B-12. TGA Thermogram of polypropyleneglycolate sinapate (Table 2-3, entry 2)

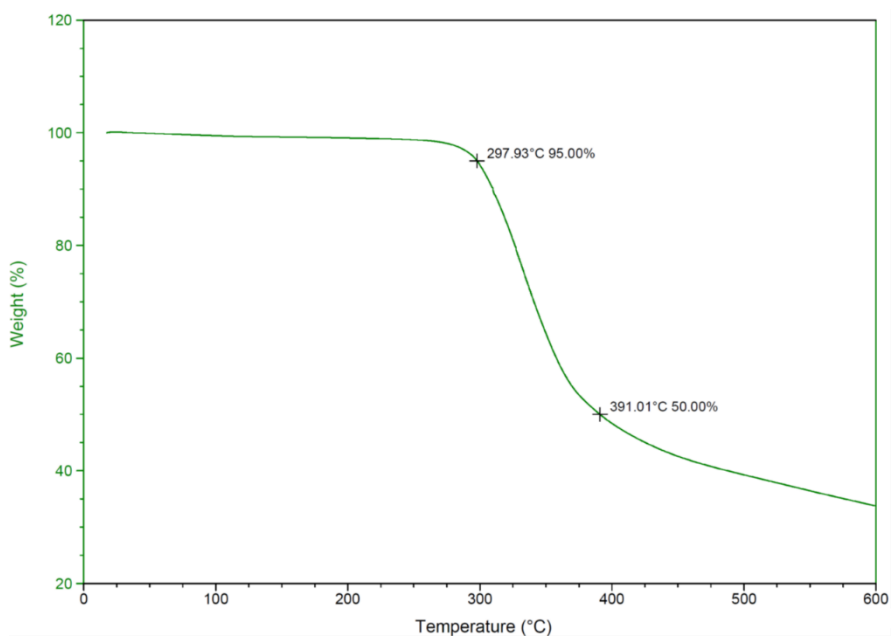


Figure B-13. TGA Thermogram of polybutyleneglycolate sinapate (Table 2-3, entry 3).

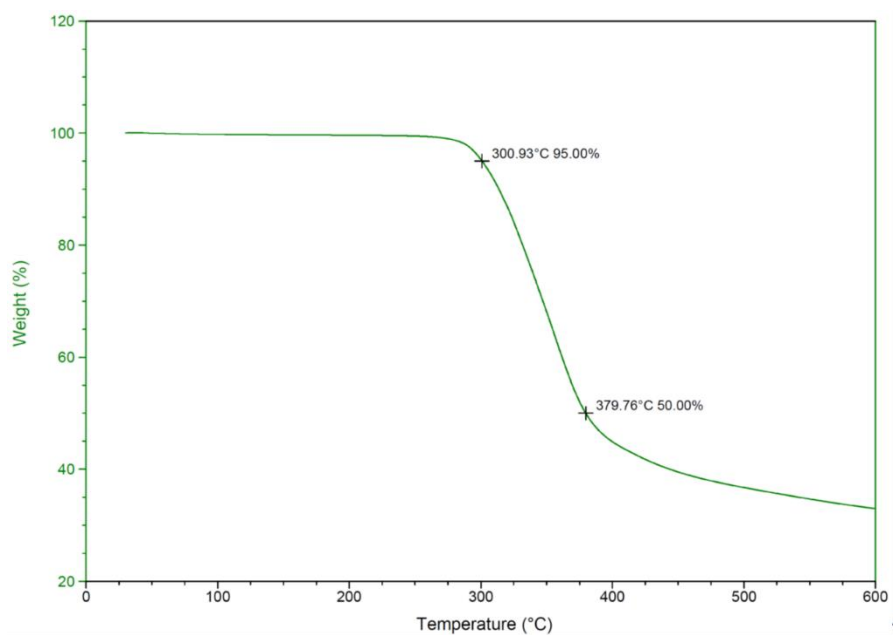


Figure B-14. TGA Thermogram of polypentyleneglycolate sinapate (Table 2-3, entry 4)

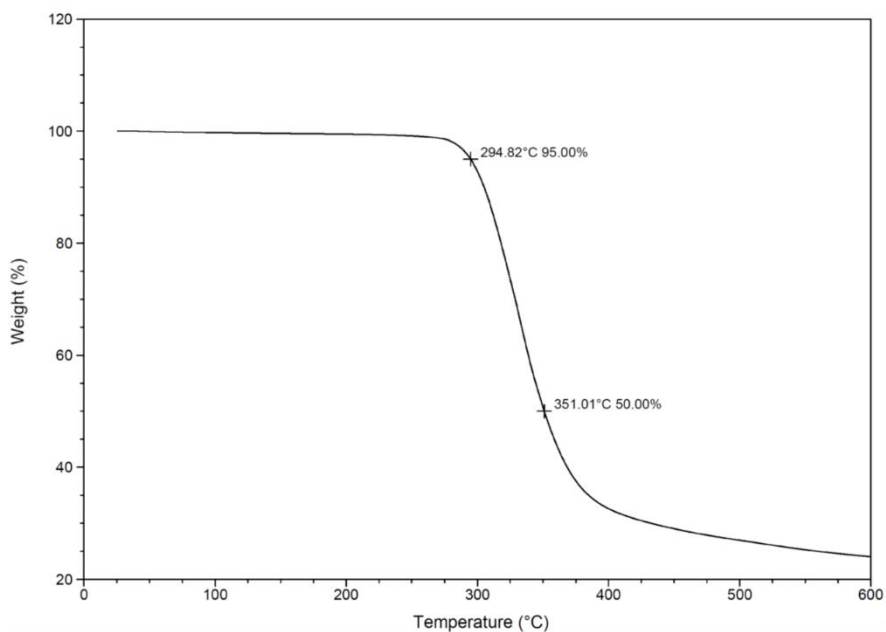


Figure B-15. TGA Thermogram of polyhexyleneglycolate dihydrosinapate (Table 2-1, entry 2).

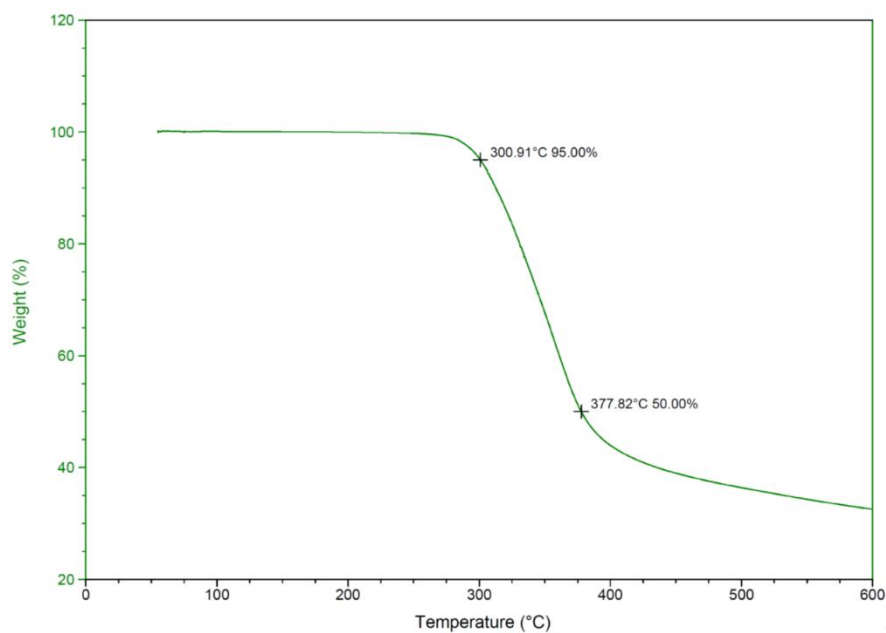


Figure B-16. TGA Thermogram of polyhexyleneglycolate sinapate (Table 2-3, entry 5).

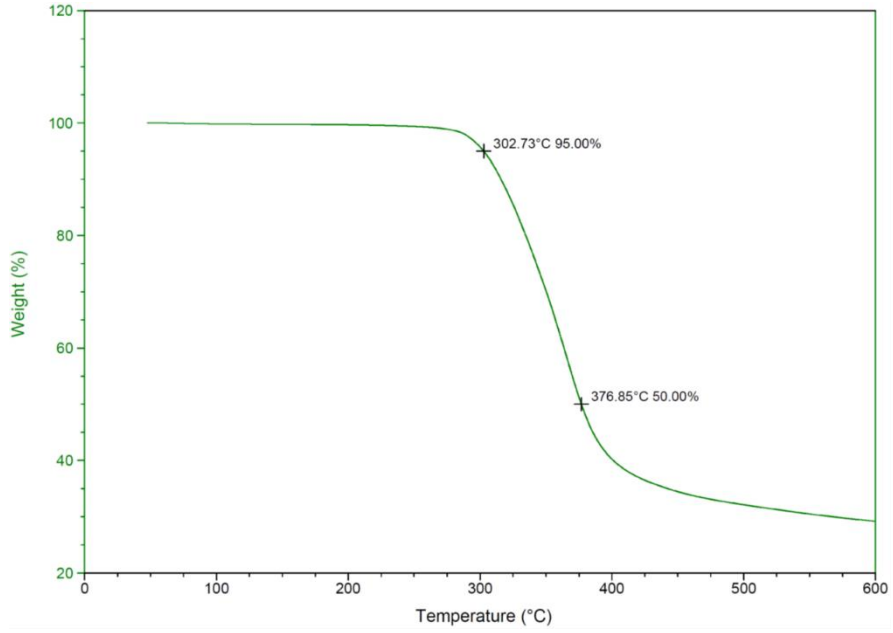


Figure B-17. TGA Thermogram of polyoctyleneglycolate sinapate (Table 2-3, entry 6)

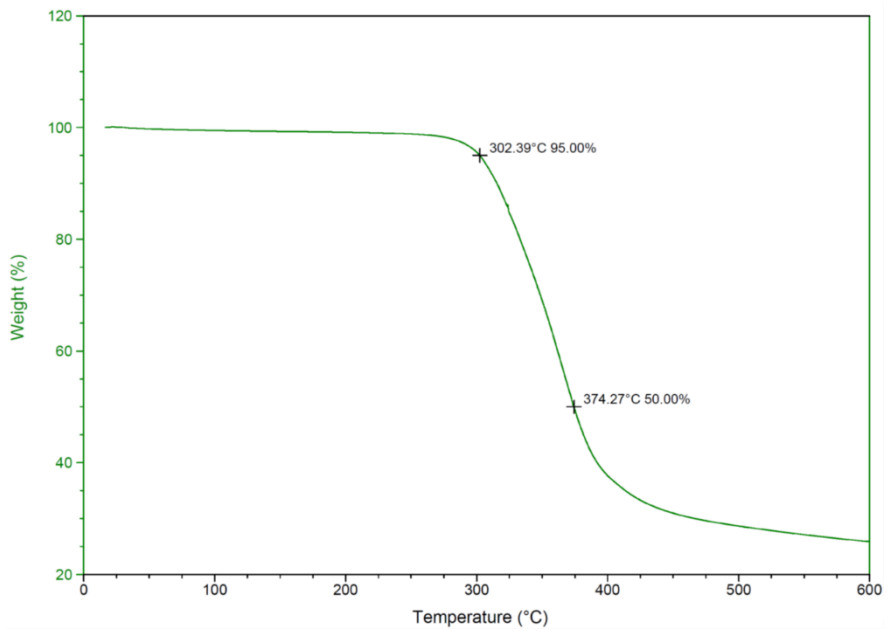


Figure B-18. TGA Thermogram of polynonyleneglycolate sinapate (Table 2-3, entry 7).

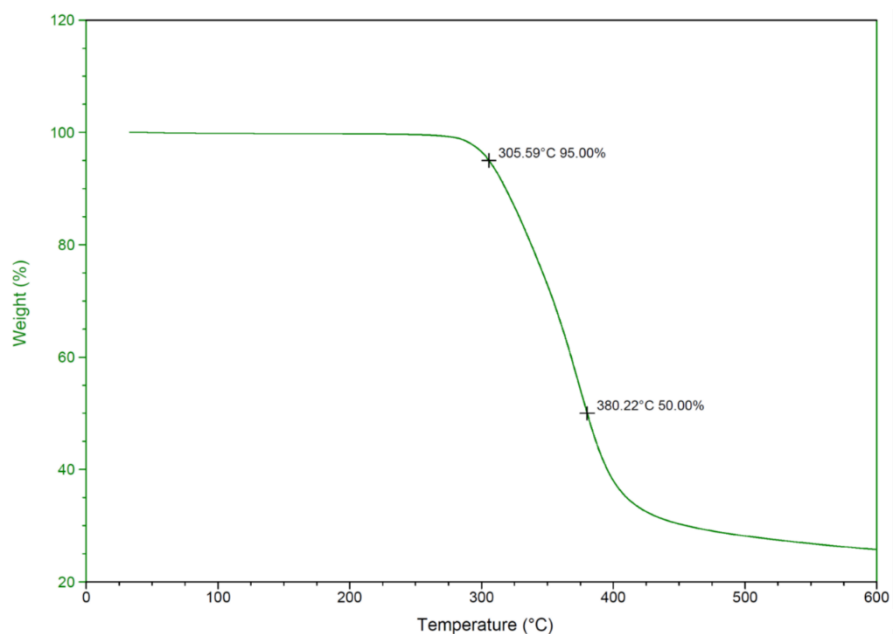


Figure B-19. TGA Thermogram of polydecyleneglycolate sinapate (Table 2-3, entry 8).

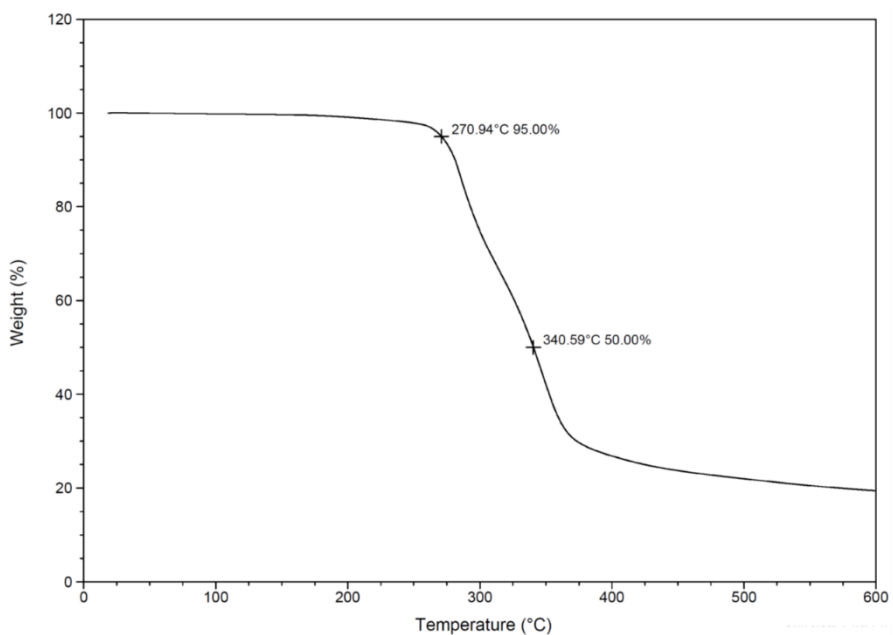


Figure B-20. TGA Thermogram of polyethylenelactate dihydrosinapate (Table 2-4, entry 1).

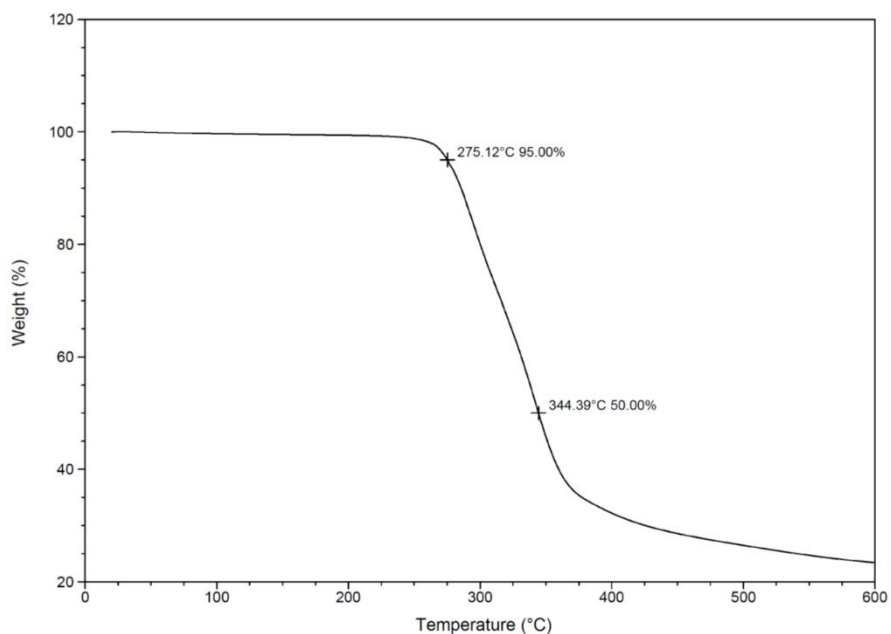


Figure B-21. TGA Thermogram of copoly(ethylenelactate dihydrosinapate/ethylenelactate sinapate) [70:30] (Table 2-4, entry 2)

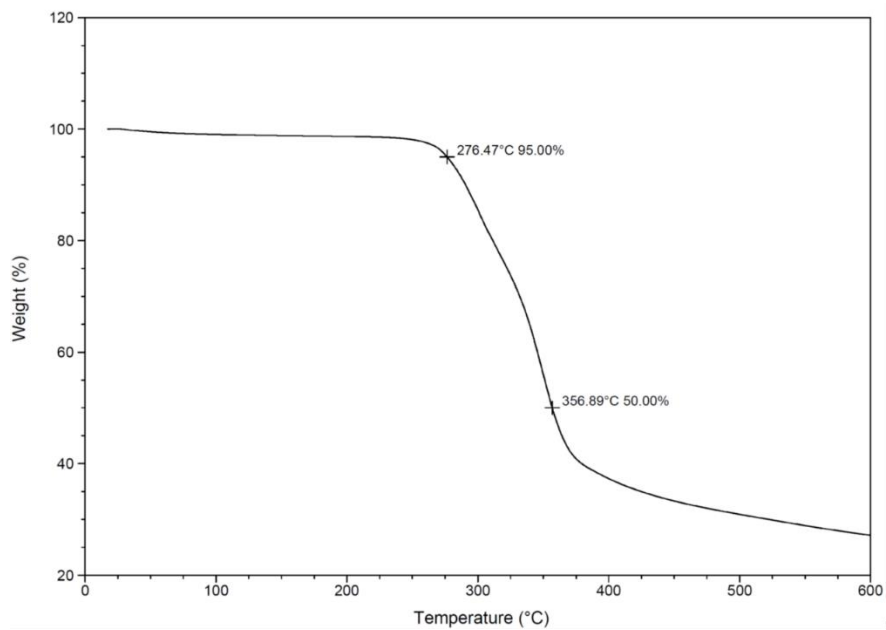


Figure B-22. TGA Thermogram of copoly(ethylenelactate dihydrosinapate/ethylenelactate sinapate) [50:50] (Table 2-4, Entry 3)

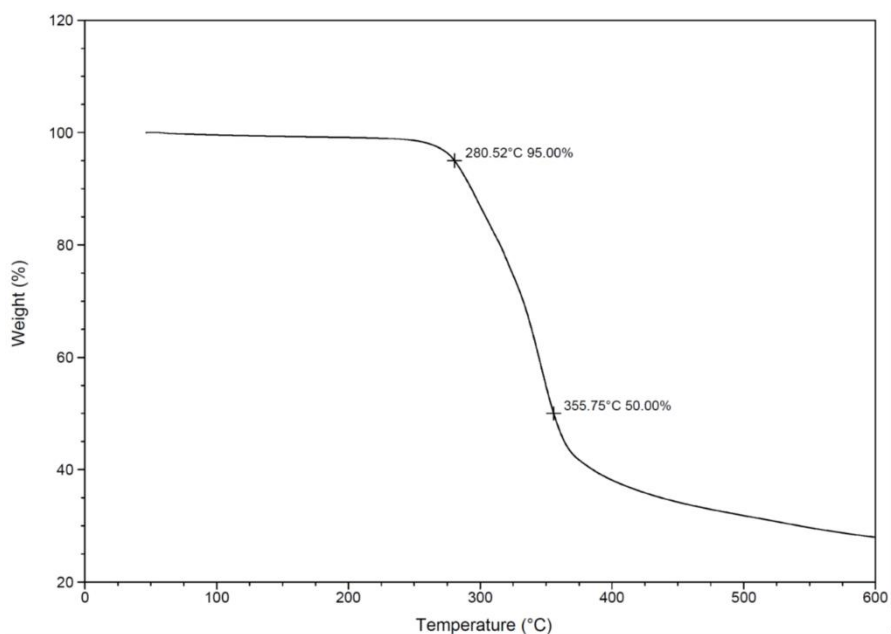


Figure B-23. TGA Thermogram of copoly(ethylenelactate dihydrosinapate/ethylenelactate sinapate) [30:70] (Table 2-4, entry 4)

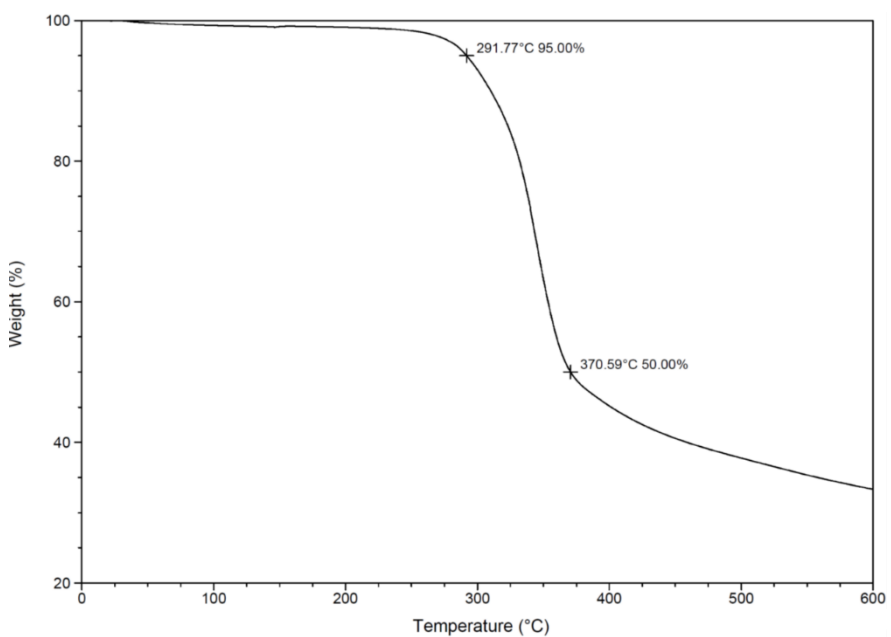


Figure B-24. TGA Thermogram of polyethylenelactate sinapate (Table 2-4, entry 5)

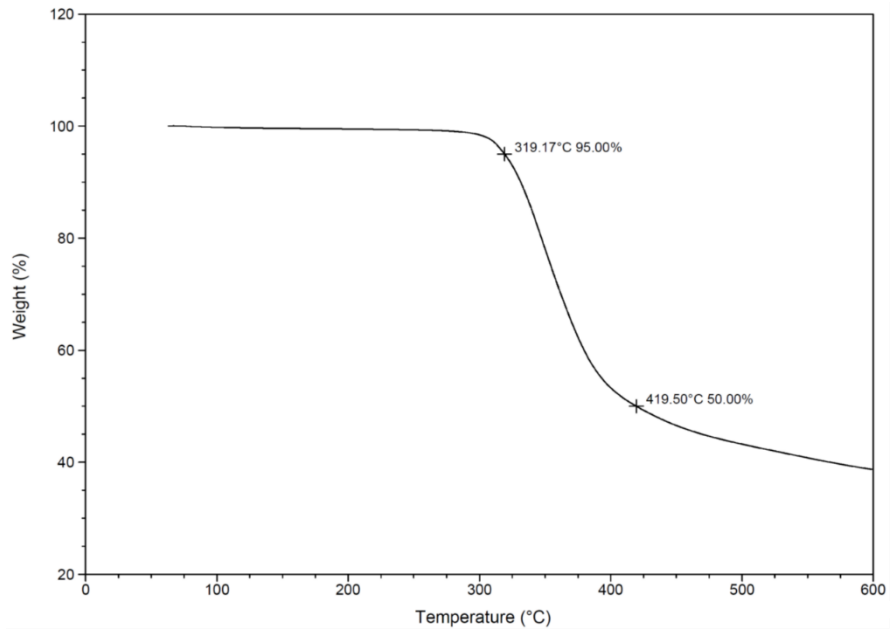


Figure B-25. TGA Thermogram of polyethyleneglycolate ferulate (Table 2-5, entry 1).

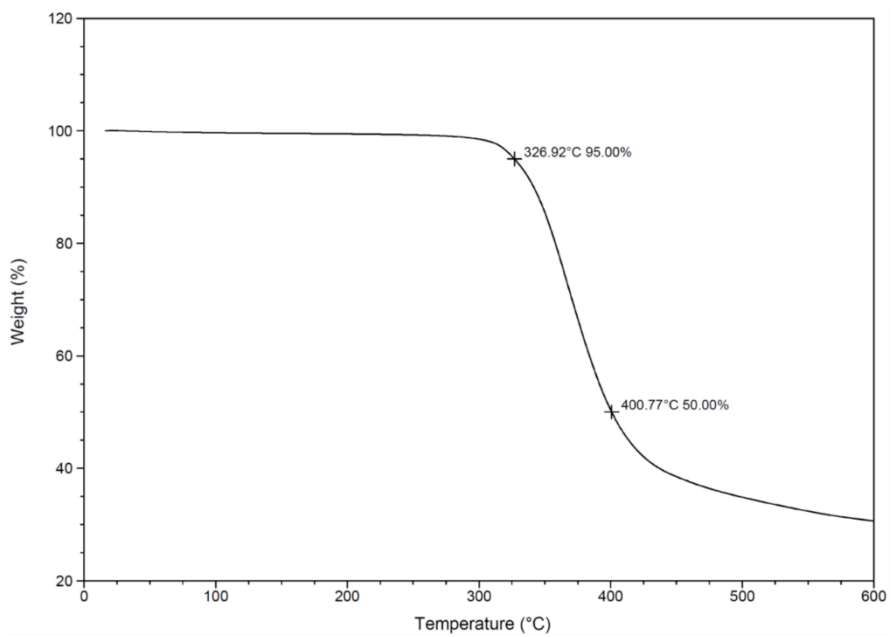


Figure B-26. TGA Thermogram of polyethyleneglycolate coumarate (Table 2-5, entry 2)

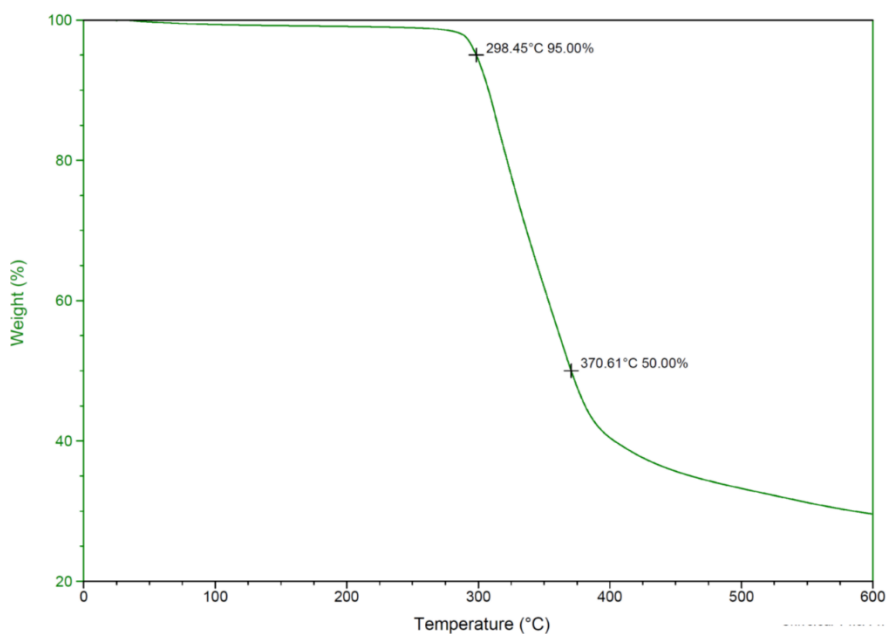


Figure B-27. TGA Thermogram of polyethylenelactate ferulate (Table 2-5, entry 3).

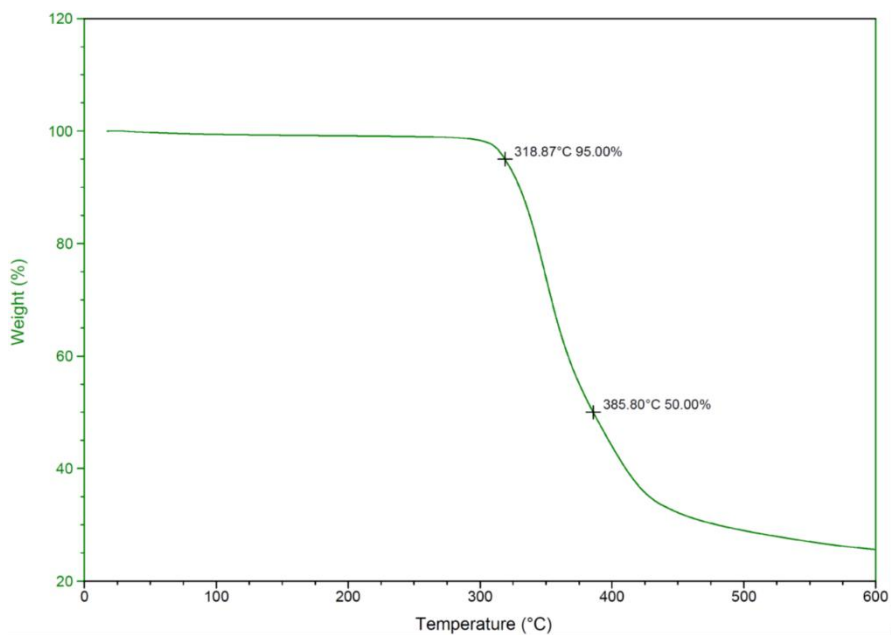


Figure B-28. TGA Thermogram of polyethylenelactate coumarate (Table 2-4, entry 4).

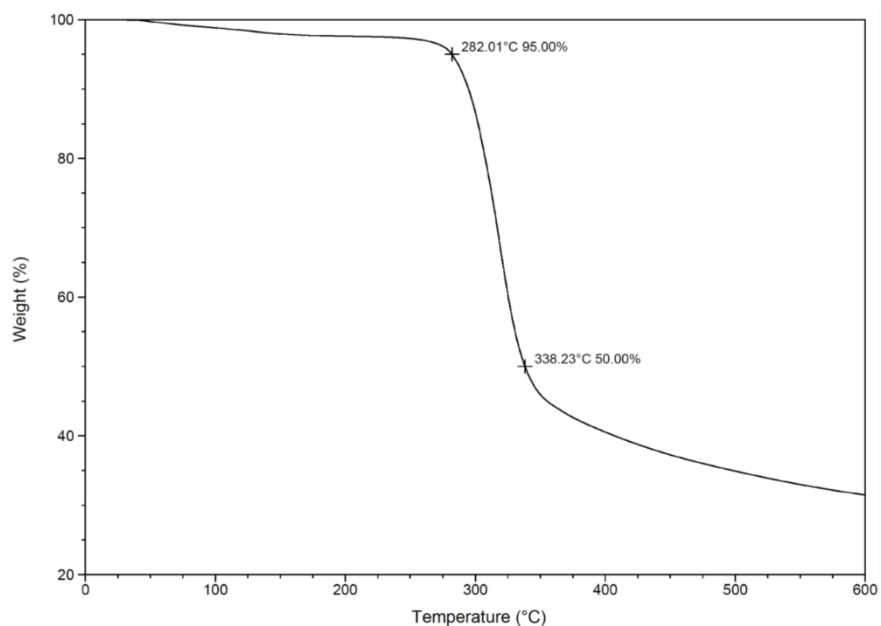


Figure B-29. TGA Thermogram of polyethyleneglycolate dihydrosinapamide (polyesteramide) (Table 2-5, entry 5).

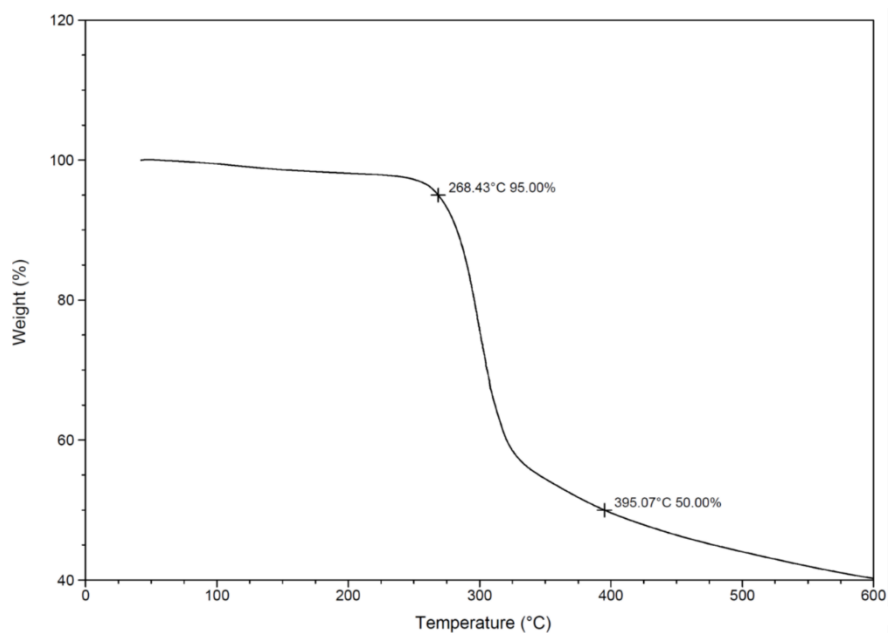


Figure B-30. TGA Thermogram of polyethyleneglycolaamide dihydrosinapamide (polyamide) (Table 2-5, entry 6).

DSC Spectra

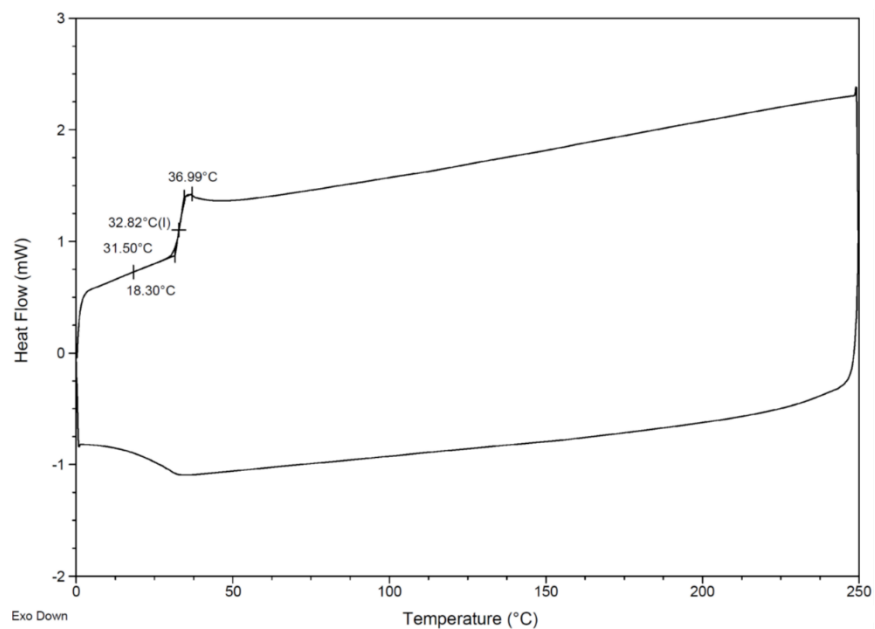


Figure B-31. DSC Thermogram of polyethyleneglycolate dihydrosinapate (Table 2-2, entry 1).

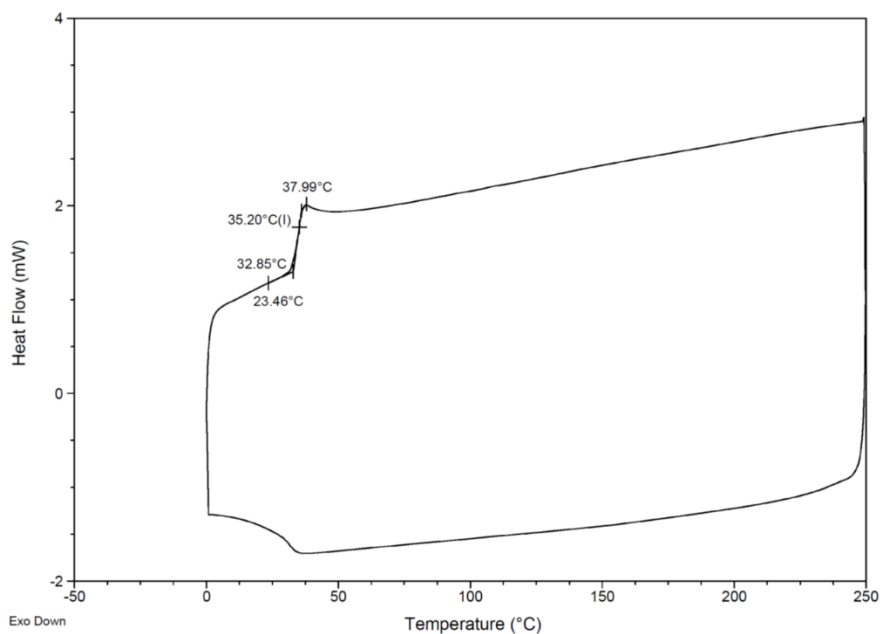


Figure B-32. DSC Thermogram of copoly(ethyleneglycolate dihydrosinapate/ethyleneglycolate sinapate) [90:10] (Table 2-2, entry 2).

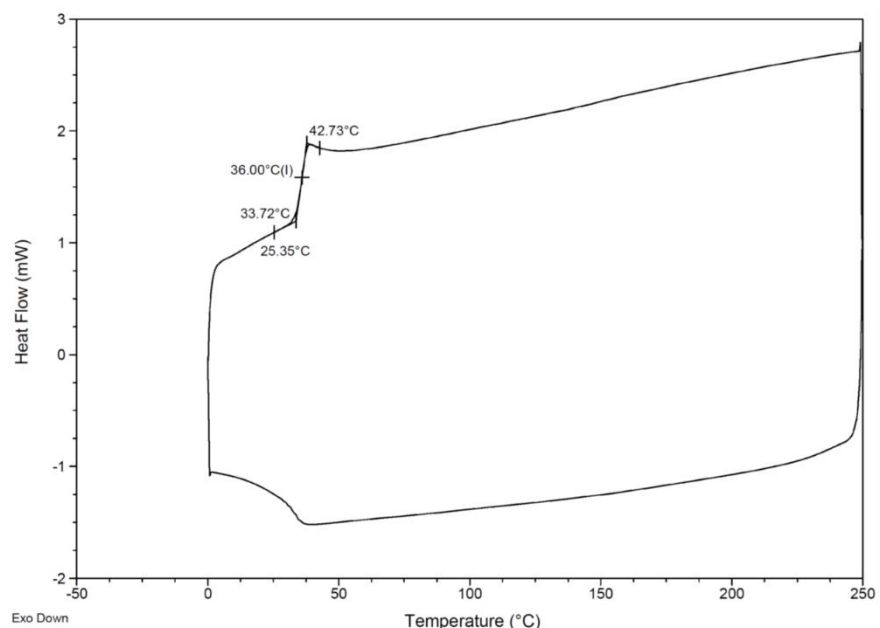


Figure B-33. DSC Thermogram of copoly(ethyleneglycolate dihydrosinapate/ethyleneglycolate sinapate) [80:20] (Table 2-2, entry 3)

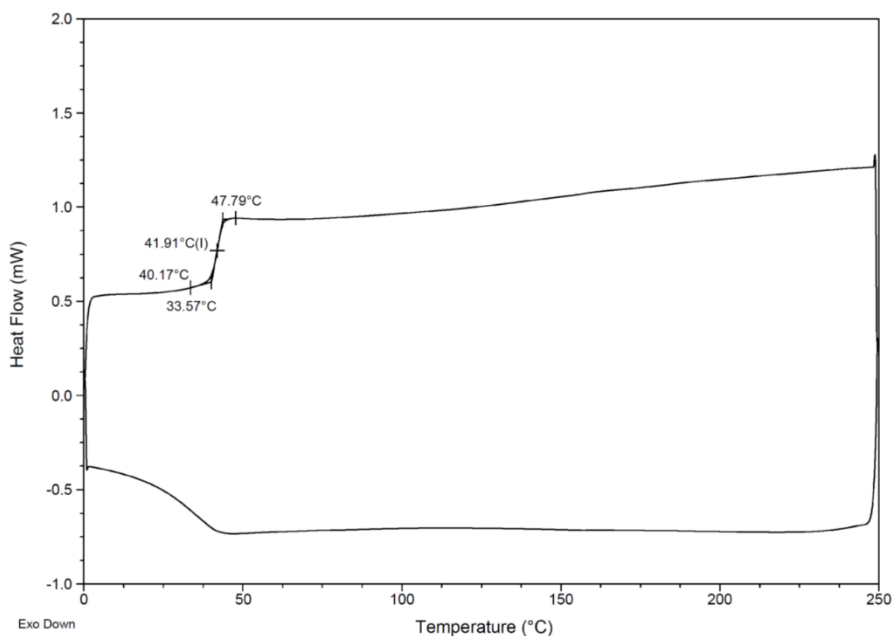


Figure B-34. DSC Thermogram of copoly(ethyleneglycolate dihydrosinapate/ethyleneglycolate sinapate) [70:30] (Table 2-2, entry 4)

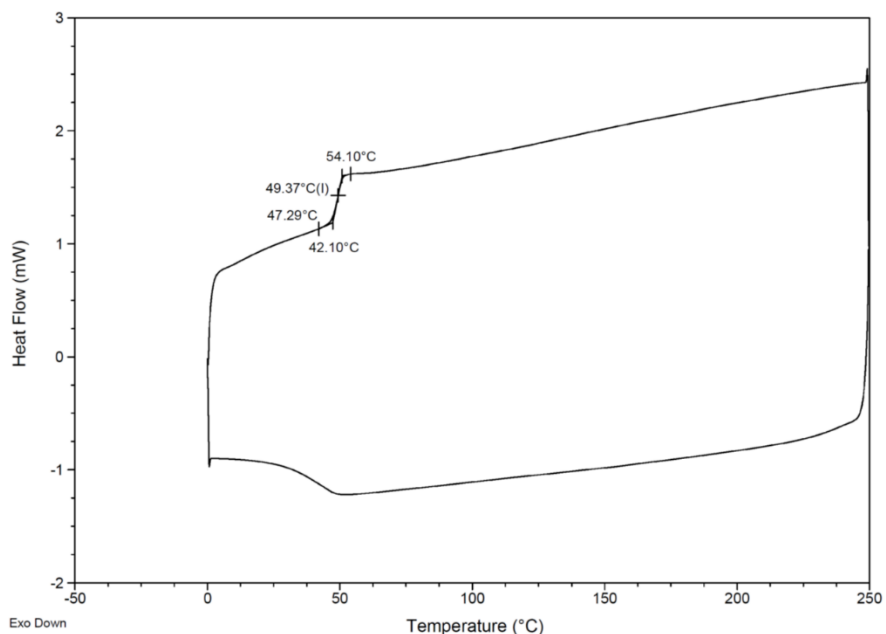


Figure B-35. DSC Thermogram of copoly(ethyleneglycolate dihydrosinapate/ethyleneglycolate sinapate) [60:40] (Table 2-2, entry 5)

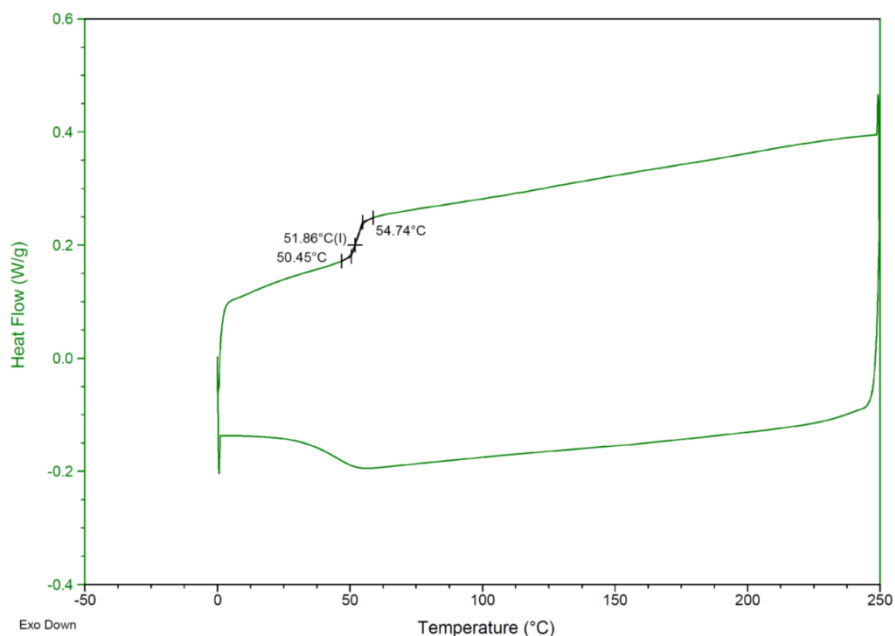


Figure B-36. DSC Thermogram of copoly(ethyleneglycolate dihydrosinapate/ethyleneglycolate sinapate) [50:50] (Table 2-2, entry 6)

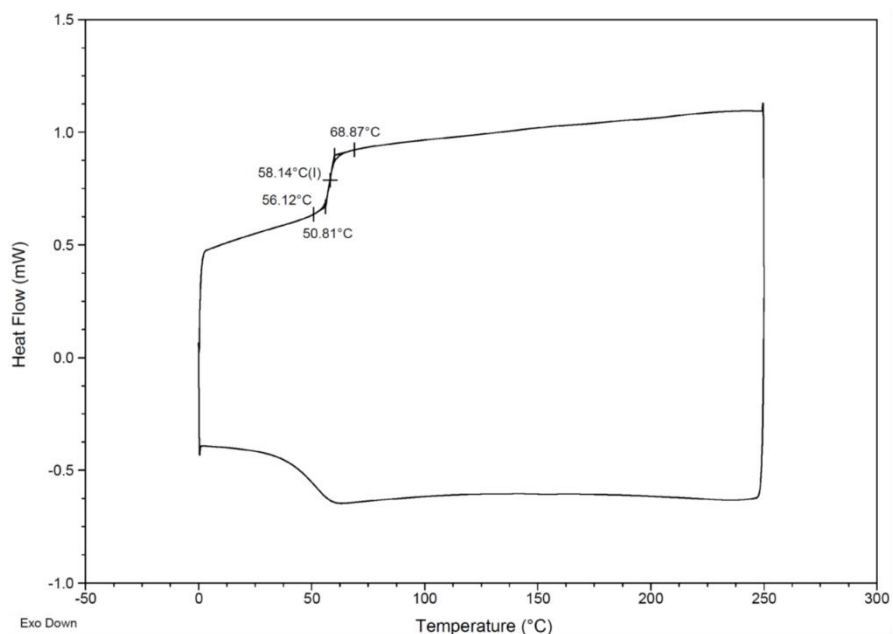


Figure B-37. DSC Thermogram of copoly(ethyleneglycolate dihydrosinapate/ethyleneglycolate sinapate) [40:60] (Table 2-2, entry 7)

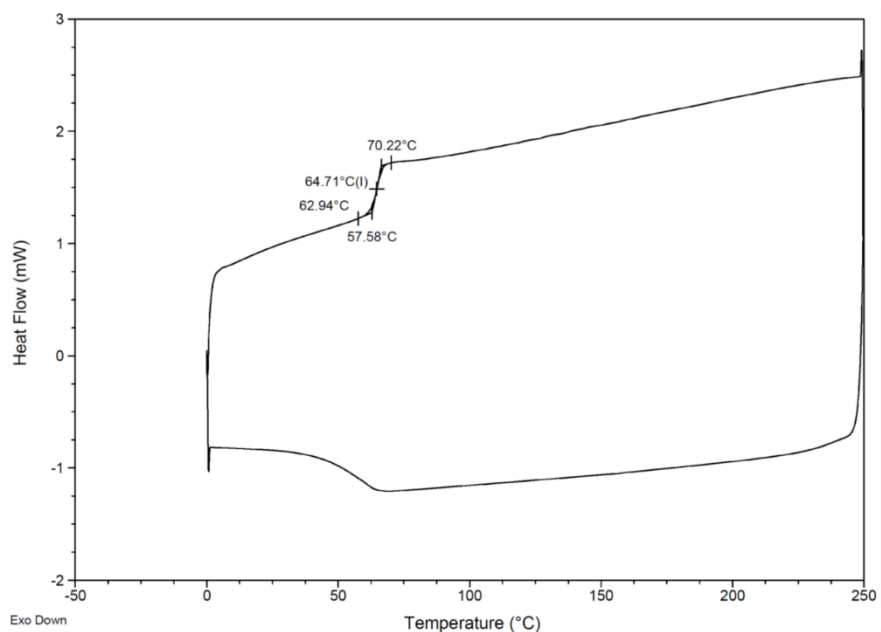


Figure B-38. DSC Thermogram of copoly(ethyleneglycolate dihydrosinapate/ethyleneglycolate sinapate) [30:70] (Table 2-2, entry 8)

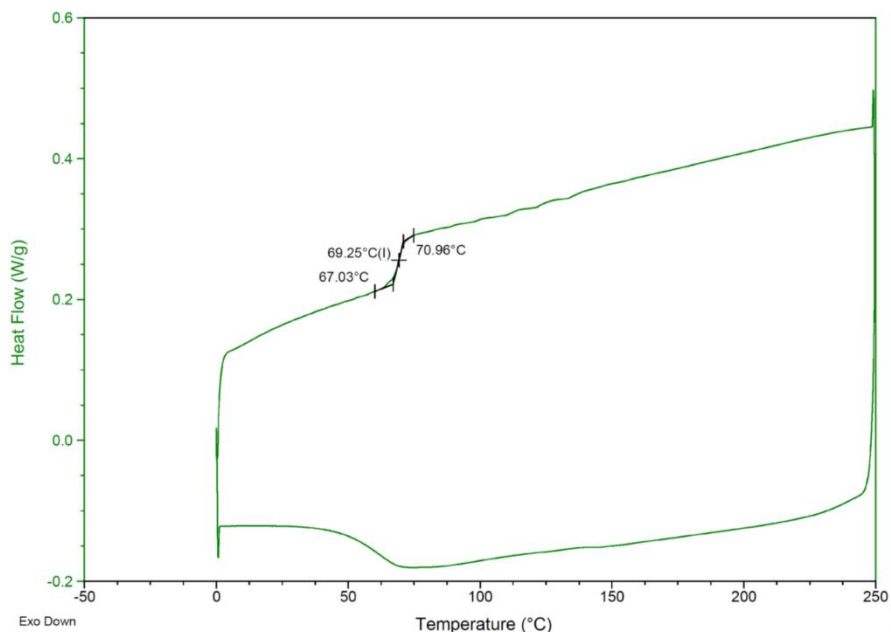


Figure B-39. DSC Thermogram of copoly(ethyleneglycolate dihydrosinapate/ethyleneglycolate sinapate) [20:80] (Table 2-2, entry 9)

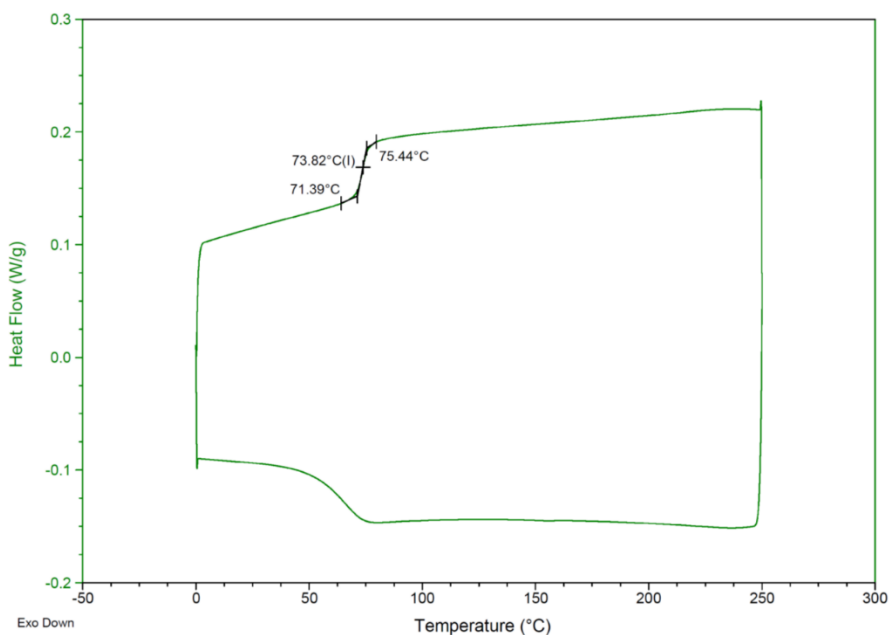


Figure B-40. DSC Thermogram of copoly(ethyleneglycolate dihydrosinapate/ethyleneglycolate sinapate) [10:90] (Table 2-2, entry 10).

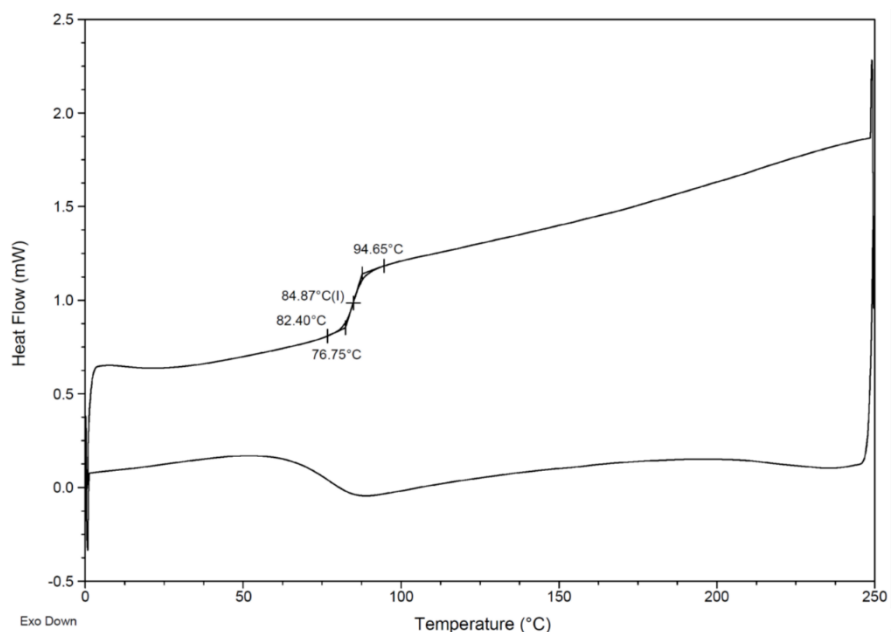


Figure B-41. DSC Thermogram of polyethyleneglycolate sinapate (Table 2-2, entry 11)

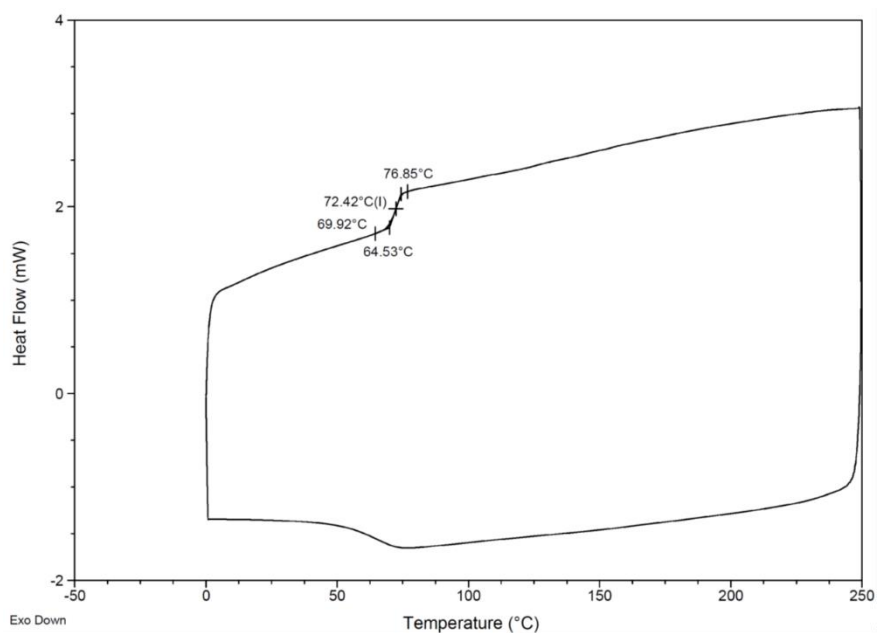


Figure B-42. DSC Thermogram of polypropyleneglycolate sinapate (Table 2-3, entry 2)

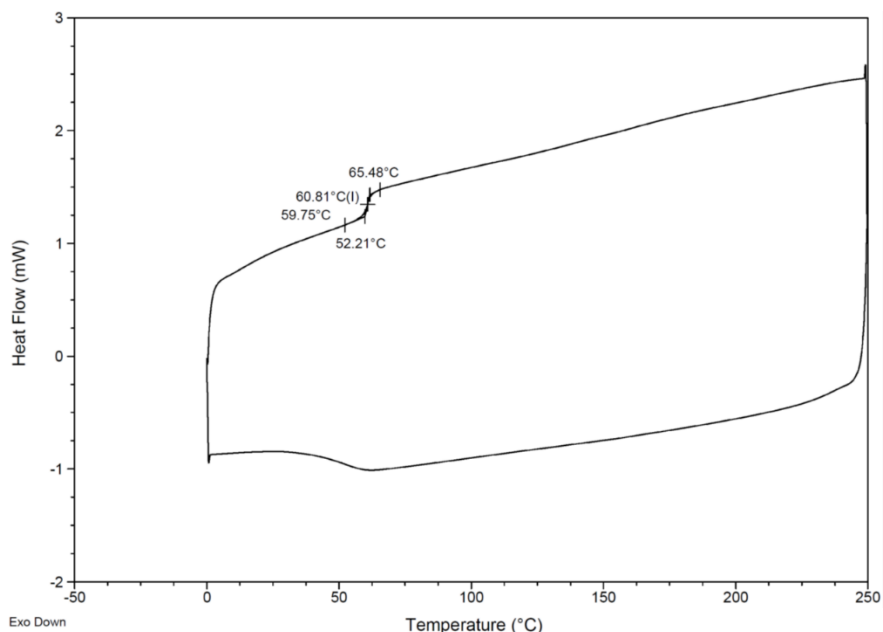


Figure B-43. DSC Thermogram of polybutyleneglycolate sinapate (Table 2-3, entry 3)

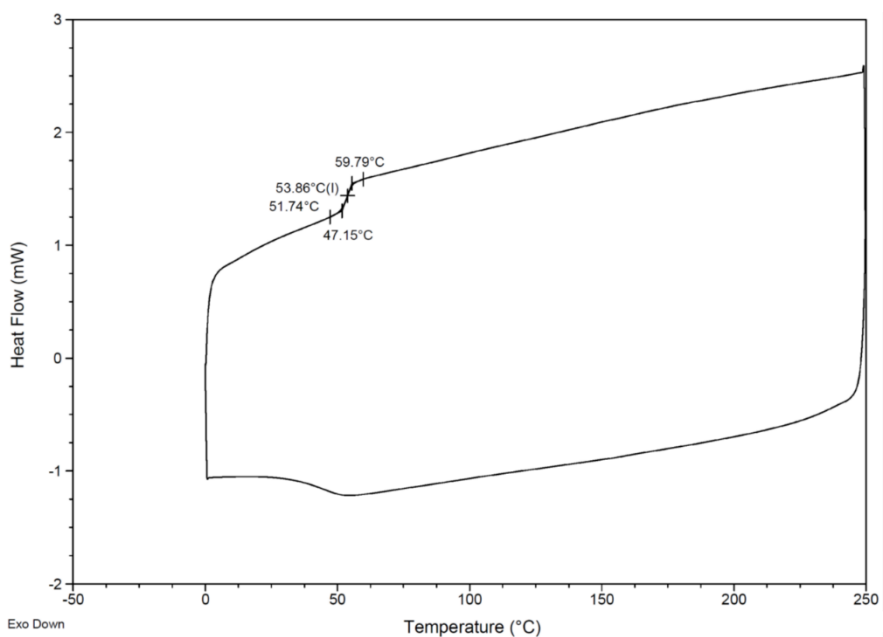


Figure B-44. DSC Thermogram of polypentyleneglycolate sinapate (Table 2-3, entry 4)

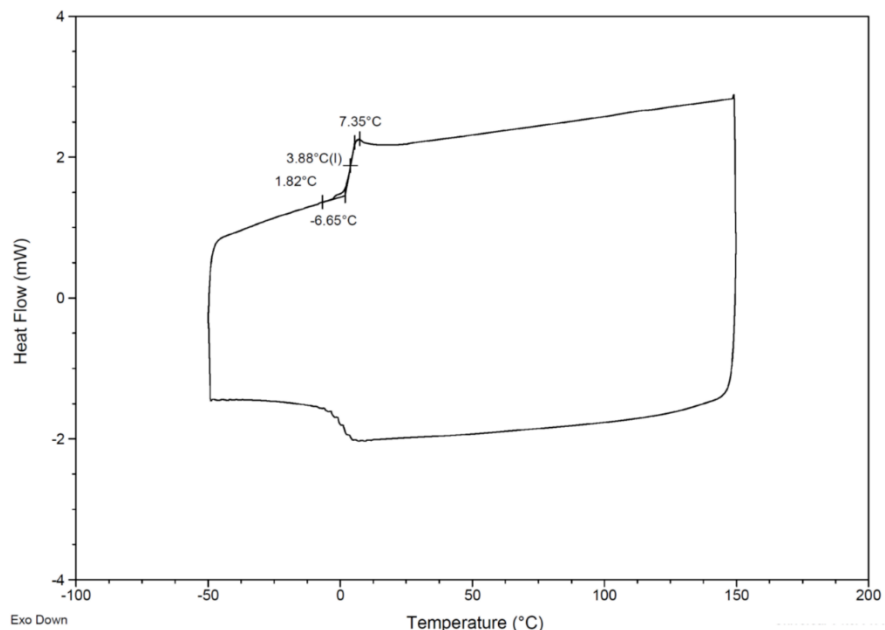


Figure B-45. DSC Thermogram of polyhexyleneglycolate dihydrosinapate (Table 2-1, entry 2)

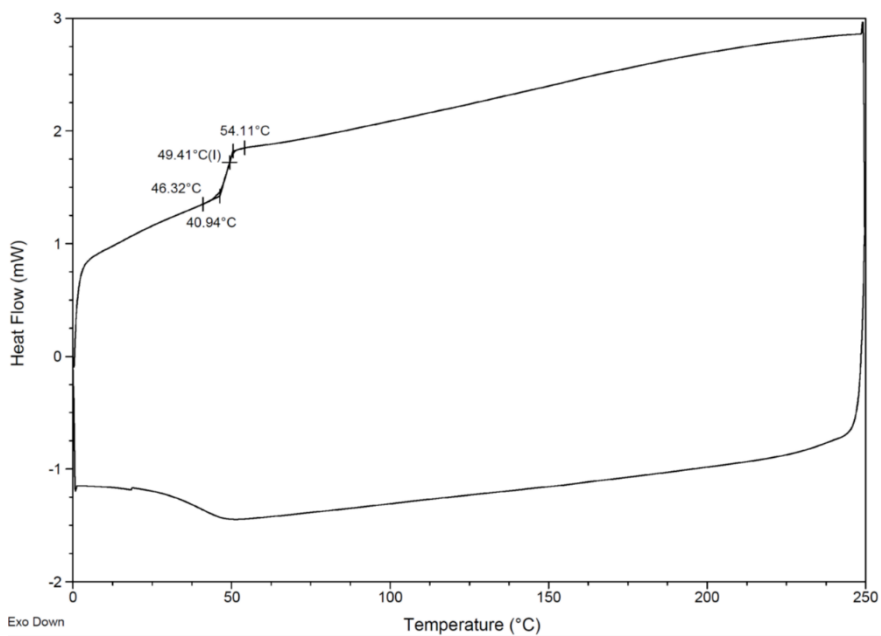


Figure B-46. DSC Thermogram of polyhexyleneglycolate sinapate (Table 2-3, entry 5)

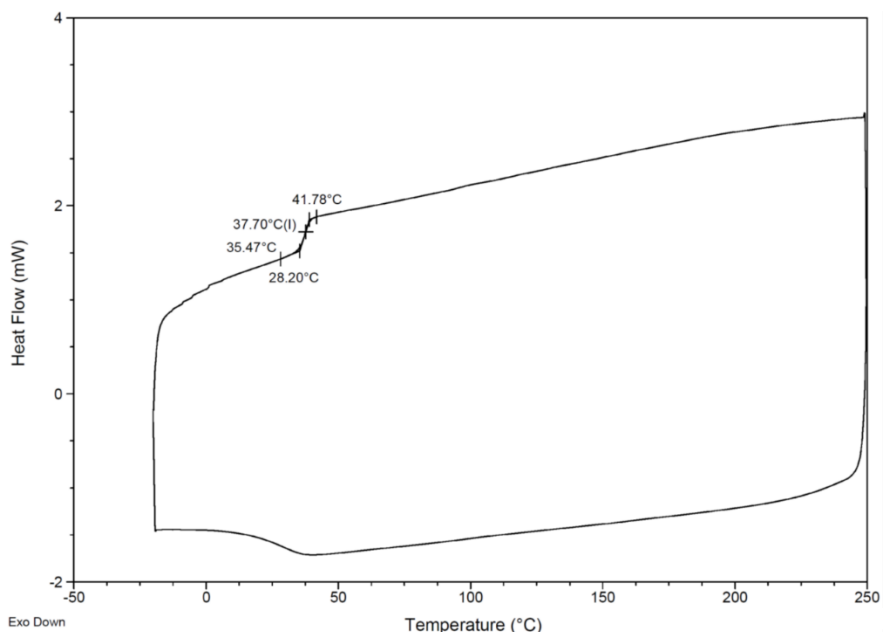


Figure B-47. DSC Thermogram of polyoctyleneglycolate sinapate (Table 2-3, entry 6)

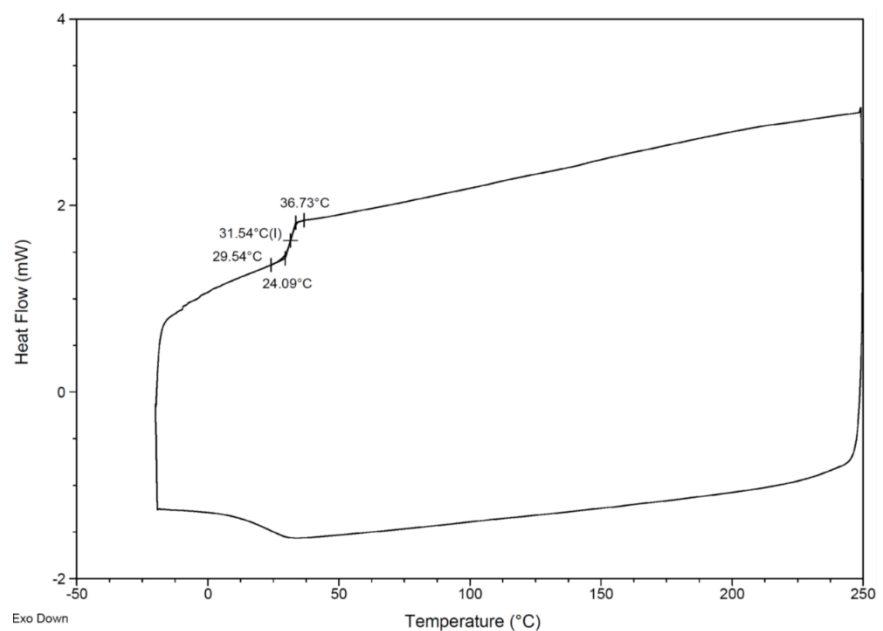


Figure B-48. DSC Thermogram of polynonyleneglycolate sinapate (Table 2-3, entry 7)

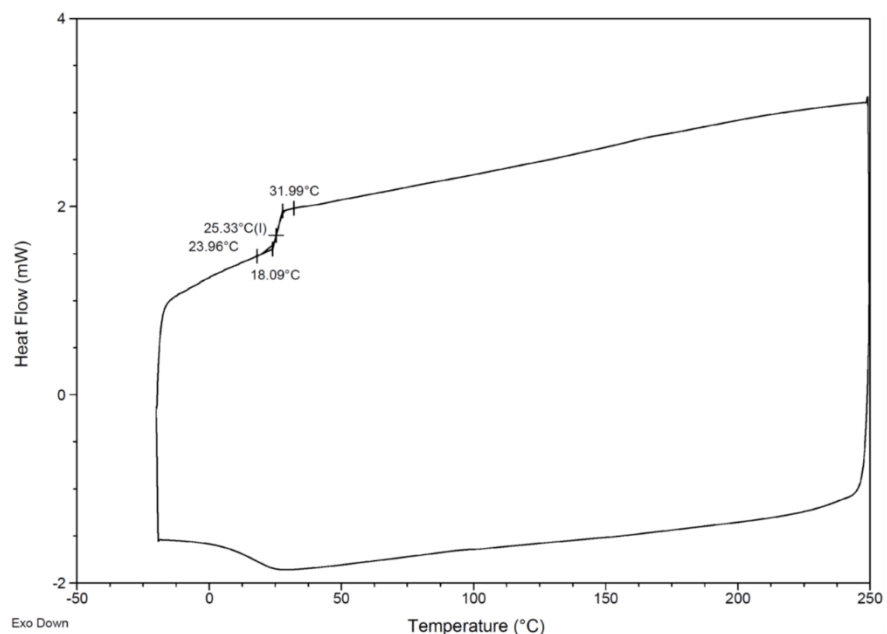


Figure B-49. DSC Thermogram of polydecyleneglycolate sinapate (Table 2-3, entry 8).

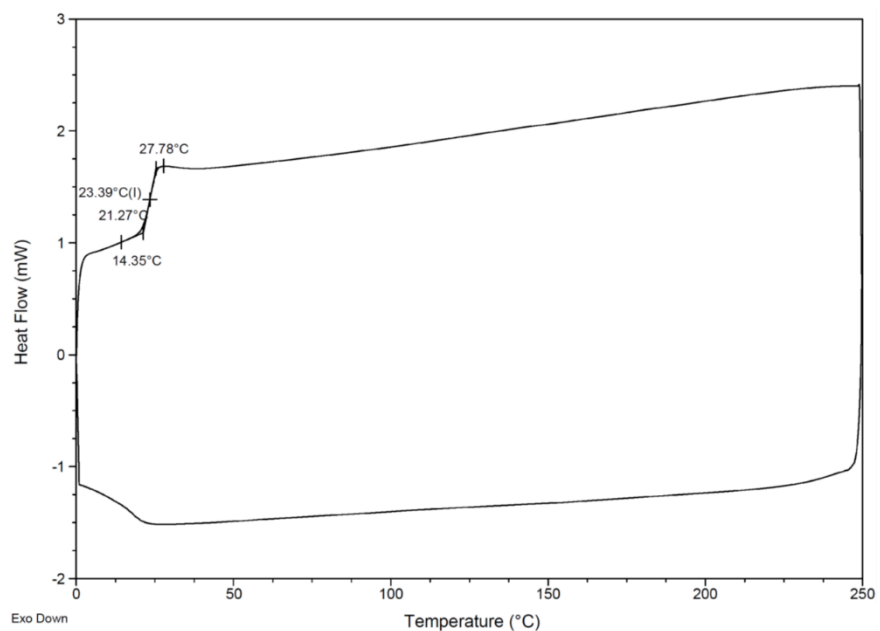


Figure B-50. DSC Thermogram of polyethylenelactate dihydrosinapate (Table 2-4, entry 1)

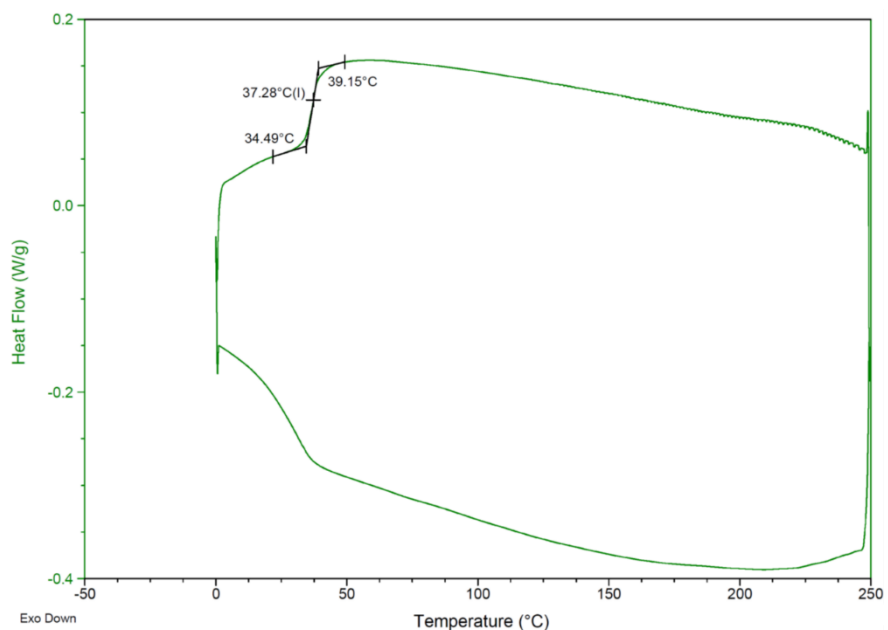


Figure B-51. DSC Thermogram of copoly(ethylenelactate dihydrosinapate/ethylenelactate sinapate) [70:30] (Table 2-4, entry 2)

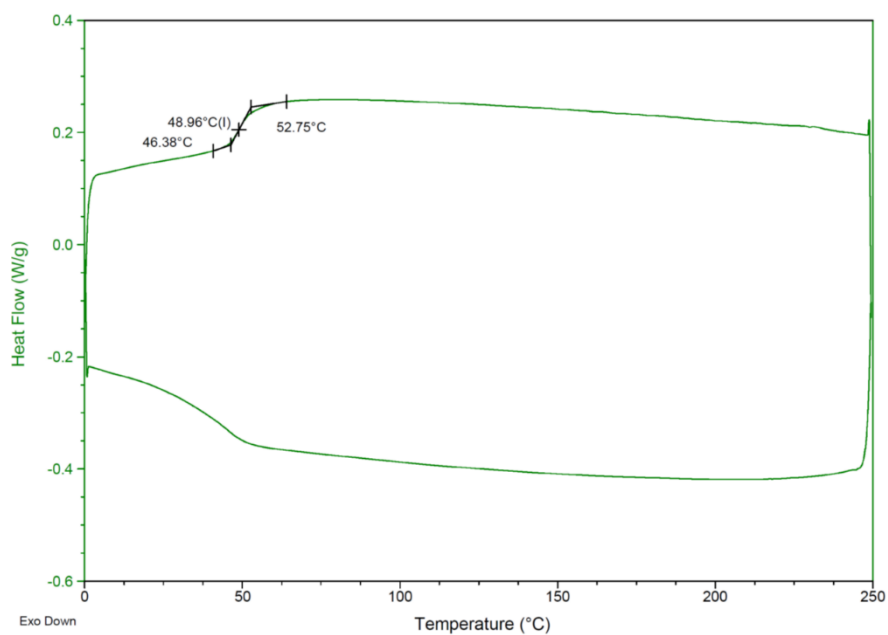


Figure B-52. DSC Thermogram of copoly(ethylenelactate dihydrosinapate/ethylenelactate sinapate) [50:50] (Table 2-4, entry 3)

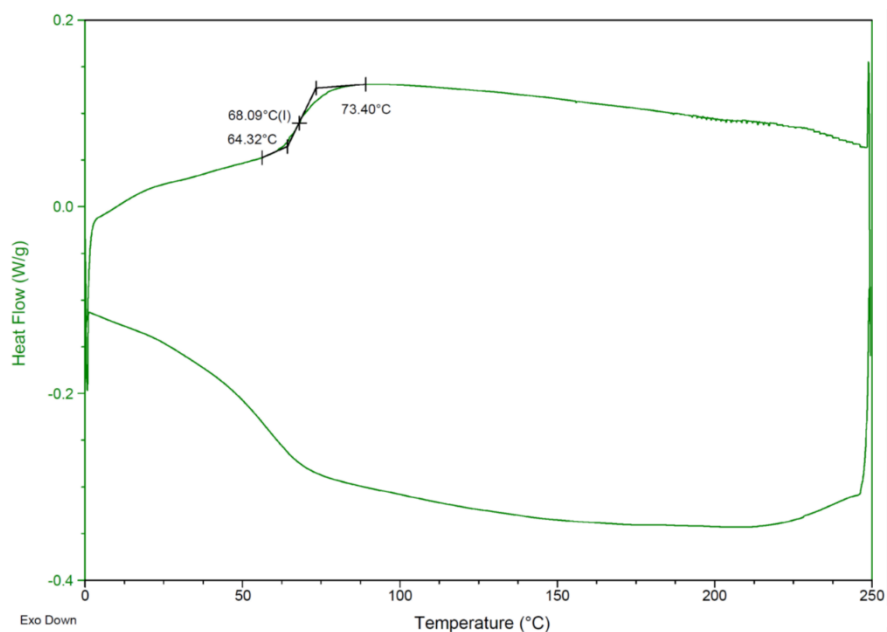


Figure B-53. DSC Thermogram of copoly(ethylenelactate dihydrosinapate/ethylenelactate sinapate) [30:70] (Table 2-4, entry 4)

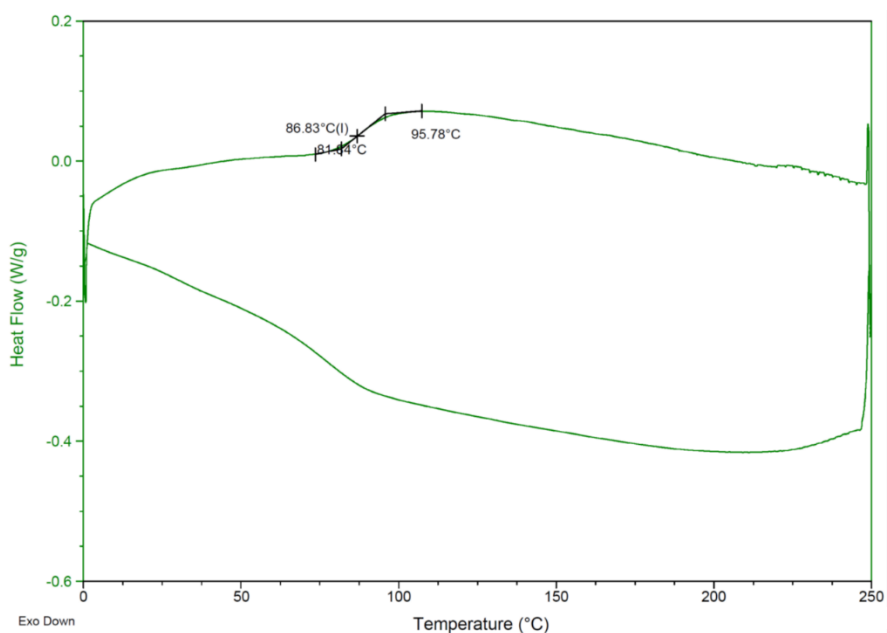


Figure B-54. DSC Thermogram of polyethylenelactate sinapate (Table 2-4, entry 5)

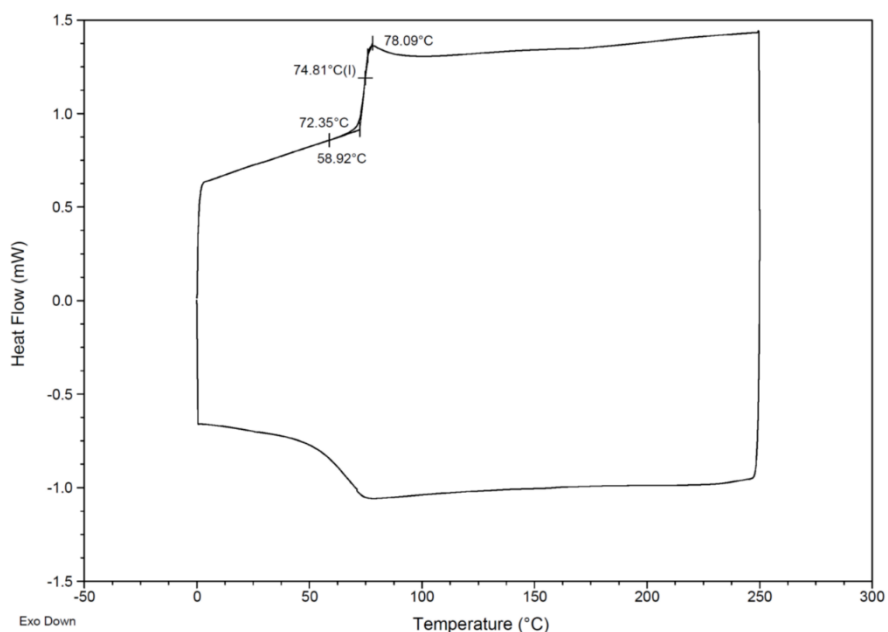


Figure B-55. DSC Thermogram of polyethyleneglycolate ferulate (Table 2-5, entry 1)

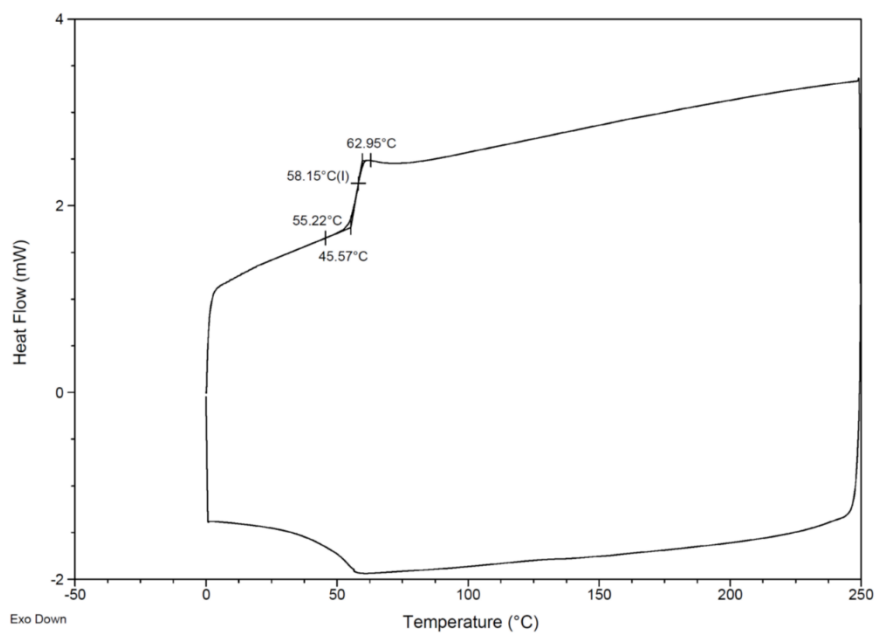


Figure B-56. DSC Thermogram of polyethyleneglycolate coumarate (Table 2-5, entry 2)

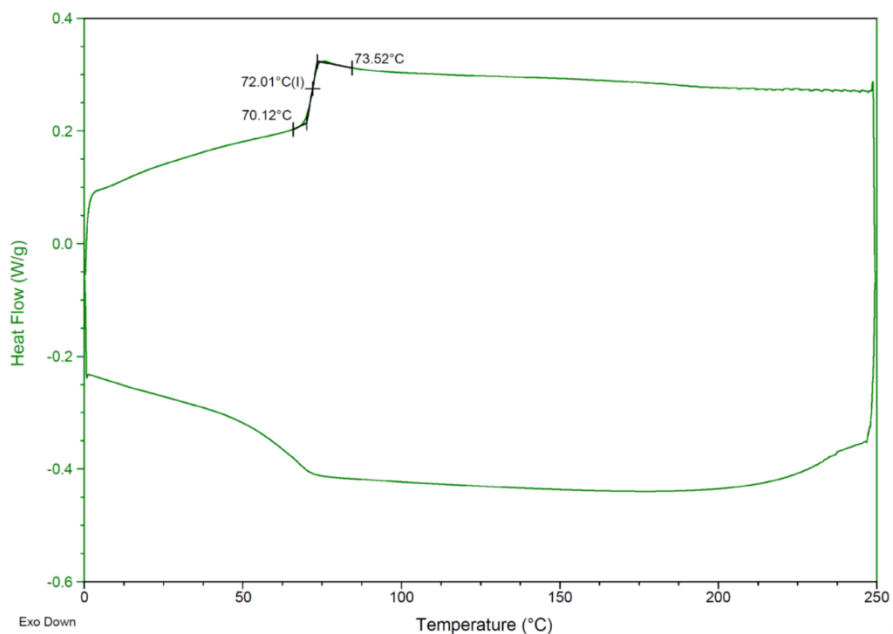


Figure B-57. DSC Thermogram of polyethylenelactate ferulate (Table 2-5, entry 3)

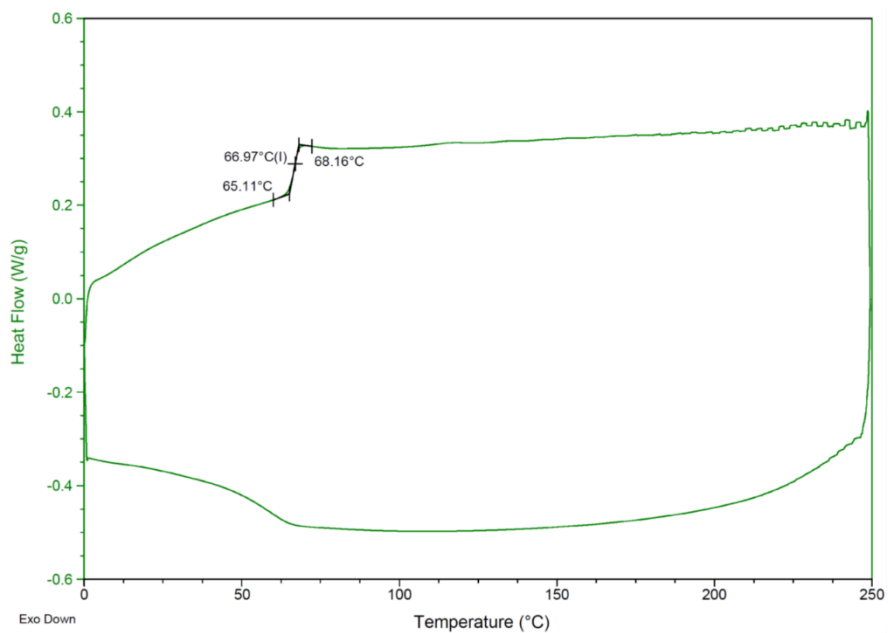


Figure B-58. DSC Thermogram of polyethylenelactate coumarate (Table 2-5, entry 4)

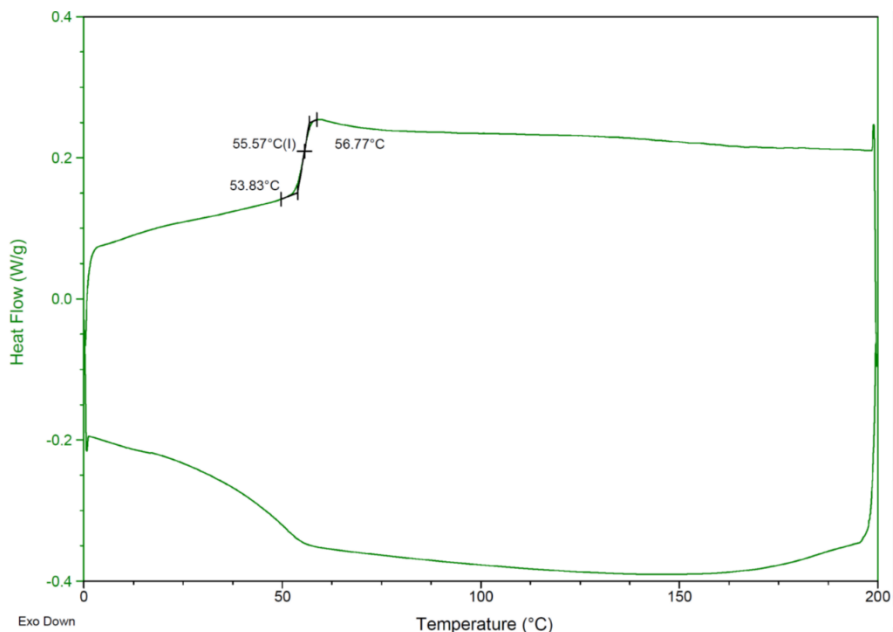


Figure B-59. DSC Thermogram of polyethyleneglycolate dihydrosinapamide (polyesteramide) (Table 2-5, entry 5)

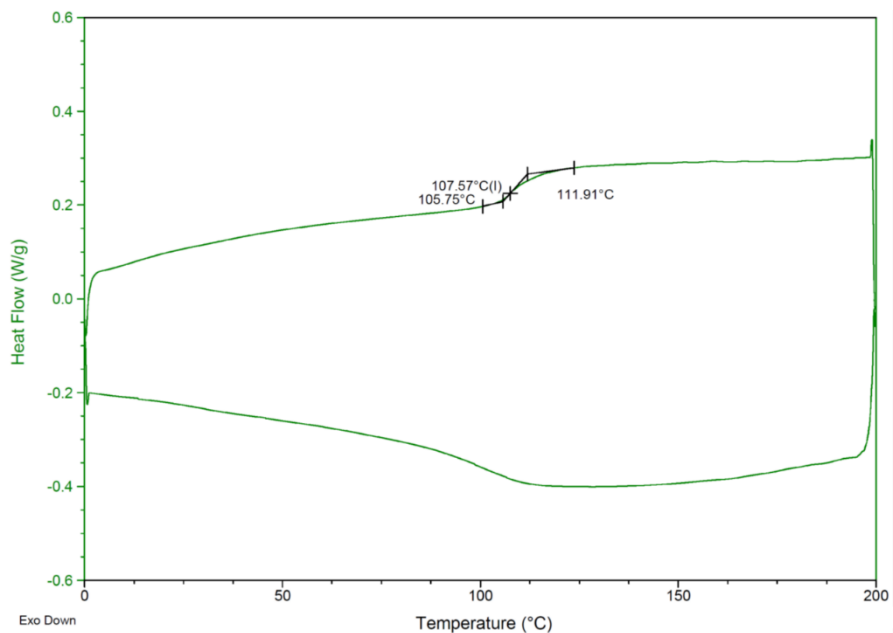


Figure B-60. DSC Thermogram of polyethyleneglycolamide dihydrosinapamide (polyamide) (Table 2-5, entry 6)

GPC Spectra

Molecular Weight Averages

| Peak | Mp | Mn | Mw | Mz | Mz+1 | Mv | PD |
|--------|-------|-------|-------|-------|--------|-------|-------|
| Peak 1 | 30636 | 16588 | 42745 | 77997 | 122667 | 72317 | 2.577 |

Peak information

| | Start (mins) | End (mins) |
|-------------------|--------------|------------|
| Baseline region 1 | 0.82 | 2.21 |
| Baseline region 2 | 29.29 | 29.86 |
| Peak 1 | 14.04 | 22.15 |

| Peak | Trace | Peak Max RT (mins) | Peak Area (mV.s) | Peak Height (mV) |
|--------|-------|--------------------|------------------|------------------|
| Peak 1 | RI | 18.19 | 3820930.747 | 20719.202 |

Chromatogram

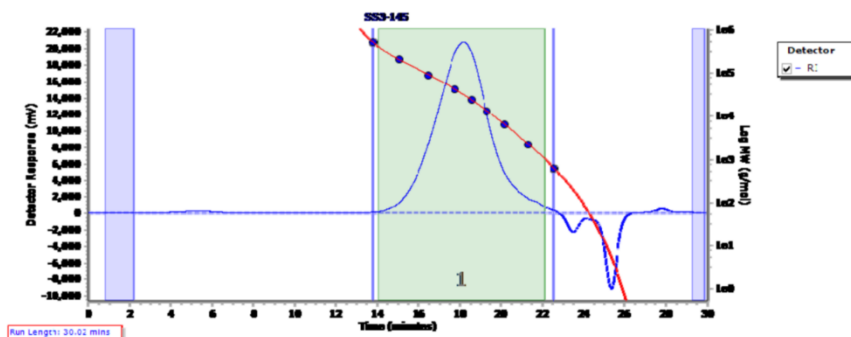


Figure B-61. GPC Chromatogram of polyethyleneglycolate dihydrosinapate (Table 2-2, entry 1).

Molecular Weight Averages

| Peak | Mp | Mn | Mw | Mz | Mz+1 | Mv | PD |
|--------|-------|-------|-------|-------|--------|-------|-------|
| Peak 1 | 23610 | 13574 | 38106 | 79906 | 142821 | 72601 | 2.807 |

Peak information

| | Start (mins) | End (mins) |
|-------------------|--------------|------------|
| Baseline region 1 | 2.00 | 2.39 |
| Baseline region 2 | 26.43 | 27.01 |
| Peak 1 | 13.57 | 22.36 |

| Peak | Trace | Peak Max RT (mins) | Peak Area (mV.s) | Peak Height (mV) |
|--------|-------|--------------------|------------------|------------------|
| Peak 1 | RI | 18.55 | 4043122.704 | 20946.221 |

Chromatogram

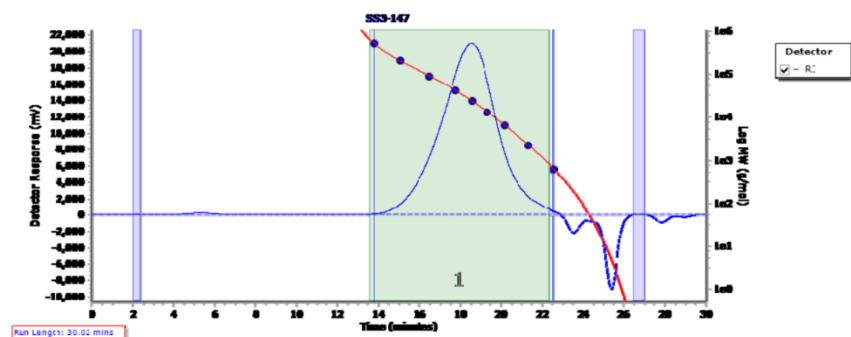


Figure B-62. GPC Chromatogram of copoly(ethylene glycolate dihydrosinapate/ethylene glycolate sinapate) [90:10] (Table 2-2, Entry 2)

| Molecular Weight Averages | | | | | | | |
|---------------------------|-------|------|-------|-------|-------|-------|-------|
| Peak | Mp | Mn | Mw | Mz | Mz+1 | Mv | PD |
| Peak 1 | 16759 | 9615 | 25838 | 51924 | 84073 | 47701 | 2.687 |

| Peak information | | |
|-------------------|--------------|------------|
| | Start (mins) | End (mins) |
| Baseline region 1 | 1.07 | 2.57 |
| Baseline region 2 | 26.54 | 27.04 |
| Peak 1 | 14.64 | 22.50 |

| Peak | Trace | Peak Max RT (mins) | Peak Area (mV.s) | Peak Height (mV) |
|--------|-------|--------------------|------------------|------------------|
| Peak 1 | RI | 18.99 | 3855601.914 | 21097.022 |

Chromatogram

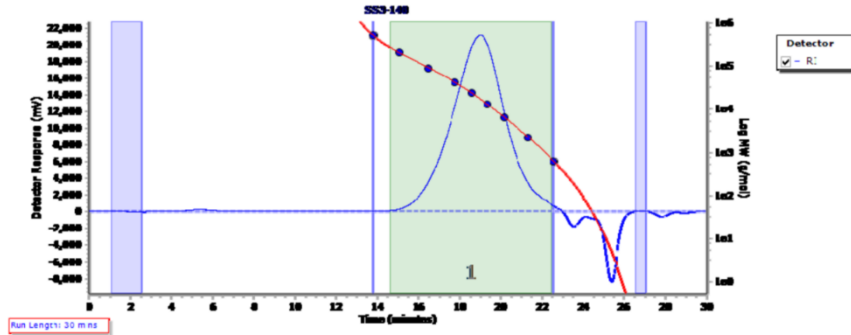


Figure B-63. GPC Chromatogram of copoly(ethyleneglycolate dihydrosinapate/ethyleneglycolate sinapate) [80:20] (Table 2-2, Entry 2)

| Molecular Weight Averages | | | | | | | |
|---------------------------|-------|-------|-------|-------|-------|-------|-------|
| Peak | Mp | Mn | Mw | Mz | Mz+1 | Mv | PD |
| Peak 1 | 26447 | 15191 | 35975 | 63750 | 98045 | 59304 | 2.388 |

| Peak information | | |
|-------------------|--------------|------------|
| | Start (mins) | End (mins) |
| Baseline region 1 | 0.64 | 2.14 |
| Baseline region 2 | 26.33 | 27.04 |
| Peak 1 | 14.43 | 22.22 |

| Peak | Trace | Peak Max RT (mins) | Peak Area (mV.s) | Peak Height (mV) |
|--------|-------|--------------------|------------------|------------------|
| Peak 1 | RI | 18.40 | 5187237.921 | 29839.338 |

Chromatogram

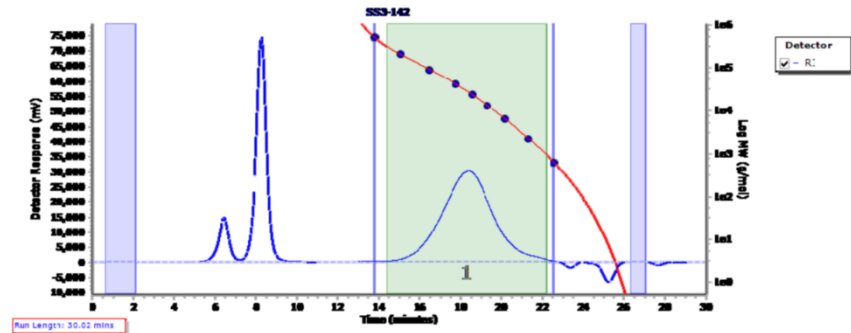


Figure B-64. GPC Chromatogram of polyhexyleneglycolate dihydrosinapate (Table 2-1, Entry 2)

| Molecular Weight Averages | | | | | | | |
|---------------------------|-------|------|-------|-------|--------|-------|-------|
| Peak | Mp | Mn | Mw | Mz | Mz+1 | Mv | PD |
| Peak 1 | 14757 | 9182 | 29090 | 66904 | 110518 | 60980 | 3.168 |

| Peak information | | |
|-------------------|--------------|------------|
| | Start (mins) | End (mins) |
| Baseline region 1 | 4.86 | 15.32 |
| Baseline region 2 | 40.95 | 44.91 |
| Peak 1 | 17.71 | 27.87 |

| Peak | Trace | Peak Max RT (mins) | Peak Area (mV.s) | Peak Height (mV) |
|--------|-------|--------------------|------------------|------------------|
| Peak 1 | RI | 23.99 | 5648652.798 | 21540.858 |

Chromatogram

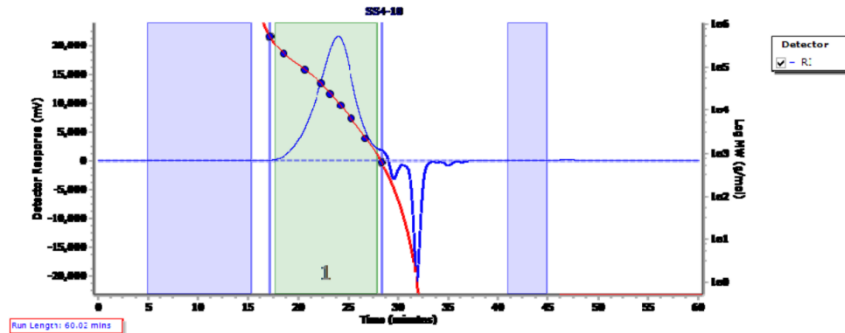


Figure B-65. GPC Chromatogram of polyethylenelactate dihydrosinapate (Table 2-4, Entry 1).

| Molecular Weight Averages | | | | | | | |
|---------------------------|------|------|-------|-------|--------|-------|-------|
| Peak | Mp | Mn | Mw | Mz | Mz+1 | Mv | PD |
| Peak 1 | 9652 | 5838 | 27646 | 82122 | 150783 | 73297 | 4.736 |

| Peak information | | |
|-------------------|--------------|------------|
| | Start (mins) | End (mins) |
| Baseline region 1 | 2.39 | 15.39 |
| Baseline region 2 | 45.51 | 56.79 |
| Peak 1 | 17.19 | 28.77 |

| Peak | Trace | Peak Max RT (mins) | Peak Area (mV.s) | Peak Height (mV) |
|--------|-------|--------------------|------------------|------------------|
| Peak 1 | RI | 24.63 | 4314429.997 | 14578.399 |

Chromatogram

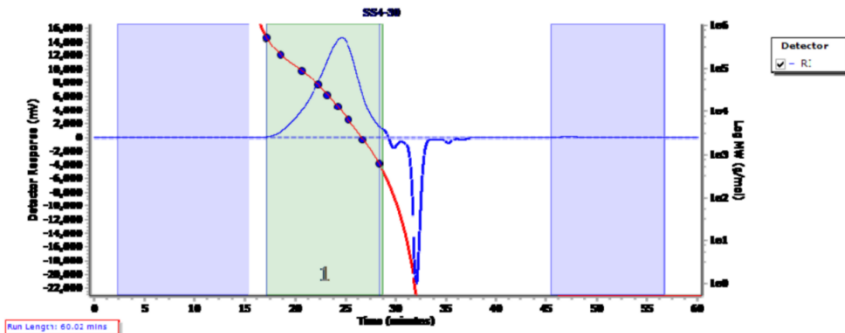


Figure B-66. GPC Chromatogram of polyethyleneglycolate dihydrosinapamide (polyesteramide) (Table 2-5, entry 5)

Molecular Weight Averages

| Peak | Mp | Mn | Mw | Mz | Mz+1 | Mv | PD |
|--------|------|------|-------|-------|-------|-------|-------|
| Peak 1 | 4843 | 2544 | 17814 | 58875 | 98450 | 53011 | 7.002 |

Peak information

| | Start (mins) | End (mins) |
|-------------------|--------------|------------|
| Baseline region 1 | 7.10 | 16.14 |
| Baseline region 2 | 45.29 | 54.33 |
| Peak 1 | 18.16 | 29.74 |

| Peak | Trace | Peak Max RT (mins) | Peak Area (mV.s) | Peak Height (mV) |
|--------|-------|--------------------|------------------|------------------|
| Peak 1 | RI | 25.63 | 5851060.052 | 17919.171 |

Chromatogram

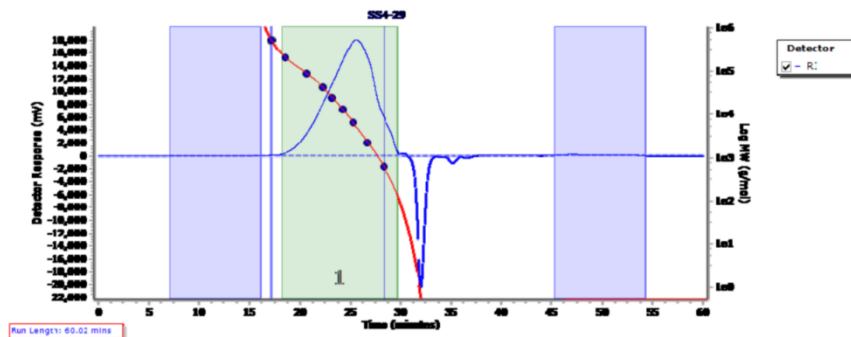


Figure B-67 . GPC Chromatogram of polyethyleneglycolamide dihydrosinapamide (polyamide) (Table 2-5, entry 6).

NMR Spectra

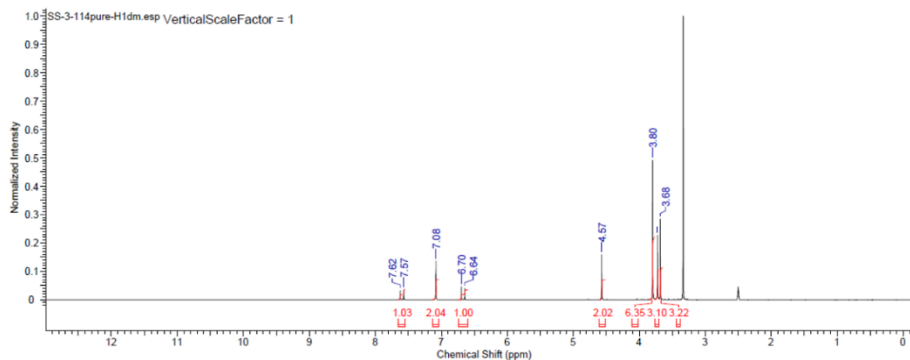


Figure B-68. ^1H NMR Spectrum of dimethylglycolate sinapate.

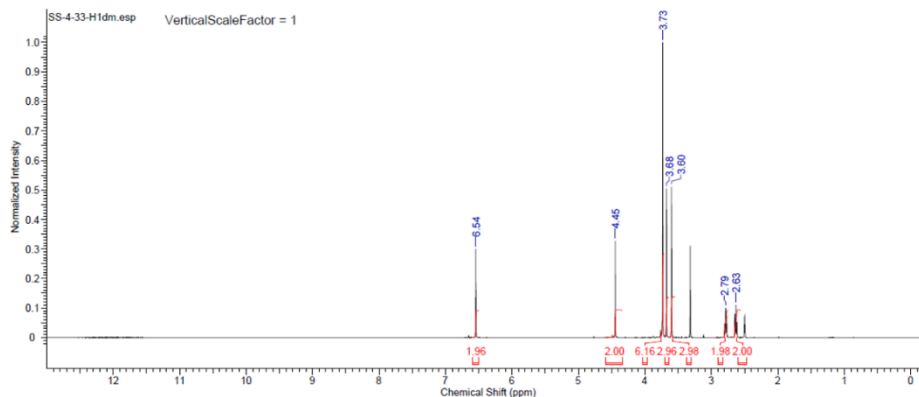


Figure B-69. ^1H NMR Spectrum of dimethylglycolate dihydrosinapate.

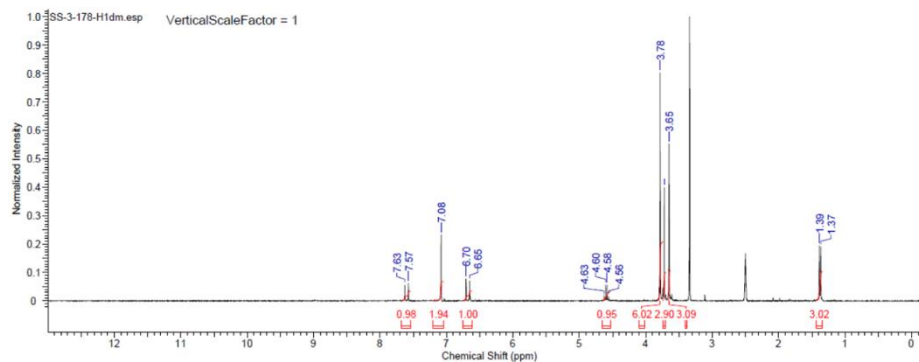


Figure B-70. ^1H NMR Spectrum of dimethyl lactate sinapate.

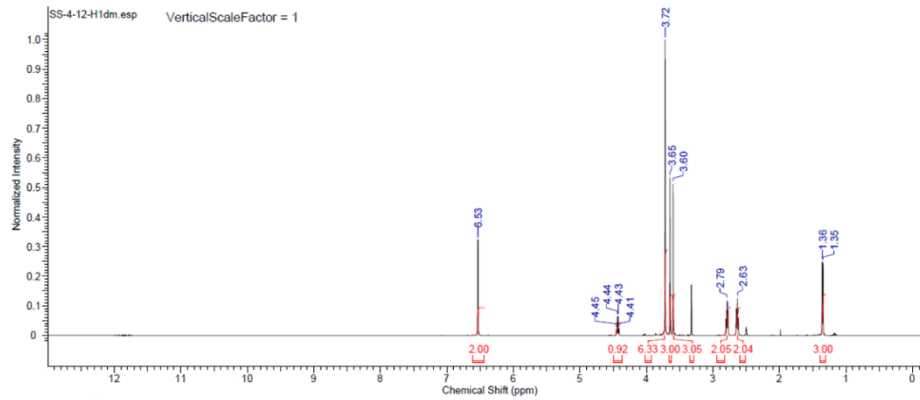


Figure B-71. ¹H NMR Spectrum of dimethylactate dihydrosinapate.

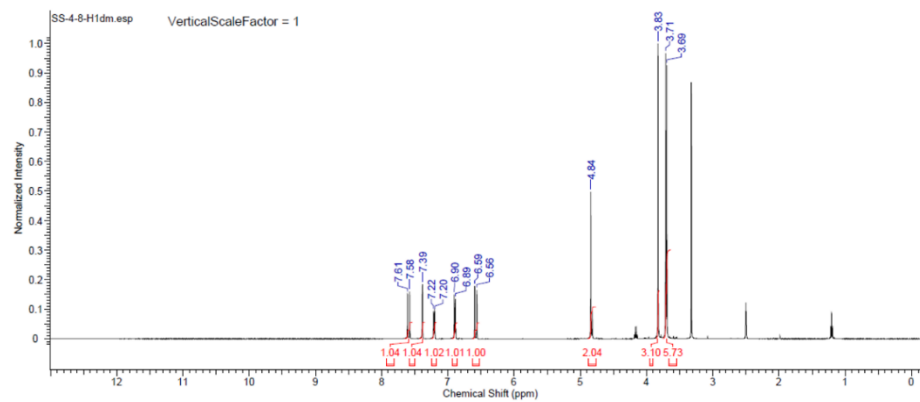


Figure B-72. ¹H NMR Spectrum of dimethylglycolate ferulate.

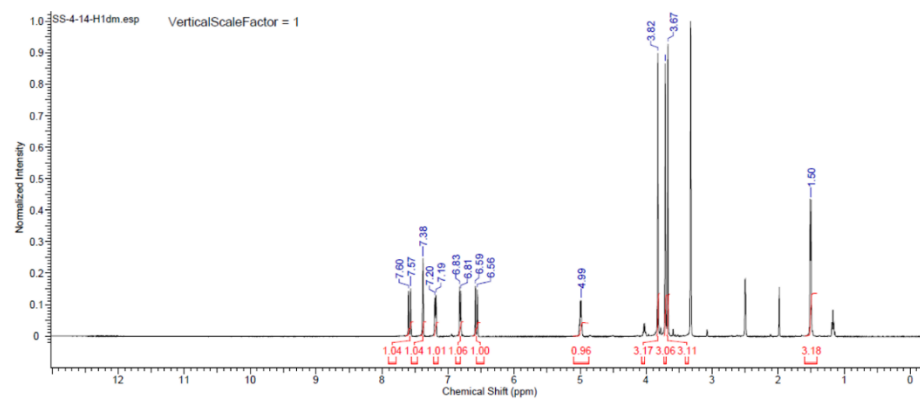


Figure B-73. ¹H NMR Spectrum of dimethylactate ferulate.

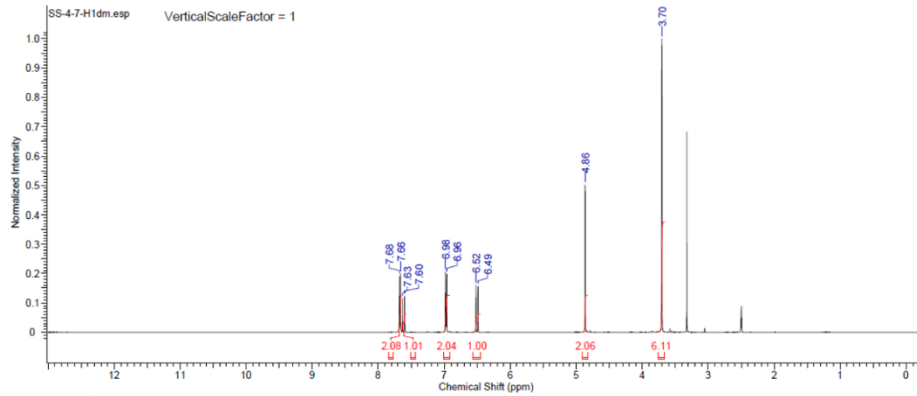


Figure B-74. ¹H NMR Spectrum of dimethylglycolate coumarate.

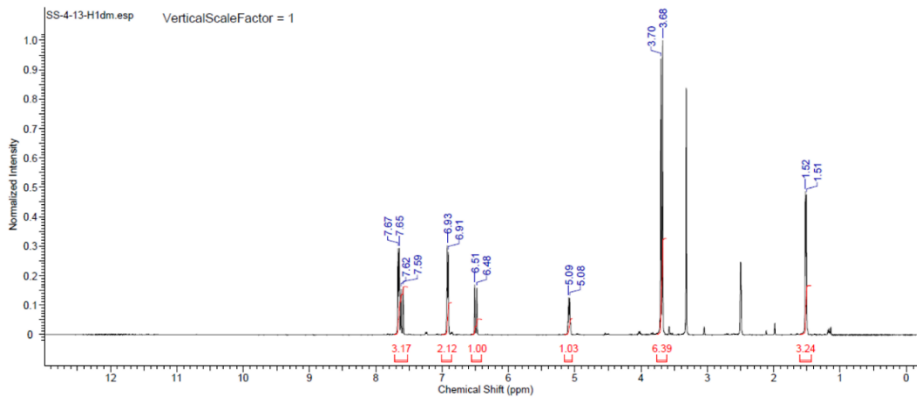


Figure B-75. ¹H NMR Spectrum of dimethyl lactate coumarate.

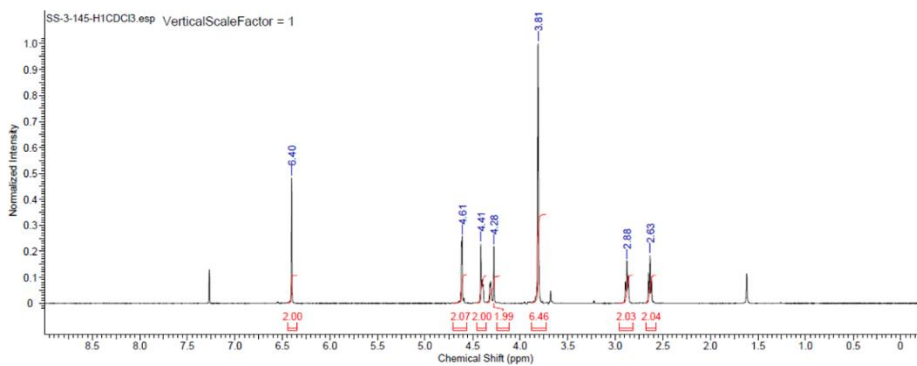


Figure B-76. ¹H NMR Spectrum of polyethyleneglycolate dihydrosinapate (Table 2-2, entry 1).

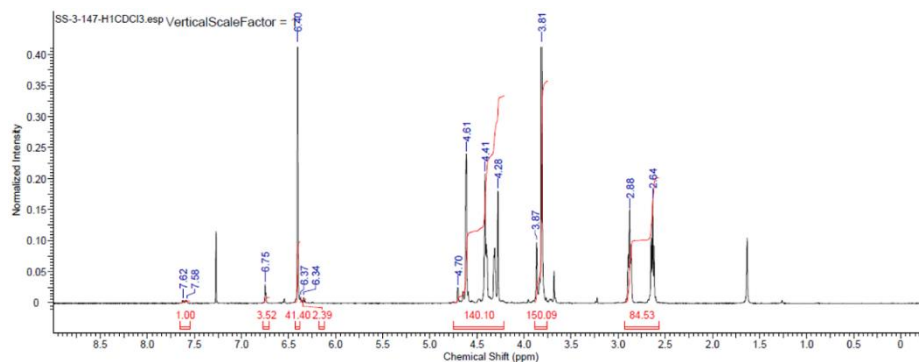


Figure B-77. ¹H NMR Spectrum of copoly(ethyleneglycolate dihydrosinapate/ethyleneglycolate sinapate) [90:10] (Table 2-2, entry 2)

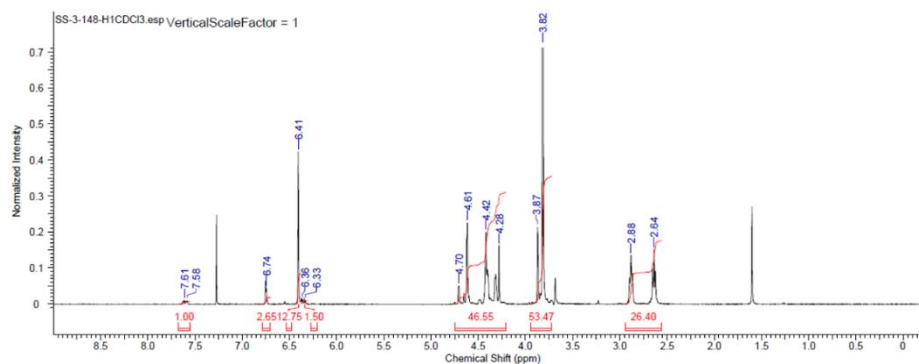


Figure B-78. ¹H NMR Spectrum of copoly(ethyleneglycolate dihydrosinapate/ethyleneglycolate sinapate) [80:20] (Table 2-2, entry 3)

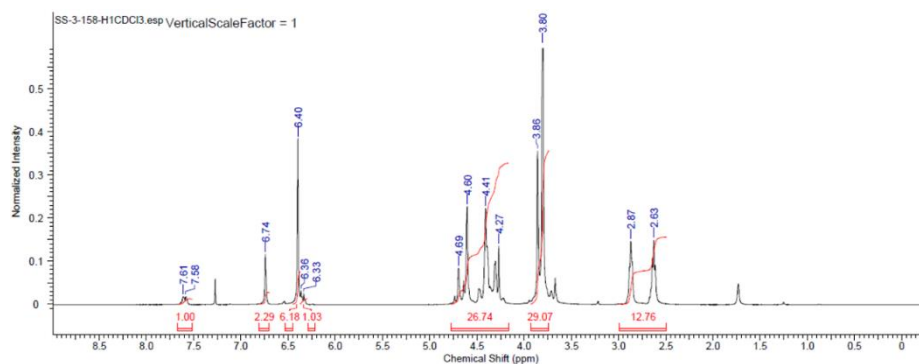


Figure B-79. ¹H NMR Spectrum of copoly(ethyleneglycolate dihydrosinapate/ethyleneglycolate sinapate) [70:30] (Table 2-2, entry 4)

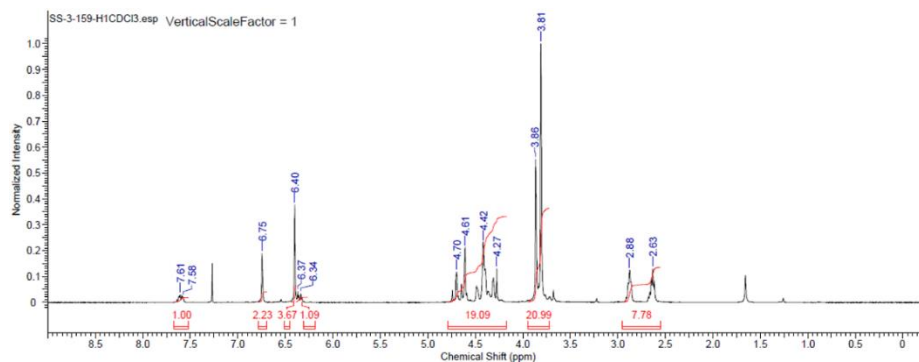


Figure B-80. ¹H NMR Spectrum of copoly(ethyleneglycolate dihydrosinapate/ethyleneglycolate sinapate) [60:40] (Table 2-2, entry 5)

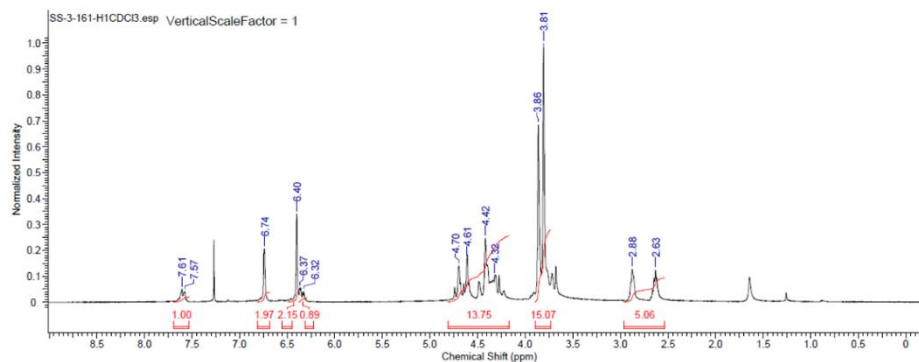


Figure B-81. ¹H NMR Spectrum of copoly(ethyleneglycolate dihydrosinapate/ethyleneglycolate sinapate) [50:50] (Table 2-2, entry 6)

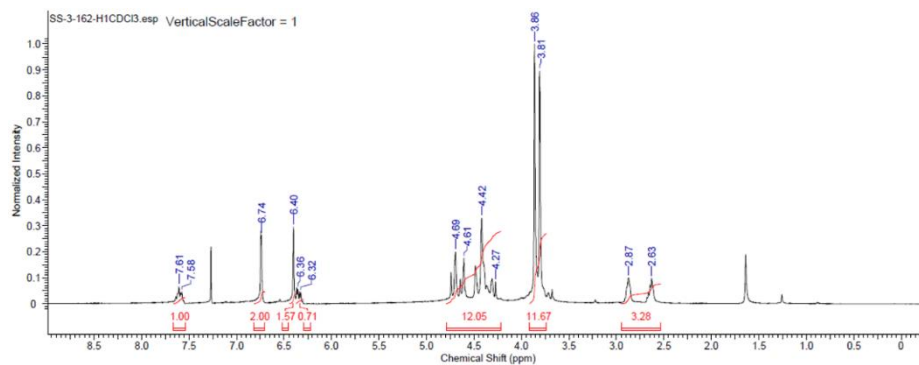


Figure B-82. ¹H NMR Spectrum of copoly(ethyleneglycolate dihydrosinapate/ethyleneglycolate sinapate) [40:60] (Table 2-2, entry 7)

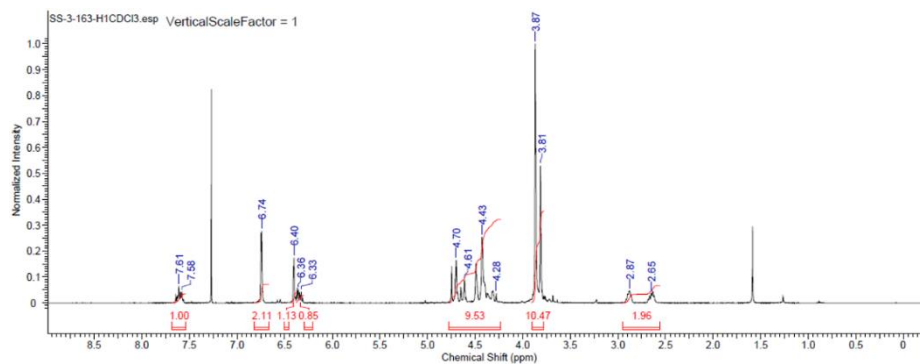


Figure B-83. ¹H NMR Spectrum of copoly(ethyleneglycolate dihydrosinapate/ethyleneglycolate sinapate) [30:70] (Table 2-2, entry 8)

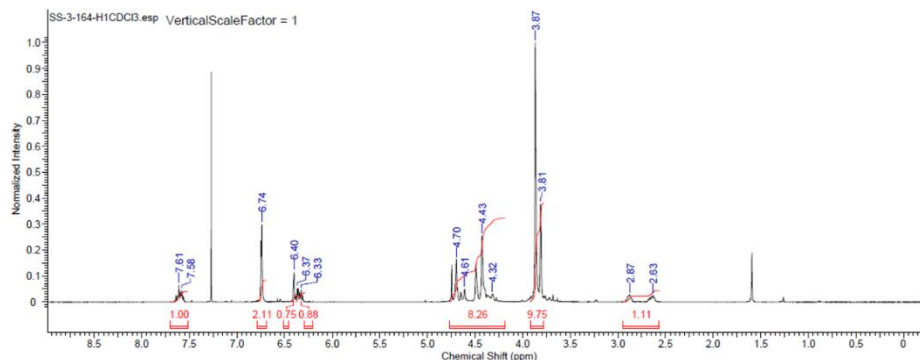


Figure B-84. ¹H NMR Spectrum of copoly(ethyleneglycolate dihydrosinapate/ethyleneglycolate sinapate) [20:80] (Table 2-2, entry 9)

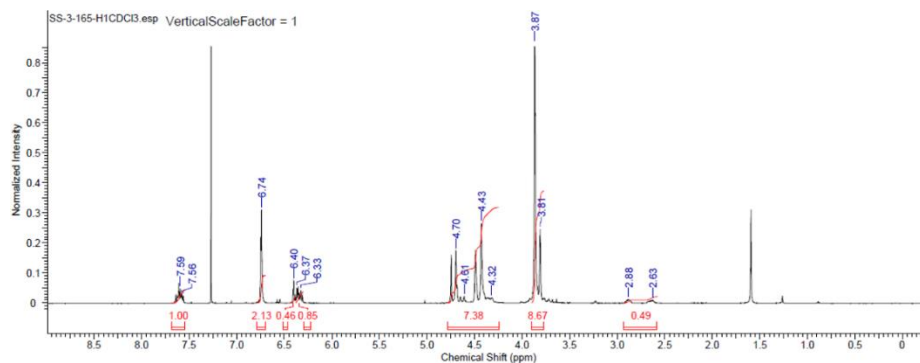


Figure B-85. ¹H NMR Spectrum of copoly(ethyleneglycolate dihydrosinapate/ethyleneglycolate sinapate) [10:90] (Table 2-2, entry 10)

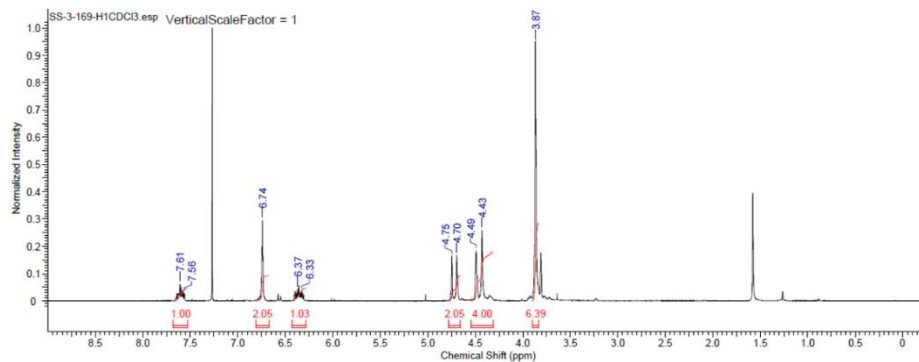


Figure B-86. ¹H NMR Spectrum of polyethyleneglycolate sinapate (Table 2-2, entry 11)

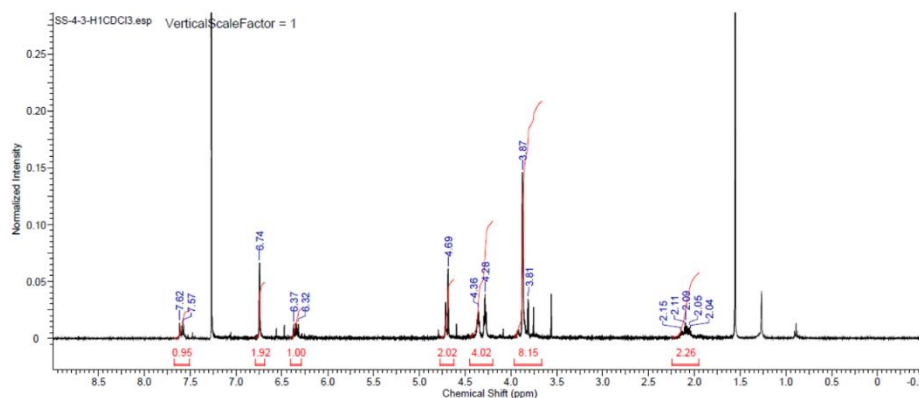


Figure B-87. ¹H NMR Spectrum of polypropyleneglycolate sinapate (Table 2-1, entry 2)

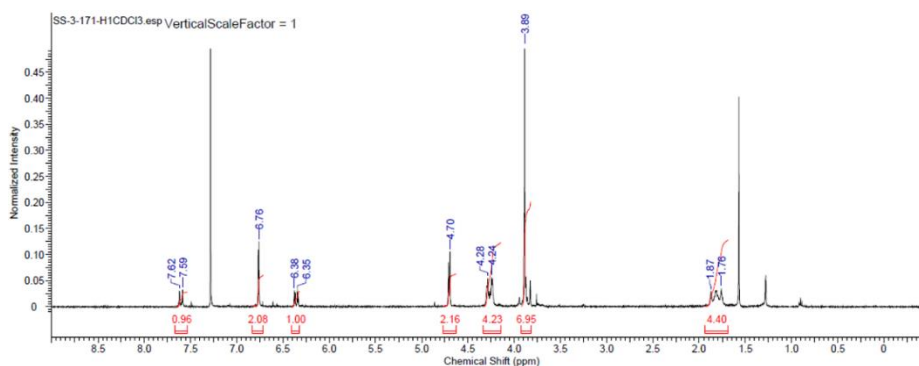


Figure B-88. ¹H NMR Spectrum of polybutyleneglycolate sinapate (Table 2-3, entry 3).

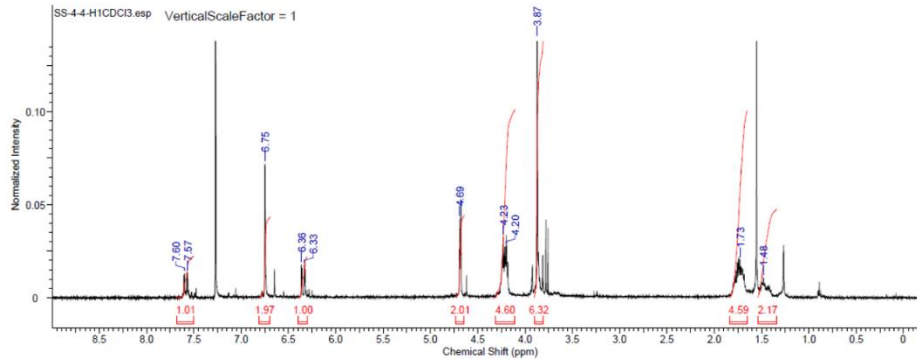


Figure B-89. ¹H NMR Spectrum of polypentylene glycolate sinapate (Table 2-3, entry 4)

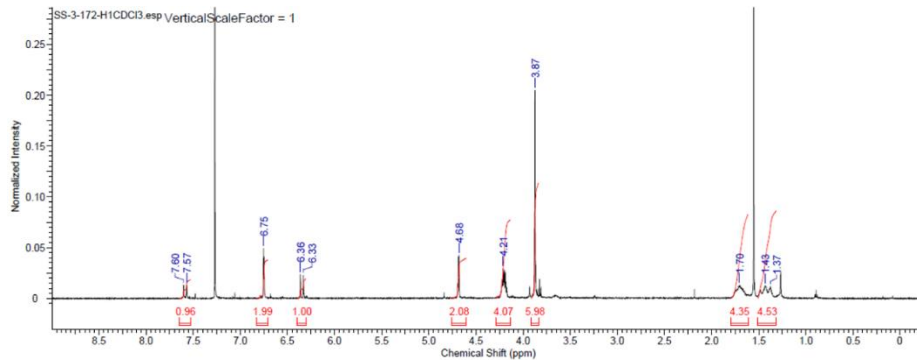


Figure B-90. ¹H NMR Spectrum of polyhexylene glycolate sinapate (Table 2-3, entry 5)

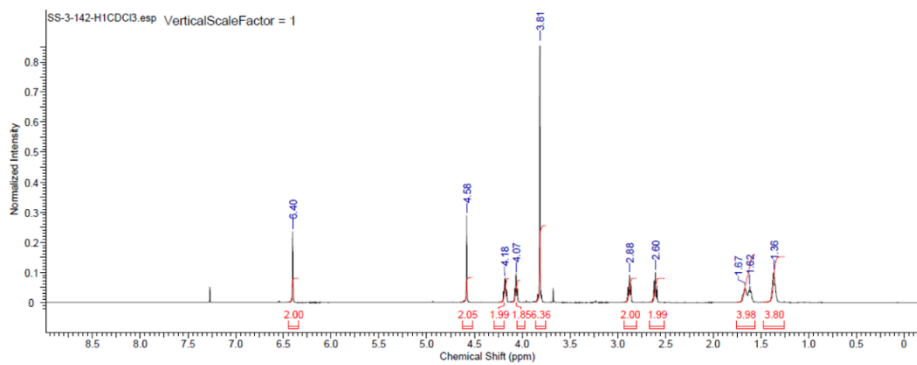


Figure B-91. ¹H NMR Spectrum of polyhexylene glycolate dihydrosinapate (Table 2-1, entry 1)

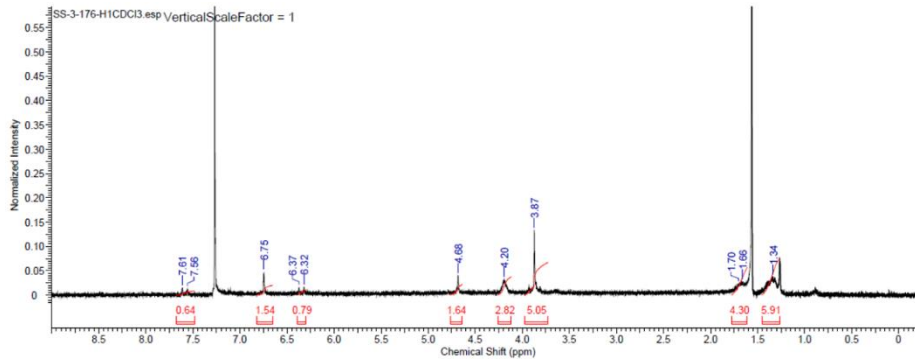


Figure B-92. ¹H NMR Spectrum of polyoctyleneglycolate sinapate (Table 2-3, entry 6)

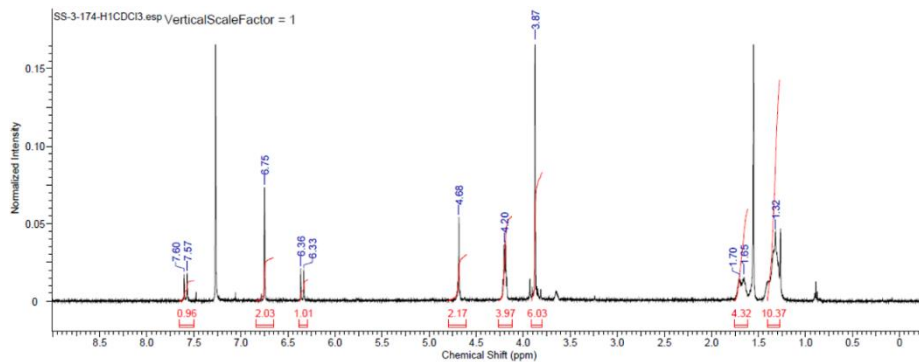


Figure B-93. ¹H NMR Spectrum of polynonyleneglycolate sinapate (Table 2-3, entry 7)

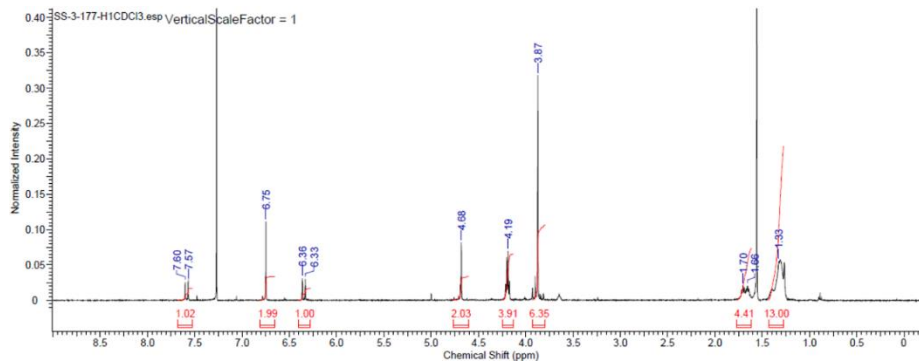


Figure B-94. ¹H NMR Spectrum of polydecyleneglycolate sinapate (Table 2-3, entry 8)

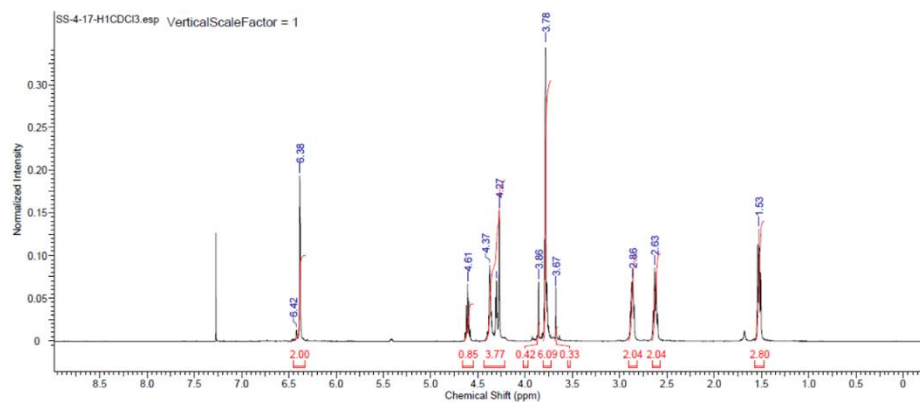


Figure B-95. ^1H NMR Spectrum of polyethylenelactate dihydrosinapate (Table 2-4, entry 1).

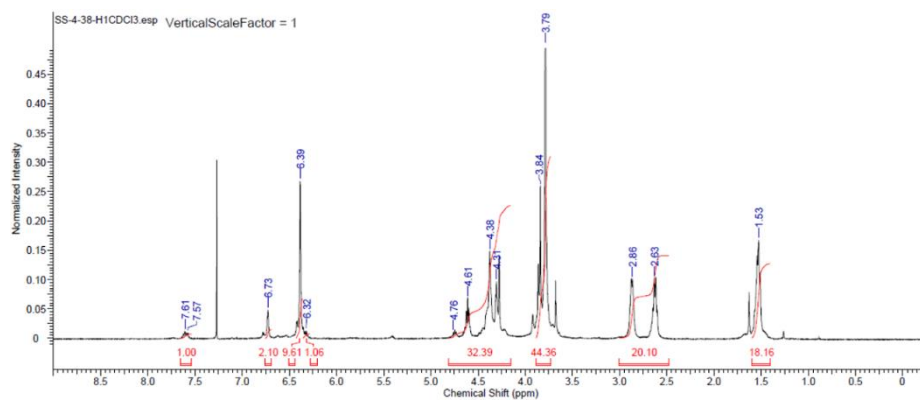


Figure B-96. ^1H NMR Spectrum of copoly(ethylenelactate dihydrosinapate/ethylenelactate sinapate) [70:30] (Table 2-4, entry 2).

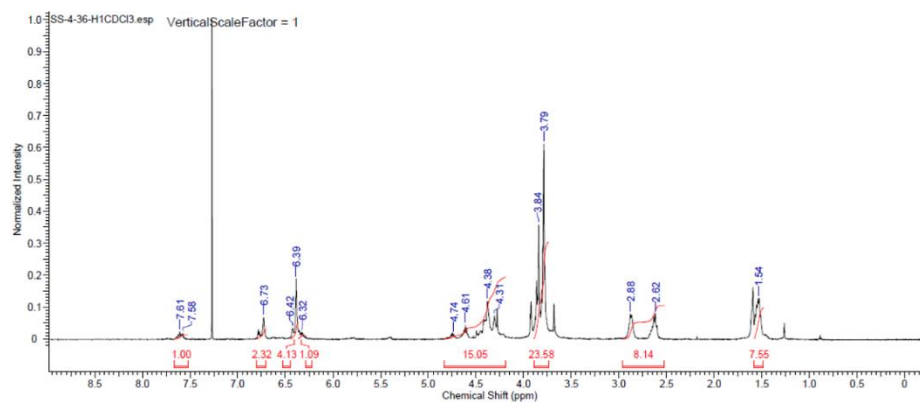


Figure B-97. ^1H NMR Spectrum of copoly(ethylenelactate dihydrosinapate/ethylenelactate sinapate) [50:50] (Table 2-4, entry 3)

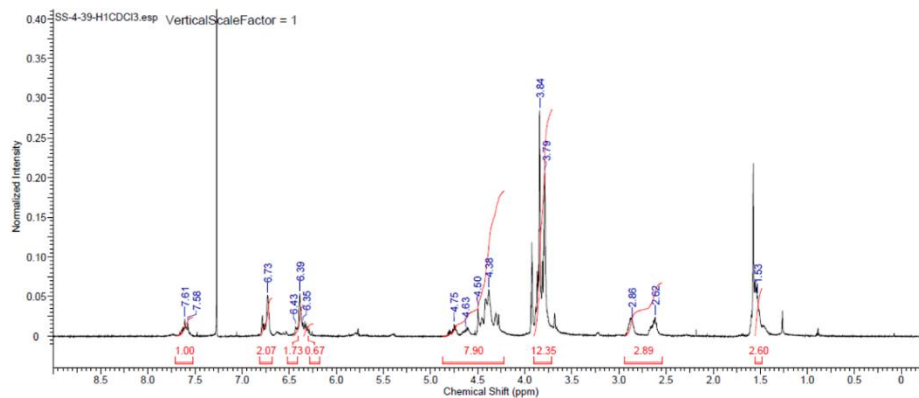


Figure B-98. ¹H NMR Spectrum of copoly(ethylenelactate dihydrosinapate/ethylenelactate sinapate) [30:70] (Table 2-4, entry 4)

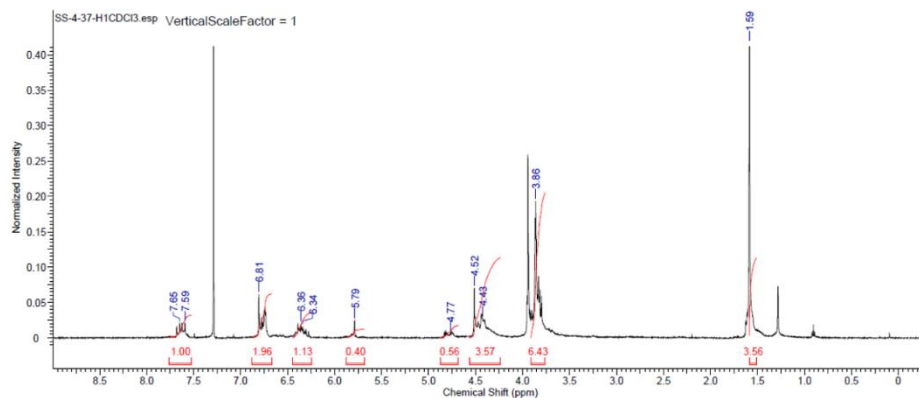


Figure B-99. ¹H NMR Spectrum of polyethylenelactate sinapate (Table 2-4, entry 5).

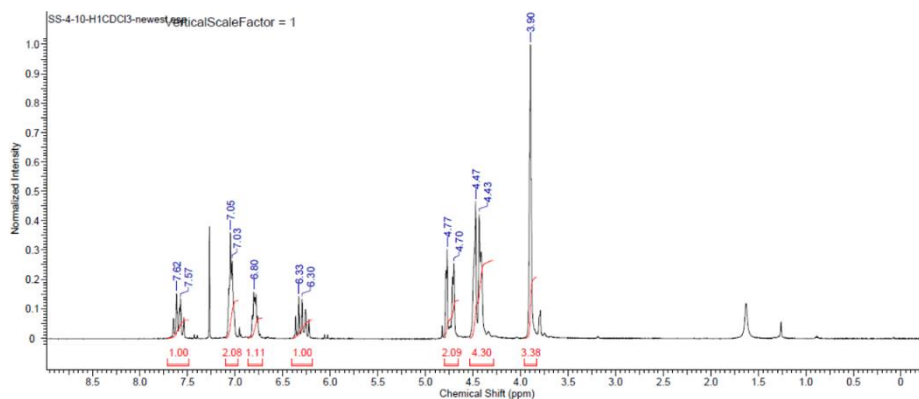


Figure B-100. ¹H NMR Spectrum of polyethyleneglycolate ferulate (Table 2-5, entry 1).

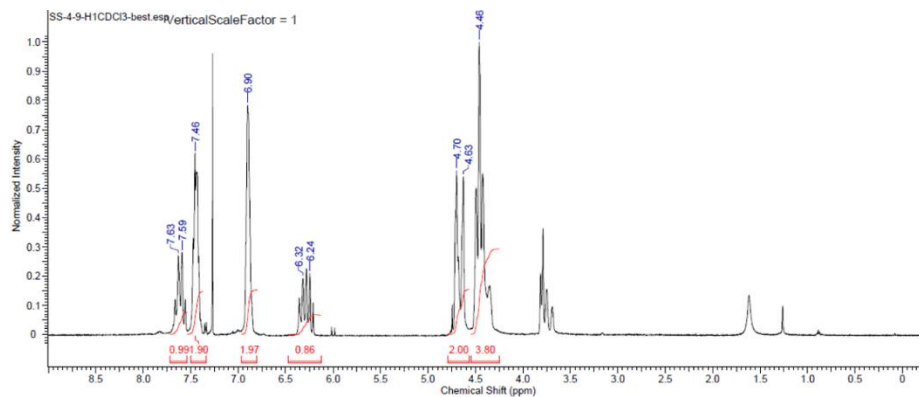


Figure B-101. ¹H NMR Spectrum of polyethyleneglycolate coumarate (Table 2-5, entry 2)

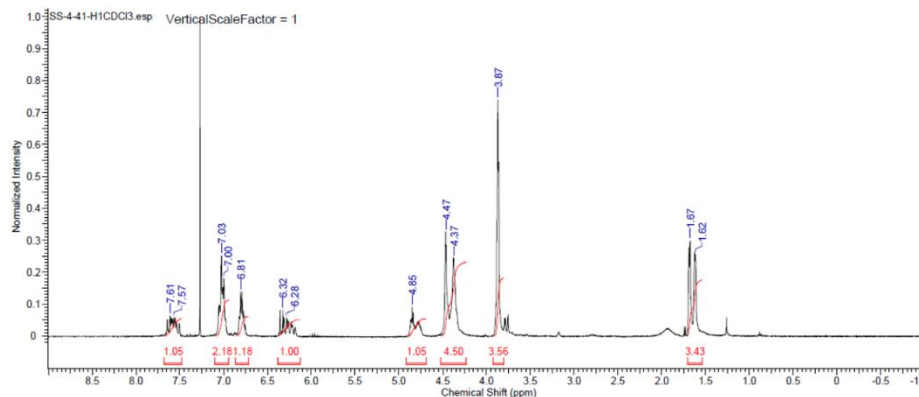


Figure B-102. ¹H NMR Spectrum of polyethylenelactate ferulate (Table 2-5, entry 3)

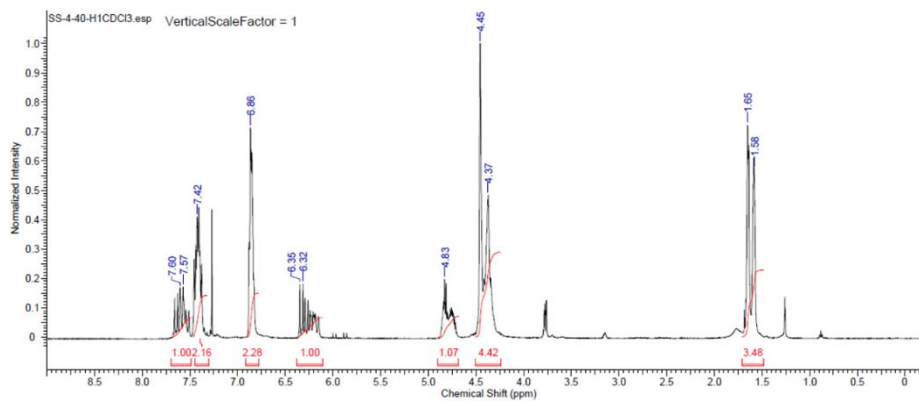


Figure B-103. ¹H NMR Spectrum of polyethylenelactate coumarate (Table 2-5, entry 4)

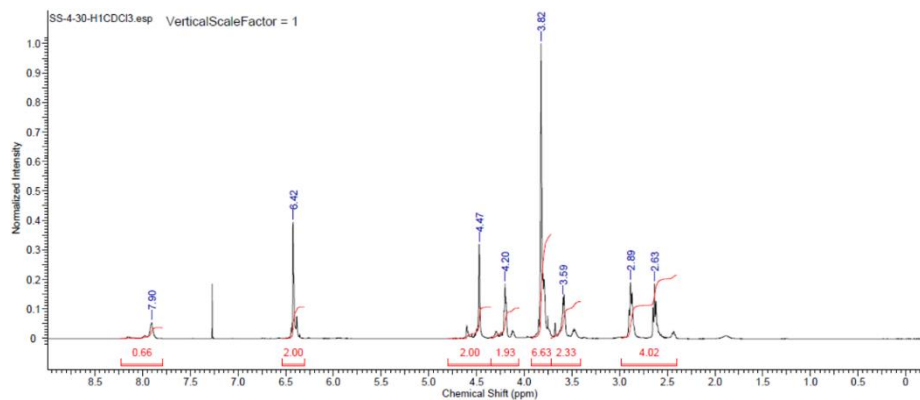


Figure B-104. ¹H NMR Spectrum of polyethyleneglycolate dihydrosinapamide (polyesteramide) (Table 2-5, entry 5)

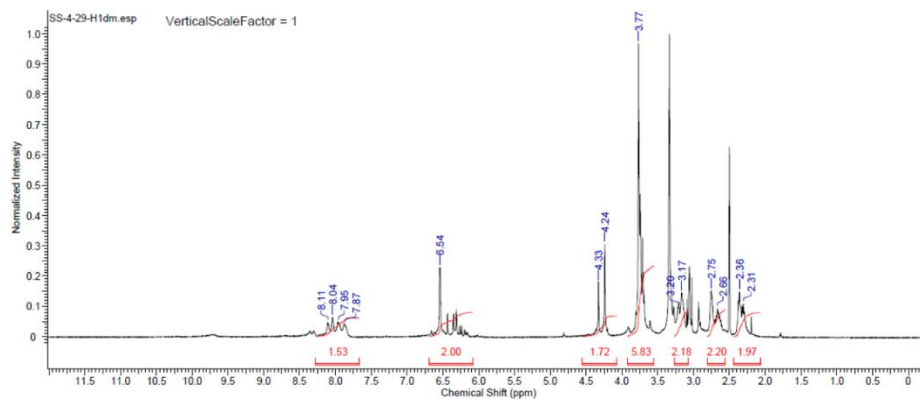


Figure B-105. ¹H NMR Spectrum of polyethyleneglycolamide dihydrosinapamide (polyamide) (Table 2-5, entry 6).

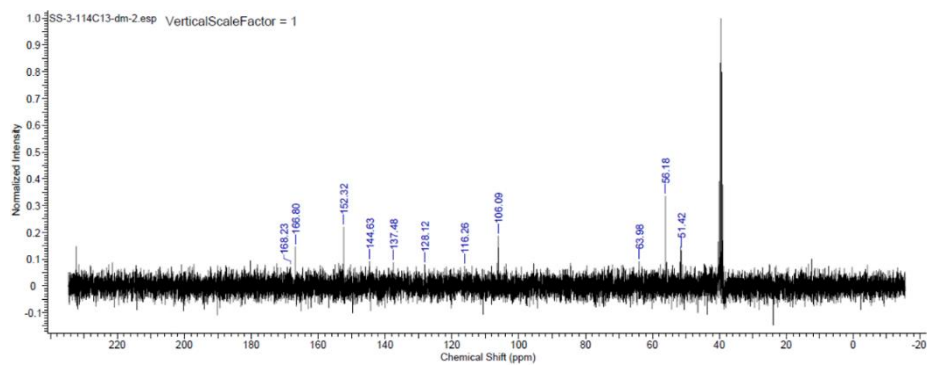


Figure B-106. ¹³C NMR Spectrum of dimethylglycolate sinapate

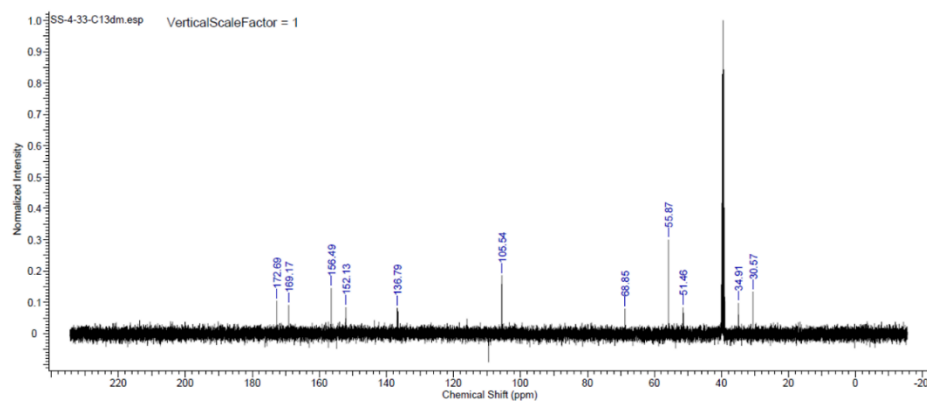


Figure B-107. ¹³C NMR Spectrum of dimethylglycolate dihydrosinapate

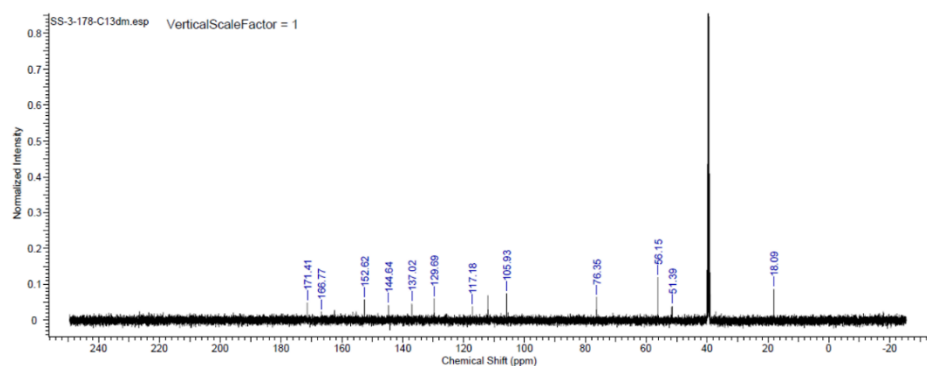


Figure B-108. ¹³C NMR Spectrum of dimethyl lactate sinapate

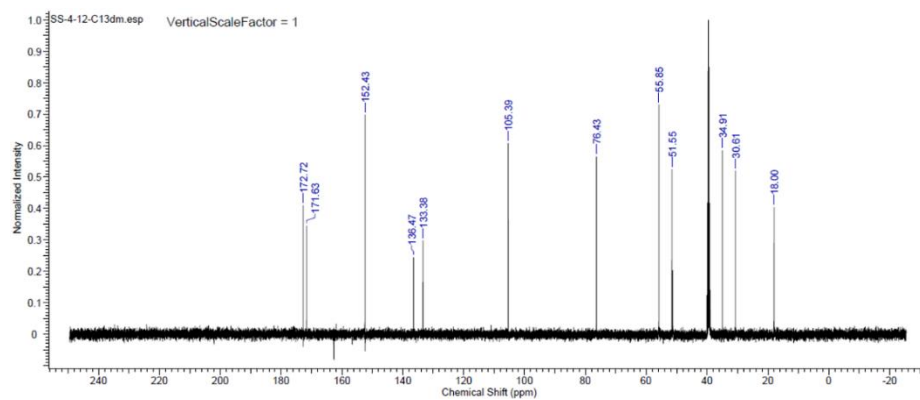


Figure B-109. ^{13}C NMR Spectrum of dimethylactate dihydrosinapate

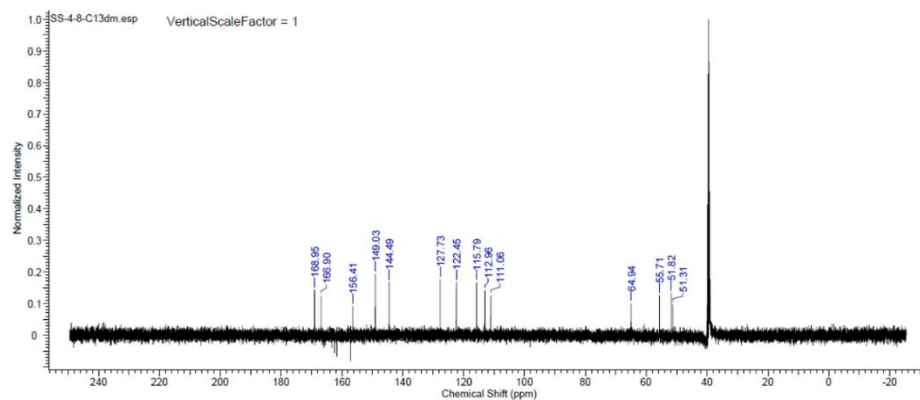


Figure B-110. ^{13}C NMR Spectrum of dimethylglycolate ferulate

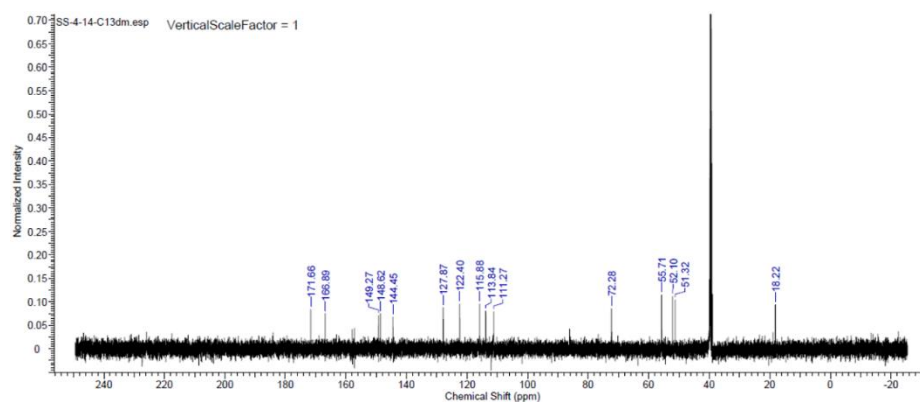


Figure B-111. ^{13}C NMR Spectrum of dimethylactate ferulate

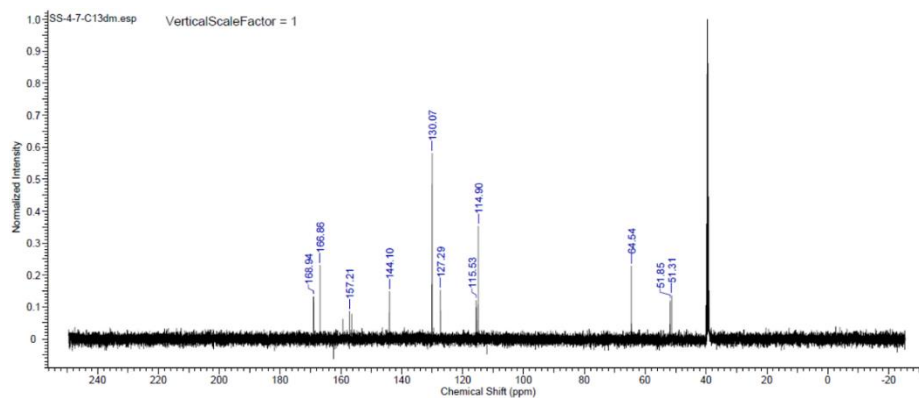


Figure B-112. ^{13}C NMR Spectrum of dimethylglycolate coumarate

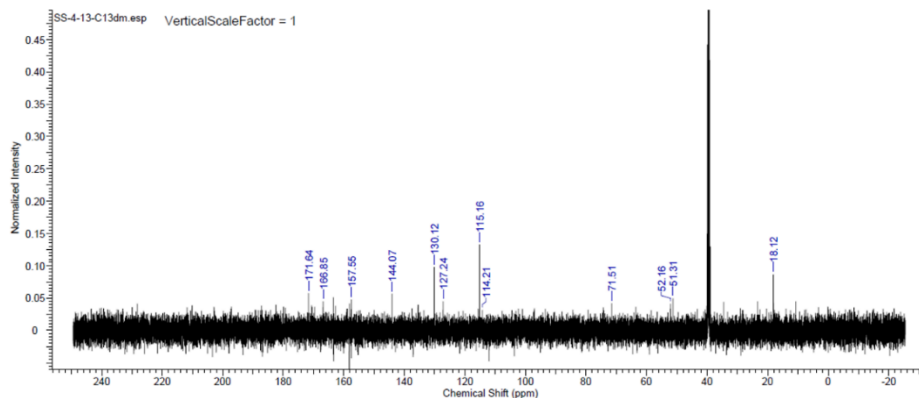


Figure B-113. ^{13}C NMR Spectrum of dimethyl lactate coumarate

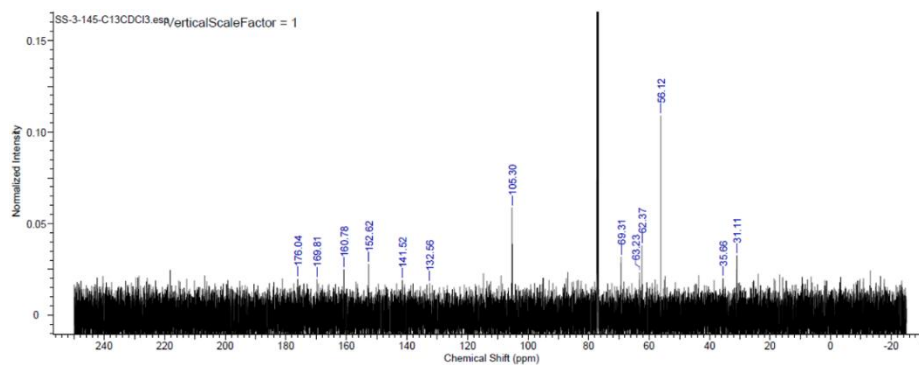


Figure B-114. ^{13}C NMR Spectrum of polyethyleneglycolate dihydrosinapate (Table 2-2, entry 1)

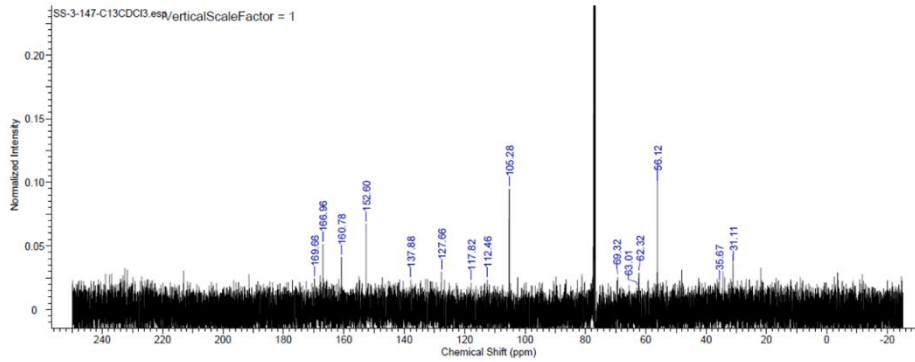


Figure B-115. ^{13}C NMR Spectrum of copoly(ethyleneglycolate dihydrosinapate/ethyleneglycolate sinapate) [90:10] (Table 2-2, entry 2)

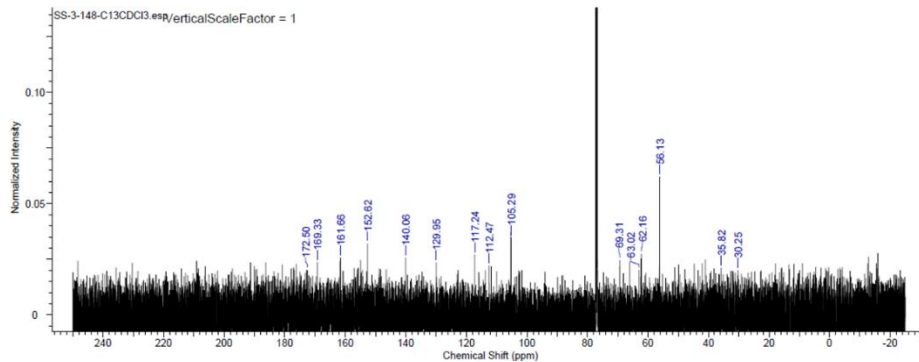


Figure B-116. ^{13}C NMR Spectrum of copoly(ethyleneglycolate dihydrosinapate/ethyleneglycolate sinapate) [80:20] (Table 2-2, entry 3).

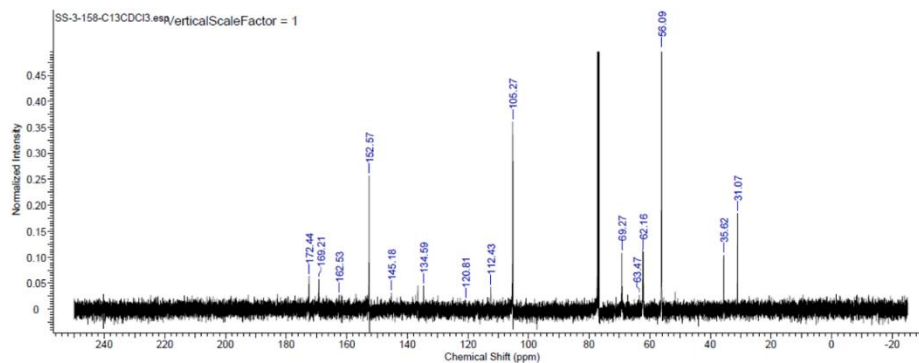


Figure B-117. ^{13}C NMR Spectrum of copoly(ethyleneglycolate dihydrosinapate/ethyleneglycolate sinapate) [70:30] (Table 2-2, entry 4)

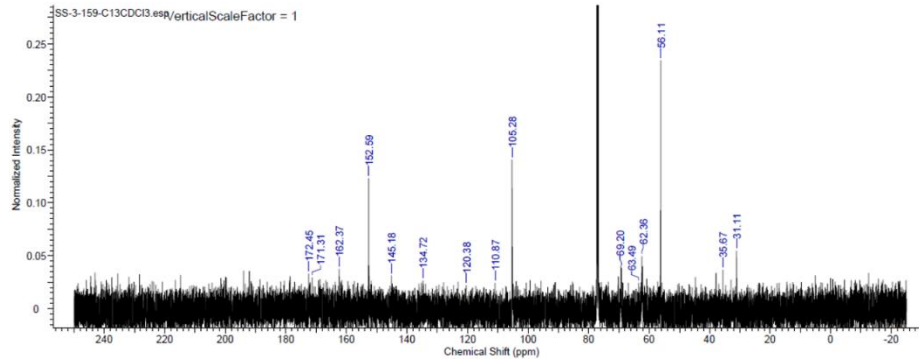


Figure B-118. ^{13}C NMR Spectrum of copoly(ethyleneglycolate dihydrosinapate/ethyleneglycolate sinapate) [60:40] (Table 2-2, entry 5)

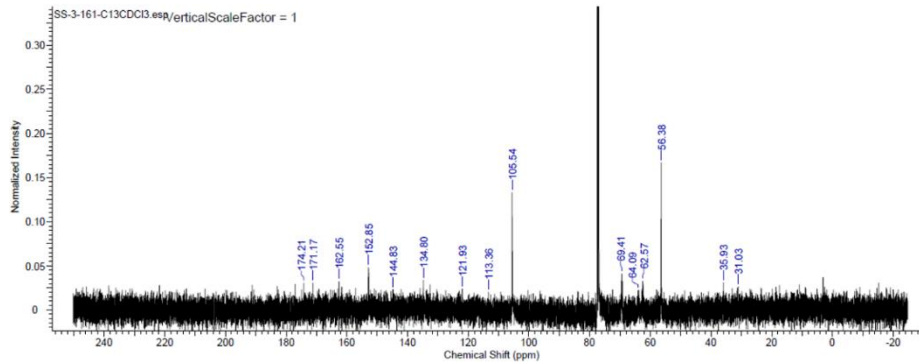


Figure B-119. ^{13}C NMR Spectrum of copoly(ethyleneglycolate dihydrosinapate/ethyleneglycolate sinapate) [50:50] (Table 2-2, entry 6)

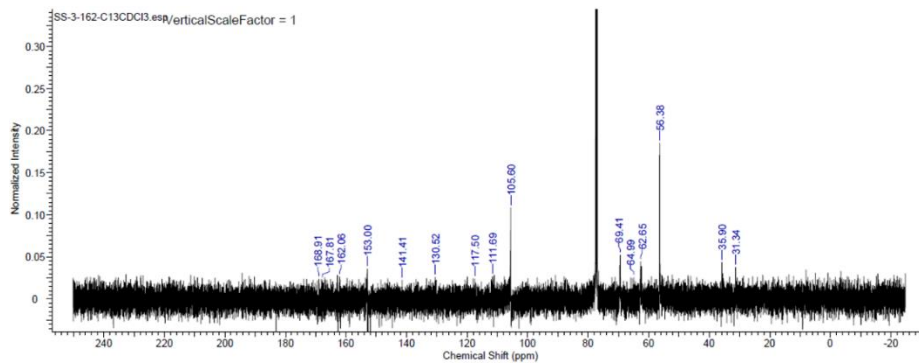


Figure B-120. ^{13}C NMR Spectrum of copoly(ethyleneglycolate dihydrosinapate/ethyleneglycolate sinapate) [40:60] (Table 2-2, entry 7)

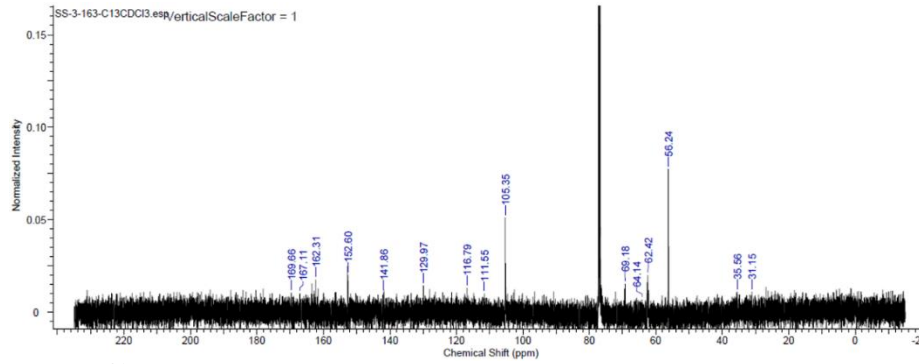


Figure B-121. ^{13}C NMR Spectrum of copoly(ethyleneglycolate dihydrosinapate/ethyleneglycolate sinapate) [30:70] (Table 2-2, entry 8)

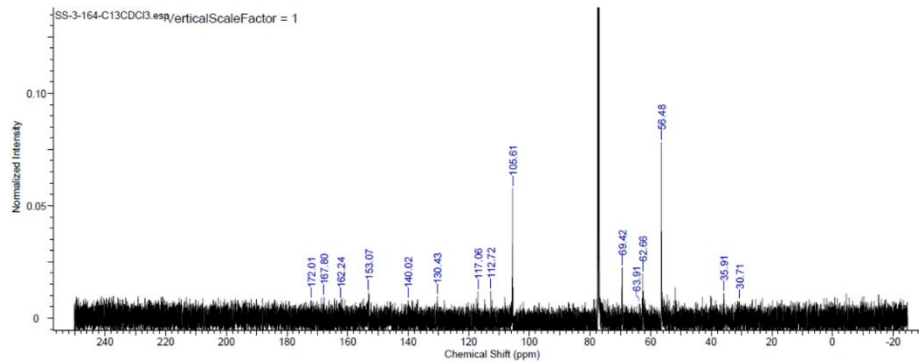


Figure B-122. ^{13}C NMR Spectrum of copoly(ethyleneglycolate dihydrosinapate/ethyleneglycolate sinapate) [20:80] (Table 2-2, entry 9)

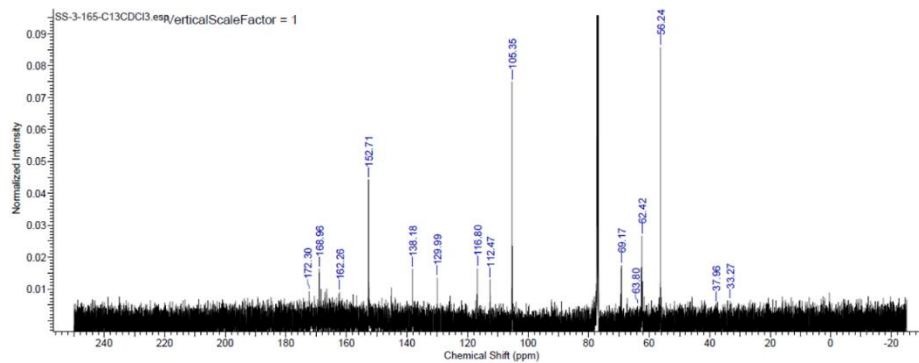


Figure B-123. ^{13}C NMR Spectrum of copoly(ethyleneglycolate dihydrosinapate/ethyleneglycolate sinapate) [10:90] (Table 2-2, entry 10)

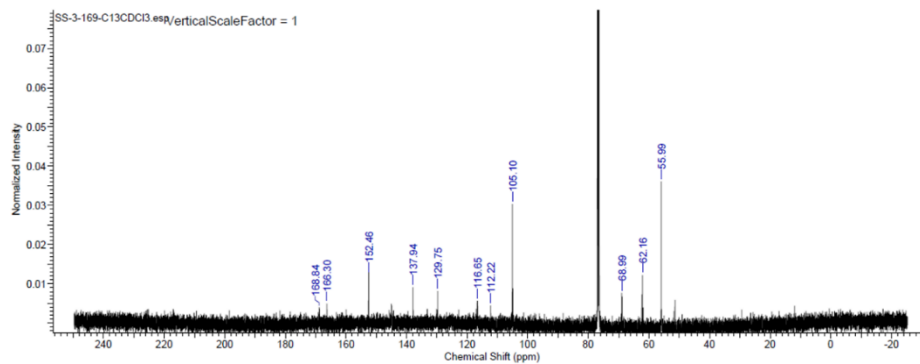


Figure B-124. ^{13}C NMR Spectrum of polyethyleneglycolate sinapate (Table 2-2, entry 11)

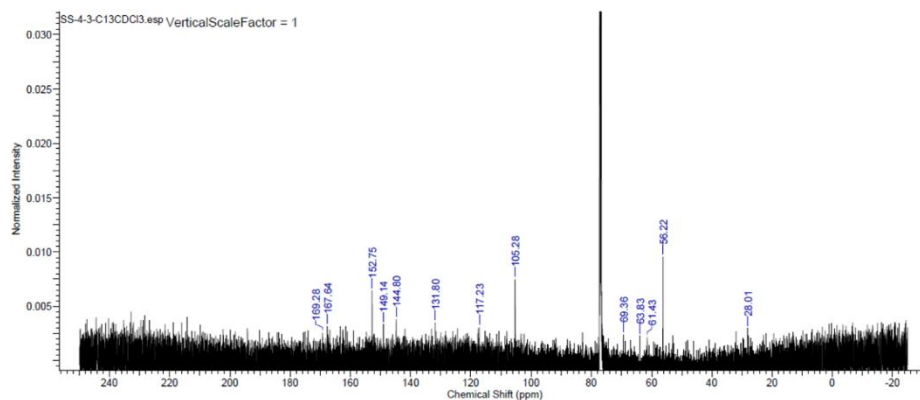


Figure B-125. ^{13}C NMR Spectrum of polypropyleneglycolate sinapate (Table 2-3, entry 2)

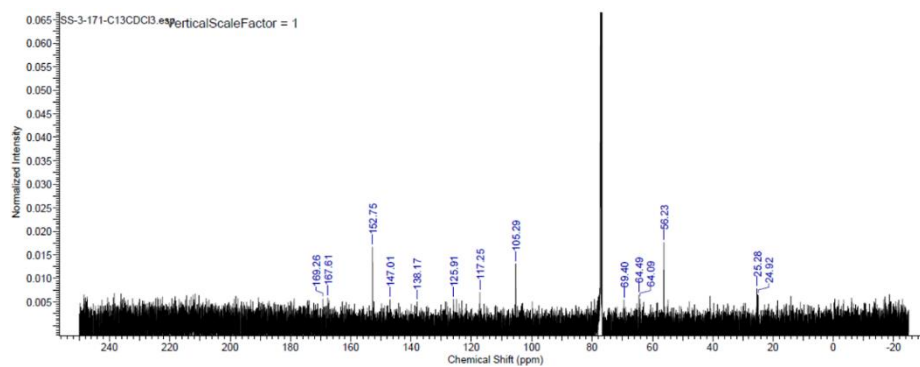


Figure B-126. ^{13}C NMR Spectrum of polybutyleneglycolate sinapate (Table 2-3, entry 3).

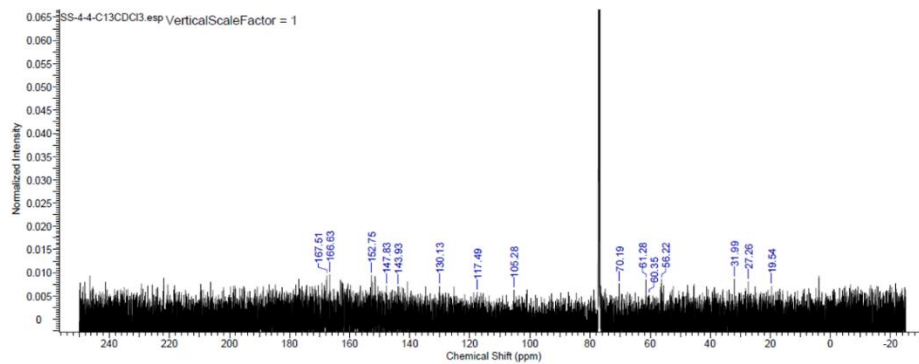


Figure B-127. ^{13}C NMR Spectrum of polypentylene glycolate sinapate (Table 2-3, entry 4)

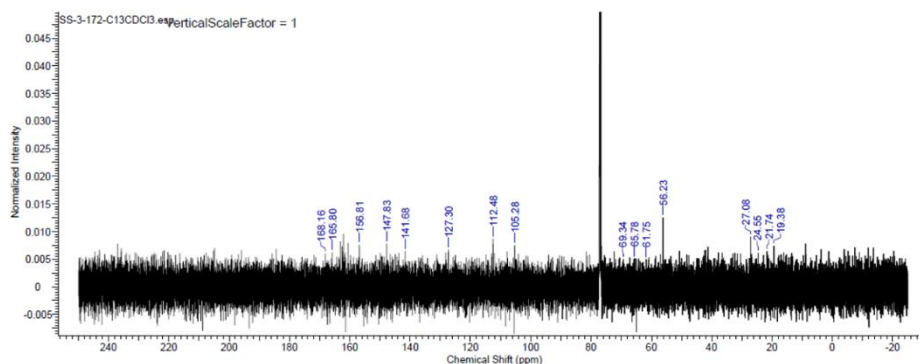


Figure B-128. ^{13}C NMR Spectrum of polyhexylene glycolate sinapate (Table 2-3, entry 5)

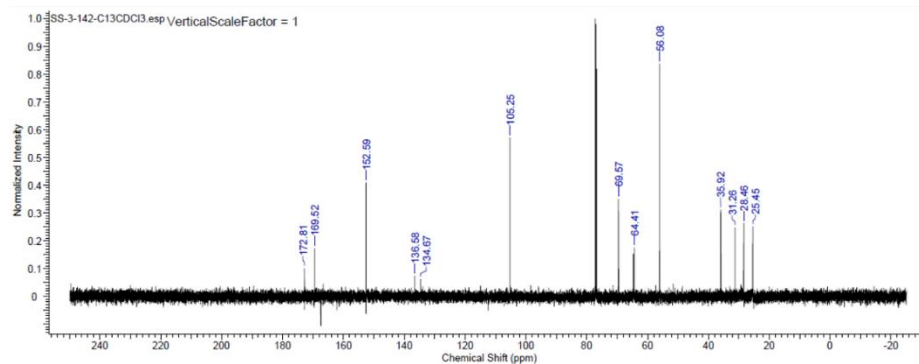


Figure B-129. ^{13}C NMR Spectrum of polyhexylene glycolate dihydrosinapate (Table 2-1, entry 2)

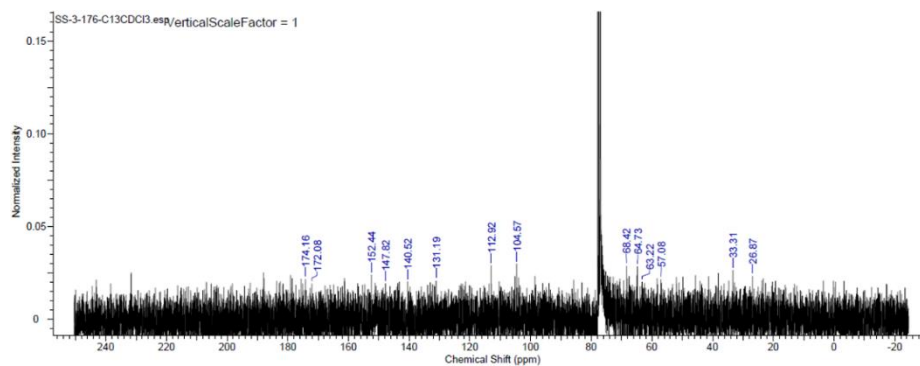


Figure B-130. ^{13}C NMR Spectrum of polyoctyleneglycolate sinapate (Table 2-3, entry 6)

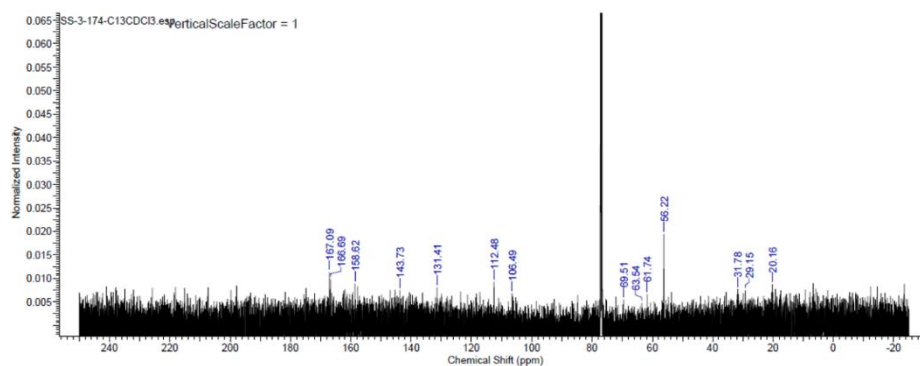


Figure B-131. ^{13}C NMR Spectrum of polynonyleneglycolate sinapate (Table 2-3, entry 7).

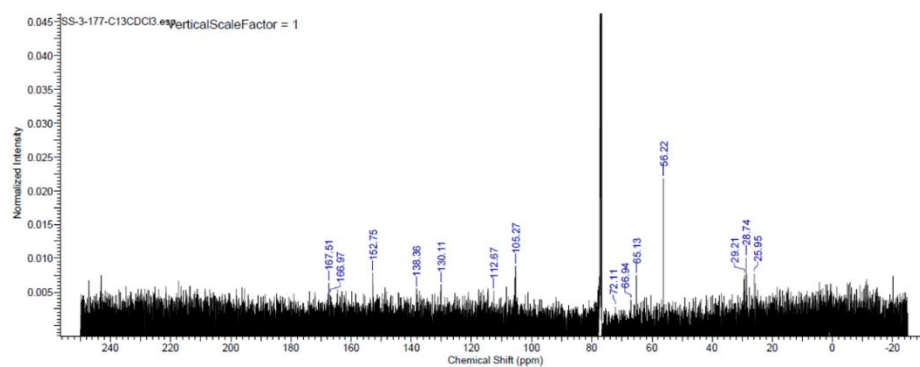


Figure B-132. ^{13}C NMR Spectrum of polydecyleneglycolate sinapate (Table 2-3, entry 8)

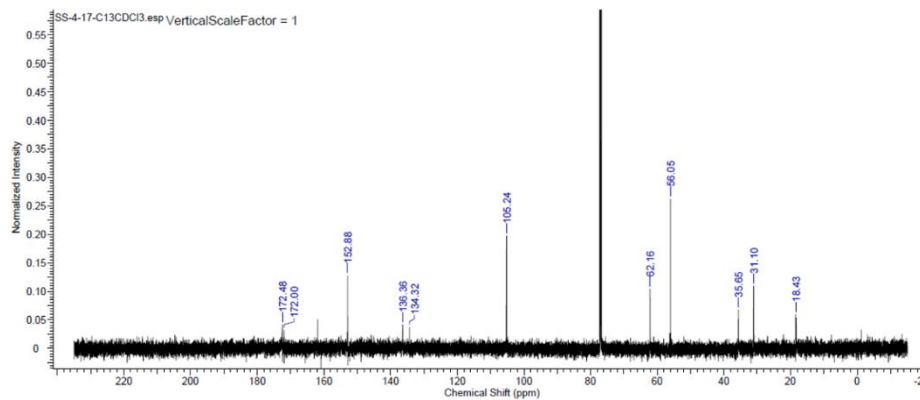


Figure B-133. ^{13}C NMR Spectrum of polyethylenelactate dihydrosinapate (Table 2-4, entry 1)

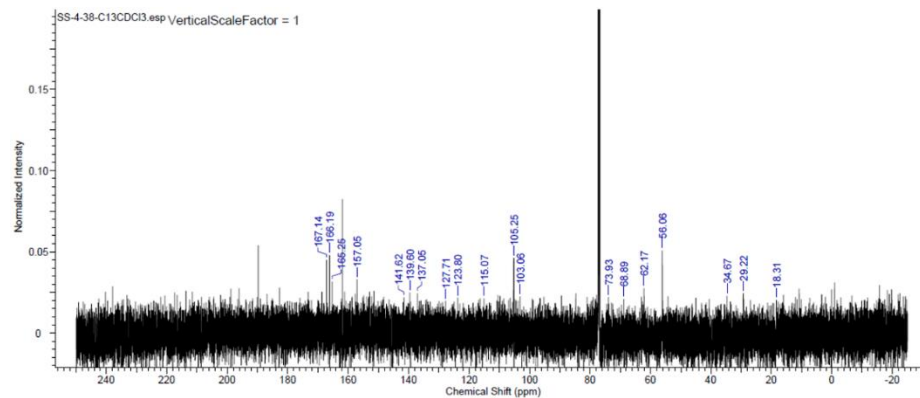


Figure B-134. ^{13}C NMR Spectrum of copoly(ethylenelactate dihydrosinapate/ethylenelactate sinapate) [70:30] (Table 2-4, entry 2)

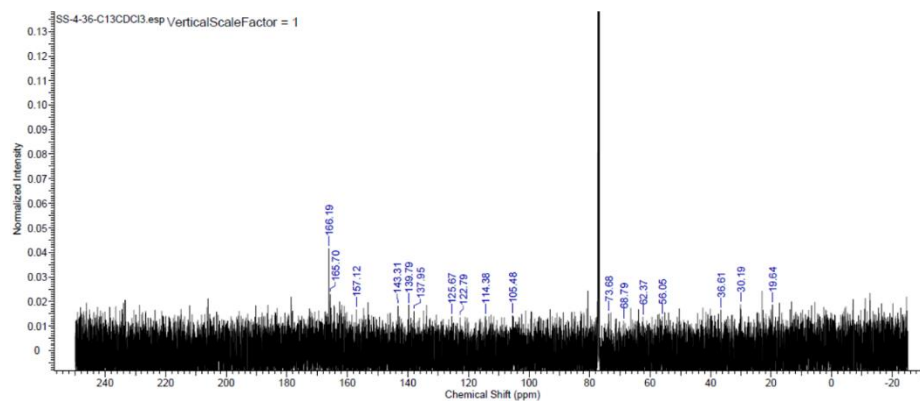


Figure B-135. ^{13}C NMR Spectrum of copoly(ethylenelactate dihydrosinapate/ethylenelactate sinapate) [50:50] (Table 2-4, entry 3)

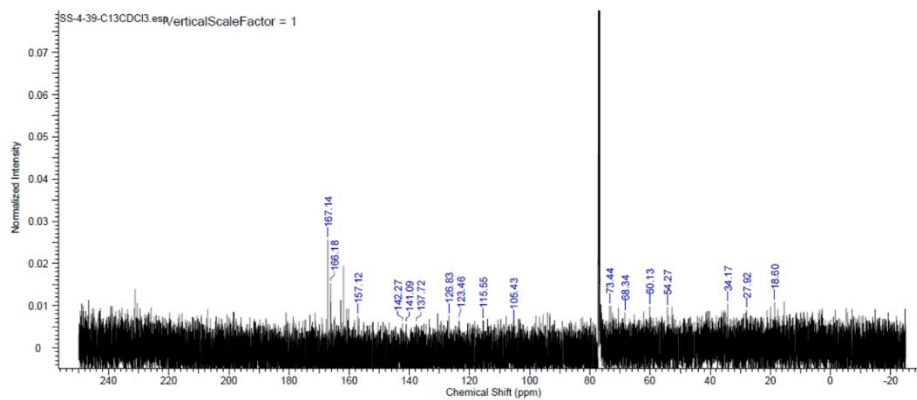


Figure B-136. ^{13}C NMR Spectrum of copoly(ethylenelactate dihydrosinapate/ethylenelactate sinapate) [30:70] (Table 2-4, entry 4)

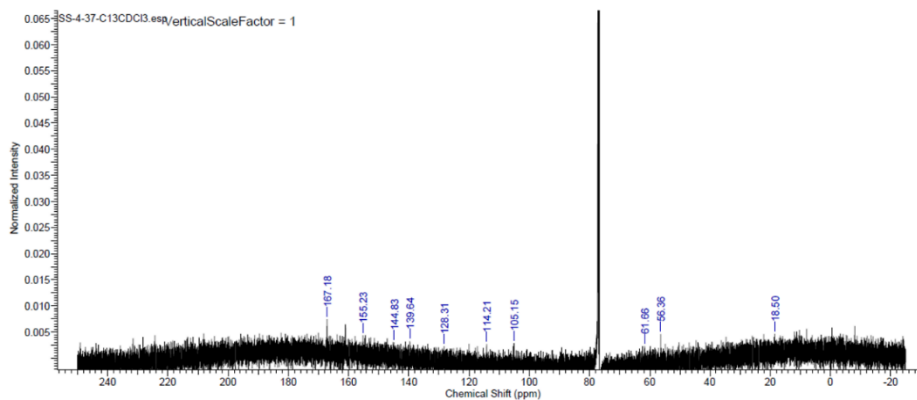


Figure B-137. ^{13}C NMR Spectrum of polyethylenelactate sinapate (Table 2-4, entry 5)

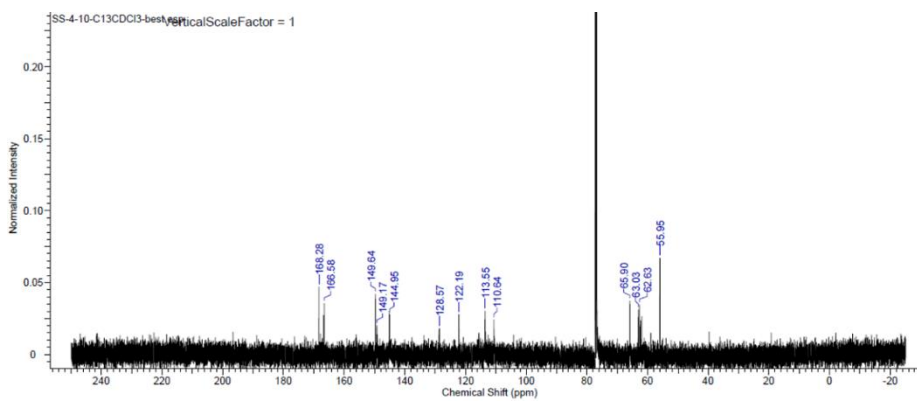


Figure B-138. ^{13}C NMR Spectrum of polyethyleneglycolate ferulate (Table 2-5, entry 1)

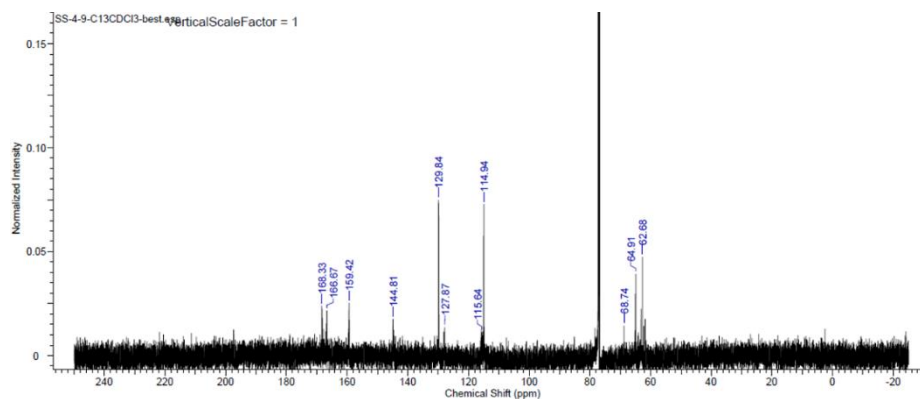


Figure B-139. ^{13}C NMR Spectrum of polyethyleneglycolate coumarate (Table 2-5, entry 2)

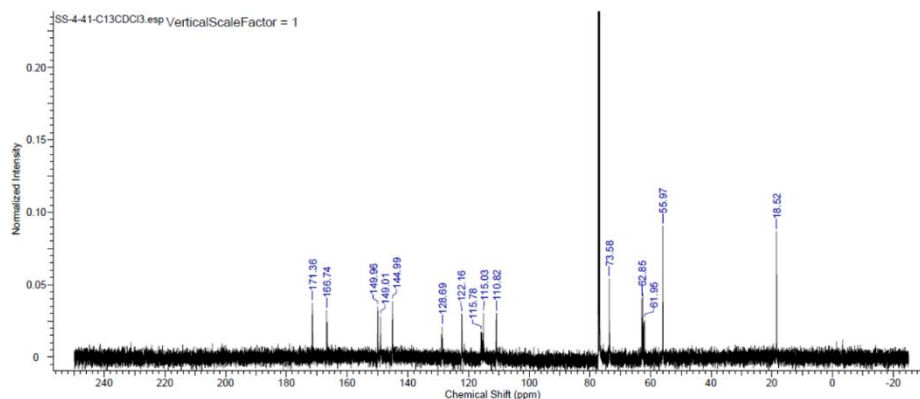


Figure B-140. ^{13}C NMR Spectrum of polyethylenelactate ferulate (Table 2-5, entry 3)

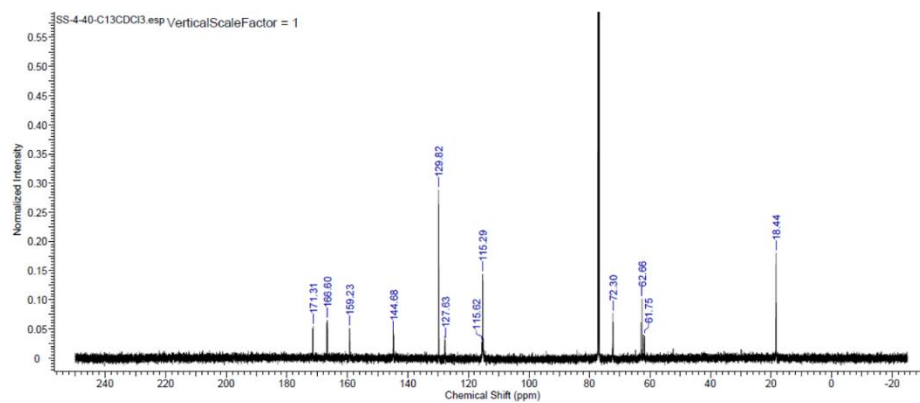


Figure B-141. ^{13}C NMR Spectrum of polyethylenelactate coumarate (Table 2-5, entry 4)

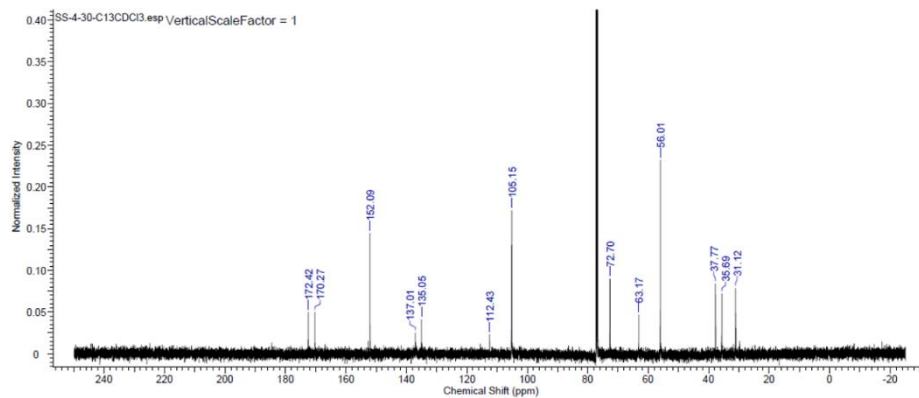


Figure B-142. ^{13}C NMR Spectrum of polyethyleneglycolate dihydrosinapamide (polyesteramide) (Table 2-5, entry 5)

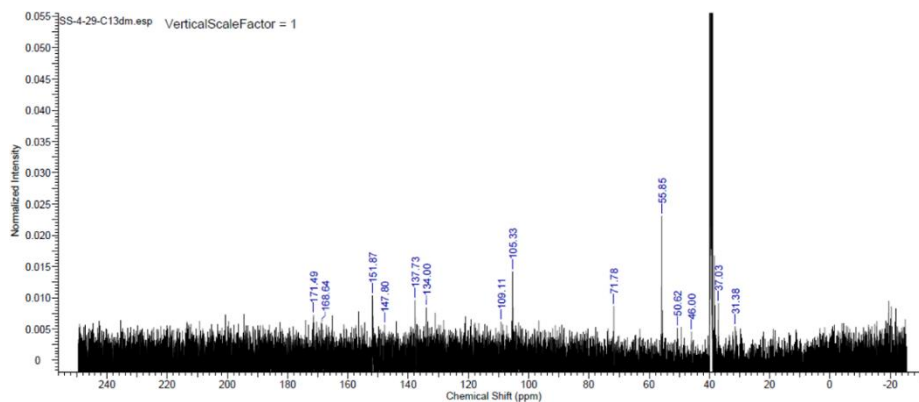


Figure B-143. ^{13}C NMR Spectrum of polyethyleneglycolamide dihydrosinapamide (polyamide) (Table 2-5, entry 6)

APPENDIX C
SUPPLEMENTARY INFORMATION FOR CHAPTER 3

NMR Spectra

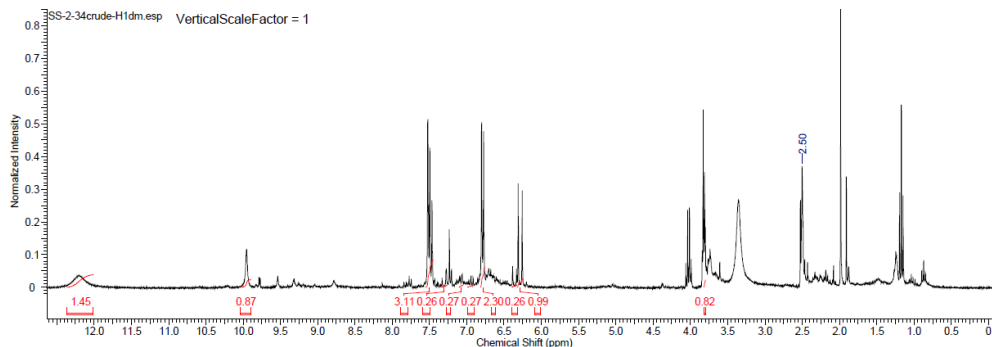


Figure C-1. ¹H NMR spectrum of crude product from large scale extraction on lignin paste.

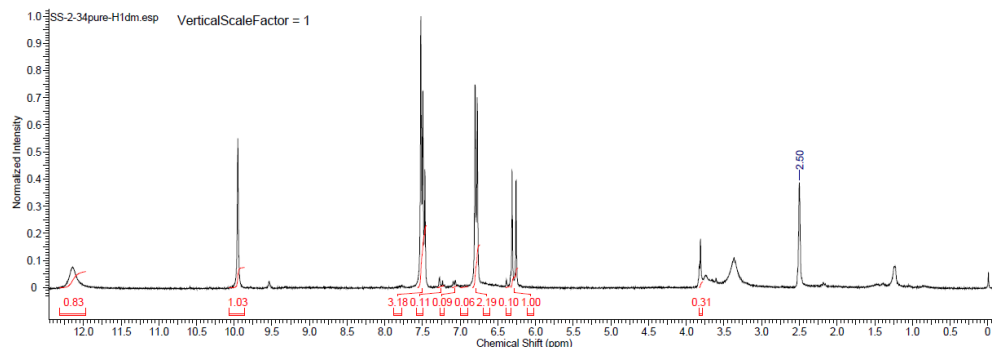


Figure C-2. ¹H NMR spectrum of recrystallized product from large scale extraction on lignin paste.

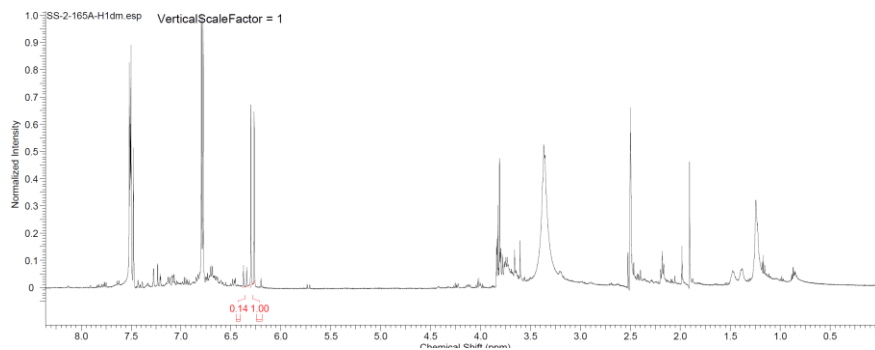


Figure C-3. ¹H NMR spectrum of 1st cycle product from reflux extraction on lignin paste (Table 3-1, entry 1).

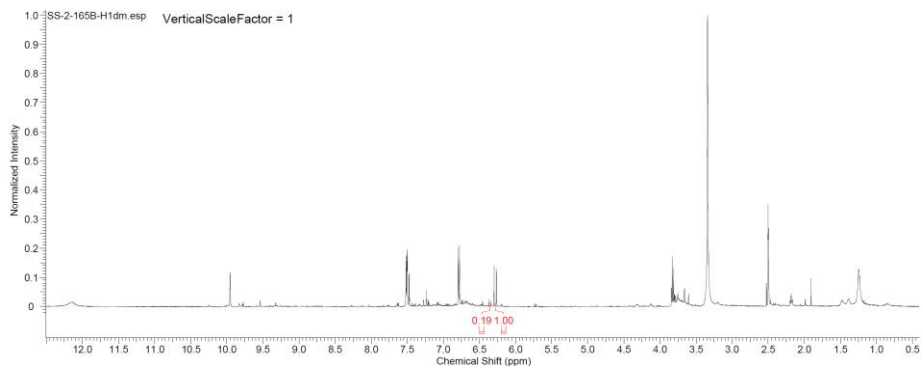


Figure C-4. ^1H NMR spectrum of 2nd cycle product from reflux extraction on lignin paste (Table 3-1, entry 2).

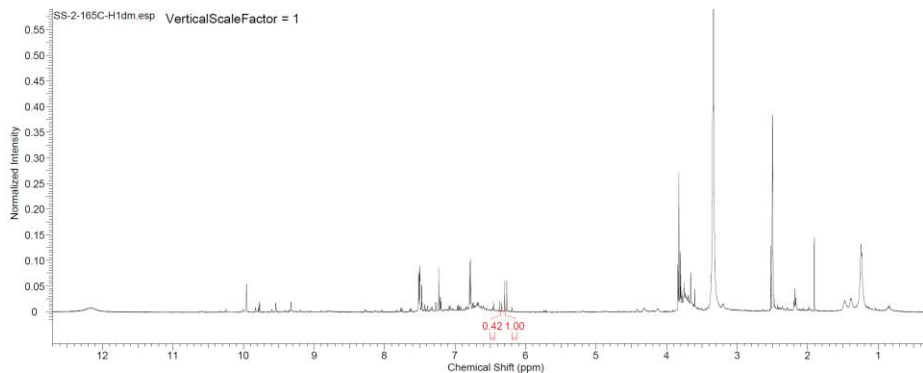


Figure C-5. ^1H NMR spectrum of 3rd cycle product from reflux extraction on lignin paste (Table 3-1, entry 3).

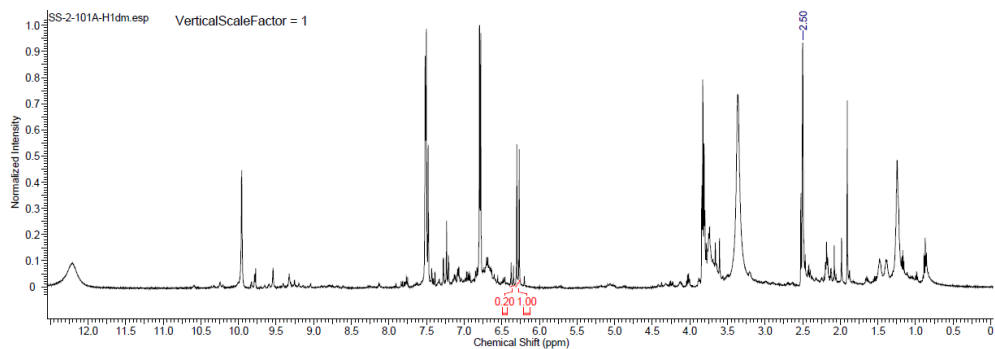


Figure C-6. ^1H NMR spectrum of 1st cycle product from pressurized extraction on lignin paste (Table 3-1, entry 1).

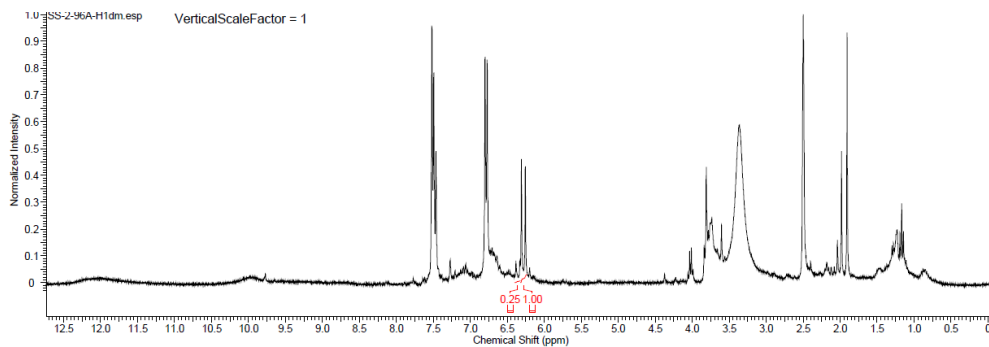


Figure C-7. ^1H NMR spectrum of 1st cycle product from ultrasound extraction on lignin paste (Table 3-1, entry 1).

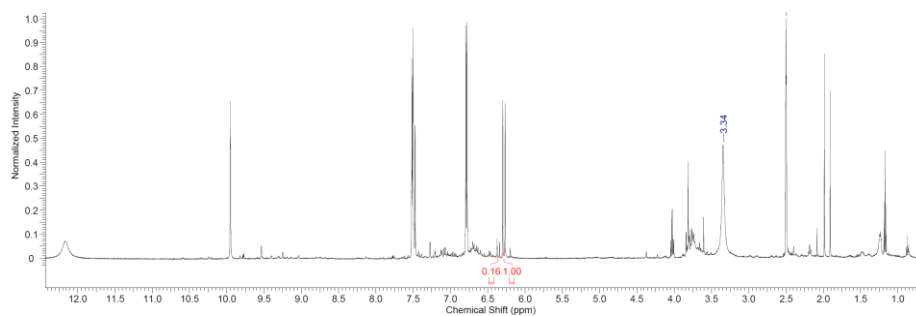


Figure C-8. ^1H NMR spectrum of 1st cycle product from microwave extraction on lignin paste (Table 3-1, entry 1).

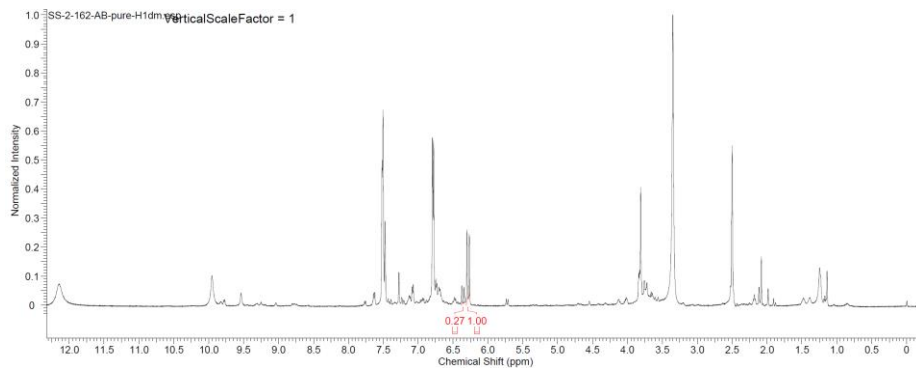


Figure C-9. ^1H NMR spectrum of 1st crop purified product from reflux extraction on sugarcane bagasse (Table 3-1, entry 6–9).

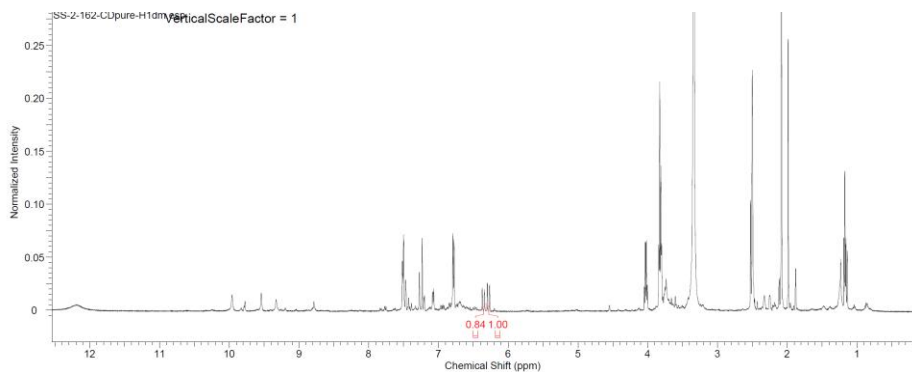


Figure C-10. ^1H NMR spectrum of 2nd crop purified product from reflux extraction on sugarcane bagasse (Table 3-1, entry 6–9).

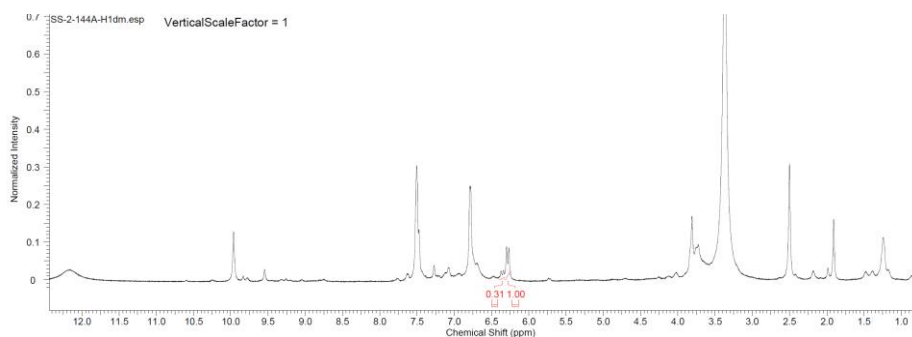


Figure C-11. ^1H NMR spectrum of 1st cycle product from pressurized extraction on sugarcane bagasse (Table 3-1, entry 6).

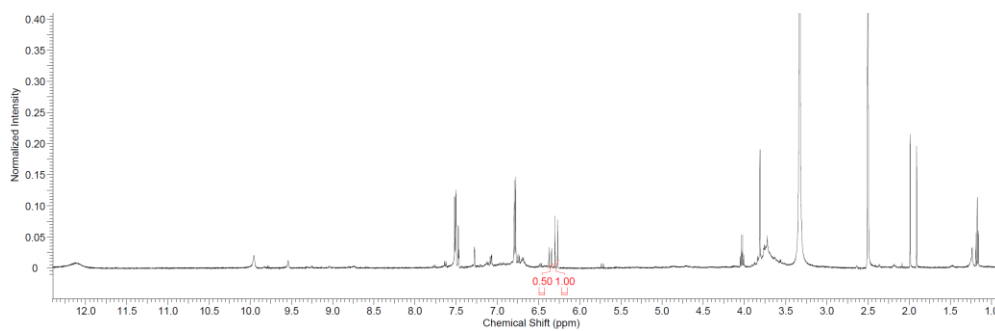


Figure C-12. ^1H NMR spectrum of 1st cycle product from ultrasound extraction on sugarcane bagasse (Table 3-1, entry 6).

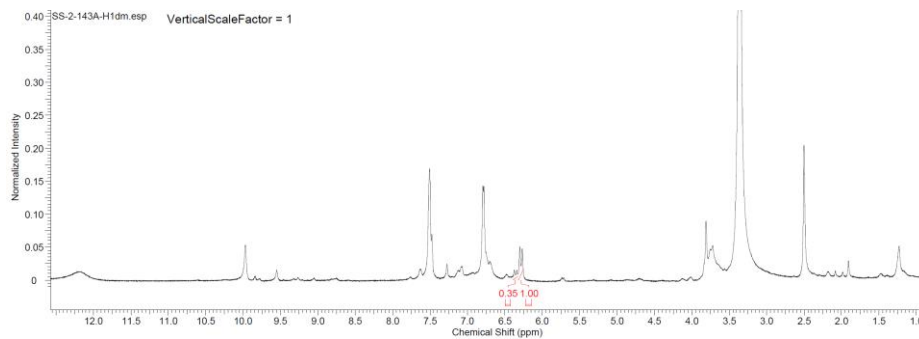


Figure C-13. ¹H NMR spectrum of 1st cycle product from microwave extraction on sugarcane bagasse (Table 3-1, entry 6).

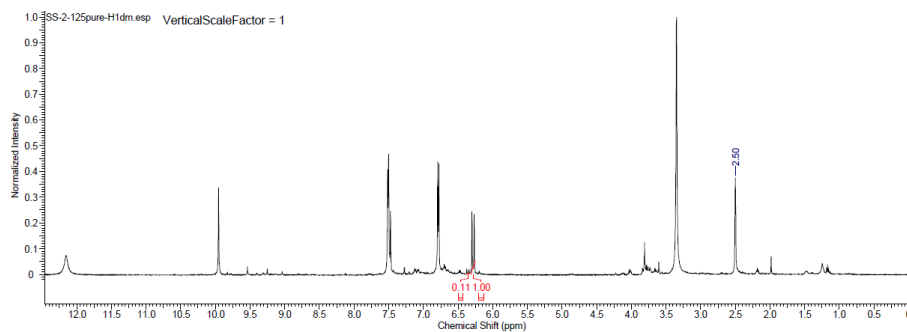


Figure C-14. ¹H NMR spectrum of purified product from ultrasound extraction on lignin paste using activated charcoal.

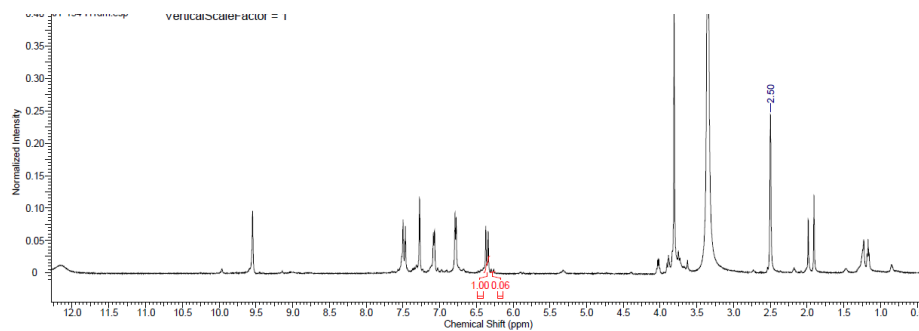


Figure C-15. ¹H NMR spectrum of product from corn bran extraction (Table 3-2, entry 1)

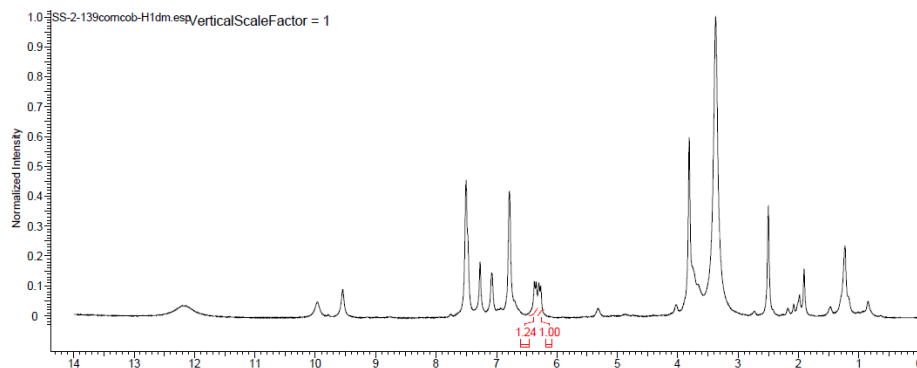


Figure C-16. ¹H NMR spectrum of product from corn cob extraction (Table 3-2, entry 2)

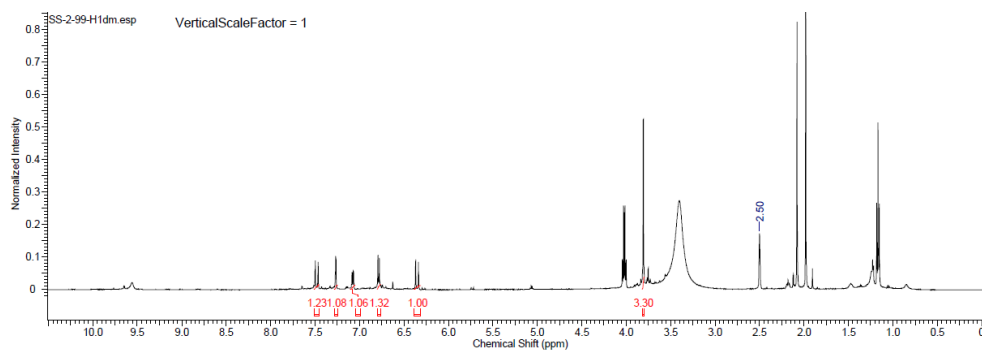


Figure C-17. ¹H NMR spectrum of product from corn silk extraction (Table 3-2, entry 3)

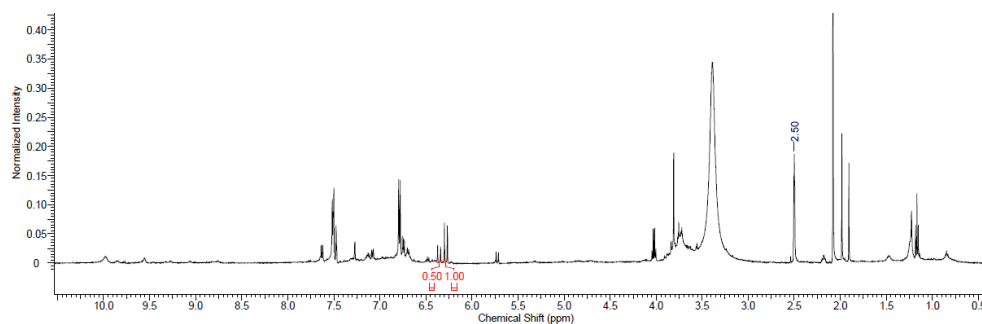


Figure C-18. ¹H NMR spectrum of product from corn tassel extraction (Table 3-2, entry 4)

APPENDIX D
SUPPLEMENTARY INFORMATION FOR CHAPTER 4

TGA Spectra

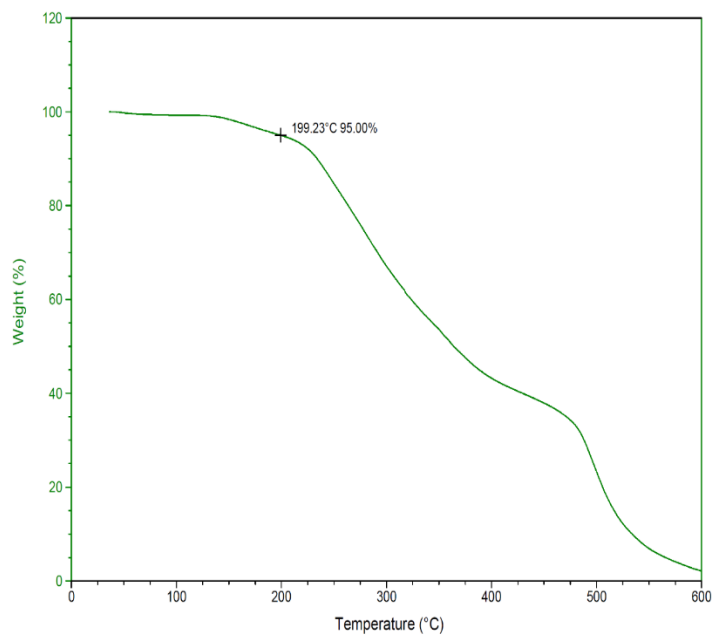


Figure D-1. TGA Thermogram of PV-VV-A (Table 4-1, entry 1).

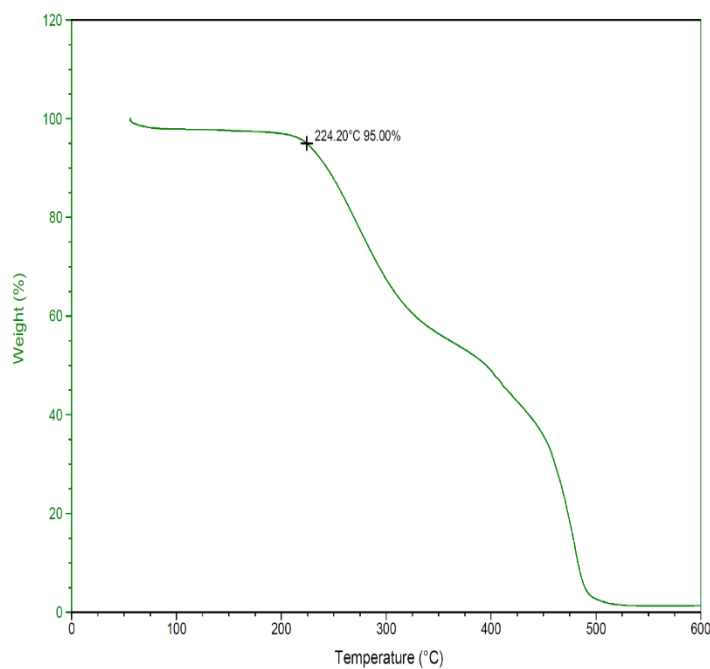


Figure D-2. TGA Thermogram of PV-HB-A (Table 4-1, entry 2).

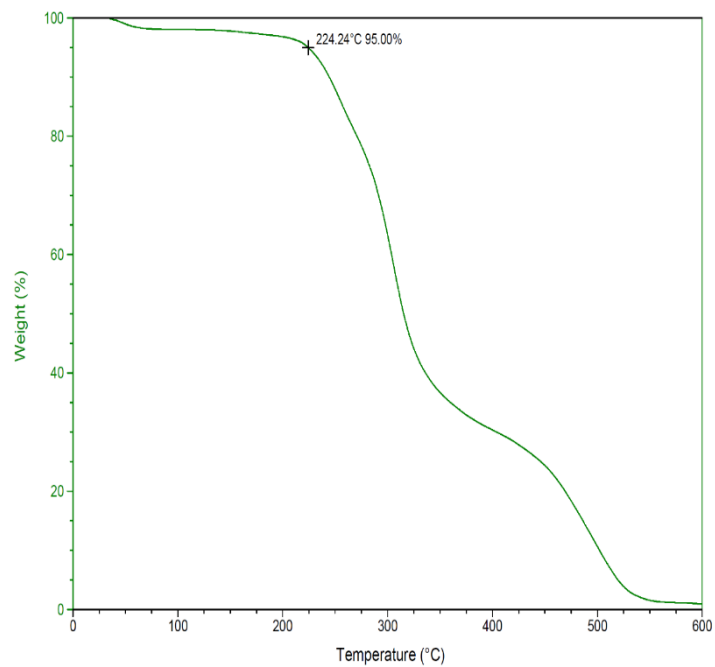


Figure D-3. TGA Thermogram of PV-SY-A (Table 4-1, entry 3).

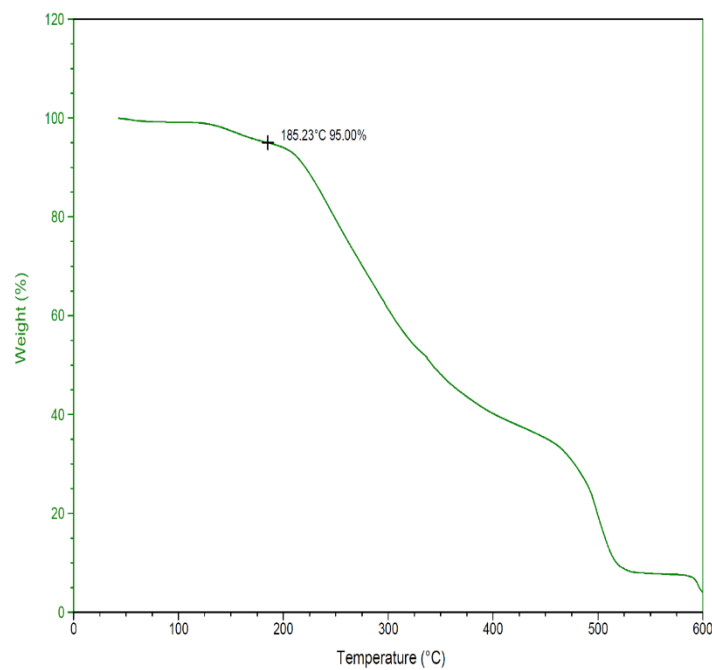


Figure D-4. TGA Thermogram of PV-EV-A (Table 4-1, entry 4).

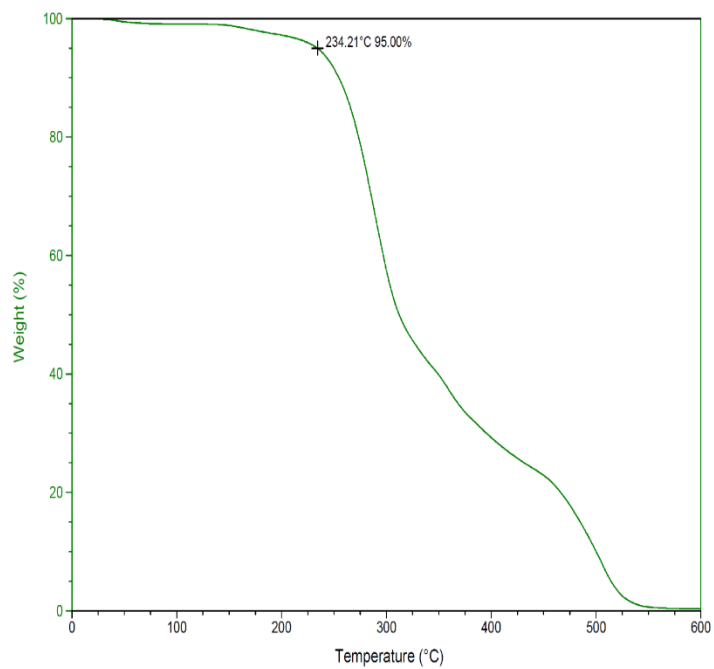


Figure D-5. TGA Thermogram of PV-OV-A (Table 4-1, entry 5).

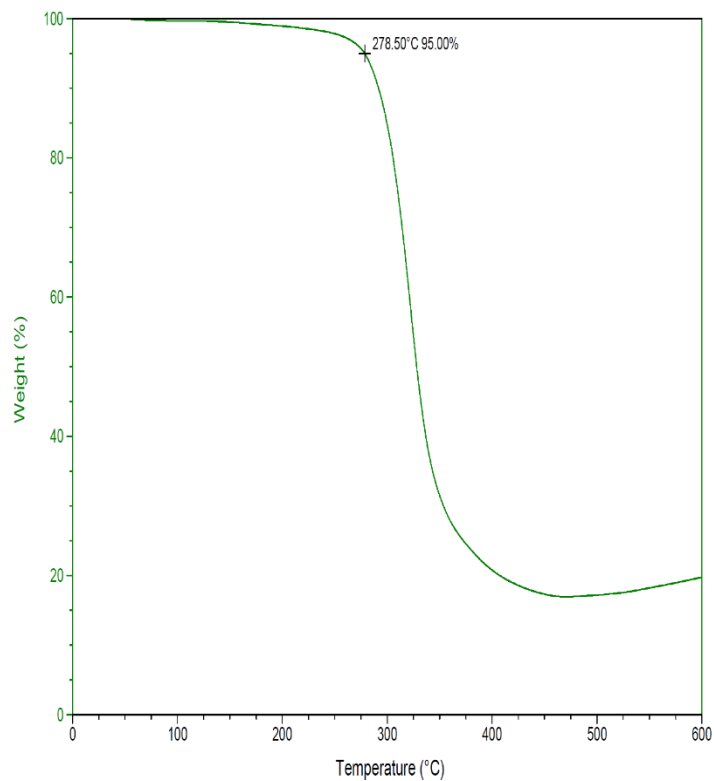


Figure D-6. TGA Thermogram of PV-IV-A (Table 4-1, entry 6).

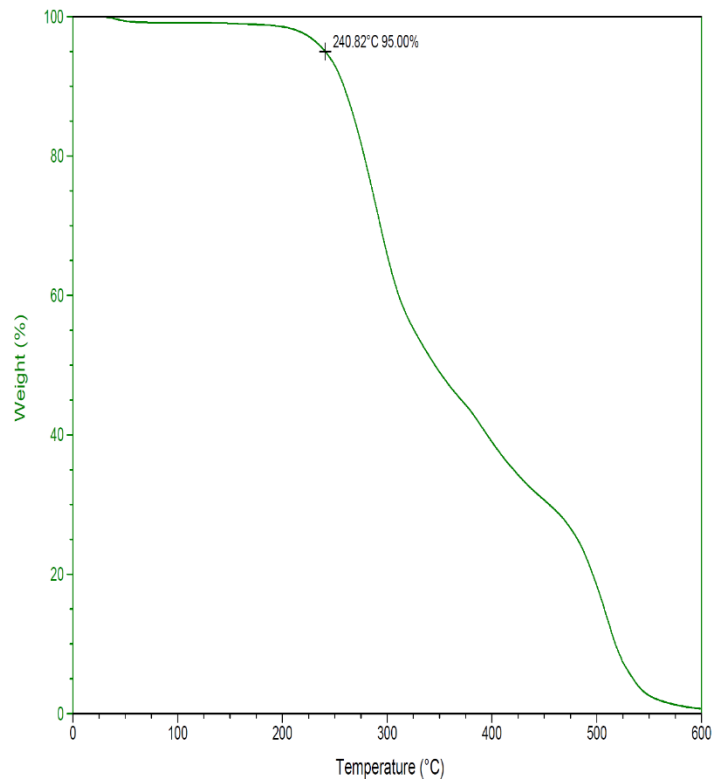


Figure D-7. TGA Thermogram of PV-SA-A (Table 4-1, entry 7).

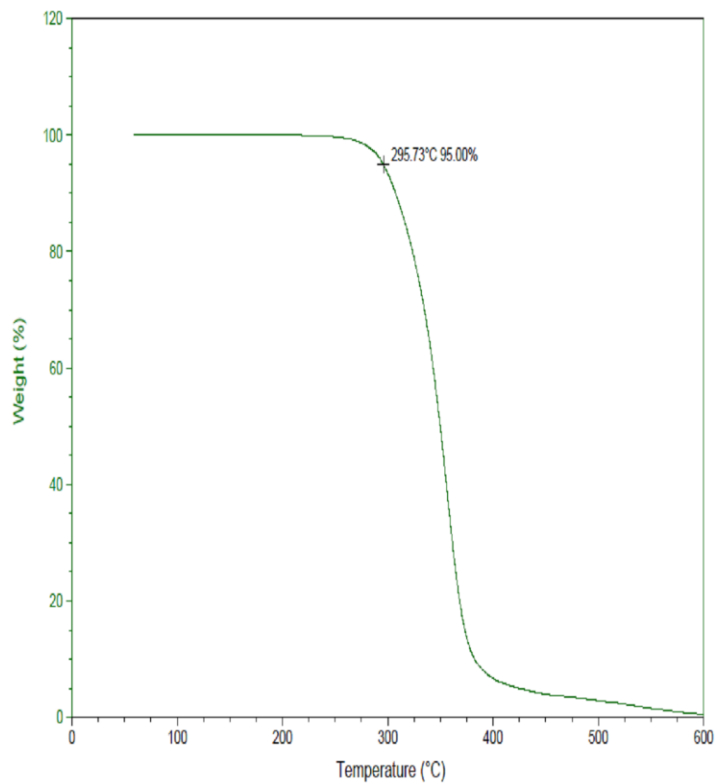


Figure D-8. TGA Thermogram of PV-OA-A (Table 4-1, entry 8).

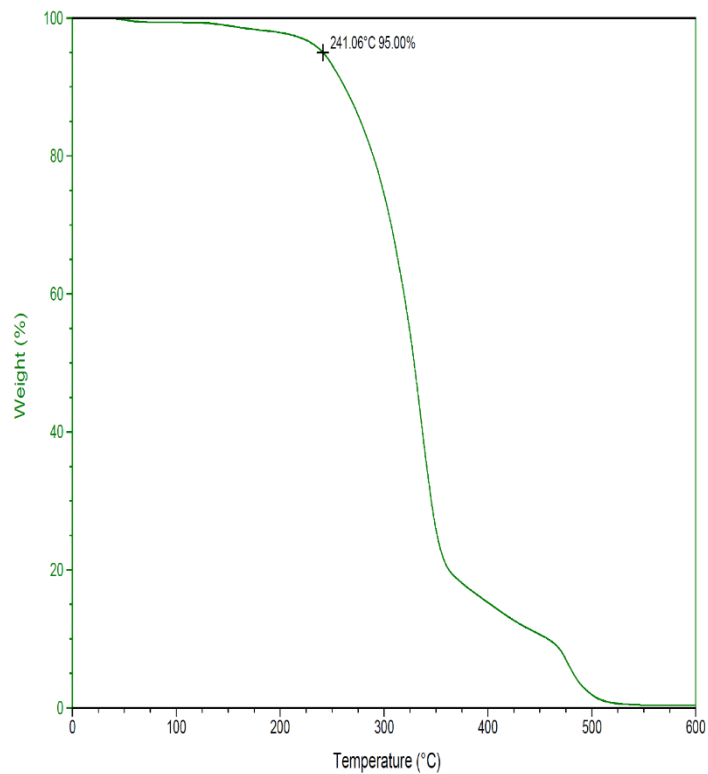


Figure D-9. TGA Thermogram of PV-PA-A (Table 4-1, entry 9).

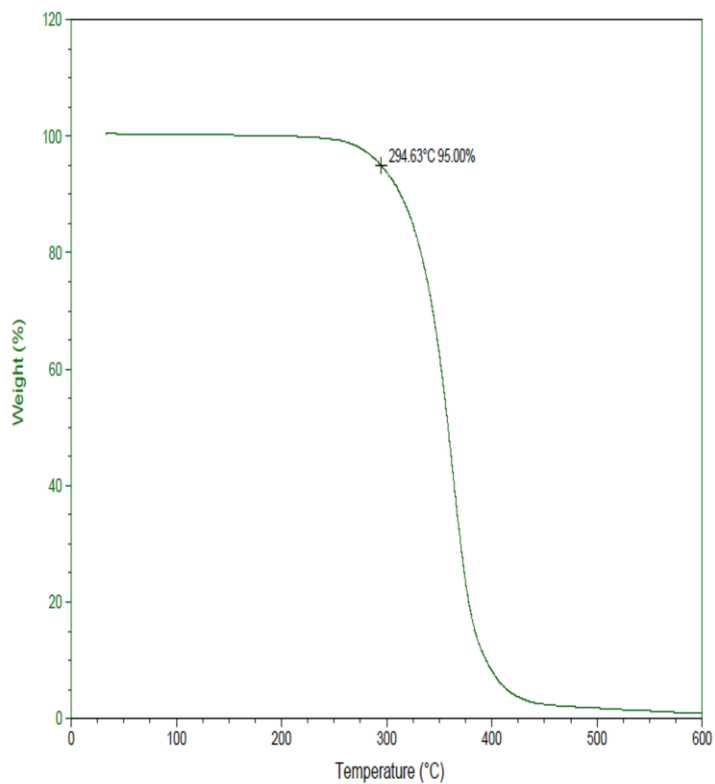


Figure D-10. TGA Thermogram of PV-BZ-A (Table 4-1, entry 10).

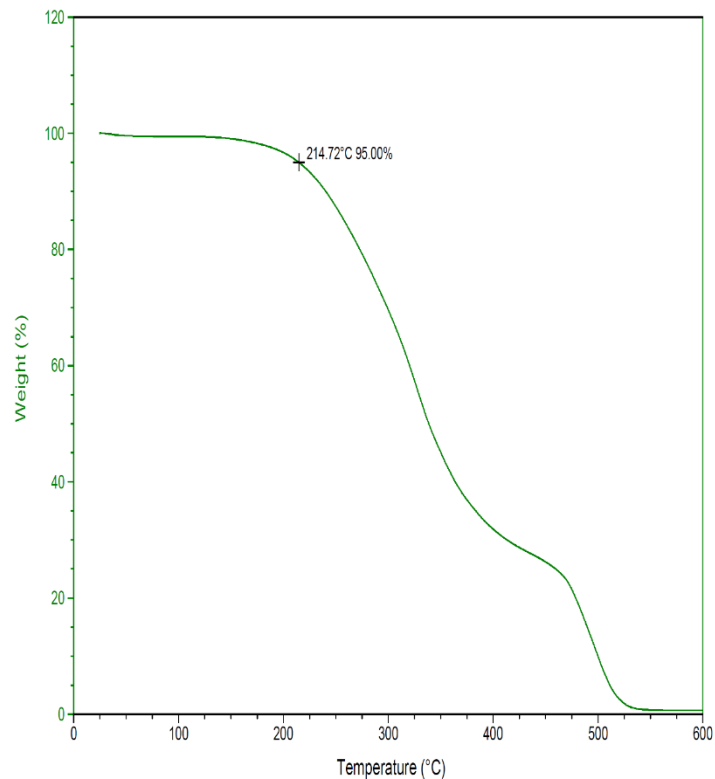


Figure D-11. TGA Thermogram of PV-CI-A (Table 4-1, entry 11).

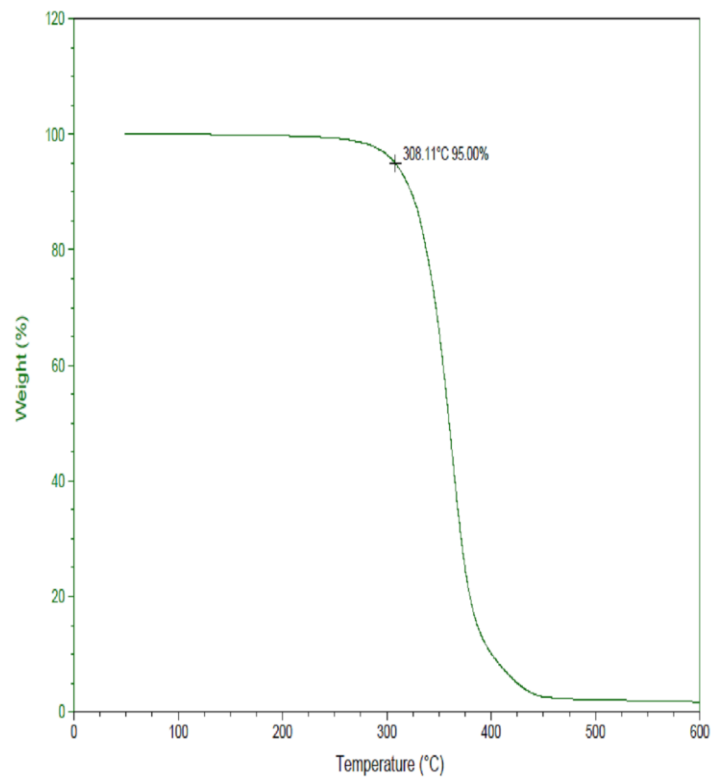


Figure D-12. TGA Thermogram of PV-CU-A (Table 4-1, entry 12).

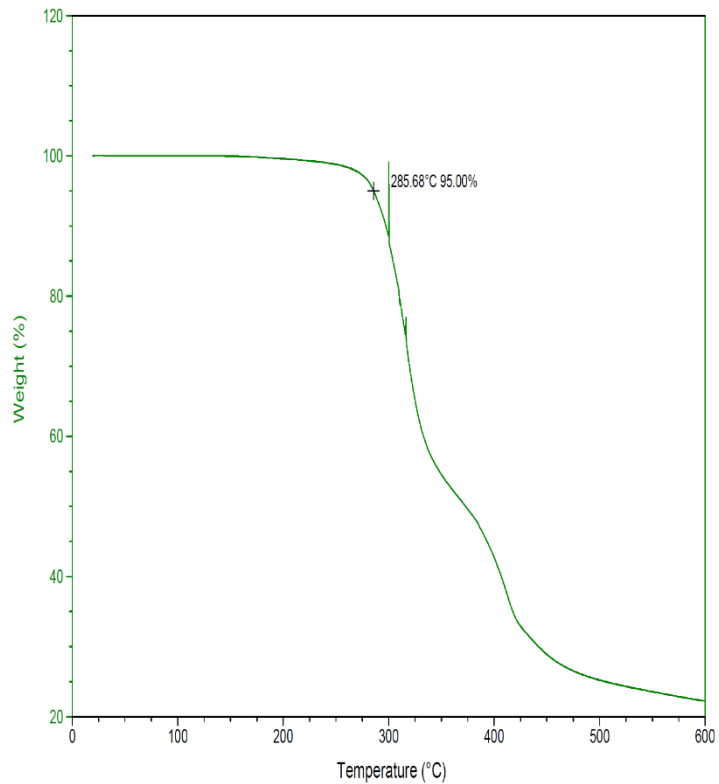


Figure D-13. TGA Thermogram of PV-HMF-A (Table 4-1, entry 13).

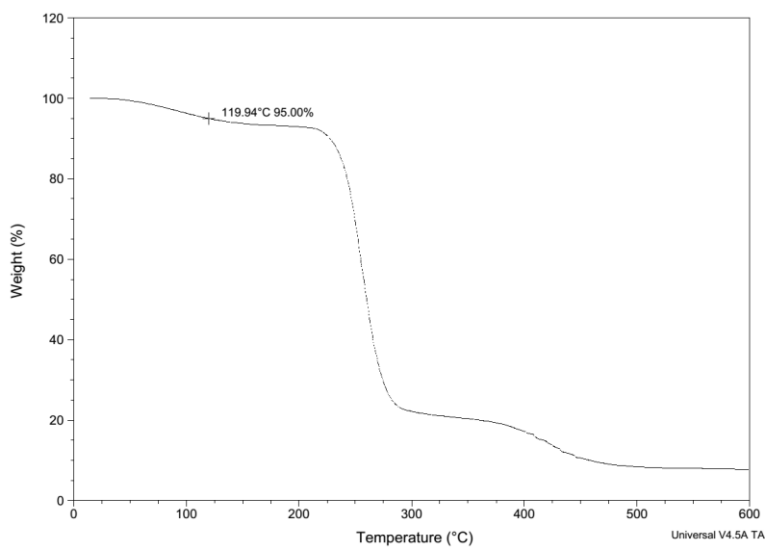


Figure D-14. TGA Thermogram of PVA High MW (Table 4-1, entry 14).

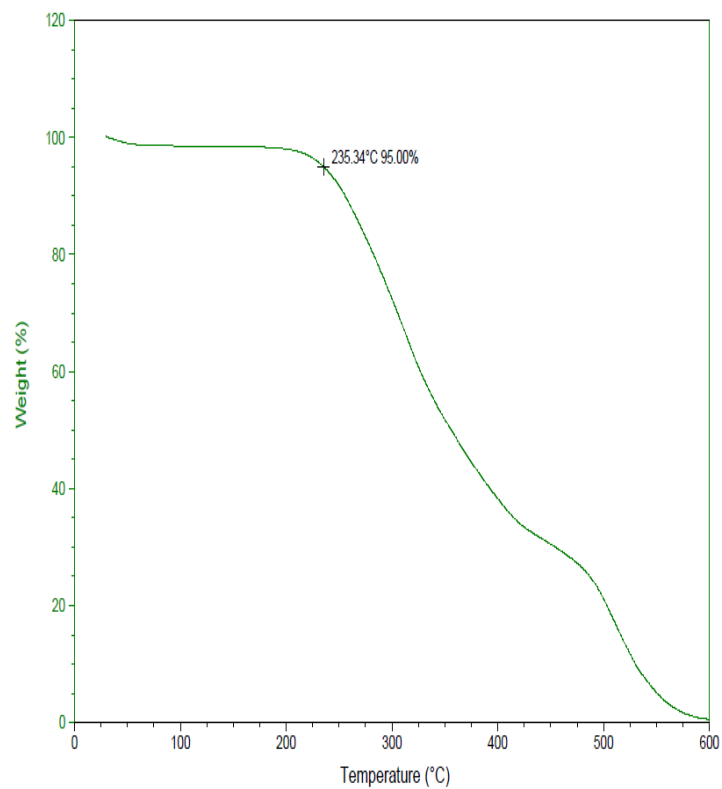


Figure D-15. TGA Thermogram of PV-VV-A High MW (Table 4-1, entry 15).

DSC Spectra

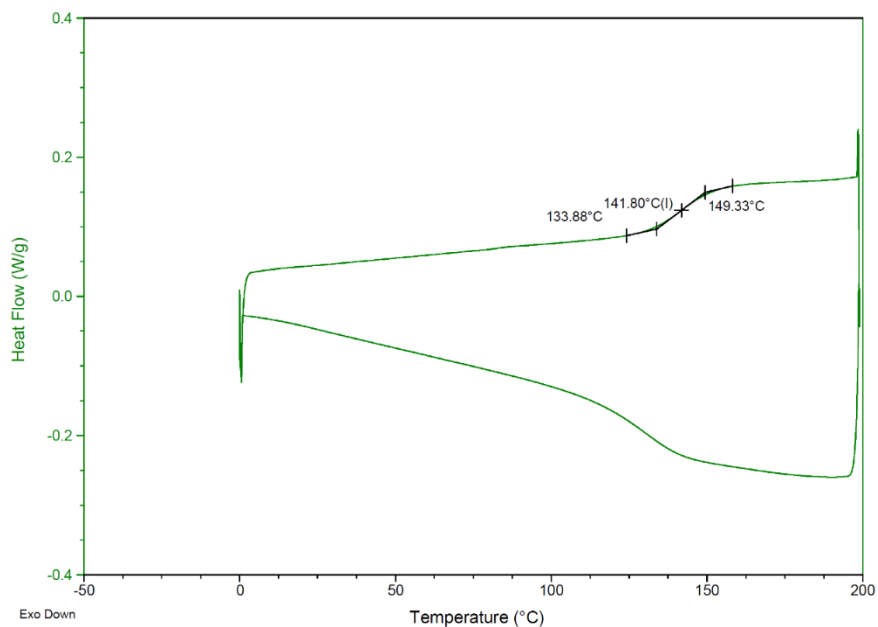


Figure D-16. DSC Thermogram of PV-VV-A (Table 4-1, entry 1).

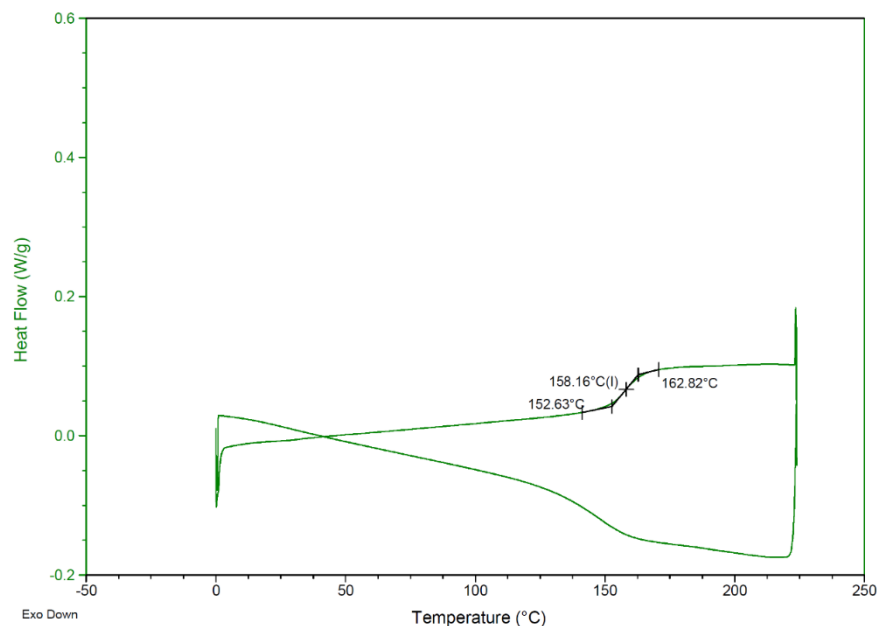


Figure D-17. DSC Thermogram of PV-HB-A (Table 4-1, entry 2).

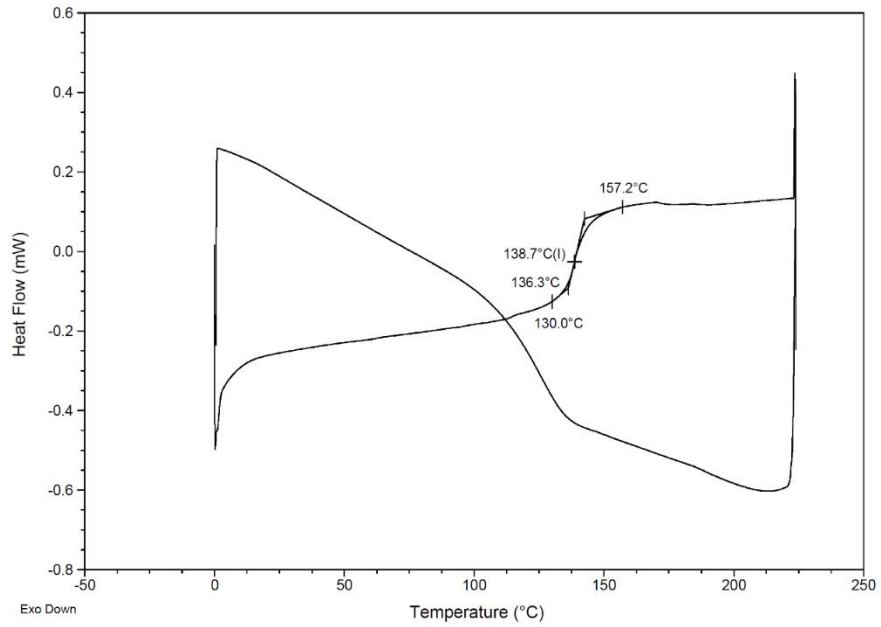


Figure D-18. DSC Thermogram of PV-SY-A (Table 4-1, entry 3).

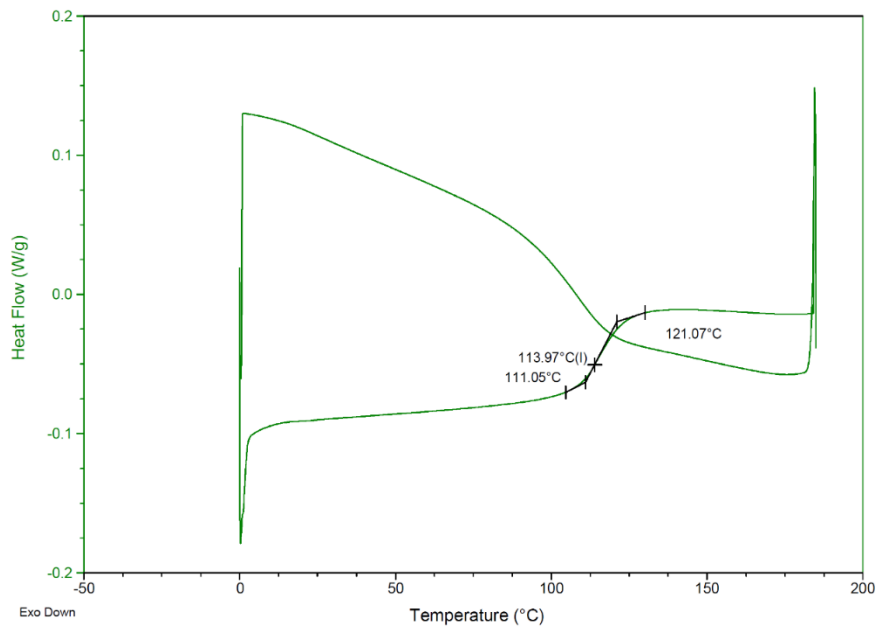


Figure D-19. DSC Thermogram of PV-EV-A (Table S1, Entry 4).

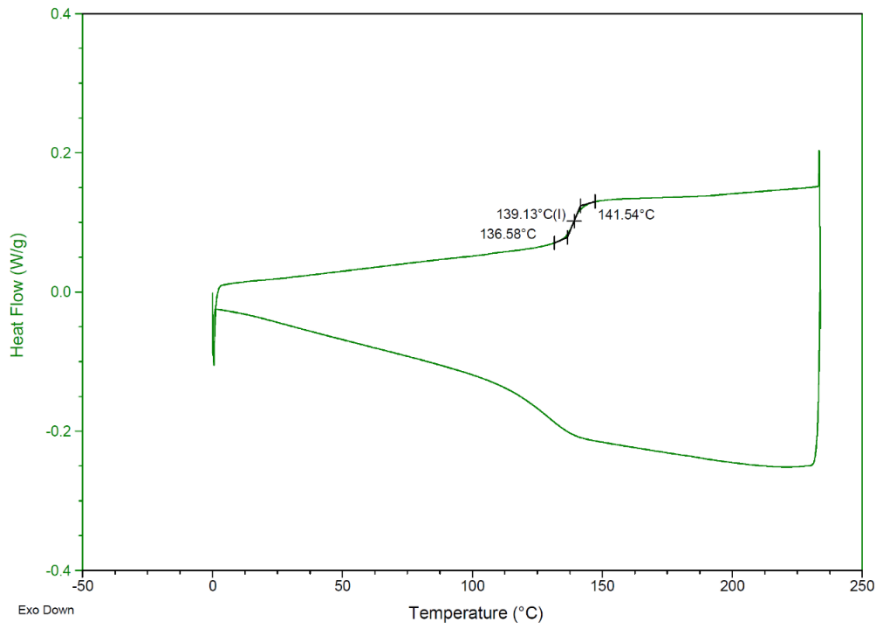


Figure D-20. DSC Thermogram of PV-OV-A (Table 4-1, entry 5).

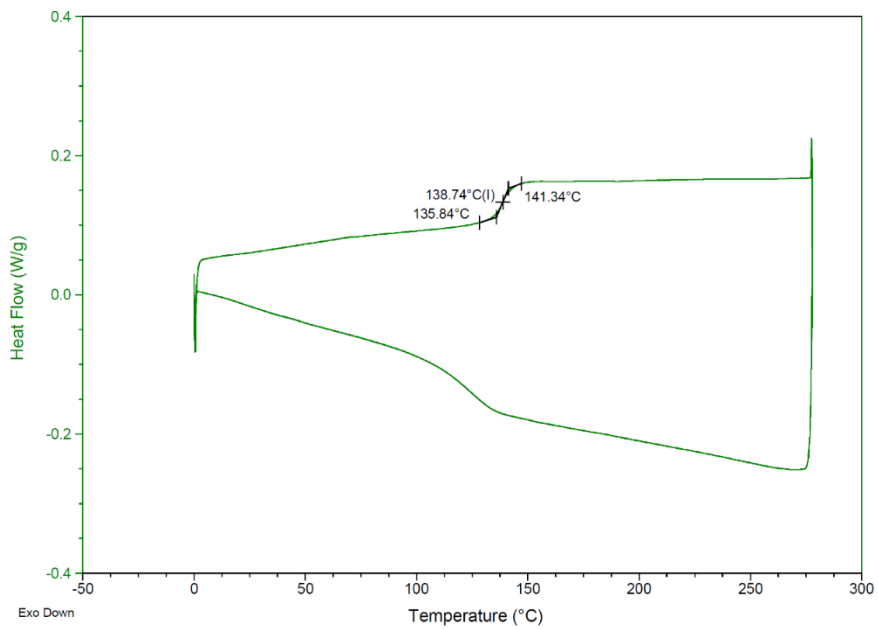


Figure D-21. DSC Thermogram of PV-IV-A (Table 4-1, entry 6).

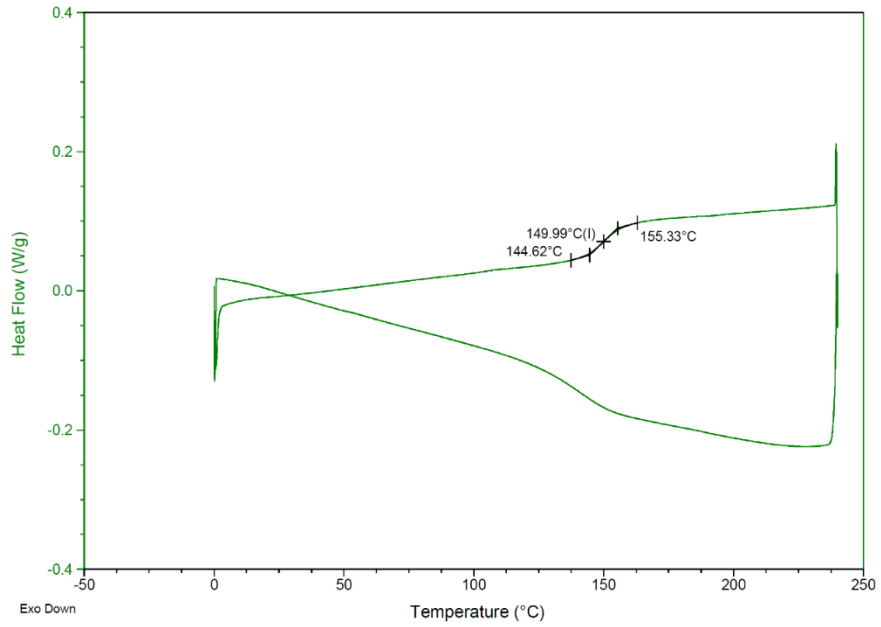


Figure D-22. DSC Thermogram of PV-SA-A (Table 4-1, entry 7).

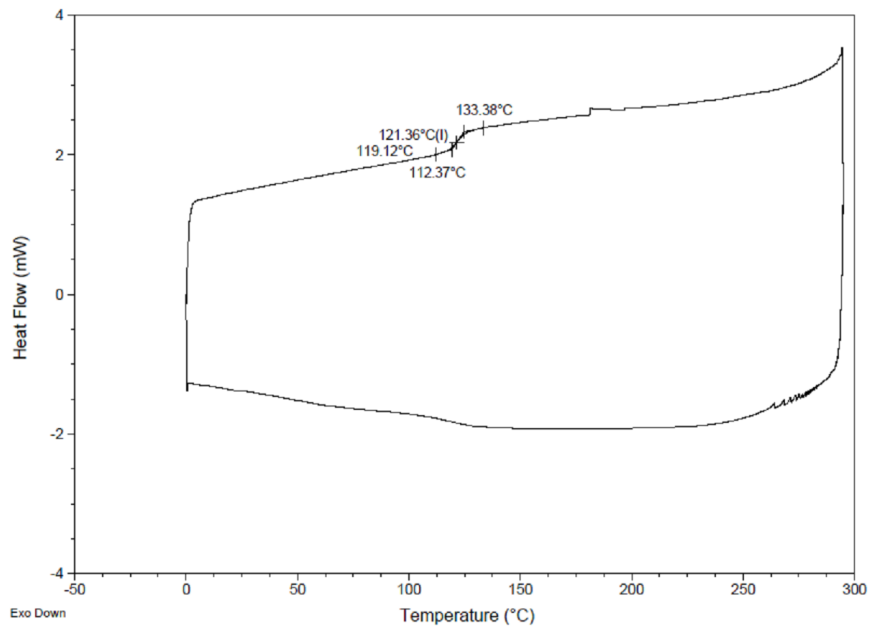


Figure D-23. DSC Thermogram of PV-OA-A (Table 4-1, entry 8).

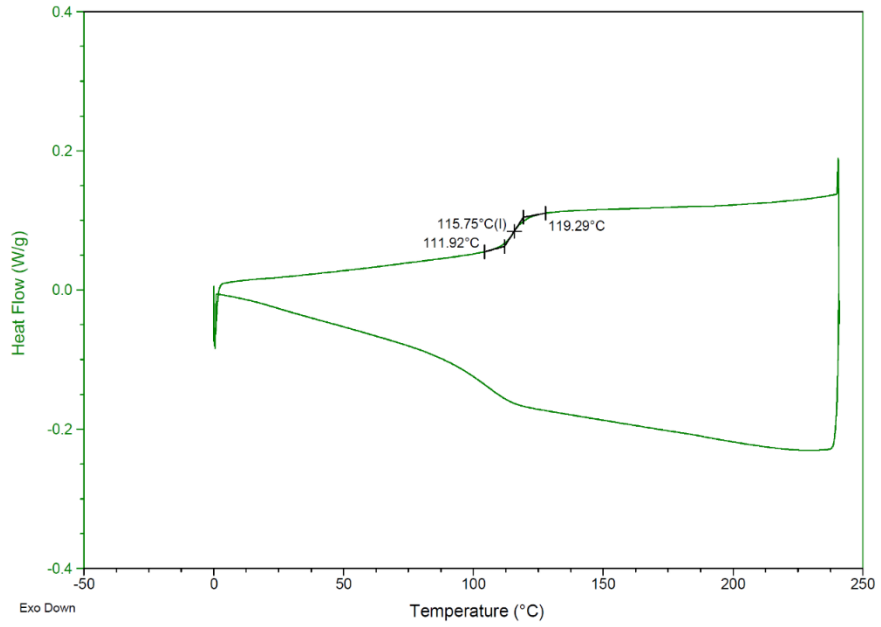


Figure D-24. DSC Thermogram of PV-PA-A (Table 4-1, entry 9).

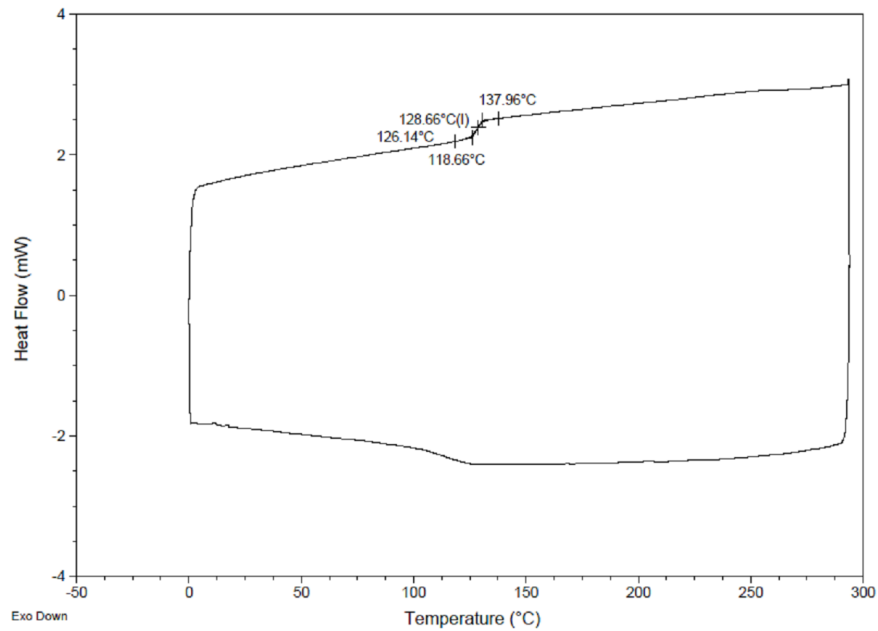


Figure D-25. DSC Thermogram of PV-BZ-A (Table 4-1, entry 10).

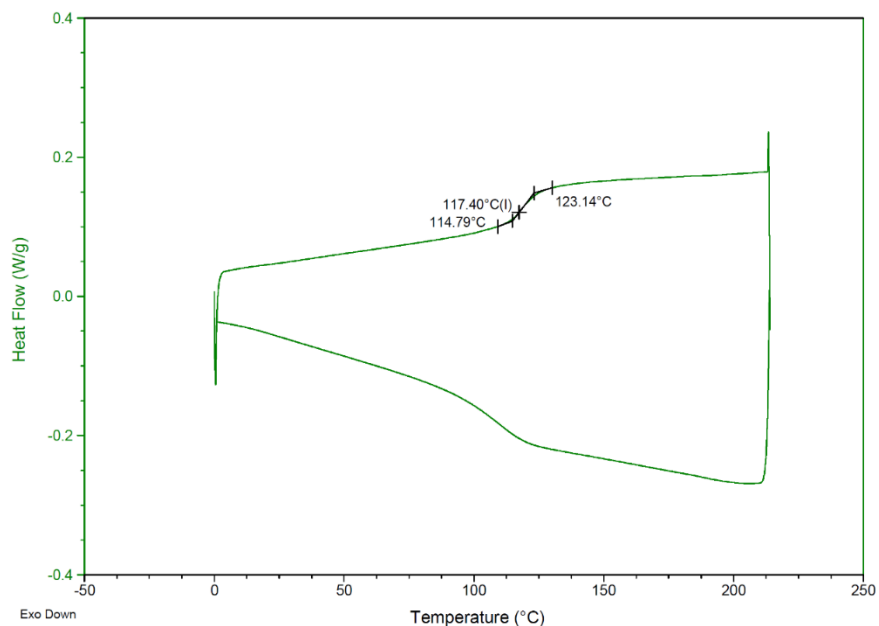


Figure D-26. DSC Thermogram of PV-CI-A (Table 4-1, entry 11).

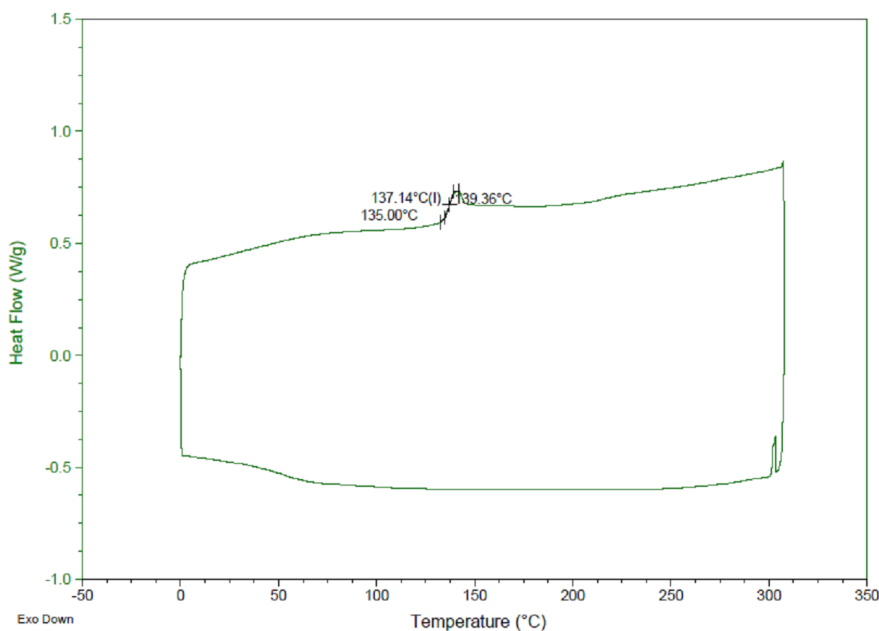


Figure D-27. DSC Thermogram of PV-CU-A (Table 4-1, entry 12).

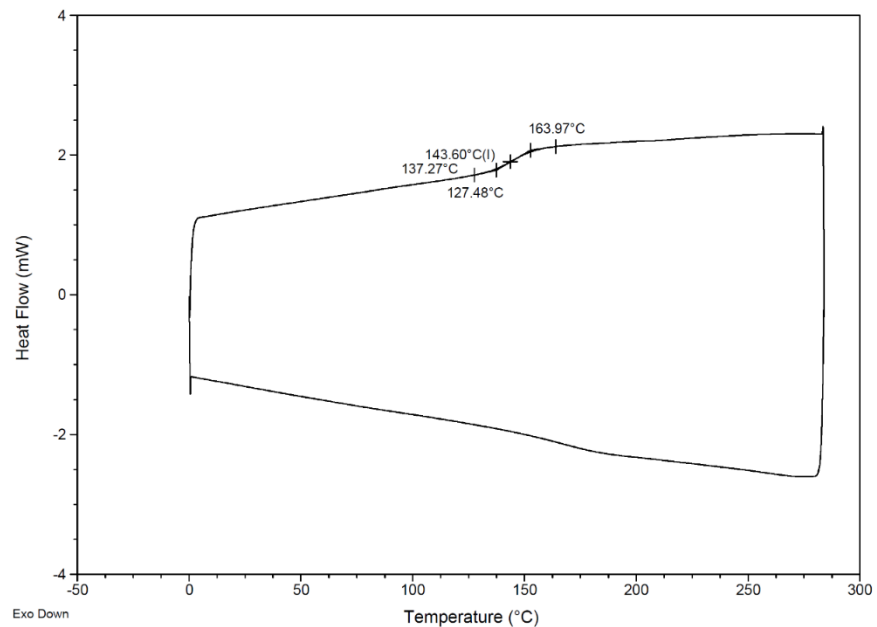


Figure D-28. DSC Thermogram of PV-HMF-A (Table 4-1, entry 13).

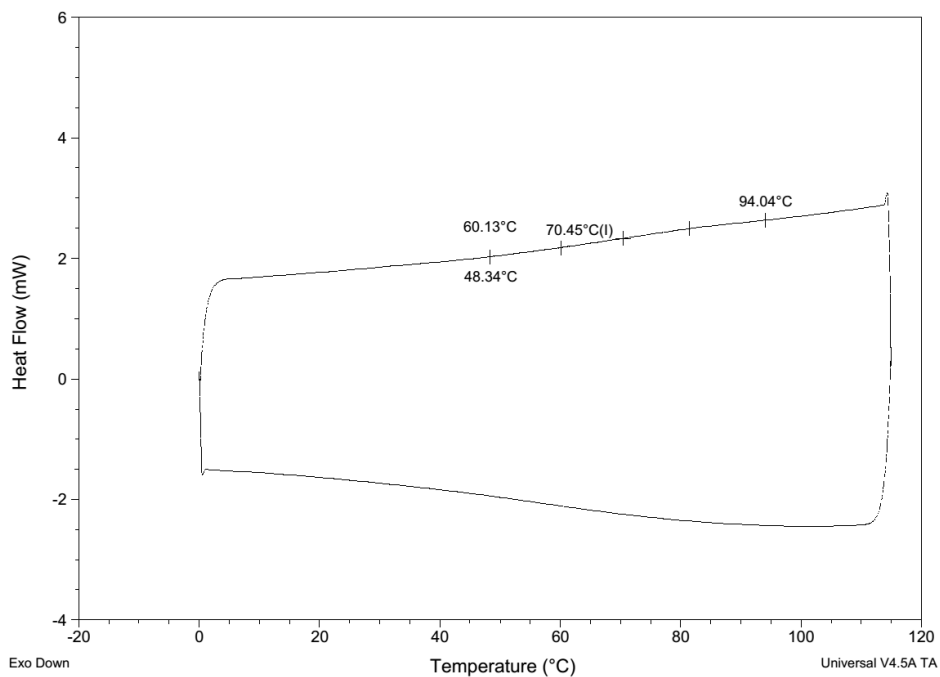


Figure D-29. DSC Thermogram of PVA High MW (Table 4-1, entry 14).

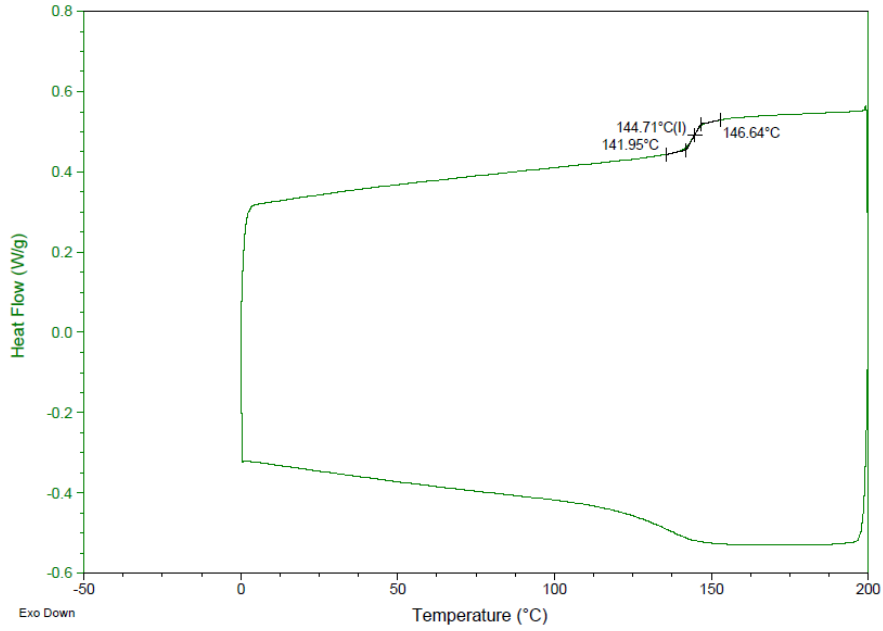


Figure D-30. DSC Thermogram of PV-VV-A High MW (Table 4-1, entry 15)

GPC Spectra

Molecular Weight Averages

| Peak | Mp | Mn | Mw | Mz | Mz+1 | Mv | PD |
|--------|-------|-------|-------|-------|-------|-------|-------|
| Peak 1 | 39963 | 22267 | 45529 | 70526 | 94466 | 67039 | 2.045 |

Peak information

| | Start (mins) | End (mins) |
|-------------------|--------------|------------|
| Baseline region 1 | 11.02 | 11.58 |
| Peak 1 | 14.17 | 20.87 |

| Peak | Trace | Peak Max RT (mins) | Peak Area (mV.s) | Peak Height (mV) |
|--------|-------|--------------------|------------------|------------------|
| Peak 1 | RI | 17.39 | 10983729.932 | 58712.592 |

Chromatogram

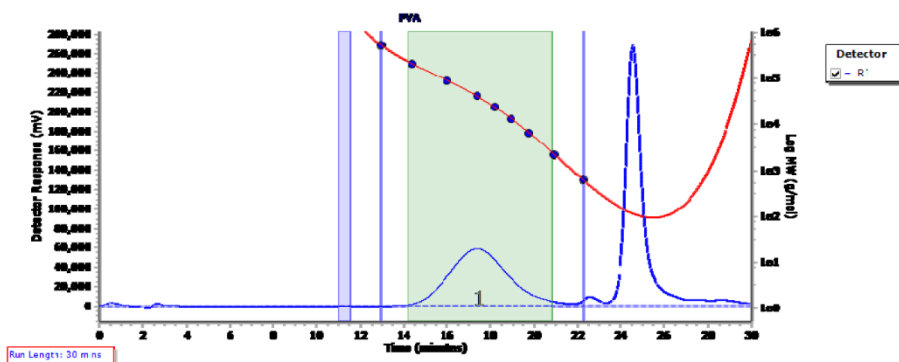


Figure D-31. GPC Chromatogram of PVA (Table 4-1, entry 0).

Molecular Weight Averages

| Peak | Mp | Mn | Mw | Mz | Mz+1 | Mv | PD |
|--------|-------|-------|-------|-------|--------|-------|-------|
| Peak 1 | 42706 | 25695 | 54906 | 97254 | 165869 | 89815 | 2.137 |

Peak information

| | Start (mins) | End (mins) |
|-------------------|--------------|------------|
| Baseline region 1 | 10.77 | 11.35 |
| Peak 1 | 12.95 | 21.42 |

| Peak | Trace | Peak Max RT (mins) | Peak Area (mV.s) | Peak Height (mV) |
|--------|-------|--------------------|------------------|------------------|
| Peak 1 | RI | 17.69 | 2221255.040 | 10983.992 |

Chromatogram

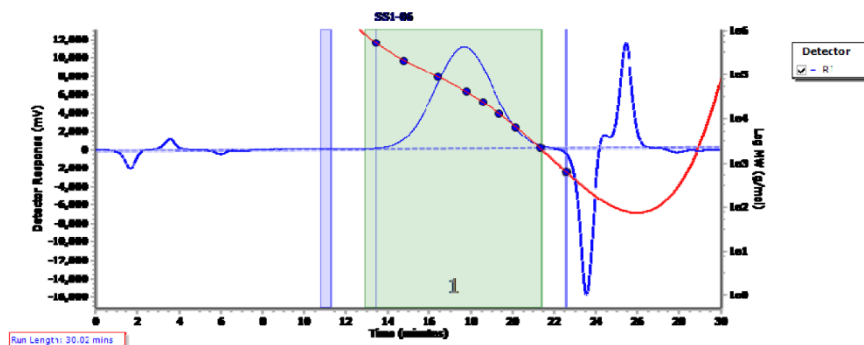


Figure D-32. GPC Chromatogram of PV-VV-A (Table 4-1, entry 1).

Molecular Weight Averages

| Peak | Mp | Mn | Mw | Mz | Mz+1 | Mv | PD |
|--------|-------|-------|-------|--------|--------|-------|-------|
| Peak 1 | 37454 | 22764 | 52523 | 101861 | 171845 | 93284 | 2.307 |

Peak information

| | Start (mins) | End (mins) |
|-------------------|--------------|------------|
| Baseline region 1 | 0.00 | 1.83 |
| Baseline region 2 | 29.47 | 29.97 |
| Peak 1 | 13.58 | 21.20 |

| Peak | Trace | Peak Max RT (mins) | Peak Area (mV.s) | Peak Height (mV) |
|--------|-------|--------------------|------------------|------------------|
| Peak 1 | RI | 17.90 | 3019497.257 | 14503.716 |

Chromatogram

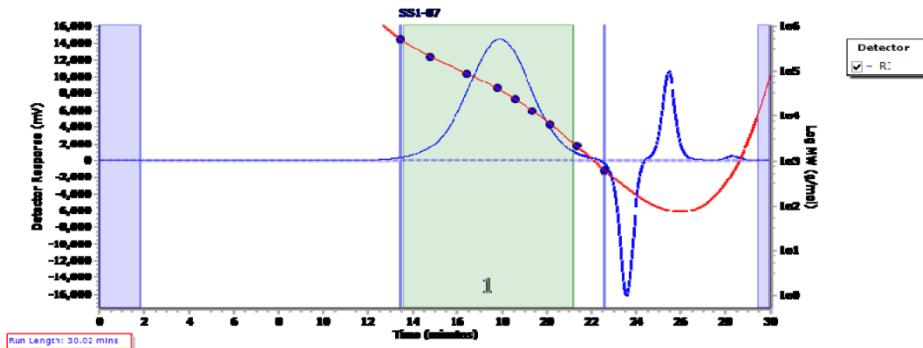


Figure D-33. GPC Chromatogram of PV-HB-A (Table 4-1, entry 2).

Molecular Weight Averages

| Peak | Mp | Mn | Mw | Mz | Mz+1 | Mv | PD |
|--------|-------|-------|-------|-------|--------|-------|-------|
| Peak 1 | 46275 | 28750 | 59666 | 99618 | 145073 | 93440 | 2.075 |

Peak information

| | Start (mins) | End (mins) |
|-------------------|--------------|------------|
| Baseline region 1 | 1.22 | 2.59 |
| Baseline region 2 | 29.11 | 29.97 |
| Peak 1 | 13.91 | 21.35 |

| Peak | Trace | Peak Max RT (mins) | Peak Area (mV.s) | Peak Height (mV) |
|--------|-------|--------------------|------------------|------------------|
| Peak 1 | RI | 17.56 | 5697828.782 | 28234.645 |

Chromatogram

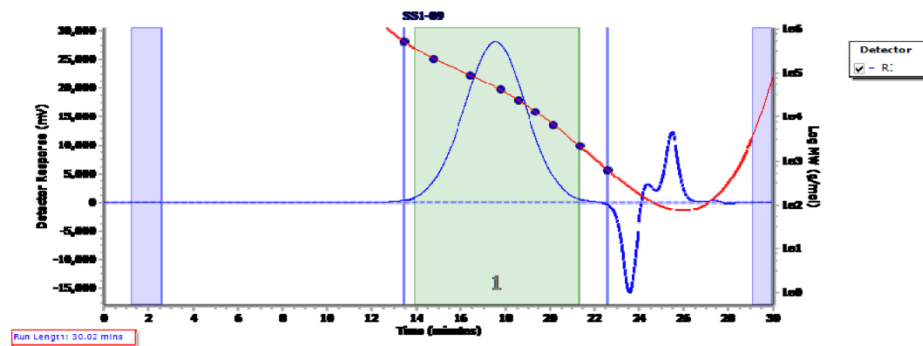


Figure D-34. GPC Chromatogram of PV-SY-A (Table 4-1, entry 3).

Molecular Weight Averages

| Peak | Mp | Mn | Mw | Mz | Mz+1 | Mv | PD |
|--------|-------|-------|-------|-------|--------|-------|-------|
| Peak 1 | 41215 | 22766 | 51597 | 85951 | 121758 | 80909 | 2.266 |

Peak information

| | Start (mins) | End (mins) |
|-------------------|--------------|------------|
| Baseline region 1 | 0.40 | 2.52 |
| Baseline region 2 | 29.50 | 29.97 |
| Peak 1 | 14.23 | 21.77 |

| Peak | Trace | Peak Max RT (mins) | Peak Area (mV.s) | Peak Height (mV) |
|--------|-------|--------------------|------------------|------------------|
| Peak 1 | RI | 17.74 | 4544257.224 | 22335.468 |

Chromatogram

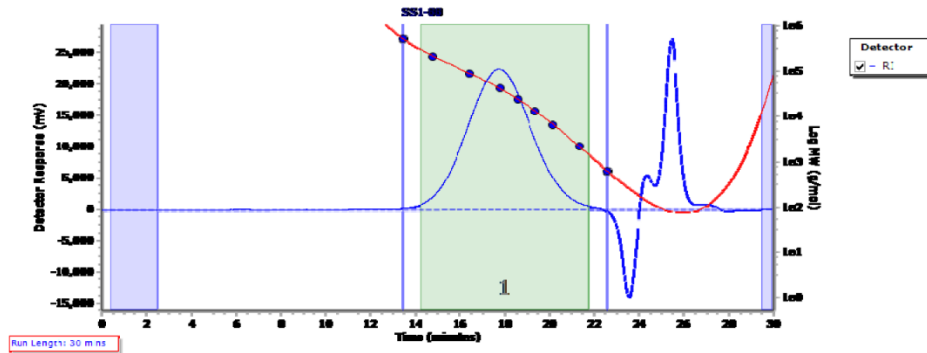


Figure D-35. GPC Chromatogram of PV-EV-A (Table 4-1, entry 4).

Molecular Weight Averages

| Peak | Mp | Mn | Mw | Mz | Mz+1 | Mv | PD |
|--------|-------|-------|-------|--------|--------|-------|-------|
| Peak 1 | 47033 | 24520 | 58929 | 102439 | 156622 | 95511 | 2.403 |

Peak information

| | Start (mins) | End (mins) |
|-------------------|--------------|------------|
| Baseline region 1 | 2.58 | 3.31 |
| Baseline region 2 | 29.64 | 30.01 |
| Peak 1 | 13.60 | 21.90 |

| Peak | Trace | Peak Max RT (mins) | Peak Area (mV.s) | Peak Height (mV) |
|--------|-------|--------------------|------------------|------------------|
| Peak 1 | RI | 17.53 | 3335915.215 | 16069.401 |

Chromatogram

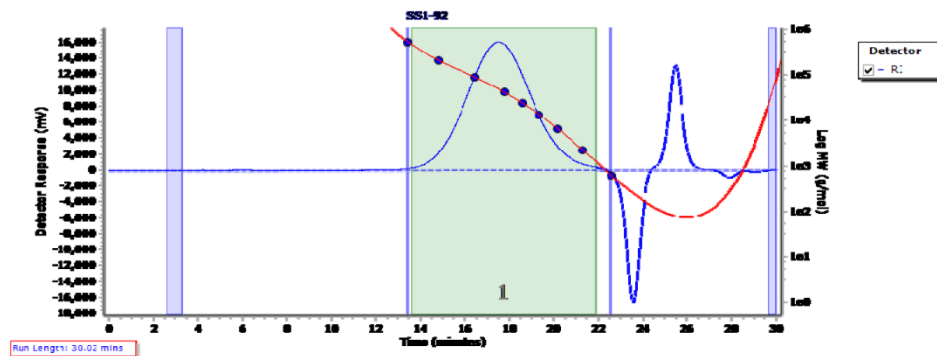


Figure D-36. GPC Chromatogram of PV-OV-A (Table 4-1, entry 5).

Molecular Weight Averages

| Peak | Mp | Mn | Mw | Mz | Mz+1 | Mv | PD |
|--------|-------|-------|-------|-------|--------|-------|-------|
| Peak 1 | 42351 | 24529 | 53368 | 91660 | 139375 | 85566 | 2.176 |

Peak information

| | Start (mins) | End (mins) |
|-------------------|--------------|------------|
| Baseline region 1 | 1.24 | 2.18 |
| Baseline region 2 | 29.82 | 30.00 |
| Peak 1 | 13.64 | 21.28 |

| Peak | Trace | Peak Max RT (mins) | Peak Area (mV.s) | Peak Height (mV) |
|--------|-------|--------------------|------------------|------------------|
| Peak 1 | RI | 17.70 | 3833001.750 | 18872.962 |

Chromatogram

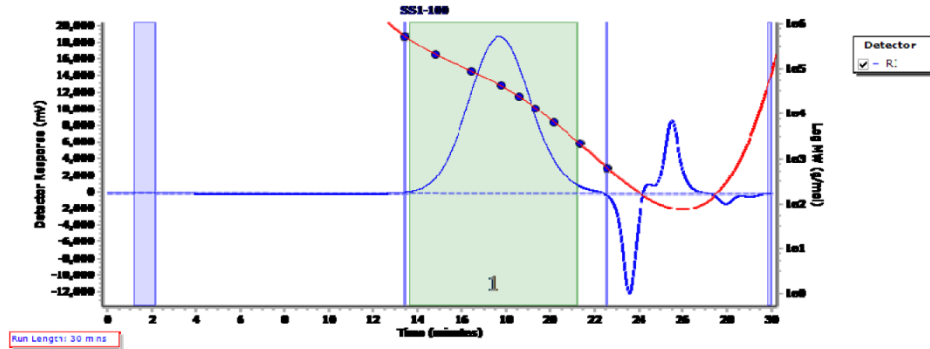


Figure D-37. GPC Chromatogram of PV-IV-A (Table 4-1, entry 6).

Molecular Weight Averages

| Peak | Mp | Mn | Mw | Mz | Mz+1 | Mv | PD |
|--------|-------|-------|-------|-------|--------|-------|-------|
| Peak 1 | 33135 | 17009 | 45024 | 85599 | 136413 | 79126 | 2.647 |

Peak information

| | Start (mins) | End (mins) |
|-------------------|--------------|------------|
| Baseline region 1 | 1.82 | 2.98 |
| Baseline region 2 | 29.57 | 30.01 |
| Peak 1 | 13.75 | 21.71 |

| Peak | Trace | Peak Max RT (mins) | Peak Area (mV.s) | Peak Height (mV) |
|--------|-------|--------------------|------------------|------------------|
| Peak 1 | RI | 18.08 | 4058974.919 | 18722.163 |

Chromatogram

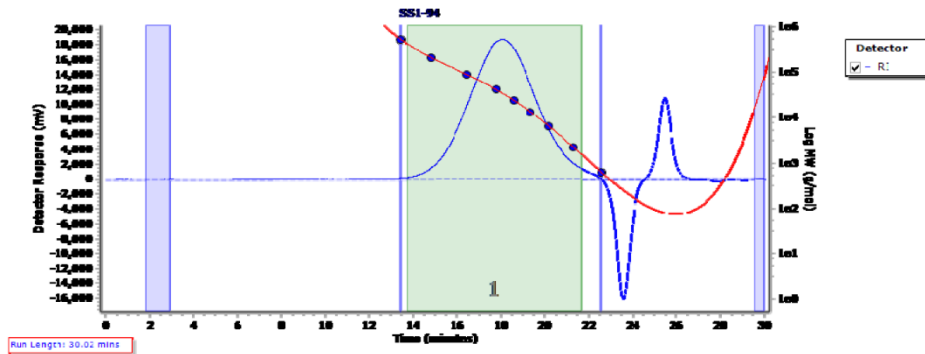


Figure D-38. GPC Chromatogram of PV-SA-A (Table 4-1, entry 7).

Molecular Weight Averages

| Peak | Mp | Mn | Mw | Mz | Mz+1 | Mv | PD |
|--------|-------|-------|-------|-------|-------|-------|-------|
| Peak 1 | 26423 | 11175 | 33113 | 59131 | 82909 | 55604 | 2.963 |

Peak information

| | Start (mins) | End (mins) |
|-------------------|--------------|------------|
| Baseline region 1 | 5.60 | 6.80 |
| Baseline region 2 | 29.57 | 30.00 |
| Peak 1 | 14.98 | 22.37 |

| Peak | Trace | Peak Max RT (mins) | Peak Area (mV.s) | Peak Height (mV) |
|--------|-------|--------------------|------------------|------------------|
| Peak 1 | RI | 18.41 | 5310695.498 | 25066.822 |

Chromatogram

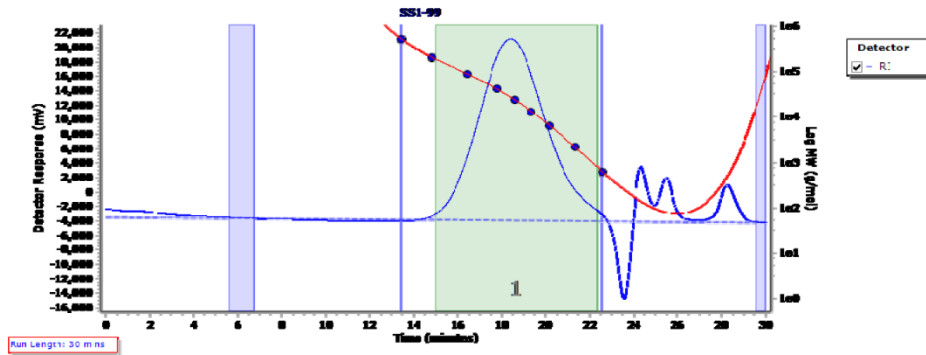


Figure D-39. GPC Chromatogram of PV-OA-A (Table 4-1, entry 8).

Molecular Weight Averages

| Peak | Mp | Mn | Mw | Mz | Mz+1 | Mv | PD |
|--------|-------|-------|-------|-------|--------|-------|-------|
| Peak 1 | 41999 | 22055 | 51153 | 85925 | 123796 | 80741 | 2.319 |

Peak information

| | Start (mins) | End (mins) |
|-------------------|--------------|------------|
| Baseline region 1 | 1.08 | 2.84 |
| Baseline region 2 | 29.18 | 29.97 |
| Peak 1 | 14.05 | 21.77 |

| Peak | Trace | Peak Max RT (mins) | Peak Area (mV.s) | Peak Height (mV) |
|--------|-------|--------------------|------------------|------------------|
| Peak 1 | RI | 17.71 | 3943358.139 | 19349.050 |

Chromatogram

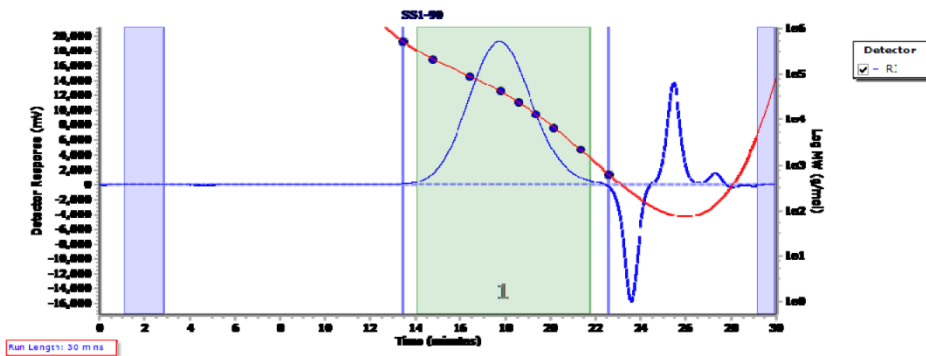


Figure D-40. GPC Chromatogram of PV-PA-A (Table 4-1, entry 9).

Molecular Weight Averages

| Peak | Mp | Mn | Mw | Mz | Mz+1 | Mv | PD |
|--------|-------|-------|-------|-------|--------|-------|-------|
| Peak 1 | 29535 | 13305 | 37040 | 66949 | 100918 | 62461 | 2.784 |

Peak information

| | Start (mins) | End (mins) |
|-------------------|--------------|------------|
| Baseline region 1 | 0.29 | 2.91 |
| Baseline region 2 | 29.13 | 30.01 |
| Peak 1 | 14.08 | 22.33 |

| Peak | Trace | Peak Max RT (mins) | Peak Area (mV.s) | Peak Height (mV) |
|--------|-------|--------------------|------------------|------------------|
| Peak 1 | RI | 18.25 | 3337716.905 | 16158.357 |

Chromatogram

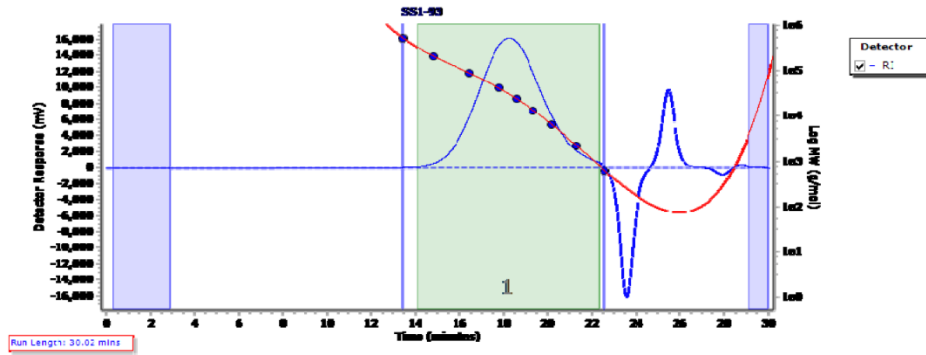


Figure D-41. GPC Chromatogram of PV-BZ-A (Table 4-1, entry 10).

NMR Spectra

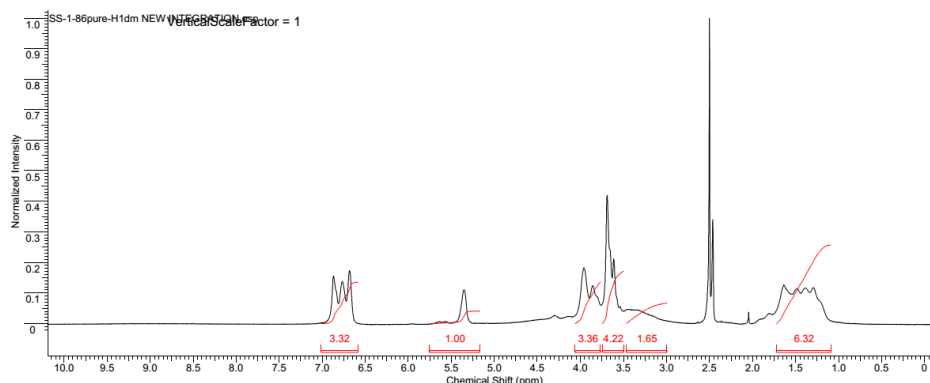


Figure D-42. ^1H NMR Spectrum PV-VV-A (Table 4-1, entry 1).

(DMSO- d_6) δ ppm 1.1-1.8 (m, 6.32 H), 3.26 (m, 1.65 H), 3.69 (m, 3 H), 3.90 (m, 3.36 H), 5.35, 5.56, 5.65 (m, 1 H), 6.68, 6.76, 6.87 (m, 3 H).

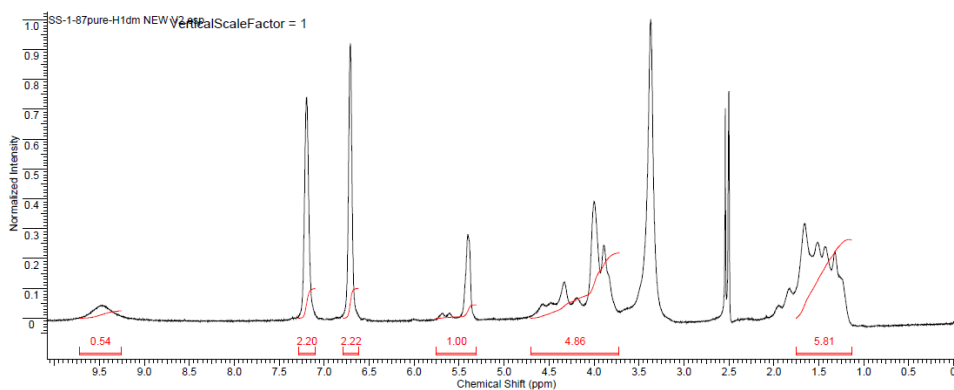


Figure D-43. ^1H NMR Spectrum PV-HB-A (Table 4-1, entry 2).

(DMSO- d_6) δ ppm 1.1-1.8 (m, 5.81 H), 3.88, 3.99, 4.33 (m, 4.86 H), 5.40, 5.60, 5.68 (m, 1 H), 6.70 (s, 2 H), 7.19 (s, 2 H), 9.47 (br, s, 1 H)

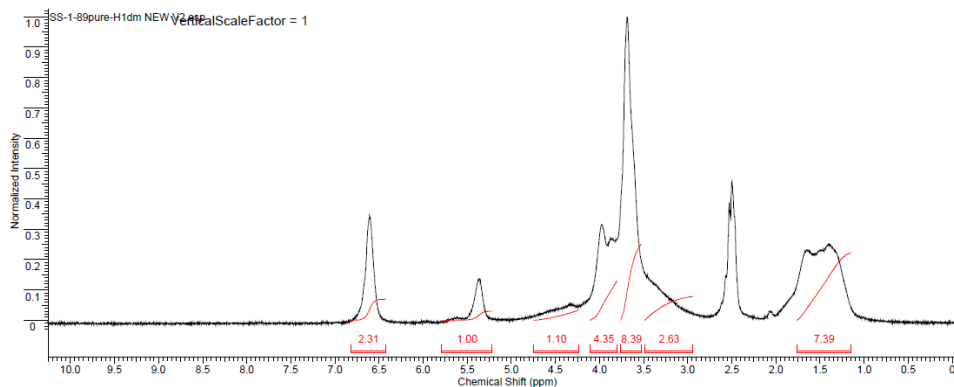


Figure D-44. ^1H NMR Spectrum PV-SY-A (Table 4-1, entry 3).

(DMSO- d_6) δ ppm 1.1-1.8 (m, 7.39 H), 3.27 (m, 2.63 H), 3.68 (m, 6 H), 3.92 (m, 4.35 H), 4.34 (m, 1H), 5.36, 5.62 (m, 1 H), 6.61 (s, 2 H).

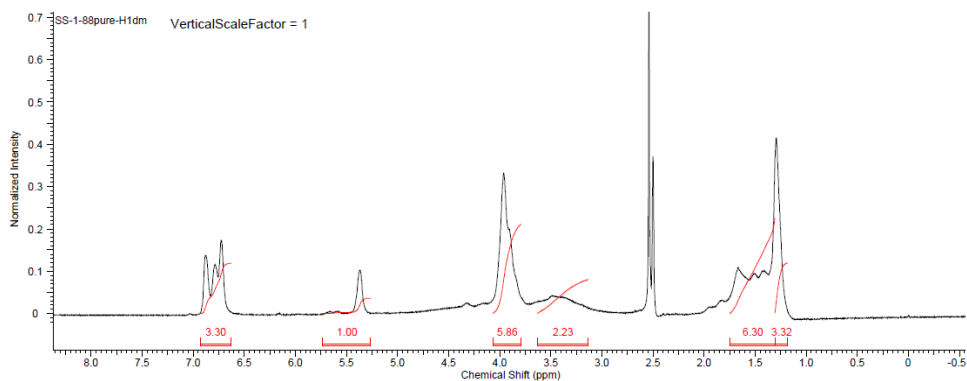


Figure D-45. ¹H NMR Spectrum PV-EV-A (Table 4-1, entry 4).

(DMSO-*d*₆) δ ppm 1.29 (s, 3 H), 1.1-1.8 (m, 6.30 H), 3.42 (m, 2.23 H), 3.90 (m, 2 H), 3.95 (m, 3.86 H), 5.36, 5.59, 5.65 (m, 1 H), 6.72, 6.79, 6.88 (m, 3H).

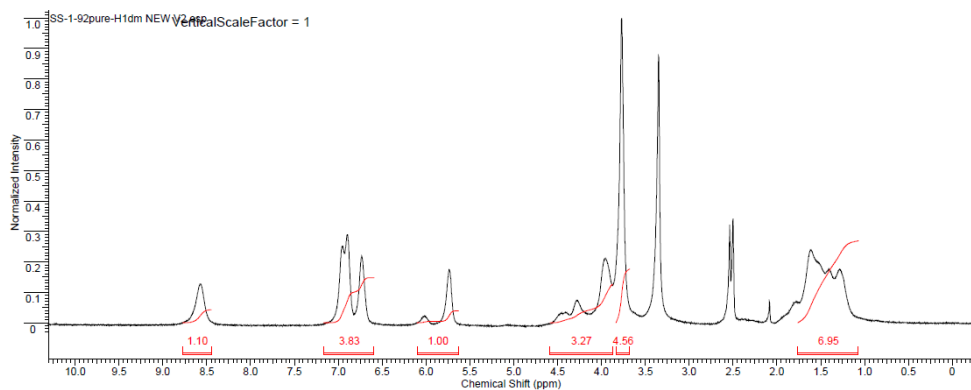


Figure D-46. ¹H NMR Spectrum PV-OV-A (Table 4-1, entry 5).

(DMSO-*d*₆) δ ppm 1.1-1.8 (m, 6.95 H), 3.77 (s, 3 H), 3.90-4.5 (m, 3.27 H), 5.74, 6.02 (m, 1 H), 6.73, 6.89, 6.97 (m, 3 H), 8.58 (br, s, 1 H).

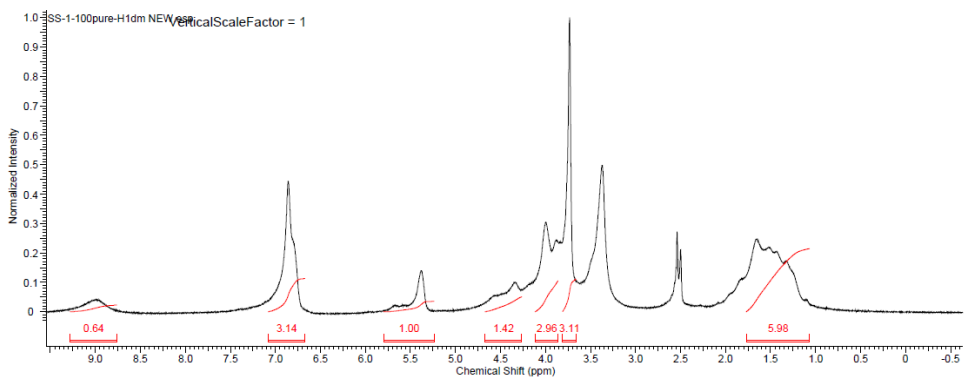


Figure D-47. ¹H NMR Spectrum PV-IV-A (Table 4-1, entry 6).

(DMSO-*d*₆) δ ppm 1.1-1.8 (m, 5.98 H), 3.73 (s, 3 H), 3.93 (m, 2.96 H), 4.42 (m, 1.42 H), 5.38, 5.56, 5.67 (m, 1 H), 6.82 (m, 3 H), 8.99 (br, s, 1 H).

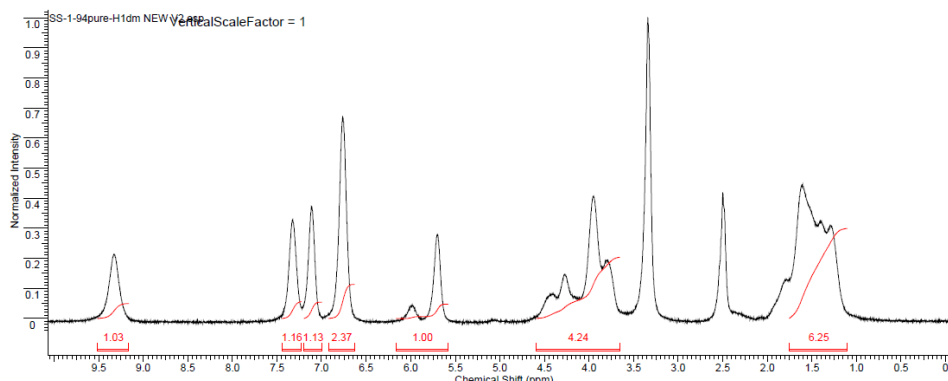


Figure D-48. ¹H NMR Spectrum PV-SA-A (Table 4-1, entry 7).

(DMSO-*d*₆) δ ppm 1.1-1.8 (m, 6.25 H), 3.79, 3.96, 4.27, 4.42 (m, 4.24 H), 5.70, 5.98 (m, 1 H), 6.77 (s, 2 H), 7.10 (s, 1 H), 7.32 (s, 1 H), 9.32 (br. s, 1 H).

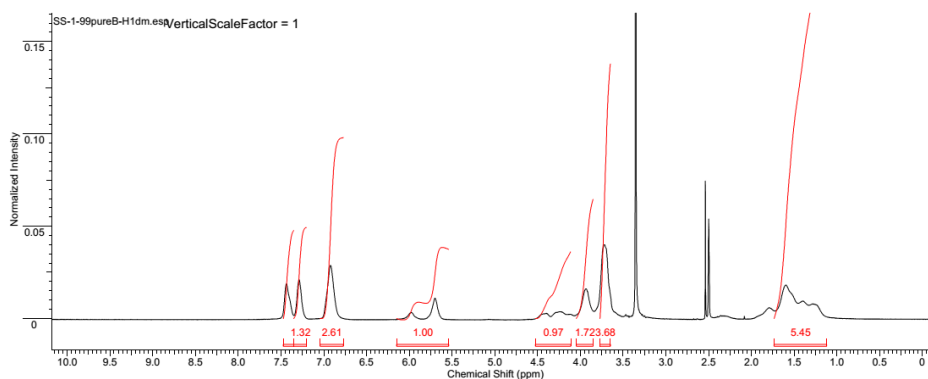


Figure D-49. ¹H NMR Spectrum PV-OA-A (Table 4-1, entry 8).

(DMSO-*d*₆) δ ppm 1.1-1.8 (m, 5.45 H), 3.72 (s, 3 H), 3.93 (m, 1.72 H), 4.29 (m, 0.97 H), 5.70, 5.97 (m, 1 H), 6.93 (m, 2 H), 7.29 (m, 1 H), 7.43 (m, 1 H).

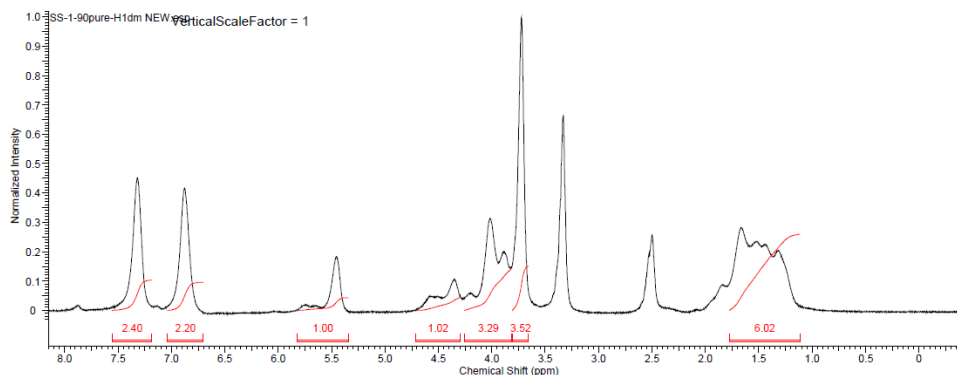


Figure D-50. ¹H NMR Spectrum PV-PA-A (Table 4-1, entry 9).

(DMSO-*d*₆) δ ppm 1.1-1.8 (m, 6.02 H), 3.74 (s, 3 H), 4.02 (m, 3.29 H), 4.43 (m, 1.02 H), 5.46, 5.64, 5.75 (m, 1 H), 6.88 (s, 2 H), 7.32 (s, 2 H).

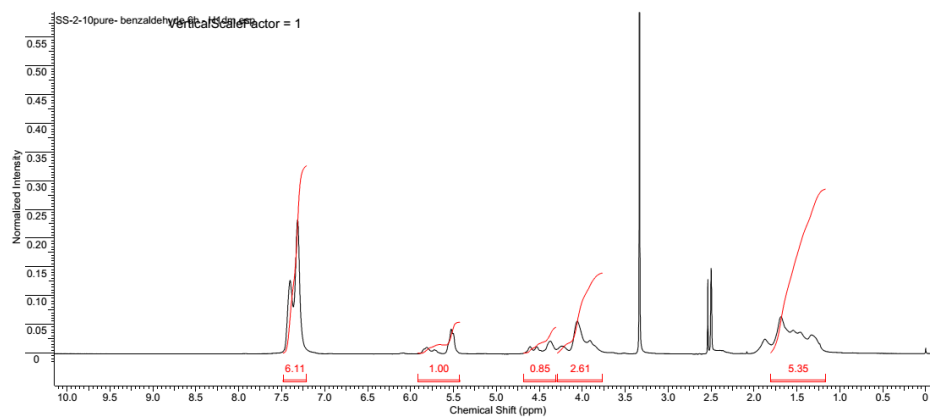


Figure D-51. ¹H NMR Spectrum PV-BZ-A (Table 4-1, entry 10).

(DMSO-*d*₆) δ ppm 1.1-1.8 (m, 5.35 H), 4.06 (m, 2.61 H), 4.50 (m, 0.85 H), 5.50, 5.76 (m, 1 H), 7.37 (m, 5 H).

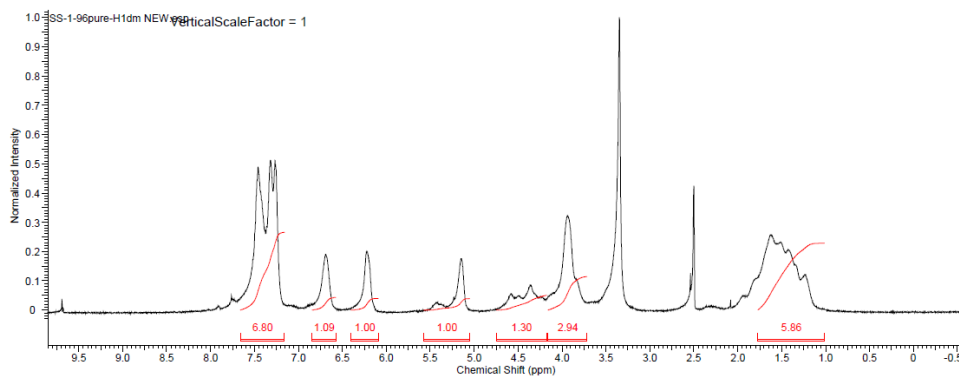


Figure D-52. ¹H NMR Spectrum PV-CI-A (Table 4-1, entry 11).

(DMSO-*d*₆) δ ppm 1.1-1.8 (m, 5.86 H), 3.94 (m, 2.94 H), 4.44 (m, 1.30 H), 5.15, 5.43 (m, 1 H), 6.23 (s, 1 H), 6.68 (s, 1 H), 7.36 (m, 5 H).

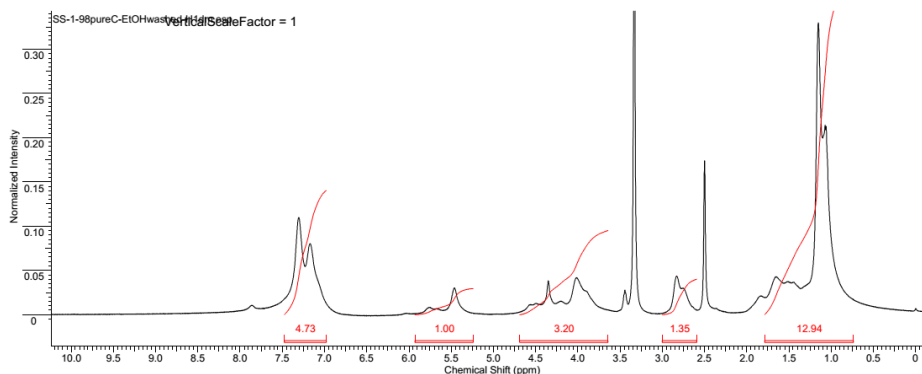


Figure D-53. ¹H NMR Spectrum PV-CU-A (Table 4-1, entry 12).

(DMSO-*d*₆) δ ppm 1.07, 1.16 (m, 6H), 1.1–1.8 (m, 6.94 H), 2.81 (m, 1 H), 3.93 (m, 3.20 H), 5.46, 5.65, 5.74 (m, 1 H), 7.26 (m, 4 H).

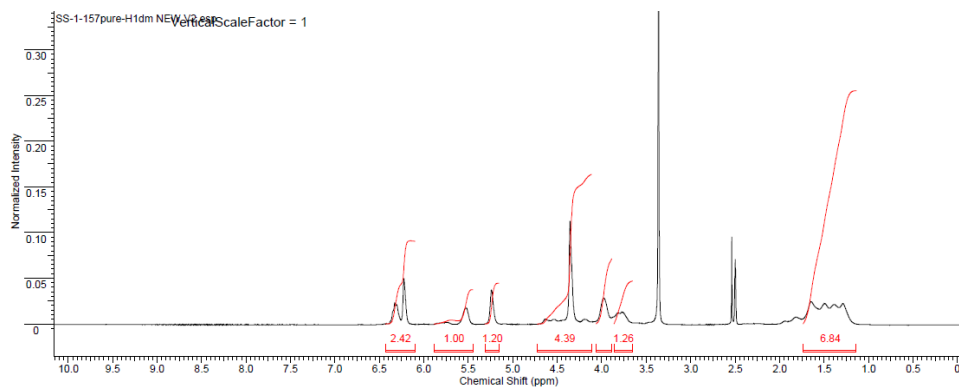


Figure D-54. ^1H NMR Spectrum PV-HMF-A (Table 4-1, entry 13).

(DMSO- d_6) δ ppm 1.1-1.8 (m, 6.84 H), 3.79 (m, 1.26 H), 3.97 (s, 2 H), 4.43 (m, 4.39 H), 5.24 (s, 1 H), 5.52, 5.77 (m, 1 H), 6.26 (m, 2 H).

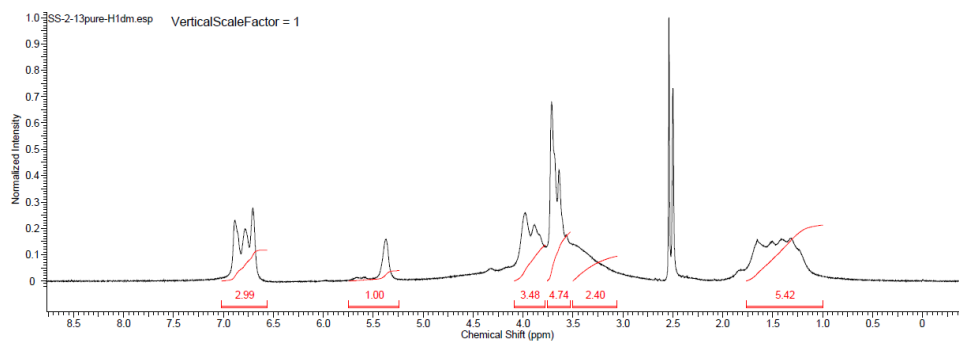


Figure D-55. ^1H NMR Spectrum PV-VV-A* High MW (Table 4-1, entry 15)

(DMSO- d_6) δ ppm 1.1-1.8 (m, 5.42 H), 3.30 (m, 2.40 H), 3.72 (m, 3 H), 3.90 (m, 3.48 H), 5.38, 5.59, 5.66 (m, 1 H), 6.71, 6.78, 6.88 (m, 3 H).

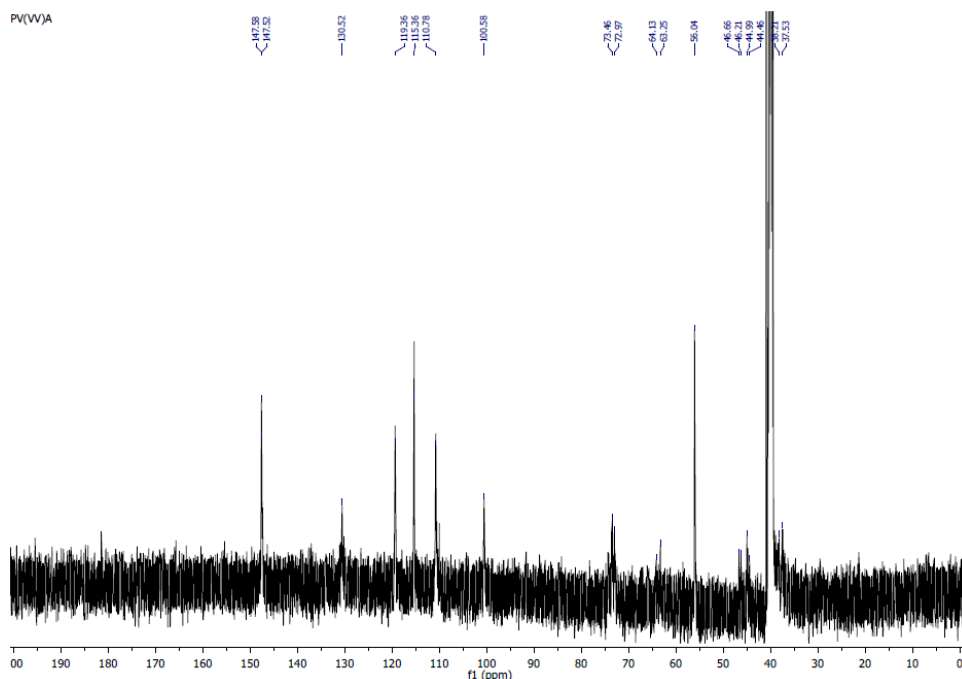


Figure D-56. ¹³C NMR Spectrum of PV-VV-A (Table 4-1, entry 1).

(DMSO-*d*₆) δ ppm 37.6, 38.2, 44.5, 45.0, 46.2, 46.7, 56.0, 63.3, 64.1, 73.0, 73.5, 100.6, 110.8, 115.4, 119.4, 130.5, 147.52, 147.56.

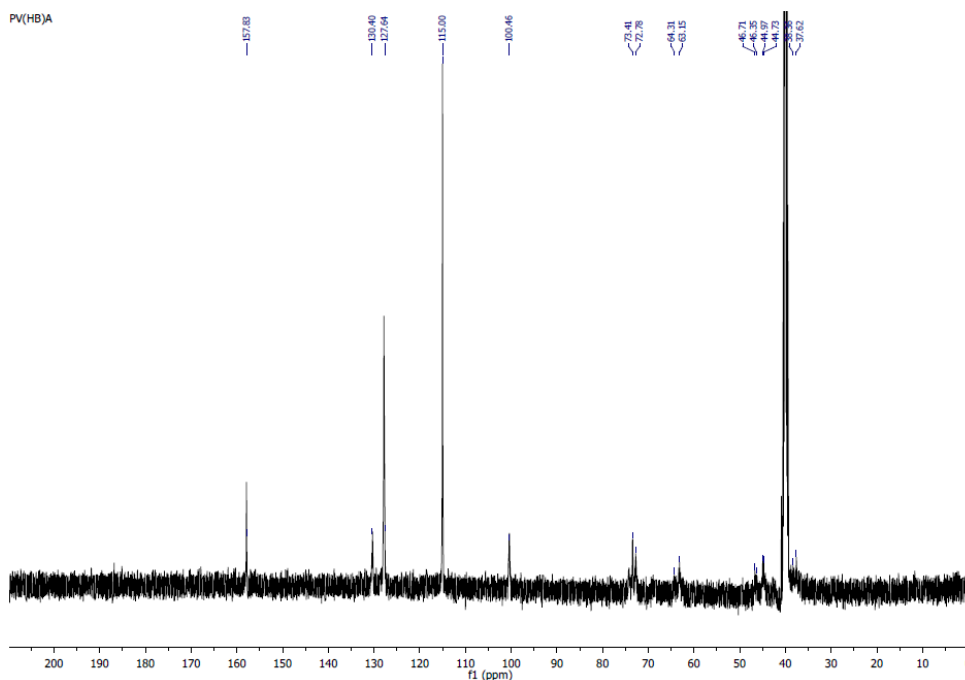


Figure D-57. ¹³C NMR Spectrum of PV-HB-A (Table 4-1, entry 2).

(DMSO-*d*₆) δ ppm 37.6, 38.4, 44.7, 45.0, 46.3, 46.7, 63.1, 64.3, 72.8, 73.4, 100.4, 115.0, 127.6, 130.4, 157.8.

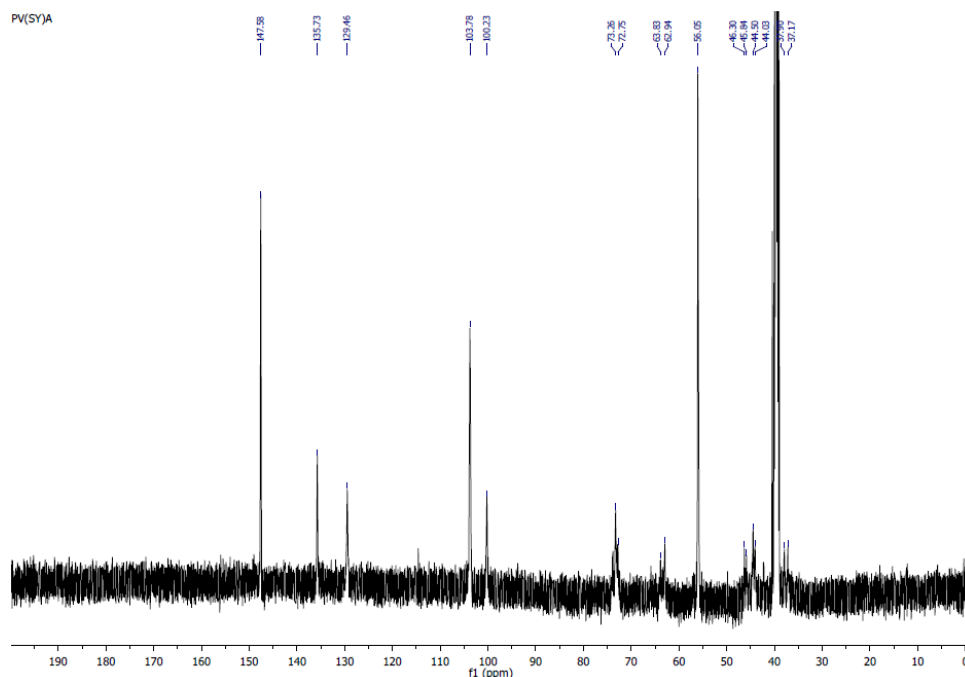


Figure D-58. ^{13}C NMR Spectrum of PV-SY-A (Table 4-1, entry 3).

(DMSO- d_6) δ ppm 37.2, 37.9, 44.0, 44.5, 45.8, 46.3, 56.0, 62.9, 63.8, 72.8, 73.3, 100.2, 103.8, 129.5, 135.7, 147.6.

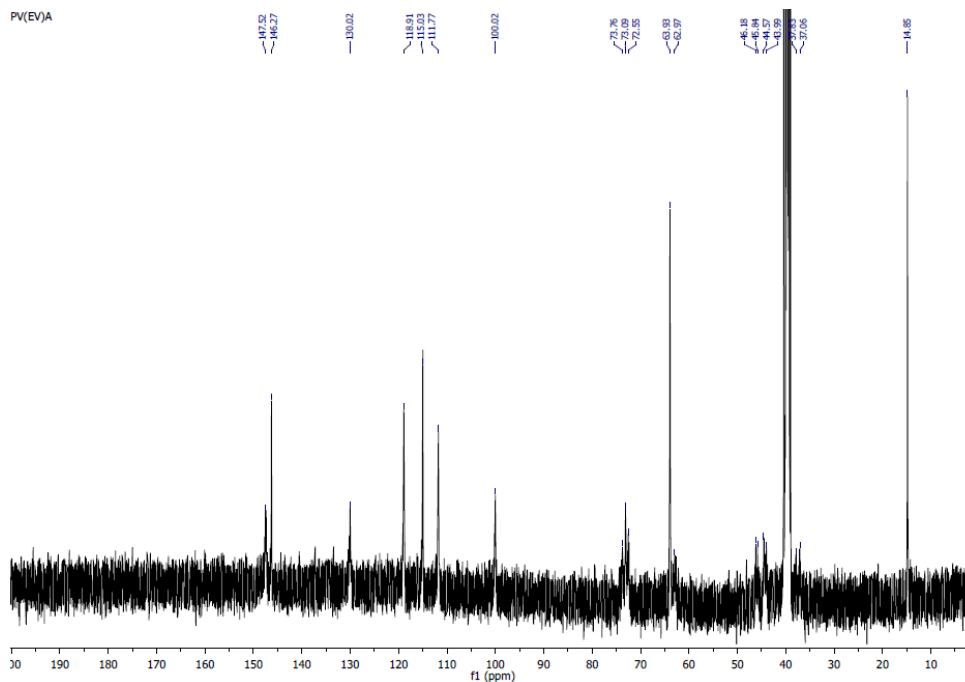


Figure D-59. ^{13}C NMR Spectrum of PV-EV-A (Table 4-1, entry 4).

(DMSO- d_6) δ ppm 14.8, 37.1, 37.8, 44.0, 44.6, 45.8, 46.2, 63.0, 63.9, 72.5, 73.1, 73.8, 100.0, 111.8, 115.0, 118.9, 130.0, 146.3, 147.5.

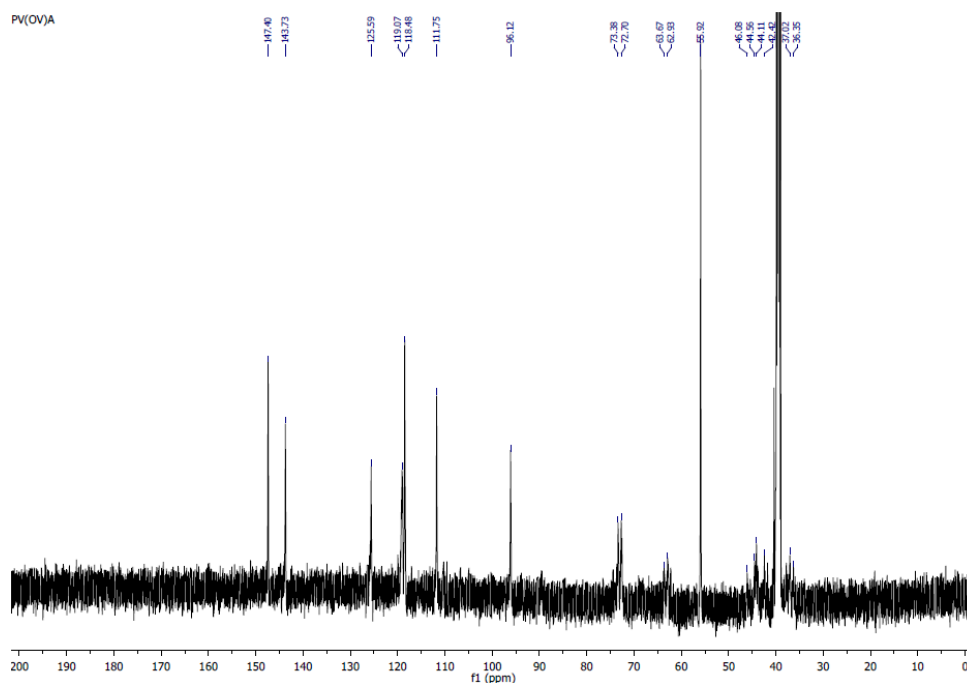


Figure D-60. ^{13}C NMR Spectrum of PV-OV-A (Table 4-1, entry 5).

(DMSO- d_6) δ ppm 36.4, 37.0, 42.4, 44.1, 44.6, 46.1, 55.9, 62.9, 63.7, 72.7, 73.4, 96.1, 111.7, 118.5, 119.1, 125.6, 143.7, 147.4.

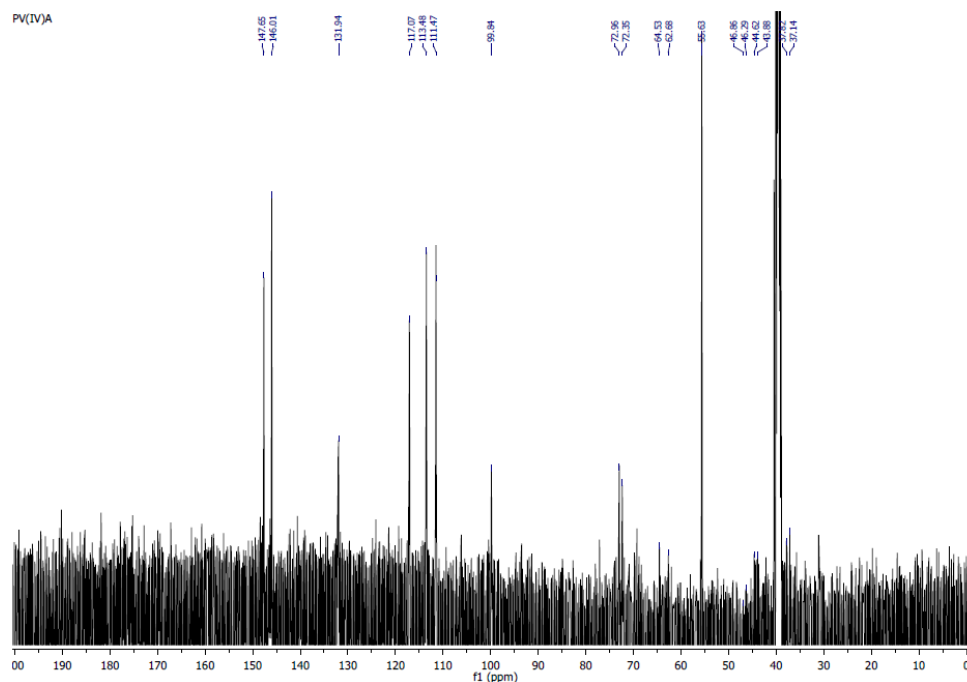


Figure D-61. ^{13}C NMR Spectrum of PV-IV-A (Table 4-1, entry 6).

(DMSO- d_6) δ ppm 37.1, 37.8, 43.9, 44.6, 46.3, 46.9, 55.6, 62.7, 64.5, 72.3, 73.0, 99.8, 111.5, 113.5, 117.1, 131.9, 146.0, 147.7.

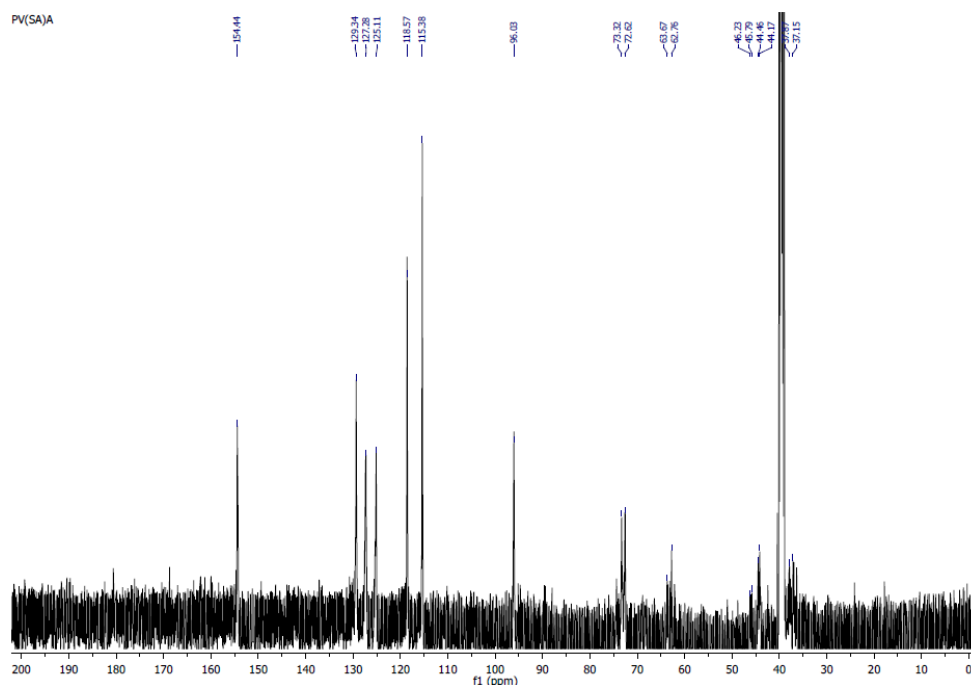


Figure D-62. ^{13}C NMR Spectrum of PV-SA-A (Table 4-1, entry 7).

(DMSO- d_6) δ ppm 37.1, 37.9, 44.2, 44.5, 45.8, 46.2, 62.8, 63.7, 72.6, 73.3, 96.0, 115.4, 118.6, 125.1, 127.3, 129.3, 154.4.

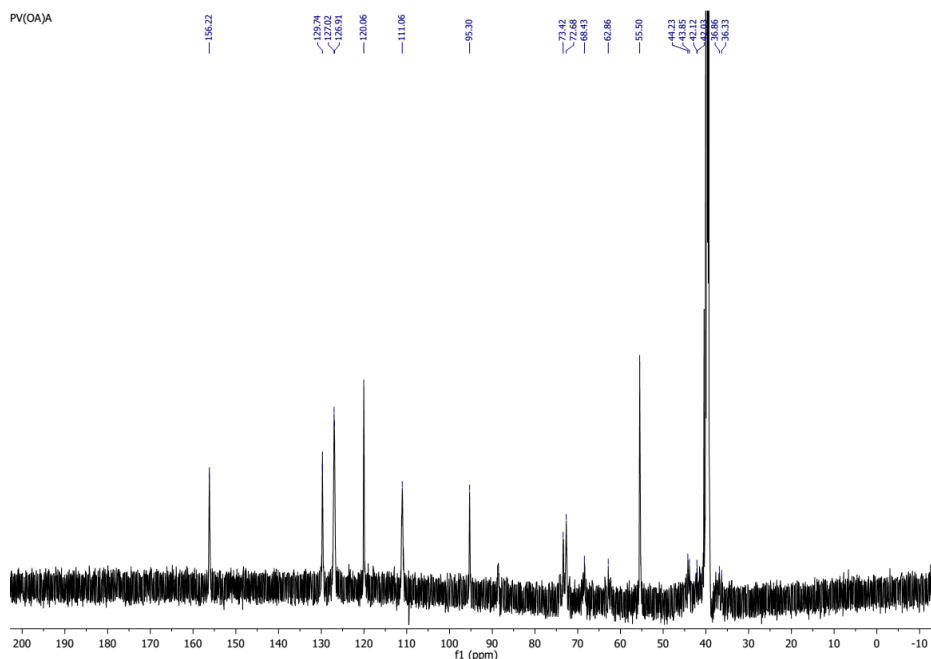


Figure D-63. ^{13}C NMR Spectrum of PV-OA-A (Table 4-1, entry 8)

(DMSO- d_6) δ ppm 36.3, 36.9, 42.0, 42.1, 43.8, 44.2, 55.5, 62.9, 68.4, 72.7, 73.4, 95.3, 111.1, 120.1, 126.9, 127.0, 129.7, 156.2.

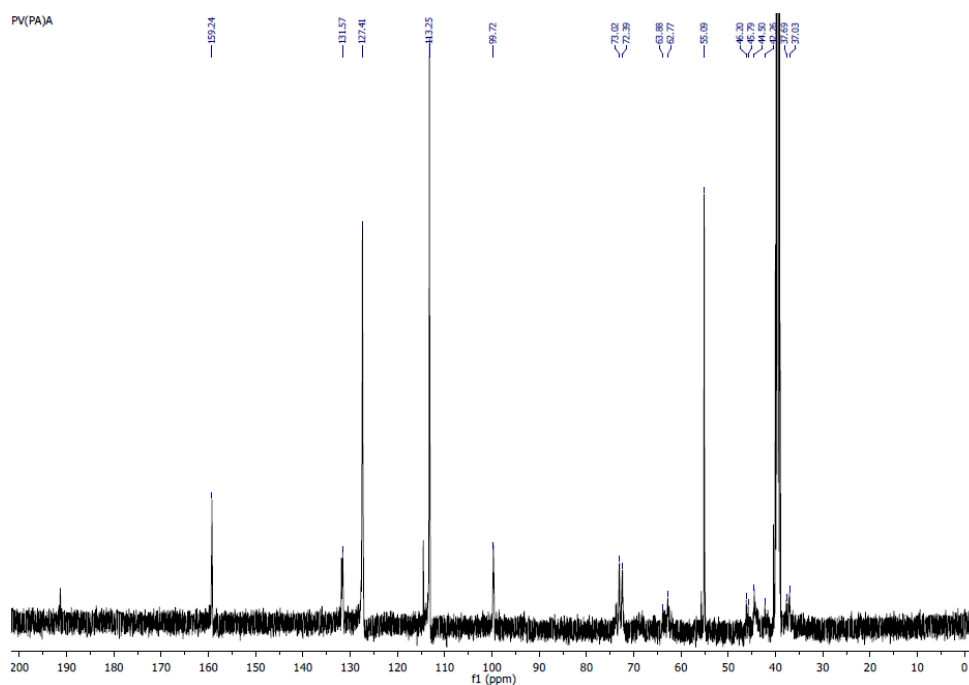


Figure D-64. ^{13}C NMR Spectrum of PV-PA-A (Table 4-1, entry 9).

(DMSO- d_6) δ ppm 37.0, 37.7, 42.3, 44.5, 45.8, 46.2, 55.1, 62.8, 63.9, 72.4, 73.0, 99.7, 113.2, 127.4, 131.6, 159.2.

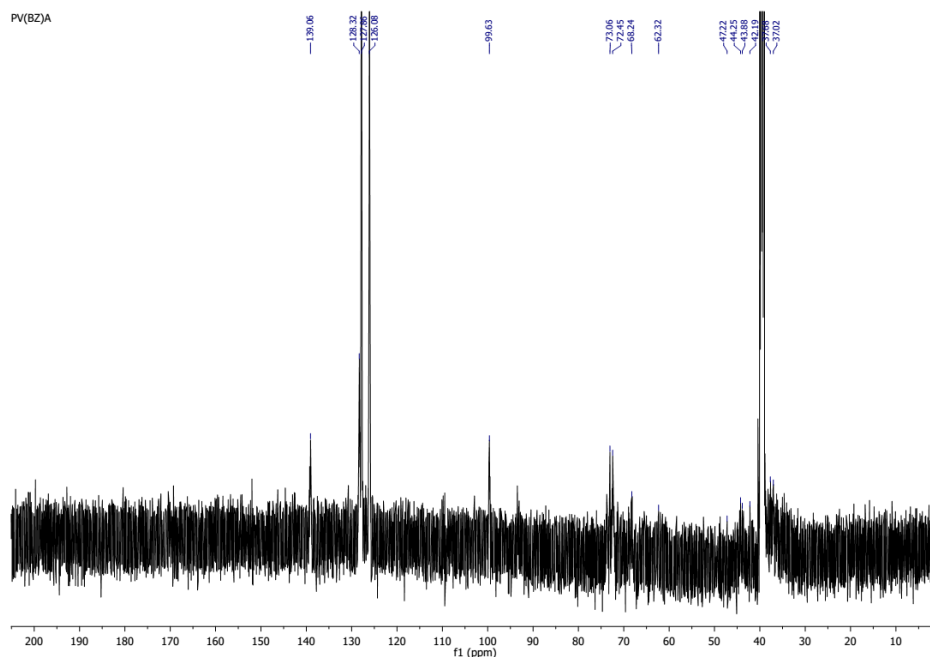


Figure D-65. ^{13}C NMR Spectrum of PV-BZ-A (Table 4-1, entry 10).

(DMSO- d_6) δ ppm 37.0, 37.7, 42.2, 43.9, 44.3, 47.2, 62.3, 68.2, 72.5, 73.1, 99.6, 126.1, 127.9, 128.3, 139.1.

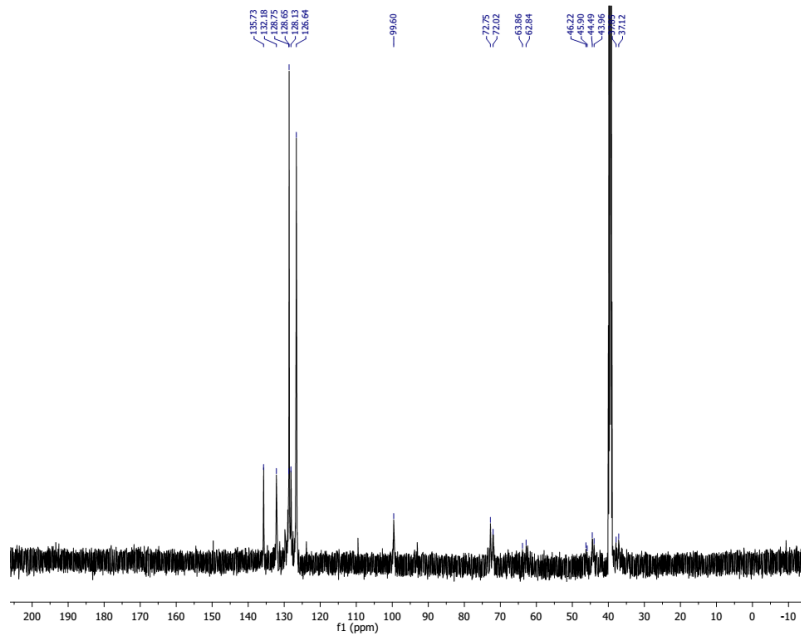


Figure D-66. ¹³C NMR Spectrum of PV-Cl-A (Table 4-1, entry 11).

(DMSO-*d*₆) δ ppm 37.1, 37.9, 44.0, 44.5, 45.9, 46.2, 62.8, 63.9, 72.0, 72.8, 99.6, 126.6, 128.1, 128.65, 128.75, 132.2, 135.7.

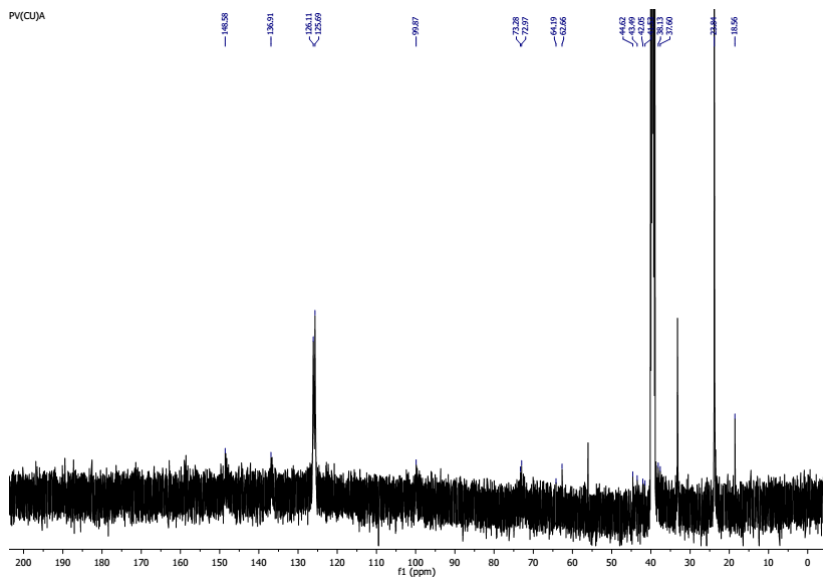


Figure D-67. ¹³C NMR Spectrum of PV-CU-A (Table 4-1, entry 12).

(DMSO-*d*₆) δ ppm 23.8, 33.2, 37.6, 38.1, 41.5, 42.0, 43.5, 44.6, 62.7, 64.2, 73.0, 73.3, 99.9, 125.7, 126.1, 136.9, 148.6 (18.6, 56.0 are from leftover ethanol).

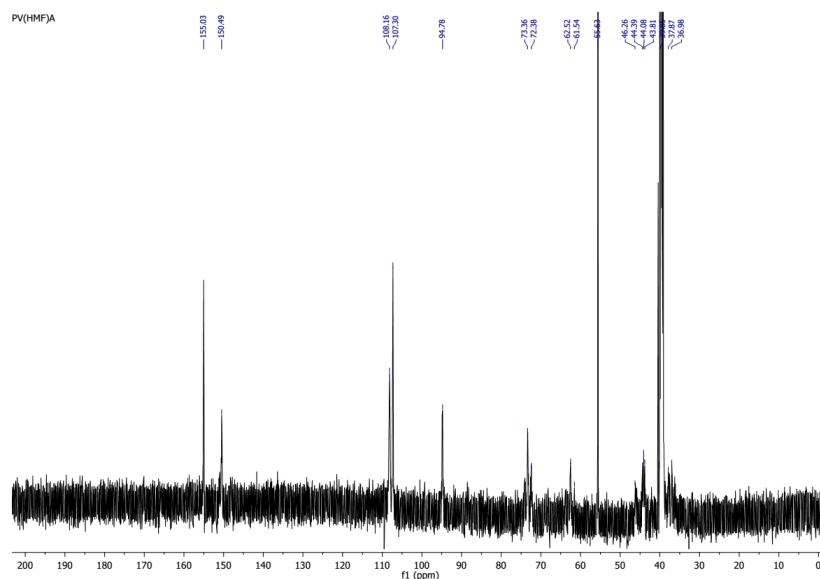


Figure D-68. ^{13}C NMR Spectrum of PV-HMF-A (Table 4-1, entry 13).

(DMSO- d_6) δ ppm 37.0, 37.9, 43.8, 44.1, 44.4, 46.3, 55.6, 61.5, 62.5, 72.4, 73.4, 94.8, 107.3, 108.2, 150.5, 155.0.

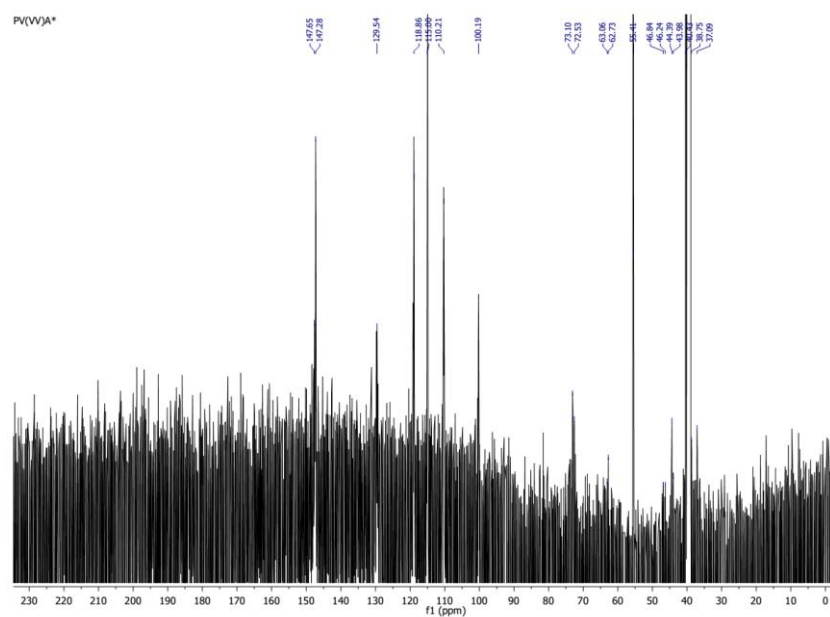


Figure D-69. ^{13}C NMR Spectrum of PV-VV-A* (Table 4-1, entry 15).

(DMSO- d_6) δ ppm. 37.1, 38.7, 44.0, 44.4, 46.2, 46.8, 55.4, 62.7, 63.1, 72.5, 73.1, 100.2, 110.2, 115.0, 118.9, 129.5, 147.3, 147.7

APPENDIX E
SUPPLEMENTARY INFORMATION FOR CHAPTER 5

TGA Spectra

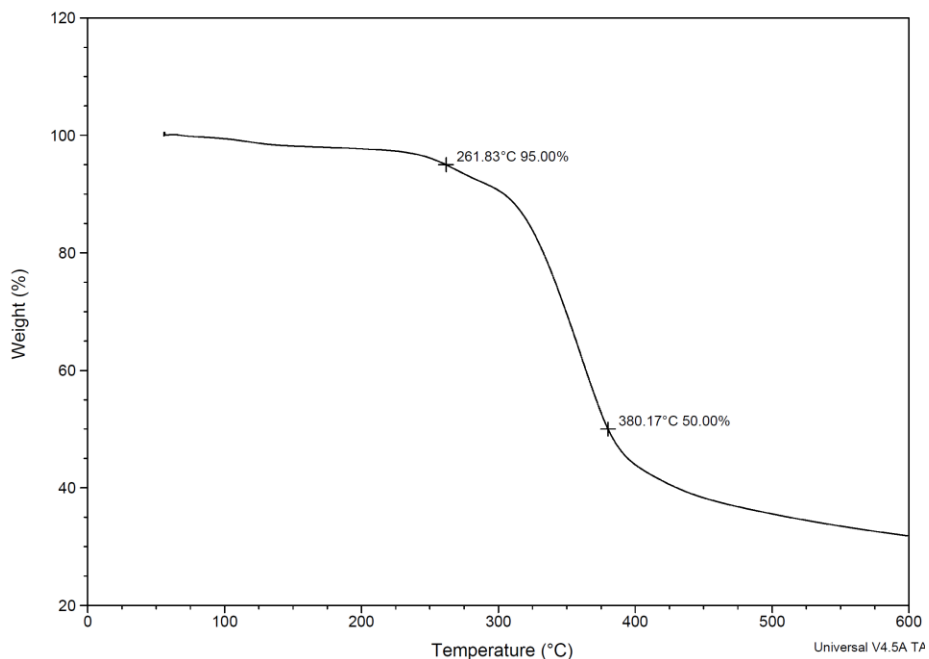


Figure E-1. TGA thermogram of poly-DHMP analogue from van-2-van and cyclopentanone (Figure 5-1, entry 1).

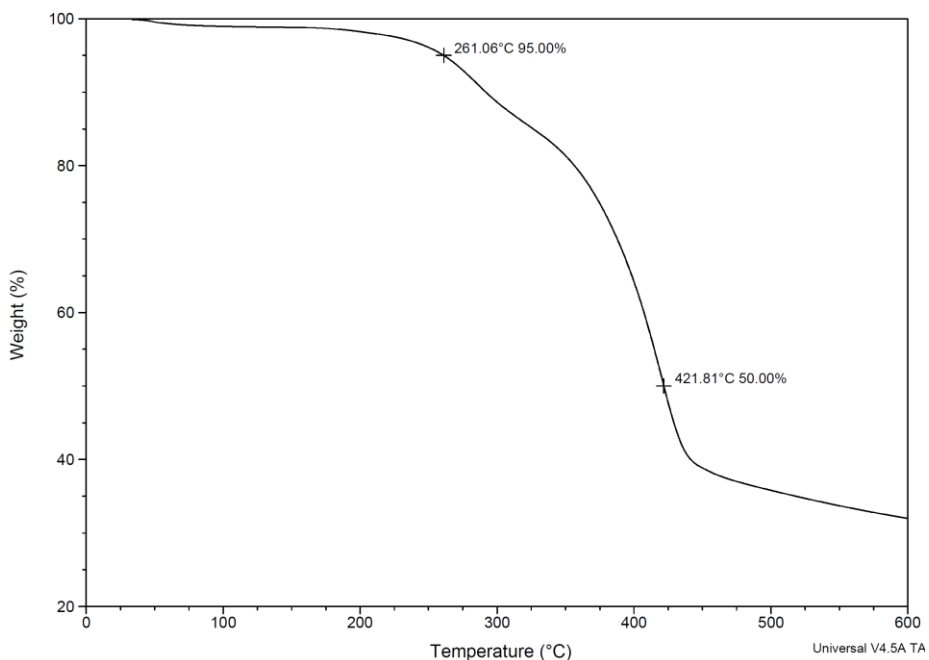


Figure E-2. TGA thermogram of poly-DHMP analogue from 4HB-2-4HB and dimethyl 3-oxoglutarate (Figure 5-2, entry 1).

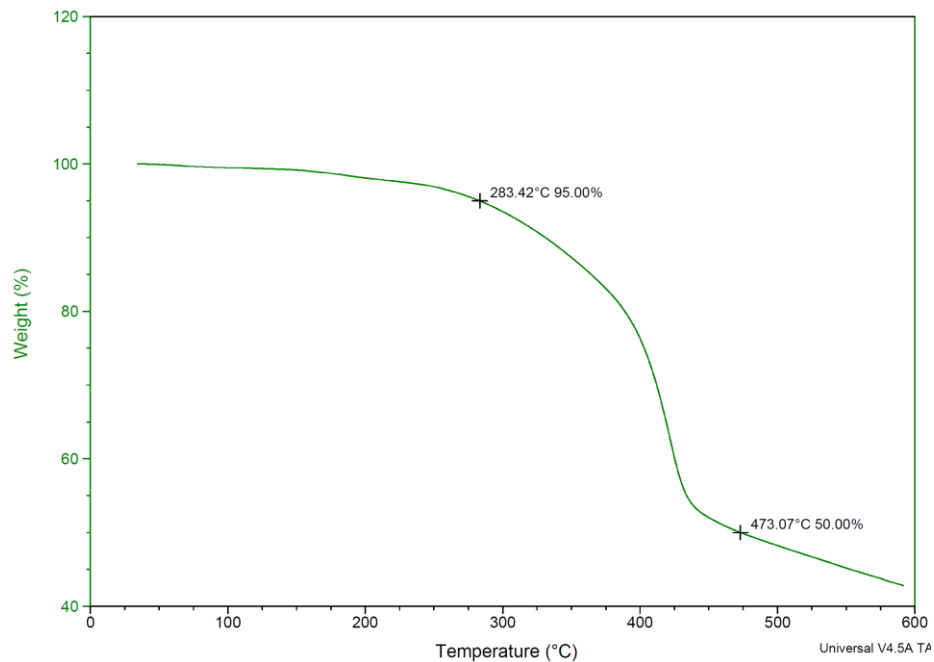


Figure E-3. TGA thermogram of poly-DHMP analogue from van-2-van and dimethyl 3-oxoglutarate (Figure 5-2, entry 2).

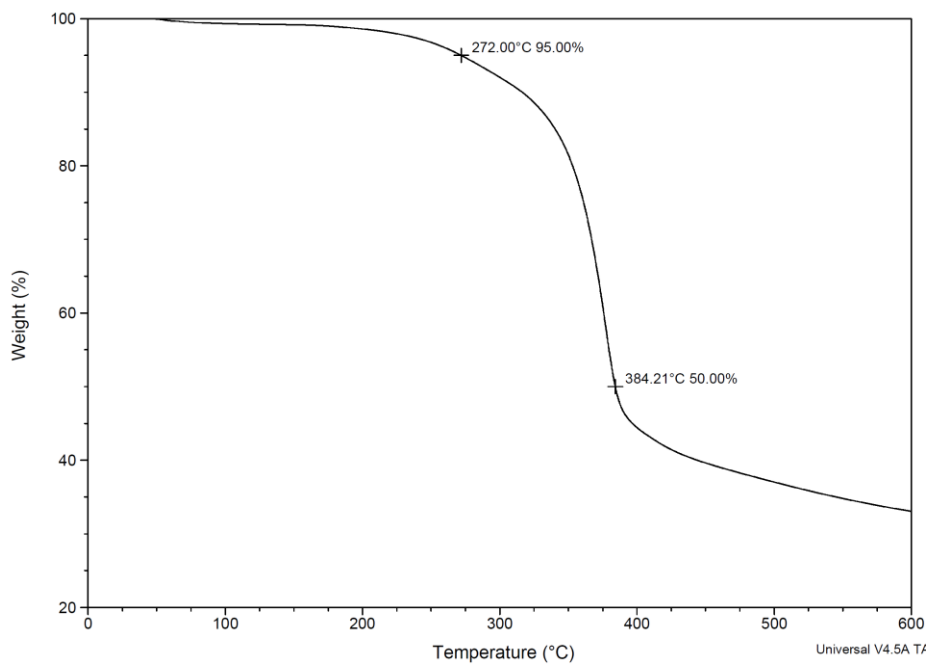


Figure E-4. TGA thermogram of poly-DHMP analogue from syr-2-syr and dimethyl 3-oxoglutarate (Figure 5-2, entry 3).

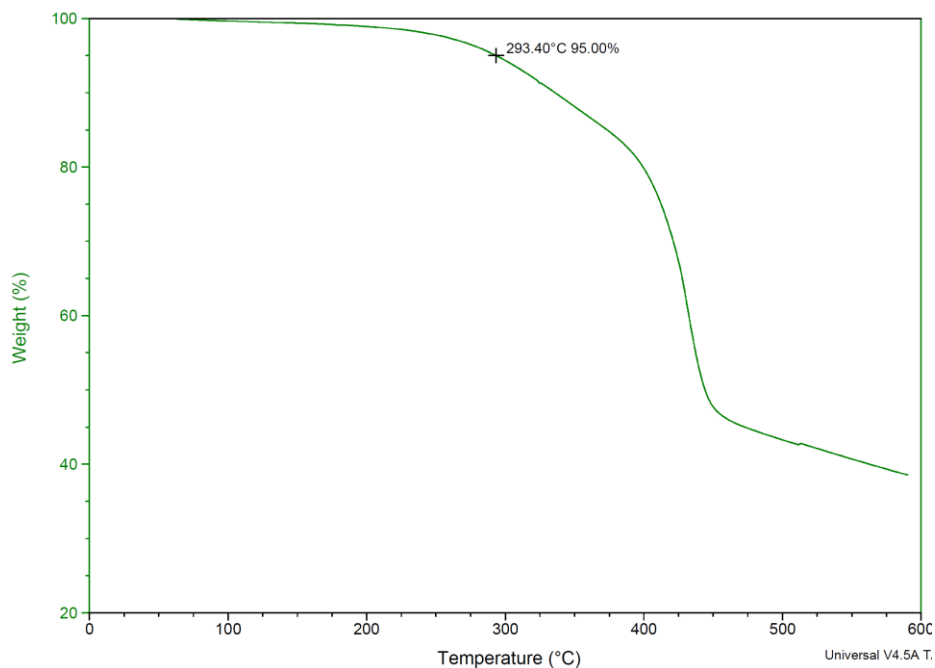


Figure E-5. TGA thermogram of poly-DHMP analogue from evan-2-evan and dimethyl 3-oxoglutarate (Figure 5-2, entry 4).

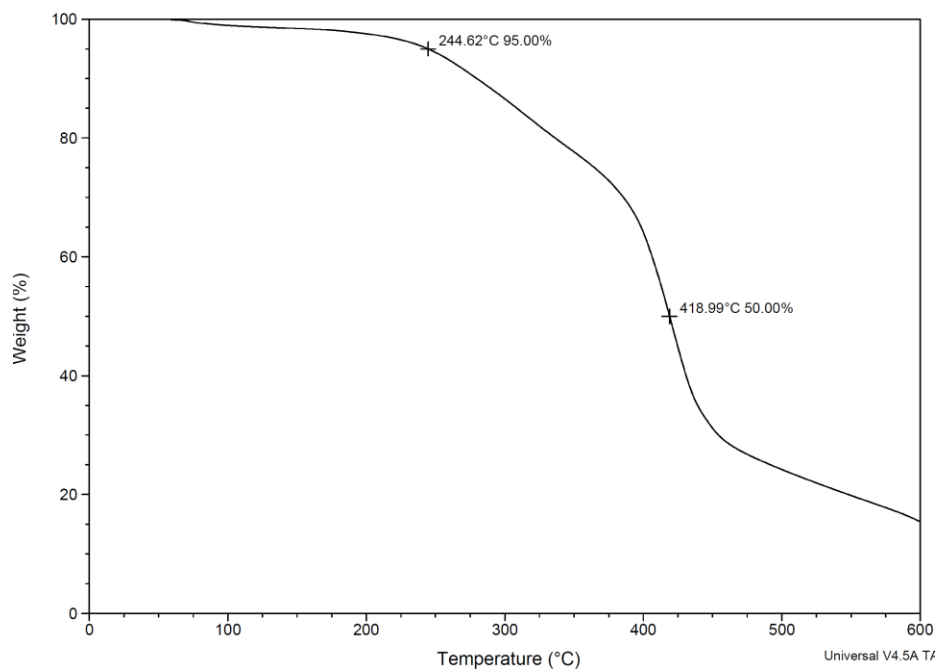


Figure E-6. TGA thermogram of poly-DHMP analogue from 4HB-3-4HB and dimethyl 3-oxoglutarate (Figure 5-2, entry 5).

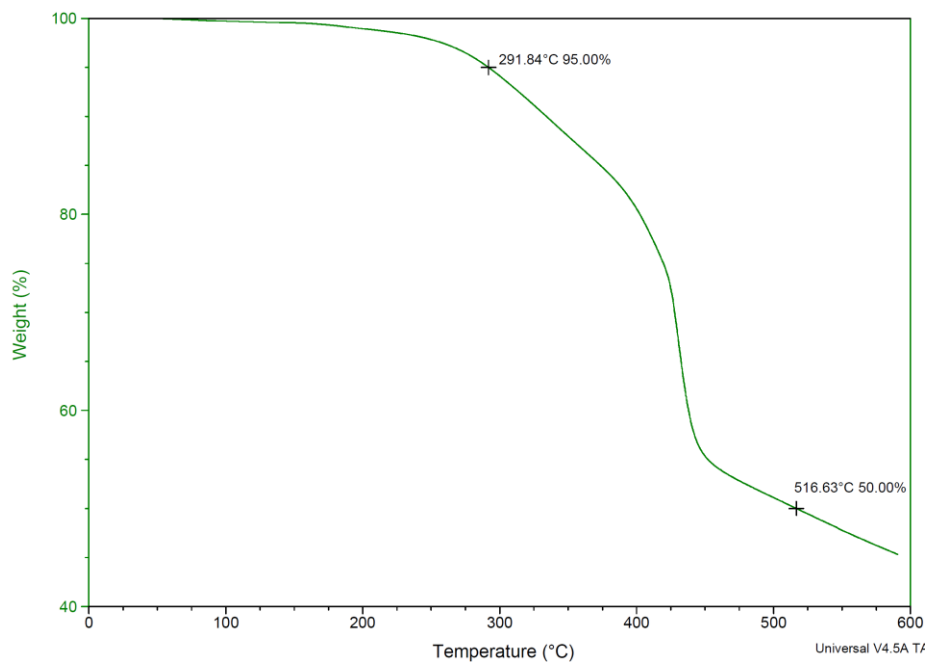


Figure E-7. TGA thermogram of poly-DHMP analogue from van-3-van and dimethyl 3-oxoglutarate (Figure 5-2, entry 6).

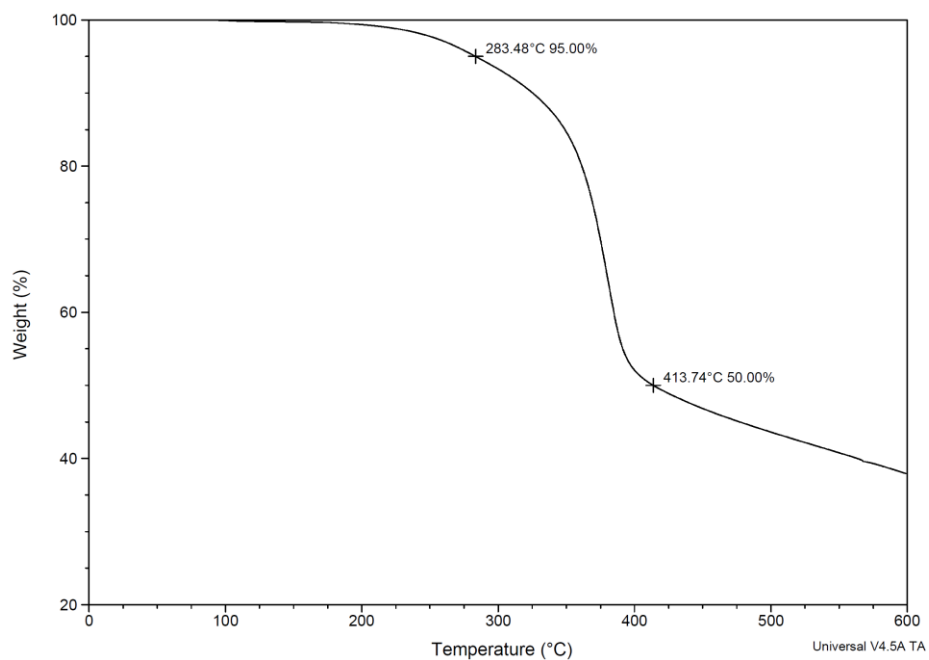


Figure E-8. TGA thermogram of poly-DHMP analogue from syr-3-syr and dimethyl 3-oxoglutarate (Figure 5-2, entry 7).

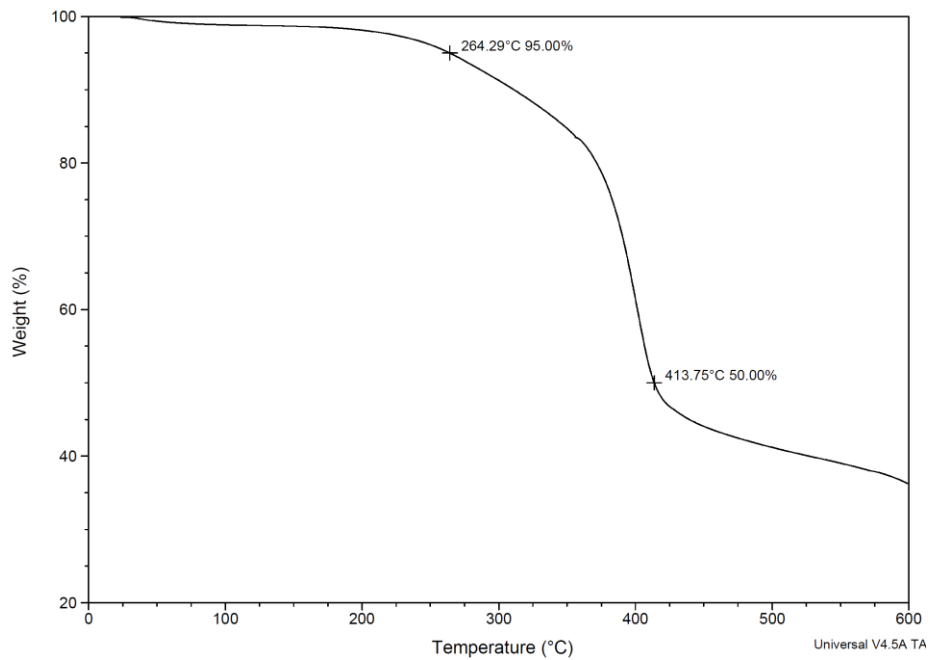


Figure E-9. TGA thermogram of poly-DHMP analogue from evan-3-*evan* and dimethyl 3-oxoglutarate (Figure 5-2, entry 8).

DSC Spectra

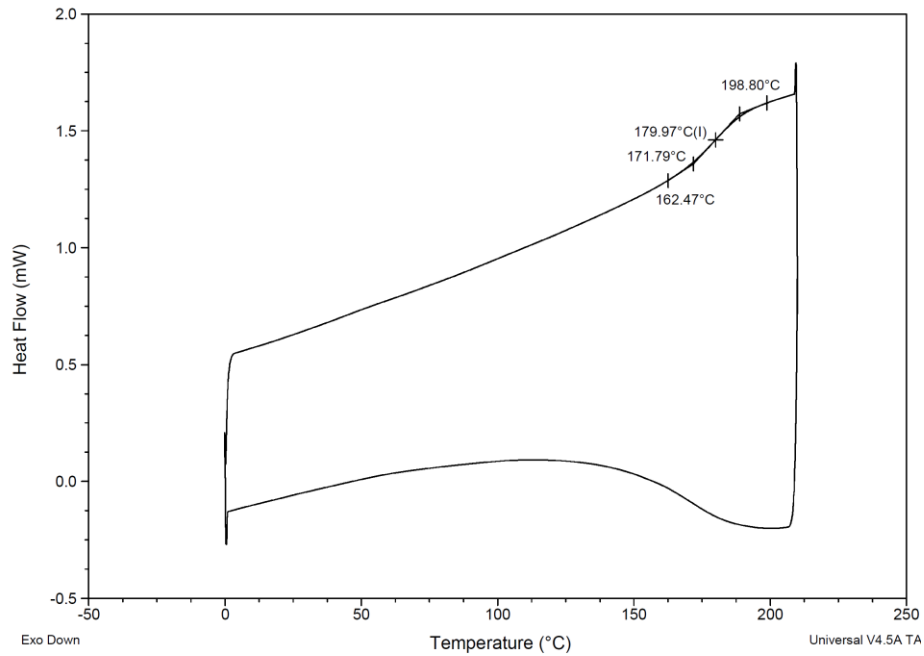


Figure E-10. DSC thermogram of poly-DHMP analogue from van-2-van and dimethyl 3-oxoglutarate (Figure 5-2, entry 2).

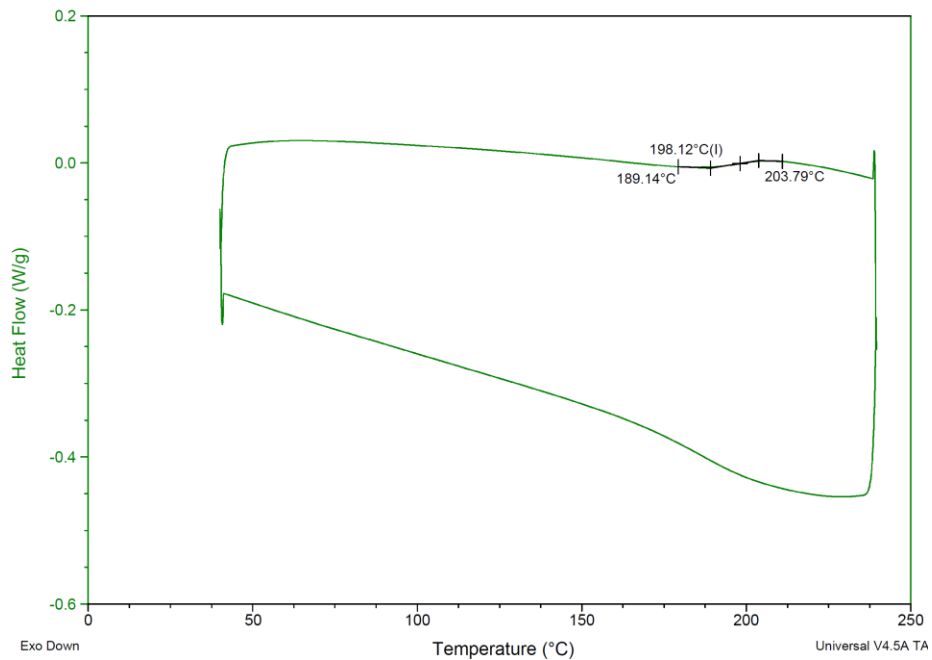


Figure E-11. DSC thermogram of poly-DHMP analogue from syr-2-syr and dimethyl 3-oxoglutarate (Figure 5-2, entry 3).

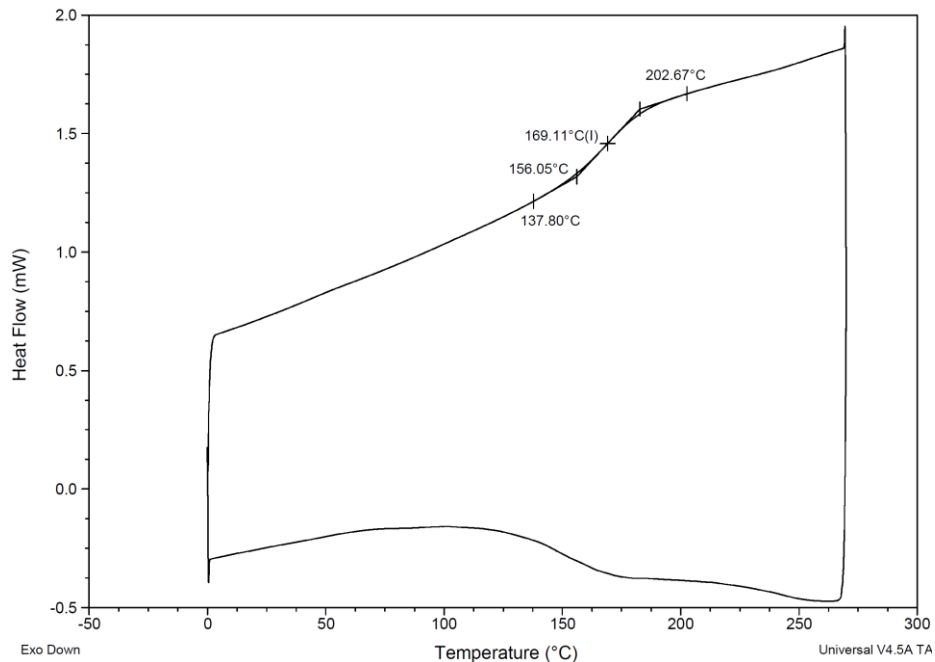


Figure E-12. DSC thermogram of poly-DHMP analogue from evan-2-evan and dimethyl 3-oxoglutarate (Figure 5-2, entry 4).

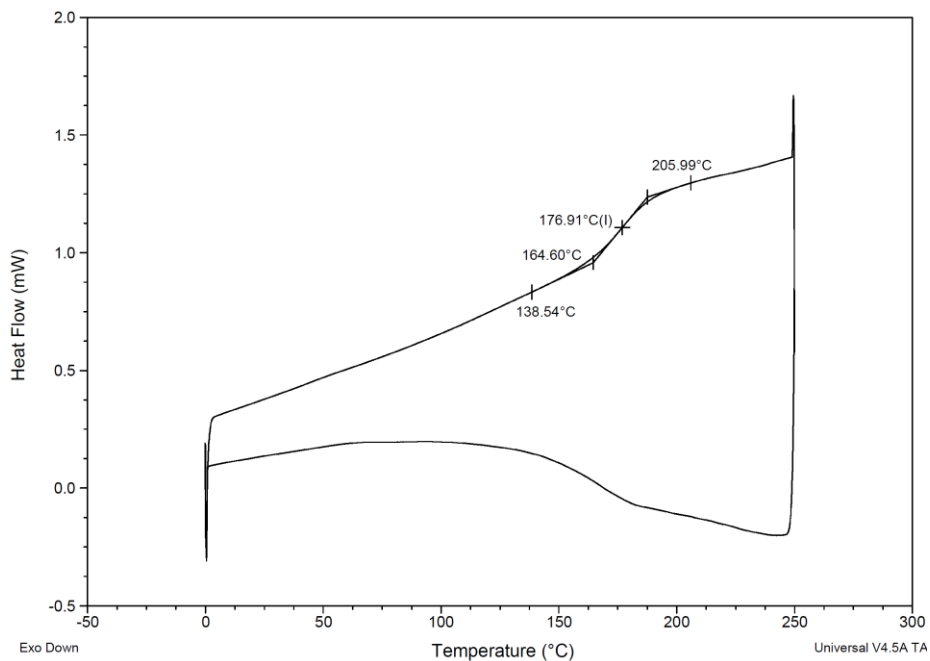


Figure E-13. DSC thermogram of poly-DHMP analogue from van-3-van and dimethyl 3-oxoglutarate (Figure 5-2, entry 6).

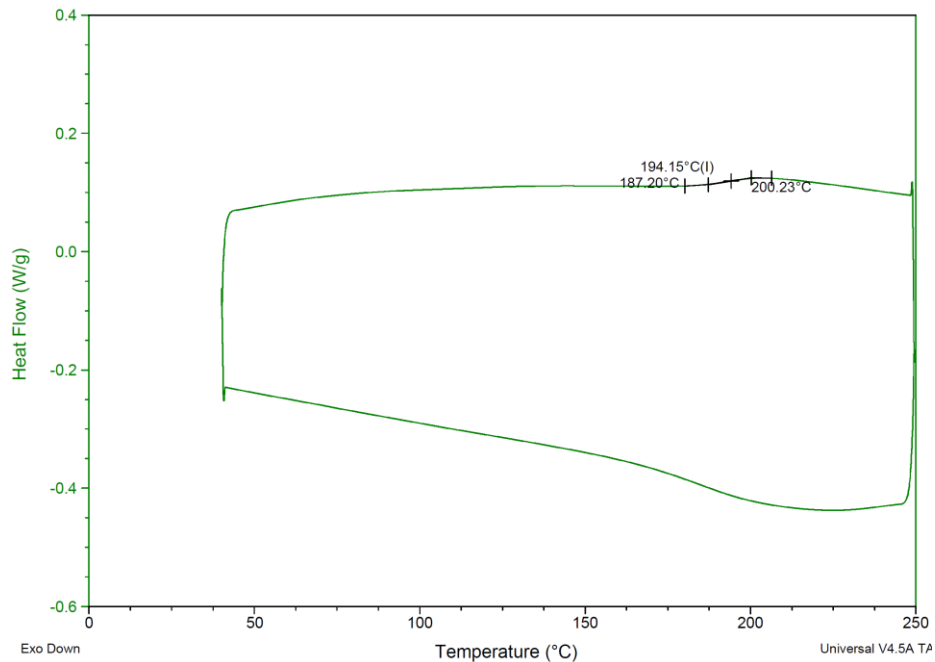


Figure E-14. DSC thermogram of poly-DHMP analogue from syr-3-syr and dimethyl 3-oxoglutarate (Figure 5-2, entry 7).

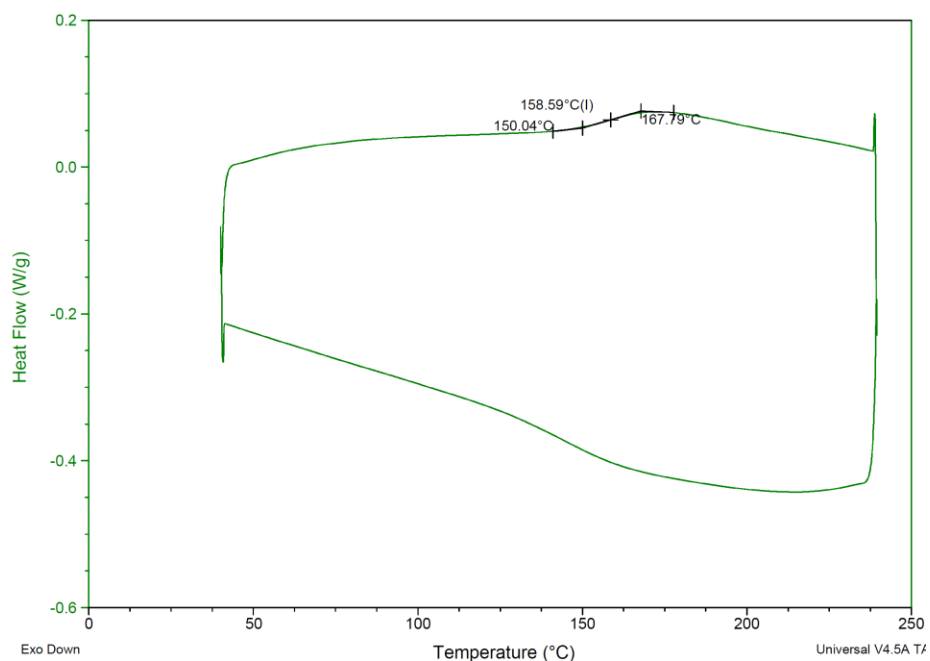


Figure E-15. DSC thermogram of poly-DHMP analogue from evan-3-evan and dimethyl 3-oxoglutarate (Figure 5-2, entry 8).

GPC Spectra

Molecular Weight Averages

| Peak | Mp | Mn | Mw | Mz | Mz+1 | Mv | PD |
|--------|-------|------|-------|--------|--------|--------|-------|
| Peak 1 | 31889 | 8184 | 55615 | 157758 | 311555 | 140481 | 6.796 |

Peak information

| | Start (mins) | End (mins) |
|-------------------|--------------|------------|
| Baseline region 1 | 0.76 | 3.64 |
| Baseline region 2 | 26.95 | 27.72 |
| Peak 1 | 13.20 | 22.66 |

| Peak | Trace | Peak Max RT (mins) | Peak Area (mV.s) | Peak Height (mV) |
|--------|-------|--------------------|------------------|------------------|
| Peak 1 | R1 | 17.99 | 2567964.056 | 8176.410 |

Chromatogram

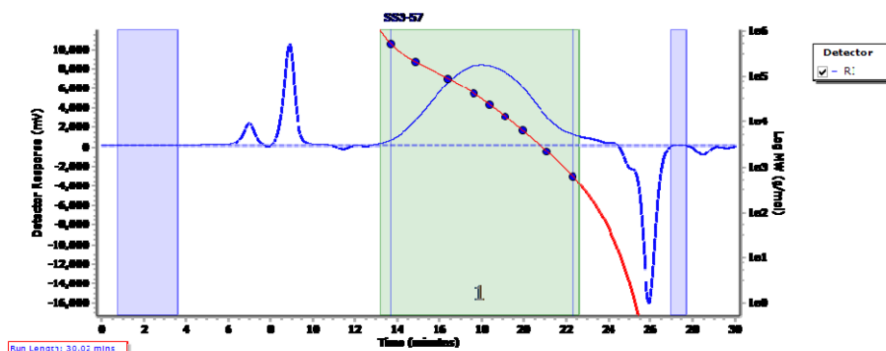


Figure E-16. GPC chromatogram of poly-DHMP analogue from 4HB-2-4HB and dimethyl 3-oxoglutarate (Figure 5-2, entry 1).

Molecular Weight Averages

| Peak | Mp | Mn | Mw | Mz | Mz+1 | Mv | PD |
|--------|-------|-------|-------|-------|-------|-------|-------|
| Peak 1 | 20292 | 11734 | 33490 | 65032 | 97999 | 60406 | 2.854 |

Peak information

| | Start (mins) | End (mins) |
|-------------------|--------------|------------|
| Baseline region 1 | 1.27 | 3.82 |
| Baseline region 2 | 26.95 | 27.42 |
| Peak 1 | 14.33 | 22.11 |

| Peak | Trace | Peak Max RT (mins) | Peak Area (mV.s) | Peak Height (mV) |
|--------|-------|--------------------|------------------|------------------|
| Peak 1 | R1 | 18.57 | 3592685.671 | 17646.893 |

Chromatogram

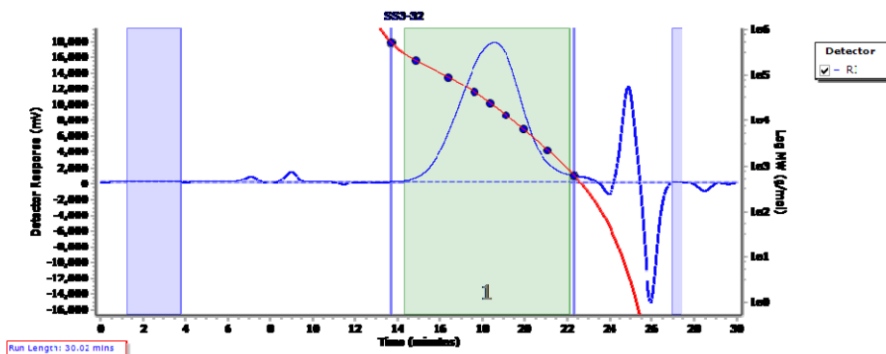


Figure E-17. GPC chromatogram of poly-DHMP analogue from van-2-van and dimethyl 3-oxoglutarate (Figure 5-2, entry 2).

Molecular Weight Averages

| Peak | Mp | Mn | Mw | Mz | Mz+1 | Mv | PD |
|--------|-------|-------|-------|--------|--------|-------|-------|
| Peak 1 | 27049 | 14557 | 49181 | 108080 | 201461 | 97812 | 3.379 |

Peak information

| | Start (mins) | End (mins) |
|-------------------|--------------|------------|
| Baseline region 1 | 1.42 | 4.33 |
| Baseline region 2 | 27.24 | 27.75 |
| Peak 1 | 13.35 | 22.30 |

| Peak | Trace | Peak Max RT (mins) | Peak Area (mV.s) | Peak Height (mV) |
|--------|-------|--------------------|------------------|------------------|
| Peak 1 | RI | 18.21 | 2321084.054 | 10496.213 |

Chromatogram

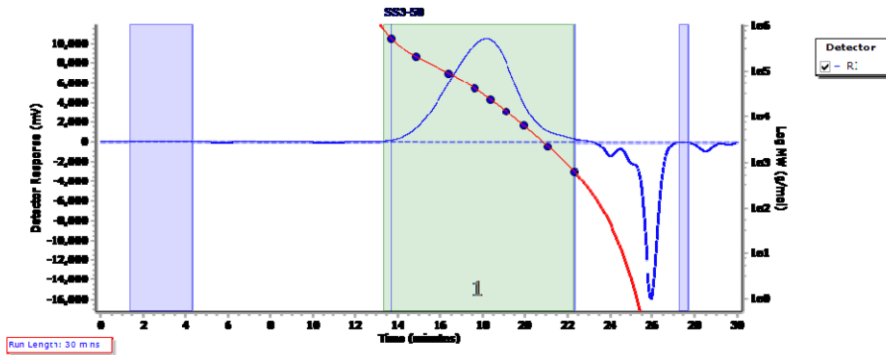


Figure E-18. GPC chromatogram of poly-DHMP analogue from syr-2-syr and dimethyl 3-oxoglutarate (Figure 5-2, entry 3).

Molecular Weight Averages

| Peak | Mp | Mn | Mw | Mz | Mz+1 | Mv | PD |
|--------|-------|-------|-------|-------|--------|-------|-------|
| Peak 1 | 22765 | 12101 | 36952 | 73331 | 114828 | 67794 | 3.054 |

Peak information

| | Start (mins) | End (mins) |
|-------------------|--------------|------------|
| Baseline region 1 | 2.44 | 4.80 |
| Baseline region 2 | 27.28 | 30.00 |
| Peak 1 | 14.11 | 22.26 |

| Peak | Trace | Peak Max RT (mins) | Peak Area (mV.s) | Peak Height (mV) |
|--------|-------|--------------------|------------------|------------------|
| Peak 1 | RI | 18.42 | 2505000.739 | 12263.069 |

Chromatogram

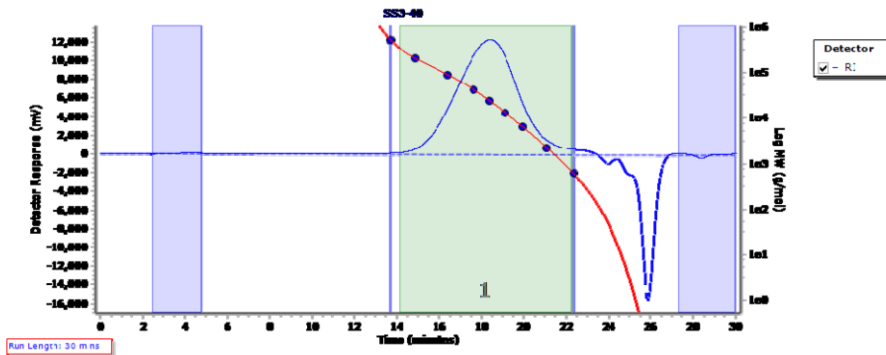


Figure E-19. GPC chromatogram of poly-DHMP analogue from evan-2-evan and dimethyl 3-oxoglutarate (Figure 5-2, entry 4).

Molecular Weight Averages

| Peak | Mp | Mn | Mw | Mz | Mz+1 | Mv | PD |
|--------|-------|------|-------|-------|--------|-------|-------|
| Peak 1 | 18605 | 8436 | 33420 | 74994 | 117239 | 69074 | 3.962 |

Peak information

| | Start (mins) | End (mins) |
|-------------------|--------------|------------|
| Baseline region 1 | 3.49 | 7.75 |
| Baseline region 2 | 27.17 | 27.68 |
| Peak 1 | 14.15 | 22.22 |

| Peak | Trace | Peak Max RT (mins) | Peak Area (mV.s) | Peak Height (mV) |
|--------|-------|--------------------|------------------|------------------|
| Peak 1 | RI | 18.67 | 2285041.902 | 9272.369 |

Chromatogram

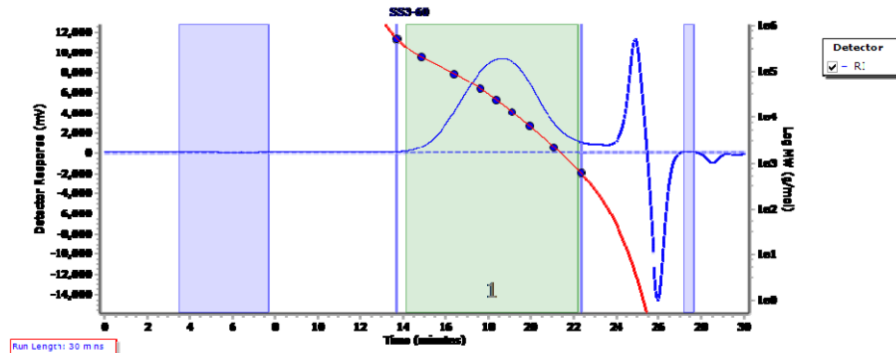


Figure E-20. GPC chromatogram of poly-DHMP analogue from 4HB-3-4HB and dimethyl 3-oxoglutarate (Figure 5-2, entry 5).

Molecular Weight Averages

| Peak | Mp | Mn | Mw | Mz | Mz+1 | Mv | PD |
|--------|-------|------|-------|-------|--------|-------|-------|
| Peak 1 | 18758 | 8960 | 30946 | 65248 | 104449 | 60030 | 3.454 |

Peak information

| | Start (mins) | End (mins) |
|-------------------|--------------|------------|
| Baseline region 1 | 2.07 | 3.89 |
| Baseline region 2 | 27.28 | 30.01 |
| Peak 1 | 14.18 | 22.48 |

| Peak | Trace | Peak Max RT (mins) | Peak Area (mV.s) | Peak Height (mV) |
|--------|-------|--------------------|------------------|------------------|
| Peak 1 | RI | 18.67 | 3135113.828 | 14992.236 |

Chromatogram

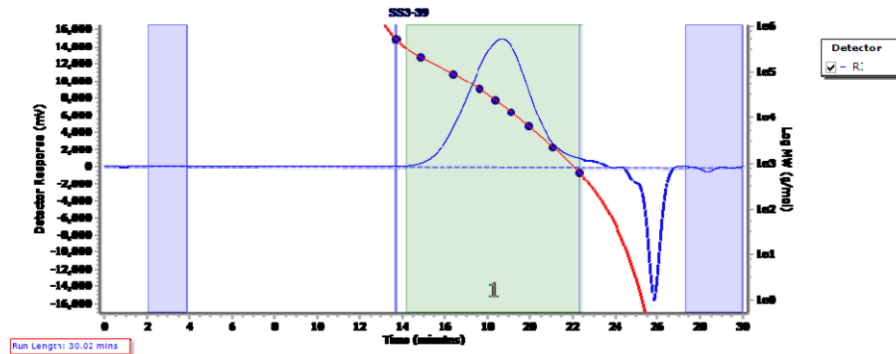


Figure E-21. GPC chromatogram of poly-DHMP analogue from van-3-van and dimethyl 3-oxoglutarate (Figure 5-2, entry 6).

Molecular Weight Averages

| Peak | Mp | Mn | Mw | Mz | Mz+1 | Mv | PD |
|--------|-------|-------|-------|-------|--------|-------|-------|
| Peak 1 | 23623 | 13667 | 37158 | 77228 | 146965 | 69961 | 2.719 |

Peak information

| | Start (mins) | End (mins) |
|-------------------|--------------|------------|
| Baseline region 1 | 1.31 | 2.98 |
| Baseline region 2 | 27.10 | 27.75 |
| Peak 1 | 13.53 | 22.11 |

| Peak | Trace | Peak Max RT (mins) | Peak Area (mV.s) | Peak Height (mV) |
|--------|-------|--------------------|------------------|------------------|
| Peak 1 | RI | 18.38 | 3896749.932 | 20554.323 |

Chromatogram

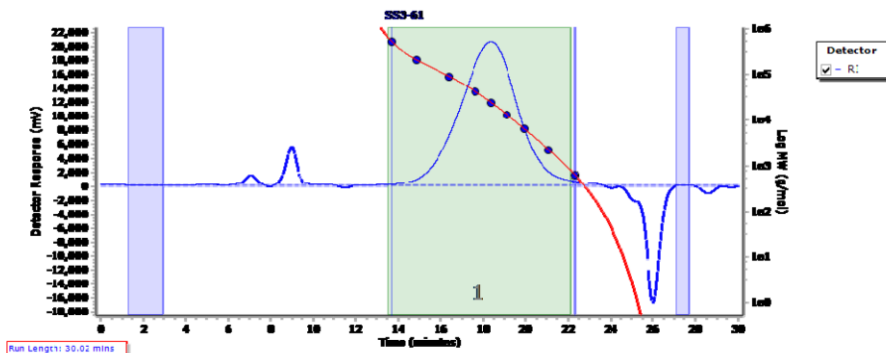


Figure E-22. GPC chromatogram of poly-DHMP analogue from syr-3-syr and dimethyl 3-oxoglutarate (Figure 5-2, entry 7).

Molecular Weight Averages

| Peak | Mp | Mn | Mw | Mz | Mz+1 | Mv | PD |
|--------|-------|-------|-------|-------|--------|-------|-------|
| Peak 1 | 23936 | 11650 | 39102 | 84300 | 148263 | 76833 | 3.356 |

Peak information

| | Start (mins) | End (mins) |
|-------------------|--------------|------------|
| Baseline region 1 | 2.29 | 4.26 |
| Baseline region 2 | 27.13 | 27.79 |
| Peak 1 | 13.57 | 22.26 |

| Peak | Trace | Peak Max RT (mins) | Peak Area (mV.s) | Peak Height (mV) |
|--------|-------|--------------------|------------------|------------------|
| Peak 1 | RI | 18.36 | 2881417.370 | 13593.723 |

Chromatogram

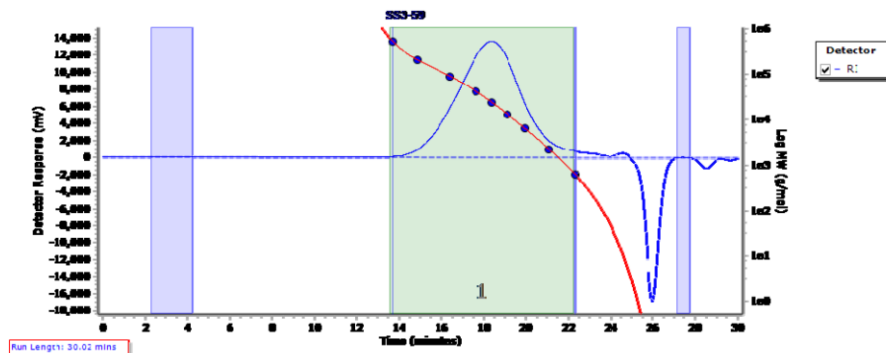


Figure E-23. GPC chromatogram of poly-DHMP analogue from evan-3-evan and dimethyl 3-oxoglutarate (Figure 5-2, entry 8).

NMR Spectra

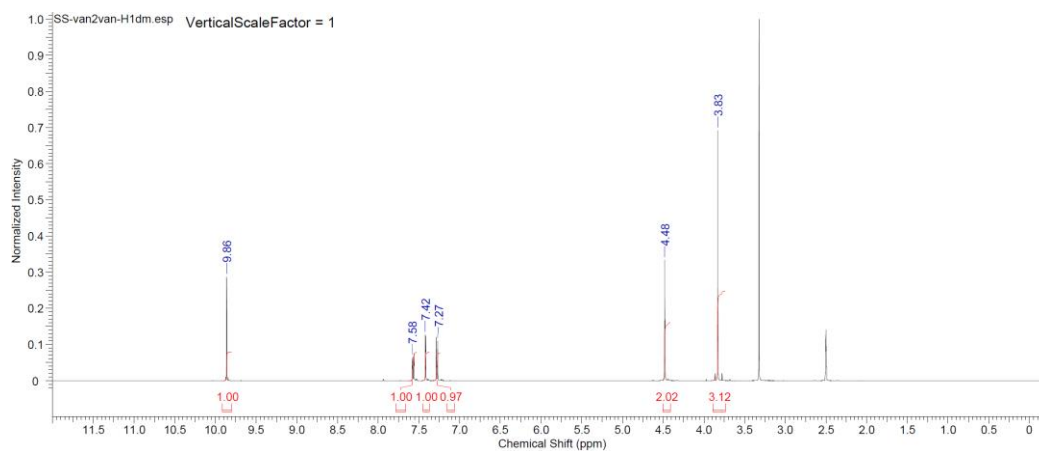


Figure E-24. ¹H NMR spectrum of van-2-van.

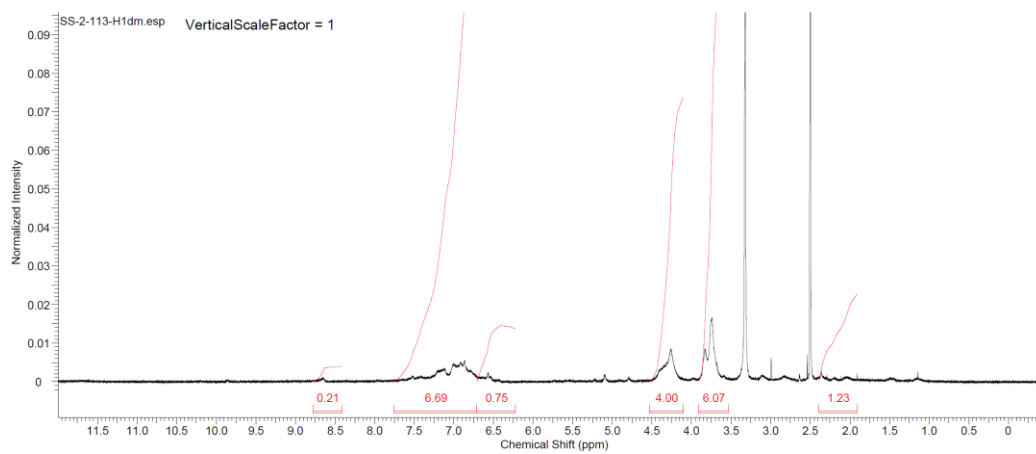


Figure E-25. ¹H NMR spectrum of poly-DHMP analogue from van-2-van and cyclopentanone (Table 5-1, entry 1).

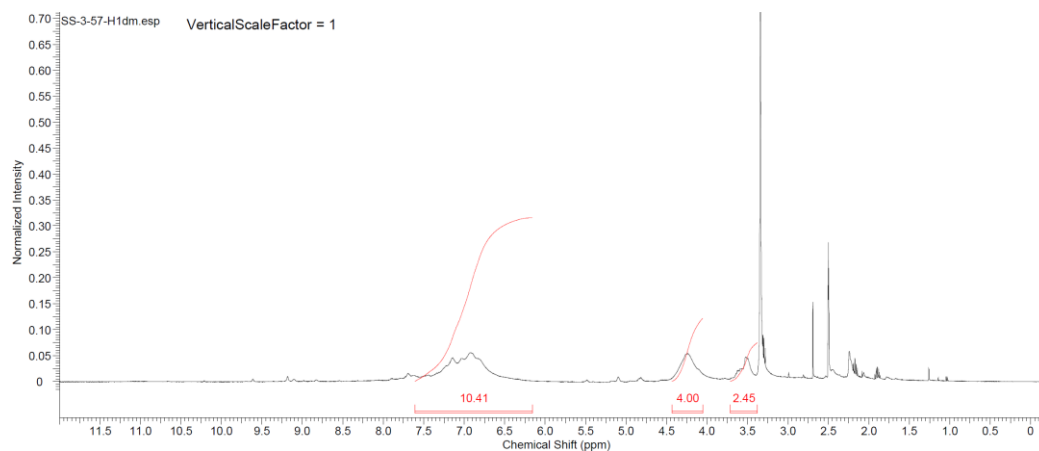


Figure E-26. ¹H NMR spectrum of poly-DHMP analogue from 4HB-2-4HB and dimethyl 3-oxoglutarate (Table 5-2, entry 1).

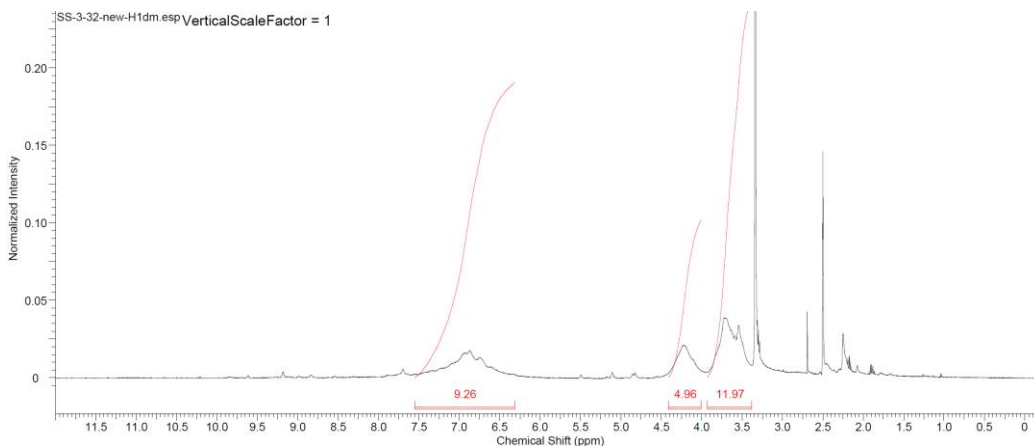


Figure E-27. ^1H NMR spectrum of poly-DHMP analogue from van-2-van and dimethyl 3-oxoglutarate (Table 5-2, entry 2).

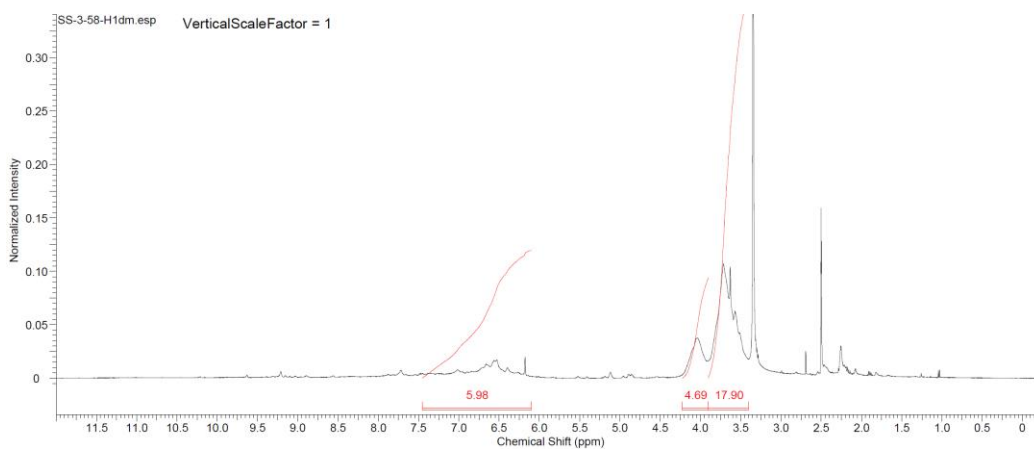


Figure E-28. ^1H NMR spectrum of poly-DHMP analogue from syr-2-syr and dimethyl 3-oxoglutarate (Table 5-2, entry 3).

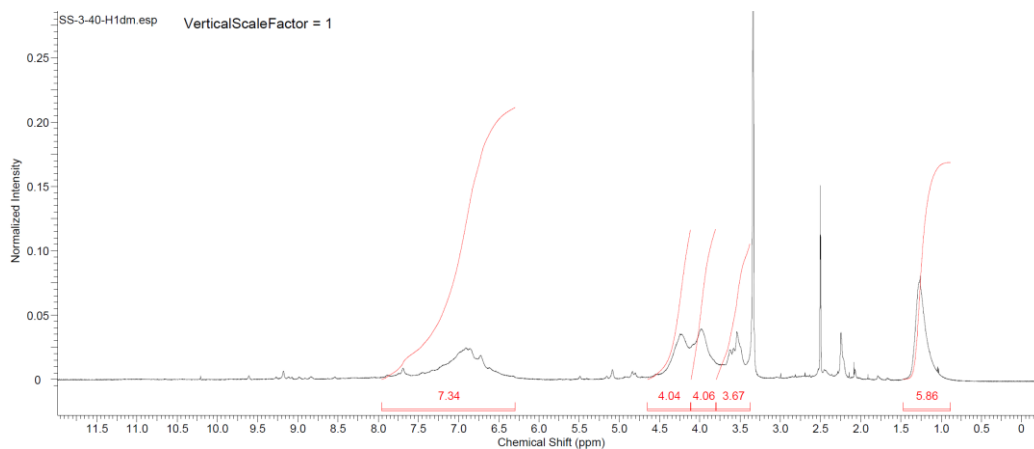


Figure E-29. ^1H NMR spectrum of poly-DHMP analogue from evan-2-evan and dimethyl 3-oxoglutarate (Table 5-2, entry 4).

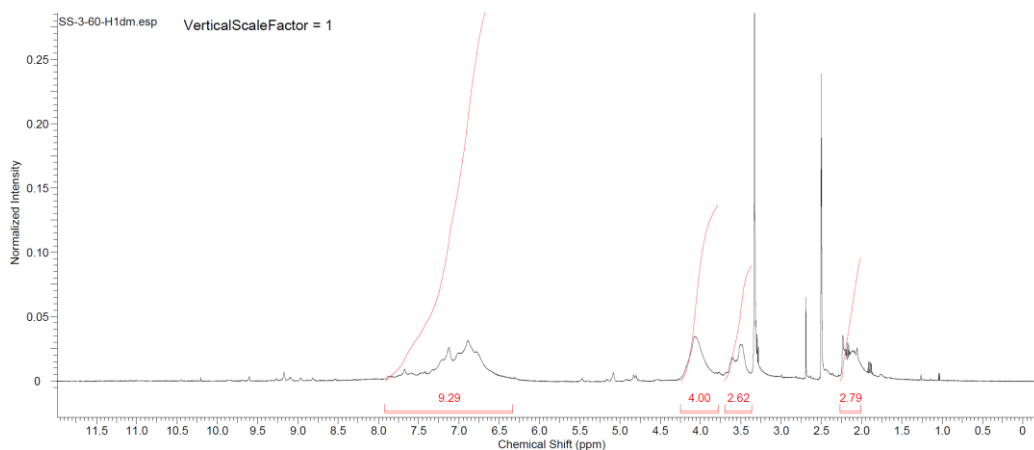


Figure E-30. ^1H NMR spectrum of poly-DHMP analogue from 4HB-3-4HB and dimethyl 3-oxoglutarate (Table 5-2, entry 5).

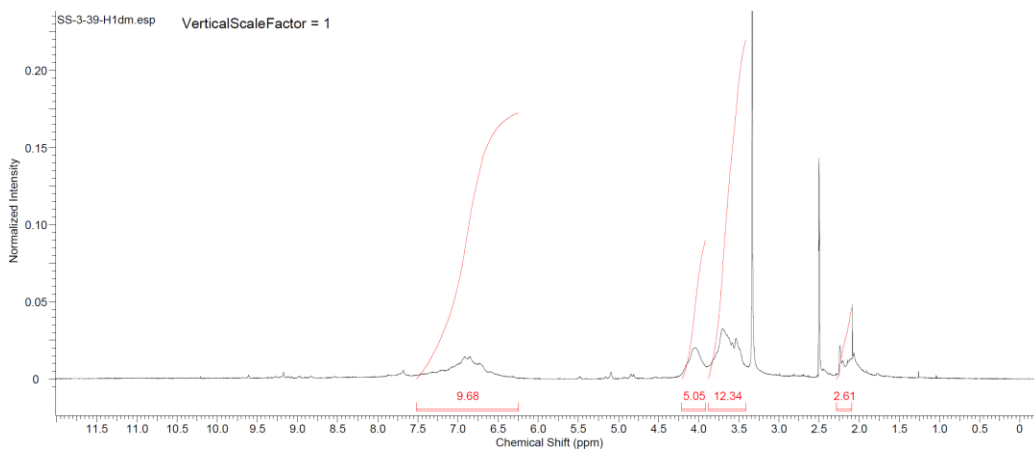


Figure E-31. ^1H NMR spectrum of poly-DHMP analogue from van-3-van and dimethyl 3-oxoglutarate (Table 5-2, entry 6).

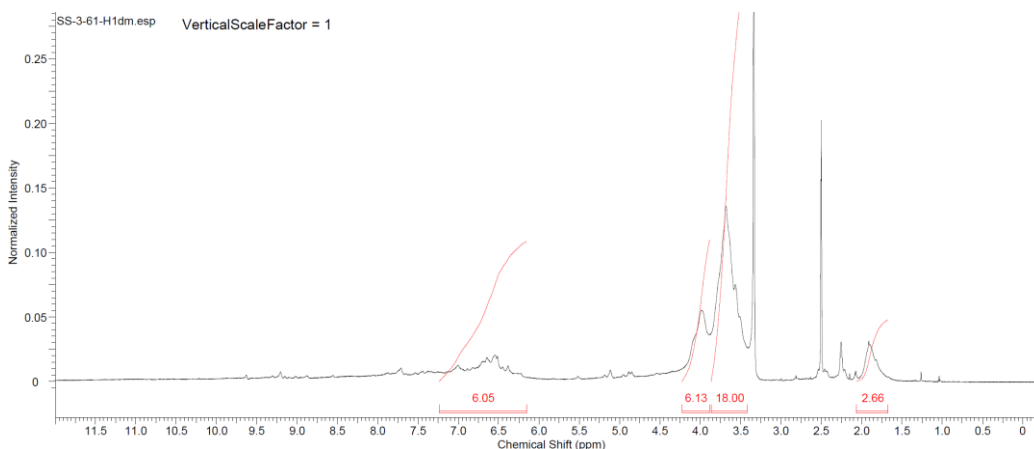


Figure E-32. ^1H NMR spectrum of poly-DHMP analogue from syr-3-syr and dimethyl 3-oxoglutarate (Table 5-2, entry 7).

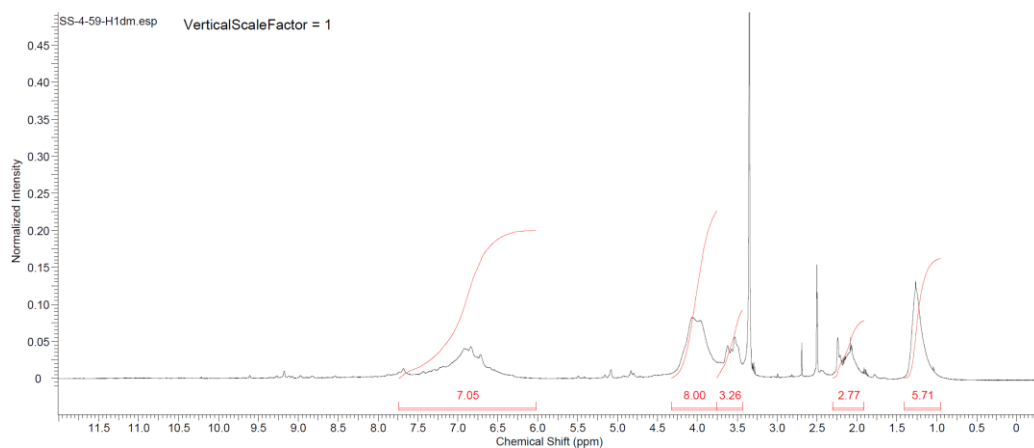


Figure E-33. ^1H NMR spectrum of poly-DHMP analogue from evan-3-evan and dimethyl 3-oxoglutarate (Table 5-2, entry 8).

BIOGRAPHICAL SKETCH

Steven Shen was born in Tanjungbalai – Asahan, North Sumatra, Indonesia. He attended Dian Harapan Daan Mogot senior high school in Jakarta, the capital city of Indonesia. He got exposed to the world of chemistry for the first time in this high school and he has been fascinated by chemistry since then. One day, he searched “the dirtiest river in the world” on the internet and he found out that the dirtiest in the world is actually located in Indonesia close to where he lived. During this time, he became aware of the plastics problem that Indonesia has faced for several decades. He hoped to do something about this problem, but he really did not know anything that he could do to help at that time, so he decided to keep studying until he found out the solution to this problem.

He obtained his bachelor’s degree in chemistry from Bandung Insititute of Technology in 2013. He landed a job as a high school chemistry teacher in SMAK1 BPK Penabur Bandung after graduation. However, his passion for chemistry and his fascination to sustainable polymers made him left this career and continued pursuing his education as a PhD in Chemistry at the University of Florida in 2014. He had enjoyed every single moments of his PhD study in Dr. Stephen A. Miller’s research group. He received his PhD from the University of Florida in 2019.

LIST OF REFERENCES

- 1 O. C. Eneh, *J. Applied Sci.*, 2011, **11**, 2084–2091.
- 2 BP Energy Economics, *BP Energy Outlook 2018 edition*, accessed February 2019, <https://www.bp.com/content/dam/bp/en/corporate/pdf/energy-economics/energy-outlook/bp-energy-outlook-2018.pdf>.
- 3 C. Pathak and H. C. Mandalia, *International Journal of Separation for Environmental Sciences*, 2012, **1**, 55–62.
- 4 M. L. Ross, *Annu. Rev. Polit. Sci.*, 2015, **18**, 239–259.
- 5 A. J. Venables, *Journal of Economic Perspectives*, 2016, **30**, 161–184.
- 6 M. Höök, R. Hirsch, and K. Aleklett, *Energy Policy*, 2009, **37**, 2262–2272.
- 7 I. Chapman, *Energy Policy*, 2014, **63**, 93–101.
- 8 REN21, *Renewables 2018 Global Status Report*, accessed February 2019, http://www.ren21.net/wp-content/uploads/2018/06/17-8652_GSR2018_FullReport_web_-1.pdf.
- 9 S. Prakash and K. Hinata, *Opera Botanica*, 1980, **55**, 1–57.
- 10 N. W. Simmonds, *Principles of Crop Improvement*, Longman, London, 1979.
- 11 T. Canam, X. Li, J. Holowachuck, M. Yu, J. Xia, R. Mandal, R. Krishnamurthy, S. Bouatra, I. Sinelnikov, B. Yu, L. Grenkow, D. S. Wishart, H. Steppuhn, K. C. Falk, T. J. Dumonceaux, and M. Y. Gruber, *Plant Science*, 2013, **198**, 17–26.
- 12 F. Zanetti, A. Monti, M. T. Berti, *Industrial Crops and Products*, 2013, **50**, 580–595.
- 13 R. S. Malik, *Exp. Agric.*, 1990, **26**, 125–130.
- 14 R. Seepaul, J. Marois, I. Small, S. George, D. L. Wright, *Agron. J.*, 2018, **110**, 1379–1389.
- 15 R. Seepaul, I. M. Small, M. J. Mulvaney, S. George, R. G. Leon, S. V. Paula-Moraes, D. Geller, J. J. Marois, and D. L. Wright, *Carinata, the Sustainable Crop for a Bio-based Economy: 2018–2019 Production Recommendations for the Southeastern United States*, UF/IFAS Extension, accessed February 2019, <https://edis.ifas.ufl.edu/pdf/AG/AG38900.pdf>.
- 16 R. Seepaul, S. George, D. L. Wright, *Industrial Crops and Products*, 2016, **94**, 872–883.
- 17 M. L. Chadha, M. O. Oluoch, D. Silue, *Acta Horticulturae*, 2007, **762**, 253–262.

- ¹⁸ S. I. Warwick, R. K. Gugel, T. McDonald, and K.C. Falk, *Genetic Resources and Crop Evolution*, 2006, **53**, 297–312.
- ¹⁹ D. C. Taylor, K. C. Falk, C. D. Palmer, J. Hammerlindl, V. Babic, E. Mietkiewska, A. Jadhav, E.-F. Marillia, T. Francis, T. Hoffman, E. M. Giblin, V. Katavic, W. A. Keller, *Biofuels, Bioprod. Bioref.*, 2010, **4**, 538–561.
- ²⁰ Food Standards Australia New Zealand, *Erucic Acid in Food: A Toxicological Review and Risk Assessment*, accessed February 2019, <http://www.foodstandards.gov.au/publications/documents/Erucic%20acid%20monograph.pdf>.
- ²¹ J. K. Kramer, F. D. Sauer, M. S. Wolynetz, E. R. Farnworth, K. M. Johnston, *Lipids*, 1992, **27**, 619–623.
- ²² A. Getinet, G. Rakow, J. P. Raney, R. K. Downey, *Can. J. Plant Sci.*, 1994, **74**, 793–795.
- ²³ A. Petersen, *Scientific Opinion on erucic acid in feed and food*, EFSA publication, Italy, 2016. DOI: 10.2903/j.efsa.2016.4593
- ²⁴ D. Biello, *The False Promise of Biofuels* in *Scientific American*, accessed February 2019, http://www.soest.hawaii.edu/oceanography/courses/OCN310_2/Fall14/files/essay3/biello.pdf.
- ²⁵ G. Fiorentino, M. Ripa, S. Mellino, S. Fahd, S. Ulgiati, *Journal of Cleaner Production*, 2014, **66**, 174–187.
- ²⁶ V. G. Semenov, D. U. Semenova, and V. P. Slipushenko, *Chemistry and Technology of Fuels and Oils*, 2006, **42**, 144–149.
- ²⁷ X. Zhao, L. Wei, S. Cheng, Y. Cao, J. Julson, Z. Gu, *Applied Catalysis A: General*, 2015, **507**, 44–55.
- ²⁸ K. Araújo, D. Mahajan, R. Kerr, M. da Silva, *Agriculture*, 2017, **7**, 32, doi:10.3390/agriculture7040032.
- ²⁹ S. G.- Garcia, C. M. Gasol, X. Gabarrell, J. Rieradevall, M. T. Moreira, G. Feijoo, *Renewable and Sustainable Energy Reviews*, 2009, **13**, 2613–2620.
- ³⁰ IRENA, *Biofuels for Aviation: Technology Brief*, International Renewable Energy Agency, Abu Dhabi, 2017.
- ³¹ Readifuels, *Applied Research Associates (ARA), National Research Council of Canada (NRC), Chevron Lummus Global (CLG), and Agrisoma Biosciences will partner to fly aircraft powered by 100% alternative jet fuel*, accessed March 2019, http://www.readifuels.com/news_sep-12.pdf.

- ³² Readifuels, *Chevron Lummus Global and ARA selected by Aemetis to Provide Technology for 100% Drop-in Alternative Fuels Production*, accessed March 2019, http://www.readifuels.com/news_sep-7.pdf
- ³³ Readifuels, *ReadiJet® Alternative Fuel Takes Flight: The world's first jet aircraft flight powered by 100%, un-blended, renewable jet fuel that meets petroleum jet fuel specifications land in Canada*, accessed March 2019, http://www.readifuels.com/includes/CSSLayouts/hometemp2_assets/Media%20Release-CLG-ARA-NRC-Flight_Oct30_12.pdf.
- ³⁴ *World First US-Australia Biofuel Flight Takes Off*, accessed March 2019, <https://www.qantasnewsroom.com.au/media-releases/world-first-us-australia-biofuel-flight-takes-off/>.
- ³⁵ J. Bachman, *Airlines' Biofuel-Powered Flights Might Soon Take Off*, accessed March 2019, <https://www.bloomberg.com/news/articles/2018-09-13/airlines-biofuel-powered-flights-might-soon-take-off>.
- ³⁶ A. P. M. M. Diniz, R. Sargeant, G. J. Millar, *Biotechnol. Biofuels*, 2018, **11**:161, <https://doi.org/10.1186/s13068-018-1158-0>.
- ³⁷ ARA, *Conversion of Carinata Oil into "Drop-In" Fuels & Chemicals*, accessed March 2019, <https://programs.ifas.ufl.edu/media/programsifasufledu/carinata/docs/pdfs/Coppola--Fuels-and-coproducts.pdf>.
- ³⁸ T. S. Schulmeister, M. R.-Moreno, G. M. Silva, M. G.-Ascolani, F. M. Ciriaco, D. D. Henry, G. C. Lamb, J. C. B. Dubeux, Jr., and N. DiLorenzo, *J. Anim. Sci.*, 2019, **97**, 1325–1334.
- ³⁹ W. R. Newson, R. Kuktaite, M. S. Hedenqvist, M. Gällstedt, and E. Johansson, *J. Am. Oil Chem. Soc.*, 2013, **90**, 1229–1237.
- ⁴⁰ USDA, *Crambe, Industrial Rapeseed, and Tung Provide Valuable Oils*, accessed March 2019, https://www.ers.usda.gov/webdocs/publications/37342/32910_ius6c_002.pdf?v=41471.
- ⁴¹ S. N. Raghallaigh, K. Bender, N. Lacey, L. Brennan, F. C. Powell, *Br. J. Dermatol.*, 2012, **166**, 279–287.
- ⁴² D. H. Katz, J. F. Marcelletti, M. H. Khalil, L. E. Pope, L. R. Katz, *Proc. Natl. Acad. Sci. USA*, 1991, **88**, 10825–10829.
- ⁴³ Glaxosmithkline Inc., *Abreva® Cream*, accessed March 2019, <https://www.abreva.com/cold-sore-products/abreva-cream/>.
- ⁴⁴ V. Chawla, S. A. Saraf, *J. Am. Oil Chem. Soc.*, 2001, **88**, 119–126.

- ⁴⁵ F. Gunstone, R. J. Hamilton, *Oleochemical manufacture and application*, CRC Press, USA, 2001, p. 325.
- ⁴⁶ H. J. Nieschlag, I. A. Wolff, *J. Am. Oil Chem. Soc.*, 1971, **48**, 723–727.
- ⁴⁷ K. D. Carlson, V. E. Sohns, R. B. Perkins, Jr., E. L. Huffman, *Ind. Eng. Chem., Prod. Res. Dev.*, 1977, **16**, 95–101.
- ⁴⁸ J. Schalau, *Backyard Gardener: Least Toxic Herbicides*, accessed March 2019, <https://cals.arizona.edu/yavapai/anr/hort/byg/archive/leasttoxicherbicides.html>.
- ⁴⁹ US EPA, *Scythe® Herbicide*, 2014, https://www3.epa.gov/pesticides/chem_search/ppls/010163-00325-20141017.pdf (accessed March 17th 2019).
- ⁵⁰ S. Ravi, D. Padmanabhan, V. R. Mamdapur, *J. Indian Inst. Sci.*, 2001, **81**, 299–312.
- ⁵¹ Industrial and Engineering Chemistry, *Children of Recovery*, 1936, **28**, 153–158. <https://pubs.acs.org/doi/pdf/10.1021/ie50314a003>.
- ⁵² H. J. Nieschlag, J. A. Rothfus, V. E. Sohns, and R. B. Perkins, Jr., *Ind. Eng. Chem., Prod. Res. Rev.*, 1977, **16**, 101–107.
- ⁵³ K.-S. Kim, and A. J. Yu, *J. Appl. Polym. Sci.*, 1979, **23**, 439–444.
- ⁵⁴ G. Impallomeni, A. Ballistreri, G. M. Carnemolla, S. P. P. Guglielmino, M. S. Nicolò, and M. G. Cambria, *International Journal of Biological Macromolecules*, 2011, **48**, 137–145.
- ⁵⁵ A. M. Bones, and J. T. Rossiter, *Physiologia Plantarum*, 1996, **97**, 194–208.
- ⁵⁶ I. A. Zasada, and H. Ferris, *Soil Biology & Biochemistry*, 2004, **36**, 1017–1024.
- ⁵⁷ T. Sotelo, M. Lema, P. Soengas, M. E. Cartea, and P. Velasco, *Appl Environ Microbiol*, 2014, **81**, 432–440.
- ⁵⁸ P. A. Egner, J.-G. Chen, A. T. Zarth, D K. Ng, J.-B. Wang, K. H. Kensler, L. P. Jacobson, A. Muñoz, J. L. Johnson, J. D. Groopman, J. W. Fahey, P. Talaly, J. Zhu, T.-Y. Chen, G.-S. Qian, S. G. Carmella, S. S. Hecht, T. W. Kensler, *Cancer Prev Res (Phila)*, 2014, **7**, 813–823.
- ⁵⁹ A. Mazumder, A. Dwivedi, J. du Plessis, *Molecules*, 2016, **21**, 416–426.
- ⁶⁰ B. Holst, and G. Williamson, *Nat. Prod. Rep.*, 2004, **21**, 425–447.
- ⁶¹ J. Alexander, G. A. Auðunsson, D. Benford, A. Cockburn, J.-P. Cravedi, E. Dogliotti, A. D. Domenico, M. L. F.-Cruz, P. Fürst, J. F.-Gremmels, C. L. Galli, P. Grandjean, J. Gzyl, G. Heinemeyer, N. Johansson, A. Mutti, J. Schlatter, R. van Leeuwen, C. van Peteghem, and P. Verger, *The EFSA Journal*, 2008, **590**, 1–76.

- ⁶² G. C. Mustakas, L. D. Kirk, E. L. Griffin, Jr., and A. N. Booth, *J. Am Oil Chem. Soc.*, 1976, **53**, 12–16.
- ⁶³ W. H. van Megen, *Can. Inst. Food Sci. Technol. J.*, 1983, **16**, 93–96.
- ⁶⁴ M. Alnsour, M. Kleinwächter, J. Böhme, and D. Selmar, *J. Sci. Food Agric.*, 2013, **93**, 918–923.
- ⁶⁵ Agrisoma, *Resonance Carinata 2015 Production Manual: A Guide to Best Management Practices*, Agrisoma Biosciences, Inc., Saskatoon, SK, Canada, 2015.
- ⁶⁶ A. C. Neish, *Ann. Rev. Plant Physiol.*, 1960, **11**, 55–80.
- ⁶⁷ N. Nićiforović, and H. Abramovič, *Comprehensive Reviews in Food Science and Food Safety*, 2014, **13**, 34–51.
- ⁶⁸ C. Chen, *Oxidative Medicine and Cellular Longevity*, 2016, Article ID 3571614, <http://dx.doi.org/10.1155/2016/3571614>.
- ⁶⁹ S. K. Nechipadappu, and D. R. Trivedi, *Journal of Molecular Structure*, 2018, **1171**, 898–905.
- ⁷⁰ K.-J. Yun, D.-J. Koh, S.-H. Kim, S. J. Park, J. H. Ryu, D.-G. Kim, J.-Y. Lee, and K.-T. Lee, *J. Agric. Food Chem.*, 2008, **56**, 10265–10272.
- ⁷¹ G. Kanchana, W. J. Shyni, M. Rajadurai, and R. Periasamy, *Global Journal of Pharmacology*, 2011, **5**, 33–39.
- ⁷² H.-L. Liu, X. Wan, X.-F. Huang, and L.-Y. Kong, *J. Agric. Food Chem.*, 2007, **55**, 1003–1008.
- ⁷³ Globe Newswire, *Butylated Hydroxytoluene Market worth \$380mn by 2025: Global Market Insights, Inc.*, accessed April 2019, <https://www.globenewswire.com/news-release/2019/04/08/1798813/0/en/Butylated-Hydroxytoluene-Market-worth-380mn-by-2025-Global-Market-Insights-Inc.html>.
- ⁷⁴ F. Aguilar, R. Crebelli, B. Dusemund, P. Galtier, J. Gilbert, D. M. Gott, U. G.-Remy, J. König, C. Lambré, J.-C. Leblanc, A. Mortensen, P. Mosesso, D. P.-Massin, I. M. C. M. Rietjens, I. Stankovic, P. Tobback, D. R. W.-Berendsen, R. A. Woutersen, M. C. Wright, *The EFSA Journal*, 2012, **10**, 25–88.
- ⁷⁵ F. Shahidi, U. N. Wanasundara, and R. Amarowicz, *Food Research International*, 1994, **27**, 489–493.
- ⁷⁶ M. H.-Roudsari, P. R. Chang, R. B. Pegg, and R. T. Tyler, *Food Chemistry*, 2009, **114**, 717–726.
- ⁷⁷ J. Dubie, A. Stancik, M. Morra, and C. Nindo, *Journal of Food Science*, 2013, **78**, 542–548.

- ⁷⁸ A. L. Flourat, G. Willig, A. R. S. Teixeira, and F. Allais, *Front. Sustain. Food Syst.*, 2019, **3**, 12. doi: 10.3389/fsufs.2019.00012.
- ⁷⁹ R. J. Mailer, A. McFadden, J. Ayton, B. Redden, *J Am Oil Chem Soc*, 2008, **85**, 937–944.
- ⁸⁰ European Bioplastics, *Bioplastics Market Data 2018*, 2018, accessed April 2019, https://www.european-bioplastics.org/wp-content/uploads/2016/02/Report_Bioplastics-Market-Data_2018.pdf.
- ⁸¹ R. S. Bezwada, US Pat., 8 318 973 B2, 2012.
- ⁸² F. D.-Néant, L. Migeot, L. Hollande, F. A. Reano, S. Domenek, and F. Allais, *Front. Chem.*, 2017, **5**, 126. doi: 10.3389/fchem.2017.00126.
- ⁸³ L. Hollande, and F. Allais, in *Green Polymer Chemistry: New Products, Processes, and Applications*, ACS Symposium Series, vol. 1310, ch. 15, pp. 221–251.
- ⁸⁴ H. T. H. Nguyen, M. H. Reis, P. Qi, and S. A. Miller, *Green Chem.*, 2015, **17**, 4503–4692.
- ⁸⁵ D. Couteau, and P. Mathaly, *Industrial Crops and Products*, 1997, **6**, 237–252.
- ⁸⁶ S. Ou, Y. Luo, F. Xue, C. Huang, N. Zhang, Z. Liu, *Journal of Food Engineering*, 2007, **78**, 1298–1304.
- ⁸⁷ S. Kennedy, and D. A. Rice, *Vet. Pathol.*, 1987, **24**, 265–271.
- ⁸⁸ B. M. L. Raun, and N. B. Kristensen, *Journal of Dairy Science*, 2011, **94**, 2566–2580.
- ⁸⁹ T. G. Fox, *Bull. Am. Phys. Soc.*, 1956, **1**, 123–124.
- ⁹⁰ J. K. Gupta, C. Jepsen, and H. Kneifel, *Journal of General Microbiology*, 1986, **132**, 2793–2799.
- ⁹¹ PlasticEurope, *Plastics – The Facts 2018*, accessed May 2019, https://www.plasticseurope.org/application/files/6315/4510/9658/Plastics_the_facts_2018_AF_web.pdf.
- ⁹² J. R. Jambeck, R. Geyer, C. Wilcox, T. R. Siegler, M. Perryman, A. Andrady, R. Narayan, K. L. Law, *Science*, 2015, **347**, 768–771.
- ⁹³ S. A. Miller, *Chem. Ind. Mag.*, 2013, **7**, 20–23.
- ⁹⁴ H. A. Neal and J. R. Schubel, *Solid Waste Management and the Environment: the Mounting Garbage and Trash Crisis*, Prentice-Hall, Englewood Cliffs, N.J., 1987.
- ⁹⁵ S. A. Miller, *ACS Macro Lett.*, 2013, **2**, 550–554.

- ⁹⁶ P. Degée and P. Dubois, Polylactides in *Kirk-othmer Encyclopedia of Chemical Technology*, John Wiley & Sons, New York, 2004, pp. 1–25.
- ⁹⁷ NatureWorks, *What is Ingeo*, accessed May 2019, <https://www.natureworkslc.com/What-is-Ingeo>.
- ⁹⁸ Total Corbion, *PLA (Poly Lactic Acid)*, accessed May 2019, <https://www.total-corbion.com/>.
- ⁹⁹ Kureha, *Kuredux® Polyglycolic Acid (PGA) Resin*, accessed May 2019, <http://www.kureha.com/pdfs/Kureha-KUREDUX.pdf>.
- ¹⁰⁰ K. Yamane, H. Sato, Y. Ichikawa, K. Sunagawa, Y. Shigaki, *Polymer Journal*, 2014, **46**, 769–775.
- ¹⁰¹ V. Singh and M. Tiwari, *Int. J. Polym. Sci.*, 2010, Article ID 652719, doi:10.1155/2010/652719.
- ¹⁰² O. Dechy-Cabaret, B. Martin-Vaca, and D. Borrisou, *Chem. Rev.*, 2004, **104**, 6147–6176.
- ¹⁰³ B. Azimi, P. Nourpanah, M. Rabiee, and S. Arbab, *J. Eng. Fibers Fabr.*, 2014, **9**, 74–90
- ¹⁰⁴ R. Auras, B. Harte, and S. Selke, *Macromol. Biosci.*, 2004, **4**, 835–864.
- ¹⁰⁵ V. Siracusa, P. Roculli, S. Romani, and M. D. Rosa, *Trends. Food. Sci. Technol.*, 2008, **19**, 634–643.
- ¹⁰⁶ G. L. Baker, E. B. Vogel, and M. R. Smith, *Polym. Rev.*, 2008, **48**, 64–84.
- ¹⁰⁷ E. Gautier, P. Fuertes, P. Cassagnau, J.-P. Pascault, and E. Fleury, *J. Polym. Sci., Part A1*, 2009, **47**, 1440–1449.
- ¹⁰⁸ H. T. H. Nguyen, P. Qi, M. Rostagno, A. Feteha, and S. A. Miller, *J. Mater. Chem. A.*, 2018, **6**, 9298–9331.
- ¹⁰⁹ M. Yin and G. L. Baker, *Macromolecules*, 1999, **32**, 7711–7718.
- ¹¹⁰ T. Liu, T. L. Simmons, D. A. Bohnsack, M. E. Mackay, M. R. Smith, and G. L. Baker, *Macromolecules*, 2007, **40**, 6040–6047.
- ¹¹¹ G. L. Fiore, F. Jing, J. V. G. Young, C. J. Cramer, and M. A. Hillmyer, *Polym. Chem.*, 2010, **1**, 870–877.
- ¹¹² K. M.-Benabdillah, J. Coudane, M. Boustta, R. Engel, and M. Vert, *Macromolecules*, 1999, **32**, 8774–8780.
- ¹¹³ K.M.-Benabdillah, M. Boustta, J. Coudane, and M. Vert, *Biomacromolecules*, 2001, **2**, 1279–1284.

- ¹¹⁴ E. Olewnik, W. Czerwiński, J. Nowaczyk, M. O. Sepulchre, M. Tessier, S. Salhi, and A. Fradet, *Eur. Polym. J.*, 2007, **43**, 1009–1019.
- ¹¹⁵ E. Olewnik and W. Czerwiński, *Polym. Degrad. Stab.*, 2009, **94**, 221–226.
- ¹¹⁶ Avantium, *Products & applications*, accessed May 2019.
<https://www.avantium.com/yxy/products-applications/>
- ¹¹⁷ A. Prieto, *Microb. Biotechnol.*, 2016, **9**, 652–657.
- ¹¹⁸ H. Hu, R. Zhang, J. Wang, W. B. Ying, L. Shi, C. Yao, Z. Kong, K. Wang, and J. Zhu, *Green Chem.*, 2019, Advance article, DOI: 10.1039/c9gc00668k.
- ¹¹⁹ H. T. H. Nguyen, G. N. Short, P. Qi, and S. A. Miller, *Green Chem.*, 2017, **19**, 1877–1888.
- ¹²⁰ A. C. Neish, *Ann. Rev. Plant Physiol.*, 1960, **11**, 55–80.
- ¹²¹ M. H.-Roudsarim P. R. Chang, R. B. Pegg, and R. T. Tyler, *Food Chemistry*, 2009, **114**, 717–726.
- ¹²² J. dubie, A. Stancik, M. Morra, and C. Nindo, *Journal of Food Science*, 2013, **78**, 542–548.
- ¹²³ S. Shen, J. A. Thomas, S. A. Miller, *Green Chem.*, 2019, **unpublished result**
- ¹²⁴ S. A. Miller, *SPARC Research Looks Beyond Fuels from Carinata in SPARC Plug May 2019*, accessed May 2019, <https://sparc-cap.org/sparc-plug-may-2019/>.
- ¹²⁵ U.-R. Samuel, W., Kohler, A. O. Gamer, and U. Keuser, *Ullmann's Encyclopedia of Industrial Chemistry*, 2012, **30**, 295–311.
- ¹²⁶ J. J. Garcia and S. A. Miller, *Polym. Chem.*, 2014, **5**, 955–961.
- ¹²⁷ O. Nsengiyumva and S. A. Miller, *Green Chem.*, 2019, **21**, 973–978.
- ¹²⁸ L. Mialon, R. Vanderhenst, A. G. Pemba, and S. A. Miller, *Macromol. Rapid Commun.*, 2011, **32**, 1386–1392.
- ¹²⁹ G. N. Short, H. T. H. Nguyen, P. I. Scheurle, and S. A. Miller, *Polym. Chem.*, 2018, **9**, 4113–4119.
- ¹³⁰ L. Mialon, A. G. Pemba, and S. A. Miller, *Green Chem.*, 2010, **12**, 1704–1706.
- ¹³¹ Y. Xiao, D. Cummins, A. R. A. Palmans, C. E. Koning, and A. Heise, *Soft Matter*, 2008, **4**, 593–599.
- ¹³² F. R. Marin, *Outlook on Agriculture*, 2016, **45**, 75–77.
- ¹³³ E. Lam, J. Shine Jr, J. D. Silva, M. Lawton, S. Bonos, M. Calvino, H. Carrer, M. C. S.-Filho, N. Glynn, Z. Helsels, J. Ma, E. R. Jr., G. M. Souza, and R. Ming, *GCB Bioenergy*, 2009, **1**, 251–255.

- ¹³⁴ D. Zhao, and Y.-R. Li, *International Journal of Agronomy*, 2015, Article ID 547386, <http://dx.doi.org/10.1155/2015/547386>.
- ¹³⁵ A. P. De Souza, M. Gaspar, E. A. Da Silva, E. C. Ulian, A. J. Waclawovsky, M. Y. Nishiyama Jr, R. V. Dos Santos, M. M. Teixeira, G. M. Souza, M. S. Buckeridge, *Plant Cell Environ*, 2008, **31**, 1116–1127.
- ¹³⁶ T. J. Rainey, G. Covey, D. Shore, *International Sugar Journal*, 2006, **108**, 640–644.
- ¹³⁷ J. Desjardins, *The World's Most Valuable Cash Crop*, accessed June 2019, <https://www.visualcapitalist.com/the-worlds-most-valuable-cash-crop/>.
- ¹³⁸ B. Leff, N. Ramankutty, J. A. Foley, *Global Biogeochemical Cycles*, 2004, **18**, GB1009, doi:10.1029/2003GB002108.
- ¹³⁹ B. Shiferaw, B. M. Prasanna, J. Hellin, M. Banziger, *Food Sec.*, 2011, **3**, 307–327.
- ¹⁴⁰ S. C. Fry, *Annu. Rev. Plant Physiol.*, 1986, **37**, 165–186.
- ¹⁴¹ R. D. Hartley, C. W. Ford, in *Plant Cell Wall Polymers, Biogenesis and Biodegradation*, ed. N. G. Lewis, M. G. Paice, ACS Symposium Series 399, American Chemical Society, Washington, DC, 1989, pp. 137–145.
- ¹⁴² H. G. Jung, D. A. Deetz, in *Forage Cell Wall Structure and Digestibility*, ed. H. G. Jung, D. R. Buxton, R. D. Hatfield, J. Ralph, ASA-CSSA-SSSA, Madison, WI, 1993, pp. 315–346.
- ¹⁴³ C. Y. Lee, A. Sharma, R. L. Uzarski, J. E. Cheong, H. Xu, R. A. Held, S. K. Upadhaya, and J. L. Nelson, *Free Radical Biol. Med.*, 2011, **50**, 918–925.
- ¹⁴⁴ L. R. Ferguson, S. Zhu, and P. J. Harris, *Mol. Nutr. Food Res.*, 2005, **49**, 585–693.
- ¹⁴⁵ K. Kikugawa, T. Hakamada, M. Hanusuma, and T. Kurechi, *J. Agric. Food. Chem.*, 1983, **31**, 780–785.
- ¹⁴⁶ M. Kampa, V. I. Alexaki, G. Notas, A. P. Nifli, A. Nistikaki, A. Hatzoglou, E. Bakogeorgou, E. Kouimtzoglou, G. Blekas, D. Boskou, A. Gravanis, and E. Castanas, *Breast Cancer Res. Treat.*, 2004, **6**, 63–74.
- ¹⁴⁷ Y. S. Lee, *Arch. Pharmacol Res.*, 2005, **8**, 1183–1189.
- ¹⁴⁸ R. Scherer and H. T. Godoy, *Rev. Bras. Pl. Med.*, 2014, **16**, 41–46.
- ¹⁴⁹ C. G. Pereira, L. Barreira, S. Bitttebier, L. Pieters, C. Marques, T. F. Santos, M. J. Rodrigues, J. Varela, and L. Custodio, *Scientific Reports*, 2018, 8:4689, doi:10.1038/s41598-018-23038-6.
- ¹⁵⁰ H. Nawaz, S. Muzaffar, M. Aslam, and S. Ahmad, in *Phytochemical Composition: Antioxidant Potential and Biological Activities of Corn*, IntechOpen, pp. 49–68.

- ¹⁵¹ Source Naturals, *Trans-Ferulic Acid*, accessed June 2019, <https://www.sourcenaturals.com/products/GP1298/>.
- ¹⁵² K. Zdunska, A. Dana, A. Kolodziejczak, and H. Rotsztein, *Skin Pharmacol. Physiol.*, 2018, **31**, 332–336.
- ¹⁵³ S. Matthew and T. E. Abraham, *Enzyme Microb. Technol.*, 2005, **36**, 565–570.
- ¹⁵⁴ T. B. T. Lam, K. Iiyama, B. A. Stone, *Phytochemistry*, 1994, **36**, 773–775.
- ¹⁵⁵ L. Saulnier, C. Marot, E. Chanliiaud, J. F. Thibault, *Carbohydr. Polym.*, 1995, **26**, 279–287.
- ¹⁵⁶ A. Saadi, I. Lempereur, S. Sharanov, J. C. Autran, M. Manfait, *J. Cereal Sci.*, 1998, **28**, 107–114.
- ¹⁵⁷ J. X. Sun, X. F. Sun, R. C. Sun, Y. Q. Su, *Carbohydr. Polym.*, 2004, **56**, 195–204.
- ¹⁵⁸ F. J. Barba, O. Parniakov, S. A. Pereira, A. Wiktor, N. Grimi, N. Boussetta, J. Saraiva, J. Raso, O. M.-Belloso, D. W.-Rajchert, O. Bals, E. Vorobiev, N. Lebovka, *Food Eng. Rev.*, 2015, **77**, 773–798.
- ¹⁵⁹ B. A. A.-Estrada, J. A. G.-Uribe, S. O. S.-Saldivar, *Food Chem.*, 2014, **152**, 46–55.
- ¹⁶⁰ H. V. Annegowda, R. Bhat, L. M.-Tze, A. A. Karim, S. M. Mansor, *J. Food. Sci. Technol.*, 2012, **49**, 510–514.
- ¹⁶¹ H. F. Zhang, X.-H. Yang, Y. Wang, *Trends Food Sci. Technol.*, 2011, **22**, 672–688.
- ¹⁶² Worldwatch Institute, *Global Plastic Production Rises, Recycling Lags*, 2015. <http://www.worldwatch.org/global-plastic-production-rises-recycling-lags-0>
- ¹⁶³ PlasticsEurope (PERMG)/Consultic *Plastics, the Facts 2015*. http://www.plasticseurope.org/documents/document/20151216062602-plastics_the_facts_2015_final_30pages_14122015.pdf
- ¹⁶⁴ World Economic Forum, *The new plastics economy, rethinking the future of plastics*, 2016. <https://www.weforum.org/reports/the-new-plastics-economy-rethinking-the-future-of-plastics/>
- ¹⁶⁵ Z. Lixin and F. Ping, China Daily Europe, *Overcapacity drives new approaches to production*, 2014. http://europe.chinadaily.com.cn/epaper/2014-09/26/content_18664501.htm
- ¹⁶⁶ V. Goodship and D. K. Jacobs in *Polyvinyl alcohol: materials, processing and applications*, ed. E. Ogur, Smithers Rapra, 2005, report 192, vol. 16, number 12.
- ¹⁶⁷ Hikasa, J.-I, in *Fibers, Poly(Vinyl Alcohol)*. *Kirk-Othmer Encyclopedia of Chemical Technology*. John Wiley & Sons: New York, 2000.
- ¹⁶⁸ M. Zhang and Y. Yu, *Ind. Eng. Chem. Res.* 2013, **52**, 9505.

- 169 V. J. Johnston, J. H. Zink, L. Chen, B. F. Kimmich and J. T. Chapman, *U.S. Patent* 8,178,715 B2, 2012.
- 170 C. Kelly, C. DeMerlis, D. Schoneker and J. Borzelleca, *Food Chem. Toxicol.*, 2003, **41**, 719.
- 171 C. DeMerlis and D. Schoneker, *Food Chem. Toxicol.*, 2003, **41**, 319.
- 172 B. L. Lopez, A. I. Mejia and L. Sierra, *Polym. Eng. Sci.*, 1999, **39**, 1346.
- 173 R. Solaro, A. Corti and E. Chiellini, *Polym. Adv. Technol.*, 2000, **11**, 873
- 174 J. Pajak, M. Ziemski and B. Nowak, *Chemik*, 2010, **64**, 523.
- 175 W. Wan, A. D. Bannerman, L. Yang, and H. Mak, in *Polymeric Cryogels: Macroporous Gels with Remarkable Properties*, ed. O. Okay, Springer International Publishing, Cham, 2014, pp. 283–321.
- 176 Analysis of 2016 polyvinyl alcohol imports, Zauba Technologies & Data Services, Ltd. <https://www.zaubacom/importanalysis-polyvinyl+alcohol-report.html>
- 177 J. W. Knapczyk in *Vinyl Acetal Polymers. Kirk-Othmer Encyclopedia of Chemical Technology*. John Wiley & Sons: New York, 2000.
- 178 JNC, Chemical products. <http://www.jnc-corp.co.jp/english/product/chemical/chemical-p.html>
- 179 Kuraray Mowital® and Pioloform®. <http://www.kuraray.us.com/products/resins/mowital-pioloform/>
- 180 Butvar® information page, Eastman. <http://www.butvar.com/en/home.aspx>
- 181 Butacite® or Trosifol® Polyvinyl Butyral (PVB) Interlayers, Kuraray. <http://glasslaminatingsolutions.kuraray.com/products/>
<http://www.kuraray.us.com/films/butacite/>
- 182 B. Yang, R. Liu, J. Huang and H. Sun, *Ind. Eng. Chem. Res.* 2013, **52**, 7425.
- 183 Eastman Butvar, polyvinyl butyral resin. Properties and uses. http://www.butvar.com/pdfs/en/butvar_properties_and_uses.pdf
- 184 Z. M. Zhou, D. J. David, W. J. Macknight and F. E. Karasz. *Turk. J. Chem.*, 1997, **21**, 229.
- 185 M. Hajian, G. A. Koohmareh and M. Rastgoo, *J. Appl. Polym. Sci.*, 2010, **115**, 3592
- 186 Y. Ogata, M. Okano and T. Ganke, *J. Am. Chem. Soc.*, 1956, **78**, 2962.
- 187 M. D. Fernández, M. J. Fernández and P. Hoces, *J. Appl. Poly. Sci.*, 2006, **102**, 5007-5017.
- 188 C. Gousse and A. Gandini, *Eur. Poly. J.*, 1997, **33**, 667.

- ¹⁸⁹ C. Gaina, O. Ursache, V. Gaina, E. Buruiana and D. Ionita, *Express Polym. Lett.*, 2012, **6**, 129.
- ¹⁹⁰ Y. A. Kurskii, L. N. Beloded, N. K. Kobayakova, V. N. Kurskaya, K. S. Ludanova, E. P. Pashkina, M. Yu. Ryabinina and A. G. Rodionov, *Russ. J. Appl Chem.*, 2011, **84**, 1828.
- ¹⁹¹ P. Chetri and N. N. Dass, *J. Appl. Poly. Sci.*, 1996, **62**, 2139.
- ¹⁹² E. Schacht, G. Desmarests, E. Goethals and T. St. Pierre, *Macromolecules*, 1983, **16**, 291.
- ¹⁹³ E. Delattre, G. Lemiere, J. Desmurs, B. Boulay and E. Dunach, *J. Appl. Poly. Sci.*, 2014, DOI: 10.1002/APP.40677.
- ¹⁹⁴ M. L. O'Neill, D. Newman and E. Beckman, *Polym. Eng. Sci.*, 1999, **5**, 862.
- ¹⁹⁵ A. Llevot, E. Grau, S. Carlotti, S. Grelier and H. Cramail, *Macromol. Rapid Commun.*, 2016, **37**, 9.
- ¹⁹⁶ H. T. H. Nguyen, E. R. Suda, E. M. Bradic, J. A. Hvozdoovich and S. A. Miller, Polyesters from Bio-Aromatics, in *ACS Symposium Series Green Polymer Chemistry III: Biobased Materials and Biocatalysis*, ed. H. N. Cheng, R. A. Gross and P. B. Smith, 2015, vol. 1192, pp. 401–409.
- ¹⁹⁷ H.-J. Jin, B.-Y. Lee, M.-N. Kim and J.-S. Yoon, *J. Polym. Sci. Part B Polym. Phys.*, 2000, **38**, 1504.
- ¹⁹⁸ A. L. Holmberg, N. A. Nguyen, M. G. Karavolias, K. H. Reno, R. P. Wool and T. H. Epps, III, *Macromolecules* 2016, **49**, 1286.
- ¹⁹⁹ A. L. Holmberg, K. H. Reno, N. A. Nguyen R. P. Wool and T. H. Epps, III, *ACS Macro Lett.*, 2016, **5**, 574.
- ²⁰⁰ H. Liu, B. Lepoittevin, C. Roddier, V. Guerineau, L. Bech, J. Herry, M. Bellon-Fontaine and P. Roger, *Polymer*, 2011, **52**, 1908.
- ²⁰¹ A. G. Pemba, J. A. Flores and S. A. Miller, *Green Chem.*, 2013, **15**, 325.
- ²⁰² S. Chikkali, F. Stempfle and S. Mecking. *Macromol. Rapid Commun.*, 2012, **33**, 1126.
- ²⁰³ B. S. Rajput, S. R. Gaikwad, S. K. Menon and S. H. Chikkali, *Green Chem.*, 2014, **16**, 3810.
- ²⁰⁴ B. S. Rajput, U. Chander, K. Arole, F. Stempfle, S. Menon, S. Mecking and S. H. Chikkali, *Macromol. Chem. Phys.* 2016, **217**, 1396.
- ²⁰⁵ S. D. Luebben and J. W. Raebiger, A Novel Renewable Thermoplastic Polyacetal by Polymerization of Glycolaldehyde Dimer, a Major Product of the Fast Pyrolysis of Cellulosic Feedstock, in *ACS Symposium Series Green Polymer Chemistry III:*

- Biobased Materials and Biocatalysis*, ed. H. N. Cheng, R. A. Gross and P. B. Smith, 2015, vol. 1192, pp. 305-328.
- ²⁰⁶ A. G. Pemba, M. Rostagno, T. A. Lee and S. A. Miller *Polym. Chem.*, 2014, **5**, 3214.
- ²⁰⁷ M. Rostagno, E. J. Price, A. G. Pemba, I. Ghiriviga, K. A. Abboud and S. A. Miller, *J. Appl. Polym. Sci.*, 2016, **133**, 44089.
- ²⁰⁸ B. M. Budhlall, K. Landfester, E. D. Sudol, V. L. Dimonie, A. Klein and M. S. El-Aasser, *Macromolecules*, 2003, **36**, 9477.
- ²⁰⁹ C. Saiz-Jimenez and J. W. De Leeuw, *Org. Geochem.*, 1986, **10**, 869.
- ²¹⁰ R. Behling, S. Valange and G. Chatel, *Green Chem.*, 2016, **18**, 1839.
- ²¹¹ Sigma-Aldrich Ingredients Catalogue: Flavors and Fragrances, 2014.
- ²¹² 3-methoxysalicylaldehyde, PubChem.
<https://pubchem.ncbi.nlm.nih.gov/compound/3-Methoxysalicylaldehyde#section=Information-Sources>
- ²¹³ Isovanillin, PubChem.
<https://pubchem.ncbi.nlm.nih.gov/compound/12127#section=Top>
- ²¹⁴ R. van Putten, J. C. van der Waal, E. de Jong, C. B. Rasrendra, H. J. Heeres and J. G. de Vries, *Chem. Rev.*, 2013, **113**, 1499.
- ²¹⁵ A. F. Sousa, C. Vilela, A. C. Fonseca, M. Matos, C. S. R. Freire, G.-J. M. Gruter, J. F. J. Coelho and A. J. D. Silvestre, *Polym. Chem.*, 2015, **6**, 5961.
- ²¹⁶ A. Scott, *BASF and Avantium join for biopolyester*, CE&En News, Volume 94, Issue 12, p. 15, March 2016. <http://cen.acs.org/articles/94/i12/BASF-Avantium-combine-bio-polyester.html>.
- ²¹⁷ D. Prat, J. Hayler and A. Wells, *Green Chem.*, 2014, **16**, 4546.
- ²¹⁸ K. Katsurayaa, K. Hatanaka, K. Matsuzaki and S. Amiya, *Polymer*, 2001, **42**, 9855.
- ²¹⁹ E. Hans-Georg in *Macromolecules*, Plenum Press, New York, 1977, vol. 2, ch. 23, pp. 815–818.
- ²²⁰ N. A. Plate and O. V. Noah, *Adv. Polym. Sci.*, 1979, **31**, 133.
- ²²¹ P. J. Flory, *J. Am. Chem. Soc.*, 1939, **61**, 1518.
- ²²² P. Chetri and N. N. Dass, *Polymer*, 1997, **38**, 3951.
- ²²³ Polymer Properties Database, *Chemical Data Retrieval on the Web (CROW)*.
<http://polymerdatabase.com/polymer%20physics/Polymer%20Tg%20C.html>.
- ²²⁴ D. B. Priddy, "Styrene Plastics" in *Kirk-Othmer Encyclopedia of Chemical Technology*, John Wiley & Sons, Inc.: New York, **2006**, Vol. 23, pp. 358–416.

- ²²⁵ B. H. Rotstein, S. Zaretsky, V. Rai, A. K. Yudin, *Chem. Rev.*, 2014, **114**, 8323–8359.
- ²²⁶ A. E. J. de Nooy, G. Masci, V. Crescenzi, *Macromolecules*, 1999, **32**, 1318–1320.
- ²²⁷ C. V. Robotham, C. Baker, B. Cuevas, K. Abboud, D. L. Wright, *Mol. Div.*, 2003, **6**, 237–244.
- ²²⁸ O. Kreye, T. Toth, M. A. R. Meier, *J. Am. Chem. Soc.*, 2011, **133**, 1790–1792.
- ²²⁹ P. Biginelli, *Ber. Dtsch Chem. Ges.*, 1891, **24**, 1317–1319.
- ²³⁰ M. Lei, M. Lei, L. Hu, *Monatsh Chem.*, 2010, **141**, 1005–1008.
- ²³¹ H. Nagarajaiah, A. Mukhophadhyay, J. N. Moorthy, *Tetrahedron Lett.*, 2016, **57**, 5135–5149.
- ²³² H. von Pechmann, *Ber. Dtsch Chem. Ges.*, 1884, **17**, 2542–2543.
- ²³³ A. Strecker, *Liebigs Annalen*, 1850, **75**, 27–45.